

AFSWP-895

THIS DOCUMENT CONSISTS OF 570 PAGES  
OF 325 SHEETS SERIES A

US DOE ARCHIVES  
326 U.S. ATOMIC ENERGY  
RG COMMISSION

Collection DAS McCRAW

Box 22 Job 1320

Folder FALL-OUT SYMPOSIUM-AFSWP-895

107366

FALL - OUT SYMPOSIUM

(██████████)

unclassified

4/12/85  
by [unclear]  
in MR  
new file

JANUARY 1955

SPECIAL HANDLING  
NOT TO BE SHOWN TO FOREIGNERS

CLASSIFICATION CANCELLED \*  
WITH DELETIONS  
BY AUTHORITY OF DOE/OC

D. Diaz 2/19/91  
REVIEWED BY DATE

\* CTR DNA SWISHER TO  
DOE MA-225, 3-5-90

Rahn 2/12/92

ARMED FORCES SPECIAL WEAPONS PROJECT  
WASHINGTON 25, D.C.

Within the  
referred to in  
any manner or  
and 704. The  
of its contents in any manner by  
person is prohibited by law."

ATOMIC ENERGY ACT 1954

AFSWP-895

FALL-OUT SYMPOSIUM

JANUARY 1955

~~This document contains information affecting the national defense of the United States within the meaning of the Espionage Laws, Title 18, U.S.C., Sections 793 and 794. The transmission or the revelation of its contents in any manner to an unauthorized person is prohibited by law.~~

~~This document contains RESTRICTED DATA within the meaning of the Atomic Energy Act of 1954. Its transmission or the revelation of its contents, in any manner not authorized by that Act, is prohibited by law.~~

~~DOE ARCHIVES~~

~~Reproduction of this document in whole or in part is prohibited except with permission of the Chief, AFSWP.~~

7/18/88

INCOMPLETE DOCUMENT REFERENCE SHEET

The archive copy of this document is incomplete.

Pages missing 2 11

Enclosures missing \_\_\_\_\_

Attachments missing \_\_\_\_\_

Other \_\_\_\_\_

cos  
signature

2-11-92  
date

2A

LETTER OF PROMULGATION

A fall-out symposium sponsored by the Armed Forces Special Weapons Project was held in the Pentagon on 10, 11, and 12 January 1955. Thirty papers were presented during the three day meeting. This report is a collection of the papers presented at the symposium; it includes a major part of the discussions which followed a number of papers and is aimed at reporting accurately an unbiased representation of those reports and discussions.

The AFSWP appreciates the wholehearted cooperation extended by the numerous Department of Defense and Atomic Energy Commission laboratories and departments and private research organizations whose personnel presented papers. The meetings were well attended and it is believed that the papers presented and the discussions which resulted served to bring into focus the numerous technical problems which exist in this important field of weapons effects.

*G. R. Luedcke*  
A. R. LUEDECKE  
Major General, USAF  
Chief, AFSWP

DOE ARCHIVES

7/18/88

INCOMPLETE DOCUMENT REFERENCE SHEET

The archive copy of this document is incomplete.

Pages missing 14

Enclosures missing \_\_\_\_\_

Attachments missing \_\_\_\_\_

Other \_\_\_\_\_

CAS  
signature

2-11-92  
date

TABLE OF CONTENTS

<u>TITLE &amp; SPEAKER</u>		<u>PAGE</u>
<u>10 January 1955</u>		
Opening Remarks (BGEN L. K. Tarrant, AFSWP)	0900-0915 hrs	1
Project 2.5a and 2.6a Results, Operation CASTLE (Dr. Edward R. Tompkins, USNRDL)	0915-0950 hrs	3
Project 2.5b and 2.6b Results, Operation CASTLE (Dr. Benjamin Barnett, CRL)	0955-1025 hrs	29
Methods, Findings, and Oceanographic Factors of Project 2.7, Operation CASTLE (Dr. Theodore R. Folsom, SIO)	1030-1110 hrs	49
Project 2.7 Radiological Aspects, Shot 6, Operation CASTLE (Dr. Lewis B. Werner, USNRDL)	1110-1135 hrs	77
Project 9.1 (Cloud Photography Results, Operation CASTLE (LTCOL Jack G. James, FC, AFSWP (DWET))	1320-1345 hrs	89
Physical and Chemical Nature of the Contaminant; Digest of Observations Prior to CASTLE (Dr. R. D. Cadle, SRI)	1347-1415 hrs	111
Physical and Chemical Nature of the Contaminant; Interpretation of CASTLE Observations (Dr. Carl F. Miller, USNRDL)	1415-1445 hrs	123
Radiological Nature of the Contaminant; Source Gamma Energy Spectra (Dr. C. S. Cook, USNRDL)	1510-1530 hrs	139
Radiological Nature of the Contaminant; Decay of the Gamma Radiation Field (Dr. N. E. Ballou, USNRDL)	1538-1600 hrs	155
Radiological Nature of the Contaminant; Radiation Field Gamma Energy Spectra (Mr. Stanley Ungar, ESL)	1610-1630 hrs	163
Radiological Nature of the Contaminant; Fraction- ation of Active Nuclides with Distance (Mr. Philip Krey, CRL)	1635-1652 hrs	175
Radiological Nature of the Contaminant; Percentage of Total Activity in Fall-out as a Function of Height of Burst (LTCOL N. M. Lulejian, ARDC)	DOE ARCHIVES	
	1655-1710 hrs	189

SECRET

REF ID: A6714  
4

TABLE OF CONTENTS

<u>TITLE &amp; SPEAKER</u>	<u>PAGE</u>
<u>11 January 1955</u>	
Atomic Cloud Height and Size as a Function of Yield and Meteorology (Dr. W. W. Kellogg, RAND)	0907-0930 hrs 193
Atomic Cloud Height and Size as a Function of Yield and Meteorology (Dr. Lester Machta, U.S. Weather Bureau)	0932-0940 hrs 205
Typical U.S. and European Weather as it Affects Fall-out, with Emphasis on Wind Structure (Dr. Lester Machta, U.S. Weather Bureau)	0940-0950 hrs 217
Prediction of Dose-rate and Dosage Contours as Functions of Yield and Meteorological Conditions, Air Weather Service Method (LTCOL Clifford A. Spohn, AWS)	1013-1024 hrs 241
Prediction of Dose-rate and Dosage Contours as Functions of Yield and Meteorological Conditions, Navy Weather Service Method (Dr. Florence W. Van Straten, O/CNO)	1025-1040 hrs 243
Prediction of Dose-rate and Dosage Contours as Functions of Yield and Meteorological Conditions, Army Signal Corps Method (Dr. Donald Swingle, OCSO)	1100-1135 hrs 253
Prediction of Dose-rate and Dosage Contours as Functions of Yield and Meteorological Conditions, ARDC Method (LTCOL N. M. Lulejian, ARDC)	1325-1355 hrs 269
Survey of Fall-out Area at Sea Following Yankee-Nectar, Operation CASTLE (Mr. Merril Eisenbud, AEC NYOC)	1400-1415 hrs 289
Prediction of Dose-rate and Dosage Contours as Functions of Yield and Meteorological Conditions, LASL Method (Dr. Gaelen Felt, LASL) (Dr. T. White, LASL)	
DOE ARCHIVES	
	1415-1445 hrs 303
	1445-1515 hrs 317

TABLE OF CONTENTS

<u>TITLE &amp; SPEAKER</u>	<u>PAGE</u>
Prediction of Dose-rate and Dosage Contours as Functions of Yield and Meteorological Conditions, RAND Method (Dr. R. Rapp, RAND) (Mr. S. M. Greenfield, RAND)	1540-1610 hrs 329 1610-1640 hrs 341
Prediction of Dose-rate and Dosage Contours as Functions of Yield and Meteorological Conditions, U.S. Weather Bureau Method (Mr. K. M. Nagler, U.S. Weather Bureau)	1640-1705 hrs 355
<u>12 January 1955</u>	
Prediction of Dose-rate and Dosage Contours as Functions of Yield and Meteorological Conditions, USNRDL Method (Mr. C. F. Ksanda, USNRDL) (Mr. J. M. McCampbell, USNRDL)	0910-0930 hrs 375 0930-0953 hrs 381
Prediction of Dose-rate and Dosage Contours as Functions of Yield and Meteorological Conditions; Predicted Contours for the CASTLE Detonations (Mr. E. A. Schuert, USNRDL)	0958-1020 hrs 387
Prediction of Dose-rate and Dosage Contours as Functions of Yield and Meteorological Conditions, ORO and Technical Operations, Inc. Method (Dr. F. C. Henriques, TOI)	1037-1118 hrs 403
Prediction of Dose-rate and Dosage Contours as Functions of Yield and Meteorological Conditions; Recent Developments in Weather Forecasting Techniques for the Pacific Proving Ground (LTCOL C. D. Bonnot & CDR D. F. Rex, JTF-7)	1300-1400 hrs 449
Prediction of Dose-rate and Dosage Contours as Functions of Yield and Meteorological Conditions; Effects of Specific Wind Structures Using the Army Signal Corps Method (Mr. Kenneth Barnett, OCSO)	1405-1430 hrs 475
Countermeasures; An Analysis of New Weapons Effects Information Required for Fall-out Countermeasures (Dr. Paul C. Tompkins, USNRDL)	1450-1530 hrs 497

DOE ARCHIVES

~~RESTRICTED~~

TABLE OF CONTENTS

<u>TITLE &amp; SPEAKER</u>	<u>PAGE</u>
Prediction of Dose-rate and Dosage Contours as Functions of Yield and Meteorological Conditions; Comparison of Problem Solutions (CDR R. W. Paine, AFSWP)	1530-1600 hrs 509
Closing Remarks (Dr. Herbert Scoville, AFSWP)	1600-1610 hrs 545
General Discussion	1610-1700 hrs 549
Attendance List	555

DOE ARCHIVES



## OPENING REMARKS

BRIGEN L. K. Tarrant, USA  
Armed Forces Special Weapons Project

I am General Tarrant, Deputy Chief of AFSWP. General Luedcke, who is out of town and unable to attend, has asked me to convey to you his regret at being unable to personally welcome you to this Symposium. It is my pleasure to extend to you General Luedcke's and my own personal and official welcome.

Significant contributions have been made in this field by a large number of agencies and individuals working on various aspects of the fall-out problem and it appeared desirable for us to provide an opportunity for a meeting of the many diverse groups involved to insure that the basic information necessary to fix a point of departure is available to all concerned, as well as to promote a free exchange of new ideas and approaches to the problem.

While we cannot minimize the inherent complexity of the fall-out processes, we do, nevertheless, recognize the urgent need for a simple, workable solution which can be applied in the operational planning by both the military and civil defense elements of our government.

We realize that close-in fall-out is only one facet of the whole contamination problem and that contamination, in turn, is only a part of the entire weapons effects picture. However, the tremendous potential effect of planned or accidental fall-out contamination makes it imperative that we achieve, as rapidly as possible, the answers which are required.

In looking at the agenda I see that you have a great deal of material to cover in the next three days, so I believe the best contribution I can make is to cut short my remarks and let you get on with it. Before I close, I feel that I must mention the ever-present security problem. First, in spite of the many recent articles in the news media, we are directed to maintain this subject in a classified category of information. Second, it is desired to maintain the fact of the occurrence of this Symposium in a classified category. Third, it has been determined that it is not in the best interests of national security for any agency to make a public release on anything related to fall-out at this time.

DOE ARCHIVES

I thank you for the interest you have shown in this meeting both by your attendance and the work that has gone into the preparation of the papers to be given.

## PROJECTS 2.5a AND 2.6a RESULTS, OPERATION CASTLE

Edward R. Tompkins  
U. S. Naval Radiological Defense Laboratory

This report summarizes the operational plan, the experimental approach, and the results of Projects 2.5a and 2.6a, Operation CASTLE. Detailed accounts of these projects are contained in the final reports. Certain specific properties of the atomic bomb debris and its distribution will be discussed at this symposium by other members from NRDL: C. F. Miller will discuss the physical and chemical nature of the contaminant; N. E. Ballou, the decay characteristics as related to the radiochemical composition; C. S. Cook, the source gamma spectra; and E. A. Schuert, the derivation of radiation contours. If some of these items are not covered in very great detail in this presentation, it is because they will be discussed later.

### Objectives

The objectives of these projects were (a) to determine the radiation contours which resulted from fall-out of atomic bomb debris, and (b) to characterize this material as to its physical, chemical and radiochemical properties. This information has been useful in developing a method for predicting the fall-out patterns from detonations of weapons of various yields at different locations and for estimating the radiation hazard and the problems associated with the contamination of military bases and other targets of military importance.

### Status of Knowledge Prior to Operation CASTLE

#### Nuclear Weapons Tests

Studies of several other contaminating events had been made prior to Operation CASTLE. At Operation CROSSROADS, the Baker shot spread radioactive contaminants over a large area around the point of detonation, but neither its distribution nor its characteristics were determined adequately.

Good measurements of the nature and distribution of the atomic bomb debris were made at Operation JANGLE for both the surface and underground shots. Here it was possible to measure the radiation field directly by the use of survey instruments. Measurements were also made of the quantity of fall-out and its rate of arrival around the shot point.

DOE ARCHIVES

At Operation IVY, the extent of the cross and upwind fall-out zone and the time and rate of arrival were measured. No samples of fall-out were collected in the down-wind direction. The pattern in the cross and

upwind directions, particularly in regard to the radiation levels, was considerably different from that predicted by scaling up JANGLE results. This indicated the need for a more refined scaling method or a model which could predict the fall-out pattern more closely.

#### High Explosive Model Tests

In addition to these contaminating events, high explosive model tests using charges ranging in size from 150 lbs. to about 50 tons have been carried out. These shots were detonated both on land and water at different depths below the surface. Non-radioactive tracers were incorporated into the charges. The fall-out was collected around the shot points. Information as to the mass of material and the fraction of the device falling per unit area and its rate of arrival at various locations was obtained. Attempts were made to scale the high explosive model results so as to compare them to JANGLE results. It was found that many parameters scaled roughly as the cube root of the yield.

#### Plan of Attack at Operation CASTLE

In planning for Operation CASTLE, an attempt was made to develop a method for measuring the distribution of the fall-out and to estimate the radiation levels that would have existed around the shot point had the fall-out occurred over land. The method adopted provided for (a) the collection of fall-out over water and on the islands of the atoll to determine the amount falling per unit area at various locations around the shot point, and (b) the measurement of the radiation fields on the islands adjacent to the collection points. Then by using the simple assumed relationship,

$$R_W = R_L \frac{FO_W}{FO_L}$$

where  $R_L$  = radiation field measured over land

$FO_W$  = the fall-out collected over water

$FO_L$  = the fall-out collected over land

the values for the radiation levels  $R_W$  at various locations which would have occurred had the fall-out arrived over land could be estimated and iso-radiation level lines drawn.

#### Planned Locations of Sampling Stations

DOE ARCHIVES

The general array of sampling stations which was planned is shown in Figure 1. The stations were to be located at the intercepts of circles, 5, 10, 20, 35 and 50 miles in radius and radii  $180^\circ$  apart extending from

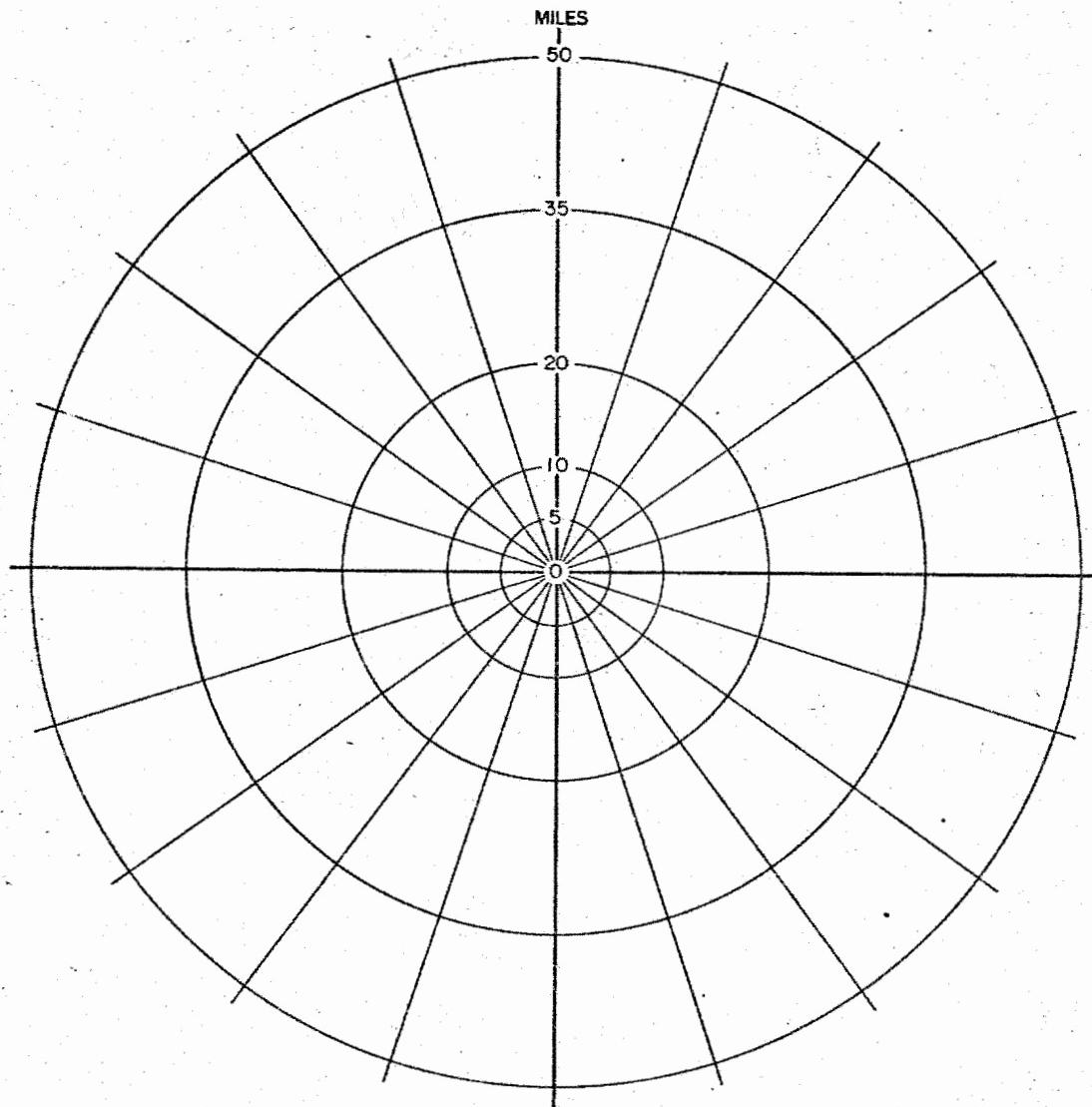


Figure 1  
Basic Sampling Array Proposed for All Shots Except Echo where  
a Smaller Array was Planned for the Lower Yield Test

5

DOE ARCHIVES



11

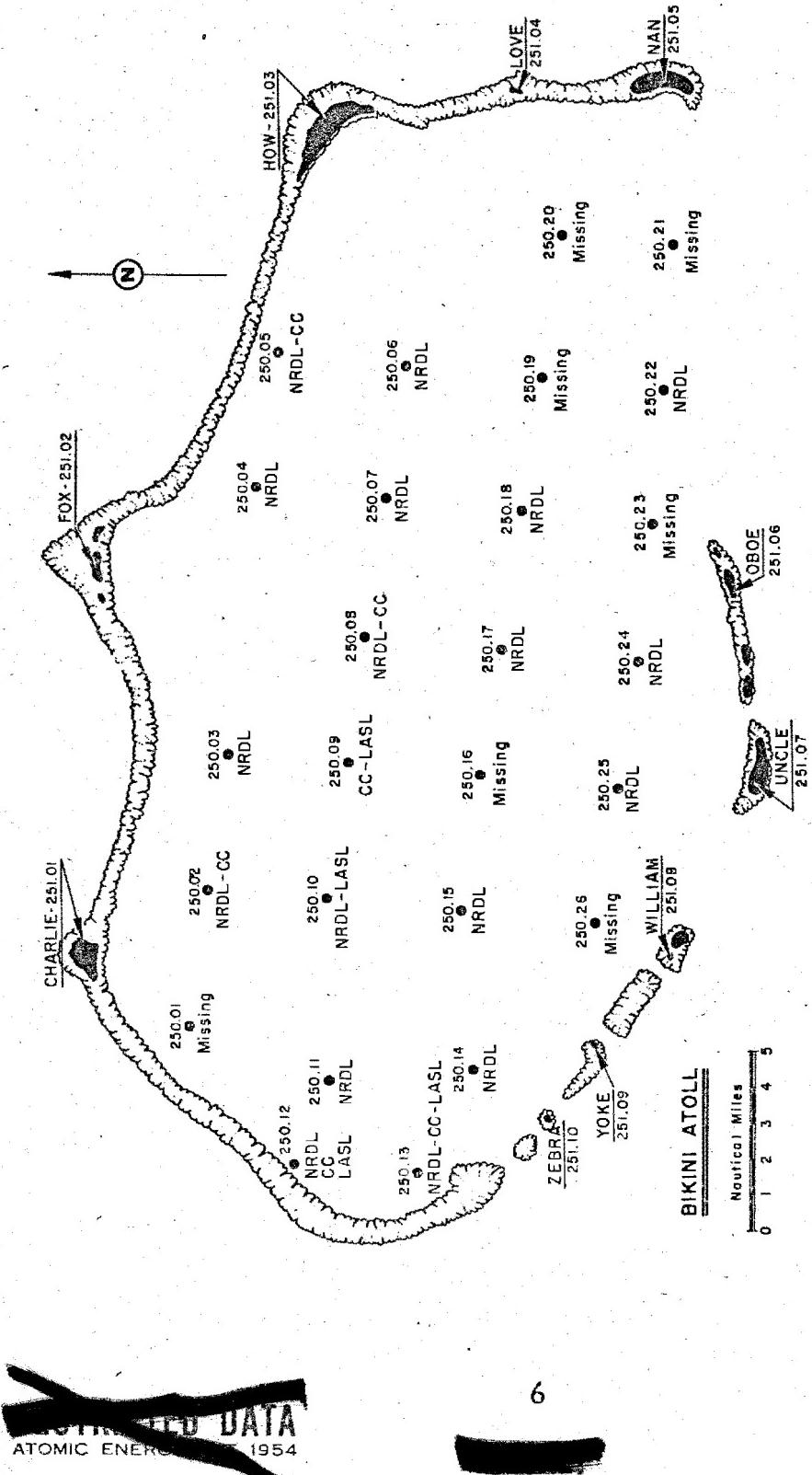


Figure 2  
Lagoon and Island Station Array for Bikini Atoll

DOE ARCHIVES

ATOMIC ENERGY 1954

the shot point. The majority of these points were located at sea thus requiring floating stations. The island and lagoon stations were not located in conformity with this pattern. The land stations were placed on high, clear ground toward the center of the islands. The lagoon stations were located on a rectangular grid. Figure 2 shows these station locations at Bikini atoll.

#### Description of Stations

Three types of stations were used: land, lagoon and sea stations.

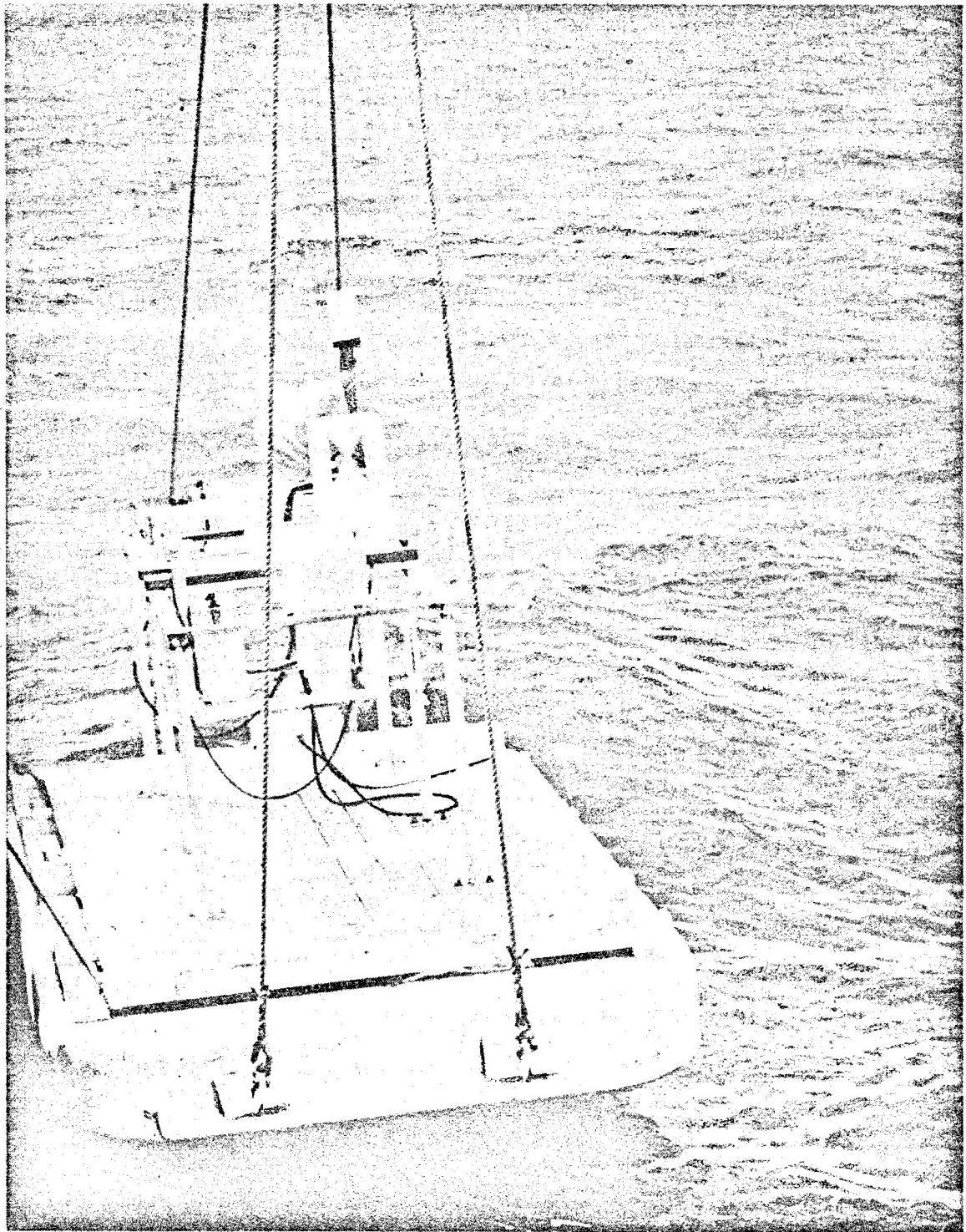
Most instrumentation at the land stations was placed in pits to shield it from blast. Total fall-out collectors and film badge dosimeters were used at all locations. Differential fall-out collectors for determining the time and rate of arrival of fall-out were located at most of the land stations. Radiation intensity recorders were located on two island stations, but only the one on station 251.03 collected useful data. Auxiliary equipment was used for starting and stopping the instruments and for furnishing power. Prototype collectors of several types were located at several island stations to test their value for use in future operations.

The lagoon stations consisted of moored rafts 7 ft. x 11 ft. Figure 3 shows one of these stations being lowered into the water. The instrumentation on these stations was similar to that at the island stations with the exception of the radiation intensity recorders. The sea stations were free-floating buoys as shown in Figure 4. They carried total collectors and film badge dosimeters. They were provided with radio transmitters for identification by the Security Force and to aid in locating them during the recovery operation.

#### Sample Collection from the Various Shots

DOE ARCHIVES

Although plans had been developed for adequate sampling of each event, a number of unforeseen circumstances made it impossible to gather more than a small fraction of the data planned. Unforeseen delays in the shot schedule and the unexpectedly rough sea conditions were the primary hindrances. As a result, most of the free-floating buoys were lost without collecting data. Also, because of the severity of the blast from Shot 1, a number of lagoon stations capsized and a fire was started on Tare which destroyed a large part of the spare equipment needed for subsequent shots. Useful information was obtained from the island stations and the surviving lagoon stations. Measurement of the radiation levels and the fall-out which arrived on the atolls east of Bikini after Shot 1 provided valuable data to assess the downwind pattern of fall-out from super weapons detonated over land. Samples collected on the Project 6.4 YAG's were useful for determining the



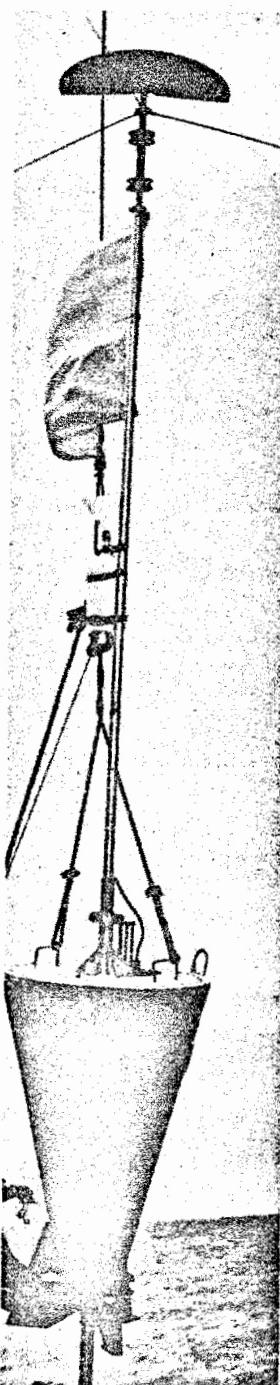
DOE ARCHIVES

Figure 3  
Lagoon Station Being Placed

8

DATA  
ATOMIC ENERGY ACT

14



DOE ARCHIVES

Figure 4  
Free-Floating Sea Station being Launched

9

SECRET

RESTRICTED DATA  
EX-1 ACT 1954

15

properties of the contaminant. On Shot 2, no fall-out arrived on the island or lagoon stations. The only samples collected were on the free-floating buoy stations. Figure 5 shows the locations of those stations which were recovered after that shot. It will be noted that the set and drift varied a great deal around the atoll. This made it difficult to determine where the buoys should be dropped in order for them to drift to the correct location at shot time. Collections were made from lagoon and island stations for Shots 3, 4 and 6. Water sampling on Shots 5 and 6 supplemented this data. This operation will be discussed by Dr. Folsom and Dr. Werner.

#### Instrumentation

Two types of total collectors were used. One was a polyethylene bottle with a 7-in. diameter funnel as shown in Figure 6; the other was a piece of gummed paper about a foot square placed in a horizontal position. The differential fall-out collector, shown in Figure 7, collected the samples in a number of small polyethylene jars through openings in a belt that was drawn over the jars. The film badge packs were supplied by Project 2.1. The radiation intensity recorder was of the same type as that used on the YAG's by Project 6.4.

#### Evaluation of Sampling Methods

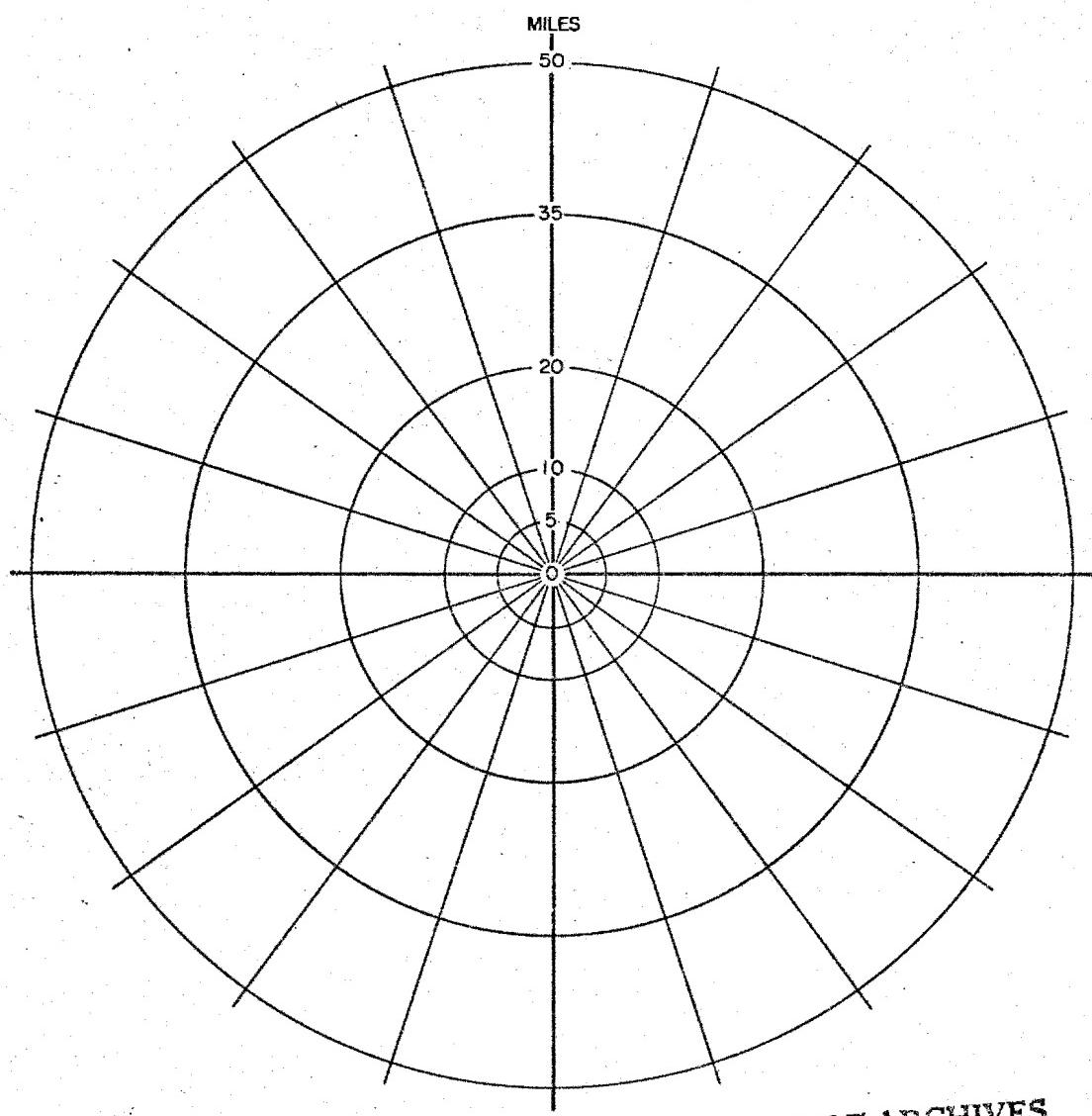
In the past, it had been assumed that the material which fell on a collecting surface of a collector was representative of what would have fallen on the same area had the collector not been there. At CASTLE, this assumption was tested.

The precision which could be expected from collections over very limited areas was tested by comparing the quantities collected in total fall-out collectors located adjacent to each other and on the circumference of a circle of 50-ft. radius. These tests showed that with either type of total collector, the largest variation between them was less than a factor of two and most values were within  $\pm 25\%$  of the mean.

An attempt was made to assess the accuracy of the collections by plotting the radiation field readings against the gamma activity of the material collected at stations located various distances from the shot point. These results shown in Figures 8 and 9 indicate that the collections on the gummed paper are proportional to the field readings while the efficiency of the bottle and funnel collector varies considerably with distance from the shot point.

DOE ARCHIVES

Because of the uncertainty of the efficiencies of various types of collectors, more extensive tests of this type are being planned for Operation TEAPOT. The accuracy and precision of several sampling methods at various locations around the shot point will be evaluated.



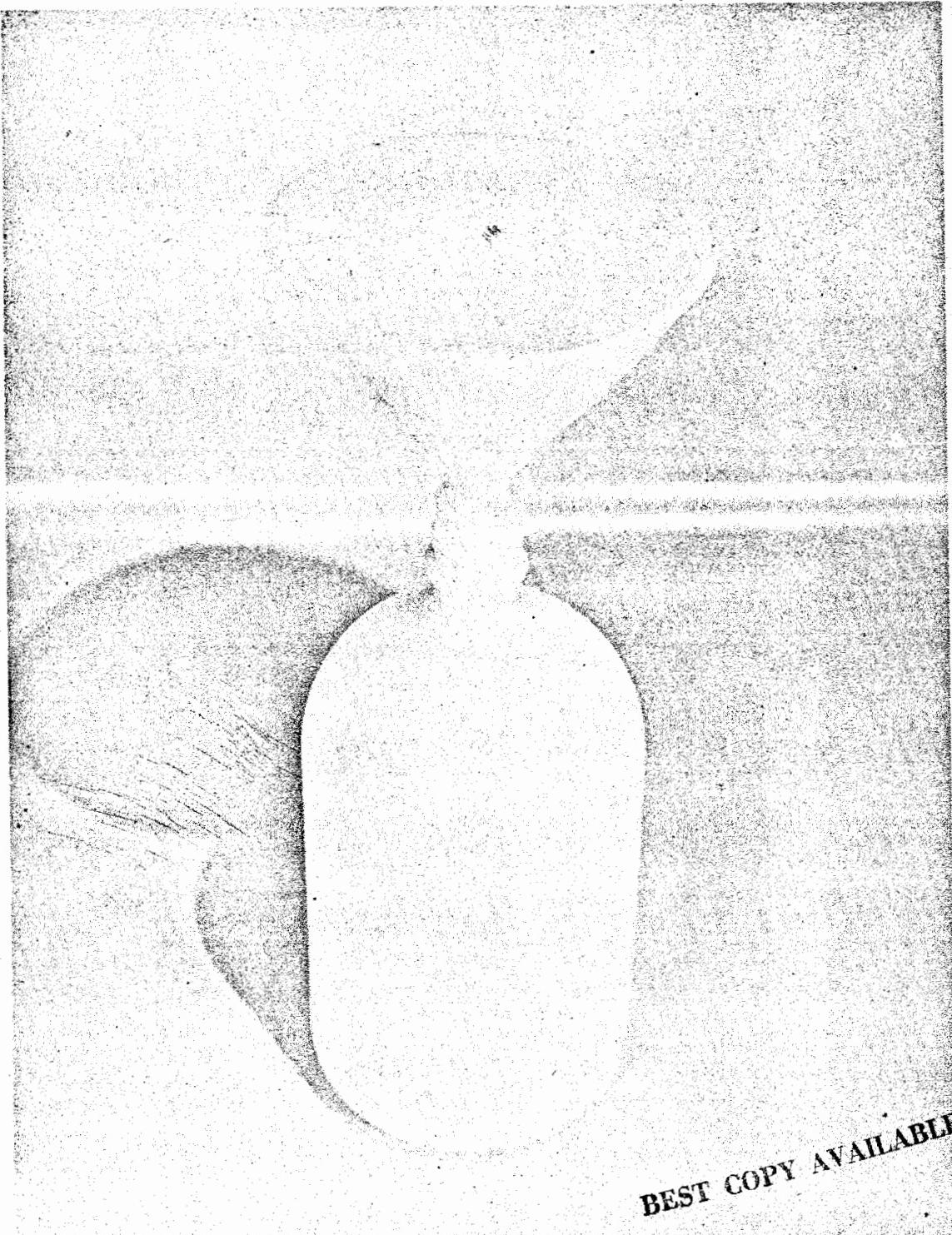
DOE ARCHIVES.

11

SECRET

RESERVE  
ENERGY ACT 1954

17



BEST COPY AVAILABLE

DOE ARCHIVES

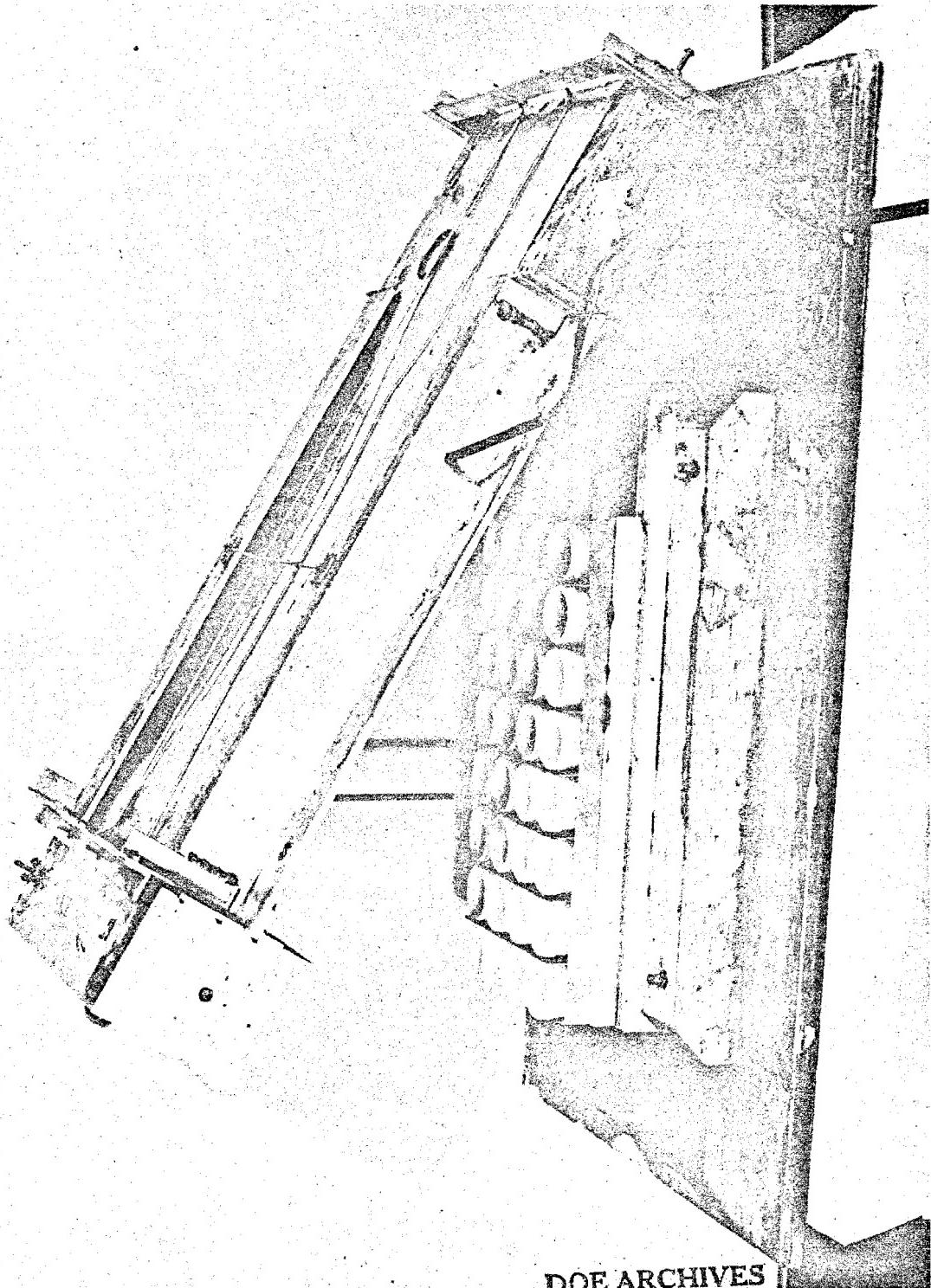
Figure 6  
Total Collectors

12

R  
OMIC ENERGY ACT 1954

18

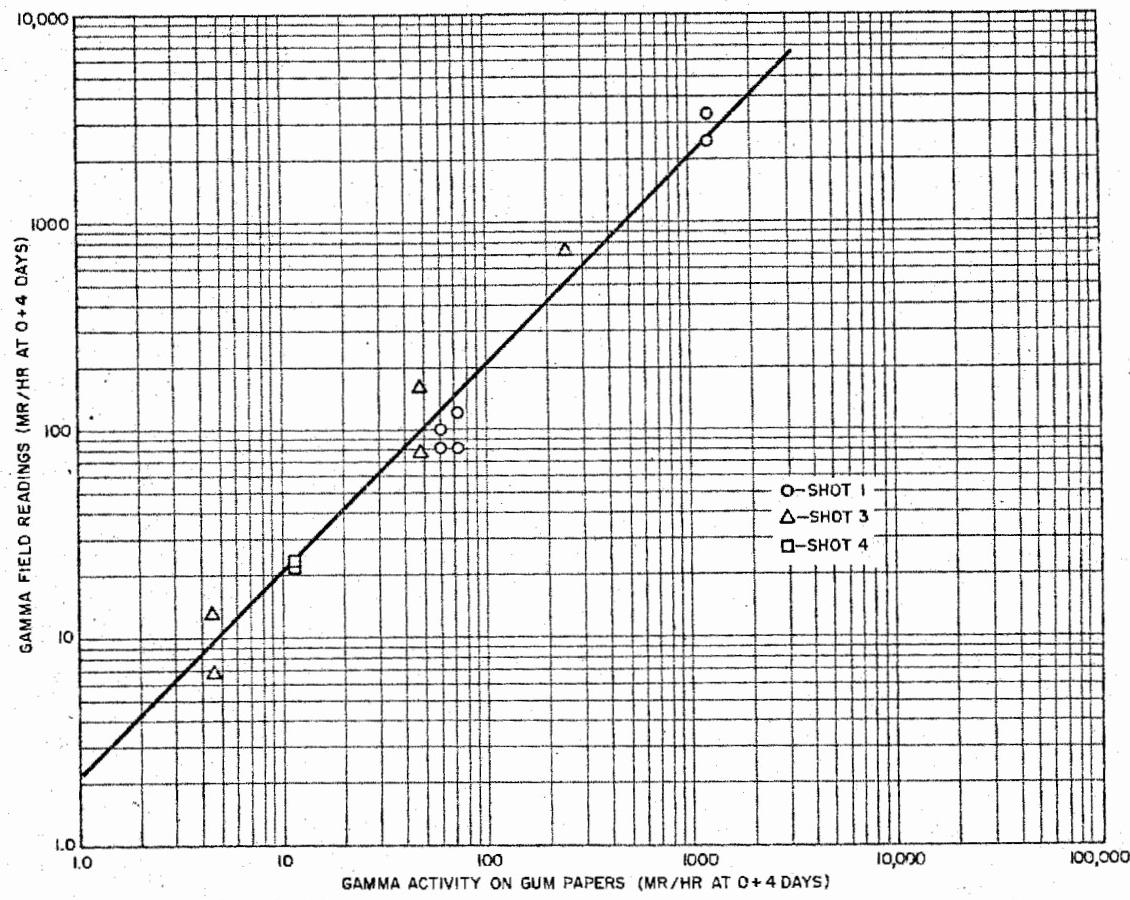
Figure 7  
Differential Fall-out Collector



13

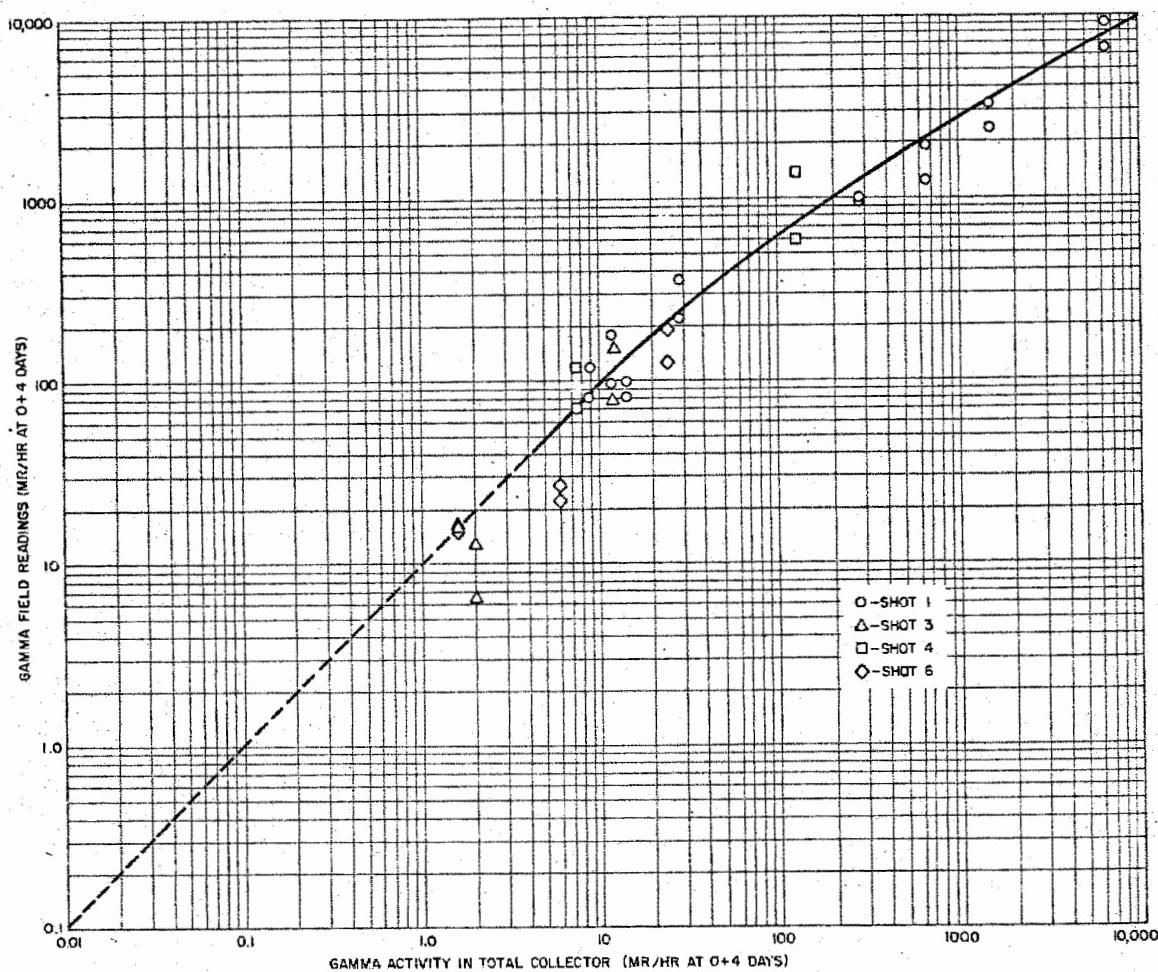
AMERICAN ENERGY ACT 1954

19



DOE ARCHIVES

Figure 8  
Ratio of Gamma Infinite Field Measurements to Equivalent Gamma Measurements from the Gummed Paper Collector (mr/hr at 0+4 days)



DOE ARCHIVES

Figure 9  
Ratio of Gamma Infinite Field Measurements to Equivalent Gamma Measurements From the Total Collector (mr/hr at 0+4 days)

### Collection and Treatment of Samples

Samples were collected by the field teams and taken to the mobile laboratory on Elmer. The approximate radiation level of each sample was determined with a survey meter. Aliquots of some samples were taken for further measurements at the site. The samples were then packaged and shipped to the Z1 for further analyses.

The measurements made at the site were limited to those which needed to be made at early times after the detonation. Gross decay measurements were started. Aluminum and lead absorption curves and gamma spectrometry measurements were made at several times starting as soon as the samples could be prepared. Analyses were performed to determine the contributions of several short-lived radionuclides including those formed by neutron reactions in the bomb components and environmental substances.

The portion of the radioactivity associated with the solid, ionic and colloidal phases was determined in the forward area after separating the phases by centrifugation and ultrafiltration. Special ion-exchange methods were developed to aid in some of the radionuclide separations. It was planned to make these measurements and determinations of some short-lived radionuclides at very early times after detonation. This was not possible because of the difficulties in collecting and transporting samples to the field laboratory.

At USNRDL, the gross decay and absorption and spectral measurements were continued. The details of these measurements will be discussed by Dr. Ballou and Dr. Cook. Also, the physical, chemical and radiochemical properties of the contaminant were studied further. The gross chemical composition was determined by spectrographic, spectrochemical and other analytical methods. Radiochemical analyses for selected species were carried out. The physical measurements included particle size and density determinations, X-ray diffraction measurements and petrographic studies.

### Summary of Results

Because results of these studies will be discussed in detail by other participants of this symposium, only a summary will be given here.

DOE ARCHIVES

### Close-in Fall-out Patterns

The fall-out patterns in the lagoon area were well documented for most of the shots. Samples from island and lagoon stations and radiation measurements on the islands furnished enough data to draw reliable contour lines. The patterns for Shots 1, 3, 4 and 6 are shown in Figures 10 through 13. Figure 14 shows estimated contours for Shot 2. These are based on the activity levels of the samples collected on the free-

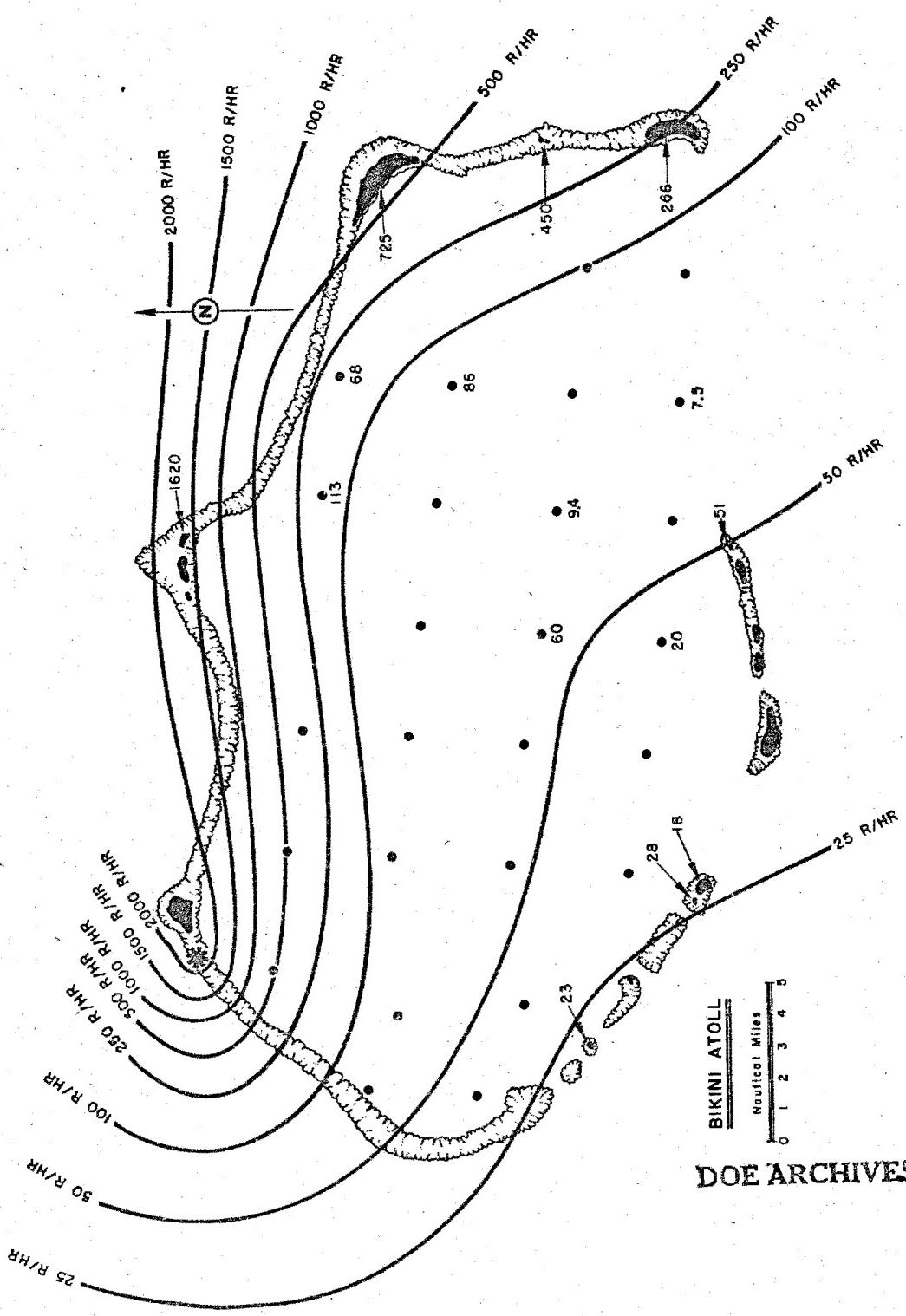
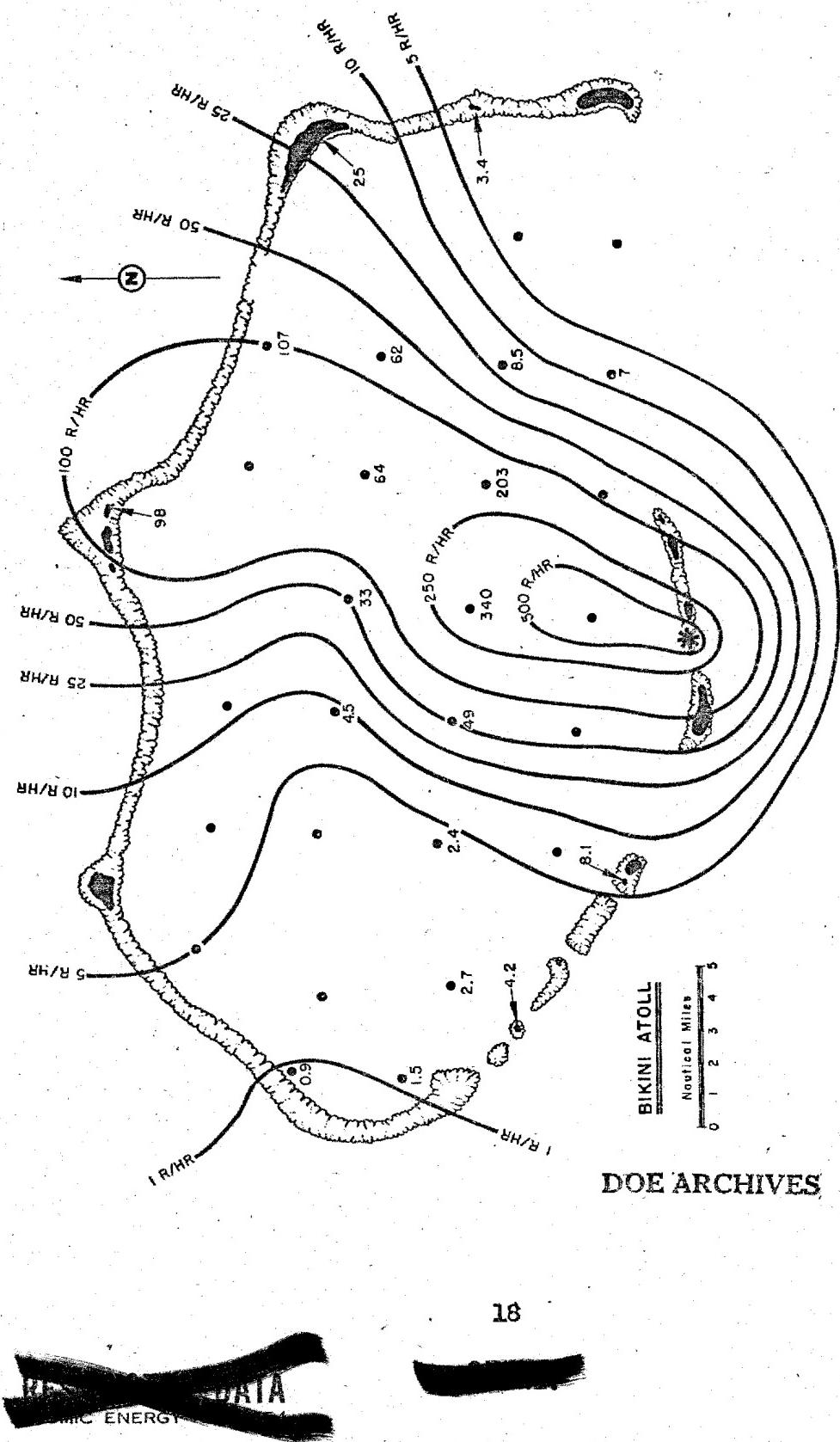
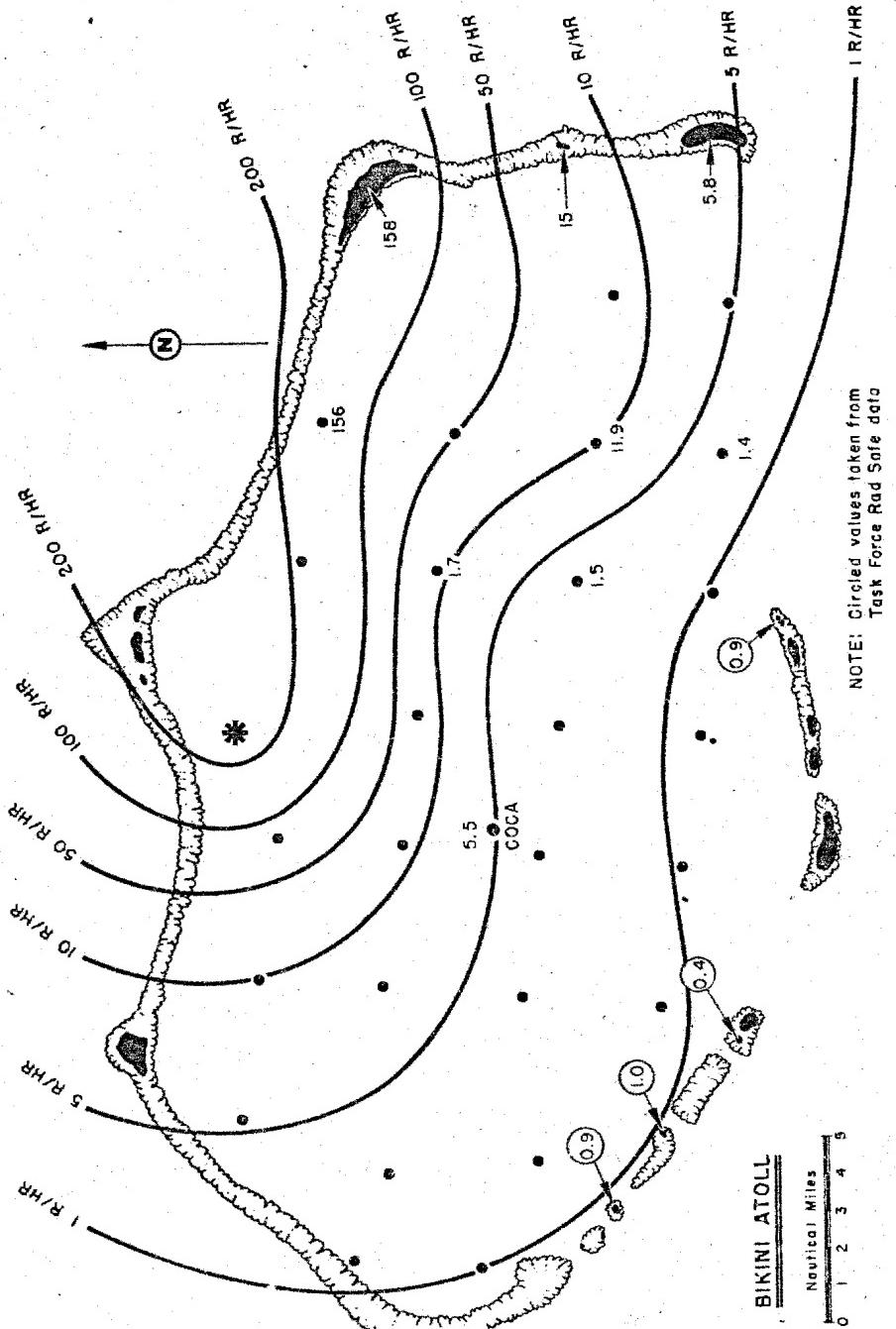


Figure 10  
Shot 1, Close-in Gamma Fall-out Pattern (r/hr at 1 hr)

23

Figure 11  
Shot 3, Close-in Gamma Fall-out Pattern (r/hr at 1 hr)





**Figure 12  
Shot 4, Close-in Gamma Fall-out (r/hr at 1 hr)**

2000

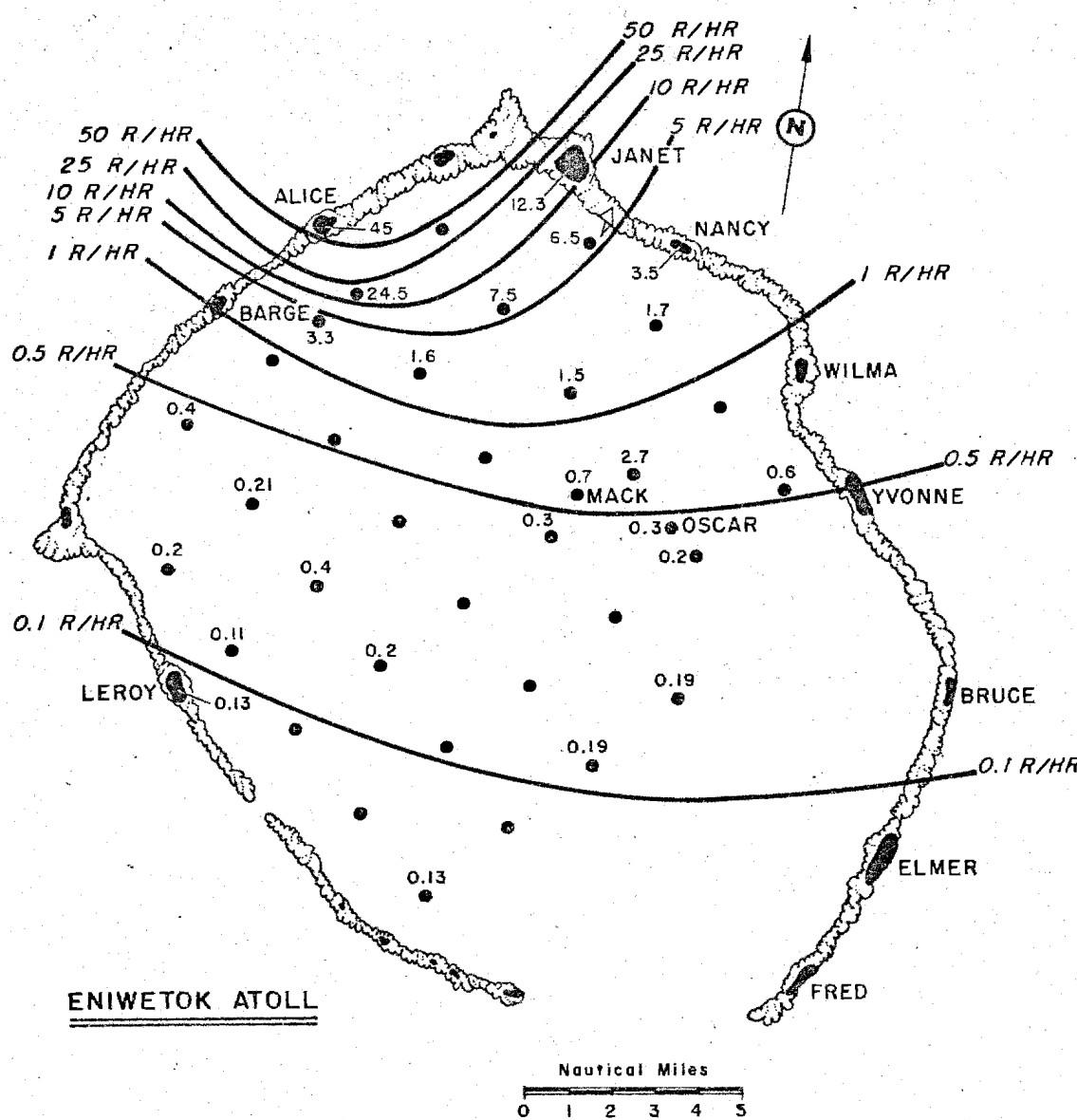


Figure 13  
Shot 6, Close-in Gamma Fall-out Pattern ( $r/\text{hr}$  at 1 hr)

20

**ATOMIC ENERGY ACT 1954**

26

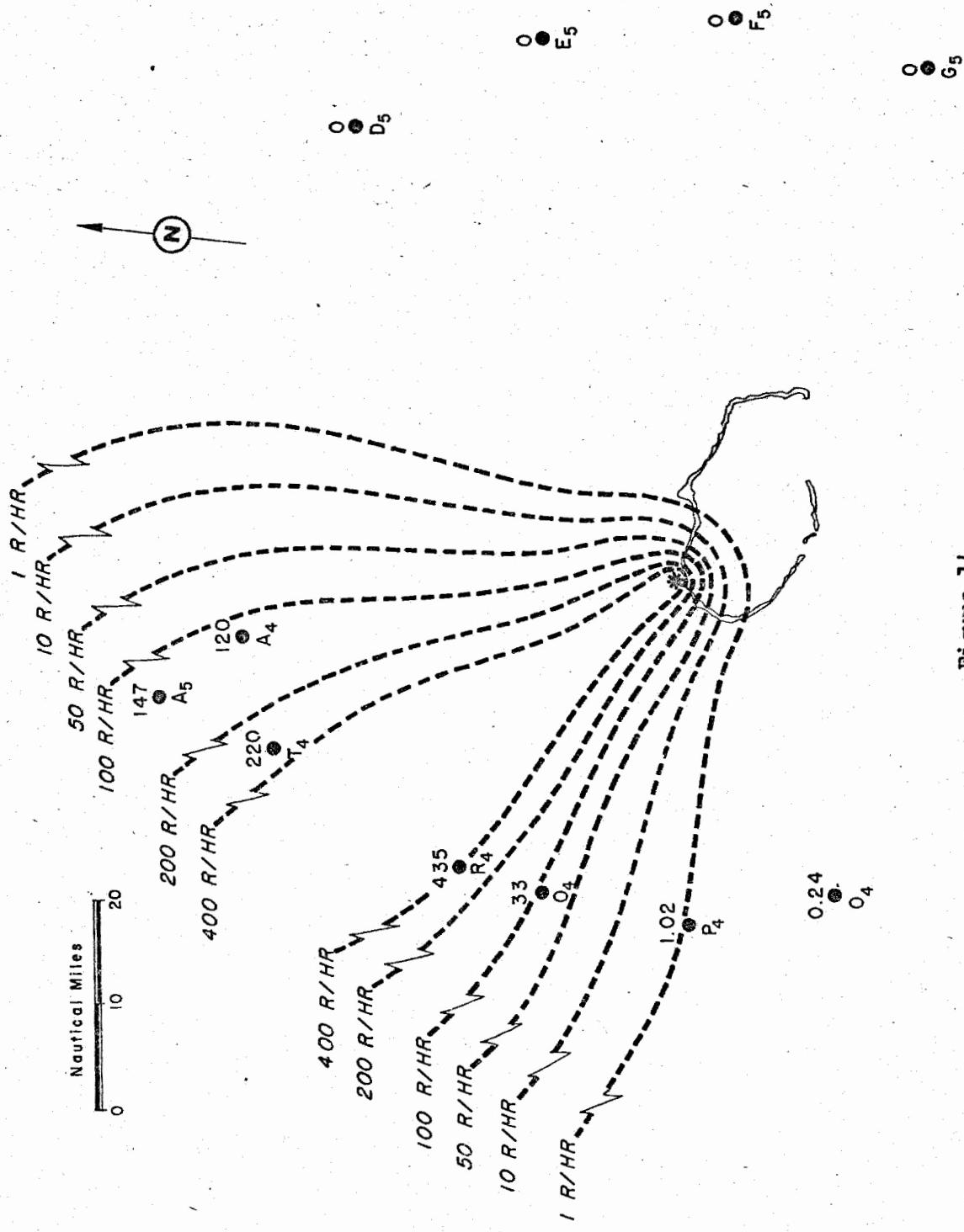


Figure 14  
Shot 2, Fall-out Pattern (r/hr at 1 hr)

floating buoy stations. No fall-out arrived at the Project 2.5a island or lagoon stations following this shot.

#### Physical Characteristics of the Fall-out

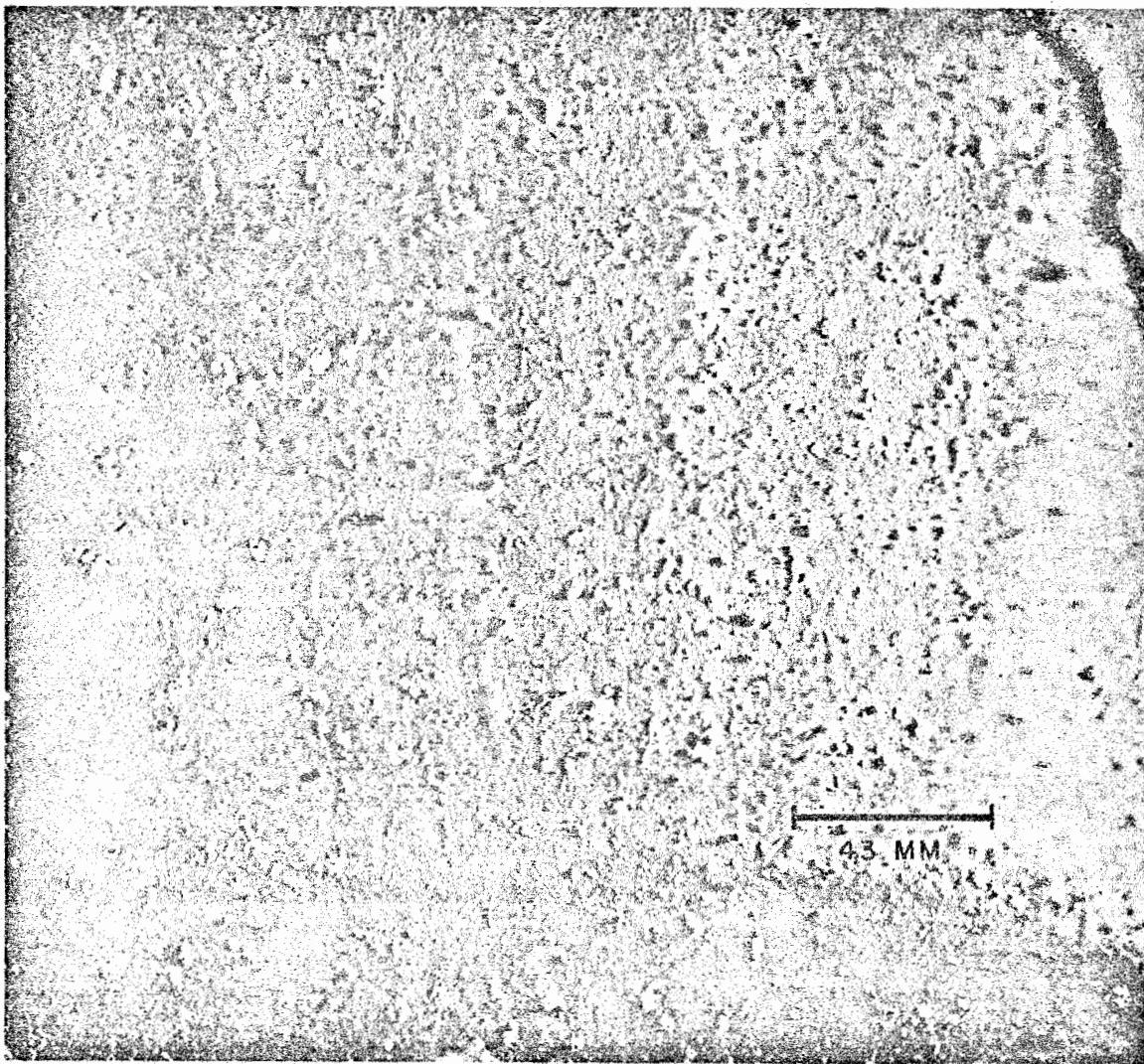
The nature of the fall-out was determined by the point of detonation and the weapon yield. Figure 15 shows a gummed paper collector from one of the lagoon stations covered with fall-out from Shot 1. This fall-out consisted largely of coral-like material, a majority of which was of large particle size. The ratio of radioactivity/mass of the particles varied considerably. No correlation was found between this ratio and the particle size. Many of the particles were fragile and could not be sieved without breaking them; therefore, the determinations of activity/unit mass of the various sized particles would not be representative of the actual fall-out. The microscopic studies of individual large particles showed that they varied considerably both as to composition and radioactivity.

The nature of the particles from the barge shots is uncertain. No visible bomb debris was collected in the total collectors. Filter samples and their radioautographs were studied microscopically. There were some small droplets observed, but it is uncertain whether these were fall-out or originated from ocean spray. Most of the particles were too small to be observed through the optical microscope, but their presence was shown by radioautography. The radioactivity in the samples from the total collectors which had collected rain after the fall-out period was found to be largely in the liquid phase. These observations as well as the contamination behavior of this fall-out as reported by Projects 6.4 and 6.5 indicate that it consisted largely of extremely fine aerosols containing the bomb debris and substances derived from sea water with a very limited amount of coral constituents.

#### Particle Size Distribution

The particle size distribution was determined by carefully mounting the fall-out samples from the differential samplers on transparent backing material and measuring them by observation through a microscope with an ocular micrometer. A radioautograph of the mounted particles was made on stripping film mounted over the backing. This was developed in place and thus permitted the identification of the radioactive particles. Nearly 7000 radioactive particles from Shot 1 were measured. Figure 16 shows the distribution of all of these particles. The distribution of the fall-out collected on several of the atoll islands east of Bikini is shown in Figure 17. The application of this information for estimating the fall-out distribution will be discussed by Mr. Schuert.

DOE ARCHIVES



DOE ARCHIVES

Figure 15  
Shot 1, Fall-out Particulate, Station 250.04

23

U.S. ENERGY ACT 1954

29

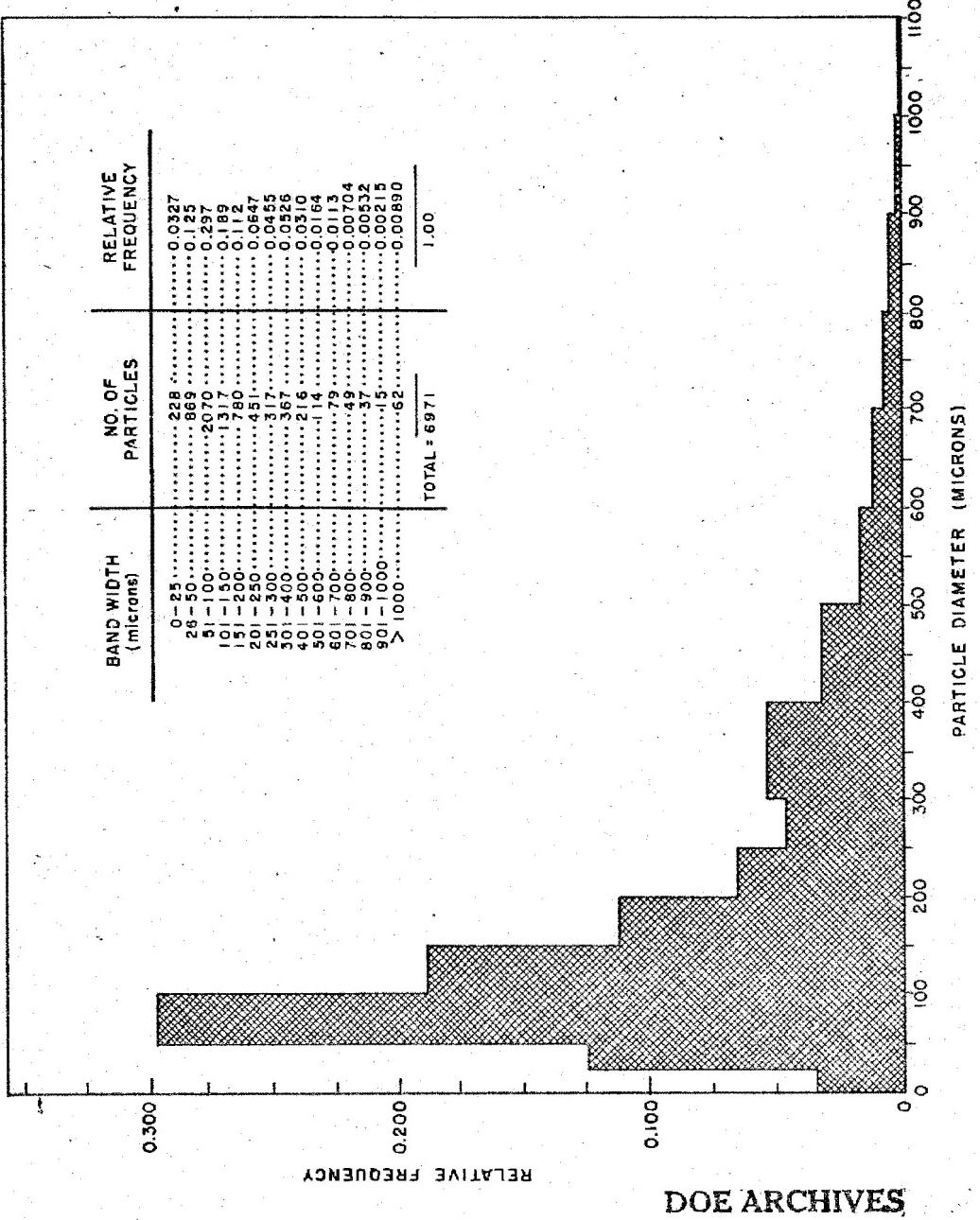


Figure 16  
Shot 1, Composite Particle Size Distribution

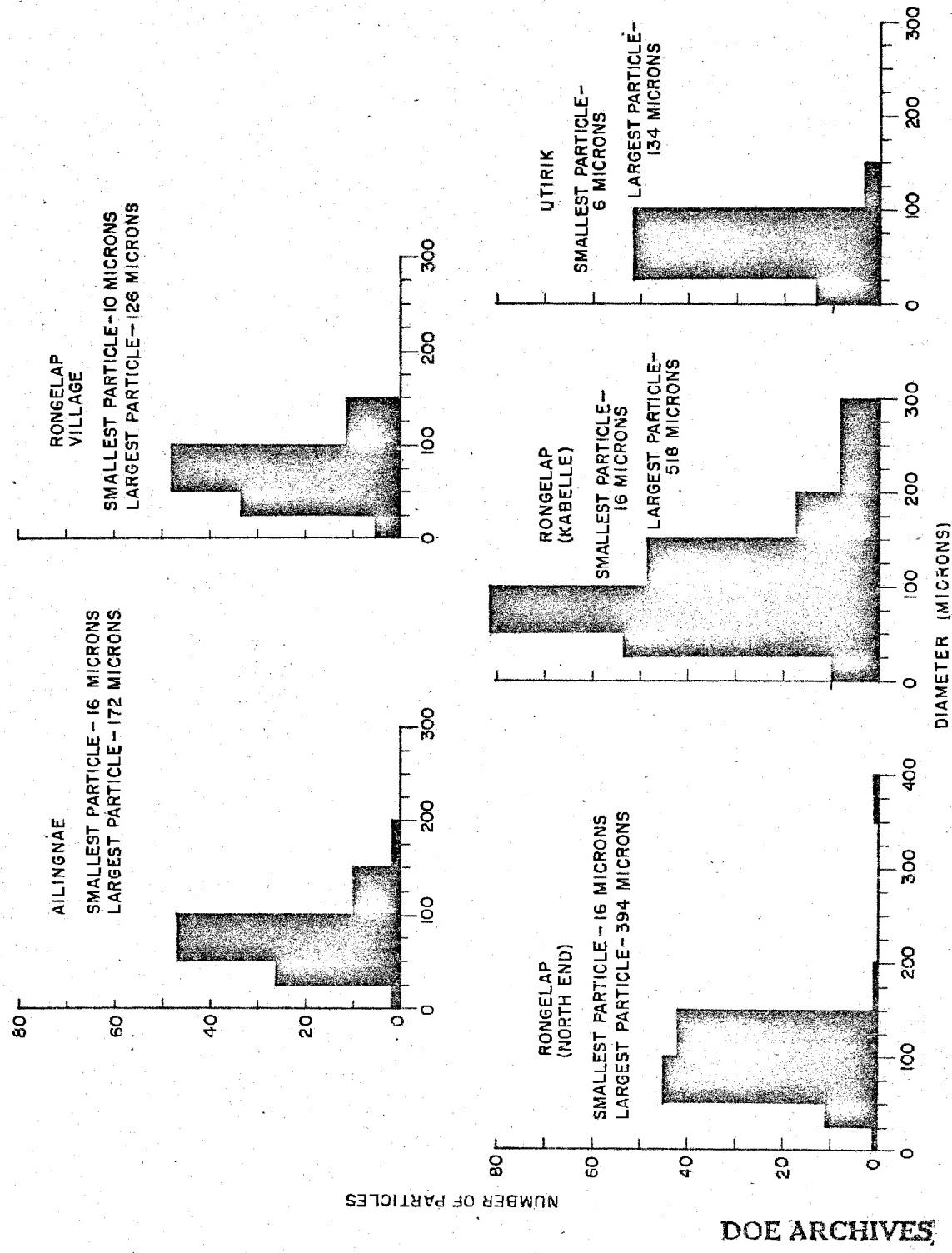


Figure 17  
Shot 1, Outer Atoll Particle Size Distribution

### Integrated Dosage at an Island Station

The data from the time-intensity recorder located at station 251.03, plotted as total dose vs. time is shown in Figure 18. This station lay in the heavily contaminated, downwind area. It may be seen from this graph that anyone caught in the open on this island would have received a lethal dosage of radiation by 4 to 5 hours after the detonation.

### Chemical and Radiochemical Properties of the Fall-out

These properties of the contaminant will be discussed by Dr. Miller and Dr. Ballou. It may be interesting here to note briefly a few results obtained in the forward area by an ion-exchange procedure developed there. Early analyses of Shot 1 fall-out for  $\text{Na}^{24}$  by standard radiochemical procedures had failed to give conclusive results because of the difficulty of purifying the sodium fraction. To eliminate this difficulty, a preliminary purification step was introduced. This consisted of passing the dissolved fall-out through a cation exchange column, washing the column with water and then eluting the alkali metal ions with dilute HCl. This fraction was then analyzed for  $\text{Na}^{24}$  in the usual manner.

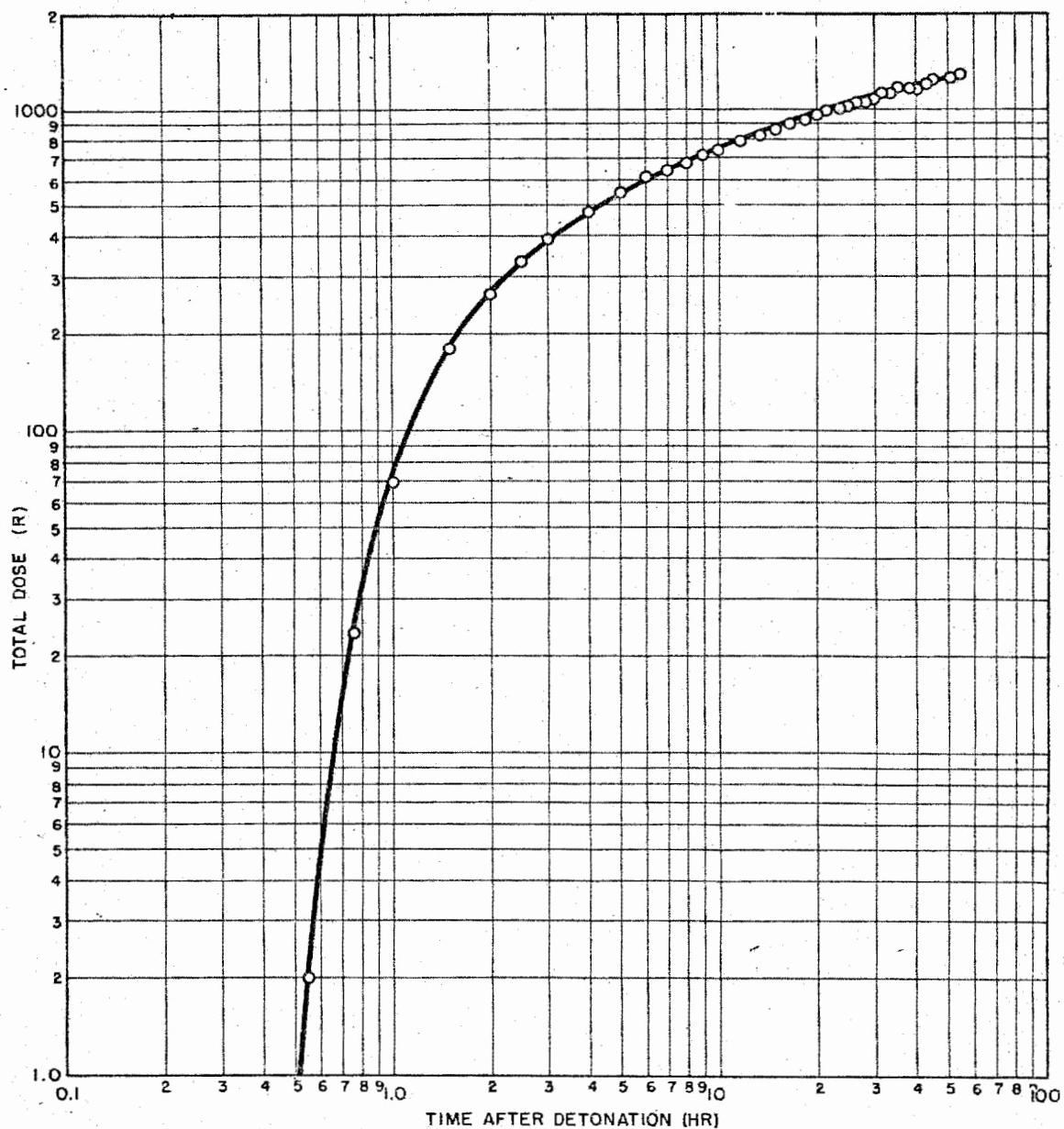
The elution curve of the radionuclides as measured by a recording rate meter for one of these experiments is shown in Figure 19. Attempts were made to identify the species in some of the other fractions as well as to ascertain the purity of the alkali metal fraction. Decay data and gamma spectra measurements led to the identification of the constituents in some of these fractions. The details of these analyses will be found in the final report of Project 2.6a.

### Summary

From this and subsequent presentations, it will be seen that a great deal of information useful in fulfilling the objectives of these projects was obtained. However, much remains to be done. The nature of the contaminant from surface land shots of super weapons over coral is well defined. More information is needed regarding its distribution. The chemical and radiochemical properties of the fall-out from surface water shots was determined. More information is needed concerning the physical characteristics and distribution of fall-out from this type of detonation. While the size and shape of the clouds have been determined photographically, the distribution of radioactivity and mass within their boundaries are entirely unknown.

**DOE ARCHIVES**

Information is also needed regarding the properties of the contaminants and their distributions from weapons of different yields in other environments. Of particular importance for the weapon effects program are detonations in clay soil and in shallow harbors of weapons of several yields.



DOE ARCHIVES

Figure 18  
Shot 1, Integrated Gamma Dose, Station 251.03

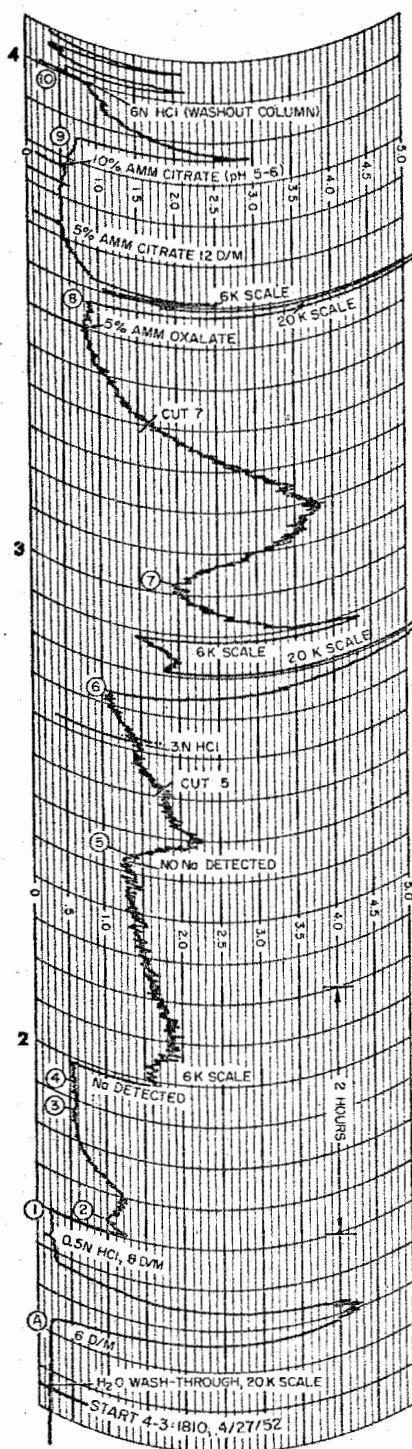


Figure 19  
Facsimile of Chromatogram Taken From the Esterline-Angus Recorder

28

DOE ARCHIVES

34

## PROJECT 2.5b AND 2.6b RESULTS, OPERATION CASTLE

Dr. Benjamin Barnett  
Chemical and Radiological Laboratories

### Introduction

The objectives of Project 2.5b and 2.6b were to document the fall-out and to determine the properties of the material.

The data were used to evaluate the contamination hazard, and to arrive at some conception of how active particles form in the fireball.

### Apparatus

To carry out these objectives two types of samplers were used. The first is shown in figure 1. This is the CmlC differential sampler. The top only is illustrated and the cover, which can be opened at any desired time after blast, is shown exposing the opening through which the fall-out enters the collecting, wedge-shaped segments, which are shown in figure 2. There are 24 of these sections on a tray, and the tray is rotated so as to expose each section for the required times.

Since samples free of aqueous fall-out were required for some of the work, a new type of sampler shown in figure 3, was devised. This consisted of a cone containing a mixture of carbon tetrachloride and chlorobenzene (together with a little aerosol OT to reduce the surface tension). Fall-out arriving at the surface was rapidly separated into an aqueous phase which remained on top, and the solid material which settled out.

### Operations

These instruments were set out at the positions shown in figure 4. The squares show where both types of samplers were located, and the circles where only the CmlC differential samplers were placed.

We also had samplers on rafts at the Bikini stations, but almost all of these were lost owing to high seas, so that our projected work on base surge could not be carried out.

### Results

DOE ARCHIVES

It seems probable that most of the activities measured came from the column, rather than the cloud, so that especially for the larger shots early arrival of fall-out was to be anticipated.

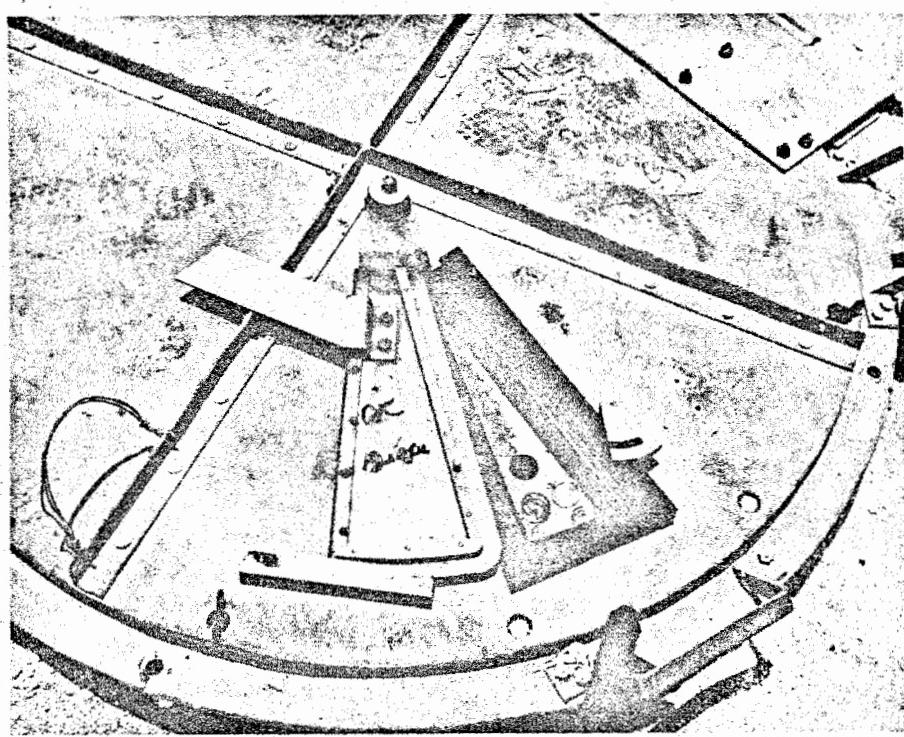


Figure 1  
Top of Chemical Corps Differential Sampler

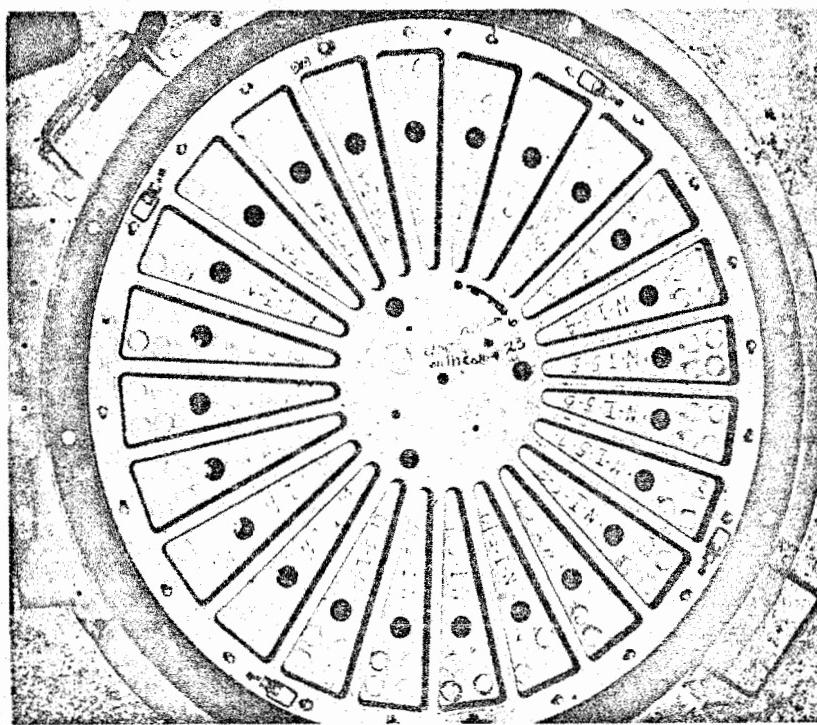
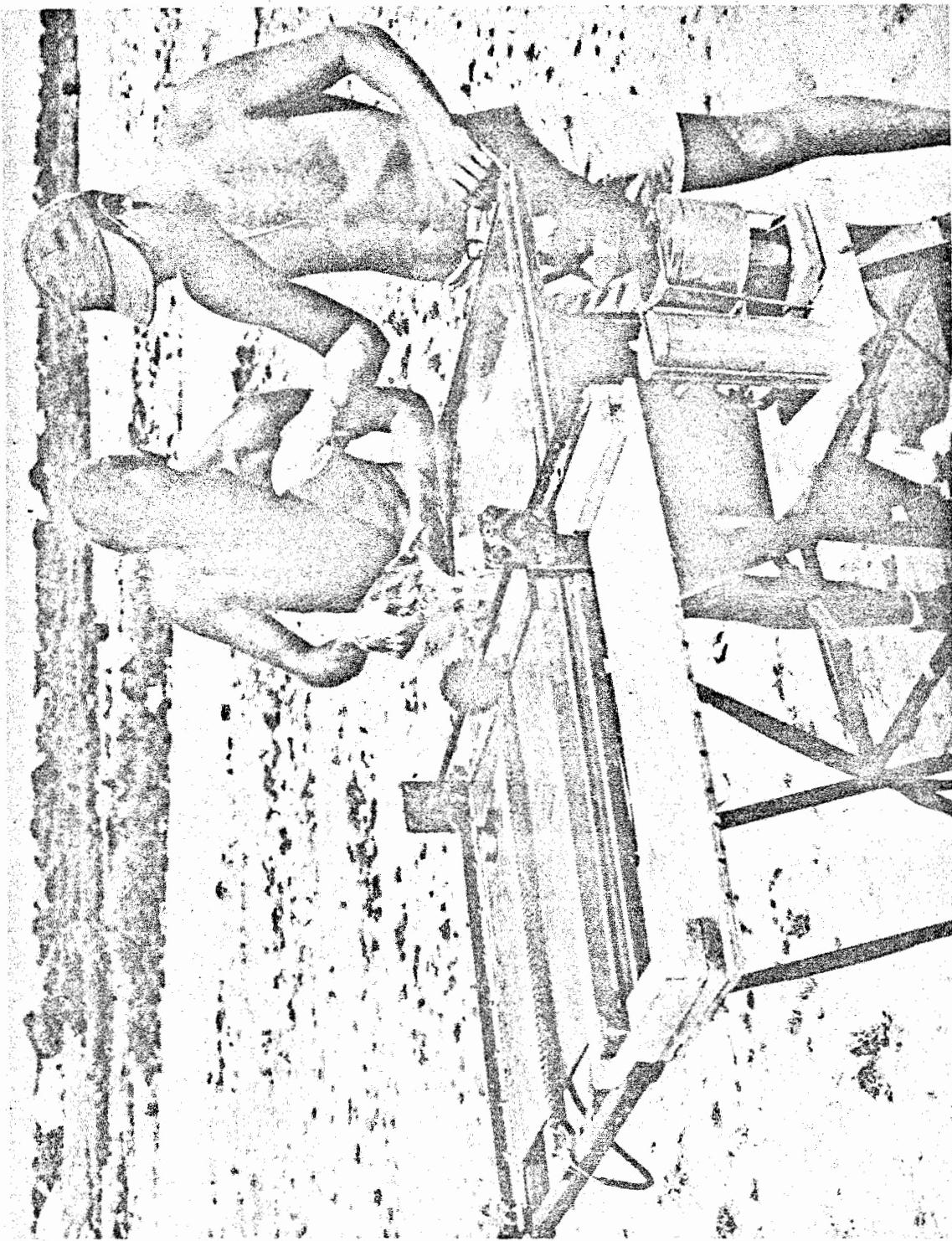


Figure 2  
Wedge-Shaped Sampling Sections of Chemical Corps Sampler



**Figure 3**  
New Cone Sampler

31

DOE ARCHIVES

37

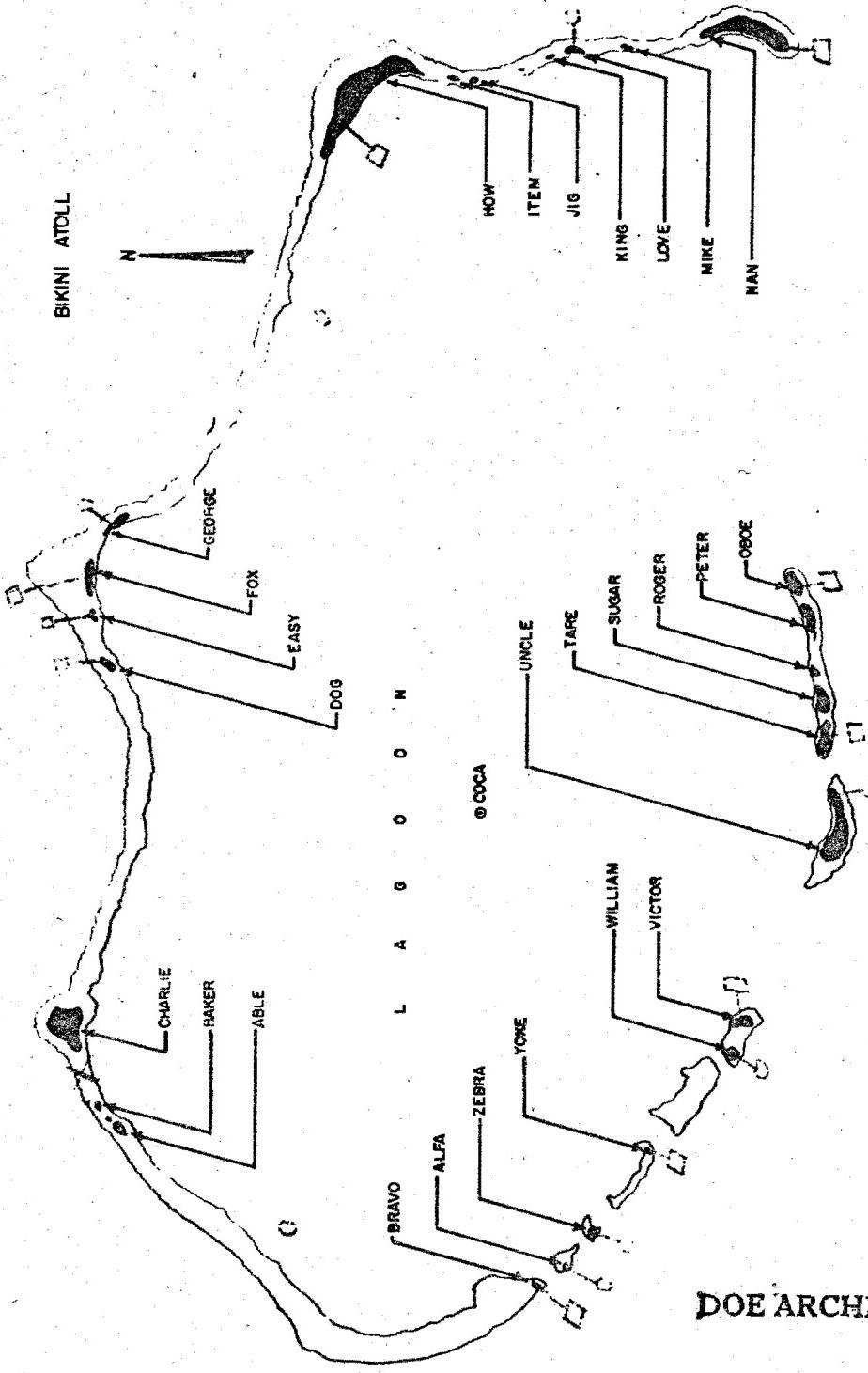


Figure 4  
Sampling Stations

~~SECRET~~

The collector located at Nan, 23 miles from ground zero, indicated that radioactive material arrived during the first six minutes sampling interval following the Bravo detonation.

In the case of the Union shot the highest activity arrived within two minutes after shot within two miles west from ground zero, whereas at stations 14 miles north fall-out arrived between  $\frac{1}{2}$  hour to  $1\frac{1}{2}$  hours after shot.

In the case of the Bravo [redacted] device the maximum activity generally arrived during the first hour after burst.

For this case the maximum  $\beta$  -field strength was  $62 \text{C}/\text{ft}^2$ . The strength of the field fell off very rapidly, as is shown in figure 5, despite the fact that fall-out continued to arrive all along this curve. This shows how rapidly the actual  $\beta$  - hazard falls off, despite the arrival of further fall-out.

Figure 6 shows isodose lines, plotted from Rad-Safe data, for gamma radiation, for the Bravo shot. The maximum dose rate at M+6 hour was 340 r/hr at Able Island. Ground zero was on the reef off Charlie Island.

A similar plot is shown in figure 7 for the third shot. The maximum dose rate was 50 r/hr at Uncle Island, and the total dose for infinite stay time was 1450 r. Ground zero was on Tare Island.

Active fall-out from surface shots of the Bravo type can give rise to illness and even death at distances far beyond those where blast and thermal effects are hazardous.

It seems also that because of the high proportion of activity in small particles, an inhalation hazard may exist for shots of this type. Figure 8 shows a plot of the total activity against particle size for a typical sample of Bravo fall-out. For all particles up to  $10\mu$  the activity amounts to as much as 15% of the total. The active particles amounted to 43% of the total particles. This evidence that activity continued down to small particles led to a study of activity as a function of particle size.

DOE ARCHIVES

A more intimate study of the activities of these active particles was made based on the relation

$$A^o = kd^m \quad (4.1)$$

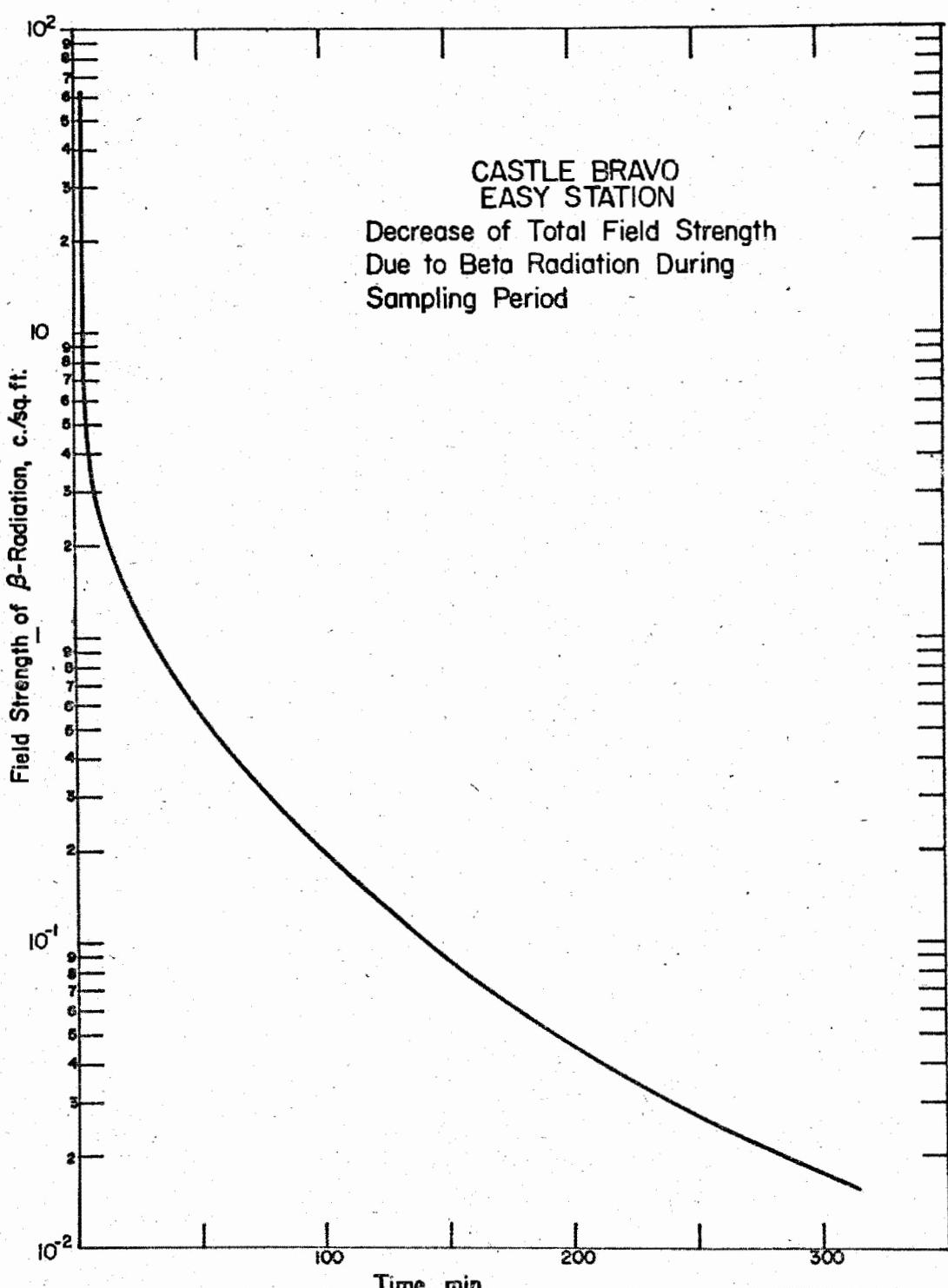


Figure 5

34

RESTRICTED  
ATOMIC ENERGY COMMISSION

4D

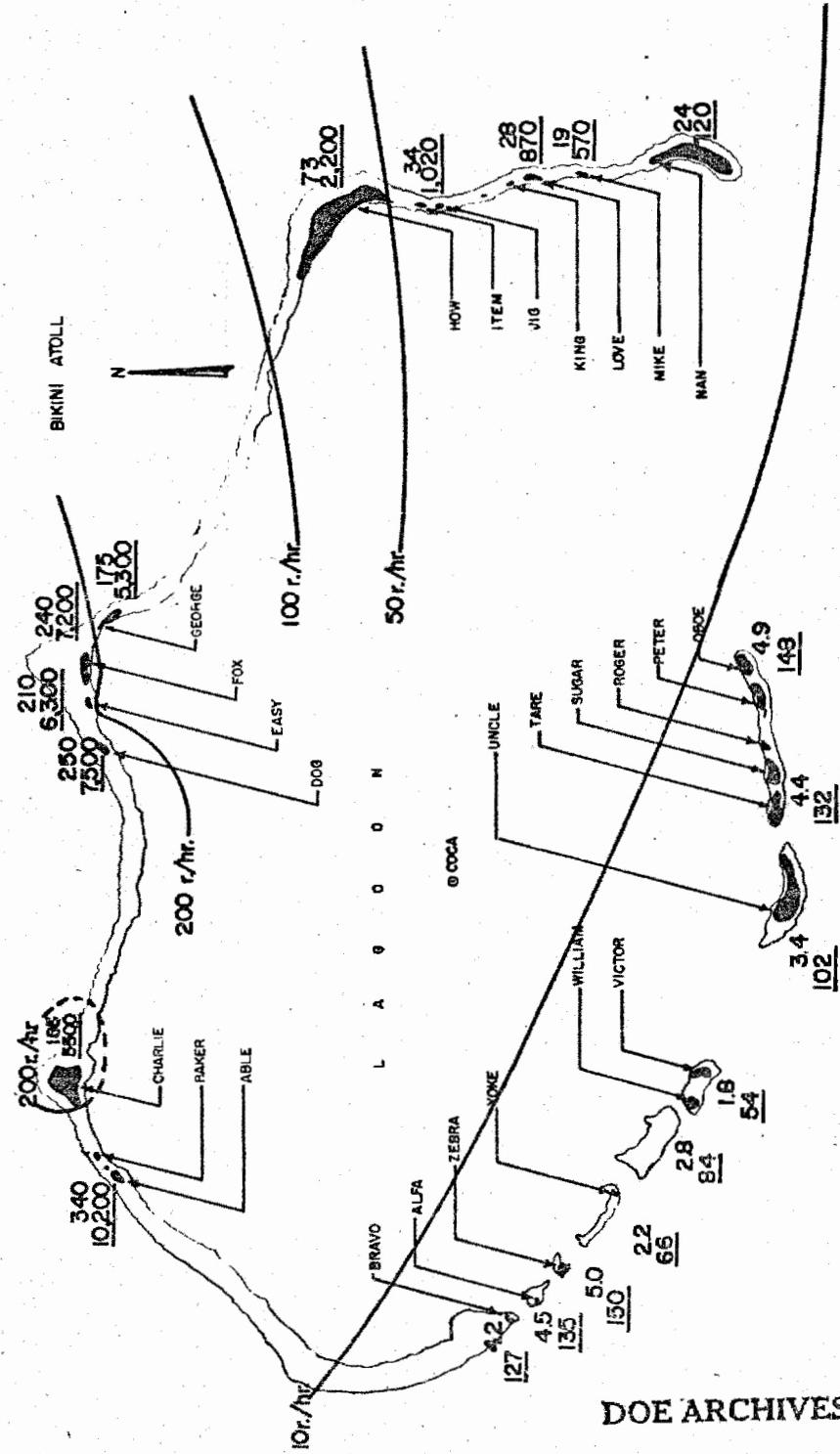


Figure 6  
Isodose Lines for First shot

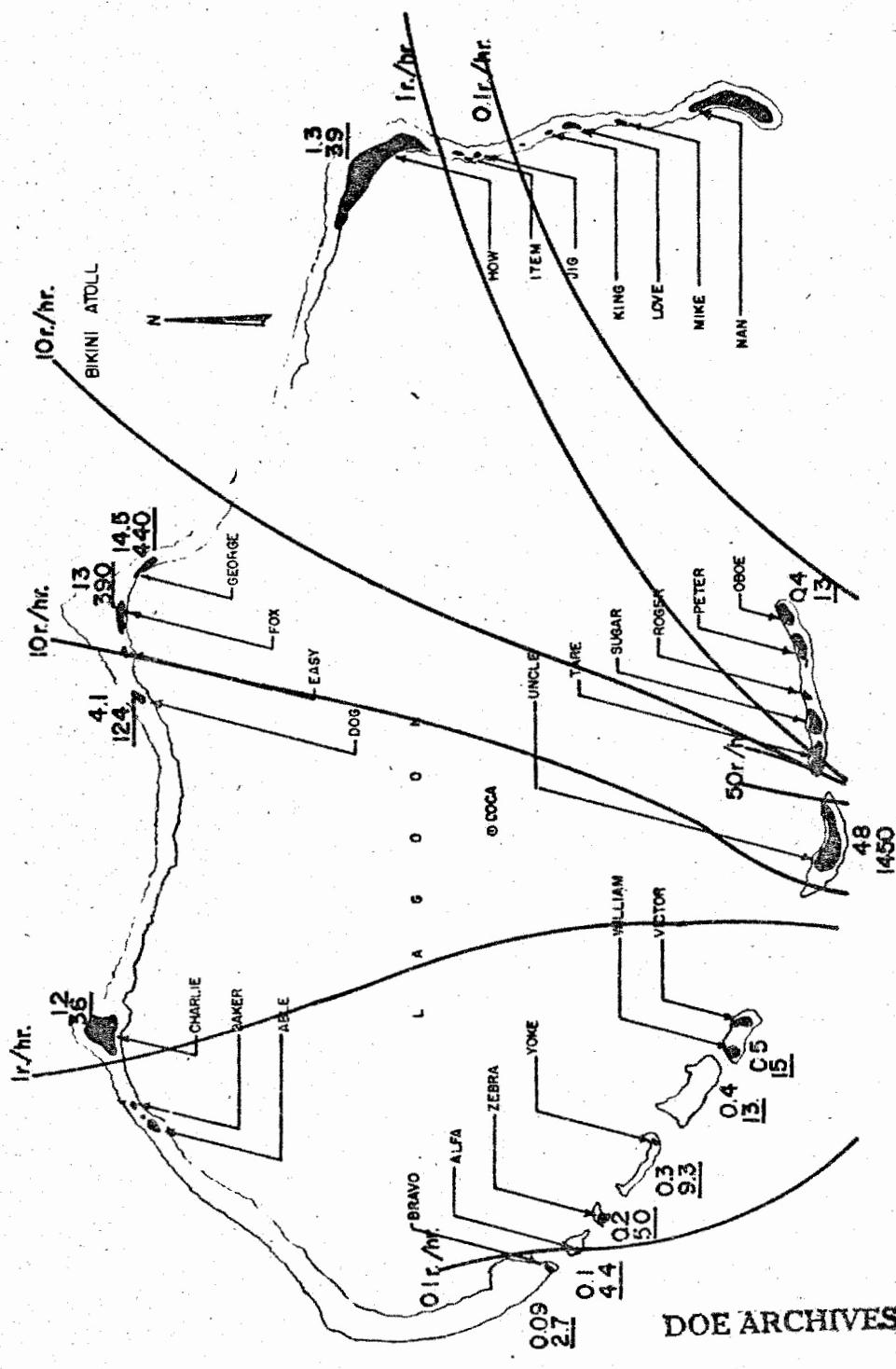
DOE ARCHIVES

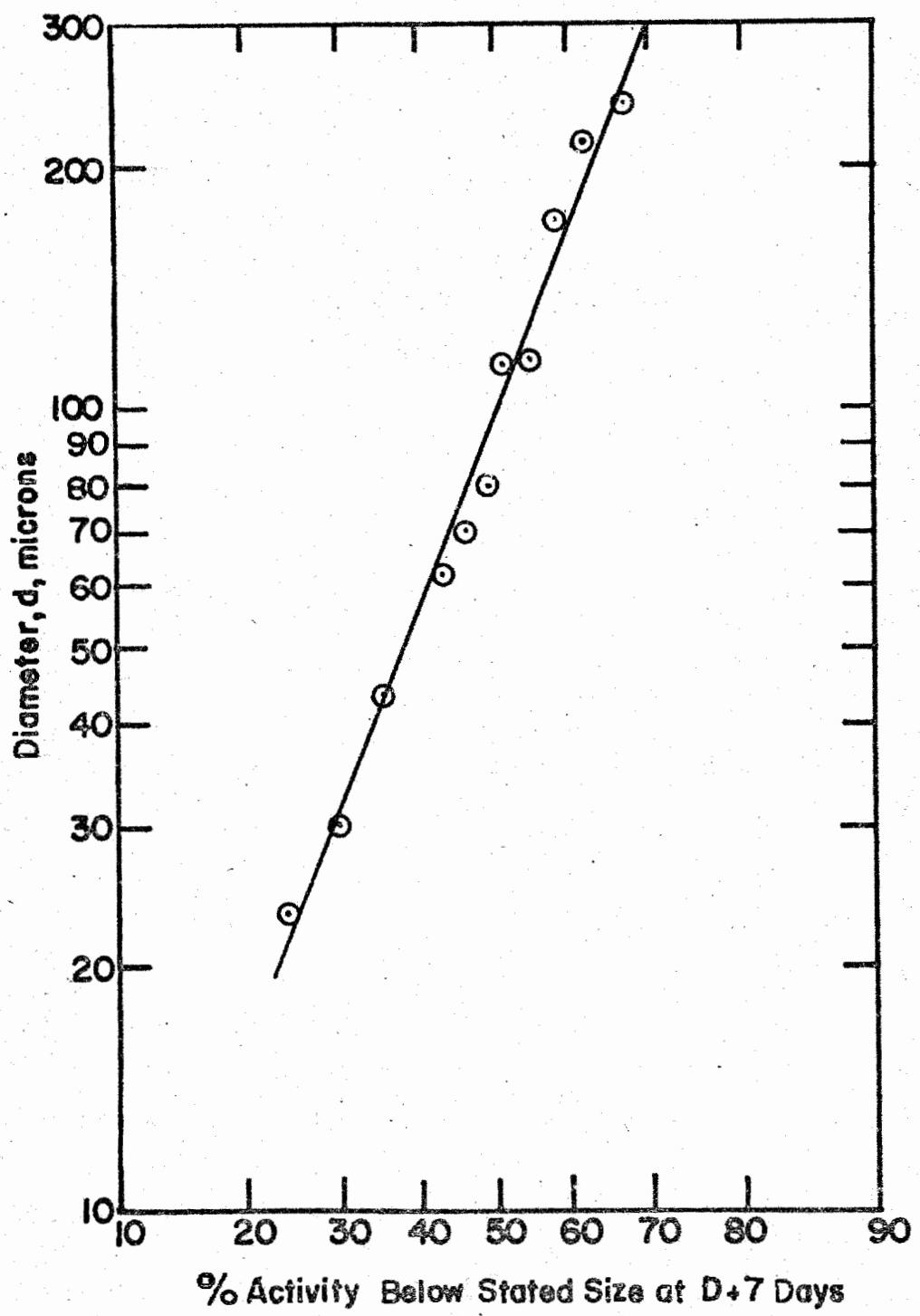
35

© E.O.P. 2007

41

Figure 7  
Isodose Lines for Third Shot





DOE ARCHIVES

Figure 8

37

SECRET

DATA

43

A study of the constant  $m$  in equation (4.1), together with other data, led to an insight into the processes in the fireball leading to the formation of active particles. In this equation  $k$  and  $m$  are constants, and  $A^0$ , the activity at zero time.

Our work has brought out the meaning of the sign and magnitude of the exponent,  $m$ . Most of the particles we studied were agglomerates and when these were broken down into their individual particles, the specific activities of the individual nuclides present in the smaller particles increased as their diameter decreased, i.e.,  $m$  was negative.

We used the Roller Analyzer for reducing the agglomerates. This is a device for size-grading particles in an air-stream.

As an example, the next figure (9) shows a plot of the  $\text{Sr}^{89}$  specific activity against particle size for a Bravo sample. (A similar curve was obtained for  $\text{Ba}^{140}$ ). This is a plot of the specific activity of  $\text{Sr}^{89}$  against the particle size. The slope of the line below  $50\mu$  is -0.88. For  $\text{Ba}^{140}$  it is -0.91.

The sharp break at  $50\mu$  is due to our size-grading procedure with the Roller Analyzer. To the right of the dotted line we have the sieve-graded aggregates, and to the left the individual particles.

The next figure (10) shows a similar plot for  $\text{Ce}^{144}$ . Note that the slope of this is much less than that for  $\text{Sr}^{89}$ .

The significance of the numerical value of  $m$  can be shown in the following way.

For any nuclide with specific activity  $A^0$  at zero time,

$$A^0 = kd^m \quad (4.1)$$

The activity referred to the whole particle, is

$$(A^0)^{\frac{1}{3}} = \frac{1}{6} \pi \rho k d^3 + m \quad (4.2)$$

where  $\frac{1}{6} \pi \rho d^3$  is the mass of the particle, assuming spherical particles and  $\rho$  is the density.

DOE ARCHIVES

Then, if experimentally, we find  $m = -1$ , the activity is proportional to the square of the diameter, i.e., to the surface area of the particle.

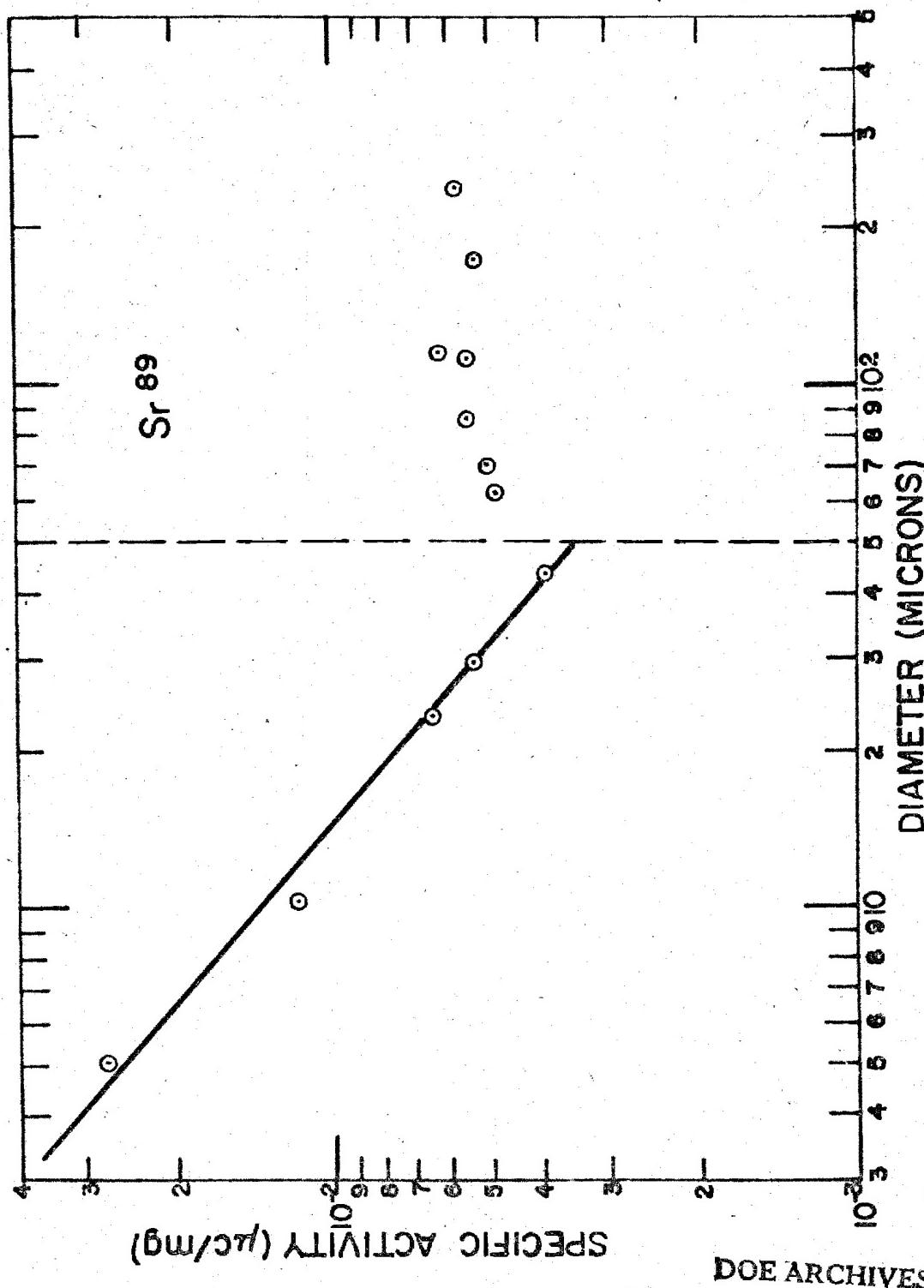


Figure 9

39

DECLASSIFIED  
ATOMIC ENERGY ACT 1954

45

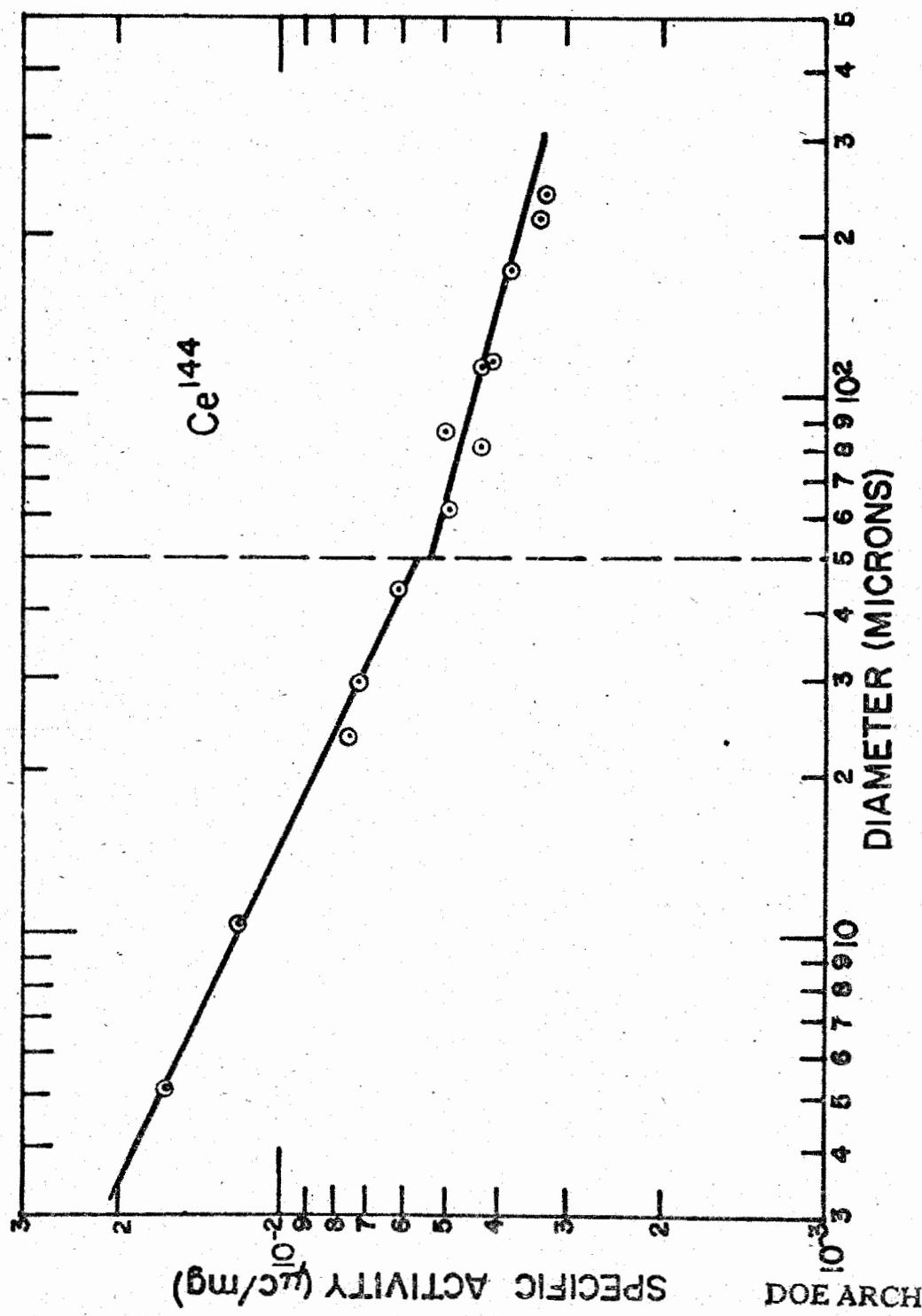


Figure 10

As was shown in the figure for Sr<sup>89</sup>, the value of m was -0.88, and for Ba<sup>140</sup> it was -0.91. Consequently, these two nuclides were concentrated essentially on the surface, as would be expected for nuclides with long-lived precursors.

If the exponent, m, were zero, the activity in equation (4.2) would be proportional to the volume, so that the activity would be distributed uniformly throughout the volume.

For activity concentrated at the center, the activity per particle is constant, and m = -3.

We have actually found values of m as low as -0.32. For example, for Ce<sup>144</sup> we found -0.47; for Mo<sup>99</sup>, -0.48, and for Zr<sup>95</sup>, -0.32. In these cases the activity is distributed in some irregular way throughout the volume. It appears that this could happen if, as particles are growing in cooler parts of the fireball, they pass across concentration gradients, i.e., there is incomplete mixing in the fireball.

Returning to equation (4.1), it is possible to relate this expression, in a formal way, with the decay slope. Since by definition

$$n = \frac{d \ln \sum A_i}{dt} = -t \frac{\sum \lambda_i A_i^0 e^{-\lambda_i t}}{\sum A_i^0 e^{-\lambda_i t}} \quad (4.3)$$

We need only substitute equation (4.1) for every nuclide, i, to obtain the desired relation.

There is also a useful relation between equation (4.1) and fractionation, as indicated by changes in the R-factor. An equation like (4.1) can be written for any two nuclides:

$$A_i^0 = k_i d^{m_i} \quad (4.4)$$

$$A_j^0 = k_j d^{m_j} \quad (4.5)$$

so that

$$\frac{A_i^0}{A_j^0} = \frac{k_i d^{m_i - m_j}}{k_j} \quad (4.6)$$

DOE ARCHIVES

and we can see that the left side is proportional to R, the proportionality constant being the value of  $A_i^0/A_j^0$  for pile fission of these two nuclides.

Note that if  $m_i \neq m_j$ , the fractionation observed will depend on the particle size, but if  $m_i = m_j$ , fractionation, if still present, is independent of the particle size. The same size particle has been assumed throughout.

We found evidence for fractionation in our CASTLE samples. Union shot samples were low in Sr<sup>89</sup> and Ba<sup>140</sup>. Table 1 shows the R-factor for Sr<sup>89</sup> and other nuclides, as a function of particle size. The trend in the R-factors is obvious.

Table 1

R Factor from Intermittent Fall-Out Collector  
Union Shot, Bikini Island

Time (after Shot) of Sample Collection in Hrs	Sr <sup>89</sup> /Mo <sup>99</sup>	Ba <sup>140</sup> /Mo <sup>99</sup>	Ce <sup>144</sup> /Mo <sup>99</sup>	Gross Decay Slope (10-20 das)
1.5- 3	0.702	0.788	0.50	-1.73
3.5- 5	1.15	1.64	-	-1.36
8- 9	0.538	0.661	0.460	-1.54
9-10	1.56	1.53	0.656	-1.60
10-11	1.81	1.43	0.31	-1.37
11-12	1.80	1.71	3.4	-1.04

We may deduce from this result that if base surge is active it will be low in Sr<sup>89</sup> and Ba<sup>140</sup>, because the base surge is due to material from the column falling back to earth shortly after shot. Since this activity leaves the fireball early, it may be low in nuclides with long-lived ancestors, so that the base surge will also be low in these.

We have found active particles in our fall-out samples which apparently must be assumed to have appeared in the base-surge. An

DOE ARCHIVES

example of such a particle is shown in figure 11. The particle, which was partially calcined coral inside, was covered, but not uniformly, with activity on the surface. Particles of this kind were found above about  $200 \mu$ , and were prepared for autoradiography by thin-sectioning.

Our decay data showed that the activities of shot 1 samples were given by equation (4.7).

~~DELETED~~

A typical decay curve, extrapolated to low times, is shown in figure 12.

~~DELETED~~

The observed decay rates of samples from certain other shots showed interference by activity due to the Bravo shot. The data for shot 2 could be represented, for example, by

$$A = A_1 (t+623)^n \quad (4.8)$$

where 623 was the time between the first and second shot, in hours; in other words, all the activity of shot 2 samples was due to shot 1. The samples from shot 3 were less affected by shot 1 activity.

#### Discussion

The results may now be collected to outline our conception of the reactions in the fireball leading to the formation of active particles.

The fireball, at the start, has, near the ground, a layer of vaporized ground material (here CaO) at the bottom, of greater density than at other points. As the hot bubble containing fission and other products rises, it carries up trailing behind it, currents of the heavier ground material layer, thus giving rise to varying concentration gradients, and to lateral eddies; in other words, conditions in the



Figure 11  
Non-uniform Surface Activity on a Large Particle ( $> 200 \mu$ )

44

DOE ARCHIVES

U.S. ENERGY ACT 1978

50

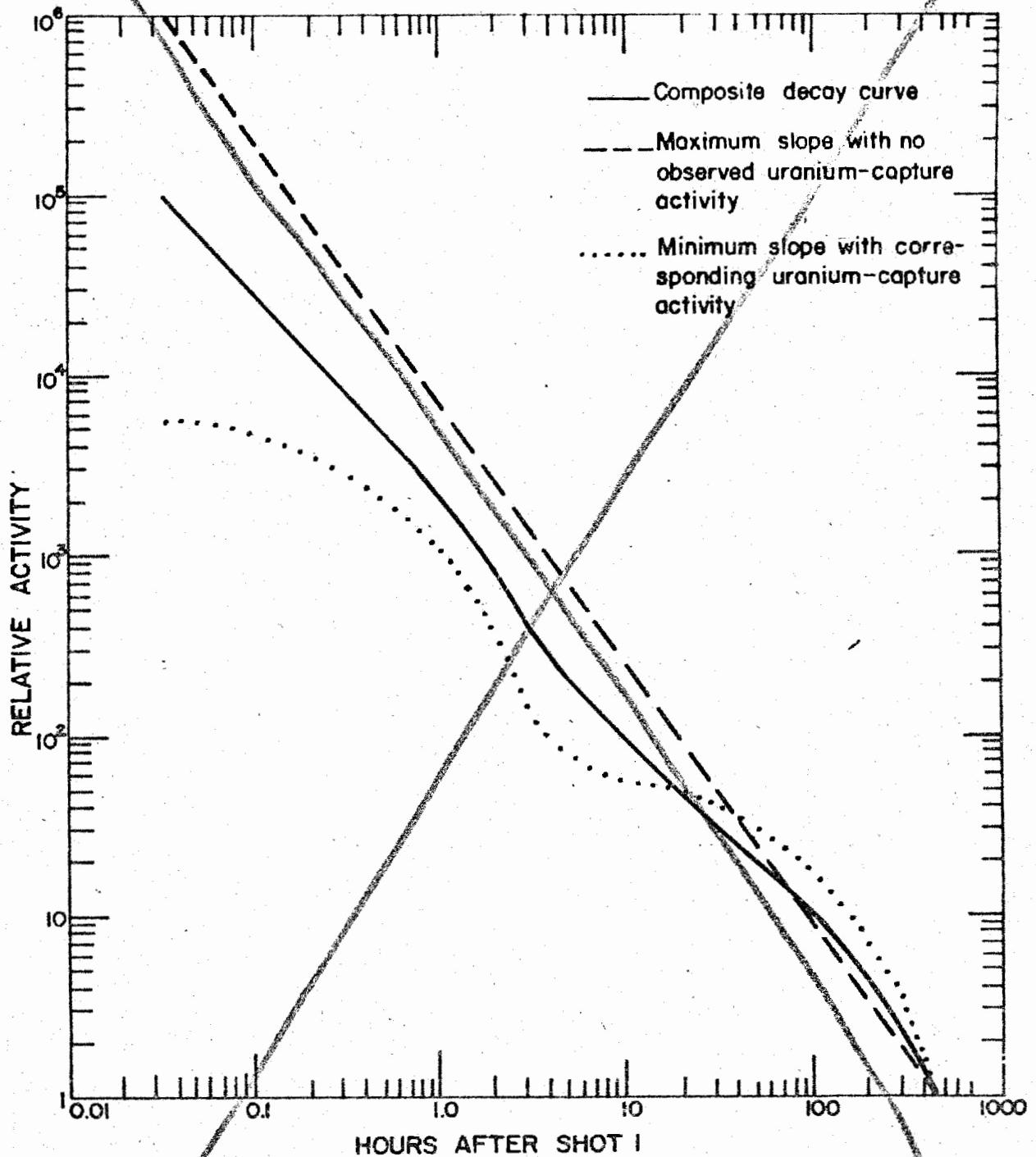


Figure 12  
Typical Gross Decay Curve

DOE ARCHIVES

fireball are such that there is poor mixing. This conclusion is supported by the low values of the exponent  $m$  in equation (4.1) for such nuclides as Ce<sup>144</sup> and Zr<sup>95</sup>, since such low values indicate particle formation under different concentration conditions.

#### Contamination of the Column and Base-Surge

At the edge of the fireball some material condenses early to fall-out, and owing to the vortex action this could be active since the eddies in the fireball may bring fission products to the edge. This fall-out, "peeling-off" and falling, may be sucked up again in the thermal draft, and become impacted on inactive material in the column. Since the base surge is believed to originate from the lower part of the column, it appears that contamination in the base surge might be explained on this basis.

The activities found would appear to be due to this effect because our stations were too close in to have received fall-out from the cloud. The photograph on figure 13 of the column collapsing over the atoll supports this.

#### Summary

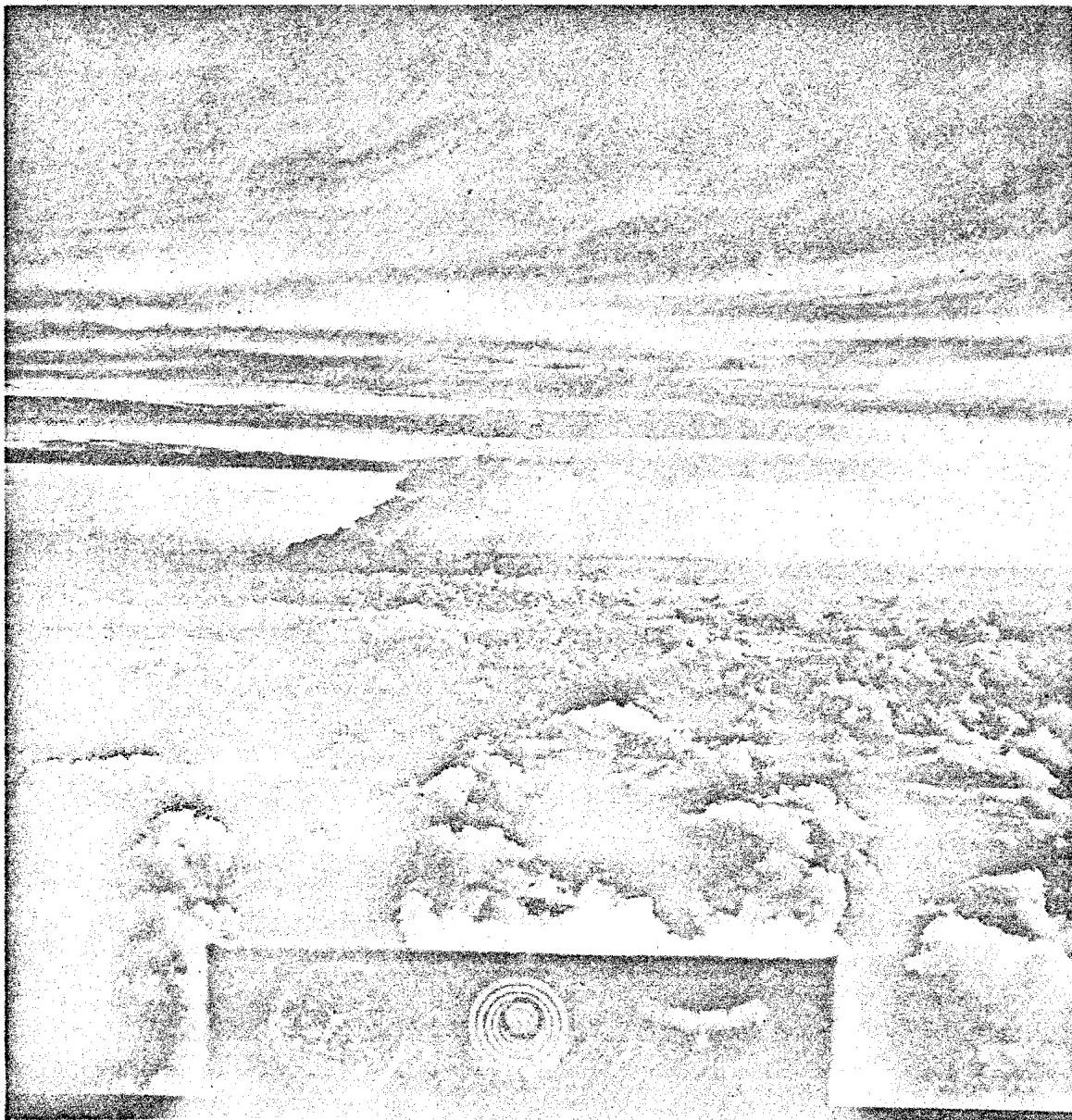
We have presented isodose lines, based on Rad-Safe Data, for the total hazard, for the various CASTLE shots.

On the basis of our decay studies, high values of the decay slope were attributed to the presence of certain capture products.

These, at 250 hrs. after the Bravo shot, corresponded to about 44% of the total activity.

Our work has advanced our more intimate understanding of the mechanism of the formation of active fall-out, and has led to a possible explanation of how the column, and eventually the base-surge, can become contaminated.

DOE ARCHIVES



DOE ARCHIVES

Figure 13  
Collapse of Column over Atoll

47



53

7/18/88

INCOMPLETE DOCUMENT REFERENCE SHEET

The archive copy of this document is incomplete.

Pages missing 48

Enclosures missing \_\_\_\_\_

Attachments missing \_\_\_\_\_

Other \_\_\_\_\_

CPS  
signature

2-11-92  
date

53A

METHODS, FINDINGS, AND OCEANOGRAPHIC FACTORS OF PROJECT 2.7,  
OPERATION CASTLE

Dr. Theodore R. Folsom  
Scripps Institution of Oceanography

Introduction

I have been asked to discuss certain aspects of a fall-out survey which was made just following Shot 5 of the CASTLE operation by personnel of both United States Naval Radiological Defense Laboratory and Scripps Institution of Oceanography operating as Project 2.7 of Task Unit 13. This survey covered a large area of open sea east of Bikini atoll, and relied to a great extent upon oceanographic methods for bringing back an evaluation of the extent of the fall-out. I will direct my remarks towards the oceanographic factors here introduced into fall-out studies for the first time, and Dr. Werner of NRDL will, in the following paper, stress the quantitative radiological results.

This expedition was planned and implemented on very short notice, and it could not have succeeded without the effective cooperation of numerous agencies and individuals within the task force. Unfortunately many of the acknowledgements, which are certainly due, will have to be omitted here.

Outfitting in Haste

This was perhaps the first time anyone had set out seriously to catch fall-out by using the ocean itself as a trap; but it so happened that no specialized and well-equipped oceanographic ship was in the Marshalls region during this particular operation. For this reason the USS SIOUX, an ATF tug which was already assigned for NRDL project work, was hastily outfitted. A contractor's winch was acquired from the Holmes and Narver yard along with about 3,000 feet of light (and very doubtful) cable. And a wire-measuring wheel, a set of standard oceanographic Nansen-type water-sampling bottles, and a set of twelve specialized oceanographic thermometers, and also a Bathythermograph and several cases of citrate bottles were loaned by the Hydrographic Office representative, Mr. Hammond. Another bathythermograph was loaned by the destroyer, USS EPPERSON.

DOE ARCHIVES

The gasoline driven winch was welded to the ship's fan-tail deck, and a hydrographer's platform and boom was rigged outboard. Project 2.5 personnel secured a rush shipment by air of gallon-sized plastic bottles for transporting water samples; and it was later found possible

to improvise from these bottles some very satisfactory though clumsy "snap-samplers" of a type which minimizes the loss of highly diluted materials.

All this was put together in about one week. One of those particular weeks memorable to many of us as "weeks of the flexible time scale" when there were several "Y - 2 days" and consequently were several repeated, disappointing, false starts. But, when the ATF SIOUX finally left Eniwetok on 4 May, she had aboard the bare elements of a hydrographer's equipment; and some of the mechanically-weak and therefore dangerous features of this equipment were remarkably well compensated for by the skill and enthusiasm discovered in a young seaman who volunteered to become the winch operator. He was a red-headed farm boy nicknamed "Booga" who apparently had learned to love the hoisting of hay gently into hay lofts. He became very good at it and for unexpected skill, we who stood at the flimsy Hydro wire will always be grateful.

#### Direct Reading Gamma Detecting Devices

The ocean is very large and very deep, and the taking of three-dimensional samplings of it is a very slow and tedious process even with the best equipment. Two hours, for example, may be required for each deep sampling cast, and four or five days may be required to merely traverse the area influenced by modern weapons. Sooner or later the oceanographer always turns to methods for interpolating between the careful measurements which he makes at "stations". Very fortunately for this particular survey a convenient interpolating device was known to be available but in sad physical condition momentarily. It was a geiger counter which had been removed from a standard Radsafe hand set and had been installed inside a section of steel tubing. It was entirely water-tight; it could be lowered to depths of about 200 feet; the gamma signals could be read on deck. It could be towed behind a ship; and it had just been tested in Bikini lagoon by Scripps people interested mainly in lagoon circulation.

DOE ARCHIVES

At the time the request for it came to Bikini, this so-called Mark I prototype, underwater, marine geiger, gamma detector was in pieces in a cardboard box, under a bench, on a ship in the lagoon. It had just passed through the propellor of an "M" boat, the captain of which having forgotten he had behind him a "tow". But so promising were the data-extending possibilities of this crude instrument, it was shipped in pieces to Parry and rebuilt. And two more, somewhat similar, underwater gamma detectors also were put together from hand set components during that period when the weather, or something, delayed the

"Yankee" event. These were really crudely-made devices; it was hoped merely that at least one of the three would survive the rough treatment expected at sea.

#### The Track of the SIOUX

Ultimately, on the morning of 5 May the ATF SIOUX, outfitted as just described, proceeded to a point south and east of Bikini, made shake down tests of all gear, took deep samples of clean water for control purposes, and then waited for permission to make a section through the fall-out area. At about 2000 hours, 5 May, the first section was started, intended to pass ground zero at a radius of about 25 miles. The gamma detecting gear was streamed out.

Figure 1 is shown to aid description of the unconventional gear used on this cruise. The cylindrical gamma detectors were towed about 200 feet astern by rubber light cords; these detectors sank six feet below the surface at the 7 to 13 knot speed which was generally held. The meters were read on deck; whenever possible two or more instruments were towed together.

Another gamma detector, an AN/PDR-TLB handset inside a steel tank was supported six feet outboard at about six feet elevation above the sea surface. It served several functions to be discussed later.

The SIOUX steamed almost 900 miles through the contaminated area during the next four days.

Along the ship's track shown in Figure 2 has been plotted the relative gamma intensity corresponding roughly to mr/hr, and the eight stations have been identified with circles. The gamma signal is plotted to the right of the track.

Somewhat before midnight the SIOUX broke abruptly into "hot" water - rapidly getting "hotter". Those who were aboard will not soon forget the ominous effect caused by the meters' climbing continuously upward and going off scale one by one. Only the above-water detector (the T1B instrument) managed to stay on scale, partly due to its heavily shielded condition.

DOE ARCHIVES

At just fifteen minutes after midnight it was discovered that the ship was reversing its course, and a dash up to the bridge brought to light the fact that the ship's Radsafe officer had been fully instructed as to procedures to carry out in the event of fall-out - but had not been prepared to recognize that event where nothing was falling on the deck but where the sea itself was radiating intensely for miles around. It also appeared from the ensuing conversation that during an earlier

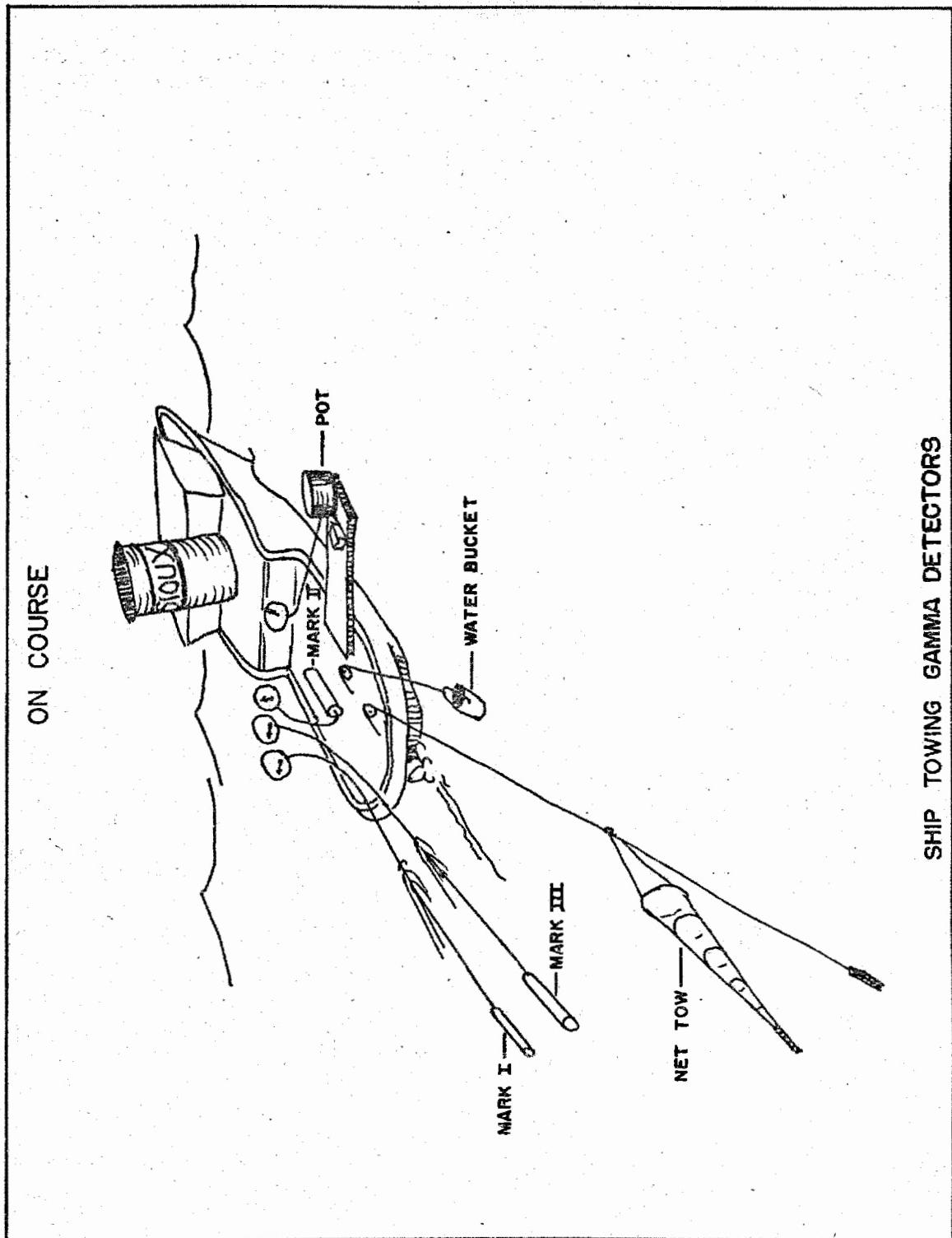
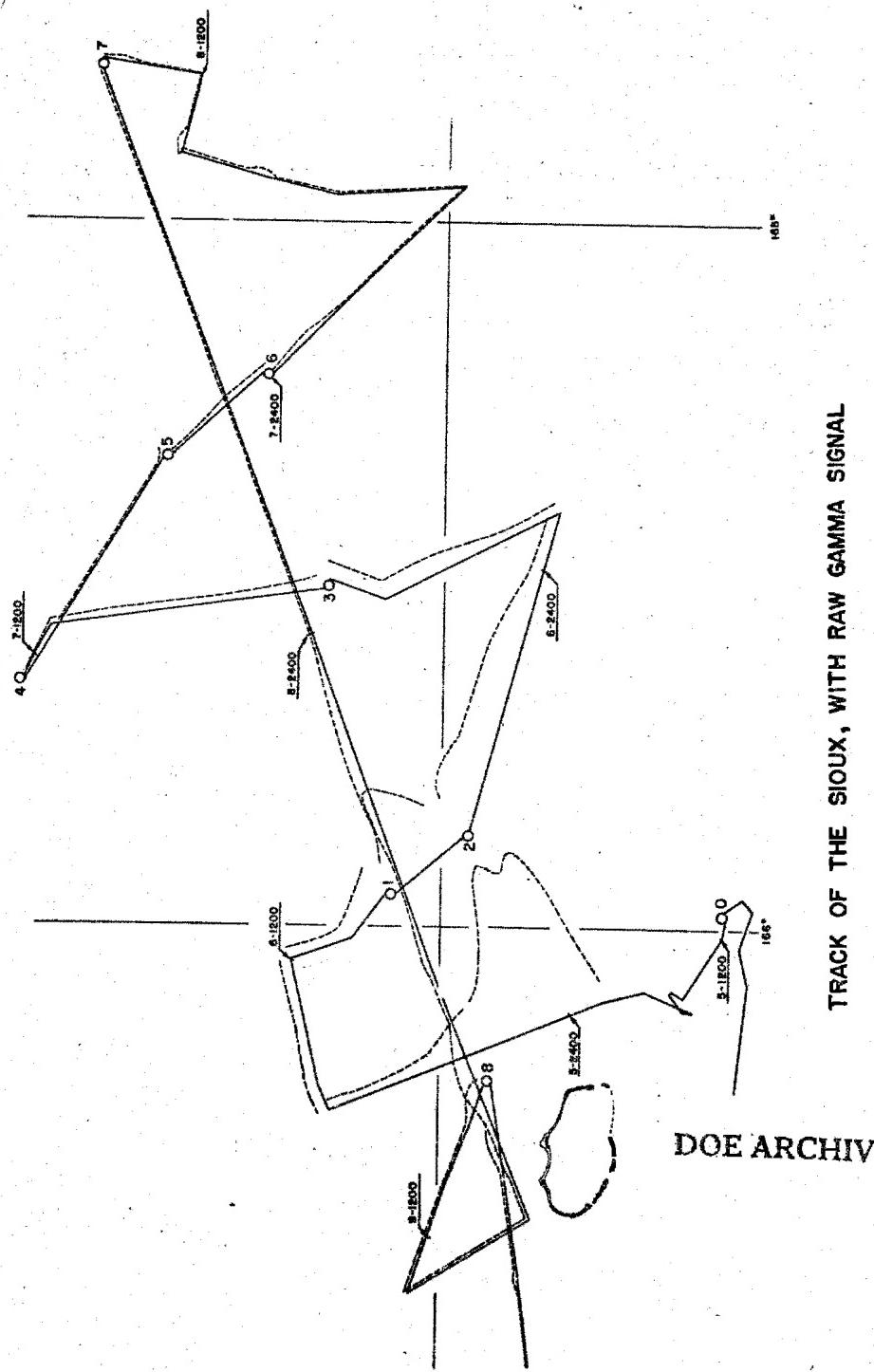


Figure 1

DOE ARCHIVES



**Figure 2**

DOE ARCHIVES

53

ENERGY ACT 1954

6

58

cruise when a similar physical situation must have existed, contaminated sea water had been pumped over the comparatively clean decks of this ship.

A simple test was demonstrated of raising the Radsafe monitoring instrument above the steel windscreens on the bridge so as to cause better exposure from the sky, and the cruise was thus prevented from ending then and there.

It will be seen that the track intercepts six areas where gamma activities far above background were detected. Since four days passed during the survey, decay alone produced a great deal of attenuation, the signals became progressively weaker, but always remained measurable.

All the gamma measurements cannot be presented in detail here, they were made at over 450 points. But some of the signal variations witnessed during the first day will be illustrated later after the measurements at fixed stations are discussed.

The winch, meter wheel, hydrographer's platform (carrying the TLB instrument in it), are shown schematically (Figure 3), as are the string of sampling bottles on the hydrographic wire.

On the left is indicated the method of lowering the Mark II gamma detector to measure the gamma intensity profile. This slide will be shown again later, but the work at fixed stations can be listed at this time.

During the eight main stations there were made: **DOE ARCHIVES**

One cast to 800 meters with seven samplers

Four casts to 500 meters with six samplers

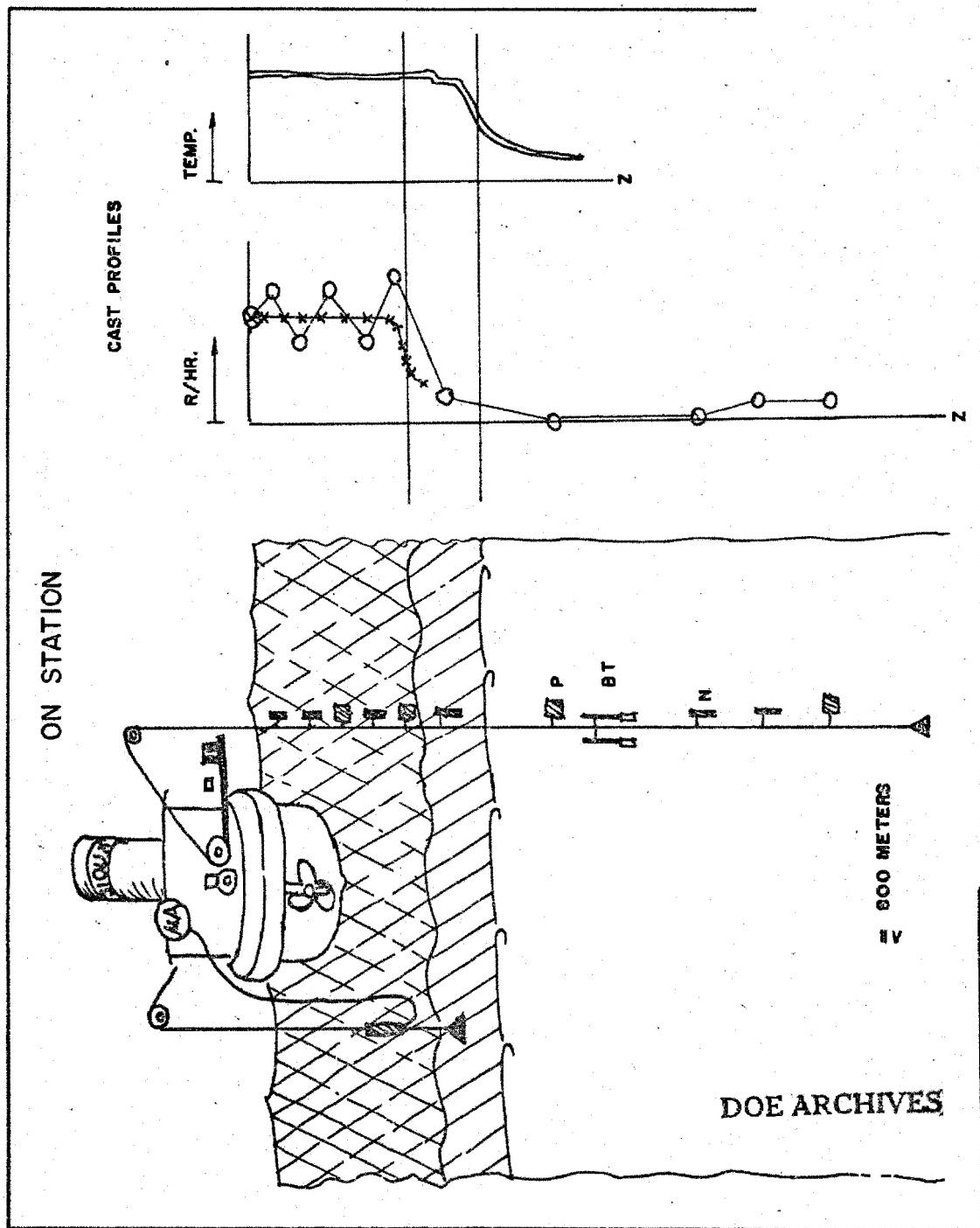
Four casts to 175 meters with six samplers

Two casts with a plankton net towed at two knots.

Four short additional stations were made where only BT instruments were lowered; all told BT's were made at 12 positions along the track.

At three stations the vertical profile of gamma signal was measured directly with the Mark II instrument.

Each Nansen bottle carried two reversing thermometers.



MEASUREMENT AND SAMPLING AT STATIONS

Figure 3

Always four of the special plastic bottles were used.

Surface water samples were taken at stations as well as along the track.

#### Disposal of the Water Samples

The water samples taken at these stations as well as samples taken at the surface during the cruise, were rushed by plane to NRDL for analysis. Dr. Werner will discuss the results of these analyses and the conclusions which can be drawn from them somewhat independent of the direct gamma measurements which will now be discussed in detail.

#### The Direct Gamma Measurements

Most of the direct measurements of dose rate were made with geiger instruments; these had many ranges and had ample sensitivity, but as with the measurements of any geiger instrument these measurements must be used with care. In this particular marine usage a number of additional reductions have to be applied to the readings to yield the approximate true dosage rates.

#### Contamination and Background

A number of steps of calibration and correction were carried out.

Several instruments were used together whenever feasible. They were intercalibrated and tested against the hand sets on board ship several times. These were new, untried instruments.

The separate records come into satisfactory numerical agreement after calibrations are applied.

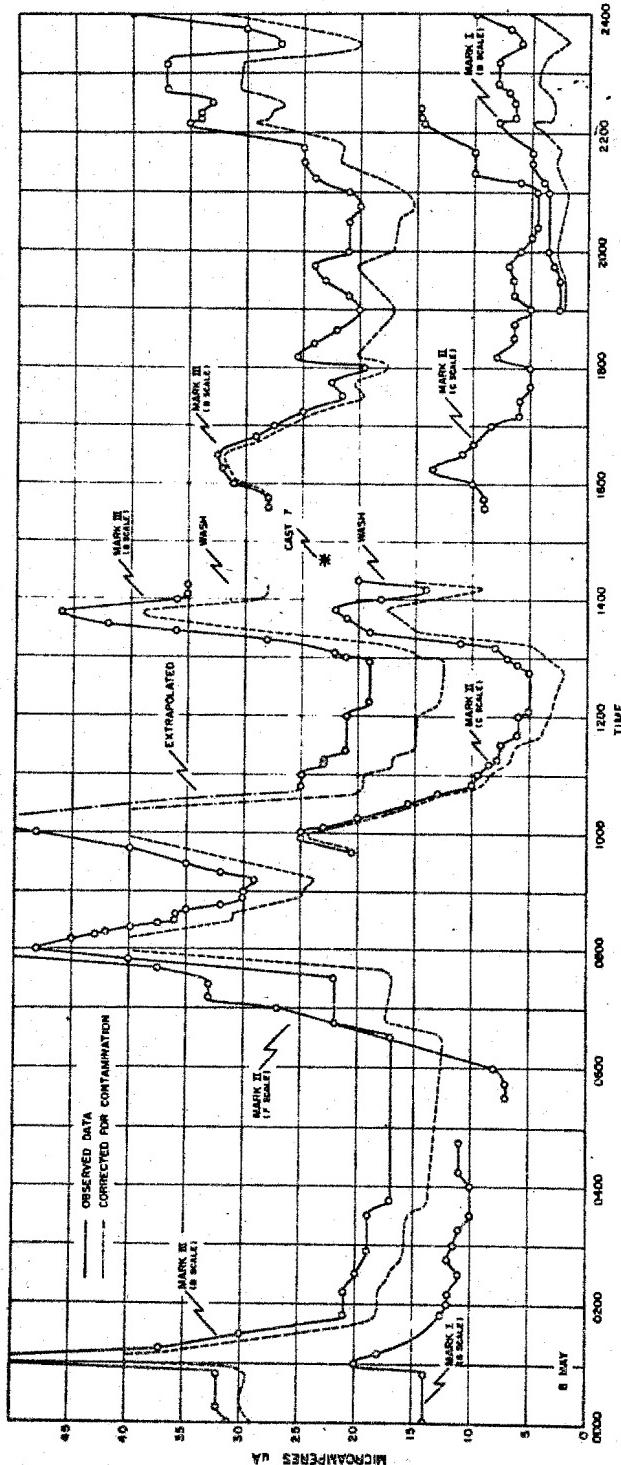
At each station - and sometimes between - the towed instruments were hauled aboard and carefully washed. The slide (Figure 4) shows the result of this washing upon the signal.

DOE ARCHIVES

At these wash-off points a reliable correction for contamination can be made; but between these positions an interpolation had to be resorted to. A simple linear proportionality was assumed for relating the rate of surface "pick-up" and concentration of activity on the sea.

Considerable thought has been given to methods to reduce pick-up and to make better corrections later - but nothing more can be presented here.

- 6 -



#### DETAILS OF SIGNAL ALONG TRACK

Figure 4

DOE ARCHIVES

57

**OMIC ENERGY ACT 1954**

62

### Calibration

All three of the towed instruments were calibrated on 10 May 1954 immediately after the cruise, at Parry Island RadSafe and against a large radium point source.

Then these instruments were immediately boxed and shipped to the United States Bureau of Standards. At the Bureau, the radium calibrations were repeated, and the instruments were then exposed to radiations having photon energies ranging from as low as 58 KEV up to 1.2 MEV.

These exposures were repeated from all incident beam angles so that a mean response corresponding to a broad source could be estimated.

The variations of response of the Mark II instrument with beam energy is shown in Figure 5.

A computed mean of responses for all angles is shown in Figure 6. This relates to a submerged exposure of the instrument inside a large, monochromatic, hypothetical, distributed source, i.e., a  $4\pi$  monochromatic source.

### Response to Estimated Field Source

Estimates of the source energy spectra which might have existed in the sea during the period of the survey were supplied by Dr. Werner of NRDL and by Dr. Scoville of the Armed Forces Special Weapons Project. An average of the estimated spectra for D+1, D+2, D+3, and D+4 days is shown in the figure second from the bottom.

By following the technique outlined in the Technical Analysis Report issued January 1954 by the Weapons Effects Division of AFSWP (AFSWP-502A), a dose histogram was computed. This represents an estimate of what energy distribution was actually "seen" by the submerged instrument. It is shown in Figure 6.

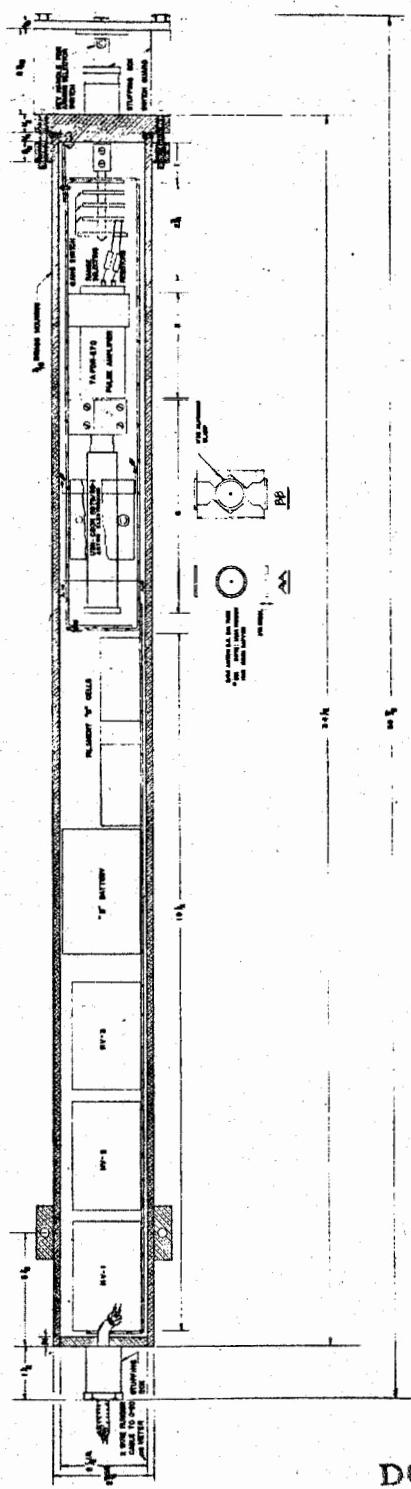
### Final Calibration Curves

DOE ARCHIVES

The results of the monochromatic response constants of the instrument may now be combined with the computed, *in situ* dosage spectrum to give an estimate of the response of the instrument to the mixed activity believed to exist in the sea.

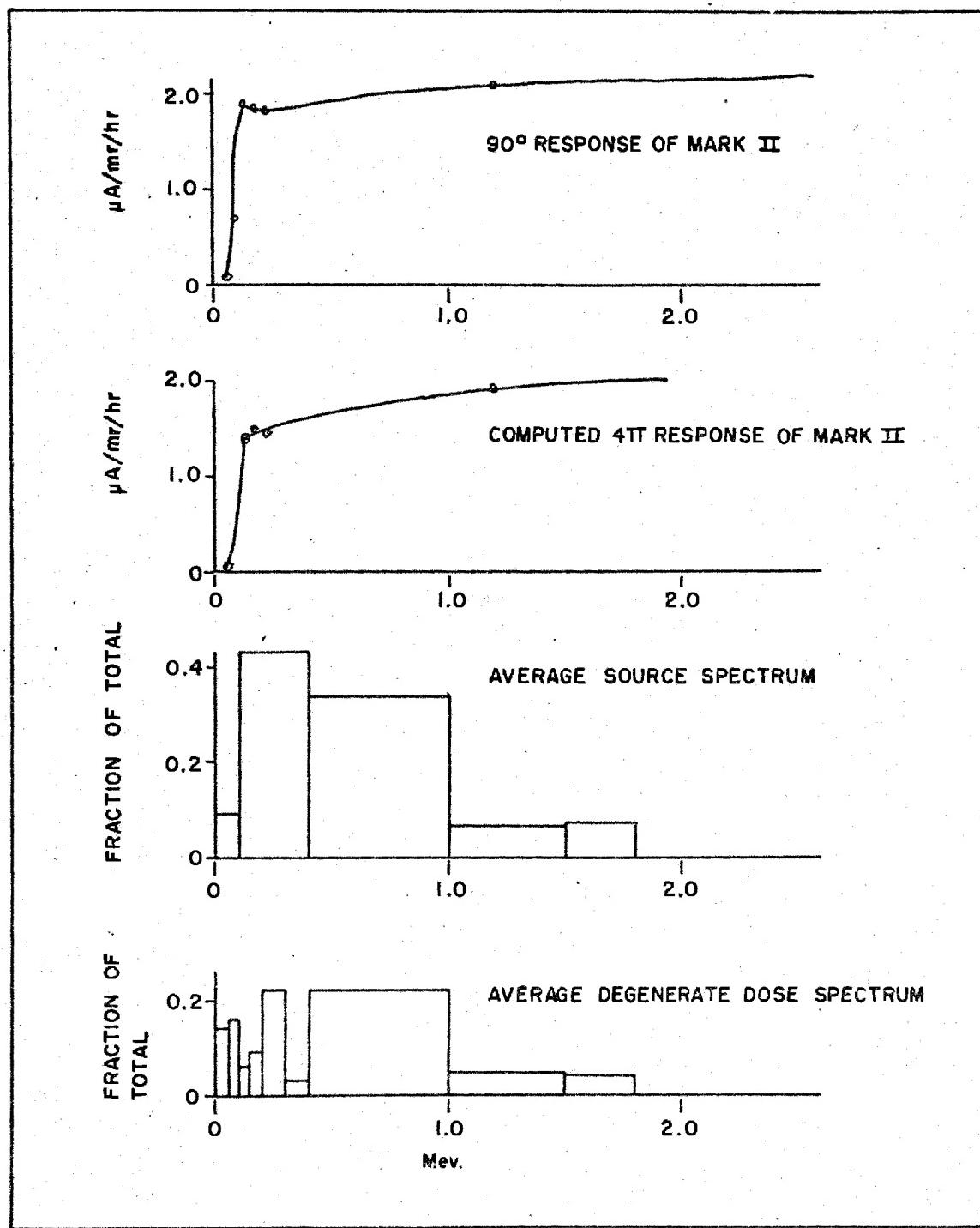
Before final application of these calibrations to the field measurements, account had to be made of the slight non-linearity of

Figure 5



DETAILS OF MARK II INSTRUMENT

DOE ARCHIVES



#### SUMMARY OF CALIBRATION STEPS

DOE ARCHIVES

Figure 6

monochromatic response of the instrument, that is the  $\mu\text{A}$ -versus- $\text{mr}/\text{hr}$  response.

The shape of the responses to radium rays is shown (Figure 7); the results from Parry Island and from the Bureau's calibrations are compared here, but for only one range.

The correction for use of the Mark II instrument inside a large distributed source of the type expected can be summarized by saying the Parry Island radium calibration curves had to be shifted upward by a factor of 1.5.

That is, this instrument calibrated against radium, underestimates the dosage rate when used to measure softer, mixed radiations underwater.

So far nothing has been said about the effects of time and vertical and horizontal motions; but the gamma signals along the track can now be reduced to apparent  $\text{mr}/\text{hr}$  in situ - that is the ionization in an air cavity under water.

#### Reduction of Hypothetical Dose at Three Feet

An underwater dose estimate has limited usefulness except perhaps for computing the exposure of personnel below decks.

It is customary to normalize fall-out dosage to that which would exist at three feet. But even over land this computation must be simplified to that unlikely case where the land is perfectly smooth - a very large hypothetical billiard table; and this imaginary, uniform distribution spread over the imaginary catchment plane is not much harder to derive from measurements made at sea than from those made on land and certainly as real.

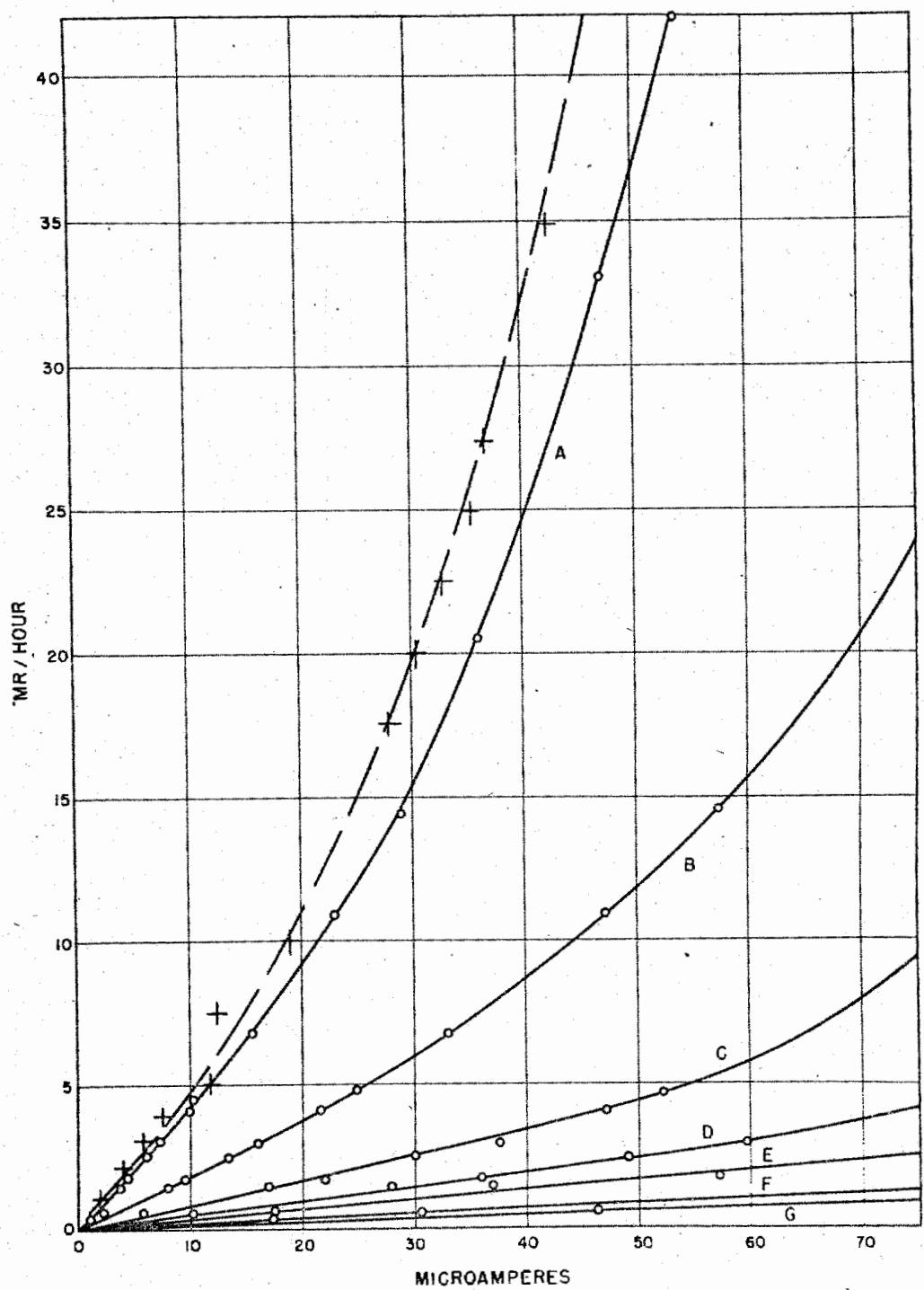
#### Absorption of Energy in Water

Apparent-dose in roentgens/hr under water can be reduced to density of radioactive energy fairly directly if the source is distributed uniformly and if the source spectrum is known.

In a large uniform distribution, energy-balance considerations require that the rate at which energy is absorbed in any unit volume of water is equal in the rate at which it is emitted from any neighboring identical volume element, that is, absorption in water equals activity density.

DOE ARCHIVES

This equation can be utilized if the apparent roentgen in situ is known since the roentgen corresponds to the amount of energy absorbed



CALIBRATION CURVE OF MARK II

DOE ARCHIVES

Figure 7

62

REC

NUCLEAR ENERGY ACT 1954

67

in a unit volume in air, which of course reduces to the energy which would have stopped in the same volume of water - by multiplying by the ratio of the appropriate "true" absorption coefficients.

#### Total Density in the Column

The total amount of fall-out energy per unit area can be obtained by summing up all activity in the water column. The field experiments indicate a surprisingly uniform mixing (Figure 8).

It can be estimated, even with the limited experimental data collected in this expedition alone, to what depth the contamination had penetrated at any time even though the cable was too short to permit direct measurement (Figure 9).

There are several reasons for giving the oceanographer confidence that the activity did not ever during the whole cruise penetrate below a fairly well established depth - the thermocline lying at about 100 meters. Twelve Bathythermograms were made during the cruise - 48 more were contributed by destroyers in the area. These and the thermometers on the hydrographic wire establish this ultimate depth of mixing within plus or minus 20%.

Only one single water sample showed any significant evidence of penetration below the thermocline. We attribute this finding to the sort of contamination which may be anticipated with Nansen-type of sampling bottles.

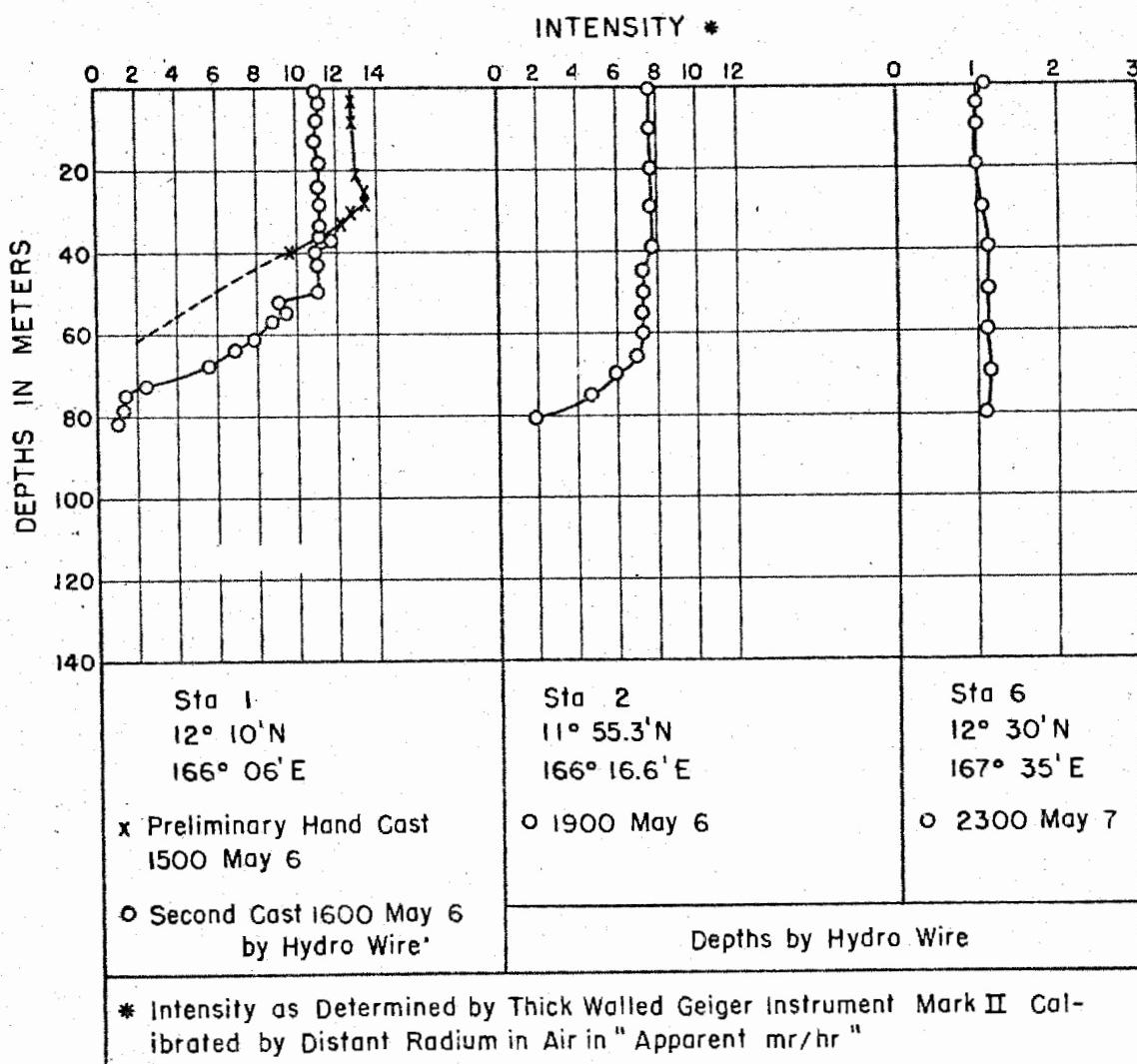
Thus the radioactive density which would have collected on the hypothetical fall-out catchment plane can be computed by simply multiplying the in situ density in MEV/cm<sup>3</sup>/sec by the depth of mixing, measured or computed in terms of centimeters of course (Figure 10).

The final step of reduction requires the use again of the tables made available in the AFSWP-502A report.

Fortunately that special case involving radiation from a uniform distribution over a plane surface has been worked out in some completeness and is presented in tabular form in this monograph. The calculations are somewhat tedious, but are straightforward; but solution does take into account the contributions from scattered rays. That is, a "build-up" factor suitable for the problem at hand has been made available by modern electronic integration.

DOE ARCHIVES

The final reduction can be summarized therefore by the formula shown at the bottom of Figure 10.



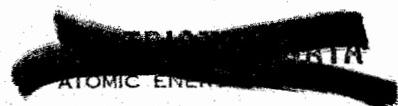
DOE ARCHIVES

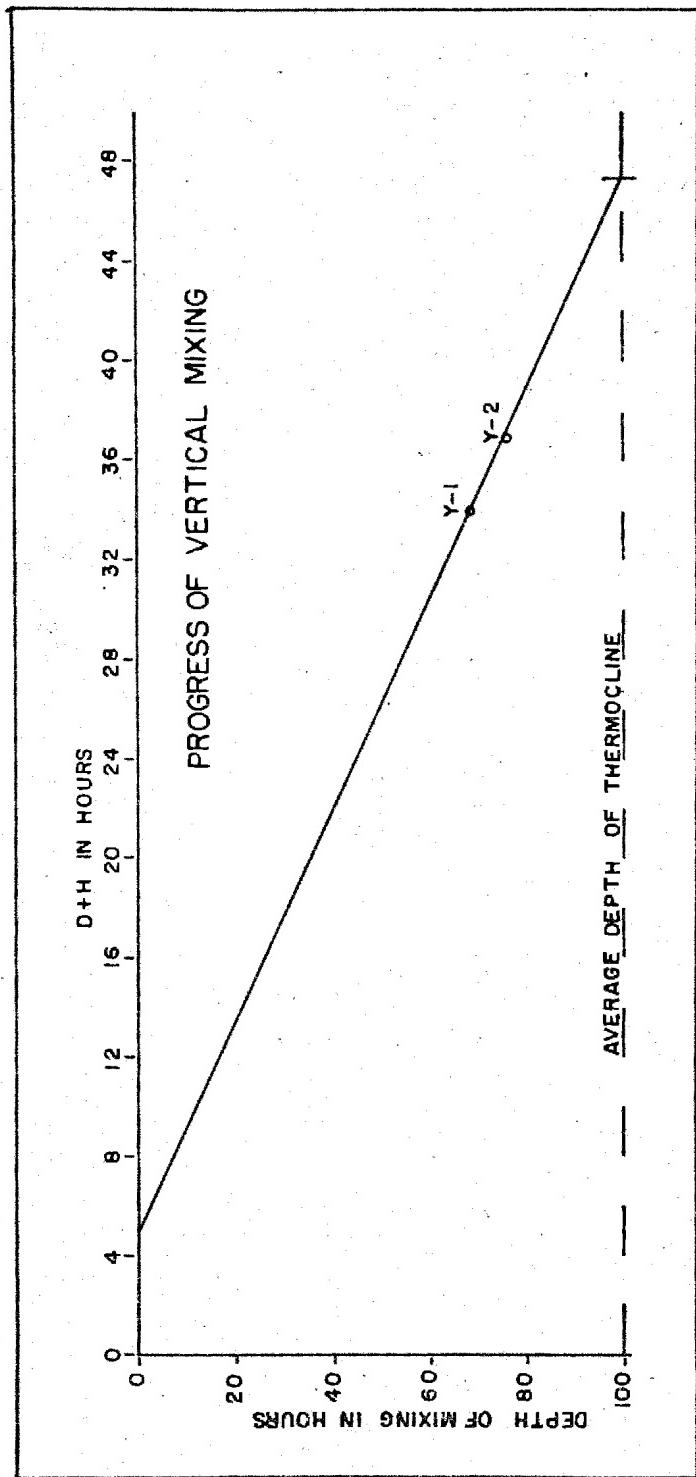
VERTICAL PROFILES OF CONTAMINATION

Figure 8

64

69





PROGRESS OF CONTAMINATION DOWNWARD

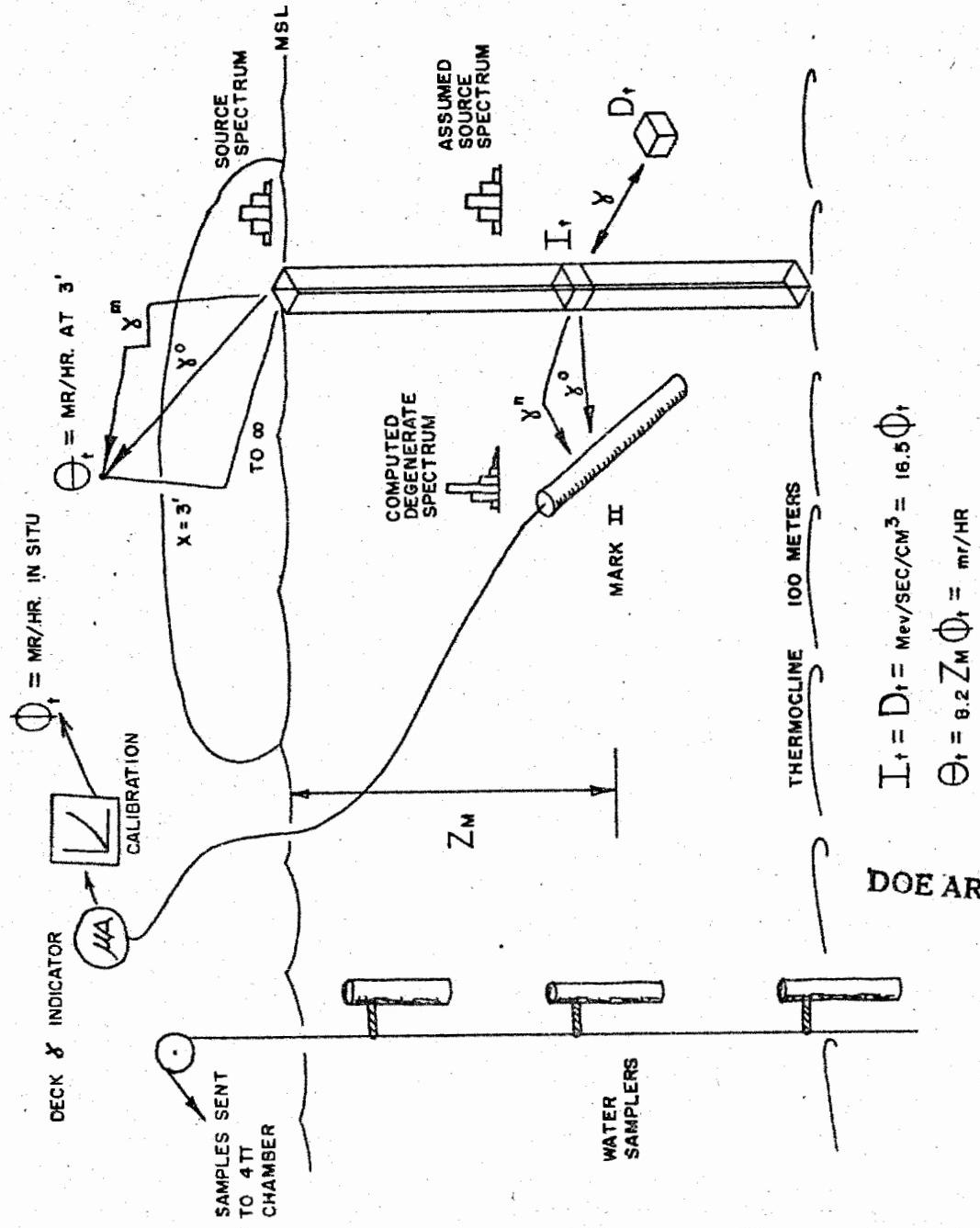
DOE ARCHIVES

65

[REDACTED]  
OMIC ENERGY ACT 1954

70

Figure 9



### SUMMARY OF REDUCTION

Figure 10

RESIDUAL ENERGY

The dose in air at three feet above the standard, smooth, fall-out plane, in mr/hr is:

$$\Theta_t = 8.2 Z_m \Phi_t = \text{mr/hr}$$

where  $Z_m$  is the mixing depth in meters and  $\Phi_t$  is the apparent dose in mr/hr read by a properly corrected dosimeter submerged in the water.

So far lateral motion and decay of activity have not been introduced. Time is still a variable.

### Decay

The amount by which the decay of the activity disguises the signals seen by a ship steaming on a slow traverse can be now illustrated. We shall now compare two plots made along the track, one of the signal unmodified (Figure 2) - the other shows it reduced to the synoptic time  $D+12$  hours (Figure 11).

For final computations an experimental decay curve supplied by Dr. Werner was used. It differs from what is given by use of the familiar "1.2 decay law".

### Lateral Displacement Due to Currents of the Sea

Finally, the effect of lateral displacement occurring after the fall-out arrives at the sea surface may now be taken into consideration.

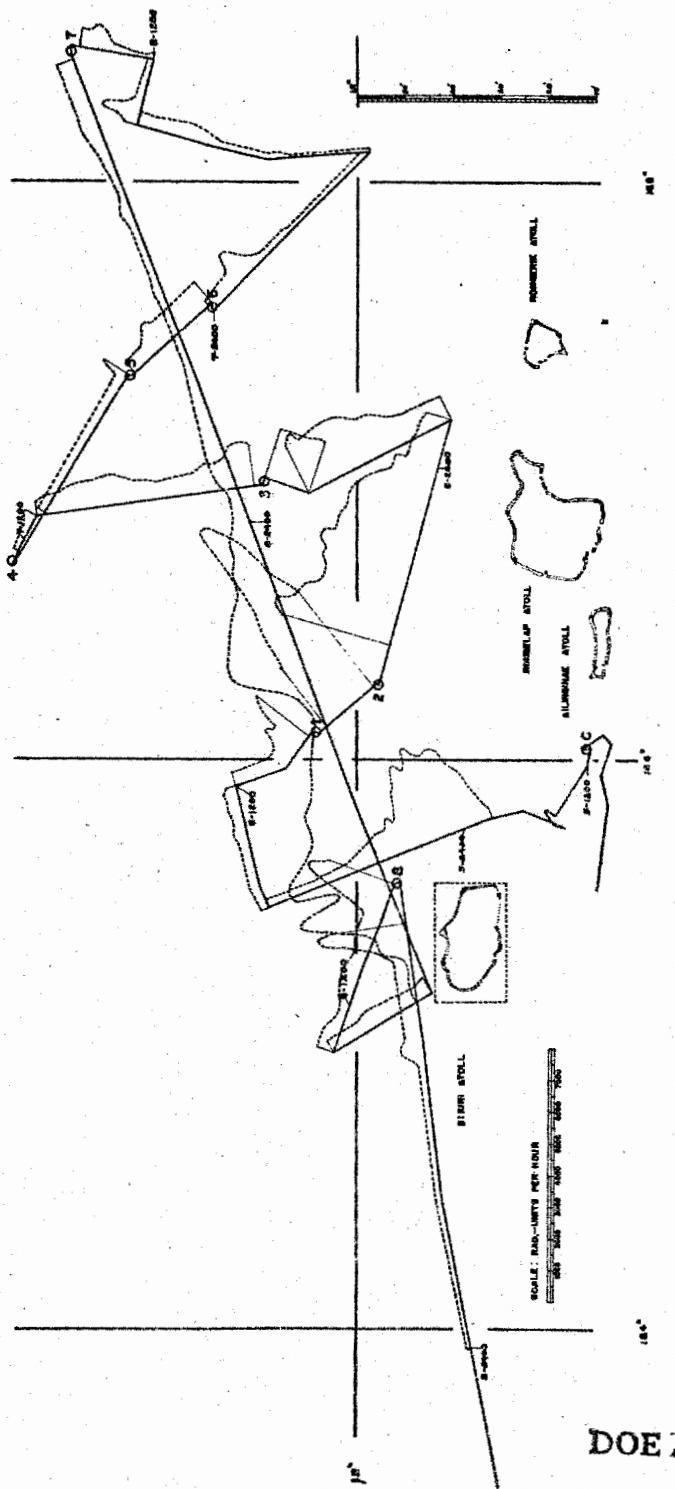
The currents near Bikini unfortunately are not stable enough to be predicted in detail with any accuracy. However, there is a fairly persistent component from east to west (Figure 12).

For the present computations, a steady east to west current of  $\frac{1}{2}$  knots was assumed. The type of error which might have been introduced is fairly apparent - it is mainly a distortion of shape of the fall-out field (Figure 13).

### Hypothetical Synoptic Track

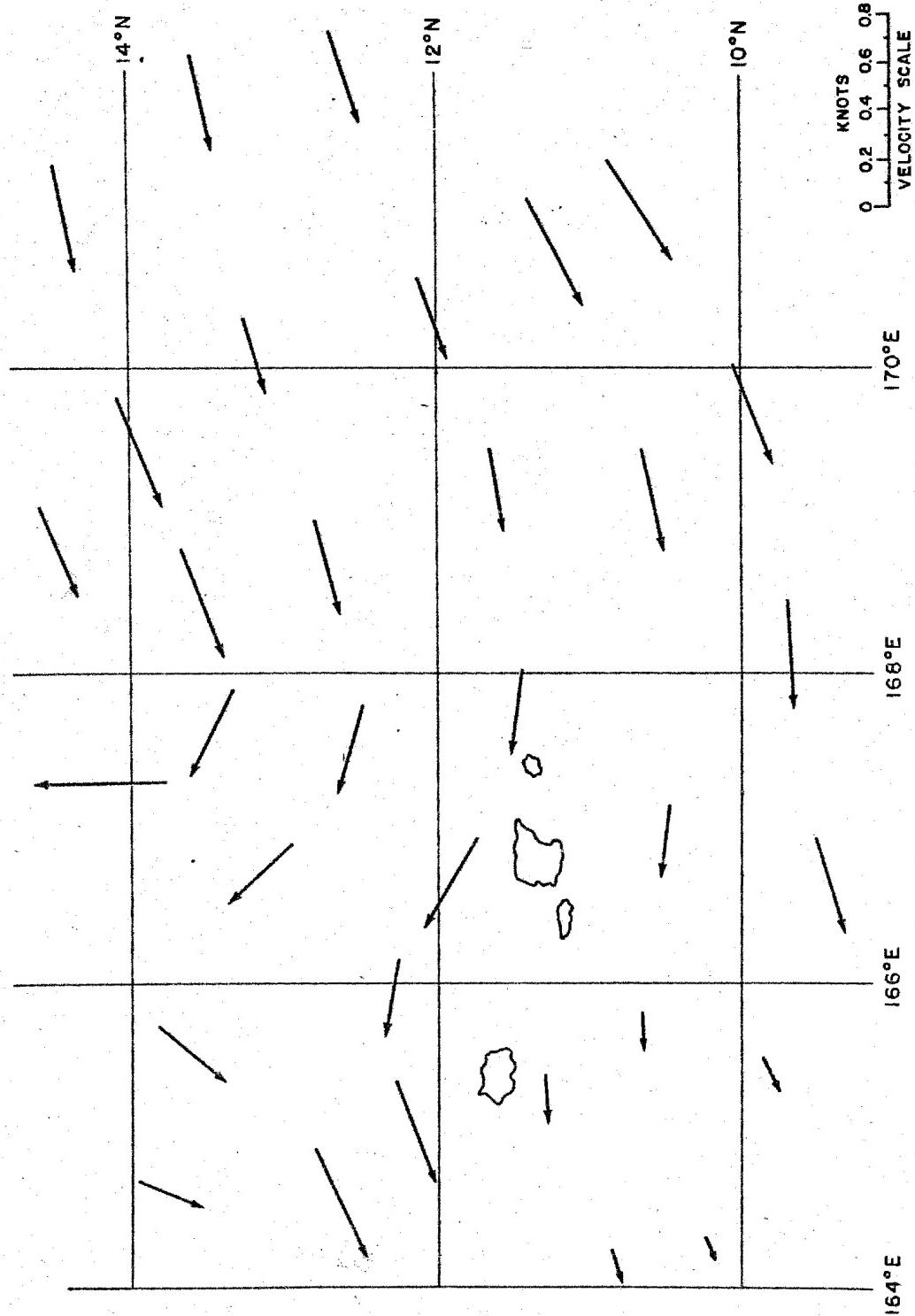
DOE ARCHIVES

It now may be computed where the fall-out material actually contacted the sea surface. The ship's track must be displaced by amounts appropriate to the time of fall-out arrival and to the sea currents. This corresponds to a route which a "Jeep" might have taken over dry land to survey the fall-out.



TRACK, APPARENT  $\text{mr/hr}$  REDUCED TO  $\gamma + 12$  HOURS

DOE ARCHIVES



VECTOR SUMMARY OF 10 YEARS OF JAPANESE OCEANOGRAPHIC STUDY IN THE AREA

Figure 12

7/18/88

INCOMPLETE DOCUMENT REFERENCE SHEET

The archive copy of this document is incomplete.

Pages missing 20

Enclosures missing \_\_\_\_\_  
\_\_\_\_\_

Attachments missing \_\_\_\_\_  
\_\_\_\_\_

Other \_\_\_\_\_

CR8  
signature

2-11-92  
date

DHA

(Figure 13 shows the results from a preliminary computation which did not take into account the variation of fall-out arrival time.)

#### Graphic Summary of Fall-out

Along the plot of this displaced track the hundreds of measurements of local dose rates now can be redistributed and joined with iso-lines in the usual manner. Intuition and artistic impulse clash at this juncture with evidence and statistics.

Two time conventions generally are adopted in fall-out presentation; reduction to D+12 hours, and reduction to D+1 hours (Figure 14).

Dose-rate reduced to D+12 hours predicts less awful results than does that dose rate reduced to D+1 hours, but the first is far more realistic.

Table I

#### Intensity and Area in Each Contour

#### Iso-dose Rate Contours at 3 Foot Elevation

Contour No.	Area (Sq. Miles)	Dose Rate	
		At H+12 Hrs.	At H+1 hr. = $22.7 \times H+12$
A	45	80	1820
B	450	60	1360
C	1190	40	910
D	3070	20	450
E	6320	10	230
F	10000	5	115
G	17850	1	25

The iso-dose contours (Figure 15) are more realistic, they imply what exposure would be accumulated by personnel on dry land within 50 hours following a large detonation. The significance of magnitudes such as these are apparent to everyone here.

DOE ARCHIVES

Figure 14

ISO - DOSE - RATE CONTOURS

DOE ARCHIVES

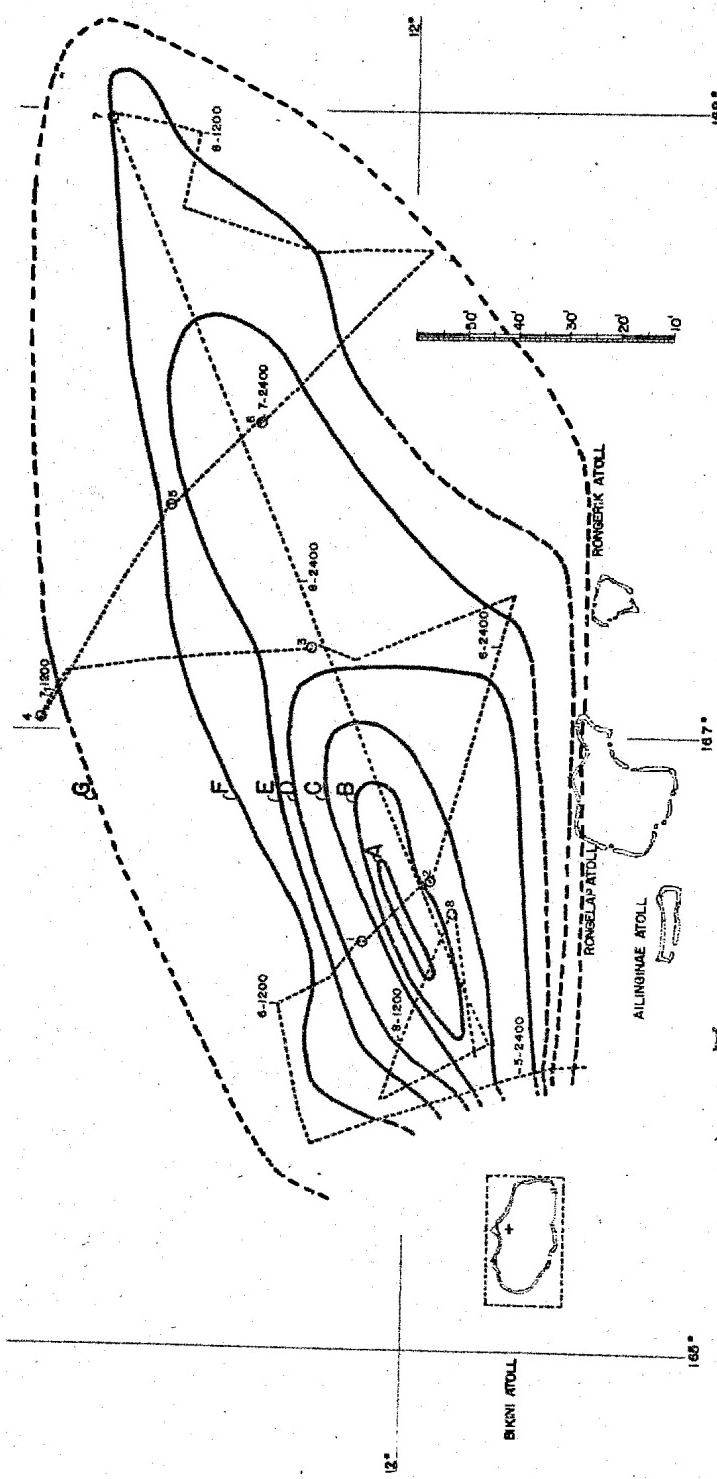


Figure 15

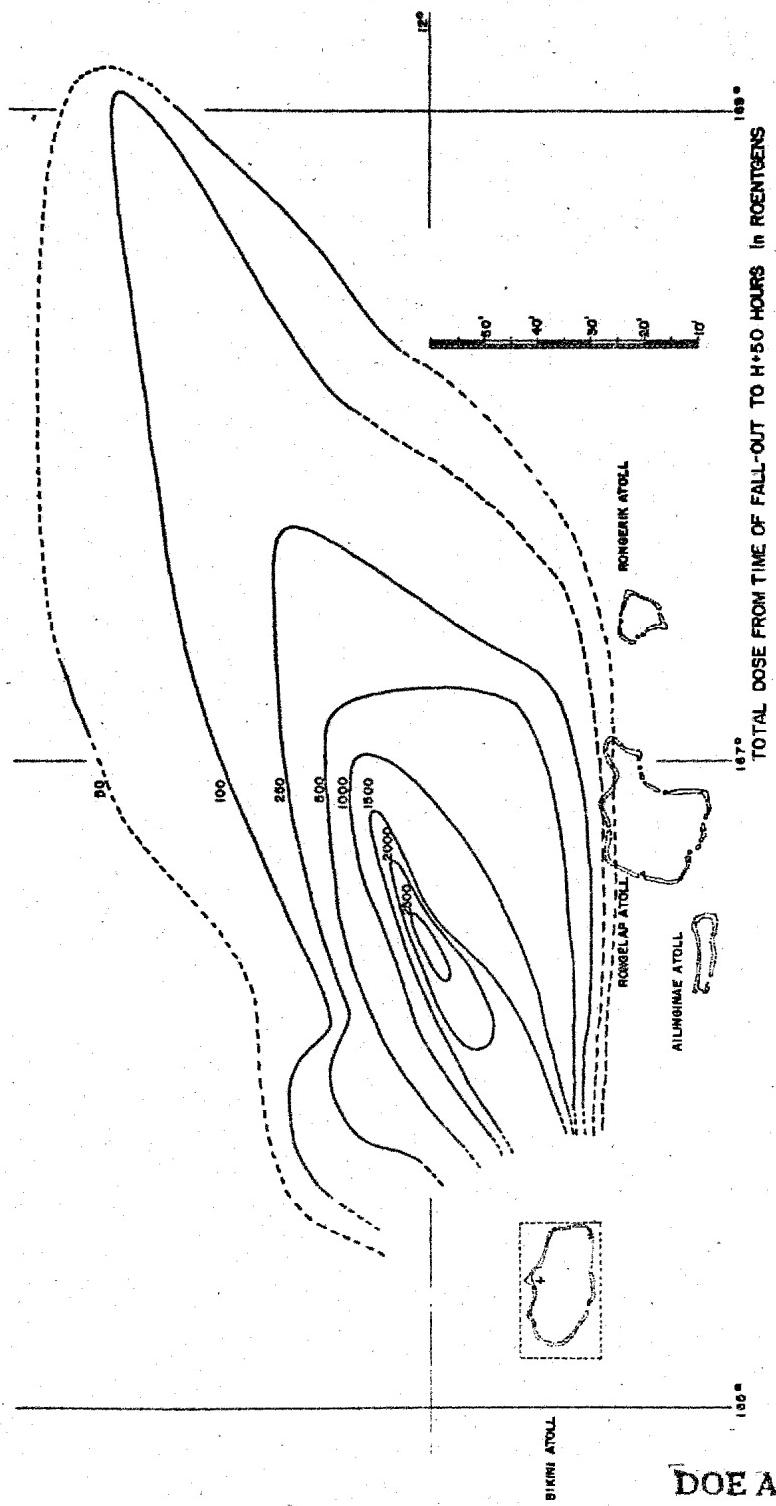


Table II

Total Dose from Fall-out Arrival Until H+50 Hours

Contour No.	Area (Sq. Miles)	Total Dose in R (Shown in Figure Itself)
Innermost	32	2500
-	210	2000
-	610	1500
-	1400	1000
-	3000	500
-	4900	250
-	9350	100
Outermost	14350	50

Discussion of Results

I believe the three accomplishments of this survey are:

Its contribution of a basis for evaluation of a promising method of studying fall-out hazard.

The approximate numerical values representing the extent of contamination from one particularly large weapon.

Some contributions to pure science, for example some actual numerical values of the rate of downward turbulent mixing of the sea - a subject of particular interest to oceanographers.

The first outcome can be amplified a little further. It does appear feasible to use the sea itself as a sampling collector - in fact there does not seem to have been a better collector devised for catching and holding in place an aerosol or fine powder. Meteorologists are aware that no instrument catches snow like a snowfield does. It appears that samples representing many of the more important features of fall-out can be retrieved safely and economically from the sea. And it appears that eventually even such data as the time of arrival of particles at distant surface points may be deduced from oceanographic measurement.

DOE ARCHIVES

Concerning the numerical fall-out values given here for a particular detonation, little more will be said, except that Dr. Werner of NRDL has recently reported that results of the water sample analyses are in surprising agreement with the direct gamma measurements just described. As to the total energy picture, it just is not

fair to expect a single little tug boat to go forth alone and bring home an accurate detailed synoptic picture of any aspect of 10,000 square miles of sea.

Conclusions

In conclusion it would appear that the greatest possible use should be made of the ocean itself during further trials.

DOE ARCHIVES

THIS PAGE IS BLANK

DOE ARCHIVES

76

NOTED  
AMERICAN ENERGY ACT 1954

80

PROJECT 2.7 RADIOLOGICAL ASPECTS, SHOT 6, OPERATION CASTLE

L. B. Werner  
U. S. Naval Radiological Defense Laboratory

The method described in this paper constitutes a means of obtaining fall-out data needed for the development and improvement of fall-out models. The method is complementary to that described by Dr. Folsom in an earlier paper and comprises a part of the Operation CASTLE Project 2.7 work. The objective of this work was to determine the dose rate above a plane which had received fall-out. The fall-out was received over wide areas of ocean surface and subsequently was mixed with sea water. The experimental approach was the collection of sea water samples and their subsequent analysis for gamma activity. Other details of the experimental method are described in the paper by Dr. Folsom. The calculation of radiation intensities was comprised of first the determination of the total gamma energy emission rate of fall-out deposited upon the ocean surface and second calculation of the dose rate for a given gamma emission rate. The method for calculating the dose rate has been described by L. D. Gates, Jr. and C. Eisenhauer in AFSWP 502A and 502A Supplement "Spectral Distribution of Gamma Rays Propagated in Air". A summary of the method is given in Tables 1 and 2.

Table 1

Calculate total dose rate  $d$  at height  $x = 3$  ft above an infinitely contaminated plane having a total energy emission rate of  $1 \text{ Mev cm}^{-2} \text{ min}^{-1}$

$$d = \sum_i n_i d_i$$

DOE ARCHIVES

where

$d_i$  = dose rate in  $\text{Mev cm}^{-3} \text{ min}^{-1}$  at height  $x$  above an infinite plane emitting photons of initial energy  $E_i$  isotropically at the rate of  $1 \text{ photon cm}^{-2} \text{ min}^{-1}$

$n_i$  = number of photons  $\text{cm}^{-2} \text{ min}^{-1}$

SECRET

Table 2

$$d = \sum_i n_i d_i$$

$$d_i = \frac{E_i h(E_i)}{2} \int_{t_1}^{\infty} \frac{e^{-\mu_i s}}{s} ds = B_i(t_1)$$

where

$E_i$  = initial photon energy

$h(E_i)$  = "true" linear absorption coefficient  
for air

$t_1 = \mu_i x$

$x = 3$  ft

$\mu_i$  = total linear absorption coefficient for  
photons of energy  $E_i$

$B_i(t_1) = \frac{1}{1-y_1}$  = build-up factor or ratio of  
dose from all photons to  
that from unscattered photons

and

$y_1$  = fraction of dose from source energy  $E_i$ ,  
delivered by scattered photons;  $y_1$  is  
obtained from Curve A, Fig 20, AFSWP  
502A.

DOE ARCHIVES

Using this method and gamma spectra supplied by Dr. C. S. Cook of  
NRDL a calculation of the dose rate produced by a source emitting  
1 Mev  $\text{cm}^{-2} \text{min}^{-1}$  is shown in Table 3.

~~SECRET~~

Table 3

Calculation of dose rate  $d$  at height  $x = 3$  ft above an infinitely contaminated plane having a total energy emission rate of 1 Mev  $\text{cm}^{-2} \text{ min}^{-1}$

Shot 5 at D + 8 days				Shot 6 at D + 7 days				
$E_i$	$\frac{n_i}{\sum n_i}$	$n_i$	$B_i(t_i)$	$n_i d_i \times 10^6$	$E_i$	$\frac{n_i}{\sum n_i}$	$n_i$	$n_i d_i \times 10^6$
.05	.261	.760	$\approx 2.5$	$\approx 7$	.05	.271	.796	$\approx 7.3$
.15	.245	.713	$\sim 1.8$	$\sim 10.5$	.15	.21	.617	$\sim 9.1$
.25	.140	.407	1.55	10.0	.25	.17	.50	12.4
.35	.016	.047	1.45	1.6	.35	.026	.076	2.69
.45	.095	.276	1.40	12.4	.45	.069	.203	9.14
.65	.087	.253	1.33	16.2	.65	.096	.282	18.1
.75	.097	.282	1.31	20.6	.75	.094	.276	20.2
.85	.0135	.039	1.29	3.1	.85	.029	.085	6.96
1.55	.0455	<u>.132</u> 2.91	1.20	<u>17.3</u> 98.7	1.55	.035	<u>.103</u> 2.94	<u>13.5</u> 99.5
.344	1.00	2.91	1.45	100	.340	1.00	2.94	100
$\therefore 1 \text{ Mev } \text{cm}^{-2} \text{min}^{-1}$ gives $\therefore 9.37 \times 10^{-8} \text{ r/hr}$				$1 \text{ Mev } \text{cm}^{-2} \text{min}^{-1}$ gives $9.45 \times 10^{-8} \text{ r hr}$				

The calculation of energy emission rate per unit volume of radioactive sea water is demonstrated in following tables.

The gamma energy emission rate of all water samples was inferred from the response produced by the samples in a high efficiency 4" geometry ionization chamber, the type described by Jones and Overman.

DOE ARCHIVES

Table 4 shows the calculation of the ratio of energy emission rate to the ionization chamber response for an arbitrary  $2.22 \times 10^6$  gamma photons per min, and using spectral data supplied by Dr. Cook.

Table 4

Calculation of Ratio of Energy Emission Rate (Mev/min) to  $4\pi$  Ionization Chamber Reading (I)

Shot 5 at D + 8 days					Shot 6 at D + 7 days				
$E_1$	$\frac{n_1}{\sum n_1}$	$I_1$	$\frac{n_1}{I_1}$	(Mev/min) $\times 10^{-6}$	$E_1$	$\frac{n_1}{\sum n_1}$	$I_1$	$\frac{n_1}{I_1}$	(Mev/min) $\times 10^{-6}$
.05	.261	.08	.0209	.0290	.05	.271	.08	.0217	.0301
.15	.245	.12	.0294	.0816	.15	.210	.12	.0252	.0700
.25	.140	.16	.0224	.0777	.25	.170	.16	.0272	.0943
.35	.016	.21	.0034	.0124	.35	.026	.21	.00546	.0202
.45	.095	.25	.0237	.0950	.45	.069	.25	.0172	.0690
.65	.087	.34	.0296	.1254	.65	.096	.34	.0326	.139
.75	.097	.38	.0368	.1614	.75	.094	.38	.0357	.157
.85	.0135	.42	.0057	.0255	.85	.029	.42	.0122	.0547
1.55	.0455	.70	.0318	.1565	1.55	.035	.70	.0245	.120
				.2037				.2176	.7543
				$\frac{(\text{Mev/min})}{I} = \frac{0.7645 \times 10^6}{0.2037} =$				$\frac{(\text{Mev/min})}{I} = \frac{0.7543}{0.20176} =$	
				$3.75 \times 10^6$				$3.74 \times 10^6$	

The data in column 3 headed  $I_1$  were obtained from a calibration curve determined by W. E. Shelberg. This curve was determined with the use of absolute standards varying in energy from approximately .2 Mev to 2 Mev. In actuality most samples were too low in intensity to permit

direct measurement in the  $4\pi$  ionization chamber. The low activity samples were therefore measured with the use of gamma scintillation counters and converted to equivalent Mev/min according to the method shown in Table 5.

Table 5

Calculation of Ratio of Mev/min emitted by Sampler to Counts/min in the Gamma Scintillation Counter

Five samples of sea water collected following Shot 5 were measured on D + 10 days in both gamma scintillation counter and the  $4\pi$  ionization chamber:

$$\frac{(I)}{(c/m)} = 1.59 \times 10^{-6}$$

since

$$\frac{(Mev/min)}{I} = 3.75 \times 10^6$$

$$(Mev/min) = 5.96 \times (c/m)$$

Finally the dose rate in r/hr at time of analysis of the samples (9 days for Shot 5 and 7 days for Shot 6) was calculated with the relationship summarized in Table 6.

Table 6

Dose Rate at 12 hr in r/hr at height  $x = 3$  ft Above an Infinitely Contaminated Plane - Calculated from Counts  $\text{cm}^{-3}\text{min}^{-1}$  at D + 9 Days

Since  $(Mev/min) = 5.96 \times (c/m)$

$$1 \text{ Mev cm}^{-2} \text{ min}^{-1} = 9.41 \times 10^{-8} \text{ r/hr}$$

$$\frac{(r/hr)}{9 \text{ days}} = 9.41 \times 10^{-8} \times 5.96 \times (c/m) \times (cm^{-3}) \times \frac{z}{9 \text{ days}}$$

where Z = depth (cm) of mixing obtained from graph, time of mixing vs depth of mixing

$$\frac{(r/hr)}{12 \text{ hr}} = \frac{0.044}{0.00135} \quad \frac{(r/hr)}{9 \text{ days}}$$

Account has been taken of the depth of the mixed radioactive surface layer of sea water as determined from the curve of time of mixing vs depth of mixing provided earlier by Dr. Folsom. The time of mixing was the difference between the time of sample collection and the time of arrival of fall-out at various distances as estimated by E.A. Schuert of NRDL. The gamma intensity in r/hr at an arbitrary reference time of 12 hours was calculated from the intensity at 9 days by use of the gamma field decay curve as given in the final report of Project 2.5a Operation CASTLE. The iso-intensity contours derived from the data for Shot 6 are shown in Figure 1. The points indicated on the figure represent the position of the sample water at the estimated time of arrival of fall-out. The areas inclosed by various dose rate contours are shown in Table 7.

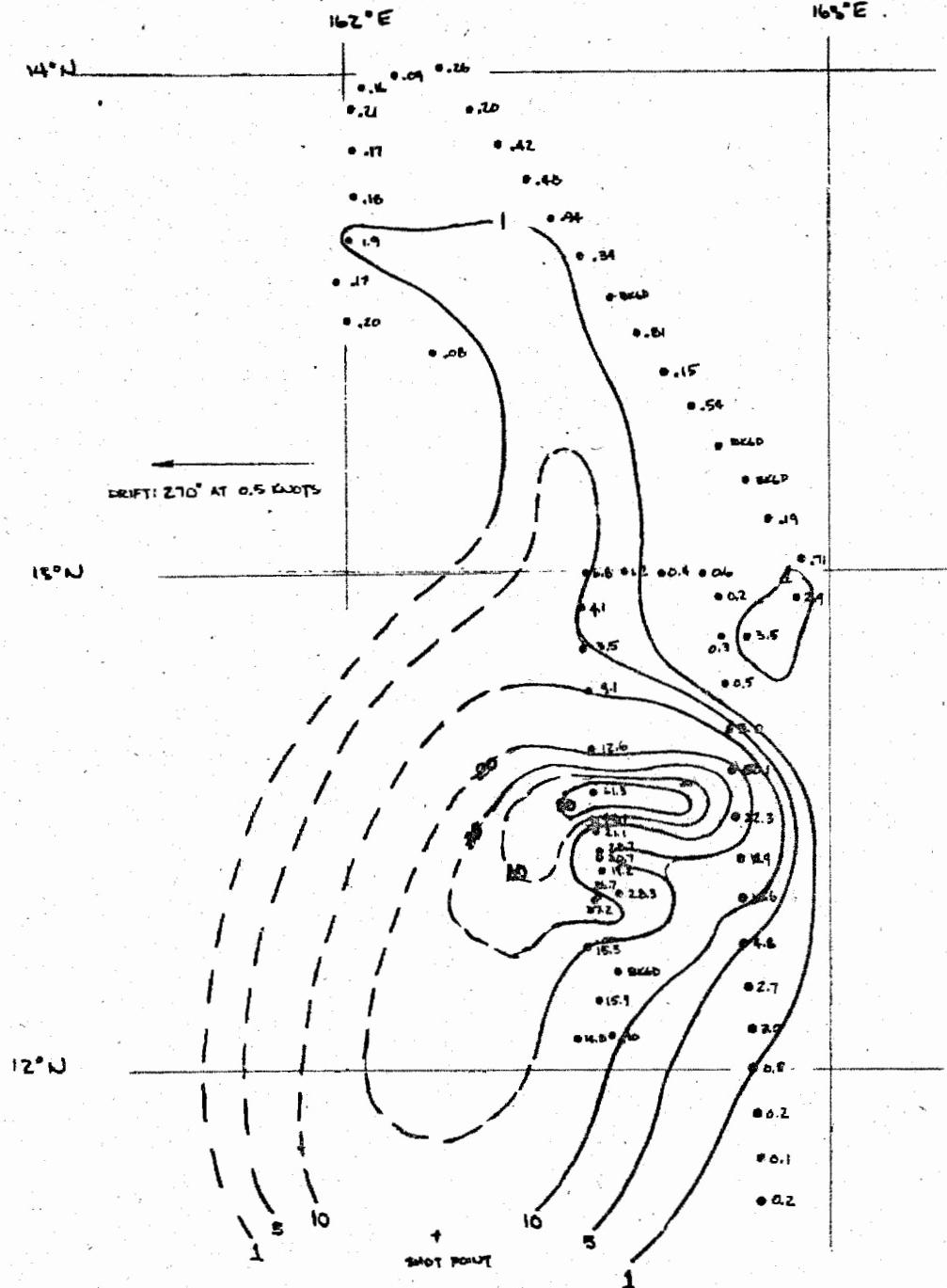
Table 7

Areas Inclosed by Various Dose-Rate Contours at 12 hrs - Shot 6

Dose Rate	Area (sq mi (stat.))
50	60
40	200
30	550
20	1600
10	3500
5	5250
1	7750

Some estimate of the reliability of the method is provided by the qualitative comparison of contours with aerial survey data kindly provided us by Mr. Levine, Head of Instrumentation Branch, NYOO, as shown in Figure 2. An indication of the precision of the method is provided by the comparison shown in Table 8.

DOE ARCHIVES



### SHOT 6 FALLOUT PATTERN DOE ARCHIVES

EXPOSURE LEVELS IN R/Hr AT D+12 HOURS

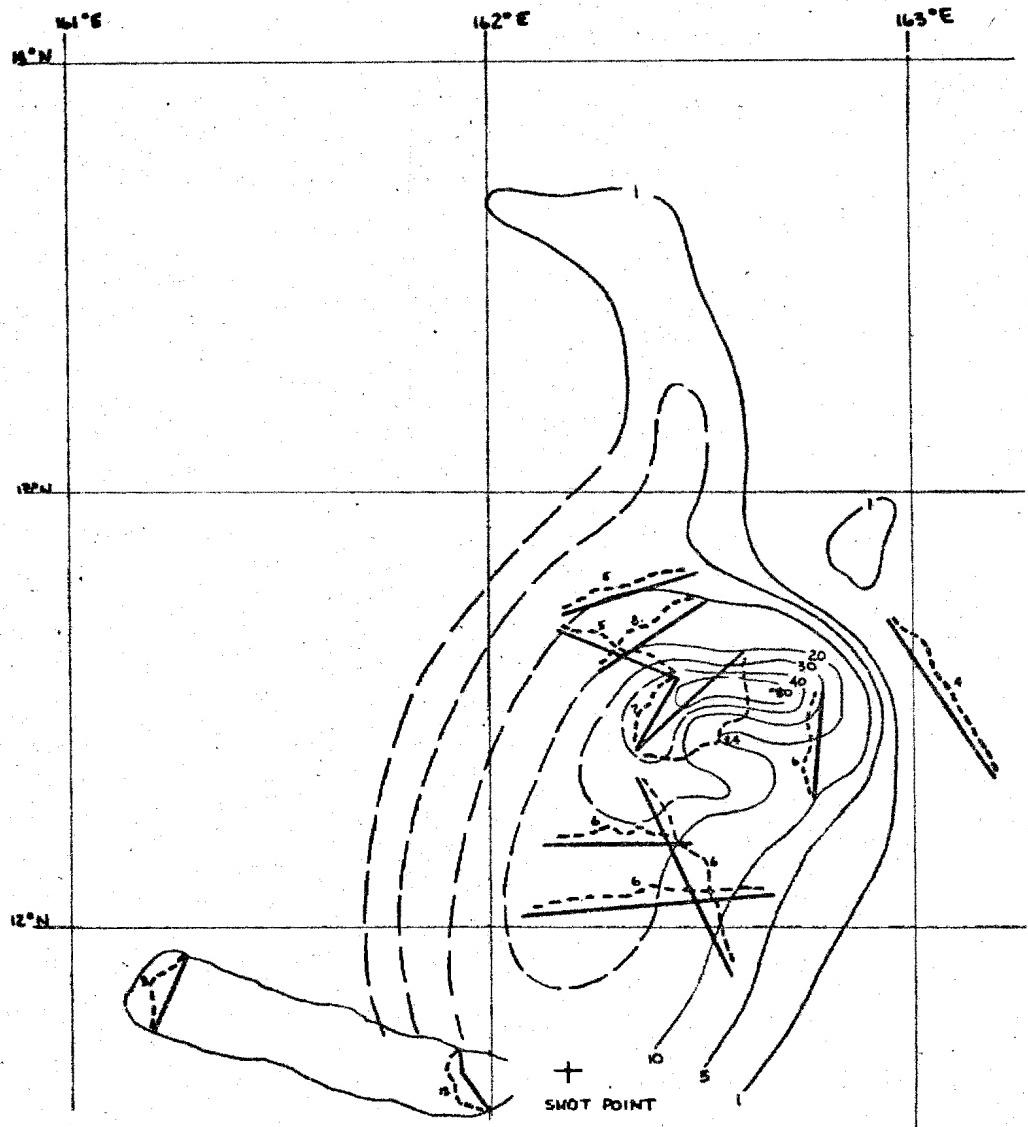
\* DENOTES SAMPLE POSITION AT MEAN ARRIVAL TIME

Figure 1  
Shot 6 Fall-out Pattern

83

NUCLEAR ENERGY ACT 1954

87



SHOT 6 DOSE RATE CONTOURS AT 0+12 HRS.

QUALITATIVE COMPARISON OF AERIAL SURVEY WITH WATER SAMPLING RESULTS

DOE ARCHIVES

Figure 2  
Shot 6 Dose Rate Contours at 0+12 hrs.  
84

~~DECLASSIFIED DATA~~  
U.S. ENERGY ACT 1954

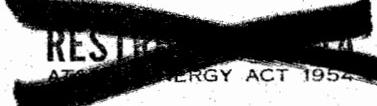
88

Table 8

Comparison of Shot 5 Gamma Field Intensities at 12 hr as Calculated from (1) Towed Probe Data; (2) Water Analysis Data; (3) Water Analysis Data and Observed Ratio of Field Gamma Intensities to Radioactivity Per Unit Area (CASTLE Project 2.5a) r/hr

Station	1	2	3
1	23	43	25
Surface	64	63	37
Surface	77	60	36
2	35	26	15
Surface	9.5	2.6	1.6
3	13	15	8.8
4	1.5	2.0	1.2
Surface	2.9	2.3	1.8
5	7.5	3.9	2.3
6	6.4	4.8	2.8
Surface	2.9	0.37	.22
Surface	18	15	8.6
Surface	8	4.9	2.7
Surface	18	16	9.3
Surface	6.1	4.2	2.5
Surface	4.5	1.8	1.1
Surface	15	11	6.7
7	8.9	6.1	3.6
Surface	38	57	34
Surface	11	13	7.9
Surface	43	56	33
Surface	7.6	9.2	5.4
8	42	52	31

Column one gives the field intensity as calculated from data taken with the towed probe as described by Dr. Folsom. The second column presents field intensity calculations from water analysis data as described in this paper. The third column presents field intensity calculations from the activity per unit area as derived from the water analysis data, and application of an observed ratio of field gamma intensity to radioactivity per unit area as presented in the CASTLE project 2.5a report. A ratio of 1:1 was considered to be most appropriate for this calculation. A third estimate of the reliability of the method is given by calculation of the fraction of the total



activity produced by the detonation which can be accounted for in fall-out.

**DELETED**

**DOE ARCHIVES**

**[REDACTED]**  
**DELETED**

In future operations it is apparent that far better supplementary data will be needed to improve the reliability of the calculations by this method. Such data must include (a) gamma spectra, (b) decay data both for source material and gamma fields, (c) characterization of the properties of fall-out throughout the area especially physical properties, (d) time of arrival data (e) careful measurement of gamma radiation fields produced on land areas and correlation of the fall-out area by unit area and correlation of the fall-out activity per unit area.

As the 2.7 Project was initiated and undertaken under the stress of actual participation in Operation CASTLE much of the necessary supplementary information had to be approximated. Nevertheless although the project was initially conceived as a feasibility study it has gone far beyond the original expectations and has produced valuable estimates of the actual radiological conditions produced by Shots 5 and 6.

For maximum effectiveness future operations should combine technique of rapid aerial synoptic survey, (2) rapid survey by multiple naval units with frequent correlation between ship and aerial measurements (3) sea water collection, (4) fall-out collections especially for detonations producing large particle fall-out and (5) thorough oceanographic characterization of the expected fall-out areas.

It is essential that for full utilization of the above technique planning for field operations scheduled for 1956 should be started immediately.

**DOE ARCHIVES**

**THIS PAGE IS BLANK**

**DOE ARCHIVES**

88

SECRET//NOFORN

92

PROJECT 9.1 (CLOUD PHOTOGRAPHY RESULTS), OPERATION CASTLE

Lt. Col. Jack G. James  
Directorate of Weapons Effects Tests

Project 9.1, Cloud Photography, Operation CASTLE, was conducted on all shots. The purpose of this experiment was to determine the dimensions and altitude of each nuclear cloud as a function of time. Primary interest lies in the early stage during which the cloud rises to maximum altitude. Secondary interest is in the intermediate interval during which the cloud extends to its maximum diameter at the stabilized altitude. The late stages during which the cloud begins to disperse receives attention, also, but to a lesser extent than the first two stages of interest. The photographic method of recording this phenomena was chosen in view of its ability to record permanently and for leisurely analysis, every visible detail of the cloud at any desired time. The extreme large dimensions of the CASTLE clouds dictated the placement of cameras at considerable distances from ground zero. The use of aircraft as camera platforms was decided on in lieu of ground stations due to the geographic locations of suitable atolls and the probability of natural cloud cover obscuring the field of view. Several aircraft were required for the purposes of triangulating on the nuclear cloud to determine its position and to provide insurance against failure of any one station procuring satisfactory data. I think it would be of interest to most of you to know something of the operational plan in order that you may better understand the results obtained on this project.

Four aircraft were used; one RB-36 operating at 40,000 feet, and three C-54's working at 10,000-14,000 feet. The planes were forty to one hundred miles from ground zero, usually at the fifty mile range. Aerial cameras were installed on A-28 Stabilized Mounts and operated by the Lookout Mountain Laboratory, U. S. Air Force. Photographs were taken of the visible cloud, from several directions, as a function of time. Supporting data was photographed automatically, and the aircraft furnished navigation logs to document the ship's position at every instant. These logs were rather less complete and less accurate than had been expected; this is attributed primarily to the heavy load the crew members had to carry in flying the ships under unaccustomed conditions.

DOE ARCHIVES

All four ships flew in every shot. Of the twenty-four missions, six were spoiled because of interference by natural clouds. Four of these were on Shot No. 3 which was fired under such bad weather conditions that, to the best of our knowledge, no decent photographs of any sort were taken from the ground or from the air.

The data obtained are more complete and more accurate than any obtained on previous operations. Good measurements of cloud height and diameter over a ten-minute interval have been worked up by Edgerton, Germeshausen and Grier, Inc. for the five shots which were photographed. It has been found possible to apply suitable corrections for the effects of earth curvature and atmospheric refraction, for the slight tilt of the camera platform, and for the altitude of the plane. The resulting data agree quite well from one plane to the other, and it has been possible to assign smaller uncertainty to the results than had been anticipated. Unfortunately, it has not been possible to evaluate the few data taken more than ten minutes after detonation.

On previous atomic tests, all cloud measurements were taken with ground-based cameras until Operation IVY when the first attempt was made at aerial documentation. The data obtained was far from perfect, but provided invaluable experience in planning the CASTLE program, and, as it turns out, the same statement can be made concerning the CASTLE results. Although the CASTLE data is incomplete, it is the best yet obtained and experience gained has shown us many ways in which our operation could have been improved. The original CASTLE 9.1 plan called for four high-altitude long-range aircraft; namely, RB-36 airplanes, but due to lack of parking space and a number of other factors, the cloud photography aircraft necessarily had to be shared with other participating projects.

Each plane was equipped with a type A-28 Automatic Stabilized Mount, which carried one modified K-17C camera and one 35mm Eclair motion picture camera. The 35mm cameras were intended to operate at about one frame per second, to document the rapid rise of the cloud during the first five minutes or so. They were equipped with timing clocks. The K-17C cameras were provided with special shutters, to permit long exposures under dim lighting conditions, and were planned to take three photographs every minute during the early stages, and to drop back to a slower schedule later on. The K-17C cameras were provided with data recording chambers to record: (a) the time at which each frame was exposed, (b) aiming of the camera by means of a gyro-controlled compass card, and (c) tilt of the stabilized platform by means of a bubble-level.

One installation was placed in the RB-36 aircraft, which was flown at about 40,000 feet on every shot. This plane was available to Program 9.1 for only the first ten minutes after detonation.

DOE ARCHIVES

Similar installations were made in three C-54 aircraft, which flew at 10,000-14,000 feet for each shot. These planes were available for an hour or more, and were shared with Task Unit 9.

The original plan called for placement of all planes in the two western quadrants to permit photography of the cloud silhouette against the dimly illuminated eastern sky. Distances and lenses were specified to cover a field of view approximately 150,000 feet high and 350,000 feet across in the vertical plane at ground zero. This requirement was based on observations taken at IVY.

The ship's navigator was requested to supply information as to the distance and bearing to ground zero every minute, together with supplementary data on the plane's heading, course and speed.

Although the schedule was tight, all equipment was installed and trial runs were made before leaving the States. These runs were apparently satisfactory. Trial runs were also made in the forward area, with the primary object the determination of the pre-dawn sky light-levels. It was found that the available light was marginally weak, but still exceeded pessimistic expectations.

The plan of operation is relatively simple in principle, but success depends upon good luck as well as on proper functioning of individuals and equipment. Serious loss of data or even complete failure of the mission can result from the failure of a single link in the chain. For example, incomplete navigation data can spoil an otherwise perfect set of films. On the other hand, failure of a clock or of a shutter or of a power source is equally ruinous.

For those of you who are interested in the method of analysis employed by Edgerton, Germeshausen and Grier, Inc., I suggest you obtain a copy of the 9.1 preliminary report which outlines the analysis method in detail. Time does not permit discussion of each event and the results obtained from the photographs; consequently, I have chosen a few selected photographs made from the RB-36 on Shot 5 (Yankee). These pictures have been reduced to 35mm slide size from 9x9 inch serial negatives made with the K-17C camera and are fairly representative of the photography obtained on this project.

Figure 1 - This is zero time, Yankee event, 6:10 A.M. You will notice at the bottom of the picture the three recording instruments which were built into the cameras. The instrument on the left is the clock time, in the center is the tilt reading, and on the right the azimuth reading. These recording chambers operated very satisfactorily except in cases where the cameraman put the cameras on runaway; thus causing a vibration which made it almost impossible to read the instruments.

Figure 2 - There has been a period here of thirty seconds where the bomb light was too intense to record any rate of rise activity with the K-17 cameras.

DOE ARCHIVES

91

卷之三

**RENEWABLE ENERGY**

95

Figure 3 - The time here is 32 seconds after zero and the cloud has reached an altitude of roughly 23,000 feet.

Figure 4 - The time here is 37 seconds after zero and you can note here the shock wave moving out across the lagoon.

Figure 5 - The time here is 41 seconds after zero and the top of the cloud at this point has reached approximately 32,000 feet.

Figure 6 - The cloud is still rising very rapidly and you can still note the shock wave in the lower right through the break in the natural cloud cover.

Figure 7 - The time here is 45 seconds after detonation and we are just at this time commencing to lose some of the extreme brilliance from the fireball.

Figure 8 - There has been a time lag here of about two minutes due to inadequate light conditions to photograph the cloud. As the cloud reaches these high-altitudes, we are able, through long exposures, to obtain reasonably good photography.

Figure 9 - The cloud is still rising quite rapidly and the characteristic skirts are forming over the stem. The white spot in the lower center foreground has nothing to do with the cloud phenomena. It is believed to be a light leak in the recording chamber.

Figure 10 - As the cloud increases in height, our chances for good photography are increased as the early dawn light is increasing rapidly at this time.

Figure 11 - Although it was not intended to do stereo pairs in this experiment, we have found that photographs, such as Figure 11, when matched under a stereoscope with a preceding picture, frequently give reasonably good stereo effects.

Figure 12 - The cloud is becoming fairly well stabilized at this time which is 4 minutes after detonation and the preliminary measurements show the top of the cloud to be at approximately 110,000 ft.

Figure 13 - We are now  $4\frac{1}{2}$  minutes after zero and the diameter of the cloud is extending very rapidly.

DOE ARCHIVES

Figure 14 - At 5 minutes after zero, the cameraman is beginning to experience difficulty keeping the cloud within the camera's field of view.

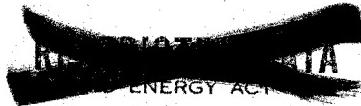


Figure 15 - At 5 minutes and 25 seconds, the cameraman generally had to resort to switching the camera from a fixed position to a left and then to a right view. This was done in order to give Edgerton, Germeshausen and Grier, Inc. an opportunity to measure the cloud diameters on every other photograph.

Figure 16 - We are coming up on 10 minutes after zero time in this photograph. Light conditions have improved considerably and we are beginning to record detail in what remains of the stem. At about the 10 minute period, the CASTLE clouds completely outgrew the capability of the cameras in all four aircraft. The solution to this problem, of course, is very simple; to conduct accurate cloud measurements by aerial photography. It is absolutely essential that the aircraft be positioned at altitudes of 30,000 feet or higher and on anything in the megaton yield range aircraft should be located at a minimum of seventy nautical miles from ground zero. On this particular event that you have just seen on the screen, the cloud reached an altitude of 44,000 feet in one minute and a diameter of 34,000 feet in one minute. The maximum altitude was measured at 110,000 feet and a spread in diameter to 270,000 feet.

Figure 17 - This is a chart taken from the preliminary report which shows you a summary of the cloud parameters in thousands of feet. This is for all CASTLE shots except Shot 3 which, as I mentioned before, was obscured by natural cloud cover. For comparison purposes, the IVY-MIKE and IVY-KING shots are included.

In conclusion, it is believed that the basic plan used during Operation CASTLE is the correct one to use and that on future operations improvements can be achieved through careful attention to details rather than by drastically altering the method of operation. For continental tests, ground-based cameras will give the best results, but for Pacific operations, high-altitude aircraft is the only presently known method of accurately recording cloud phenomena. We believe that in future Pacific tests, the program should provide automatic means of recording every bit of information it needs without too much reliance on the aircraft crew; for example, it is essential to know aircraft position, altitude, course, attitude, air speed and ground speed, also, the camera parameters such as aiming, timing, aperture and shutter settings. Judgment is sometimes impaired while working at high-altitudes and the photography interval program should not be placed at the discretion of the operator. We firmly believe that the photographer must be free of as many manual duties as possible. He should not have too many cameras to operate and the controls should be simple, clearly labeled, and as automatic as possible. In fact, the camera installation should try and do the cameraman out of his job. If he has nothing to do except check for malfunctions, the probability of success on the mission should be very high. If and when we are called upon again to conduct a cloud photography program, I can assure you the lessons learned on CASTLE will be of tremendous value to us in planning and instrumenting on any future test series.

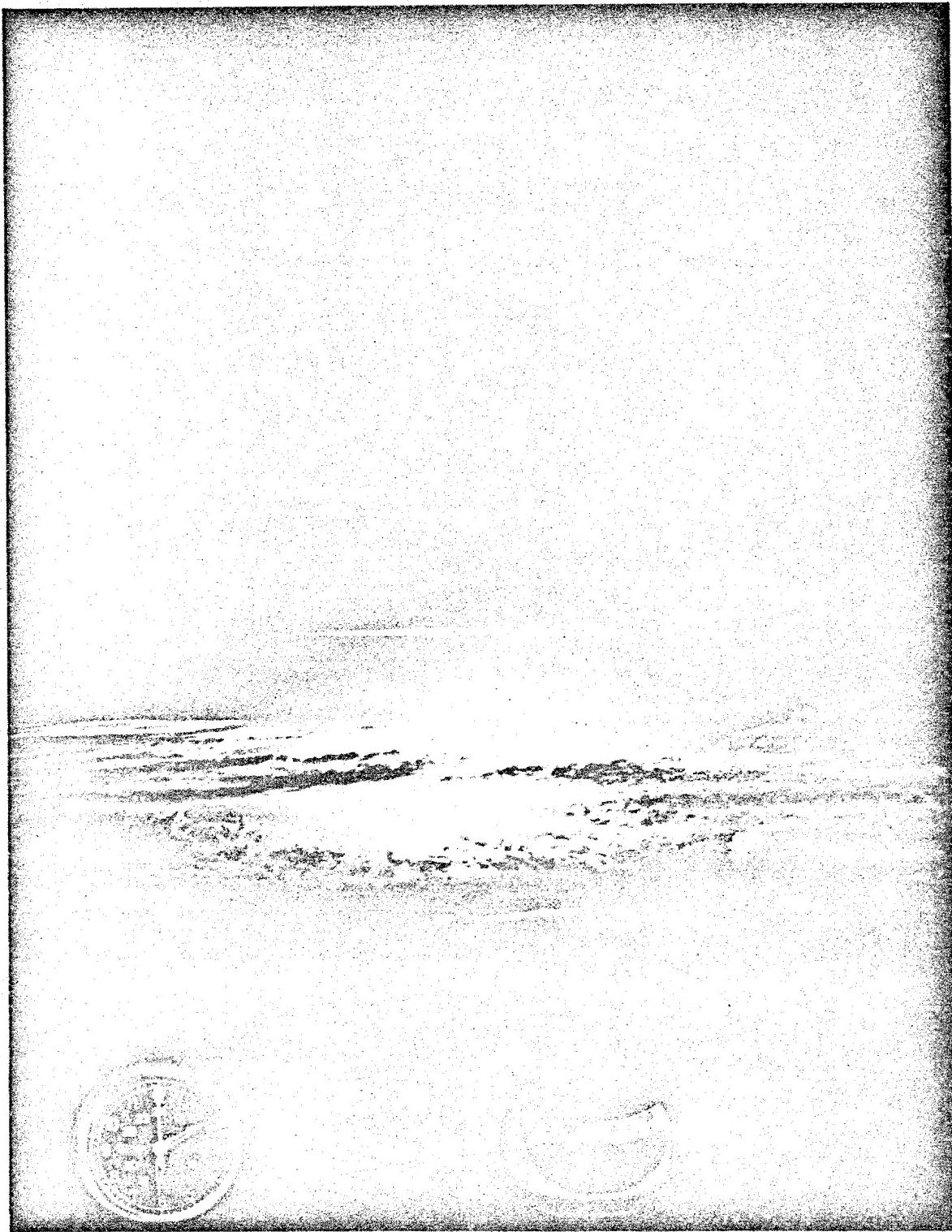


Figure 1  
94

DOE ARCHIVES

98

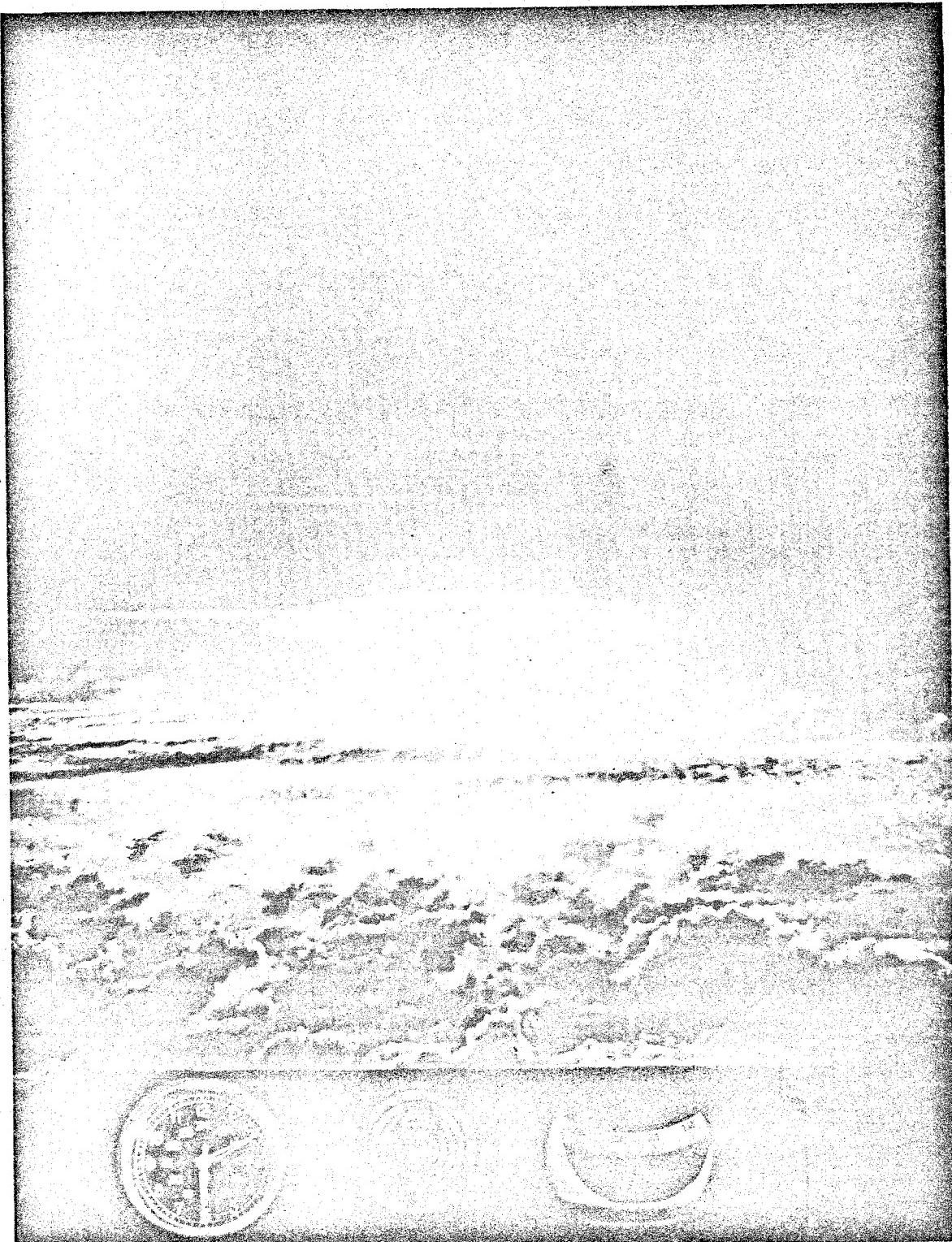


Figure 2

95

~~SECRET~~

DOE ARCHIVES

~~DATA~~  
OMIC ENERGY ACT 4

99



Figure 3

96

DOE ARCHIVES

100

**AT&T**

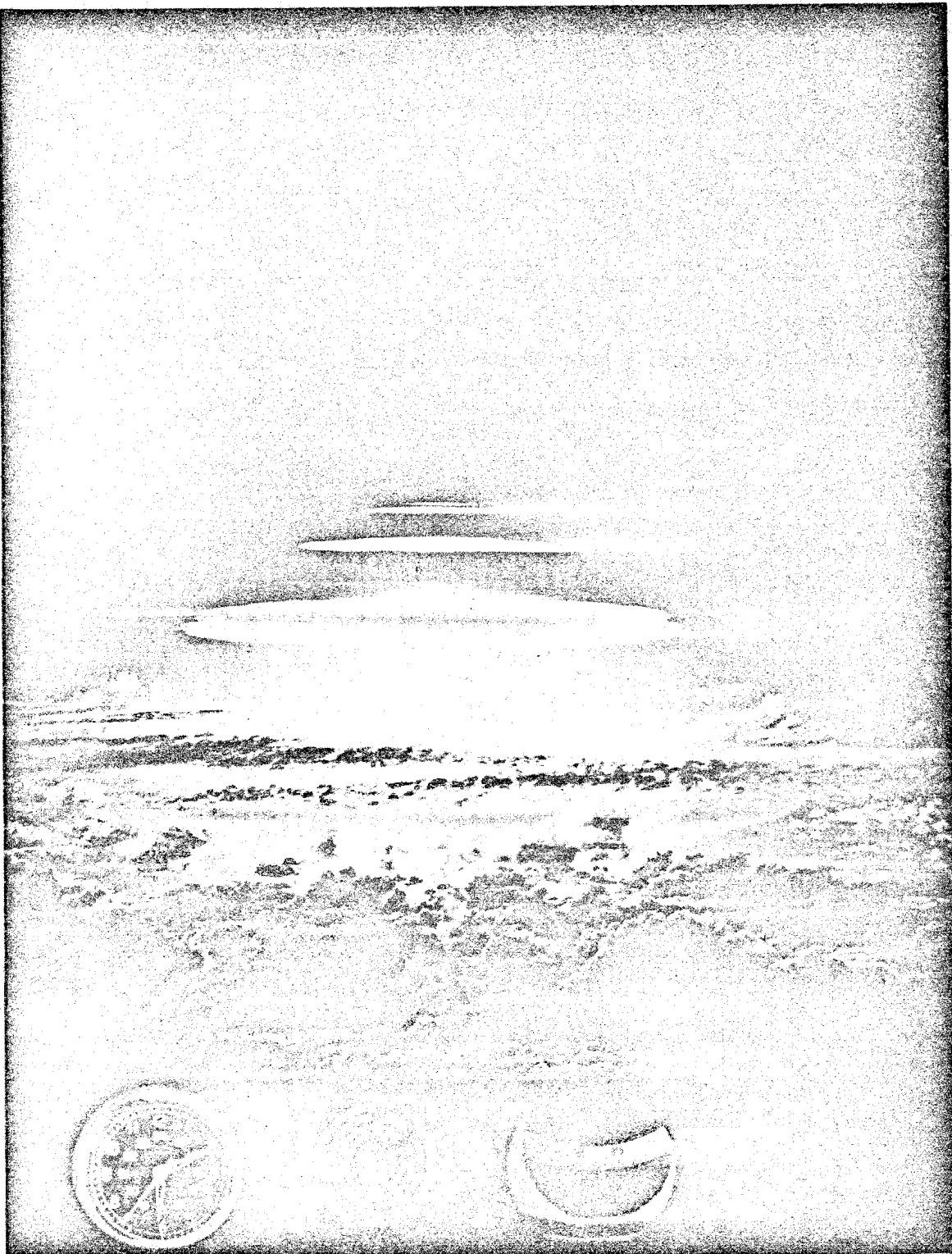


Figure 4

97

DOE ARCHIVES

REF ID: A11111111  
ATOMIC ENERGY ACT 1954

101

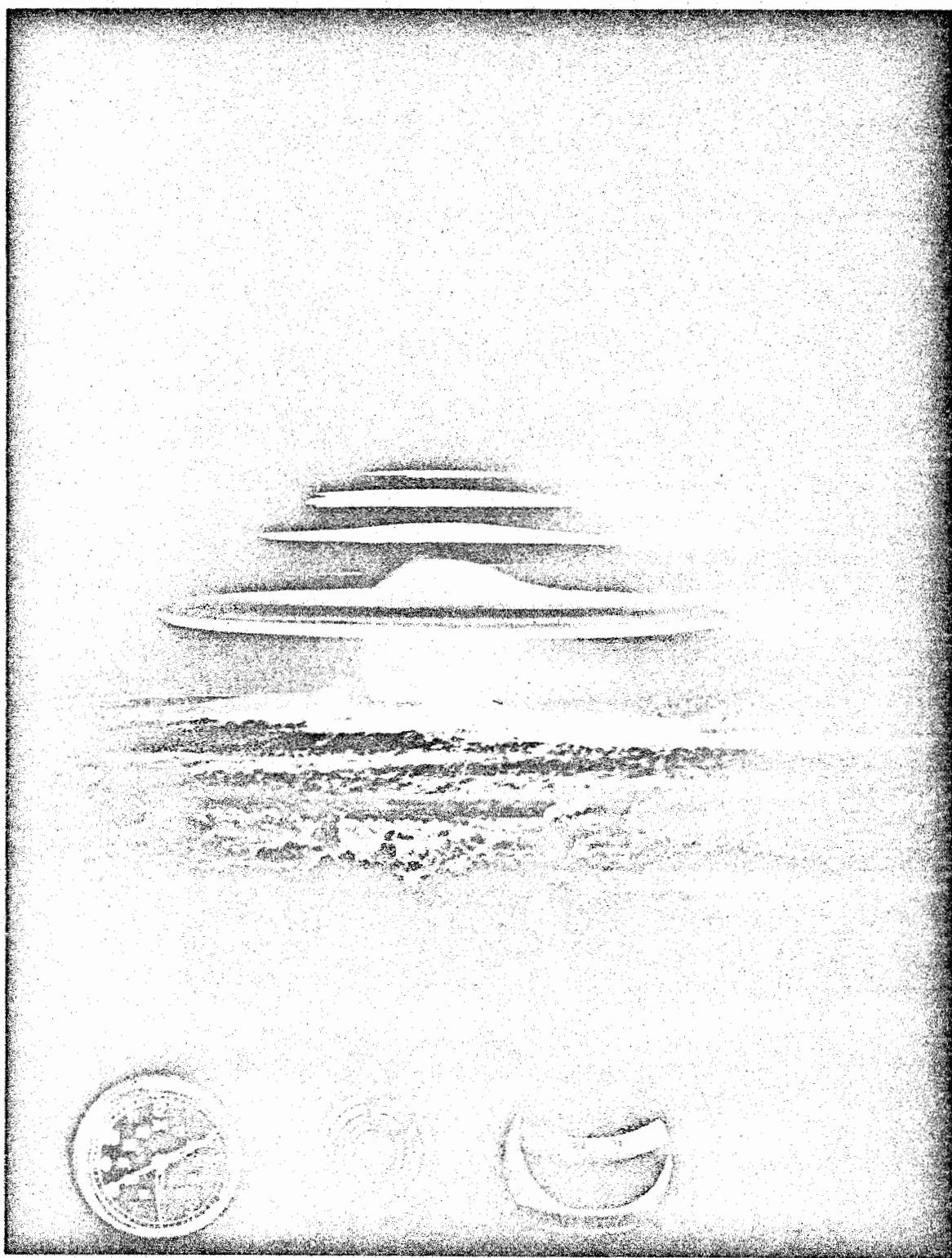


Figure 5  
98

DOE ARCHIVES

REDACTED  
REDACTED  
ENERGY ACT 1950

102

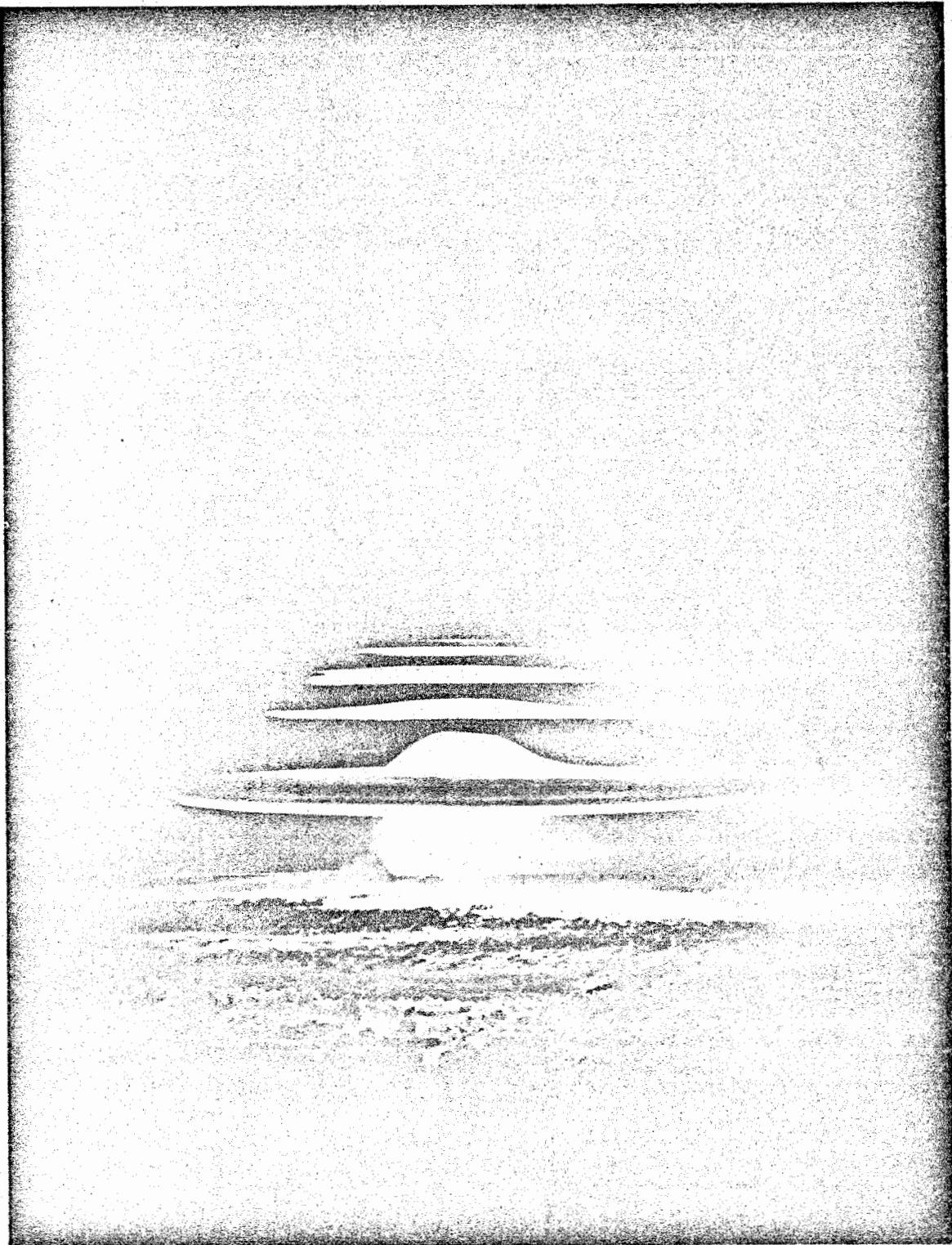


Figure 6

99

DOE ARCHIVES

AMERICAN ENERGY ACT 1954

103

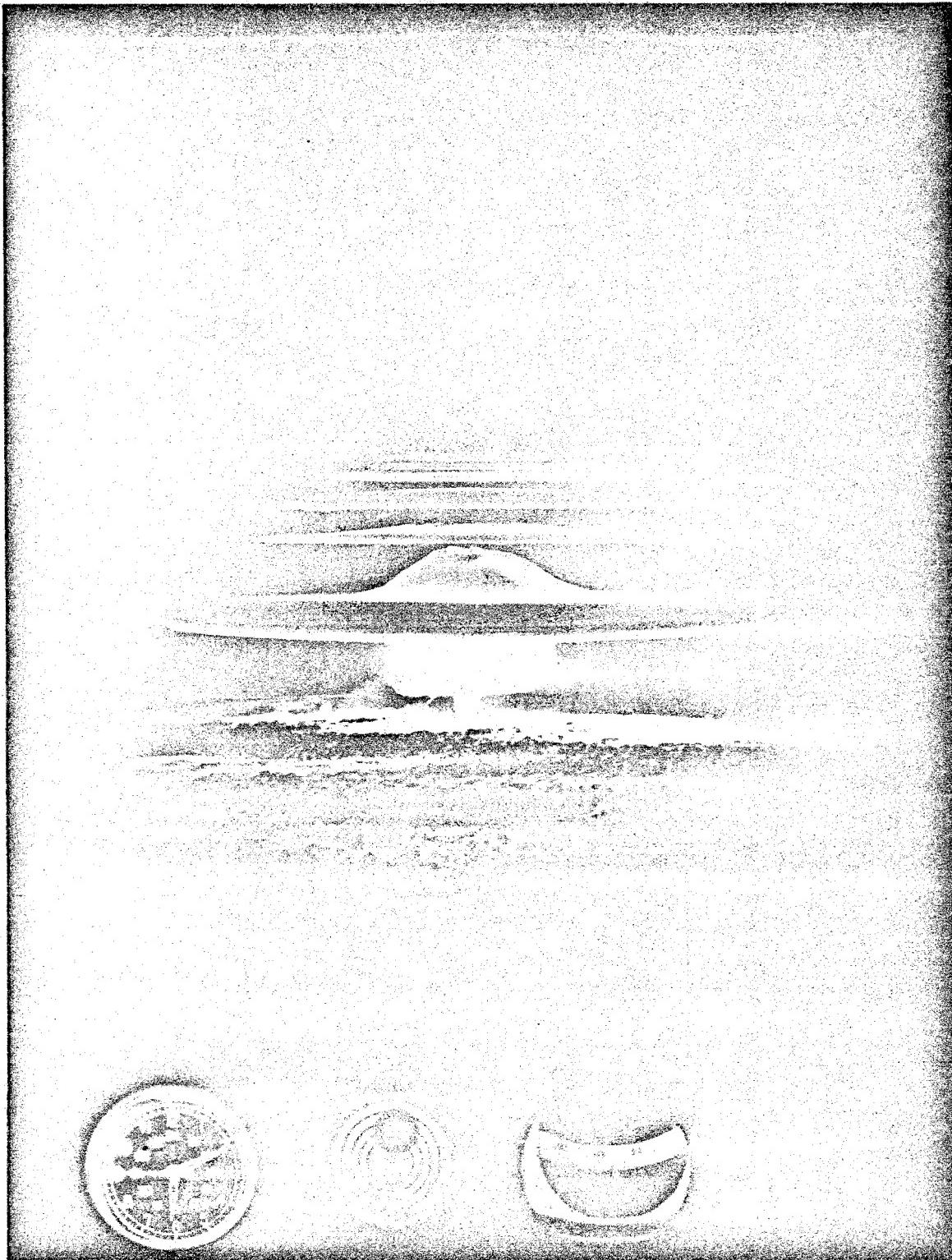


Figure 7

100

AMERICAN ENERGY ACT 1980

DOE ARCHIVES

104

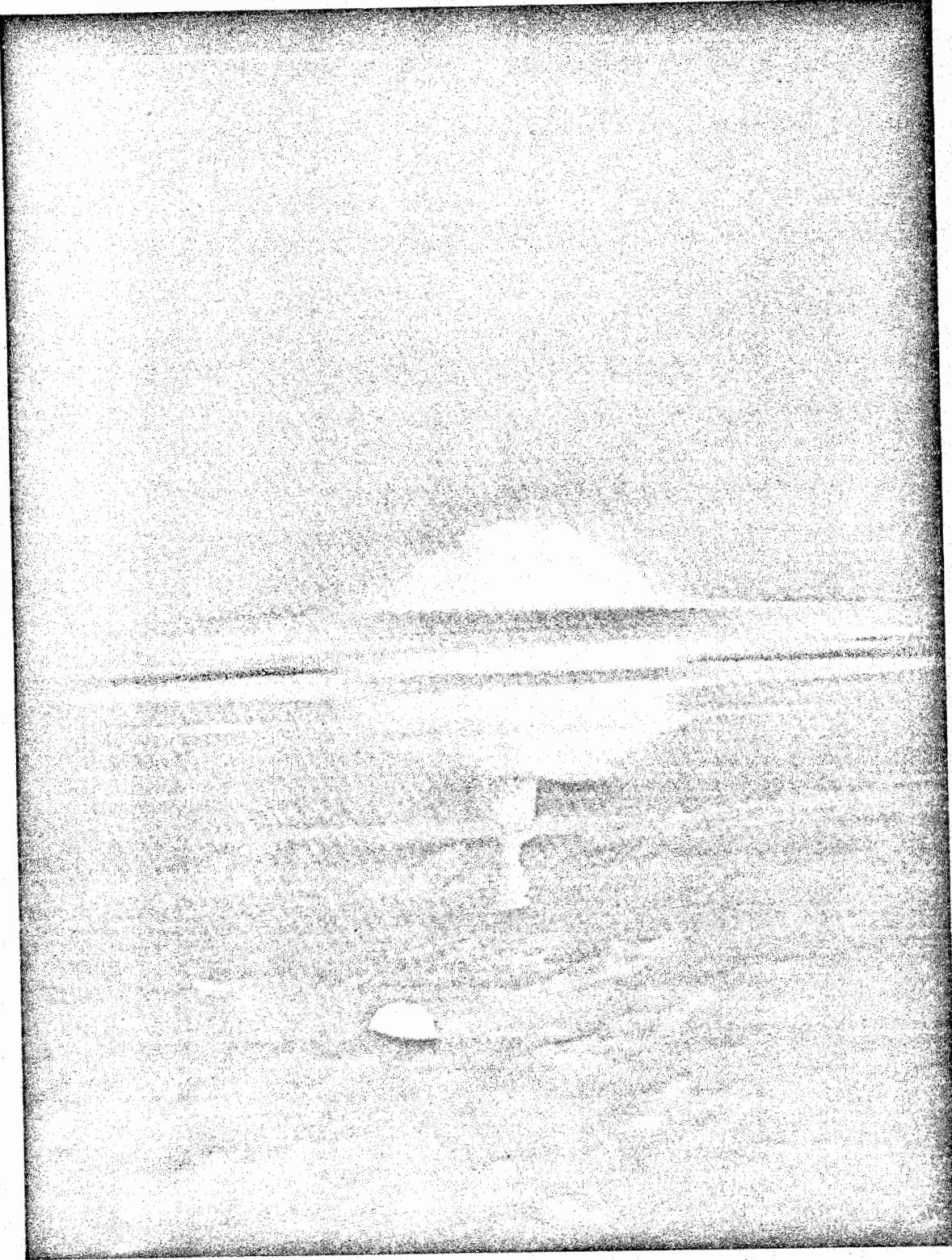


Figure 8

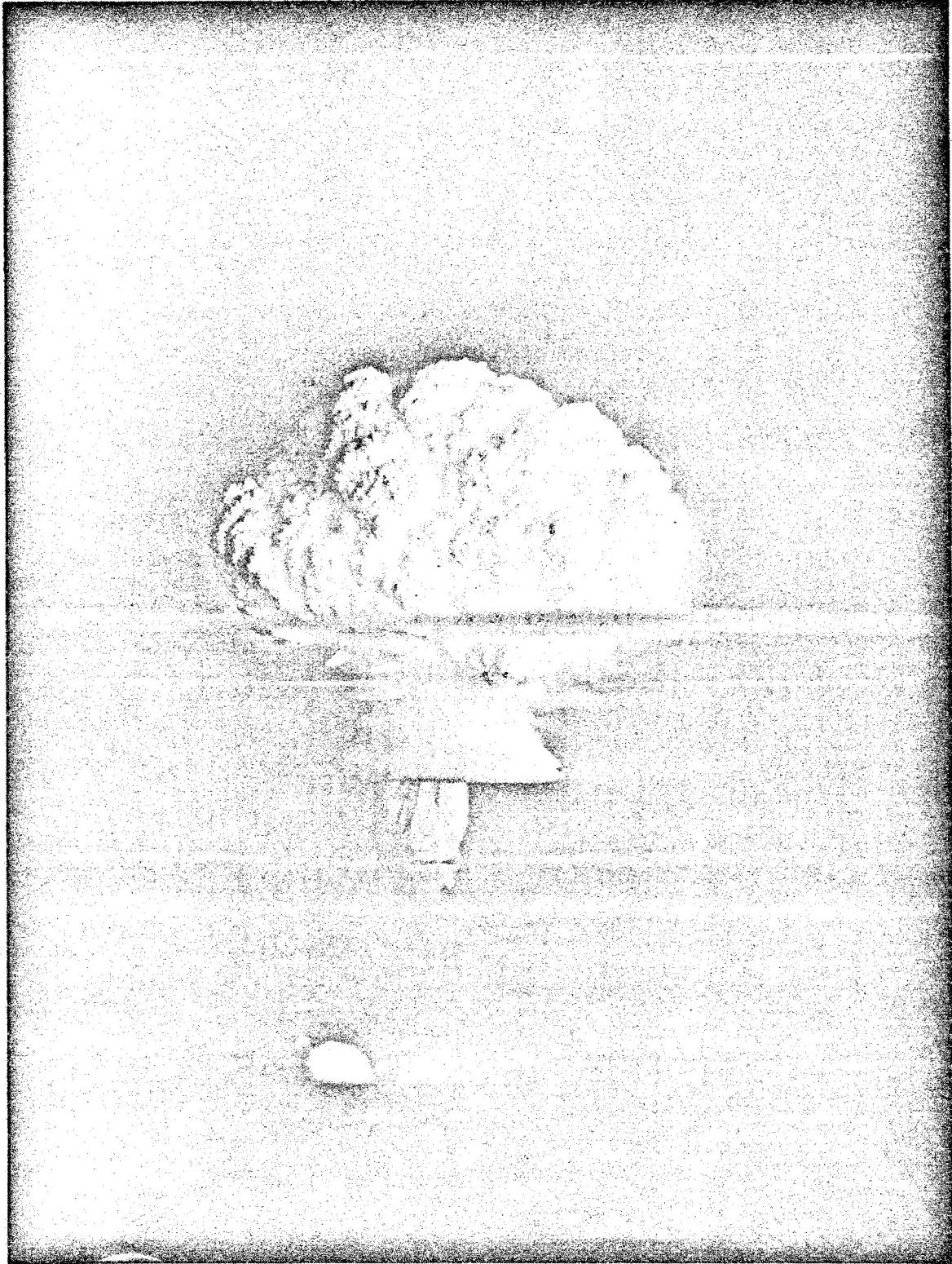
101

DOE ARCHIVES

DOE DATA

DOE ENERGY

105



DOE ARCHIVES

Figure 9

102

REFUGEE

106

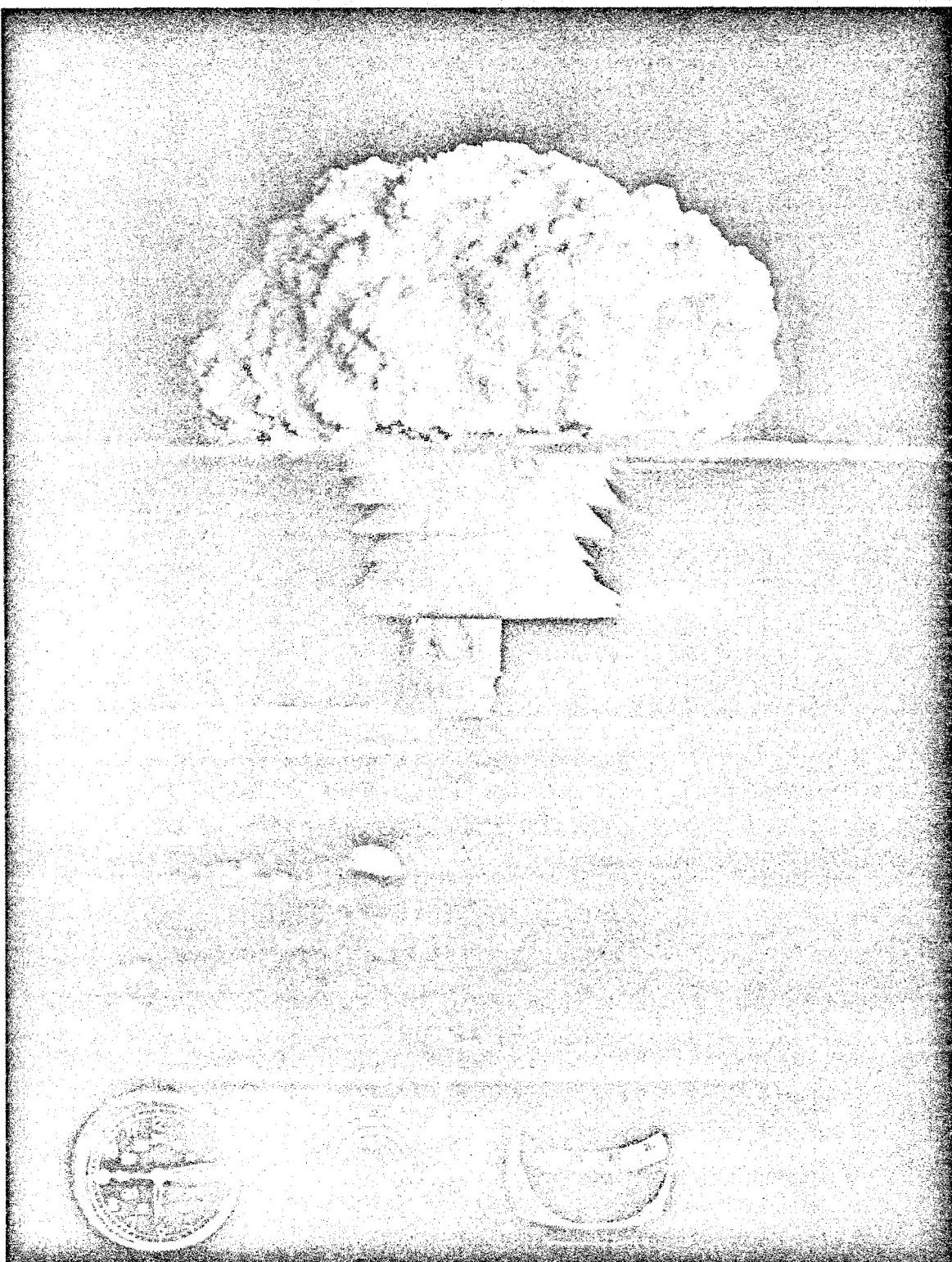
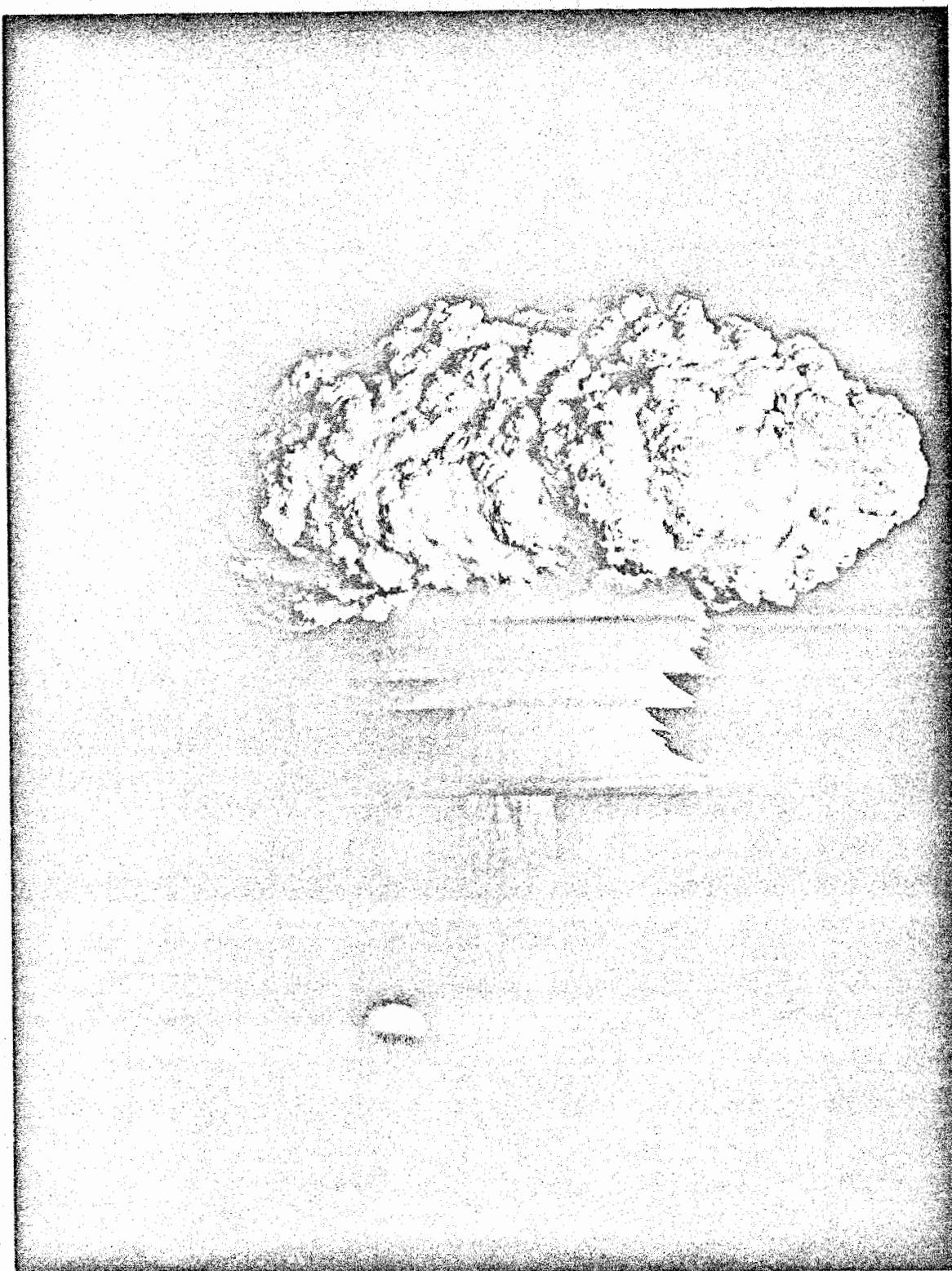


Figure 10

103

DOE ARCHIVES

107



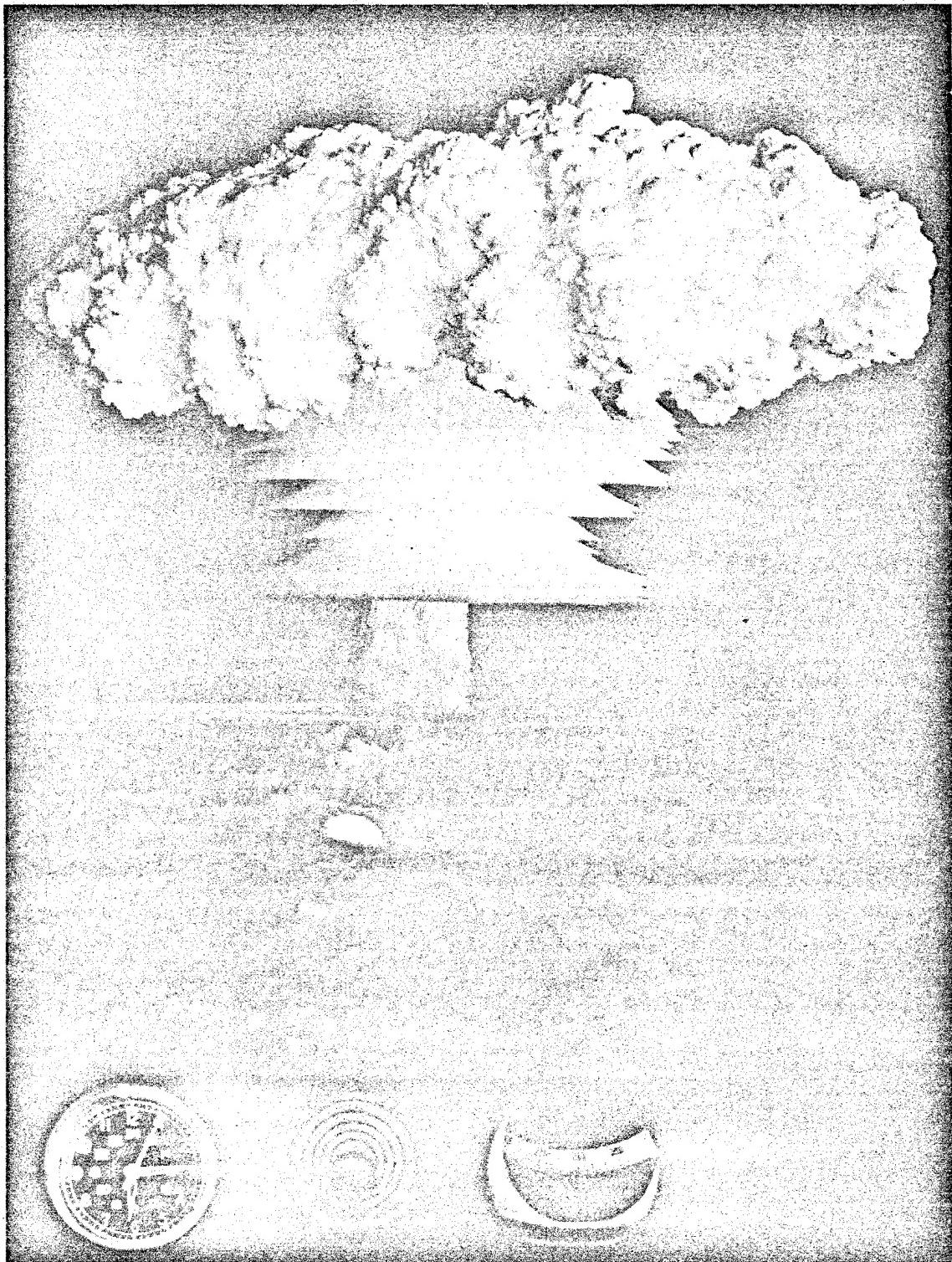
DOE ARCHIVES

Figure 11

104

RESTRICTED

108



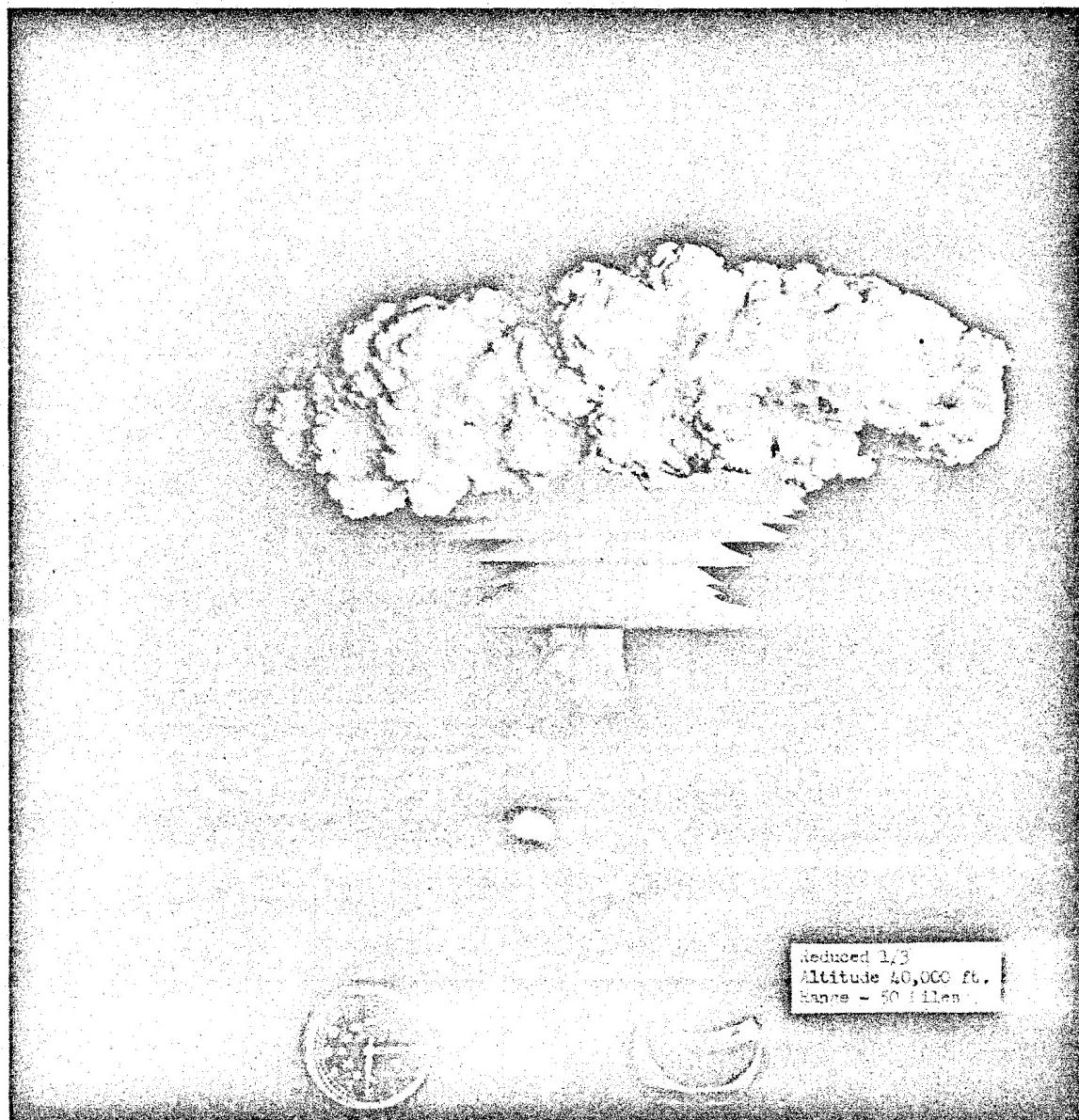
DOE ARCHIVES

Figure 12

105



109



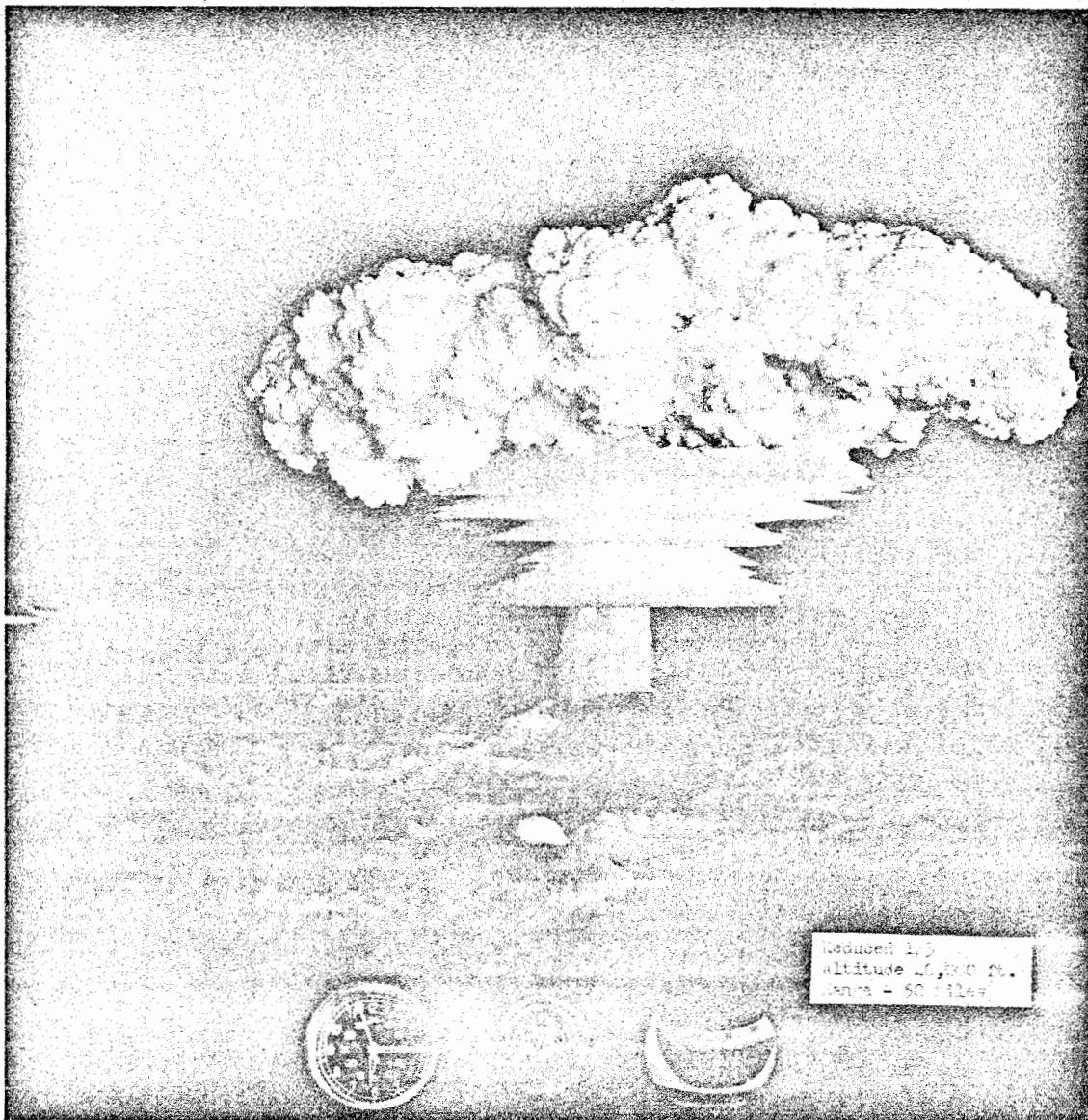
DOE ARCHIVES

Figure 13  
106

Re

ATOMIC ENERGY ACT 1954

110



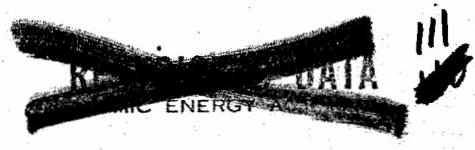
Reduced 1/3  
altitude 46,800 ft.  
range = 50 miles

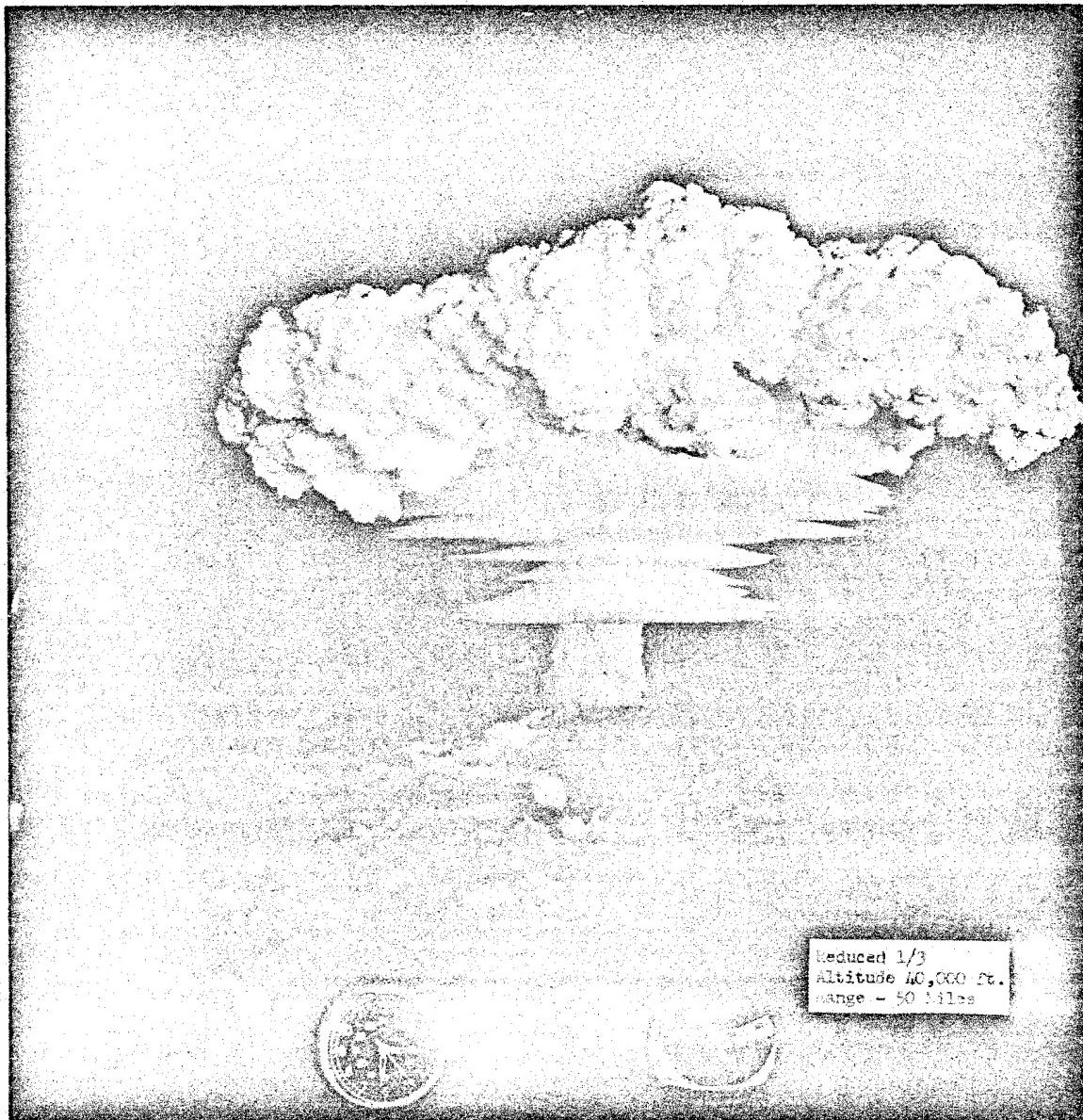
DOE ARCHIVES

Figure 14

107

SECRET

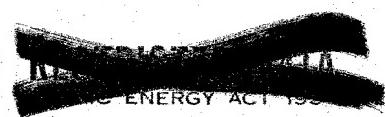




DOE ARCHIVES

Figure 15

108



112

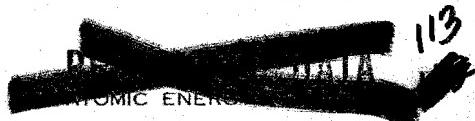


DOE ARCHIVES

Figure 16

109

113



# SUMMARY CLOUD PARAMETERS

THOUSANDS OF FEET

SHOT	HEIGHT - TOP		DIAMETER	
	MAX	1 MIN	1 MIN	10 MIN
CASTLE 1	114	47	38	370
CASTLE 2	110	44	33	316
CASTLE 4	94	35	26	125
CASTLE 5	110	44	34	270
CASTLE 6	72	25	19	147
IVY M	98	39	30	200
IVY K	76	28	11	90

DOE ARCHIVES

Figure 17

**PHYSICAL AND CHEMICAL NATURE OF THE CONTAMINANT;  
DIGEST OF OBSERVATIONS PRIOR TO CASTLE**

R. D. Cadle  
Stanford Research Institute

Pre-Jangle Fall-Out Studies

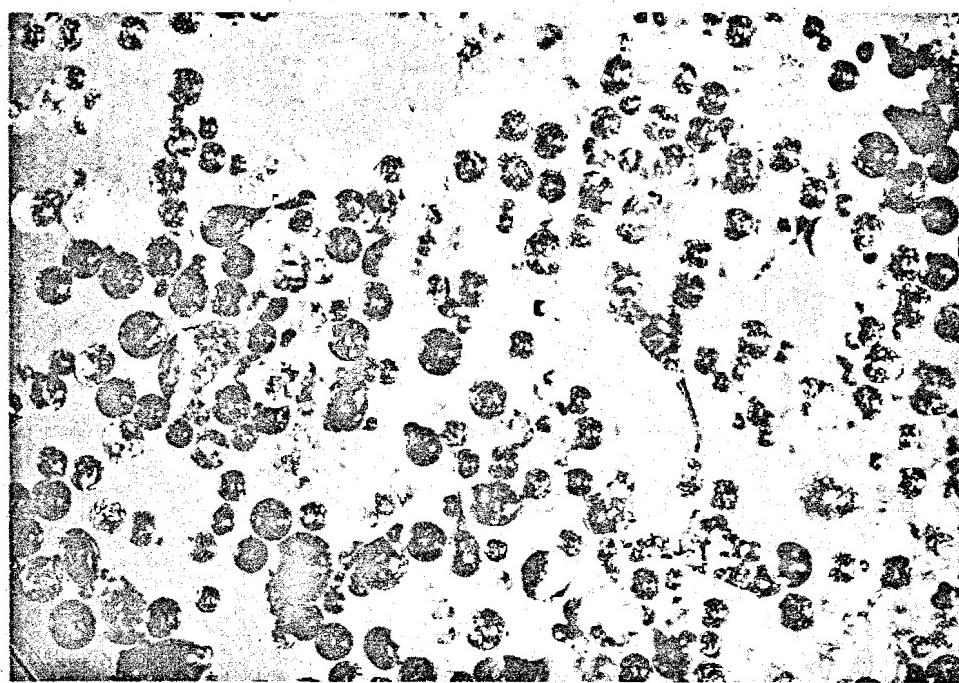
Most of the pre-Castle fall-out studies were made on three shots: Jangle Surface, Jangle Underground, and Ivy Mike. However, some investigations of cloud and fall-out particles were conducted at Sandstone and Greenhouse.

Cloud particles were sampled at Greenhouse by means of aircraft and were studied by means of an electron microscope. The median diameters were about 0.5 micron, although there was considerable variation from shot to shot and with altitude. Active fall-out particles collected at Greenhouse were classified either as spheres or as active coral grains. The median diameter of the spheres was about 5 microns and of the grains, about 20 microns.

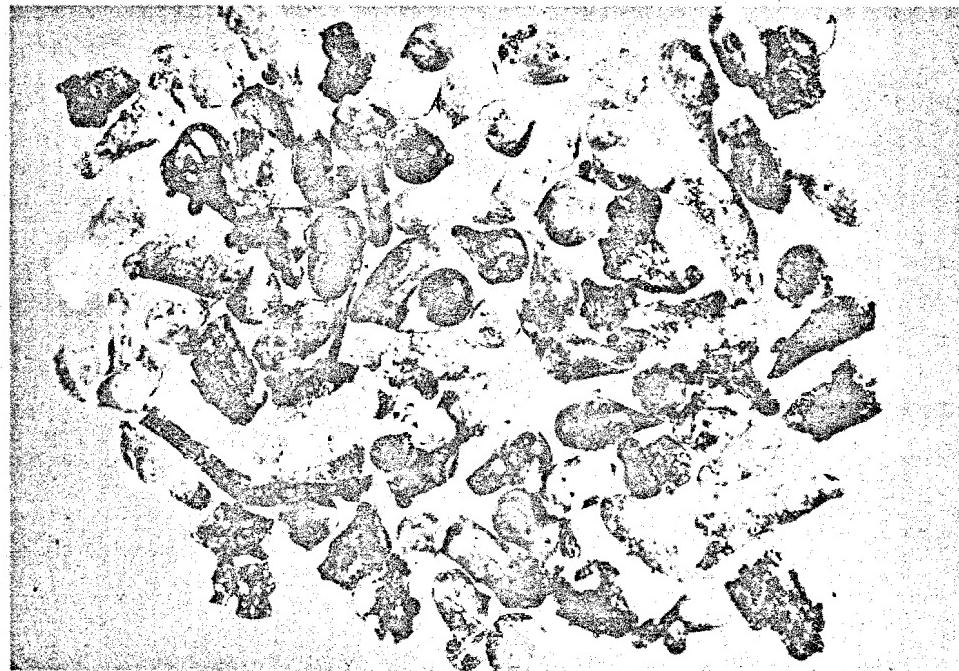
Jangle Tests

Extensive sampling of the fall-out from the Jangle Surface and Underground shots was conducted by several groups. The fall-out consisted of both radioactive and inactive fractions. The inactive fraction appeared to be essentially unchanged soil and the active material appeared to have been formed by fusion or condensation. The particle size distribution of the gross fall-out was essentially that of the original soil. The percentage of active particles in the gross fall-out varied with particle size but was about 5% to 10% for both shots.

The general appearance of the active particles is shown in the photomicrographs in Figure 1. Most of the active particles contained glassy material which was often vesicular; they varied from almost colorless to jet black, the darker particles being the most active. Some of the particles appeared to contain essentially unchanged earth. Spherical particles were found in both surface and underground shot fall-out, although a larger percentage was found in the former. Possibly the surface shot particles were formed at a higher average temperature than the underground shot particles. Figure 2 is a photomicrograph of a particle found in the crater from the underground shot. It demonstrates the complex nature of many of the particles. When found, it was covered with a black, glassy, ferromagnetic crust which was removed.



(a)



(b)

DOE ARCHIVES

Figure 1  
Typical Radioactive Particles from Fall-Out of Operation JANGLE  
(a) Surface Shot, (b) Underground Shot

Several groups prepared thin sections of the particles and studied them with the petrographic microscope. The particles were found to contain, in addition to the glassy material, fragments of quartz, feldspar, olivine, serpentine, and other minerals which were presumably part of the original soil. A few active particles were found which contained small spheres or irregular fragments of a ferromagnetic metal, presumably iron (Figure 3). Since the black material with which so much of the activity was associated seemed to consist of iron oxides, the discovery of free metal suggested the interesting possibility that both reducing (or inert) and oxidizing conditions existed at various times or places within the clouds produced by the explosions.

Emission spectrographs of black glassy particles and of the original soil showed that the former contained much higher concentrations of iron and copper than the latter. The black particles were ferromagnetic and may have contained considerable iron oxide, possibly from the bomb casing. This dark material may have been produced by condensation of vapors of soil, bomb casing, and fission products, which constituted the "fireball."

More than 99% of the mass of the underground shot active fall-out was composed of particles larger than 10 microns in diameter, and 50% was larger than 180 microns. Few data are available concerning the size distribution of active fall-out from the surface shot, but work reported by NRDL shows that almost all activity of the surface shot fall-out was associated with particles larger than 100 microns in diameter.

Thin sections of active particles were autoradiographed. The autoradiographs were enlarged and compared with photomicrographs of the sections. Some of the results are shown in Figures 4 and 5. Activity was distributed rather uniformly throughout some particles but was mainly associated with specific regions of others. The darker portions of the particles were usually more active than the lighter portions. Very rarely the activity was concentrated near the outside of the particle. Apparently, glassy droplets of relatively low activity often came in contact with other droplets which were more active and usually dark colored. Various degrees of mixing occurred, depending on the viscosity (temperature?) of the droplets, the time which elapsed before cooling, and the turbulence of the gases bearing the particles.

Ivy Mike

DOE ARCHIVES

Ivy Mike was a thermonuclear surface shot at Eniwetok. The active fall-out particles were usually white, hard grains having a

113

ATOMIC ENERGY ACTIVITIES

117

124



Figure 2  
Part of a Large Radioactive Particle Found in  
a Sample of the Soil from the JANGLE Underground  
Shot Crater. The largest black sphere was 240  
microns in diameter. A magnetized needle showed  
that the spheres were ferromagnetic.

DOE ARCHIVES

114

REPRODUCED BY ENERGY AGENCE

118

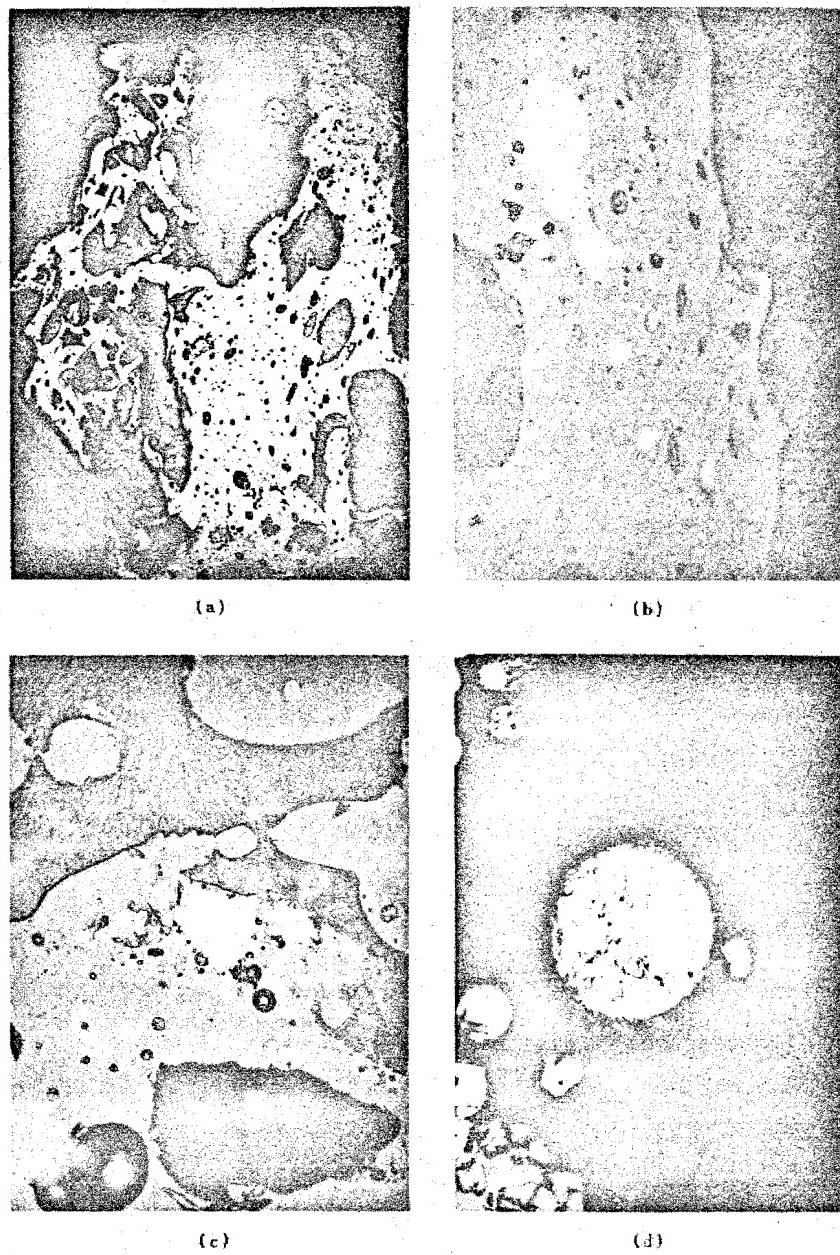


Figure 3

Photomicrographs of Thin Sections of Particles, under Vertical Illumination. Photographs (a) and (b) show an active particle from the JANGLE Underground shot with essentially white, metallic particles imbedded in the larger particle. The particle in (c) was etched with nitric acid and had a surface structure similar to the Widmanstätten figure. Photograph shows an etched section of a particle from the fume of an open hearth furnace which exhibited typical Widmanstätten figures.

DOE ARCHIVES

microcrystalline structure. Occasionally the particles were colored grey or brown. The composition of active fall-out particles was investigated using petrographic methods, chemical tests, X-ray diffraction measurements, and emission spectroscopy. Particles examined at Stanford Research Institute were composed almost entirely of calcium carbonate in the form of calcite. The original coral sand was also calcium carbonate, but almost entirely in the form of aragonite.

A large percentage of the active particles studied by NRDL were reported to consist of calcium hydroxide coated with calcium carbonate. Calcium nitrate was tentatively identified in a number of the particles.

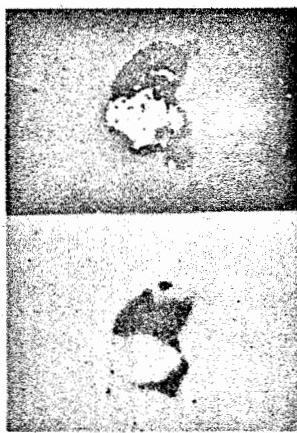
Autoradiographs were prepared of sections of Ivy Mike particles (Figure 6). Activity was usually concentrated near the surface of the particles, although they were often, and possibly always, somewhat active throughout.

DOE ARCHIVES



Figure 4 (a - i)      DOE ARCHIVES

Photomicrographs of Active JANGLE Fall-out Particles with Corresponding Autoradiographs. Figures a, m, p, q, r, s, and t were from the surface shot. The remainder were from the underground shot.



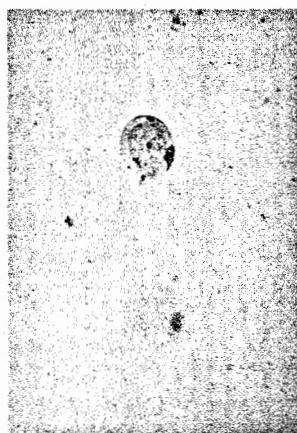
(j)



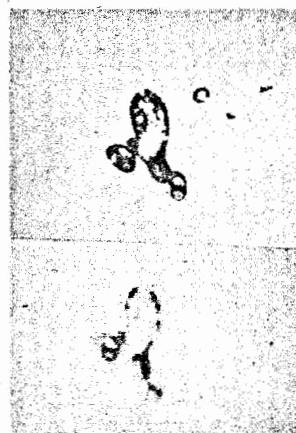
(k)



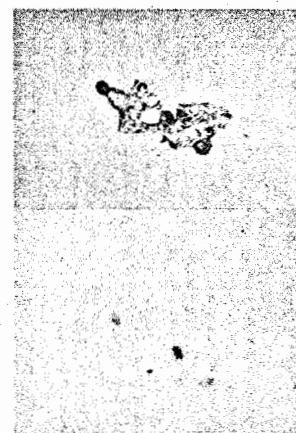
(l)



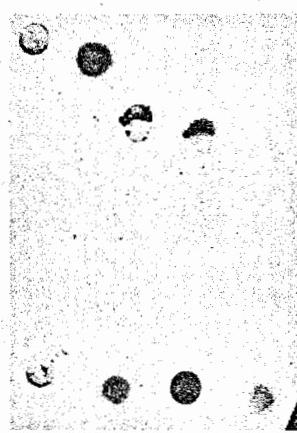
(m)



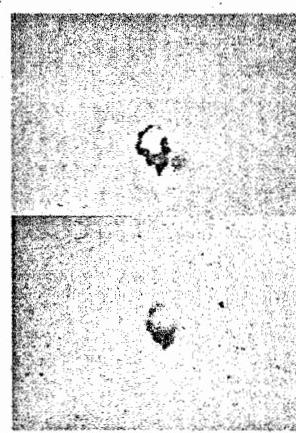
(n)



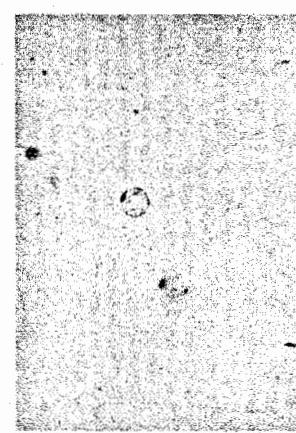
(o)



(p)



(q)



(r)

Figure 4 cont. (j - r)

DOE ARCHIVES

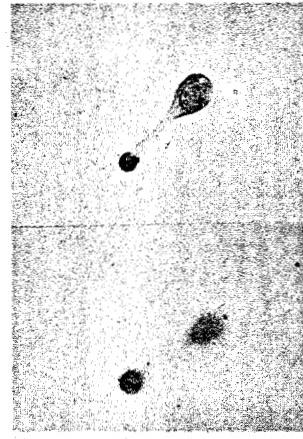
~~SECRET~~



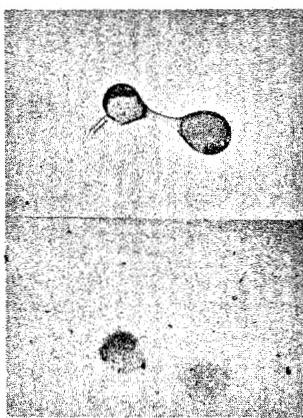
(s)



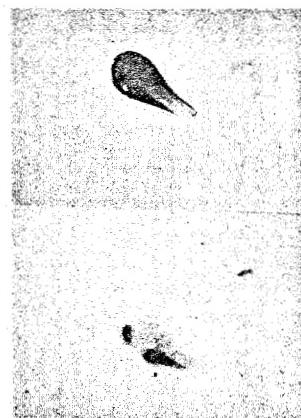
(t)



(u)



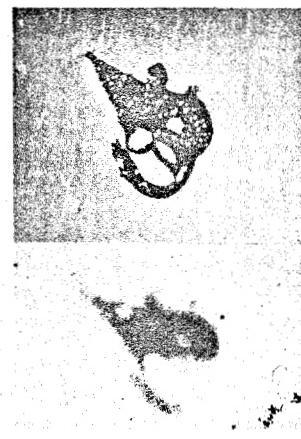
(v)



(w)



(x)



(y)

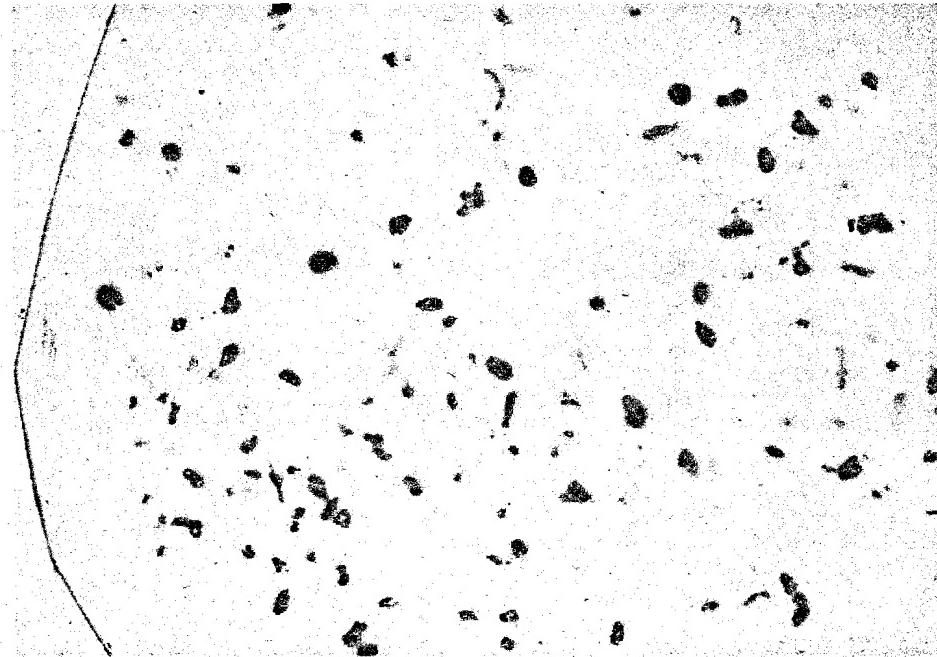
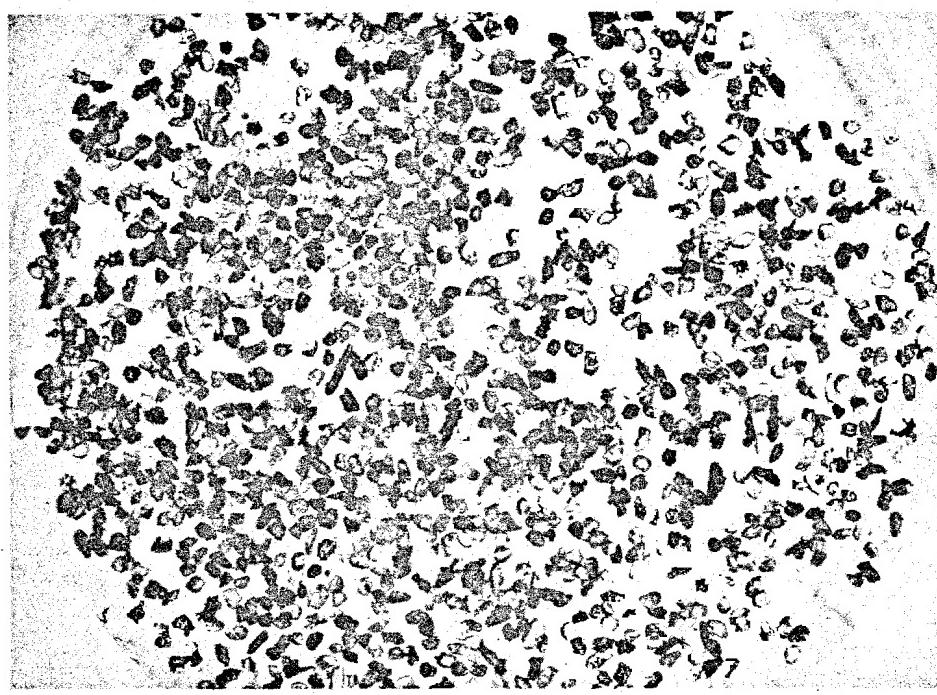
DOE ARCHIVES

Figure 4 cont. (s - y)

119.

~~RESTRICTED DATA~~  
ATOMIC ENERGY ACT 1954

123



DOE ARCHIVES

Figure 5  
Photomicrographs (above) and Corresponding Autoradiographs (below) of JANGLE Underground Shot Fall-out Mounted and Sectioned in Plastic. The various types and relative abundance of active particles can be observed.

120

124

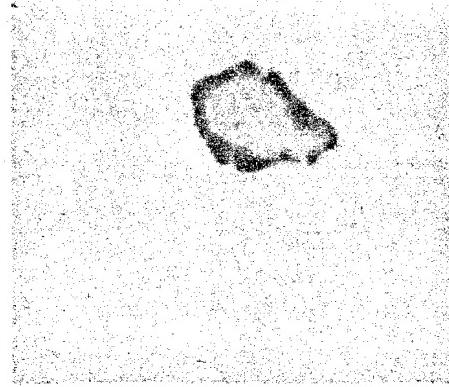
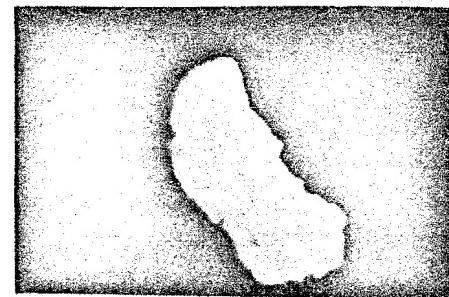
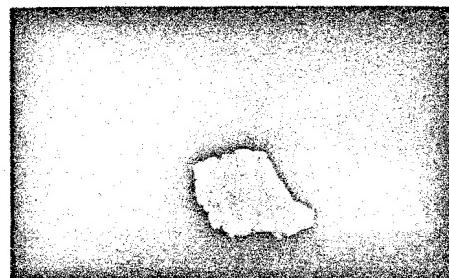
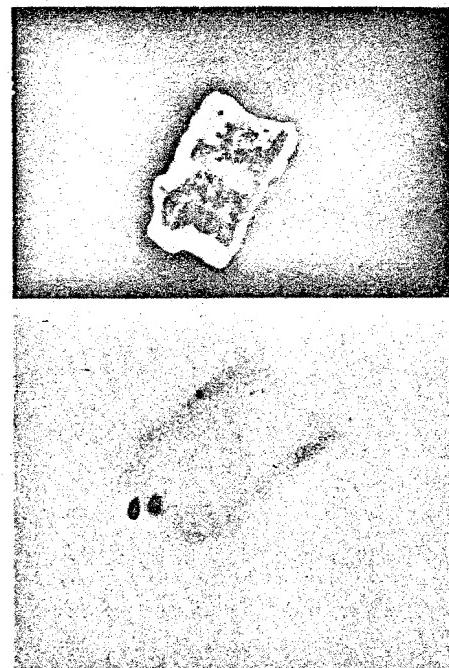
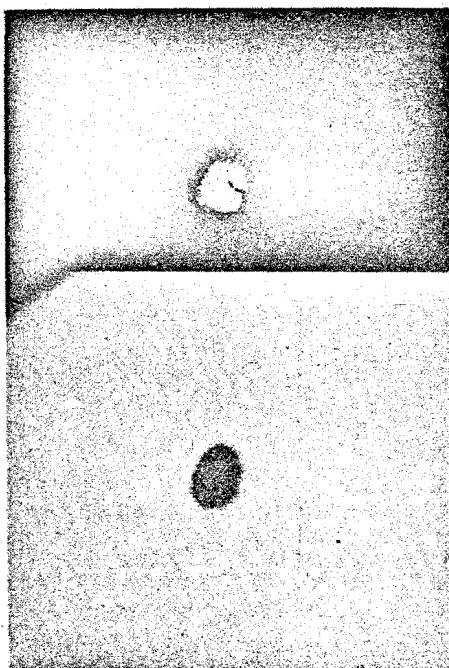


Figure 6  
Photomicrographs of sections of IVY-Mike Particles with Corresponding  
Autoradiographs

121

DOE ARCHIVES



THIS PAGE IS BLANK

DOE ARCHIVES

122



126

**PHYSICAL AND CHEMICAL NATURE OF THE CONTAMINANT  
INTERPRETATION OF CASTLE OBSERVATIONS**

Dr. Carl F. Miller  
U. S. Naval Radiological Defense Laboratory

The main objective of part of Project 2.6a was to determine the properties of the fall-out which were directly or indirectly related to countermeasures - that is, decontamination of the fall-out. In addition, many of the measured properties are those which determine the fall-out pattern.

A specific object of this paper is to show how the data can be used to specify, in a thermodynamic sense, a contaminated system. Such a system can be defined for a surface burst when four variants are given:

Site of detonation (environmental materials).

Yield of the device or weapon.

Amount of elemental structural components in the device.

Radiation contour in r/hr at 1 hour.

Once the above four items are given, data from the CASTLE Operations can be utilized to determine the kind and amount of materials which comprise the contaminated system produced by a surface burst.

The fall-out samples from which the data were derived are discussed in detail in the Project 2.6a final report. In general, the samples contained impurities of various kinds which had to be taken into account in interpreting the data. Fall-out from the first four shots was analyzed.

The contaminant properties of interest were of two general kinds: (1) contour properties and (2) chemical and physical properties. Both types, however, may be considered as giving a detailed picture of a given contour or the over-all fall-out pattern.

The contour properties are given by relationships between the radiation field and (1) the total mass of fall-out per unit area, (2) the specific activity or fraction of the device per unit area, and (3) the radiation characteristics of radioactive materials. Only the first two will be discussed at this time.

DOE ARCHIVES

The physical and chemical properties which were determined included (1) distribution of the radioactivity into solid, liquid,

123

DOE ARCHIVES  
ATOMIC ENERGY ACT 127

and colloidal fractions (or solubility of active constituents), (2) particle size distribution, (3) composition and structure of particles, (4) oxidation state of a few important radionuclides, (5) gamma spectra of the bulk radioactive source material, and (6) chemical composition of the fall-out.

A summary of the physical state fractionation of gamma activity (essentially solubility) is given in Table 1. An analysis of lead absorption data into three component energies for the various fractions is given in Table 2. The data in Table 1 are to be viewed as solubility effects. The weight of solid, for example, depended upon how much rain water, etc., fell into the sample collectors. The colloidal fraction was probably ionic material absorbed onto the ultrafilter membrane as indicated by the constancy of the fraction of ionic in the liquid phase for all shots and times of analysis. Decay of a sample from an island shot is given in Figure 1 and from a barge shot in Figure 2.

The particle size distributions are given in both Projects 2.5a and 2.6a final reports. The particles themselves were of several types: (1) inactive, unchanged coral particles (greater fraction of these from Shot 3 than Shot 1), (2) unchanged coral particles with radioactivity on the outside, (3) particles unchanged in the center with CaO or Ca(OH)<sub>2</sub> towards the exterior of the particle containing activity diffused inwards, (4) particles completely pyrolyzed with CaO or Ca(OH)<sub>2</sub> interiors with a thin shell of CaCO<sub>3</sub> around the exterior and radioactivity diffused inwards, and (5) particles of a very fluffy fragile nature containing spots of activity in them (apparently a "condensed" or agglomerated particle - like snowflakes). The most numerous or typical of the particles containing radioactivity were those typified by those given as (4) above of which an example of a thin section of a particle is given by Figure 3 in which the picture with polarized light shows the CaCO<sub>3</sub> shell, and the radioautograph shows the radioactivity diffusing into the Ca(OH)<sub>2</sub> center. The so-called "condensed" particles were relatively few in number. Hence, it is concluded that by far the majority of the radioactive particles were formed by the condensation of gaseous radioactive atoms (or particles of molecular size) onto larger solid particles which had never been vaporized, but which swept up through the radioactive gas cloud collecting both radioactive material as well as some vaporized environmental material. Later, as the cloud cooled, H<sub>2</sub>O and CO<sub>2</sub> could have again reacted with calcined particles to form Ca(OH)<sub>2</sub> and the CaCO<sub>3</sub> shells. No definite information was obtained on the particles resulting from the water shots excepting that, as the fall-out reached the earth's surface, they must have been extremely small; the fall-out contained very little, if any, water.

DOE ARCHIVES

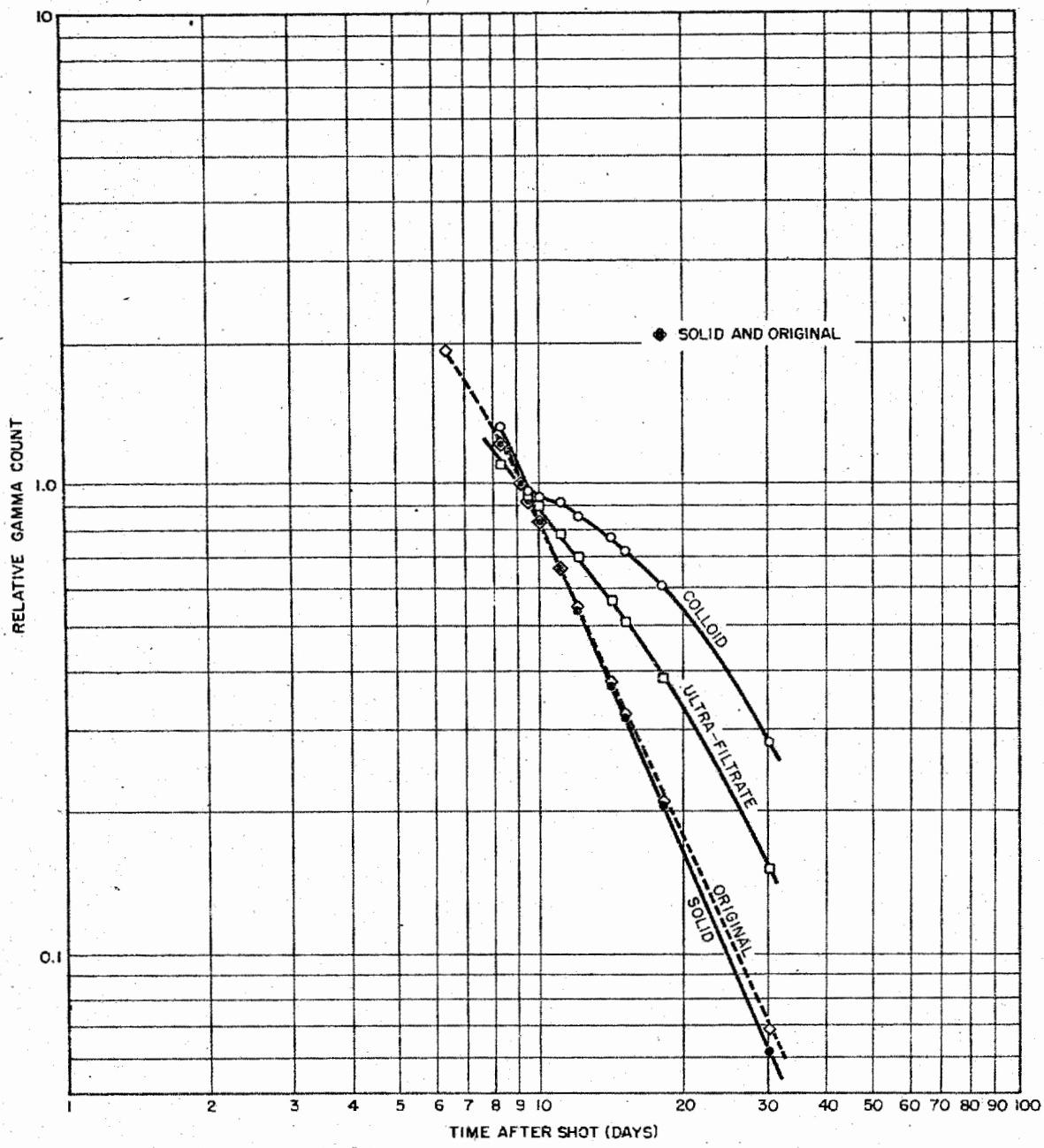
Table 1  
Summary, Physical State Fractionation of Gamma Activity

Shot Type	No.	Number of Samples	Time After Detonation (days)	Wt. of Solid (%)	pH	Solid (%)	Ionic (%)	Colloidal (%)	Amount Ionic Phase (%) (a)
Island	1	3	6.5-8.3	0.85-9.2	9.0-12.3	92.1-98.1	1.9-7.7	0.06-0.2	97.0-97.5
	3	2	4.2-5.5	0.18-0.23	10.5-11.2	92.4-94.2	5.6-7.3	0.23-0.23	96.1-97.0
Barge	2	1	3.4	0.01	7.5	24.7	72.9	2.4	96.8
	4	1	1.8	0.01	7.7	40.2	57.9	1.9	96.8

(a) Gamma count in ionic, as fraction of gamma count in liquid phase

Table 2  
Average Photon Energy and Distribution of Apparent Photon Energies  
in Physical State Fractions

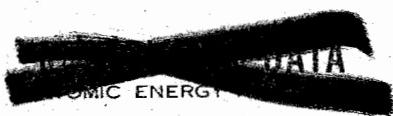
Shot Position	Low Energy Component Amount (Mev)	Medium Energy Component Energy (Mev)	High Energy Component Energy (Mev)	Average Photon Energy (Mev)
Island	0.15	50.3	0.34	22.2
	0.15	45.0	0.34	23.4
Barge	0.16	44.1	0.41	19.7
	0.15	55.4	0.34	24.2
Island	0.17	22.0	0.40	20.0
	0.15	41.5	0.34	23.4
Barge	0.17	22.0	0.40	1.37
	0.15	41.5	0.34	35.1



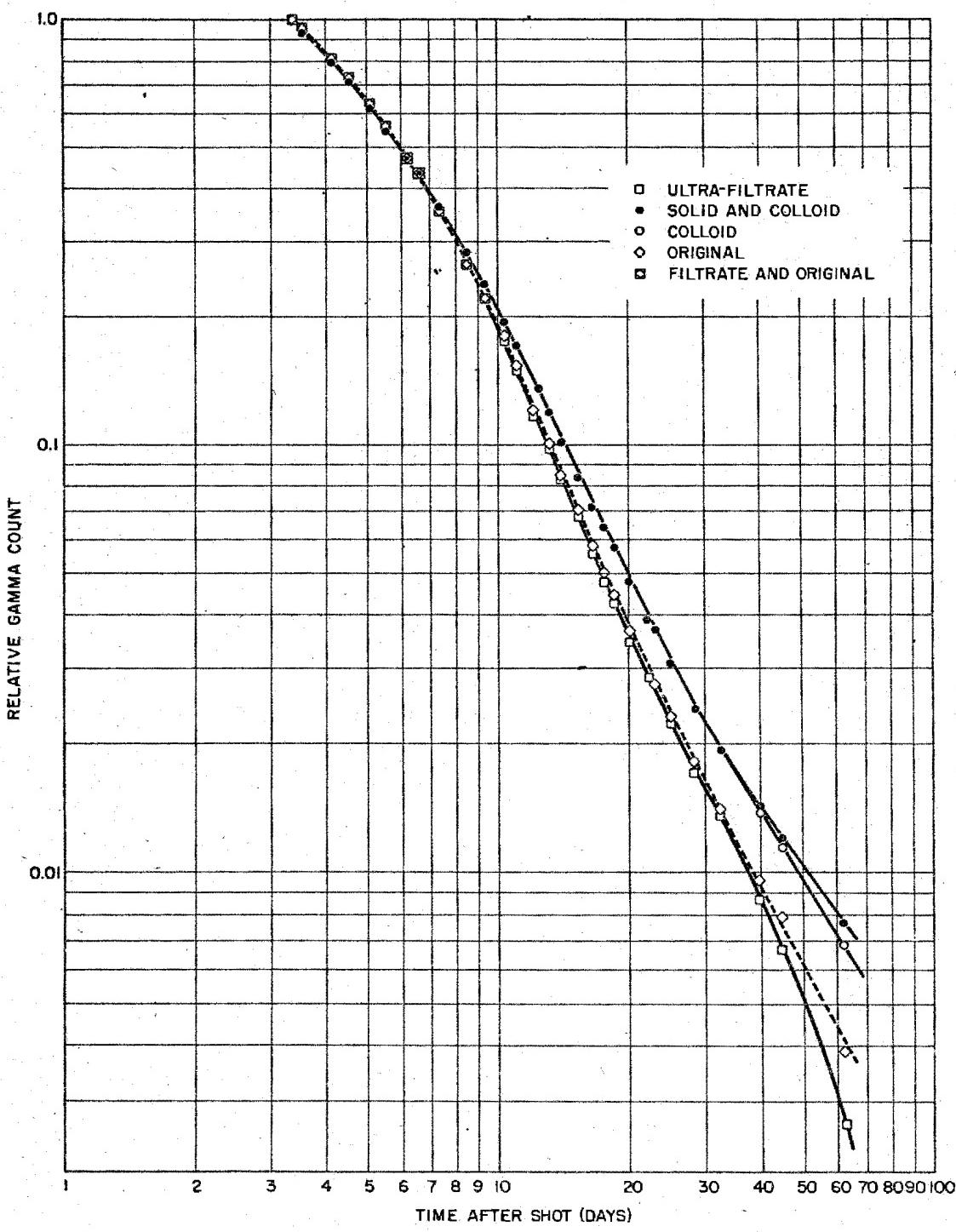
DOE ARCHIVES

Figure 1  
Gamma Decay of Physical State Fractions of Sample 1-251.03

126



130

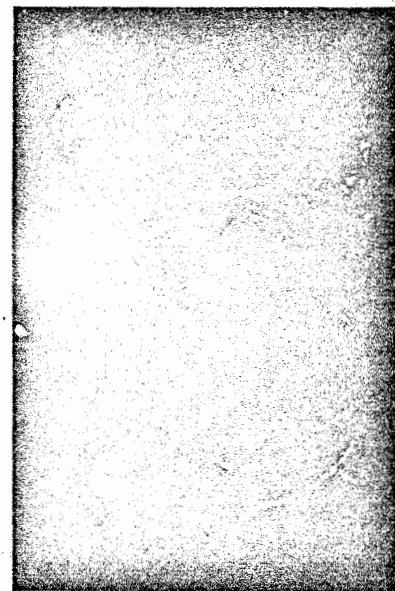


DOE ARCHIVES

Figure 2  
Gamma Decay of Physical State Fractions of Sample 2-Al



a. Photographed in ordinary light



b. Photographed in  
polarized light



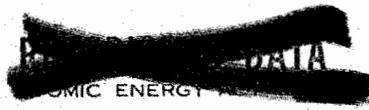
c. Radioautograph

1 mm

DOE ARCHIVES

Figure 3  
Typical Fall-out Particle from Operation CASTLE  
Consisting Almost Entirely of Calcium Hydroxide

128



132

The oxidation states of Np and I were investigated. Np was found to be about 2/3 as NpIV and 1/3 as NpV and NpVI. For the barge shots, I was found in the liquid fraction, while for the island shots it was mainly in the solid fraction. With two phases present, I was apparently present in the -1 oxidation state (I as iodine is subject to air oxidation which is fairly rapid in the dry state).

Some 800 gamma spectral determinations were made in one month at the site. With a 1 in. NaI crystal, the data could not readily be reduced quantitatively but were used to demonstrate that, for samples obtained from various locations in the fall-out area up to about 200 miles distant from shot point, fractionation of the radioactive elements did not occur to any appreciable extent. The coincidence of the decay of such samples agree with the spectral data in this respect. The data do not prove that fractionation does (or did) not occur; they prove that if it did occur, the degree to which fractionation occurred was not sufficient to alter the over-all gamma spectral distribution and decay of the fall-out (each source sample was a dissolved aliquot representative of all the particles which fell out over a 7 in. diameter area). Spectral data for single particles have been taken and do, in fact, show a different gamma spectrum.

The chemical composition of the fall-out was determined by analyzing for Na, K, Mg, Ca, Sr, Al, Cl, Br, Cu, and Fe. Samples of the lagoon water, sea water, and coral were similarly analyzed as background constituents to obtain a ratio of the elements for coral and sea water. Using the ratios and the analysis of the fall-out samples, it was possible to reduce the composition of the fall-out into coral, sea water, and device-product components. The residual iron in the sea water and coral components was found to be about the same order of magnitude as that used in the device (barge, etc.). From the data, then, it was possible to determine the mass of coral per sq. ft., the mass (or apparent volume) of sea water per sq. ft., and the fraction of the device per sq. ft. which fell into each collector. Then knowing, or estimating, the radiation at each of the stations in r/hr (at 1 hr), a ratio can be calculated between the radiation field and each of the surface density quantities. For a given shot, the ratio should be constant providing the component in question has been thoroughly mixed with the total radioactive material available. The data are plotted as histograms in Figures 4 through 9. In the case of "double" distributions, it was noted that samples collected in the lagoon or at sea were high in sea water; samples collected on the islands were high in coral. In such cases, the lower distribution was considered a more reliable estimate of the quantity. The data are summarized in Table 3. The mass equivalents are in terms of weight of original material - coral or sea water - which was used to produce the stated ratio. For

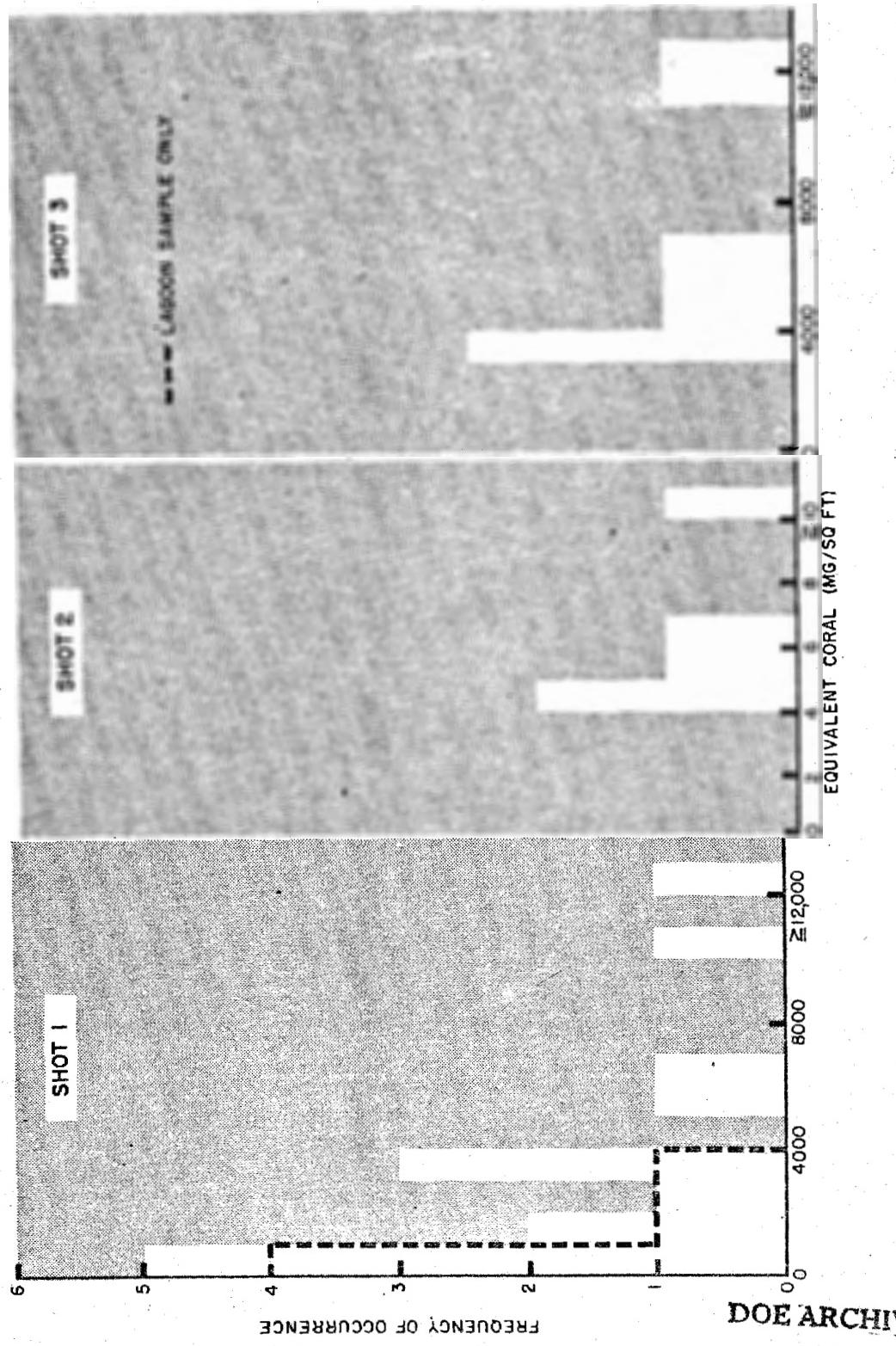
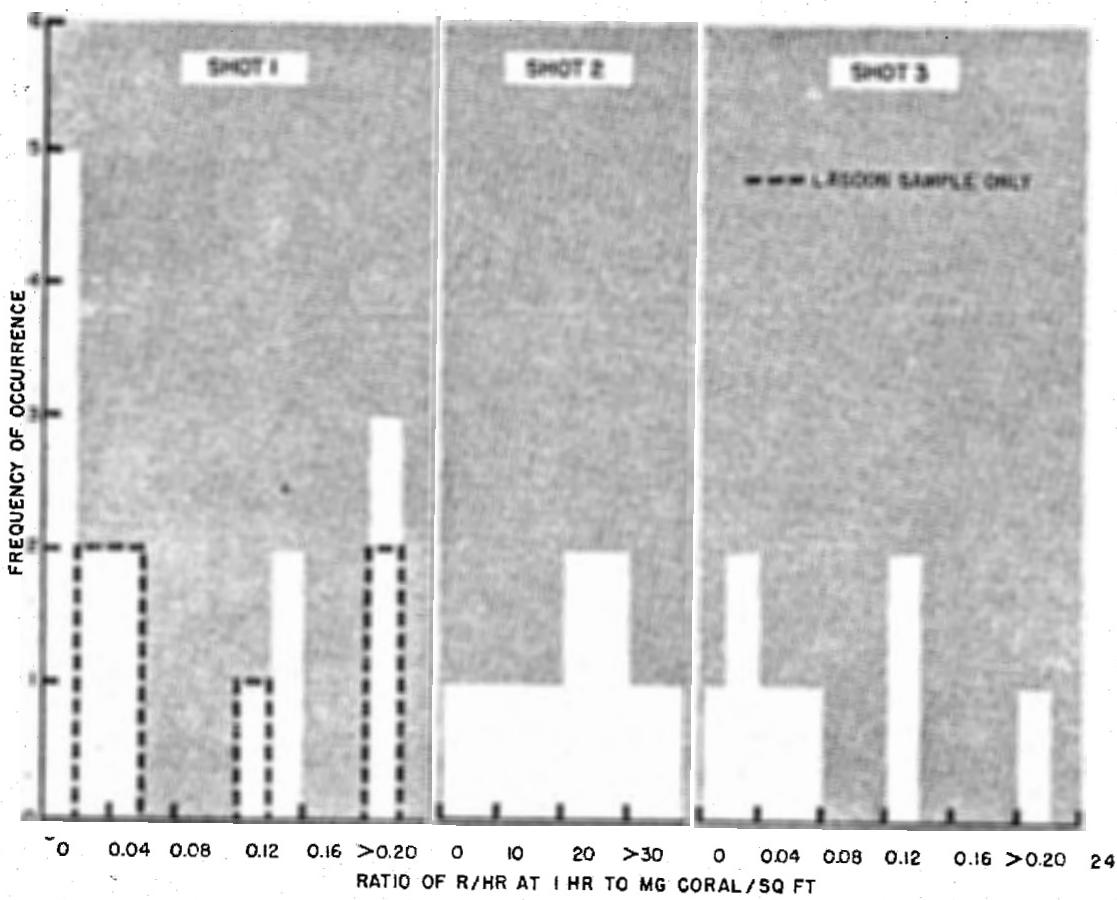


Figure 4  
Density Distribution of Equivalent Coral for Shots 1, 2, and 3



**DOE ARCHIVES**

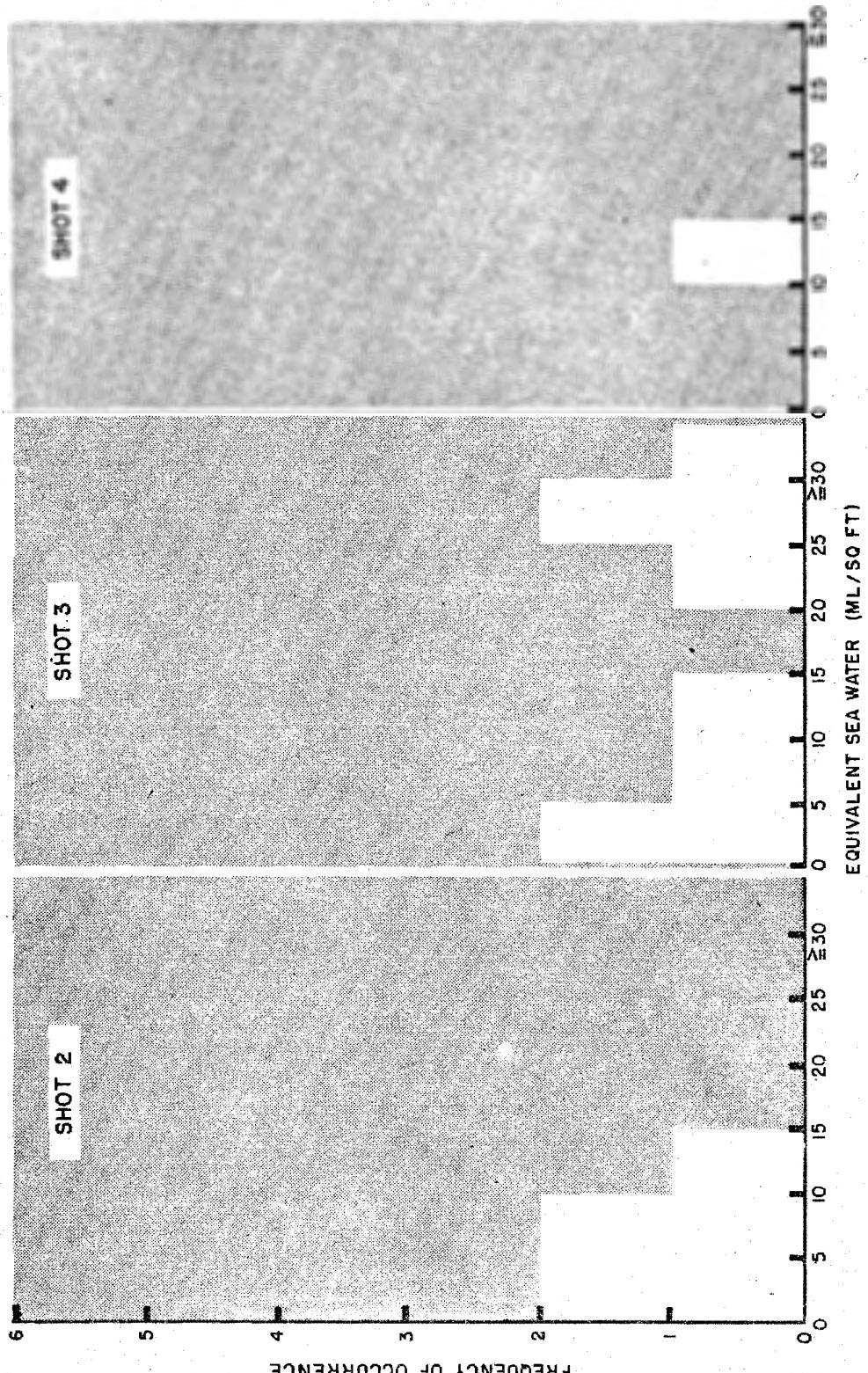
**Figure 5**  
**Distribution of the Ratio of the Radiation Field**  
**to the Surface Density of the Coral Component**

131

REF ID: A6479



135



DOE ARCHIVES

132

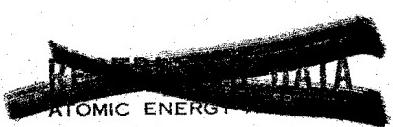


Figure 6  
Density Distribution of Equivalent Sea Water for Shots 2, 3, and 4

136

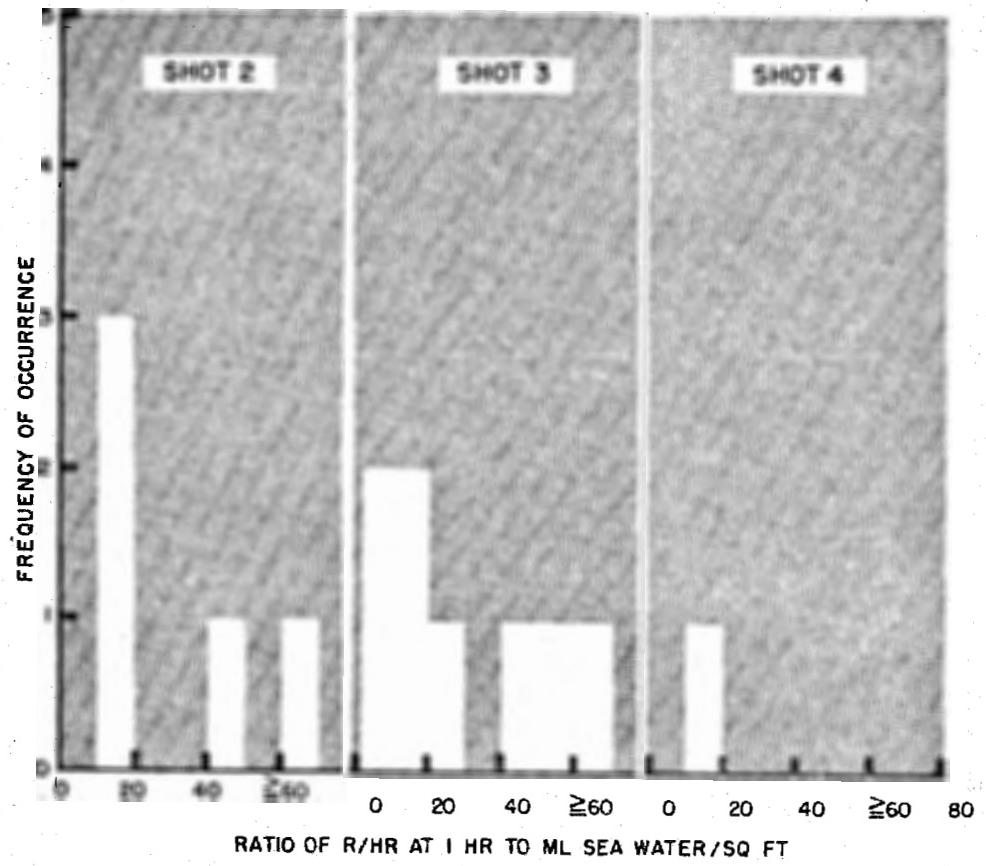
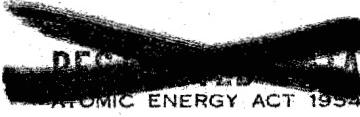


Figure 7  
Distribution of the Ratio of the Radiation Field  
to the Surface Density of the Sea Water Component

DOE ARCHIVES

133



137

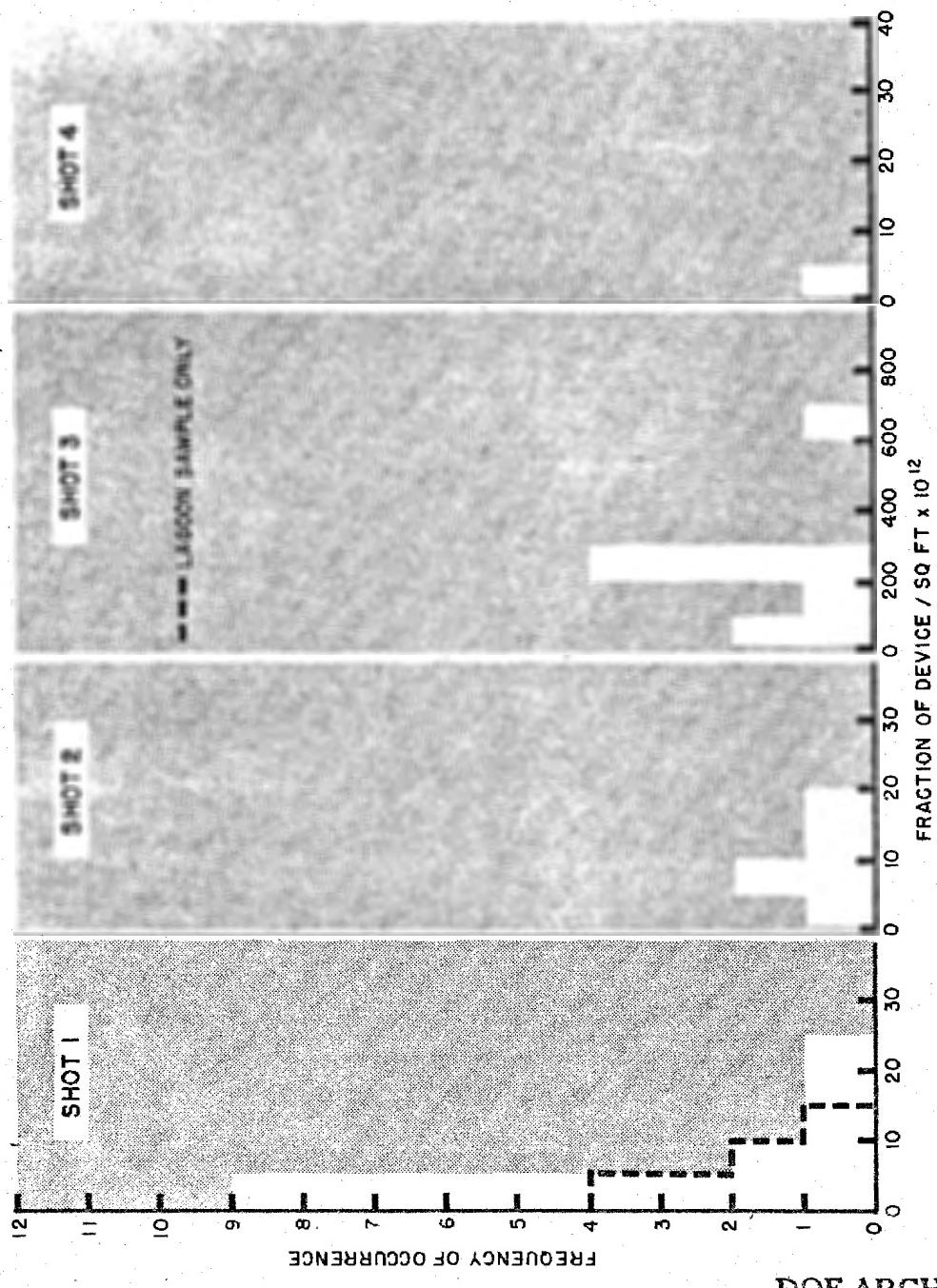


**Figure 8**  
Density Distribution of Device Fraction for Shots 1, 2, 3, and 4

TESTED  
1954

134

138

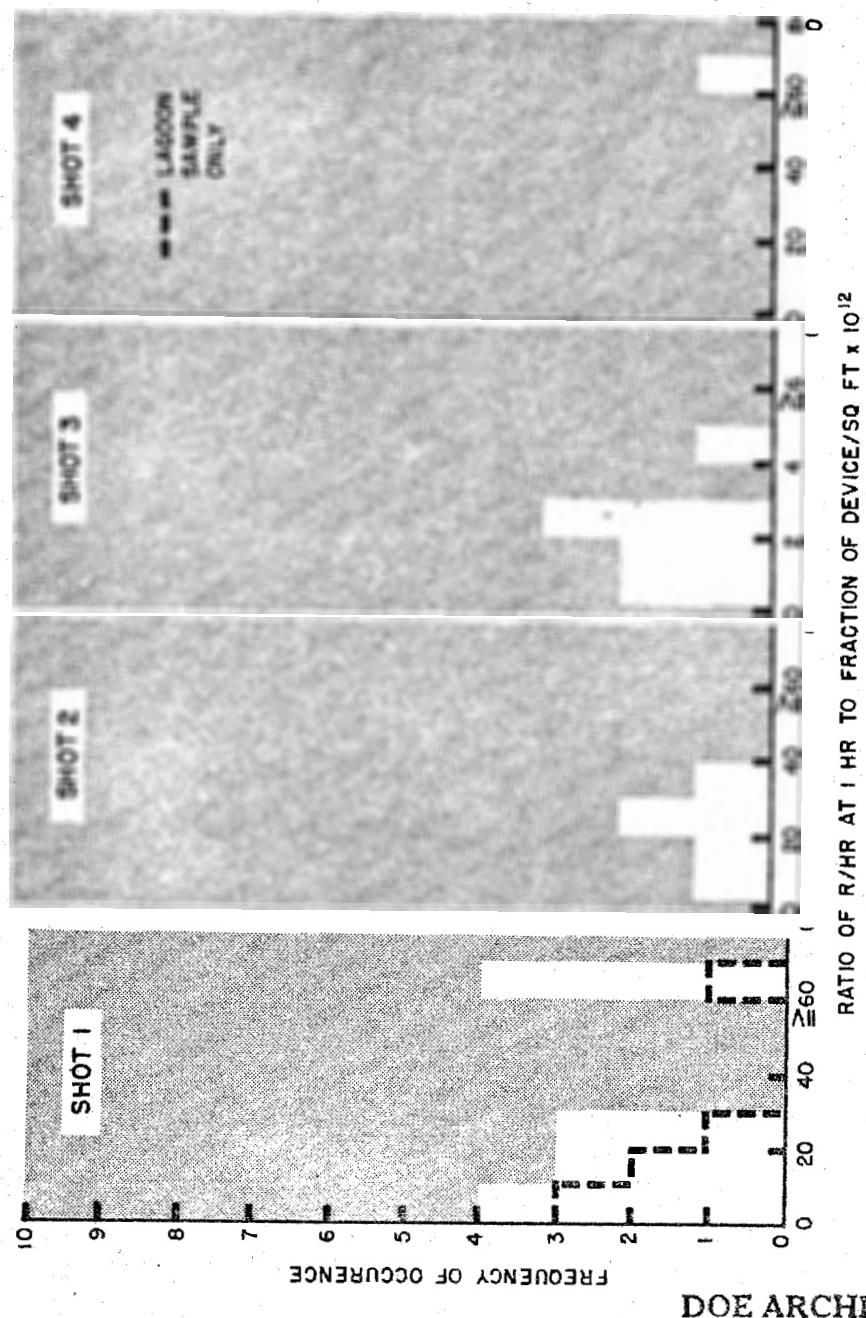


**Figure 9**  
Distribution of the Ratio of the Radiation Field  
to the Surface Density of the Device Fraction Component

135

RESTRICTED BY  
ATOMIC ENERGY ACT 1954

139

Table 3  
Contour Property Ratios

Event	mg.eq. coral/ft <sup>2</sup>		mg.eq. seawater/ft <sup>2</sup>		Total mass in mg/ft <sup>2</sup>		(a) Fraction Device/ft <sup>2</sup>	
	r/hr at 1 hr	r/hr at 1 hr	r/hr at 1 hr	r/hr at 1 hr	r/hr at 1 hr	r/hr at 1 hr	r/hr at 1 hr	Yield
Castle No. 1	25	0	0	0	25	25	4 x 10 <sup>-14</sup>	14.5MT
Castle No. 2	0.04	0.04	77	77	77	77	5 x 10 <sup>-14</sup>	10.5MT
Castle No. 3	20	20	5	5	25	25	30 x 10 <sup>-14</sup>	110KT
Castle No. 4	0	0	91	91	91	91	2 x 10 <sup>-14</sup>	7MT
Jangle "S"	-	-	-	-	26	26	-	1.2KT

(a)  $R_{f,d} = 2.4 \times 10^{-12} \cdot Y^{-0.42}$  (Y in KT)

DOE ARCHIVES

Shots 2 and 4, for example, a ratio of 80 mg. sea water per sq. ft. to 1 r/hr at 1 hr would produce only an actual ratio of 2.7 mg. of residual salts per sq. ft. to 1 r/hr at 1 hr. The coral values would not be changed much by using  $\text{Ca}(\text{OH})_2$  for  $\text{CaCO}_3$ . For the JANGLE surface shot, the mass change would be less yet. The data show that the total mass contour ratio is essentially invariant with yield with the surface water shots producing a ratio greater by about a factor of [density (soil)/density (sea water)+1]. The contour ratio for the fraction of the device varies with yield (from the Effects of Atomic Weapons, the variation of the ratio with yield would be  $3 \times 10^{-11}/Y$ ). A more precise method for obtaining this contour ratio would be from a FP radiochemical analysis. The iron analytical are consistent within themselves but give a set of contour ratios which are apparently too high. This may be due to inadequate sampling of the background materials.

For Shot 1, the fall-out consisted of coral (mostly pyrolyzed) and device products (surface-land shot).

For Shot 2, the fall-out consisted of sea water (salts), device products, and small amounts of coral (surface-deep harbor shot).

For Shot 3, the fall-out consisted of coral smaller amounts of sea water (salts), and device products (surface-land shot on beach or harbor dock area).

For Shot 4, the fall-out consisted of sea water (salts), and device products (surface-water shot).

The above summary of the composition of the gross fall-out neglects rain water which fell during the collecting period by some of the sample collectors.

The following conclusions may be made from the data:

The site, or point of detonation, is the determining factor in the production of fall-out debris and its chemical and physical composition.

The contour properties which define a contaminated system (fall-out on a surface) can be utilized to specify experimental systems to evaluate countermeasures of various types for estimating the time, cost, and efficiency of a given recovery procedure. Such information is necessary for a practical countermeasure doctrine.

The chemical and physical properties not directly related to the contour properties are essential to the testing of experimental

systems; they serve as criteria by which a synthetic - or laboratory prepared - fall-out can be compared to the real fall-out. In addition, such determinations lead to a better understanding of the production and distribution of the fall-out and furnish such required data as are used in the calculation (or prediction) of the fall-out patterns themselves.

DOE ARCHIVES

138

142

ATOMIC ENERGY A

RADIOLOGICAL NATURE OF THE CONTAMINANT; SOURCE GAMMA ENERGY SPECTRA

Dr. C.S. Cook  
U.S. Naval Radiological Defense Laboratory

Using a NaI(Tl) scintillation spectrometer, gamma-ray spectra have been determined for selected samples returned from the Pacific Proving Grounds to USNRDL.

The spectrometer is a single-channel analyzer developed in our laboratory. The block diagram of its electronics is shown in Fig. 1, and a photograph of the apparatus is shown in Fig. 2.

A 4-in. diameter by 4-in. high cylindrically-shaped crystal was used for the analysis in order to enhance the total absorption peak. The effect of a large crystal on this enhancement is seen by comparing the spectra of Cs<sup>137</sup> as obtained by a 1-in. diameter by 1-in. high crystal, uncollimated (Fig. 3), and a 4-in. diameter by 4-in. high crystal (Fig. 4). The number of quanta at a given energy is determined through measurement of the area of the total absorption peak, followed by a peak-to-total area correction and a correction for the number of quanta which pass through the crystal without undergoing either a photoelectric or Compton interaction.

Further reduction to a dosage spectrum is made by correcting as a function of energy for the relative ionization produced in a unit mass of air per photon per unit time in accordance with the work of Marinelli et al.

The dosage spectrum as a function of time after shot is shown in Table I for a sample from CASTLE, Shot 4, (Union). This was one of the best sources from the point of view of having sufficient strength to produce relatively good statistical accuracy (approximately  $\pm 10$  per cent).

The time-dependent characteristics of the spectra should be noted. Prior to ten days following the detonation, a large fraction of the radiations are concentrated in the vicinity of 100 kev. This is primarily the result of induced activities in the nuclear device. After ten days a growth in the relative amounts of activity in the regions of 500 kev and 1.6 Mev are noted. This can be attributed to the presence of the Ba<sup>140</sup>-La<sup>140</sup> radiations. As this dies away, a concentration of the spectra in the 700 kev region is noted. The primary contributant to this is the Nb<sup>95</sup>-Zr<sup>95</sup> fission product chain.

DOE ARCHIVES

It should be remembered that the figures quoted are percentages. The absolute activity is constantly decaying.

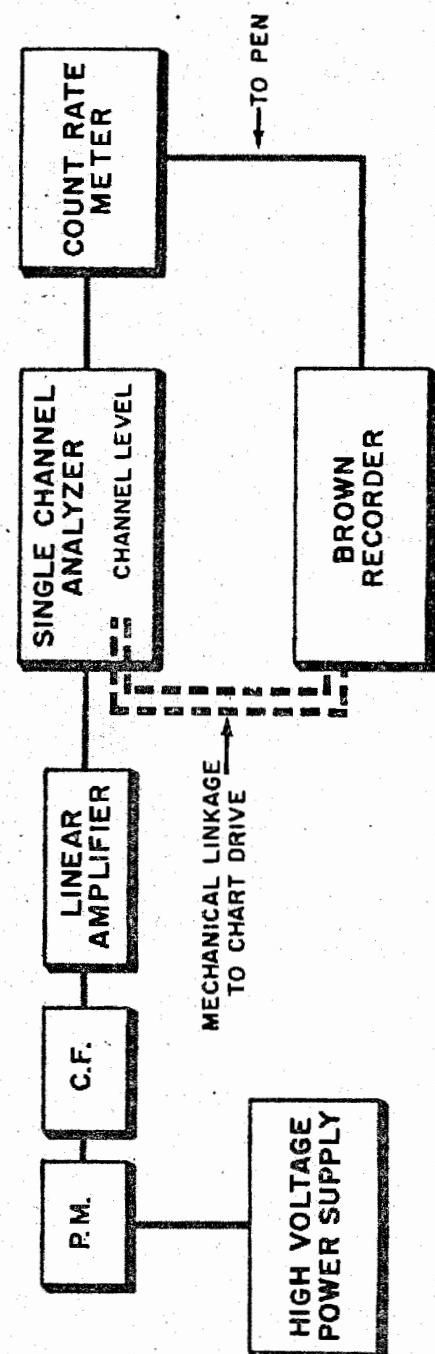
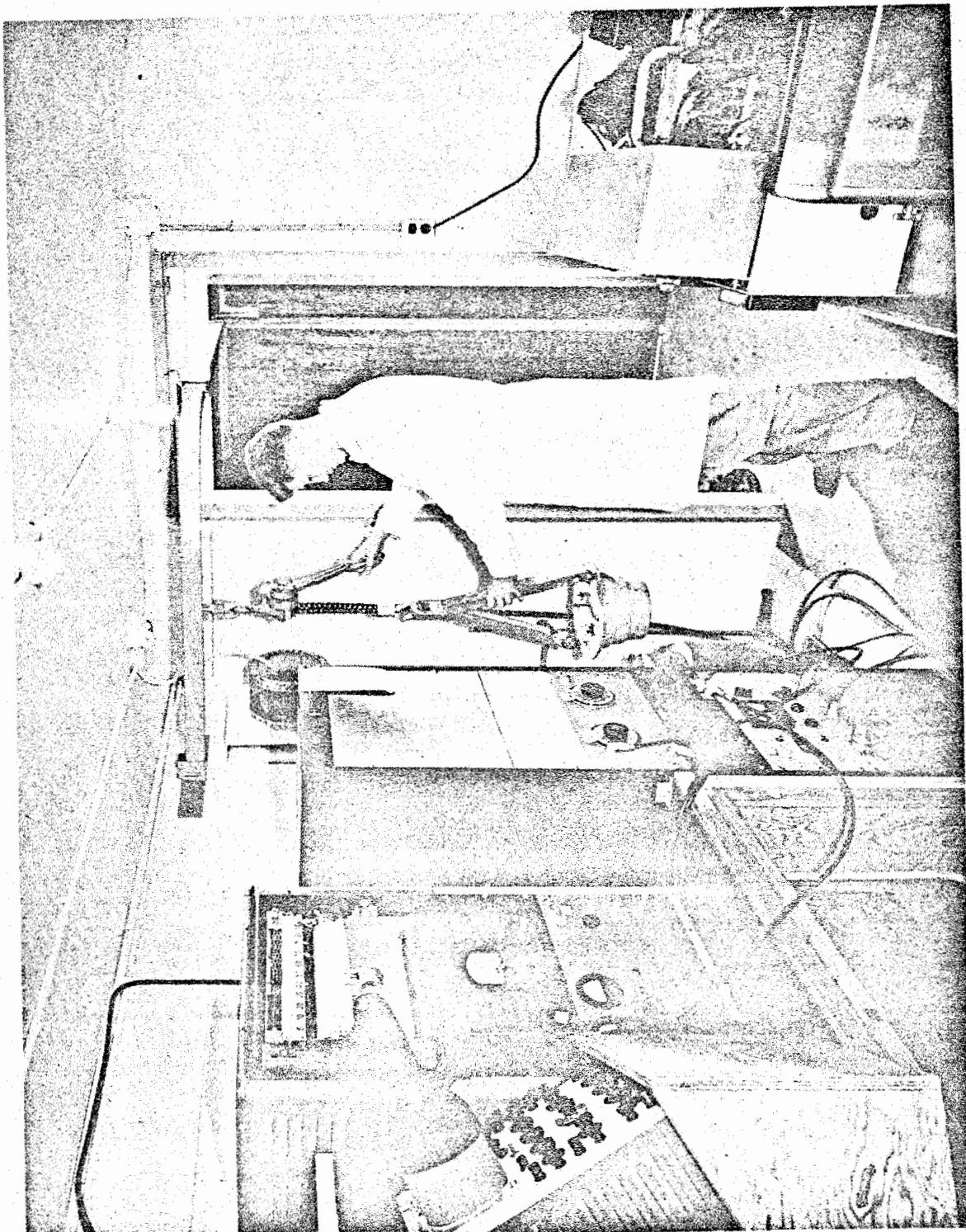


Figure 1  
Block diagram of the Electronics for the Single Channel  
Scintillation Spectrometer. P.M. = Photomultiplier Tube,  
C.F. = Cathode Follower.

DOE ARCHIVES

Figure 2  
Single Channel Scintillation Spectrometer



DOE ARCHIVES

141

ATOMIC ENERGY ACT

145

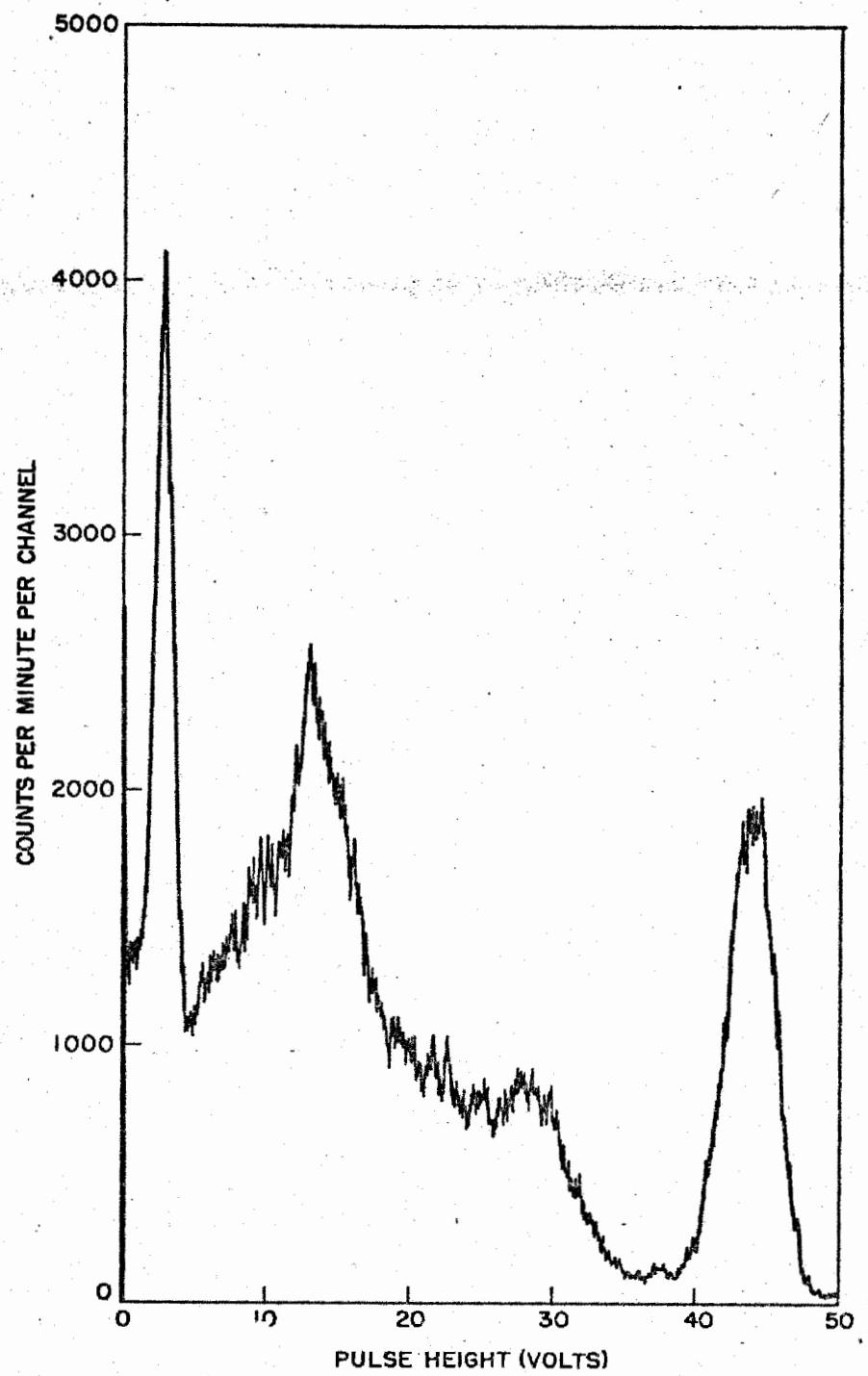
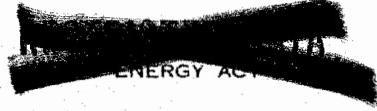


Figure 3  
Spectrum of  $\text{Cs}^{137}$  as obtained by a 1-in. diameter  
by 1-in. high Crystal

DOE ARCHIVES

142



146

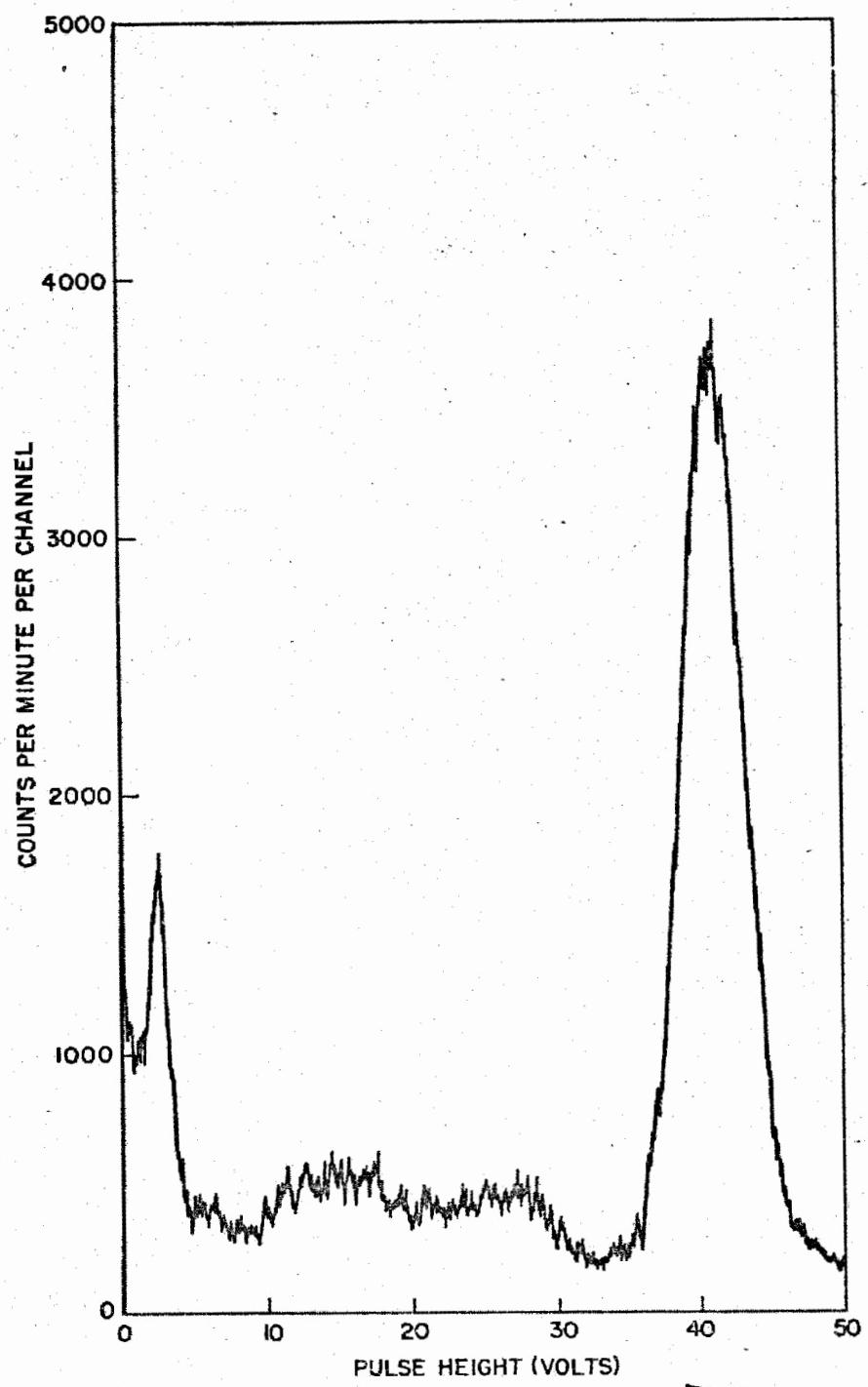
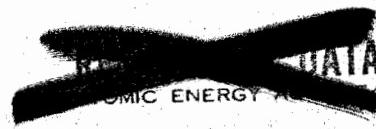


Figure 4  
Spectrum of  $\text{Cs}^{137}$  as obtained by a 4-in. diameter  
by 4-in. high Crystal

DOE ARCHIVES

143



147

TABLE I

Dosage Spectra for Sample 4-L in Per Cent of  
Dosage per 0.1 Mev Energy Interval

Days After Shot	0	.1	.2	.3	.4	.5	.6	.7	.8	.9	1.0	1.1
5.1	44.3	5.1	10.0	6.8	6.4	9.4	11.5	3.3	13.2	3.6	13.4	
5.3	31.1	8.3	7.0	1.6	8.9	12.0	12.7					
7.9	22.1	8.0	5.6	1.8	8.9	12.5	13.2	3.9	22.5			
9.9	22.3	8.3	10.0	2.8	11.2	11.0	12.6	5.3	22.2			
11.9	17.1	8.3	6.4	4.2	16.4	7.0	13.7	4.7	25.1			
14.9	12.5	4.6	8.1	3.5	15.6	6.2	13.9	4.7	31.3			
16.9	8.6	5.3	4.9	2.6	14.2	5.4	13.5	5.8	34.9			
18.9	6.9	8.7	4.7	4.7	3.1	18.0	5.5	13.5	6.0	37.9		
22.0	8.0	4.0	3.1	2.6	18.3	5.9	14.4	6.7	35.3			
24.1	7.1	3.8	3.2	2.5	18.7	7.6	17.7	7.0	37.4			
26.1	5.3	3.7	2.1	2.6	17.5	7.9	16.9	9.0	32.4			
29.0*	5.6	4.0	3.4	3.4	21.2	23.2	23.0	5.9	35.0			
29.1*	5.2	3.2	2.8	3.0	21.0	23.1	6.3					
31.0	7.6	2.9	2.3	3.2	21.5	26.2	5.0					
33.0	38.1	7.8	3.2	2.6	3.4	21.5	27.1	6.0	28.4			
44.0	6.6	2.1	2.4	2.8	21.2	33.0	6.2					
49.9	7.7	2.1	2.6	3.5	20.8	37.0	3.9					
79.0	5.1	1.9	2.0	2.9	21.8	54.0						
137.0		1.5		2.6	17.7	78.2						

\* Sample 4-L consisted of two parts. Each contained approximately one cubic centimeter of liquid but one was prepared to have ten times the specific activity of the other. Measurements at 29.0 days and earlier were made on the lower specific activity source, and at 29.1 days and later on the higher specific activity source.

OMIC ENERGY ACT

144

DOE ARCHIVES

148

**TABLE II**  
**Dosage Spectra in Per Cent of Dosage Per 0.1 Mev Energy**  
**Interval for Several Samples, Each Recorded at**  
**Approximately 8 Days after Detonation**

Days After Shot	0	.1	.2	.3	.4	.5	.6	.7	.8	.9	1.0	1.1	1.2	1.3	1.4	1.5	1.6	1.7	1.8	1.9	2.0	2.1	2.2
Sample																							
1-1	8	8.8	8.0	10.5	2.9	9.0	4.6	17.1	15.2	7.8													
1-1	5	14.5	8.3	17.0	2.7	9.9		16.8	14.9	5.9													
2-1	7	18.1	7.0	18.5	3.1		10.8	15.1	9.4														
2-1	8	14.0	8.1	15.5	2.8	10.6		11.7	14.5	2.8													
3-2	8	21.5	3.5	13.8	6.6	8.3		14.3	11.0	2.4													
4-1	5	31.1	10.0	8.3	8.9		12.0	12.7	3.6														
4-1	8	22.1	8.3	7.0	1.6	8.9		12.5	13.2	2.9													
4-2	8	14.4	8.1	9.3	1.6	13.0		11.0	14.1	6.6													
4-3	8	23.9	10.2	16.6	3.7	9.7		8.6	11.6	5.0													
5-1	7	15.9	9.3	13.9	2.3	24.6		11.2	13.4	4.0													
5-1	8	12.7	6.6	9.5	1.6	13.7		15.7	20.5	2.3													
6-1	5	11.9	5.2	13.1	2.9	10.7		17.6	22.0	6.1													
6-1	7	13.0	6.4	11.0	2.4	10.0		17.5	19.9	7.1													
6-1	11	11.1	4.6	8.1	2.3	13.5		17.8	18.2	5.0													

DOE ARCHIVES



TABLE III

Dosage Spectra in Per Cent of Dosage per 0.1 Mev  
Energy Interval for Several Samples, Each Recorded  
at Approximately 17 Days after Detonation

Days After Shot	0	.1	.2	.3	.4	.5	.6	.7	.8	.9	1.0	1.5	2.0	2.4
Sample	1-L	17	2.6	2.6	2.9	2.4	9.7	7.0	7.3	17.2	10.2	38.1		
	2-1	17	7.3	2.8	4.6	4.2	19.2		3.0	20.5	3.4	35.0		
	2-2	18	6.4	2.7	5.0	3.1	18.9		14.7	19.8	5.2	24.2		
	3-1	17	12.4	10.8	3.2	10.3	17.3			11.4	6.4	21.9	6.3	
	3-4	17	17.1	8.0	7.2	12.2	16.3		11.0	11.8		14.0	2.4	
	4-1	17	8.6	4.6	8.1	3.5	15.6		5.4	13.5	5.8	34.9		
	4-2	17	11.1	4.4	7.7	3.6	17.0		8.1	14.6	6.6	26.9		
	4-3	17	13.4	4.1	7.4	3.4	15.5		5.0	17.0	6.9	27.3		
	5-1	17	7.0	2.9	5.8	2.9	19.2		10.0	16.5	7.5	28.8		
	6-1	20	9.4	4.4	6.4	3.7	16.6		11.6	17.4	6.6	23.9		

DOE ARCHIVES

146

150

ATOMIC ENERGY

To answer questions regarding variations in spectra from different detonations of the CASTLE series, intercomparisons have been made in the vicinity of 8 days following the detonation and 17 days following the detonation. These are respectively recorded in Tables II and III. Where a measurement at 8 days or 17 days was not available, measurements are shown at the nearest data recording time.

It will be noted that the spectra of all samples except those from Shot 3 show considerable agreement. Only from Shot 3 were radiations noted of energy higher than the 1.59 Mev  $\text{La}^{140}$  gamma-ray. No information is available to indicate the source of these radiations.

Energy and rate of decay measurements of the total absorption peaks allow most of the peaks of the spectrum of sample 4-L to be associated with particular radioisotopes. In the low-energy region, peaks were found whose energies and decay characteristics identified them with either  $\text{Np}^{232}$  or  $\text{U}^{237}$ . Otherwise the identified peaks are associated with known fission products. Figure 5 indicates the relative contribution to the dosage spectrum. All peaks can be identified, with two exceptions. The contributions of the unidentified peaks are indicated by curves X and Y.

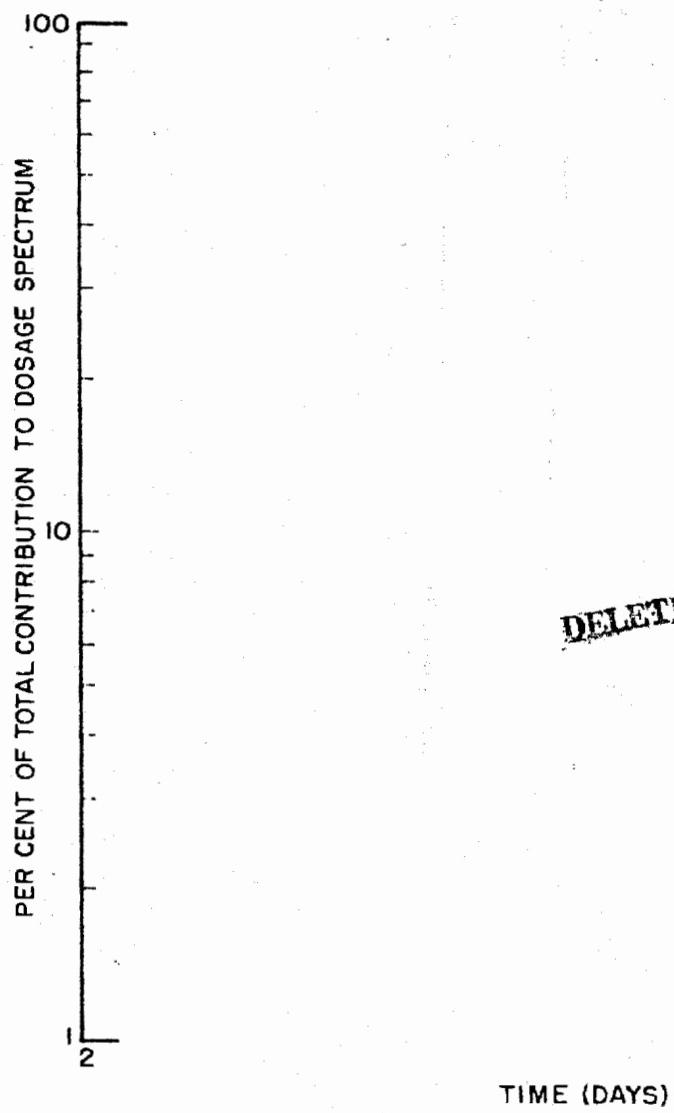
The results plotted in Fig. 5 are in reasonably good agreement with Heiman's predictions. The chief exceptions are the presence of two unknown radiations, X and Y, and the absence of iodine, also noted in the UPSHOT-KNOTHOLE report.

The unknown line, X, at approximately 75 to 85 kev, possesses decay characteristics similar to those of the  $\text{Ba}^{140}\text{La}^{140}$  gamma-ray lines. In line with prior discussion it appears that at least part of this line may be spurious, attributable to the effect of a lower absorption coefficient immediately below the energy of the lead K-shell absorption edge. Although it makes an appreciable contribution to the quantum spectrum, its contribution to the dosage spectrum is quite small.

The higher energy unknown line has a half-life of approximately seven days. Its energy is not known uniquely since it appears in a group of at least three lines which overlap in the pulse height spectrum. However, if the total area under these lines is plotted as a function of time, normalized to the standard  $\text{Cs}^{137}$  peak, two half-lives expected in this energy region from the fission products and the unknown seven day half-life are observed. A search for possible sources of this gamma-ray was not too successful. One of the few which appeared feasible was the decay of  $\text{Bi}^{206}$  to  $\text{Fb}^{206}$ . It appears possible to fit the radiations of  $\text{Bi}^{206}$  into the pulse height gamma-ray analysis for sample 4-L.

Gummed paper samples were placed for observation in a test tube having walls  $0.028 \text{ gm/cm}^2$  thick. The aluminum cover for the

DOE ARCHIVES  
DOE ARCHIVES



DOE ARCHIVES

Figure 5  
Relative Contributions to the Dosage Spectrum

148

crystal was  $0.068 \text{ gm/cm}^2$  thick and the MgO powder reflector approximately the same as the aluminum. No betas having energies less than 500 kev should penetrate this material. However, there are several fission products, whose gamma-rays were observed in the spectrum, which emit beta radiation whose maximum energy end point is above 500 kev. To see whether a sufficient number of beta particles are able to get into the crystal to produce an error in the gamma-ray dosage spectrum, a number of tests were made in which the gamma-ray pulse height spectrum was recorded, both in the normal manner and with an aluminum cap whose minimum wall thickness was  $0.880 \text{ gm/cm}^2$  covering the end of the Lustroid test tube. Typical plots are shown in Fig. 6 of the results in the low energy region at times when beta energies up to at least 1.5 Mev are expected. The black line is the spectrum as recorded without the aluminum cap and the white line as recorded with the aluminum cap. The only difference is observed below 75 kev and this can be explained by the absorption of the low energy gamma radiation in the aluminum cap. Therefore, it is concluded that no correction is required for the underlying continuous beta spectrum in the pulse height spectrum, and no such correction was made in this study.

The Shot 1 samples of radioactive coral from the four locations of Table 1 were initially treated as four radioactive sources. From three to six pieces of coral had been removed from each gummed paper and collected together as individual samples for analysis in the pulse height spectrometer. Although similar spectra were obtained, there were sufficient differences to introduce questions regarding possible fractionation of the samples as a function of position of the sample collector. Because of these differences, the pulse height spectra from individual coral particles were observed. The particles were found to fall into two classifications with regard to spectra, and both classifications appeared both downwind and crosswind. The two general types of pulse height spectra, henceforth called type 1 and type 2, are shown in Figs. 7 and 8, respectively. The spectrum of type 1 appears to consist primarily of radiations from  $\text{Ba}^{140}\text{La}^{140}$ , with perhaps a small amount of  $\text{Zr}^{95}\text{Nb}^{95}$  radiation. On the other hand the spectrum of type 2 shows very little  $\text{Ba}^{140}\text{La}^{140}$  radiation, but sizable quantities of  $\text{Ru}^{103}$ ,  $\text{Zr}^{95}$ , and  $\text{Nb}^{95}$  radiations.

DOE ARCHIVES

These measurements begin at approximately five days after detonation. Source spectral measurements should be made at earlier times. Such measurements are contemplated for Operation TEAPOT. Overlapping times with the currently reported measurements will allow comparisons between low and high yield weapons. Although there is no reason to believe that there should be any drastic difference except for differing amounts of induced activities, spectral measurements at times corresponding to the currently reported measurements will be made.

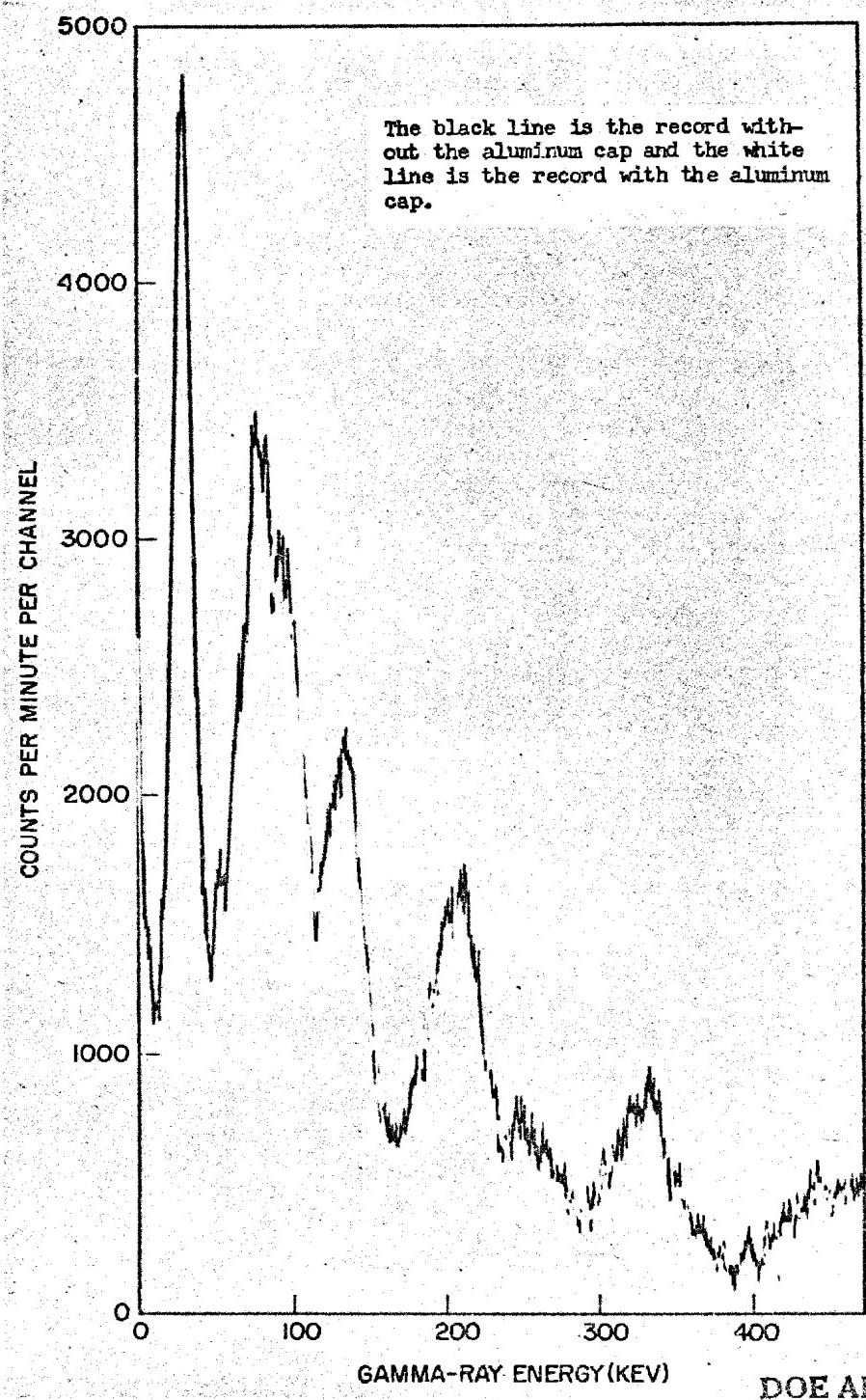
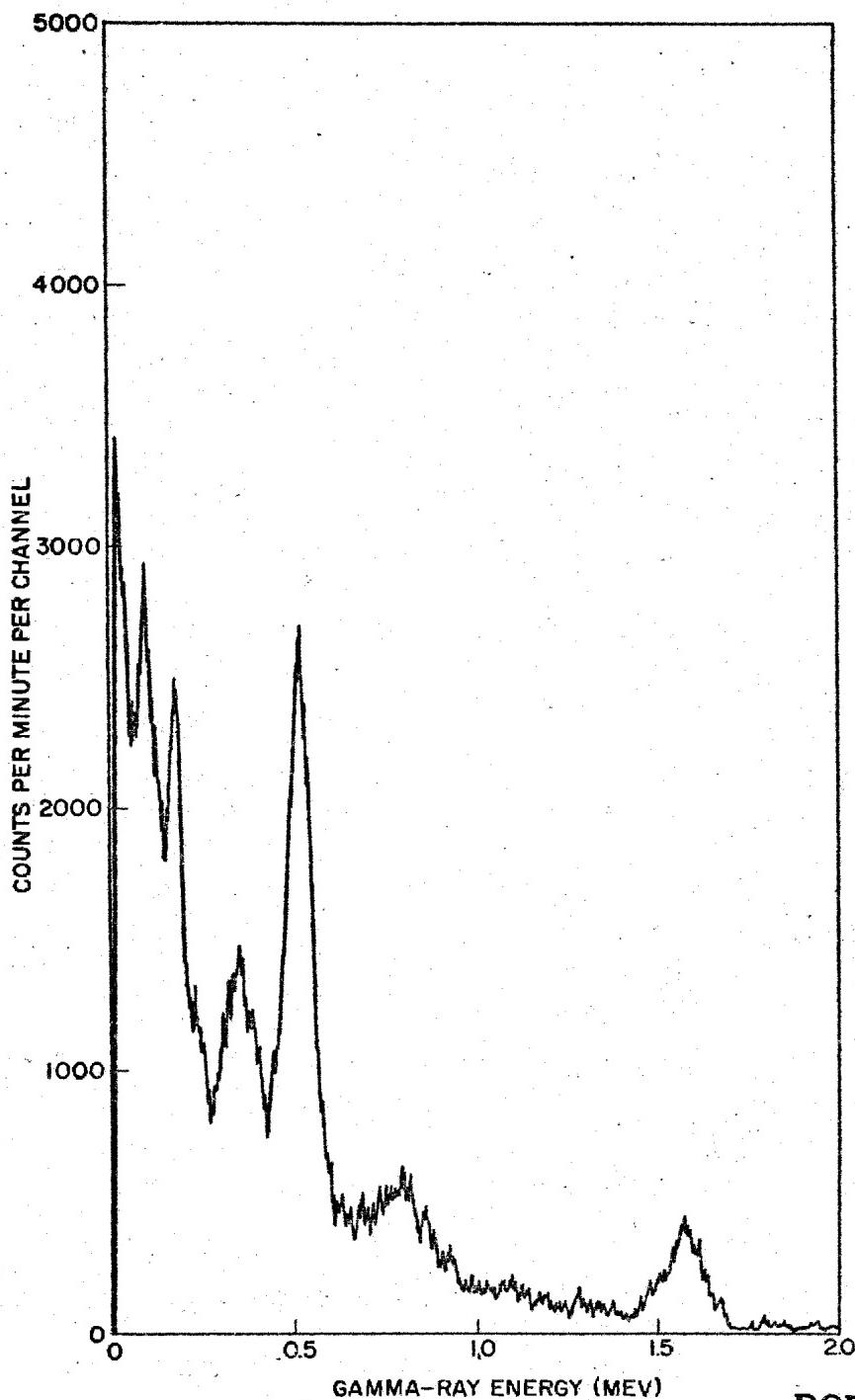


Figure 6  
Low Energy Region Spectra

150

ATOMIC ENERGY ACT

154



DOE ARCHIVES

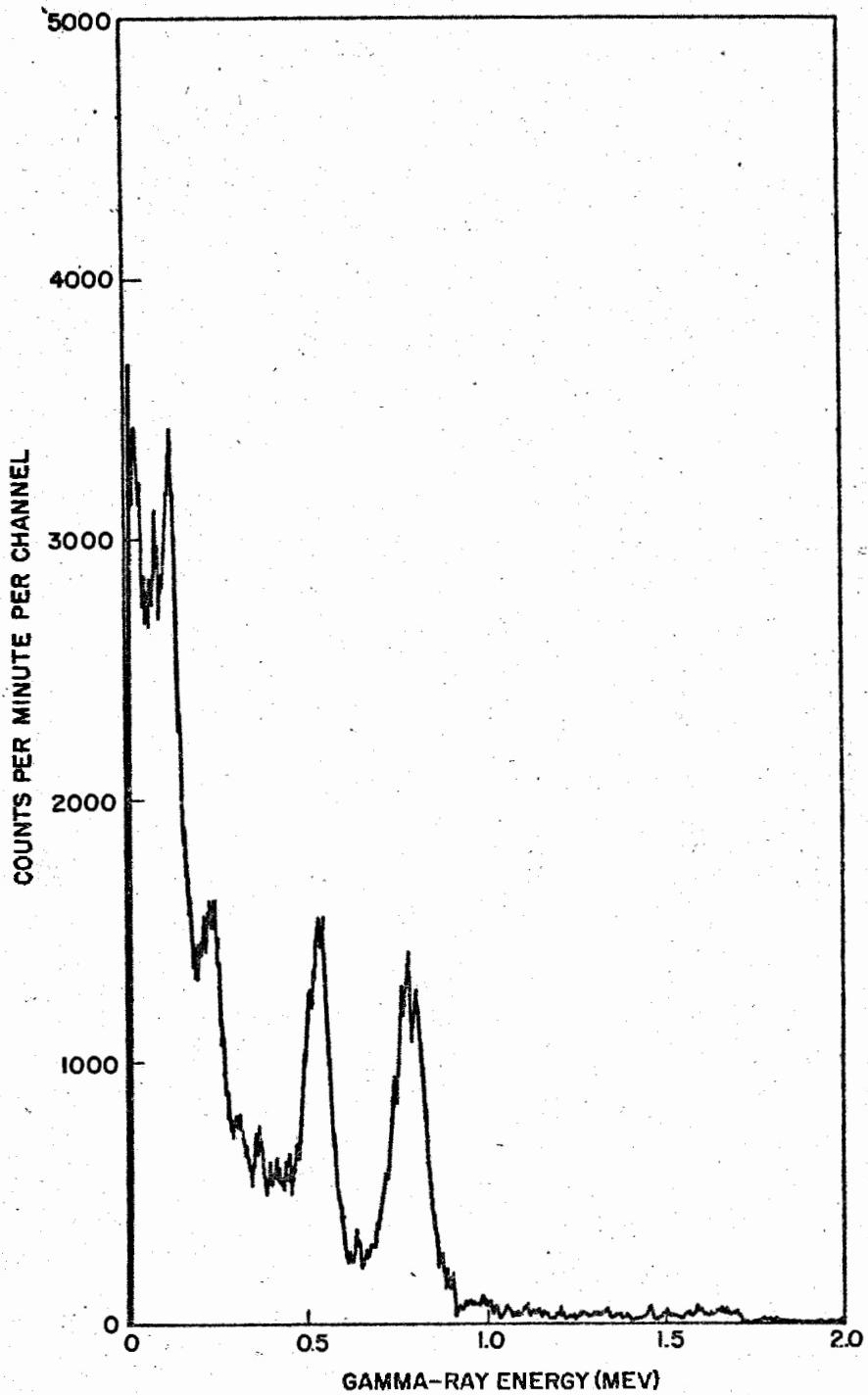
Figure 7  
Type 1 Pulse Height Spectrum

151

~~CONFIDENTIAL~~

~~DATA~~  
NUCLEAR ENERGY ACT 1954

155



DOE ARCHIVES

Figure 8  
Type 2 Pulse Height Spectrum

152

ATOMIC ENERGY

156

Controlled experimental determinations of the spectra from distributed sources are also needed. These are relatively straight forward, although time consuming once experimentally determined source spectral characteristics are known. A limited amount of this type of information can be obtained at weapons effects tests, and some measurements of this type will be made at TEAPOT.

DOE ARCHIVES

153

OMIC ENERGY ACT

157

THIS PAGE IS BLANK

DOE ARCHIVES

154



158

RADIOLOGICAL NATURE OF THE CONTAMINANT;  
DECAY OF THE GAMMA RADIATION FIELD

N. E. Ballou  
U. S. Naval Radiological Defense Laboratory

It is the purpose of this paper to present a general discussion of decay and radiation characteristics of nuclear weapons debris and to report on the results of measurements of these characteristics of fallout material produced in Operation CASTLE. It is clear that the decay and radiation properties of nuclear bomb debris are necessarily among the predominant determinants of radiation hazards resulting from such detonations, and thus good information on them is required for many purposes.

The contributing species to the radiation field consist of fission product radionuclides in addition to other radionuclides formed by neutron induced reactions. The relative amounts of the various fission products are determined by their fission yields; the fission yields are functions of the identity of the nuclide undergoing fission and the energies of the neutrons causing fission. The non-fission product radionuclides result from neutron reactions with the components of the nuclear devices and with the environmental materials in the detonation area. The relative amounts of these products depend on the quantities of material exposed to neutrons, the cross-sections for the reactions producing them, and the total number of neutrons to which the material is exposed.

Determination of gross decay curves from nuclear detonations can be made either by direct observations on the debris or by calculations. In order to calculate a gross decay curve, knowledge of the yields and half-lives of all contributing radionuclides must be known. At the present time, there is much good information available on yields and half-lives of fission products whose half-lives are approximately one hour or longer. The yields of neutron induced radionuclides vary from one weapon type to another and with the nature of the surrounding detonation medium. The contributions of induced radionuclides have been determined radiochemically in a large number of nuclear detonations. Under most circumstances, the major contributors are those derived from the components of the nuclear weapon and only to a small extent from the materials present in the detonation area.

DOE ARCHIVES

It is of importance to measure the gross decay curves from various nuclear detonations and to compare them to the calculated curves. The main cause of lack of agreement between such curves would be the use of inaccurate fission yield and half-life values in the calculations and

the existence of fractionation among the products of a nuclear detonation. Since half-life and yield values are believed to be fairly well known, fractionation is the most likely source of discrepancy. Fractionation has been observed radiochemically in some detonations, especially in the surface type shots. This was markedly demonstrated in measurements on Operation JANGLE debris.

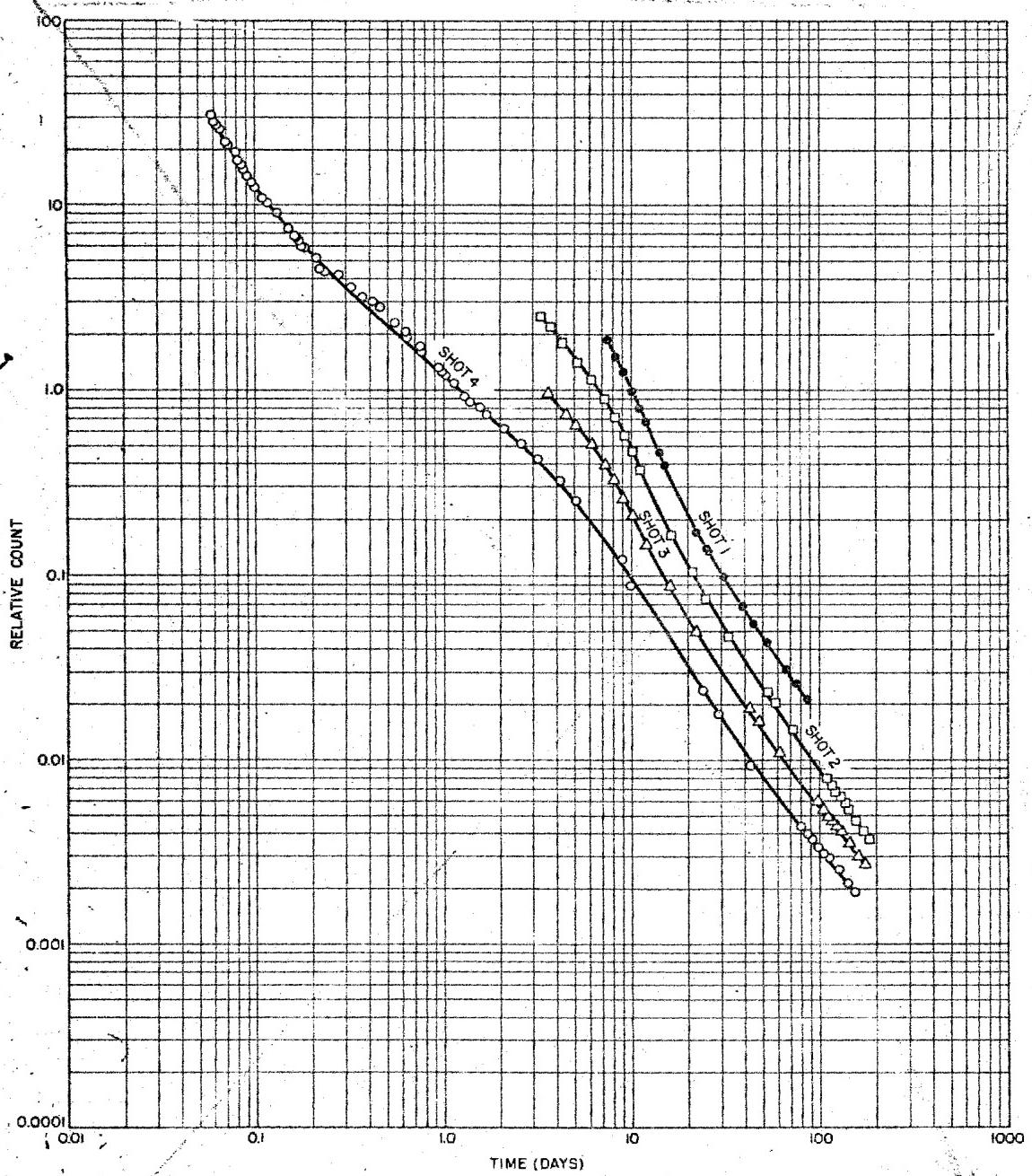
Because of these and other considerations, it seemed worthwhile to measure the gross decay curves of material resulting from Operation CASTLE. Both beta and gamma ray decay curves were measured. In order to obtain information on beta and gamma ray energies as a function of time, decay rates were measured with various lead and aluminum absorbers placed between the sample and detector. The measurements were started at the site as soon after detonation as possible and were eventually continued at USNRDL. The beta and gamma ray decay curves (Figure 1 and Figure 2, respectively) have the same shape except at longer times, approximately two weeks, at which times the gamma curves have a somewhat steeper slope. Although the gamma ray counting rates were rather low by this time, the differences may be real. Computations of the gamma ray decay curves have not been completed, consequently, the extent of similarity to be expected between the beta ray and gamma ray decay curves is as yet not known. In order to compare beta ray disintegration rate and gamma ray ionization decay curves, measurements of these two were made at the site for approximately two weeks following detonation. The shapes of the two were the same. Comparisons between observed and calculated beta ray decay curves (Figure 3) show that there is moderately good agreement among these curves. Absorption curves on samples of fallout material gave information on beta ray and gamma ray energies. Although details cannot be derived from the curves, the expected occurrence of soft and hard beta and gamma ray components was found. The results are in general agreement with the more detailed information on energies obtained from spectral measurements, as reported by Dr. Cook in the preceding paper.

**DELETED**

**DOE ARCHIVES**

The slopes of the logarithmic beta ray decay curves can be approximated by certain values over given periods of time. For most of the CASTLE shots, the slope was approximately -1.0 from about three hours to six days. From

this page stays  
was marked in  
my mistake



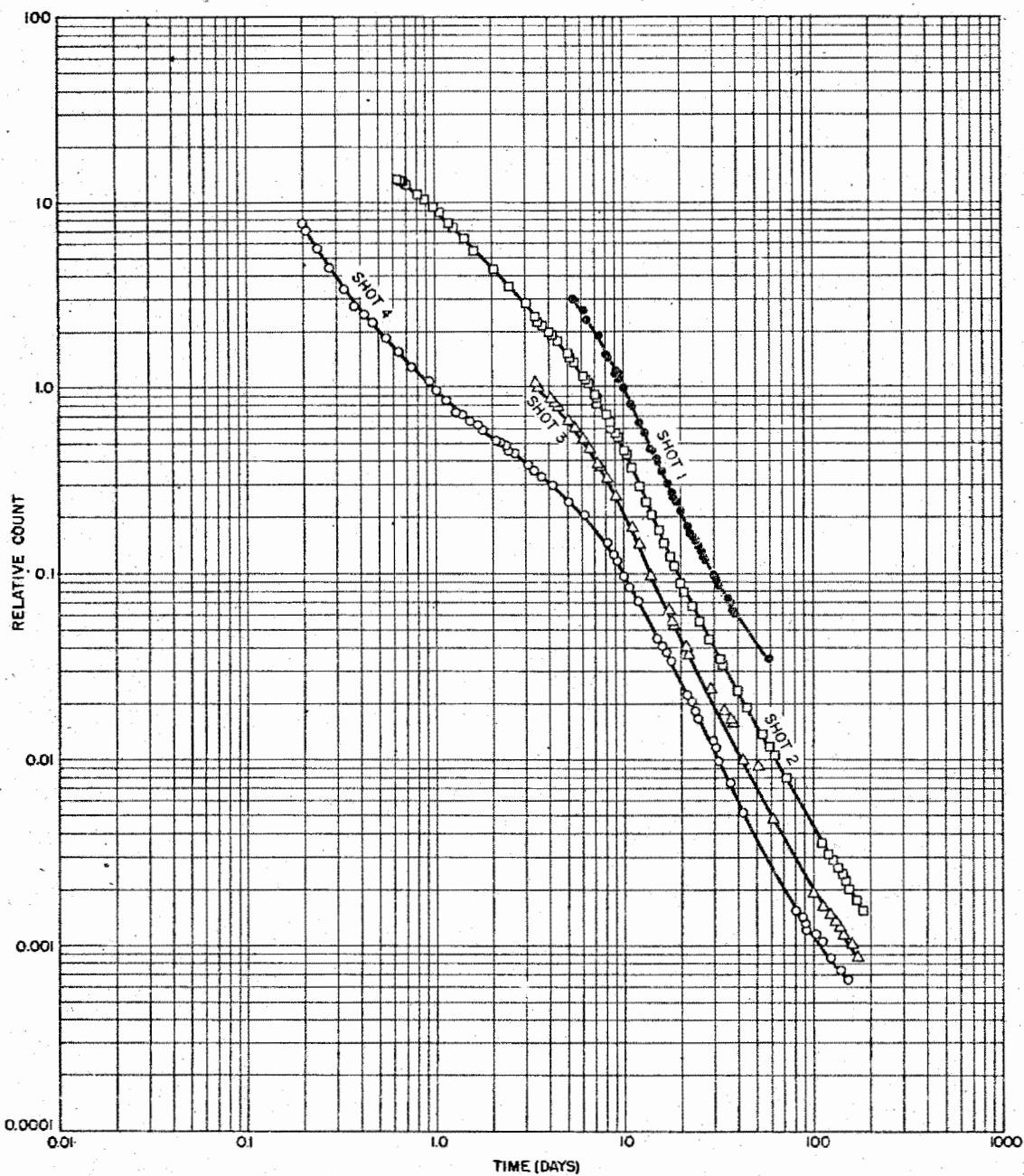
DOE ARCHIVES

Figure 1  
Gross Beta-Ray Decay of Fall-out Samples from Shots 1, 2, 3, and 4

157

OMIC ENERGY ACT

161



DOE ARCHIVES

Figure 2  
Gross Gamma-Ray Decay of Fall-out Samples from Shots 1, 2, 3, and 4

158

A black and white photograph of a bridge at night. The word "STATE" is written in capital letters across the top of the bridge's structure, and the word "ENERGY" is written in capital letters across the bottom. The bridge has multiple arches and is illuminated from below, creating a dramatic silhouette against the dark sky.

162

**DELETED**

**DOE ARCHIVES**

Calculated and Observed Gross Beta-Ray Decay Curves of Fall-out Sample

159

ATOMIC ENERGY ACT 1954

163

six days to fifty days, the slope was about -1.7. The observed slope at the earlier times agrees with the calculated value. The slope at later times is somewhat greater than the calculated value of -1.5.

It is now possible, as a result of radiochemical measurements, to make certain statements about gross decay rates of debris from various types of weapon detonations. Relative production of non-fission product radionuclides is in general greatest with thermonuclear weapons of the type tested so far; is appreciably less with normal fission type weapons; and is very small with the type of gun weapon tested in the UPSHOT-KNOTHOLE test series. Gross beta ray decay curves of debris from representative weapons of these three types are given in Figure 4.

**DELETED**

On the basis of studies made so far, several conclusions can be reached. First, the radiochemical composition of unfractionated nuclear weapons debris is moderately well established for weapons of various types. Second, fractionation of products of nuclear weapons detonation does occur, especially in surface type shots. Third, calculated gross beta ray decay curves agree with the experimentally observed curves for unfractionated material. Fourth, in the absence of well established gamma ray decay curves, calculated beta ray decay curves can be used to approximate the gamma ray decay curves.

In view of the present state of knowledge, it is recommended the following be done in order to obtain necessary information on radiation characteristics of nuclear weapons debris:

Calculate beta and gamma ray energies as a function of time for various weapon types.

**DOE ARCHIVES**

Measure radiochemical composition of debris from nuclear weapons test and determine nature and extent of fractionation.

**DELETED**

**DOE ARCHIVES**

**161**

~~DATA~~  
~~NUCLEAR ENERGY ACT~~

**165**

Figure 4  
Calculated Gross Beta-Ray Decay Curves from Thermonuclear,  
Fission and Gun Type Nuclear Weapons

Measure gamma ray decay curves and energy spectral distributions of nuclear weapons debris and determine extent of agreement between measured and calculated curves.

DOE ARCHIVES

162

RECORDED DATA

SECRET

166

RADIOLOGICAL NATURE OF THE CONTAMINANT; RADIATION  
FIELD GAMMA ENERGY SPECTRA

Mr. Stanley Ungar  
Evans Signal Laboratory

Radiation survey instruments are used in monitoring dose rate levels in contaminated areas. Design requirements for these detectors call for an energy response of  $\pm 20\%$  down to 80 Kev. In order to determine the adequacy of present specifications, a determination of the fraction of the radiation dose due to photons in the energy range below 80 Kev is essential. In addition, knowledge of the spectral distribution of the gamma ray fields is desirable in order to predict the relative biological effectiveness of the radiation. This paper will concern itself with a brief survey of previous field determinations of parameters of the gamma spectra of residual contamination and a summary of the techniques and results of scintillation spectrometer measurements made during Operation UPSHOT-KNOTHOLE.

Several experimental approaches to these determinations have been made. The gamma spectral quality was investigated at Operation GREENHOUSE and at subsequent test operations. Data available have been obtained by essentially three techniques: absorption measurements, energy dependent chambers, and scintillation crystal spectrometers.

Absorption Type Measurements

Depth dose studies have been made by several groups during past operations. In these measurements, dosages are obtained as a function of depth from surface. Pressed wood phantom men and spherical absorbers made of tissue-equivalent or unit density materials are unusable in the field as effective energy measuring devices. Numerous experiments have demonstrated that the shape of the depth dose curve is not very sensitive to the effective energy of the gamma radiation over a wide range of energies. This is due in part to the fact that the radiation is incident on all sides and to the high ratio of scatter to actual absorption taking place. Comparison of various absorption curves indicates that the high surface readings obtained are due to high energy  $\beta$  particles which are rapidly attenuated by the first two  $\text{gm}/\text{cm}^2$  of absorber, rather than low energy gamma radiation.

DOE ARCHIVES ~~STANION HED~~

Aluminum lined and air wall chambers used in depth-dose studies have shown that the effective energy inside the phantom decreased relative to the effective energy of the gamma radiation near the surface of the phantom. This was attributed to the increased effect of scatter within the phantom.

Measurements have also been made with film badges as detectors using copper spheres of various thicknesses around the film as absorbers. The results of measurements of residual radiation quality were expressed in the form of copper absorption curves. No evaluation was attempted, however, of the effective energies of the composite spectra.

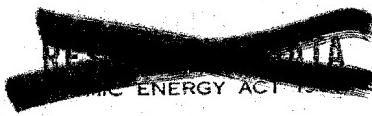
Although these absorption measurements did not provide the gamma spectral distribution or the effective energy of the residual contamination, the depth-dose curves may be of use in themselves for predicting total-body dose from readings of surface detectors. In addition information was obtained regarding the presence of  $\beta$  particles in the soft component of the radiation.

#### Energy Dependent Chambers

Lining the walls of an ionization chamber with a material which is not air equivalent changes the relative response such as to make the instrument energy dependent. This response will depend on the true absorption coefficient of the wall material and its stopping power for electrons. Numerous measurements have been made using ionization chambers lined with materials such as aluminum, copper, tin and lead of various liner thicknesses. Prior to field use, theoretical and experimental curves were obtained for the chamber response as a function of energy, heavily filtered X-ray beams being used in these calibrations as well as any monoenergetic gamma sources available. Field measurements were made using both lined and unlined chambers. The ratio of lined and unlined chambers gave an indication of an "effective" energy of the radiation. The effective energy value at any one time or place was in general somewhat dependent upon the liner material used. This is due in part at least to the fact that instruments calibrated by beams of relatively narrow photon energy distribution were used to evaluate a photon beam containing a broad band of energies. The significance of such effective energy determinations is reduced as the broadness of the photon energy distribution increases. Extensive sets of data on effective energies at various positions and times have been obtained. Effective energies for a number of distances for two shots at Operation GREENHOUSE ranged from 83 to 127 Kev. At Operation JANGLE over a large area of contamination the effective energy measured near a surface burst and an underground burst ranged from 84 to 140 Kev and 113 to 144 Kev respectively. Measurements during UPSHOT-KNOTHOLE gave effective energies ranging from 96 to 230 Kev. The effective energies were highest in the crater and fall-out areas and were observed to decrease for several days subsequent to detonation after which time they increased.

#### **DOE ARCHIVES**

Data obtained during UPSHOT-KNOTHOLE with lined chambers were used to determine mixtures of X-ray beams which would yield results



equivalent to those obtained in the field measurements. These field equivalent X-ray beam mixtures were then considered to be representations of the quality of the gamma radiation. Considering these mixtures, the UPSHOT-KNOTHOLE field results indicated the percentage of energy flux of photons of energy below 200 Kev varied from approximately 5 to 25 percent of the total energy flux.

An attempt was made to obtain more spectral information by extending the lined ionization chamber technique. Here use was made of the fact that the energy response curves of aluminum, copper, tin and lead peak at different energies. An estimate was made of the percent of gamma dose rate contributed by gamma rays of energy less than 200 Kev as well as the approximate spectral extent. The Operation JANGLE results indicated, for a number of locations within several days after detonation in the fall-out area, that the soft component contributed 60 to 70 percent of the total dose for the surface shot and 40 to 50 percent of the total dose for the underground shot and that the hard band extended to beyond 1 Mev in energy. The Operation SNAPPER data indicated that for the times after detonation and distances from ground zero over which measurements were made 15 to 35 percent of the gamma dose was contributed by gamma rays less than 200 Kev in energy. Operation UPSHOT-KNOTHOLE results indicated for the first two days after detonation 9 to 30 percent of the total being contributed by gamma rays with less than 200 Kev energy.

#### Scintillation Spectrometers

Gamma spectral distribution curves were obtained during Operation UPSHOT-KNOTHOLE using a scintillation crystal-type spectrometer. Measurements were made for several shots at various times after detonation and at various distances from ground zero. This instrument is well suited as a field device as it can be made relatively compact with a minimum of shielding and can readily be moved to various locations in the fall-out area. The gamma ray energy distribution was determined over the approximate photon energy range from 40 Kev to 2 Mev. The spectrometer incorporated a low energy NaI-Tl crystal detector head to cover an energy range from 40 Kev to 200 Kev and a high energy anthracene crystal detector head which covered an energy range from 200 Kev to 2 Mev.

DOE ARCHIVES

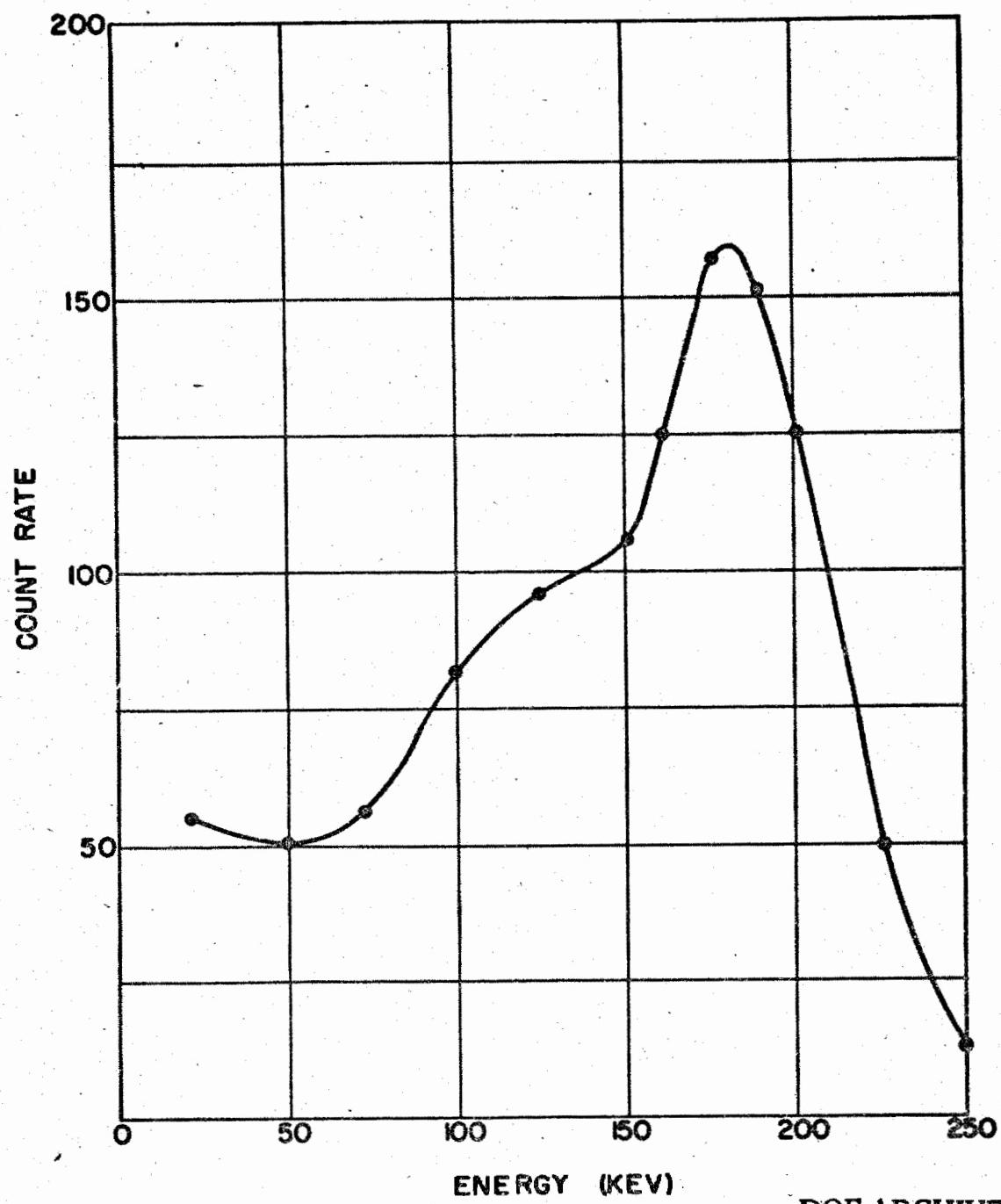
The gamma ray photons incident on the NaI and anthracene crystals undergo photoelectric and Compton absorption, producing secondary electrons. These electrons for the most part are completely stopped within the crystal, giving rise to the emission of a quantity of light of a quality characteristic of the crystal. The integrated light flux of each incident photon is proportional to the energy of the secondary

electron produced. The pulses from the photomultiplier which are amplified are therefore proportional in height to the energies of these secondary electrons produced. Knowing the absorption processes taking place, an analysis of the pulse height distribution of the secondary electrons leads to a determination of the incident photon spectrum. Measurements made were of the detected count rate per channel width versus pulse height using a single channel analyzer.

The response of the NaI-Tl crystal is due predominantly to the photoelectric absorption process, Compton interactions being minimized by low Compton absorption cross section and small crystal thickness (0.2 cm). A thick tin absorber around the crystal decreased the total number of events. In order to correct for Compton electrons due to higher energy photons contributing to the observed pulse height distribution measurements were made with and without a removable tin disc of 1.75 gm/cm<sup>2</sup> thickness over the top face of the crystal and the difference in these two curves was considered to represent the pulse height distribution of the photoelectrons. An In<sup>114</sup> source of known strength was used to absolutely calibrate the NaI crystal used, and to determine energy scale (Figure 1). The effects present and the assumptions employed in the analysis were such as to somewhat over estimate the photon intensity at the low energy end of the spectrum so that if the low energy region of the gamma dose spectral distribution is not of great importance, then it may be concluded that present radiation survey instrument design parameters are adequate.

The portion of the spectrum extending from 200 Kev to 2 Mev was determined using the anthracene crystal. In this energy region Compton absorption predominates and with the anthracene crystal used is the only process of importance. Analysis of the data obtained is based on the assumption that the pulse height distribution due to absorption of monoenergetic photons may be approximated by a rectangle, the area of this rectangle being proportional to the incident photon flux. The gamma ray spectrum is then given by the derivative of the measured pulse height distribution curve, correcting for crystal efficiency and energy scale distortion. Absolute calibrations of the anthracene crystal used were performed using both Co<sup>60</sup> and Cs<sup>137</sup> sources of known intensities (Figure 2). Co<sup>60</sup> was used to determine the energy scale. The calibration procedure was performed both prior and subsequent to each field run in a radiation free area. The assumption of the rectangular distribution limits the resolution of the results in this region although the general shape of the spectrum may be obtained. The intensities measured with the two crystals were normalized using the absolute calibration of each crystal.

DOE ARCHIVES



DOE ARCHIVES

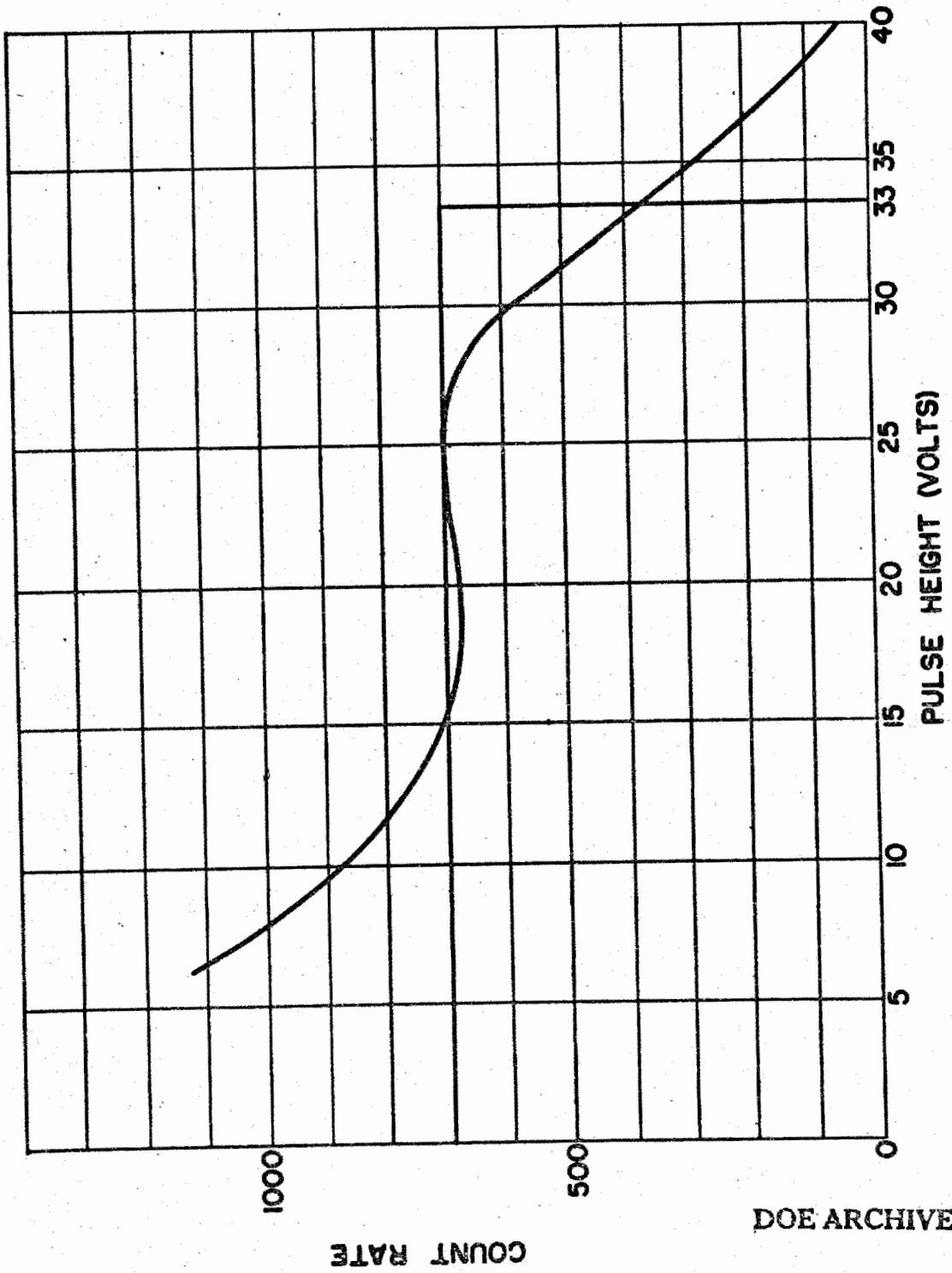
Figure 1  
NaI-Tl Response for In<sup>114</sup>

167

GEORGE

ATOMIC ENERGY ACT 1954

171



DOE ARCHIVES

168

ENERGY ACT

172

Figure 2  
Anthracene Crystal Response for  $\text{Cs}^{137}$

Comparison of the results of scintillation spectrometer and lined ionization chamber measurements taken at the same location at the same time showed excellent agreement. Insufficient data was obtained to make any generalizations regarding the variations of spectral quality with distance. Indications were that the spectrum softens for several days subsequent to the shot after which time a progressive hardening occurs. Results (Figures 3, 4, 5, 6) also disclose a large contribution to the gamma dose rate by photons with energies up to approximately 2 Mev. In addition to the low energy peak below 200 Kev, most of the data indicated peaks in the 600 to 800 Kev and 1.5 to 1.8 Mev energy regions. Results indicate that for measurements made on subsequent days and closer distances from the point of detonation, the peak in the highest energy region becomes increasingly important. In general, as was to be expected because of multiple scattering, the contribution to the low energy peak was greatest from the upward direction. It was concluded that for the tower and air detonations following which there was an extensive contaminated area, the contribution to the gamma dose rate by photons with energies less than 100 Kev is but a small percentage of the total. When making gamma measurements in these residual fields, currently used radiac instruments with their associates energy response are adequate. For surface and subsurface detonations the spectral distribution in the fall-out area is significantly altered so that additional information is required before adequacy of radiation detectors under these conditions may be determined.

The use of a total absorption spectrometer for future measurements will enable better resolution of the spectral distribution and eliminate the need for normalization of two crystals, thereby increasing the overall accuracy. It is recommended that these measurements include the energy region down to 20 Kev, that the angular dependence be investigated in greater detail, that more data be obtained regarding the variation of spectral quality with distance from ground zero, and that lined chamber measurements be made simultaneously for the subsurface detonation to enable further conclusions regarding the adequacy of this technique for rapid evaluation of spectral quality. It is further recommended that the spectral measurement be absolute so that a comparison of the integrated dose rate with radiac readings can be made.

DOE ARCHIVES

169

THE SUBJECT DATA

173

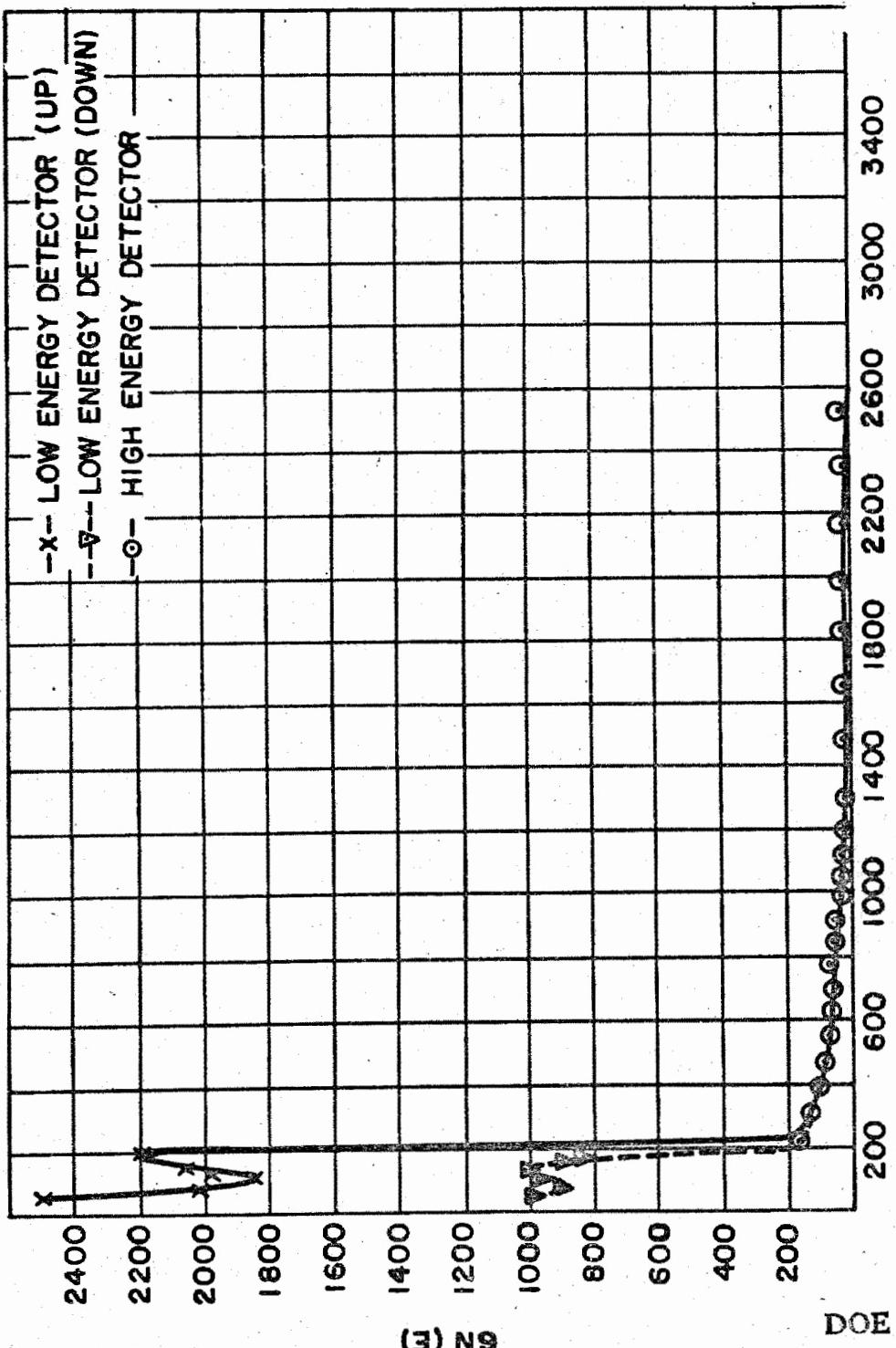


Figure 3  
Photon Spectral Distribution - Shot 8 (D + 2)

REDACTED  
DATA  
ENERGY

170

174

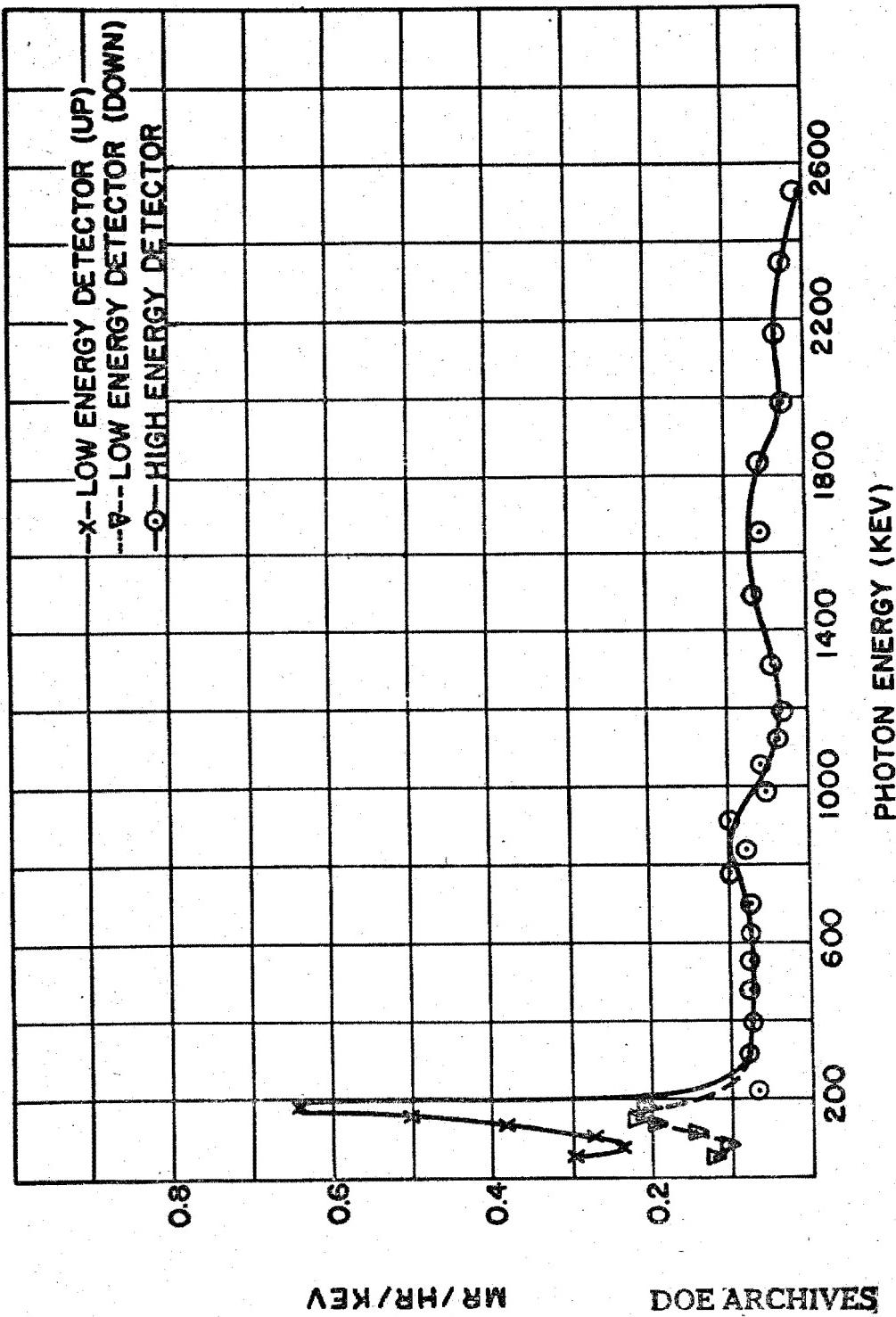


Figure 4  
Dose Rate Spectral Distribution - Shot 8 (D+2)

171

175

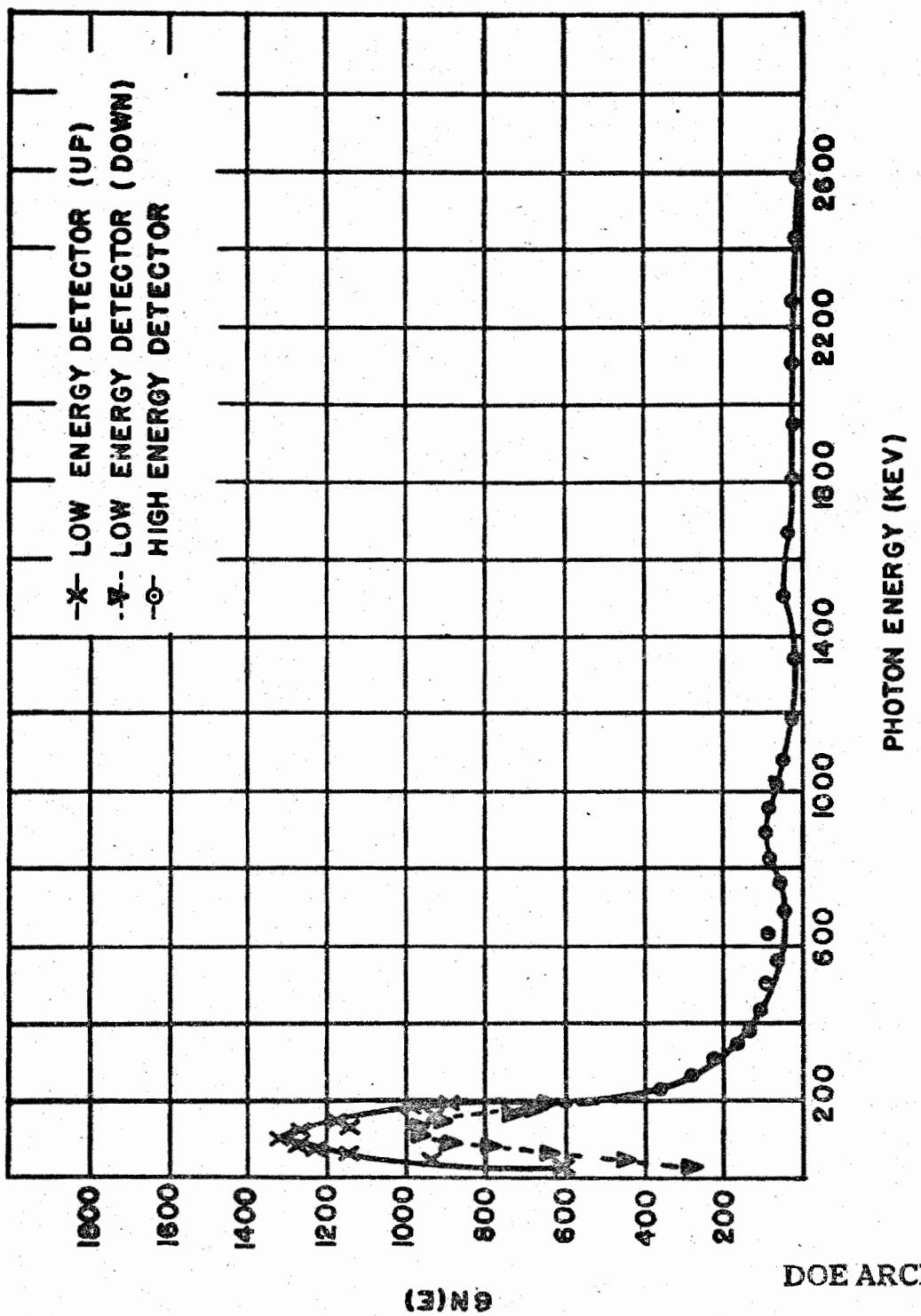


Figure 5  
Photon Spectral Distribution - Shot 11 (D)

~~RESTRICTED DATA~~  
ATOMIC ENERGY ACT 1954

172

~~SECURITY~~

176

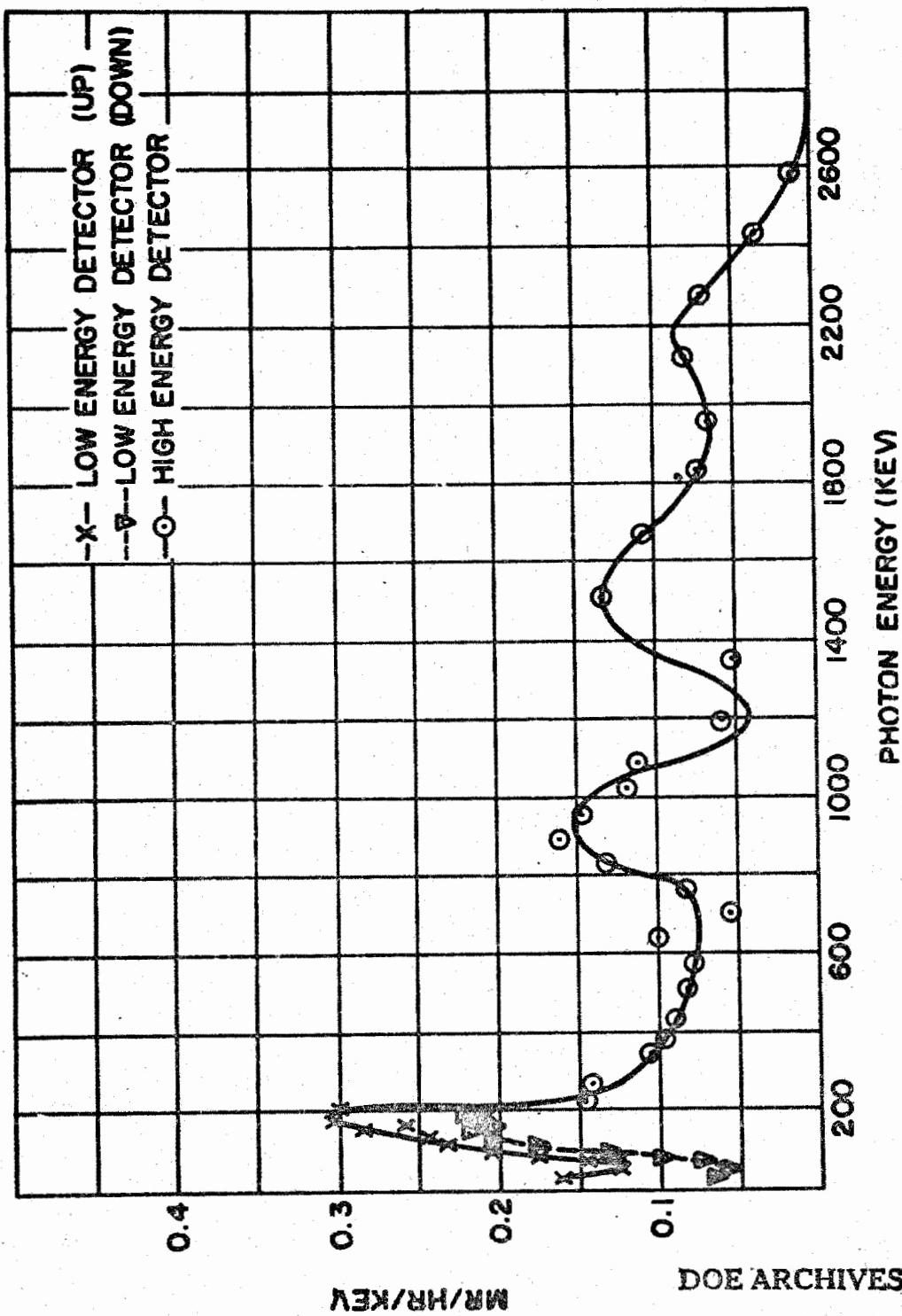


Figure 6  
Dose Rate Spectral Distribution - Shot 11 (d)

**THIS PAGE IS BLANK**

**DOE ARCHIVES**

**174**

**RES**  
A ENERGY ACT 1954

**178**

RADIOLOGICAL NATURE OF THE CONTAMINANT;  
FRACTIONATION OF ACTIVE NUCLIDES WITH DISTANCE

Philip Krey  
Chemical and Radiological Laboratories

Introduction

Before going into the main topic which is, Fractionation as a Function of Distance From Ground Zero, it may be useful to explain what we mean by fractionation. Fractionation is any change in the relative concentrations of the radioactive nuclides present in one sample as compared to another sample of the same event. It is a relative concept such that one nuclide cannot fractionate alone but must fractionate with respect to another constituent in the same sample. For example, consider the hypothetical situation shown in Table I. The  $Ba^{140}$  activity in sample 1 is four times the  $Sr^{89}$  activity and twenty times the  $Ce^{144}$  activity. In sample 2 the magnitude of these activities have changed but their relative concentrations are the same. Consequently, there is no fractionation. In sample 3,  $Ba^{140}$  activity is still four times the  $Sr^{89}$  activity but the  $Ce^{144}$  activity has increased from one-twentieth to one-fourth of the  $Ba^{140}$  activity. Here there is fractionation.  $Ce^{144}$  fractionates with respect to  $Sr^{89}$  and  $Ba^{140}$  in sample 3 as compared to the other two, but the  $Sr^{89}$  and  $Ba^{140}$  still do not fractionate with respect to each other.

Table 1 - Activities in Microcuries

DOE ARCHIVES

Nuclide	Sample 1	Sample 2	Sample 3
$Sr^{89}$	10	1.0	0.10
$Ba^{140}$	40	4.0	0.40
$Ce^{144}$	2	0.2	0.10

Fractionation between samples can be identified in three ways. First, a radiochemical analyses of the samples, as would be expected, reveals this effect. Secondly, different decay rates between samples indicate corresponding changes in the relative concentrations of the radioactive nuclides present. Small variations in decay rates signify large changes in the radiochemical composition. The dosage accumulated over a period of time is also very sensitive to decay rates. For example, if we are given the dose rate in an area at ten days after detonation and if we assume that the dose rate decayed as the equation,

$D = kt^{-n}$ , what would be the dosage accumulated by a person in this area during one to ten days? A change in the exponent from 1.2 to 1.4 increases the accumulated dose by 28 per cent. An increase in the exponent from 1.2 to 1.7 doubles the cumulative dose over this same period of time. Finally, different energy spectra (either beta or gamma) between samples indicate that fractionation has taken place.

This phenomenon of fractionation has received considerable attention in the last few years of atomic weapons testing. Oddly enough there is only a limited amount of data describing this behavior as a function of distance from ground zero. However, if fractionation can be shown to be dependent upon such variables as particle size of fall-out, altitude in the cloud, and time of collection after shot, then its dependence upon distance from ground zero is a necessary conclusion. This follows because each of the previously mentioned conditions will of itself produce fractionation with distance from the point of detonation. Therefore, a review of the existing data from previous operations is in order to point out the frequency and magnitude of these effects.

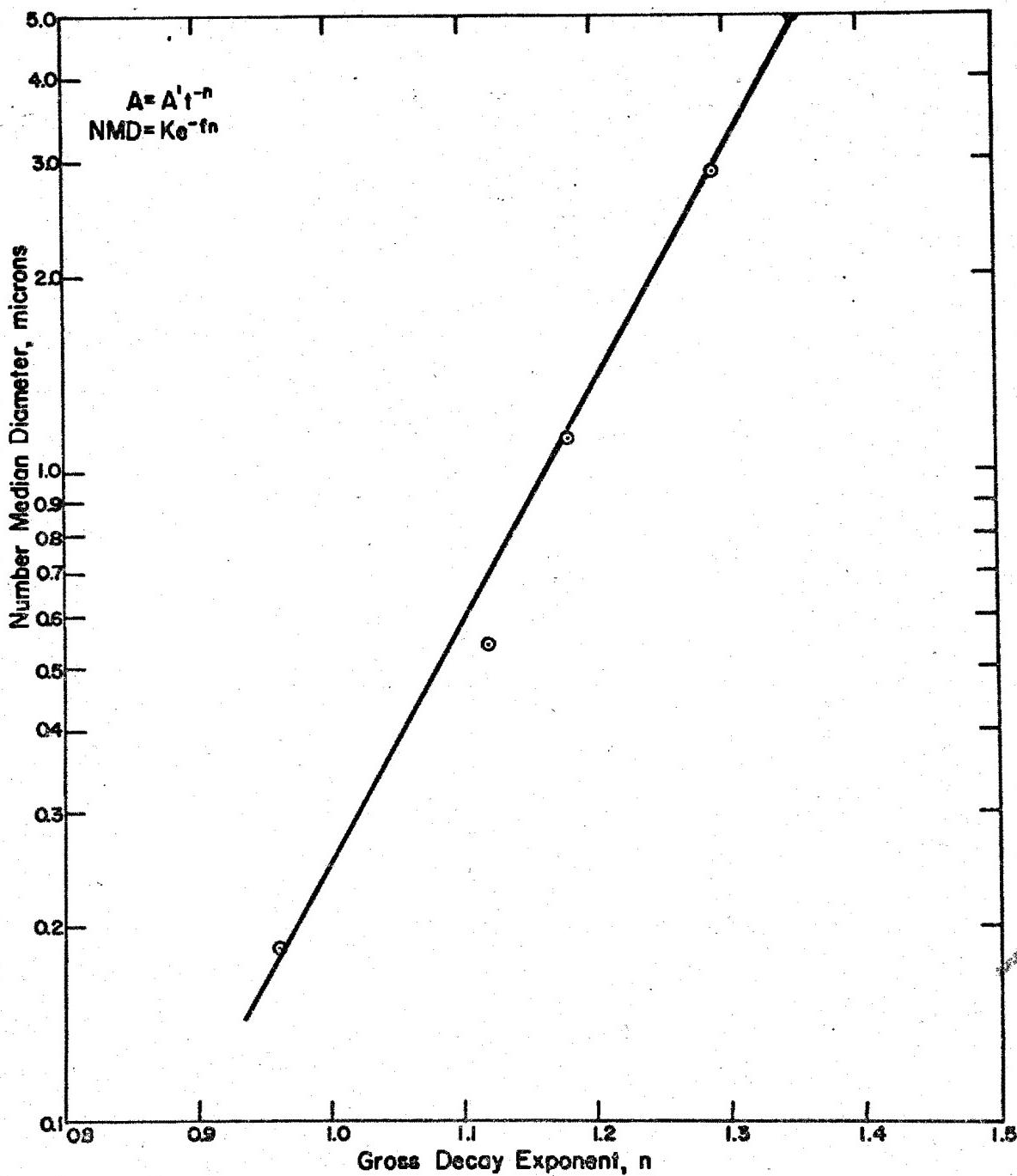
#### Experimental Data and Discussion

##### Operation GREENHOUSE

Fractionation at Operation GREENHOUSE was clearly established. The dependence of radiochemical composition on particle size is shown by the cascade impactor data presented in Figure 1. The cascade impactor separates particles below 10 microns into size ranges by the impaction of each size range on separate glass or plastic slides. The gross beta decay of each slide was measured from about 250 to 1300 hours after shot time and it followed the equation,  $A = A't^{-n}$ . A definite relationship existed between the exponent ( $n$ ) of the decay equation and the particle size on the slide. In this figure, the logarithm of the number median diameter is plotted against the exponent ( $n$ ). The number median diameter is that diameter for which 50 per cent by number of the particles measured are less than this size. The actual relationship is  $NMD = k e^{fn}$ . This particular cascade impactor sampled the Dog shot cloud at 30,000 feet. Similar relationships were found in the Easy and George shots at this operation.

DOE ARCHIVES





DOE ARCHIVES

Figure 1

177

181

**DELETED**

**DOE ARCHIVES**

178

~~RESTRICTED~~

182

**DELETED**

Table 3 - Relative Fractionation

	Ce <sup>144</sup> / Mo <sup>99</sup>	Zr <sup>95</sup> / Mo <sup>99</sup>	Ba <sup>140</sup> / Mo <sup>99</sup>	Ag <sup>111</sup> / Mo <sup>99</sup>	Cd <sup>115</sup> / Mo <sup>99</sup>	Sr <sup>89</sup> / Mo <sup>99</sup>
<b>Surface Shot</b>						
Crater Area	1	1	0.6	0.7	0.4	0.1
Low Altitude	3.4	1.3	0.5	1.5	2	0.3
High Altitude	1.8	0.9	4	4.6	6	7
Long Range (1200 mi)	1	1	6	8	8	10
<b>Underground Shot</b>						
Crater Area	0.8	0.7	0.5	0.3	-	0.1
Low Altitude	1.3	1.0	9.3	12	9	8
High Altitude	1.5	1.8	46	28	29	96
Long Range (1200 mi)	17	11	97	55	-	200

**DOE ARCHIVES**

### Operation JANGLE

The most severe fractionation to date was observed at Operation JANGLE. (Table 3) This table of relative fractionation was calculated by taking the average R values for the different sampling areas and dividing by the corresponding R values obtained at Operation RANGER, Able shot. An R value is the counting rate ratio of two fission products obtained from a shot sample divided by the counting rate ratio of these same fission products obtained from the thermal fission of U<sup>235</sup>.

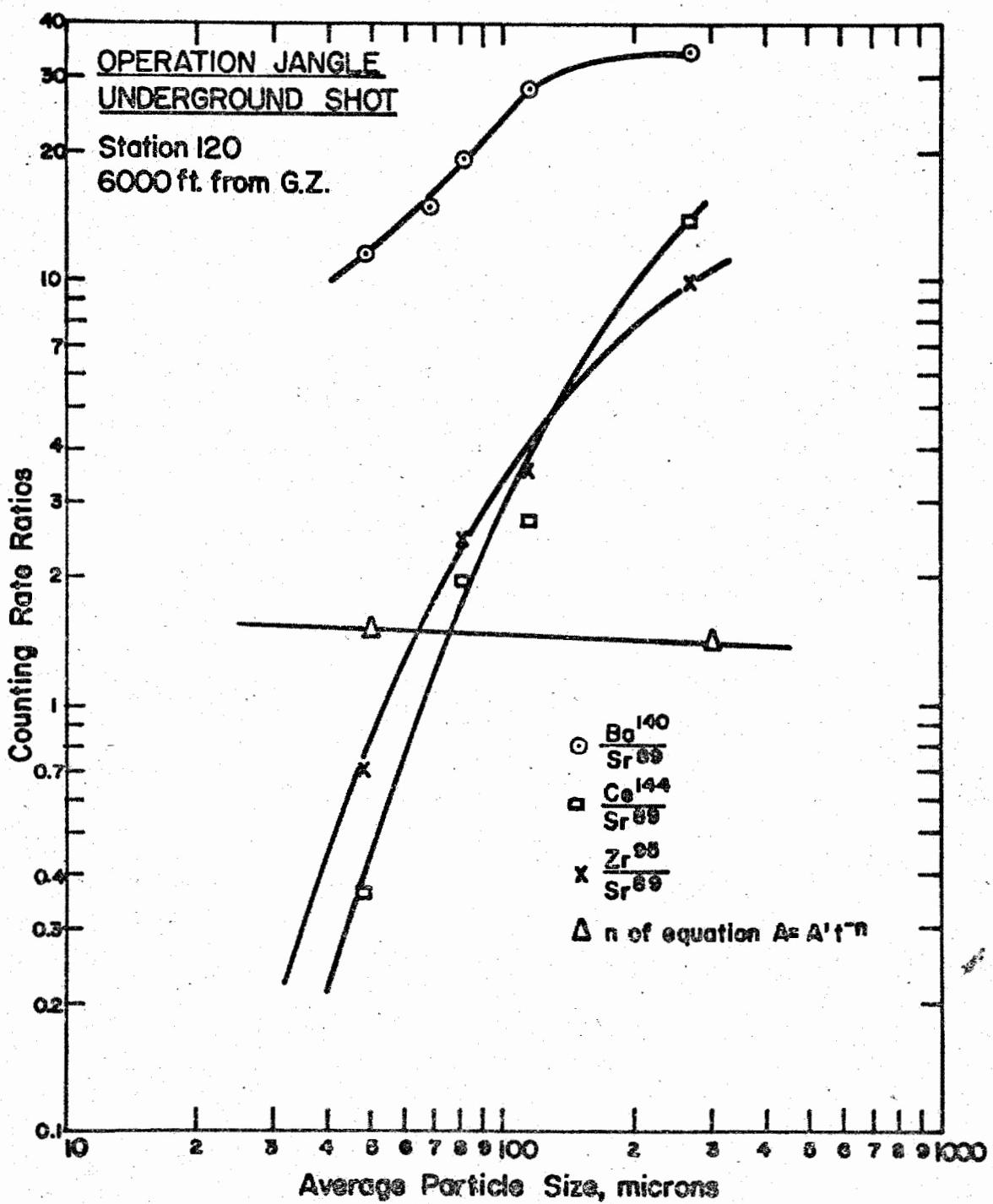
For the surface shot the Ce<sup>144</sup> and Zr<sup>95</sup> to Mo<sup>99</sup> values do not change drastically while the Ba<sup>140</sup>, Ag<sup>111</sup>, Cd<sup>115</sup> and Sr<sup>89</sup> to Mo<sup>99</sup> ratios all show a definite increase with overall distance from ground zero. In the Underground shot all six fission products fractionate with respect to Mo<sup>99</sup> in the same way. The Sr<sup>89</sup> and Ba<sup>140</sup> are the most severe followed by Cd<sup>115</sup>, Ag<sup>111</sup> and then by Ce<sup>144</sup> and Zr<sup>95</sup>. The Ce<sup>144</sup> and Zr<sup>95</sup> to Mo<sup>99</sup> ratios increase at the same rate which indicate that perhaps the Mo<sup>99</sup> activity might be falling off very rapidly with distance from ground zero and causing the ratios to Mo<sup>99</sup> to soar. A similar possibility of an odd behavior of Mo<sup>99</sup> was pointed out in discussing the GREENHOUSE results. Rather than attempt a lengthy explanation here, I would prefer to just mention that the Sr<sup>89</sup> and Ba<sup>140</sup> behavior can be explained on the basis of their relatively long-lived rare gas precursors, Kr<sup>89</sup> and Xe<sup>140</sup>. The fractionation of Ag<sup>111</sup> and Cd<sup>115</sup> to Mo<sup>99</sup> is more difficult to explain since the proper physical properties are lacking.

The dependence of radiochemical composition upon particle size was also verified at JANGLE as shown in Figure 2. This is a log-log plot of fission product counting rate ratios against particle size of the fall-out. The Zr<sup>95</sup> and Ce<sup>144</sup> to Sr<sup>89</sup> ratios behave similarly, both decreasing with decreasing particle size. Ba<sup>140</sup> also follows this trend but not so steeply. It is obvious that if two JANGLE samples did not have the same particle size distribution, there was a corresponding difference in the radiochemical composition. As further support the gross decay of these samples measured from 1000 to 2000 hours after shot did change with particle size. There was a good deal of scatter of the original points but the general trend was as indicated, a gradual increase of the decay exponent with decreasing particle size.

### Operation TUMBLER-SNAPPER

DOE ARCHIVES

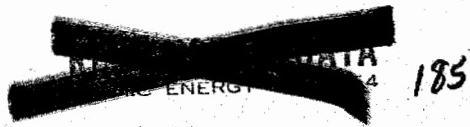
At Operation TUMBLER-SNAPPER, fractionation as a function of distance from ground zero can be clearly seen even though the data are



DOE ARCHIVES

Figure 2

181



185

very limited. (Figure 3) The University of California collected the small amount of fall-out resulting from the tower shot, SNAPPER 6, at downwind distances of almost 60 miles. The logarithm of the average gross decay exponent for each station is plotted against the logarithm of the station distance from ground zero. The general trend indicates that a relatively greater concentration of a faster decaying nuclide or nuclides is present in areas closer to ground zero.

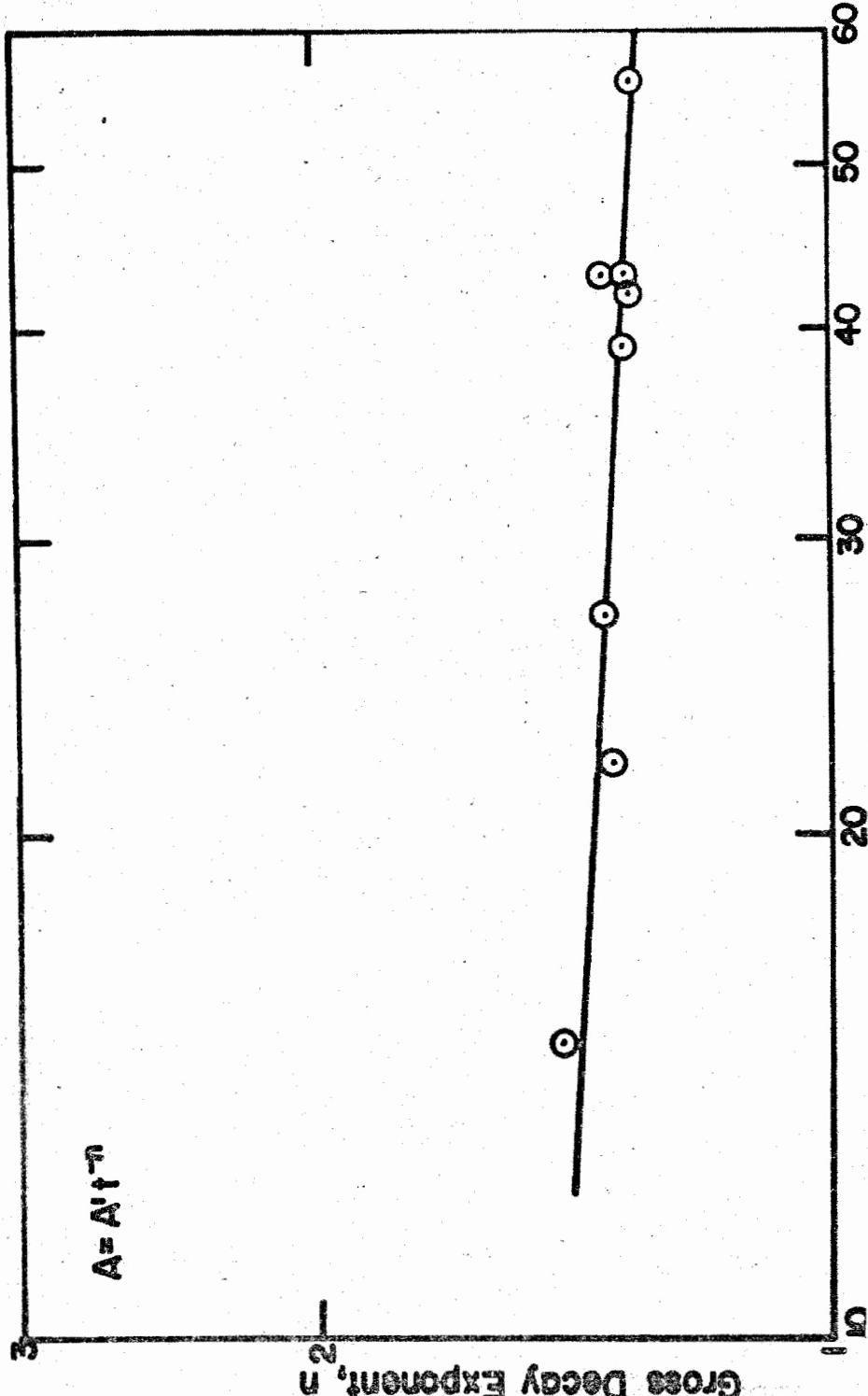
#### Operation IVY

The first large scale thermonuclear device detonated at Operation IVY produced fractionation but it was not well documented. A total fall-out sample was separated into various particle size fractions and the decay rates of each fraction was measured from 600 to 1100 hours after shot. The variation of rate of decay with particle size is shown in Figure 4. Radiochemical analyses for Sr<sup>89</sup>, Zr<sup>95</sup>, Mo<sup>99</sup>, Ru<sup>103</sup>, Ru<sup>106</sup>, Ba<sup>140</sup> and Ce<sup>144</sup> performed on these IVY size-separated samples indicated only a slight amount of fractionation among these nuclides. The radiochemical results cannot explain the decay variations.

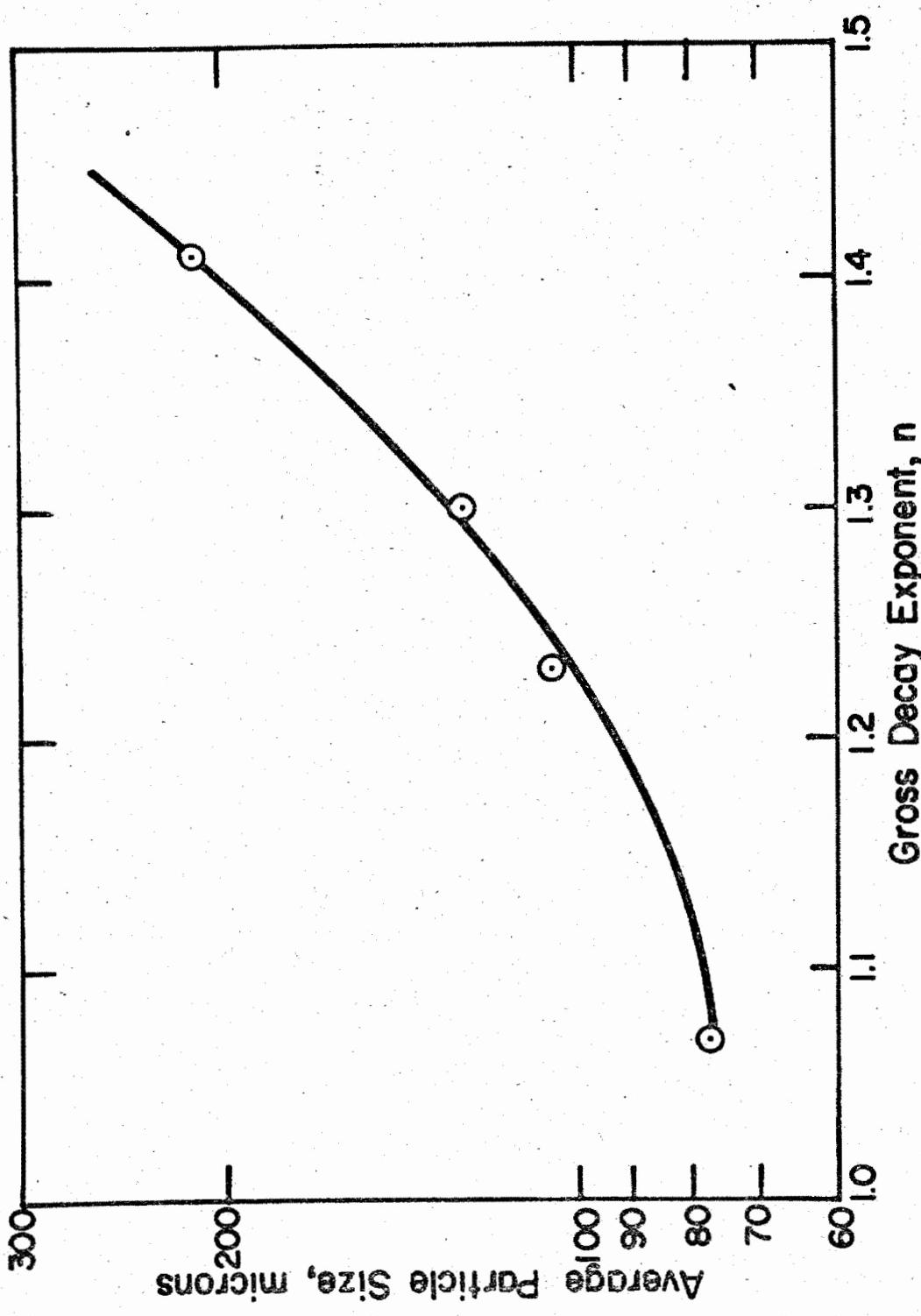
DELETE.

#### Operation CASTLE

Operation CASTLE was much more successful with regard to the study of fractionation. The dependence of radiochemical composition upon particle size of fall-out at Bravo shot is clearly shown in Figure 5. Here the logarithm of the R value is plotted against the logarithm of the particle size. The Ba<sup>140</sup> pattern is the same as the Sr<sup>89</sup> pattern which indicates that Ce<sup>144</sup>, Ba<sup>140</sup> and Sr<sup>89</sup> both Ce<sup>144</sup> fractionate with respect to Ce<sup>144</sup> but they do not fractionate with respect to each other. The Mo<sup>99</sup>/Ce<sup>144</sup> data shows how the relative concentrations of these nuclides vary with particle size. The discontinuity at 50 microns, as was explained this morning by Dr. Barnett, is caused by the methods used to separate the particles of the fall-out into their respective sizes. Here as at JANGLE, samples having different particle size distributions, had corresponding changes in radiochemical composition. The gross beta decay of these samples was measured from 110 days to 170 days after detonation and the exponent of the decay equation ( $A = A_0 t^{-n}$ ) is plotted against particle size. There is good correlation with the radiochemical data and the decay data because any increase in the relative Sr<sup>89</sup> concentration at this time will increase the decay rate of the sample. The contributions of the Mo<sup>99</sup> and Ba<sup>140</sup> have decayed below significant levels, at the time these decay measurements were made.



DOE ARCHIVES



DOE ARCHIVES

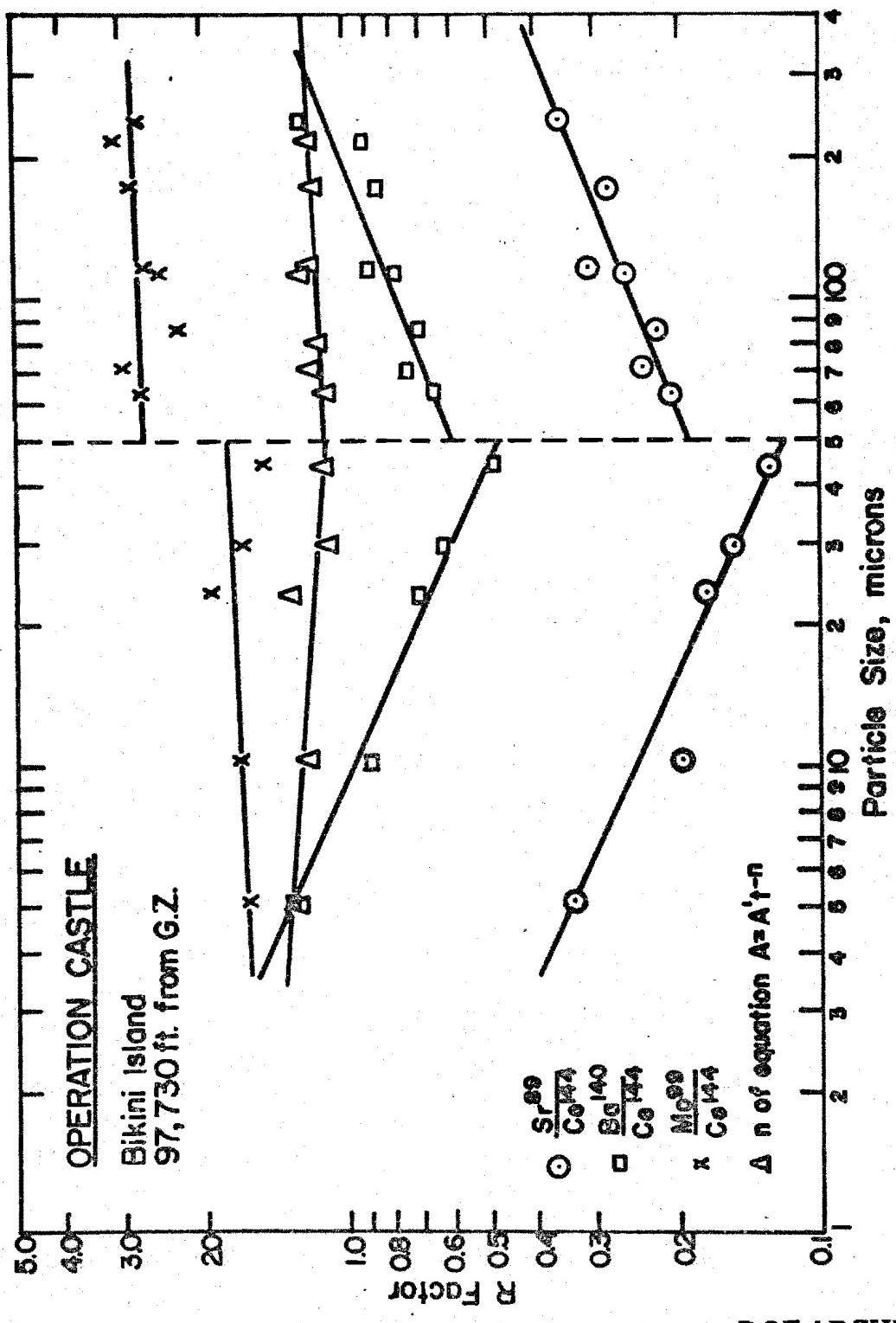
Figure 4

184

ATOMIC ENERGY

188

Figure 5



DOE ARCHIVES

185

SECRET

DATA  
ATOMIC ENERGY

189

Analyses of a few time differentiated samples at Union shot (a surface water detonation) revealed a change in the radiochemical composition with time of collection after shot. Figure 6 is a logarithmic plot of the R values against the time the sample was collected. It can be seen that Sr<sup>89</sup> and Ba<sup>140</sup> fractionate with respect to Mo<sup>99</sup> at different times but are fairly consistent with each other. The Cs<sup>134</sup> data are included but are not too reliable. The gross beta decay of these samples was measured from 7 to 20 days after shot. The exponents of the gross decay equations are also included in this figure to substantiate the presence of severe fractionation.

#### Summary

To summarize briefly, the limited amount of fall-out sampling at significant downwind distances from ground zero indicates that there is fractionation as a function of distance. The existence of fractionation as a function of particle size of fall-out, altitude in the atomic cloud and time of collection lends additional weight to this observation.

Further investigation of this phenomenon is essential for a better understanding of the vital processes that take place following an atomic detonation. Such information has very important applications. How can one confidently predict the residual contamination patterns caused by an atomic detonation under a variety of conditions if he is not certain of how the fission products are associated with the fall-out material? The value of any scaling law suffers when different decay rates of the same isodose line may cause wide variations in the cumulative dose acquired over a period of time. The agencies determining the fission yields of the weapons by radiochemical methods are well aware of the existence of fractionation. For nominal weapons these effects may be significant for only small localized areas. However with the advent of thermonuclear weapons by which casualty producing radiation effects can be realized over a 100 mile downwind direction, the possible effects of fractionation assume alarming proportions. The studies of fireball mechanics and fractionation will proceed simultaneously until a complete understanding of the effects and capabilities of these weapons are realized.

DOE ARCHIVES

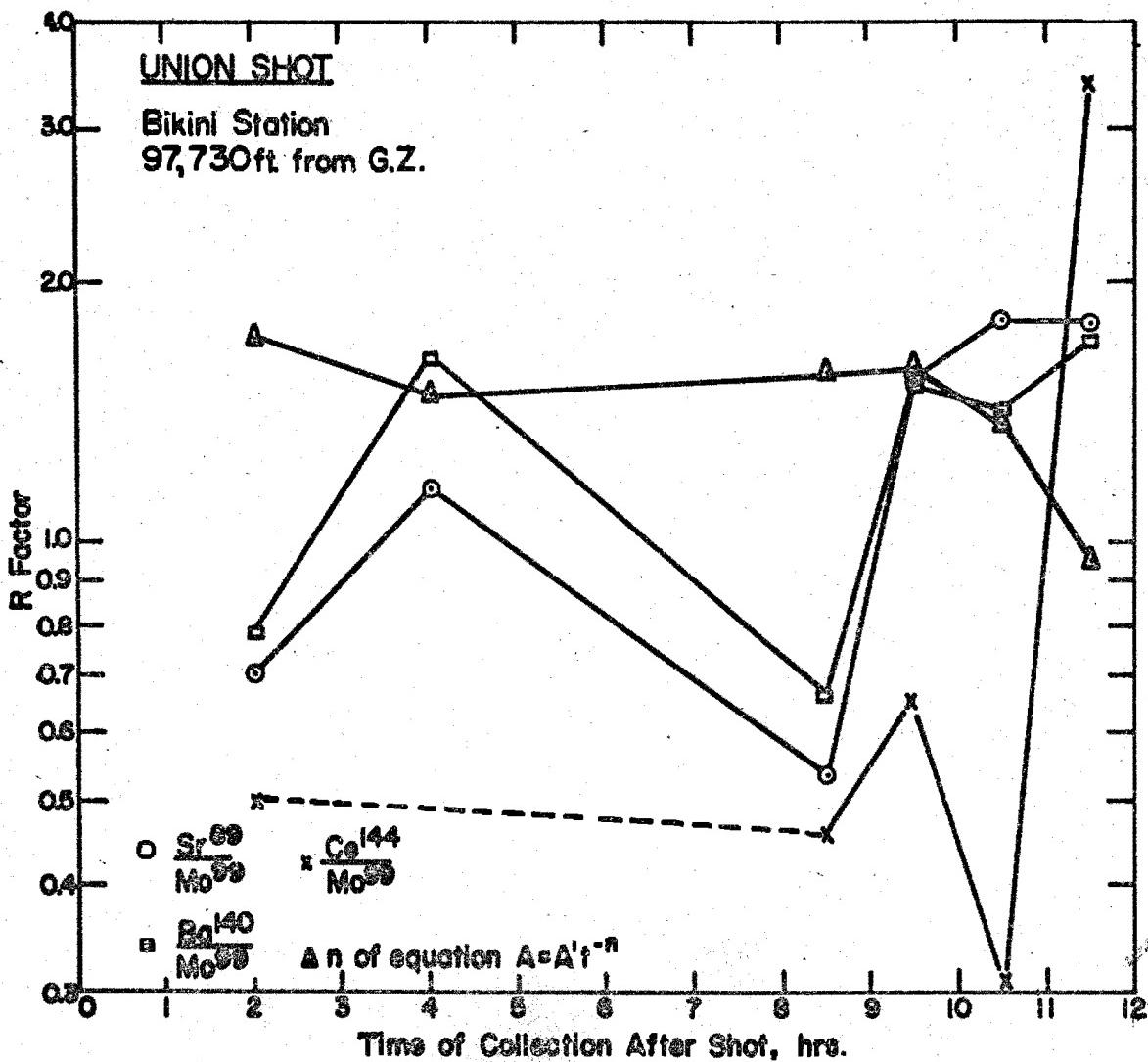


Figure 6

187

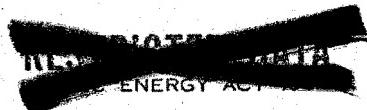
REDACTED  
DOE ENERGY

191

**THIS PAGE IS BLANK**

**DOE ARCHIVES**

**188**



**192**

RADIOLOGICAL NATURE OF THE CONTAMINANT; PERCENTAGE OF  
TOTAL ACTIVITY IN FALLOUT AS A FUNCTION OF HEIGHT OF BURST

Lt. Col. N. M. Lulejian  
Air Research and Development Command

By studying the fallout from the TUMBLER-SNAPPER and UPSHOT-KNOTHOLE atomic test operations, we were able to determine that there was some simple function of the percentage fallout as a function of scaled height. Figure 1A shows this simple curve. We have also plotted in this figure the JANGLE-Surface and JANGLE-Underground as well as the IVY-Mike and the CASTLE-Bravo shots. The data for this curve was obtained from Headquarters, ARDC Report C3-36417 and its supplement, and ARDC Report No. C4-23676. In this work, we define scaled height as  $\lambda$ , where

$$\lambda = \frac{h}{W^{1/3}}$$

$h$  = height of burst in feet above target

$W$  = kiloton yield of bomb

Percentage fallout is defined by  $P$ , where  $P = \frac{\sum AR}{k W^{1/3}}$

where  $A$  = area covered by fallout in nautical square miles

$R$  = dose rate in r/hr at time of fallout

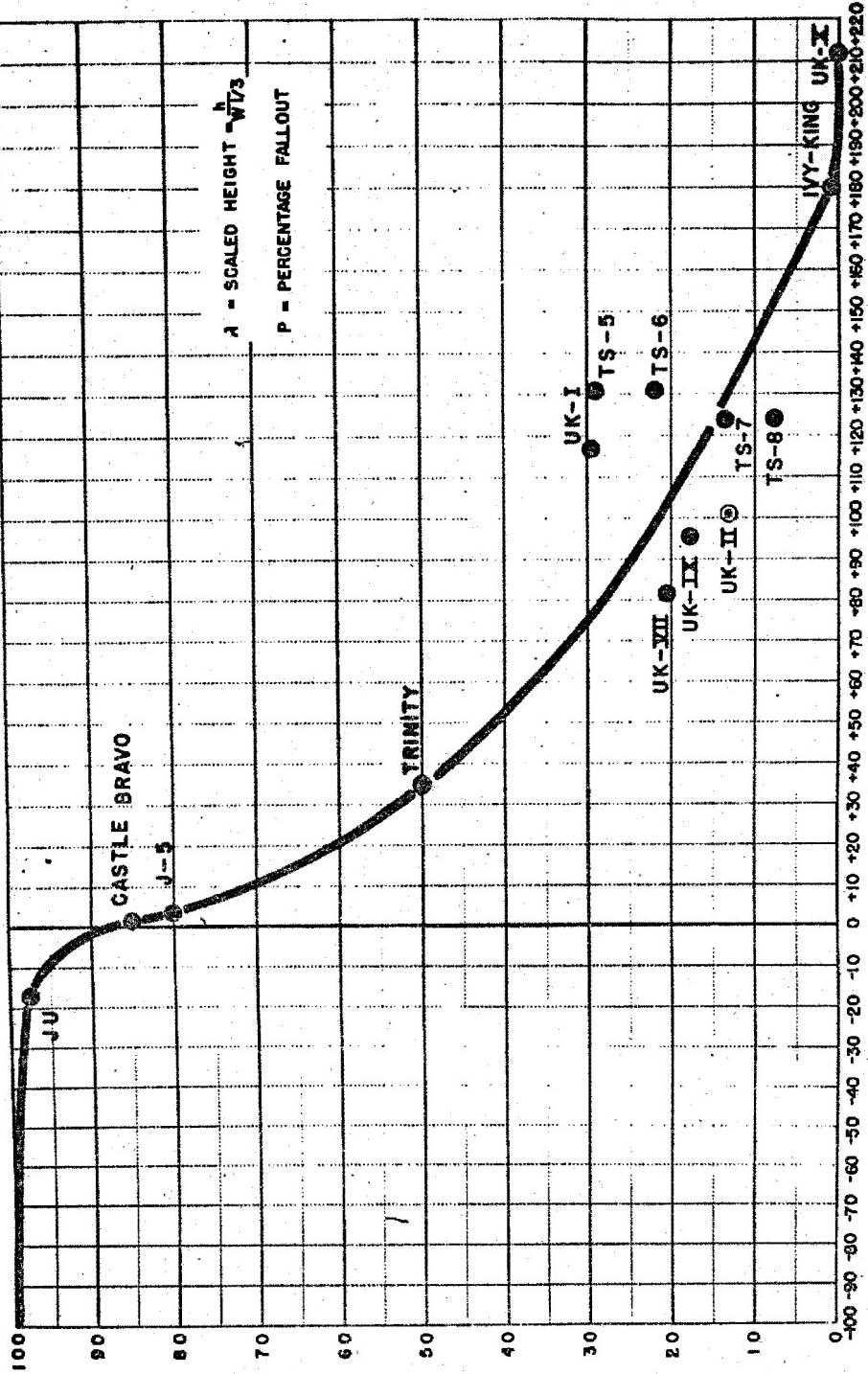
$t$  = time of start of fallout

$W$  = bomb yield in kilotons (fission yield)

$k$  = constant (we have taken this as 10 in our reports)

As we study the curve shown in Figure 1A, we see that between 70 and 90% of the total residual activity is assumed to fall out downwind within 24 hours or less. This fallout is that due to those particles that are sufficiently large to have significant rate of fall (1000 to 30 microns). Many organizations analyzed in detail fallout from the JANGLE-Surface and JANGLE-Underground shots. They concluded that only 10 to 15% of the JANGLE-Surface residual activity was found within 3 to 5 miles downwind of ground zero. This data closed the 100 roentgen/hr contour line. Now the 10 - 15% fallout from JANGLE-Surface shot perturbed us greatly because we had developed a curve (Figure 1A) which showed that surface fallout ( $\lambda = 0$ ) should be above 50% and probably less than 90%. This gave us the strong suspicion that either our beloved curve was wrong, or the

**PERCENTAGE FALLOUT IN 24 HOURS**  
**VERSUS**  
**SCALED HEIGHT OF DETONATION**



DOE ARCHIVES

Figure 1A

workers in the field of fallout had only measured a very small portion of the total. To this end, we started hunting the classified literature. We found that in AFSWP Report WT-370, hidden under Project 2.1c-1, there were figures showing that fallout occurred 50 to 100 miles downwind of ground zero. Unfortunately, this fallout data was in relative units and contact with the project officer indicated that he had no idea of the actual amount of contamination on the ground. He agreed it could have been in roentgens or tenths of roentgens. Further search brought out the fact that the Air Force Special Weapons Center of ARDC had made repeated aerial survey of the downwind area for both JANGLE-Surface and JANGLE-Underground shots at D-day and also at D+1 day. This excellent work done by SWC under the direction of Colonel Fackler resulted in the fallout plot shown in Figure 1C. We were able to prepare this fallout plot by utilizing the following attenuation factors with height:

<u>Height Above Ground in Ft</u>	<u>Attenuation Factor</u>
3	1.
10	1.2
20	1.4
30	1.5
40	1.7
50	1.8
100	2.6
200	4.0
300	5.1
400	6.8
500	8.5
1000	30.

A study of Figure 1C shows that the total fallout downwind is not 10 or 15%, but more in the order of 70 ± 20%. This quite satisfactorily fits our curve shown in Figure 1A.

I would now like to touch on one more point in our analysis which I consider to be very significant. During TUMBLER-SNAPPER test operations, the percentage fallout from the stem of the cloud was approximately equal to that coming from the mushroom. Now the TUMBLER-SNAPPER tower shots were from 12 to 14 KT bombs detonated from 300 ft. towers. During the UPSHOT-KNOTHOLE test operation, however, the yields varied from 17 KT to 50 KT (I am now referring to the large yield tower shots) and the tower heights were 300 feet. During UPSHOT-KNOTHOLE, where the scaled heights were significantly lower than during TUMBLER-SNAPPER, the percentage activity in the stem was two to three times the percentage fallout coming from the mushroom. This was amazing to us at the time. We had anticipated that as the tower height remained constant while the

yield was increased (by a factor of 2 or 3), then the percentage fallout coming from the taller and wider mushroom would be greater. We found the contrary to be true. Also, as we studied Figure 1C, we noted that approximately 50% of the fallout came from the stem and only 15 to 25% came from the mushroom. It was this increased percentage fallout from the stem that made us take the gamble of predicting in November 1953 (see ARDC Report No. C3-36417) that if a 5 to 10 MT weapon were detonated on the surface in Washington, D. C., then Baltimore, which is 40 miles downwind, may have to be evacuated. We further stated in this report that 50 to 75% of the total activity of a surface detonated multi-megaton weapon would fall out downwind and cover an area of approximately 5000 square miles. We also stated that this prediction was based only on small yield weapons and that it had to be proof-tested in a high yield test before we developed any confidence in it.

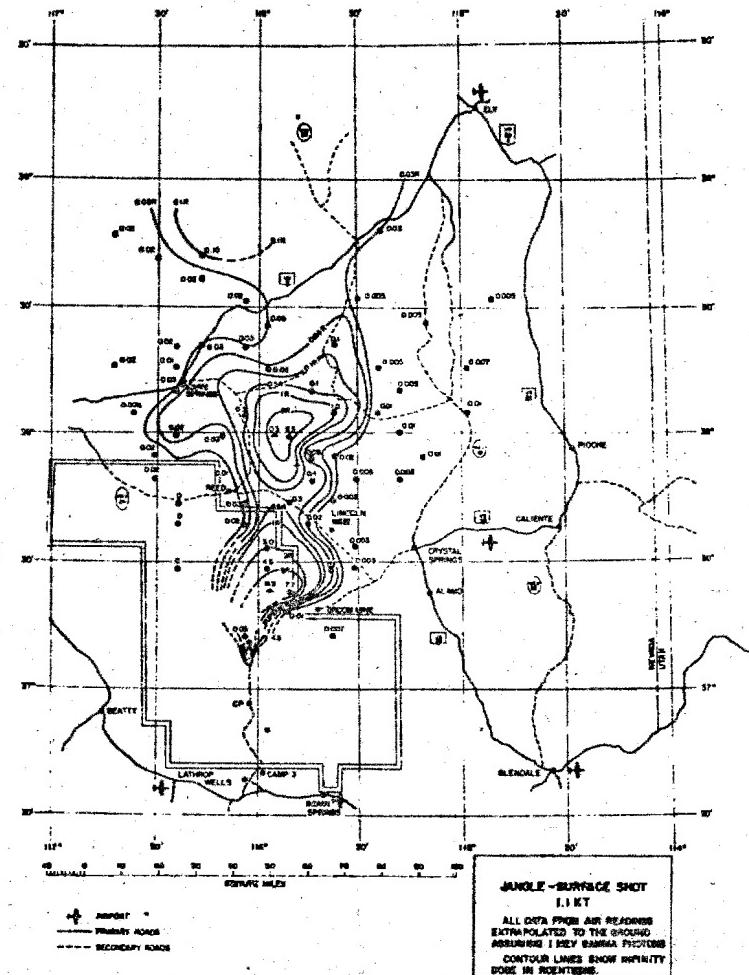


Figure 1C

DOE ARCHIVES

## ATOMIC CLOUD HEIGHT AND SIZE AS A FUNCTION OF YIELD AND METEOROLOGY

Dr. W. W. Kellogg  
Rand Corporation

### Introduction

Yesterday we were in the microscopic realm of micron-sized particles. Today we abandon the particles--for a while at least--and talk about the very biggest part of an atomic explosion, the cloud which forms after the blast has gone off.

Why, you may ask, are we particularly concerned with the cloud in a symposium devoted to fall-out? The answer is simple--only by a careful study of all the available evidence on the behavior of the atomic cloud can we hope to determine where the radioactive debris goes initially. In a very real sense the atomic cloud defines the initial spacial boundary condition for the fall-out process.

With this in mind, the purpose of the present paper should be twofold:

To get an idea of the circulation which an atomic explosion sets up, in order to tell where, within the cloud, the radioactive debris of the fireball will go.

To describe the dimensions and heights of atomic clouds as precisely as possible. These will vary primarily with yield, of course, but the meteorological situation also has an effect.

### Early Development and Circulation

In order to fix our ideas a bit, consider the first few minutes in the life of an atomic cloud (Figure 1). It will not be necessary to dwell on this schematic diagram at any length, but a few points are very pertinent to the question of fall-out.

Notice that, in the high air burst, the surface material never reaches the mushroom. In the low air burst it often does reach the mushroom, and we have looked at many pictures (for example, BUSTER Easy) where the material from the ground passes completely through the doughnut-shaped mushroom, and then flows out and around the outside. Yet, in such cases there is no fall-out, as LTCOL Lulejian pointed out. The toroidal circulation is so strong, apparently, that the dirt can only circulate around the doughnut which contains the fission products, and never comes in contact with them.

DOE ARCHIVES

**SCHEMATIC CROSS-SECTION, SHOWING THE WAY IN WHICH  
SURFACE MATERIAL RESPONDS TO THE INDRAFT  
CAUSED BY THE RISING ATOMIC CLOUD.**

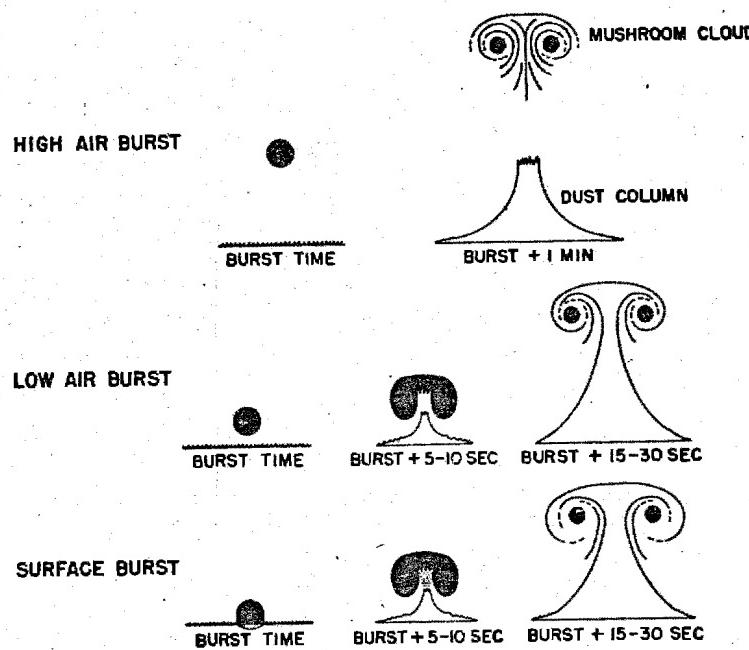


Figure 1

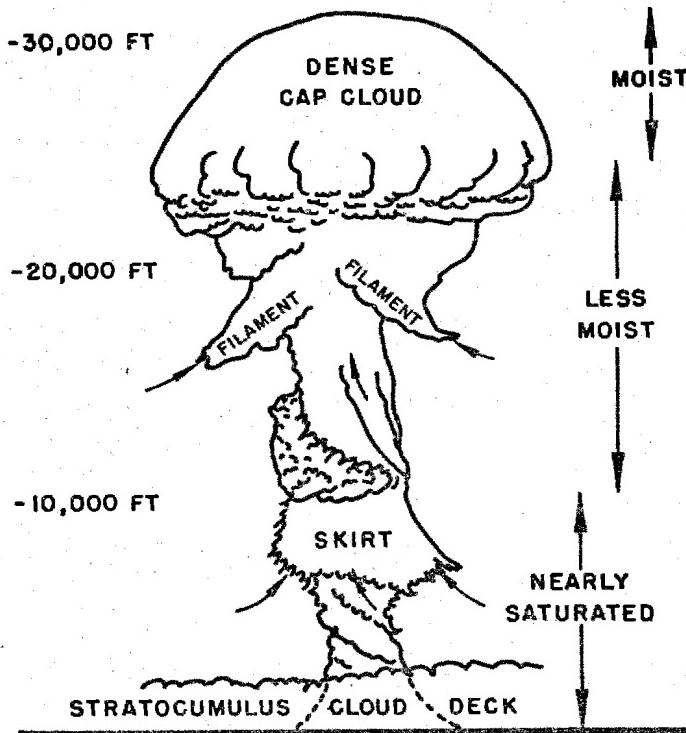


Figure 2

DOE ARCHIVES

In the surface burst, contact between the dirt and the fission products is achieved initially, and the dirt is drawn up with the fireball in a mixture of vapor, liquid, and solid particles. The evidence from the particle sampling makes this fact quite certain. After a few seconds, however, one would expect exactly the same influences that dominated the low air burst to exert themselves, and there will be little or no further mingling of soil and fission products.

Now follow the cloud upwards. From the outside it may look like the sketch of the **DELETED** cloud (Figure 2). We cannot actually see the inside, but we can deduce a good many things about the circulation just the same. First, we are certain of the strong convergence and updrafts along the stem. The existence of the skirts and filaments, which are an invariable feature of these clouds, is proof that there is an upward motion, since only by a forced lifting will the air be made to form a cloud. Moreover, we can get an idea of the rate of the toroidal circulation of the mushroom by a simple experiment. In a movie, taken with a fixed camera, mark with a pointer on the screen some bump or spur on the side of the upward rushing mushroom. You may be surprised to find that, relative to the ground, the outside of the mushroom is standing still or even descending slightly (Figure 3).

**SKETCH OF TORUS OF A 30 Kt WEAPON ABOUT  
1 MIN AFTER BURST**

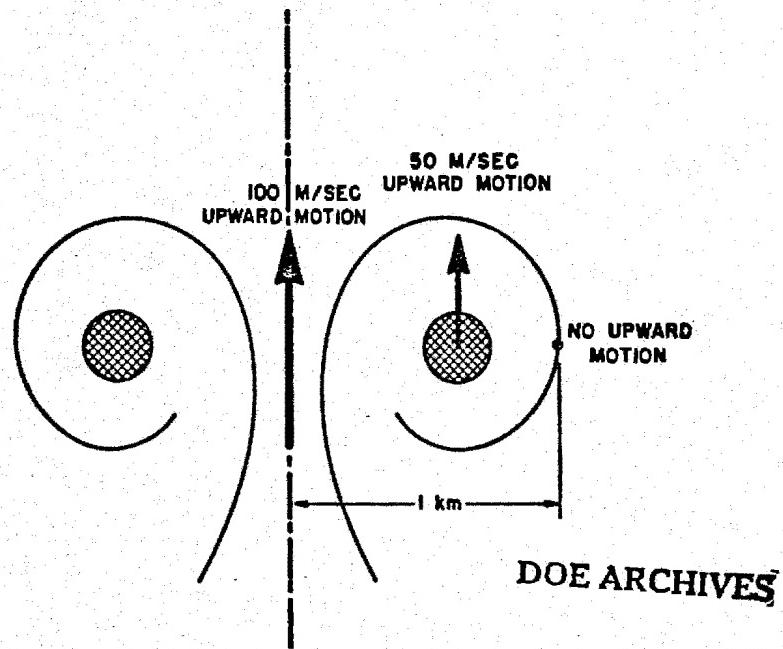


Figure 3

195

SECRET

RECORDED UNDER THE  
NATIONAL SECURITY ACT 1947  
199

This means that the material in the middle of the mushroom must be moving upward even faster than the cloud as a whole. The figure shows a 30 KT case (a schematic drawing of the situation in TUMBLER-SNAPPER 3). Imagine the upward motion in the larger clouds, such as CASTLE Bravo, which, as LTCOL James showed, were moving at the rate of about 150 meters per second during the first minute or two!

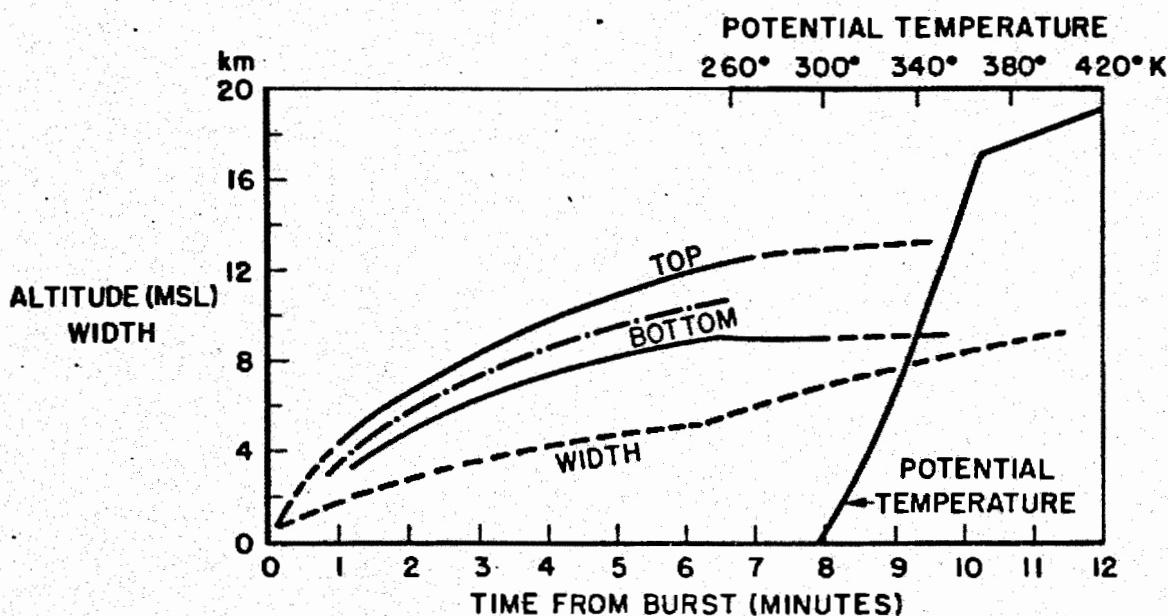
It is clear, from these considerations, that very little debris from the mushroom could ever remain behind in the stem. It would be swept upward far too rapidly. If there are any particles left behind, they must be large particles which have been thrown outward by the two or three "g" force of the toroidal motion, and fall in a thin veil outside of the stem. Actually, when the light is right one can sometimes see this thin fall-out veil around the stem--though it must constitute but a small fraction of the total radioactive material.

There always comes a time in the life of an atomic cloud when it reaches its ceiling. The cloud, as it rises, draws in or "entrains" a great deal of the surrounding air, and its mass increases by a factor of over 100 in going from, say, 5 or 10 seconds, to its stabilization height. This large entrainment, coupled with the natural stability of the atmosphere, means that it will eventually use up all its thermal energy and acquire the same temperature and density as the surrounding air at its level. However, it may still have the kinetic energy of its toroidal circulation, and if it is a cloud from a large yield weapon it will have a great deal of this kind of energy.

There are two good pieces of evidence for this in the larger yield clouds. First, a study of pictures of these clouds shows that they keep on turning and boiling after they stabilize. In addition, to clinch the matter, the cloud often behaves just the way a smoke ring behaves when it stops moving—it suddenly starts to grow radially. The GREENHOUSE George cloud showed this, and the Easy cloud did to a lesser degree (Figure 4). Several of the larger Nevada clouds have shown this behavior also. In the case of the very large clouds, in the megaton range, this rapid expansion is so pronounced that, as we heard yesterday, the mushroom quickly grows right out of the picture, and we hardly know how large it did get before it settled down. All we know is that, according to EG&G's analysis, at 10 minutes after shot time the rate of horizontal growth for several of the CASTLE clouds was two or three hundred miles per hour—far too fast to be accounted for by the prevailing winds and wind shears.

DOE ARCHIVES

This feature will be noted again in the next section.



RISE AND GROWTH OF GREENHOUSE EASY CLOUD

DELETED

RISE AND GROWTH OF GREENHOUSE GEORGE CLOUD

DOE ARCHIVES

Figure 4

197

REF ID: A6424

DOE ARCHIVES  
OMIC ENERGY 1954 201

### Measurements of Size and Altitude

In the earlier atomic tests, TRINITY, CROSSROADS, SANDSTONE, and RANGER, the emphasis of the observations was on the devices themselves, and on the events of the first few seconds or milliseconds. After the fireball glow died and the boiling mushroom cloud started rising the test was "over", and what went on after that was the province of the documentary photographers--and a handful of weather men with theodolites who tried excitedly to get angles on the rushing cloud. If it has not been for these weather men, I believe that we would have virtually no information on the heights to which these clouds went.

Starting with the GREENHOUSE tests, however, carefully planned programs to observe the cloud were instituted, and photographic measurements were made. You have heard from LTCOL James about the most recent--and most elaborate--efforts to photograph the CASTLE clouds. So now we do have a fairly good set of data on a number of atomic clouds, covering a wide range of yields.

Before showing you the collected data on all the shots to date, a few caveats are in order about the quality and accuracy of these measurements. (I believe Dr. Machta will have more to say about this matter.) Whether the measurement is by theodolite or by camera, the basic observation is a set of angles. Before these angles can be reduced to dimensions two important factors must be taken into account:

Wind drift

Cloud shape

It will not be necessary to go into the details of just how these are handled in the analysis, but you should understand how an erroneous treatment can introduce large errors.

First, concerning the wind drift, the motion of the cloud relative to the observer will change the distance, and this will give the impression of a vertical motion or a change of size. For example, movement towards the observer of the cloud top will give the impression that the cloud is still rising. Fortunately, wind observations are nearly always available at the test site, so, though the correction may be laborious, it can be made with some degree of confidence.

The cloud shape is more illusive and has resulted, I believe, in some rather serious errors in height estimates. The natural assumption to make about a mushroom cloud is that it is round on top (Figure 5). This is not a bad assumption for the smaller yield clouds, but even here it must be noted that there may be an appreciable difference

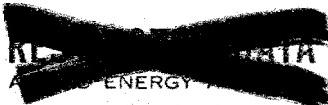
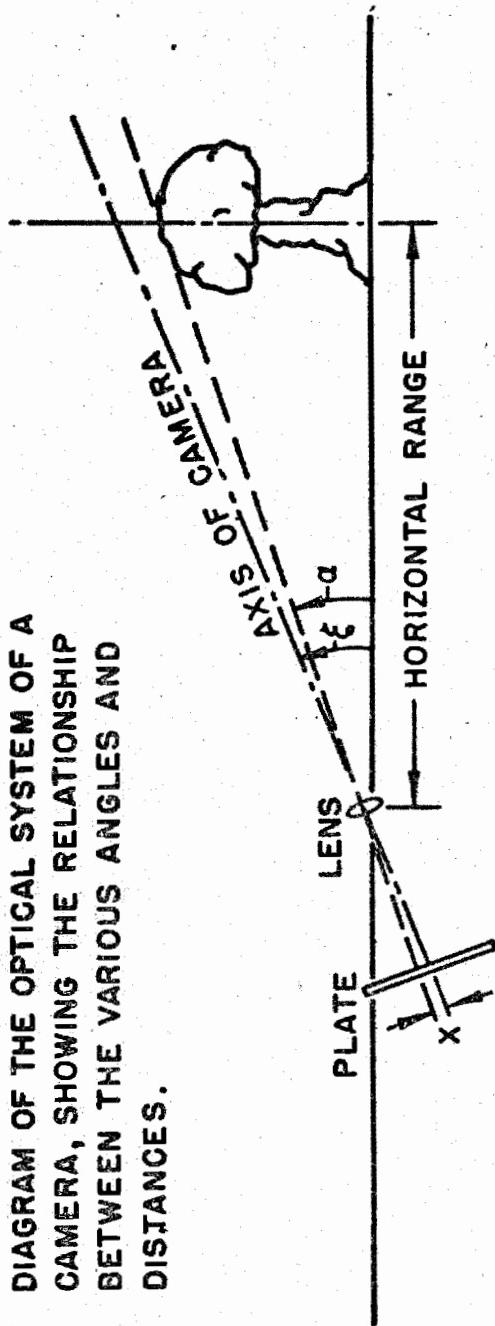
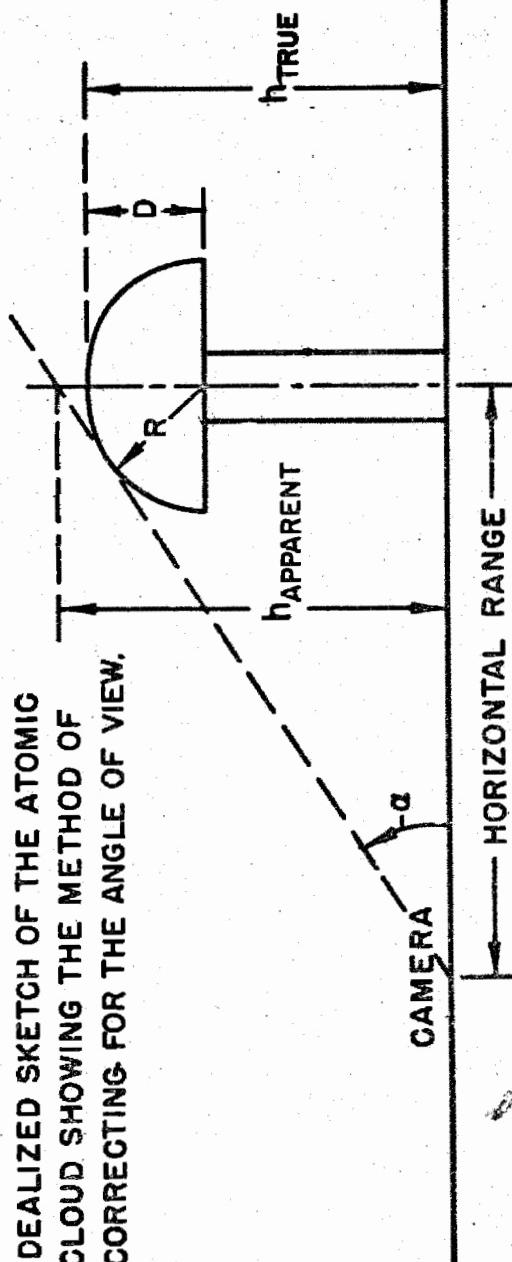


DIAGRAM OF THE OPTICAL SYSTEM OF A  
CAMERA, SHOWING THE RELATIONSHIP  
BETWEEN THE VARIOUS ANGLES AND  
DISTANCES.



IDEALIZED SKETCH OF THE ATOMIC  
CLOUD SHOWING THE METHOD OF  
CORRECTING FOR THE ANGLE OF VIEW.



DOE ARCHIVES

Figure 5

between the true height and the apparent height, as indicated in the figure.

Imagine, now, that the rapid expansion of diameter, shown in Figure 4, takes place while the observer is measuring the elevation angle,  $\alpha$ , between the horizon and the cloud edge nearest him. Clearly, the expansion will push the edge towards him, and he may interpret this as a continued increase in height instead of an increase in size. Of all the clouds which I have studied carefully, none have, as far as I could judge, continued to rise for more than six to seven minutes, and many stabilize at four to five minutes. However, at around six minutes many have shown the pronounced diameter increase, with its accompanying flattening. Therefore, where height versus time curves are presented which show the cloud continuing upward for eight, ten, or even fifteen minutes, it is probably justified to chop it off at around six minutes, and to ascribe the remainder to an illusion in space.

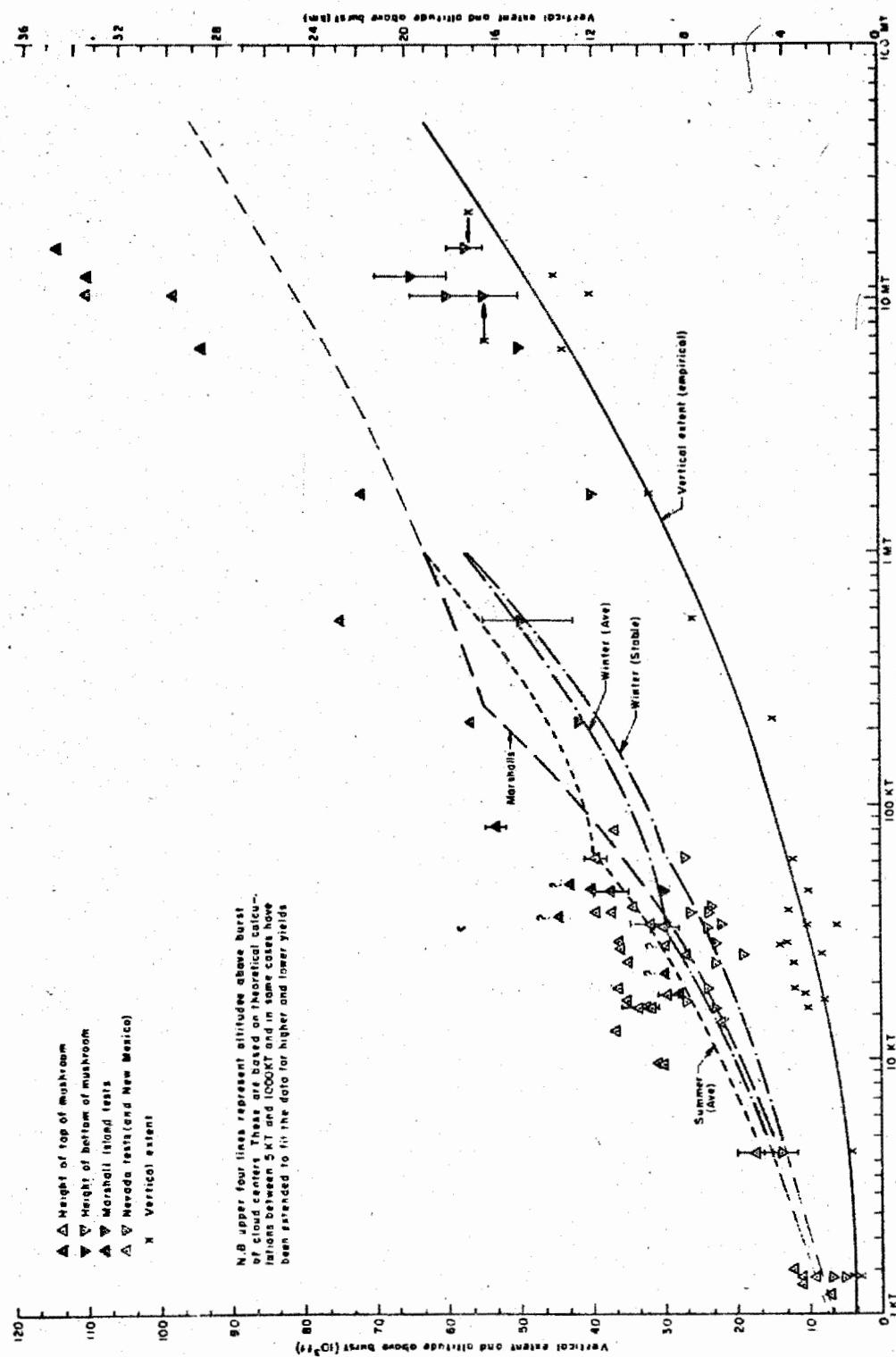
The results of all the observations which are available to date are shown in the next two figures. In the height data (Figure 6) I have taken the best estimates, and in two cases (SANDSTONE Yoke and X-Ray) have cut them down, in line with the previous statement about stabilization time. You should note that these are heights of centers. Should you want height of top or bottom, the vertical extent is shown as a solid line.

The various curves through the data points are theoretical curves, whose derivations are described in the Rand "Aursole Report" and so will not be repeated here. They show the effects of atmospheric stability and the height of the tropopause, and appear to agree fairly well with the data. The extension of the Marshall Islands curve to yields above 1 MT is done so as to roughly fit the data, and the same applies to the extension of the two winter cases below 5 KT.

You have all noticed, by now, that there is quite a discouragingly large spread in the data points. Part of this is certainly due to poor measurements, and part is a real effect due to the change in atmospheric conditions of stability and wind or wind shear between shots of the same yield. It is also possible that certain characteristics of the device, in addition to the yield, have an effect on the cloud behavior.

The yields, incidentally, have all been corrected to sea level by the ratio of the sea level pressure (standard) to the pressure at burst altitude. This is to take into account in a rough way the fact

Figure 6



DOE ARCHIVES

201

OMIC ENERGY ACT

205

that a burst at, say, 750 mb pressure has to do less work in pushing outward against the atmosphere than a burst at sea level, and so will grow bigger. This correction factor amounts in some cases to 20 to 25 percent of the yield.

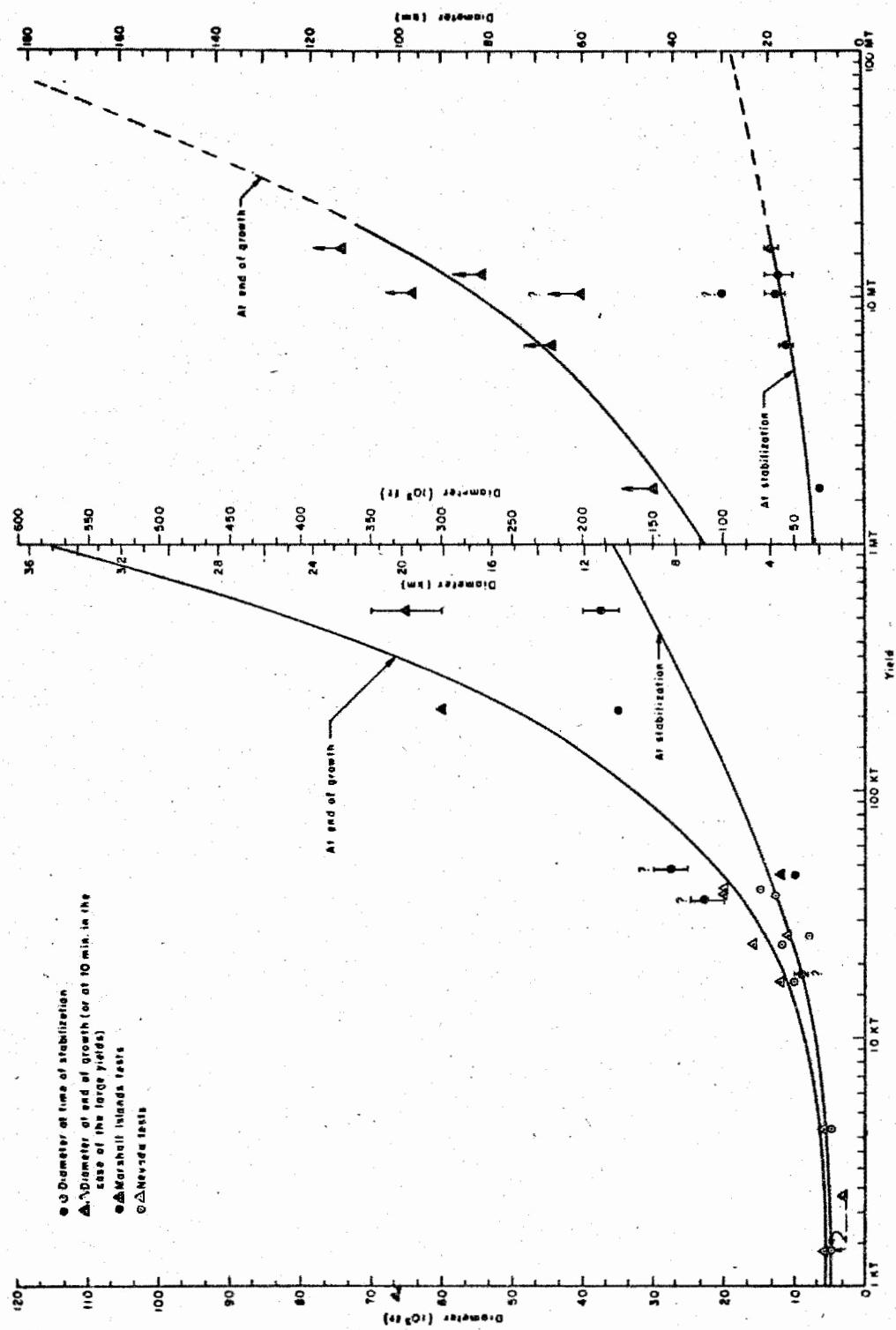
Figure 7 shows the diameters versus yield. Note the change in scale at 1 MT to accomodate the tremendous growth in the megaton range. The curves here are drawn as best fits to the data. You will note the arrows attached to the points showing the 10 minute diameters above 1 MT. As previously mentioned, these clouds, even at 10 minutes from shot time, were still growing at a rate which was too great to be accounted for by wind shear, so their "final" diameters, a difficult thing to define even if we could observe it, may be considerably larger than shown.

In conclusion it should be admitted that our information on atomic cloud dimensions and heights leaves much to be desired from the point of view of precision, but I have the feeling that these clouds share to some degree the sloppy behavior of natural clouds. Turbulence, winds, layers of stable and unstable air encountered during the atomic cloud's rise are bound to have some effect, and make each case a unique one. Therefore, I doubt if we will ever be able to be much more precise than we are now.

Fortunately, as you will see later in the day, a few thousand feet in positioning of the cloud will not have any great effect on the fall-out computation.

DOE ARCHIVES

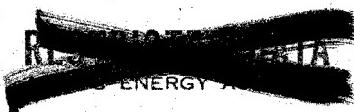
Figure 7



THIS PAGE IS BLANK

DOE ARCHIVES

204



208

## ATOMIC CLOUD HEIGHT AND SIZE AS A FUNCTION OF YIELD AND METEOROLOGY

Dr. Lester Machta  
U. S. Weather Bureau

The Weather Bureau under contract to the AFCRC in connection with TEAPOT Project 9.4 is attempting to determine whether there is any relationship between the physical characteristics of the various atomic clouds and available meteorological parameters.

The study has just begun so that only a limited field of interest can be reported upon today; namely, the tops of the clouds detonated in the Nevada Test Site. These data were examined first because they are most numerous and probably most reliable. Any conclusions derived from such a study of Nevada shots would then be applied to both kiloton and megaton weapons in the Pacific as well as being useful in the forthcoming TEAPOT series.

It is evident that the quality of the cloud top and meteorological information will bear strongly on the success of the study. The conventional upper air weather data collected by the Air Weather Service for the test operations is among the best that weathermen may work with, although it is true that we may not be measuring all of the pertinent meteorological elements because of lack of proper instruments as, for example, the failure to measure vertical currents or atmospheric turbulence.

The matter of the cloud tops is another question, however, and some background information is necessary.

### DOE ARCHIVES

It is perhaps, convenient to review the three methods by which we may ascertain the tops of the atomic clouds in Nevada. First and simplest is to fly an airplane at the same level as the cloud and read the altimeter. This is routinely done and except for small altimeter corrections and cases where the cloud is well above the aircraft one should assign relatively small errors to this method. However, I understand that this determination of the cloud top data is not a primary function of the pilots and probably no attempt is made to obtain precise measurements.

A second method of height determination is the measurement of the elevation angle of the cloud top and together with a knowledge of the point of burst and the drift of the cloud compute the cloud rise. This may be done either by theodolite or by photography. Uncertainties in the drift and inability to sight the top of the cloud are the main limitations in this method. In general, when the elevation angle is

~~SECRET~~

small and the cloud outline still sharp, during and immediately following the ascent, the errors ought to be small.

The third method uses two or more cameras or theodolites focused on the same point at the cloud top and applies trigonometric computations to find the cloud rise. Drift corrections are unnecessary, but for this benefit we substitute the uncertainty in the location of the same point on the cloud. Only during BUSTER-JANGLE has there been any attempt to use this method--by EG&G with photographic film.

There are some minor ambiguities in the definition of the irregular cloud top which may account for some of the discrepancies to be seen later. EG&G, for example, uses the average top rather than the highest point of the cloud while I suspect that the theodolite measurements are based on the highest point of the cloud. Further, since the cloud frequently overshoots the final levelling off height, it is not always clear which height; (the absolute maximum or the final maximum) is being referred to. In time, some sort of agreement should be reached as to the definition of a cloud top.

I have surveyed, to the best of my ability, the documented heights of all the atomic clouds detonated in Nevada, discarding insofar as possible, values which were subsequently changed by later computations. I should like to illustrate a few of the cases of discrepancies which were found by the different methods. Table 1 shows two BUSTER-JANGLE

Table 1  
Examples of Cloud Top Observations  
Heights in feet MSL

BUSTER/BAKER				
AWS Theodolite	27,000	at	15 minutes	
EG&G Photographs	22,000	at	8 minutes and still rising	
Rand Photographs	29,000	at	7 minutes and still rising	
Aircraft (at 26,500)	25,000	at	50 minutes	
Value used 27,000				
BUSTER/DOG				
AWS Theodolite	(48,000)	at	20 minutes	
	-(46,000)	at	8 minutes (data confusing)	
	(21,000)	at	21 minutes	
EG&G Photographs	40,000	at	8 minutes & rising fast	
Rand Photographs	37,000	at	7 minutes and still rising	
Aircraft (at 41,000)	41,000	at	1 hr., 50 minutes	
Value used 40,000				

DOE ARCHIVES

~~RESTRICTED~~  
BY THE UNITED STATES  
ATOMIC ENERGY COMMISSION

~~SECRET~~

cases—illustrations of poor agreement. Let me make it clear that the individuals making the observations during these early series make no pretense of great accuracy. Nevertheless, this is what we must work with.

These BUSTER shots were selected for illustration because there were four sets of measurements available. EG&G used double triangulation—Rand, single camera and drift, but checked their results from second observing point. The differences between the cloud tops speak for themselves. In the case of BUSTER Dog the cloud moved toward both the theodolite and cameras so greater credence was associated with the aircraft, tempered by the photographic analysis which incorporates the spherical shape of the cloud.

Table 2 shows two of the UPSHOT-KNOTHOLE clouds. In the case of Shot 4, the discrepancy between EG&G and the others is more than might

Table 2  
Examples of Cloud Top Observations  
Heights in feet MSL

UPSHOT-KNOTHOLE-DIXIE (4)			
AWS Theodolite	43,000	at	12 minutes
EG&G Photographs	38,500	at	10 minutes
Aircraft	43,000		
Value used 41,000			
UPSHOT-KNOTHOLE-ENCORE (8)			
AWS Theodolite	43,000 & 41,500		
	42,500	at	13 minutes
EG&G Photographs	42,000	at	9 minutes
Aircraft	40,500		
Value used 42,000			

be expected. In the case of Shot 8, only the aircraft is out of line and the 42,000 feet value looks fairly reliable. The two AWS numbers: 43,000 and 41,500 are the tops reported by two different theodolite observations — the 42,500 number is a compromise. The comparison between various methods of measurements for the UPSHOT-KNOTHOLE cloud tops reveals better agreement than the earlier series suggesting a trend toward better observations.

In summary, I feel that the cloud top data are acceptable for this study in no more than half of the 29 cases.

DOE ARCHIVES

It is evident that a more powerful explosion will, in general, yield a cloud which rises higher than a weaker blast. Figure 1, typical of the kind which everyone working in this field prepares, shows a plot of the adjusted yield of the device as the abscissa against the amount of rise of the cloud as the ordinate. This adjusted yield is the fireball yield multiplied by the standard sea level pressure (1013 millibars) and divided by the pressure at the point of burst. The correction factor for pressure, about 1.2, is roughly the same for all shots except the two high air bursts--shown by the double circles--so that the results of this and later figures would be just about the same if we used the actual rather than the adjusted yields. The amount of rise is the difference between my interpretation of the top of the atomic cloud and the height of the burst. The circles represent air bursts and the crosses tower bursts (all 300-foot towers); the gun shot by a circle and cross since it was a true air burst, but detonated much lower than the other air bursts. The letters and numbers denote the names and numbers of the Nevada test series - R for Ranger, B/J for BUSTER-JANGLE, S/T for SNAPPER-TUMBLER, and U/K for UPSHOT-KNOTHOLE. The curve denotes my subjective interpretation of a best fit of the data.

It is clear that up to about 15 KT, the rise is generally greater the larger the yield, but between about 20 and 75 KT, I suspect that a least squares analysis would indicate almost a horizontal line showing little or no dependence of the amount of rise on the yield.

Since, in Nevada, the tropopause lies in the range of about 30-45,000 ft. above mean sea level, the same height range at which the bombs over 10 to 15 KT appear to stop, it seems logical to see what the relationship between the top and the tropopause may be. Figure 2 shows the adjusted yield as the abscissa once again with height above sea level as the ordinate this time rather than the amount of rise. For those shots which rose above 20,000 feet, the corresponding tropopause is given as either a line or a thin or a broad shaded area. The line indicates a weak tropopause with little tendency to stop the rising cloud, while the broad area indicates an intense tropopause with a strong tendency to stop the cloud. The narrow shaded area lies between the two extremes and the question marks on two cases mean that the tropopause has not yet been reached at the indicated heights. Up to about 15 or 20 KT none of the tops really rise above the tropopause but between 20 and 40 KT adjusted yields there are cases in which the clouds tops overshoot and undershoot the tropopause. All three cases above 40 KT exceeded the height of the tropopause slightly. Aside from these remarks there appears to be very little relationship between the height of the tropopause and the height at which the atomic clouds stop.

DOE ARCHIVES

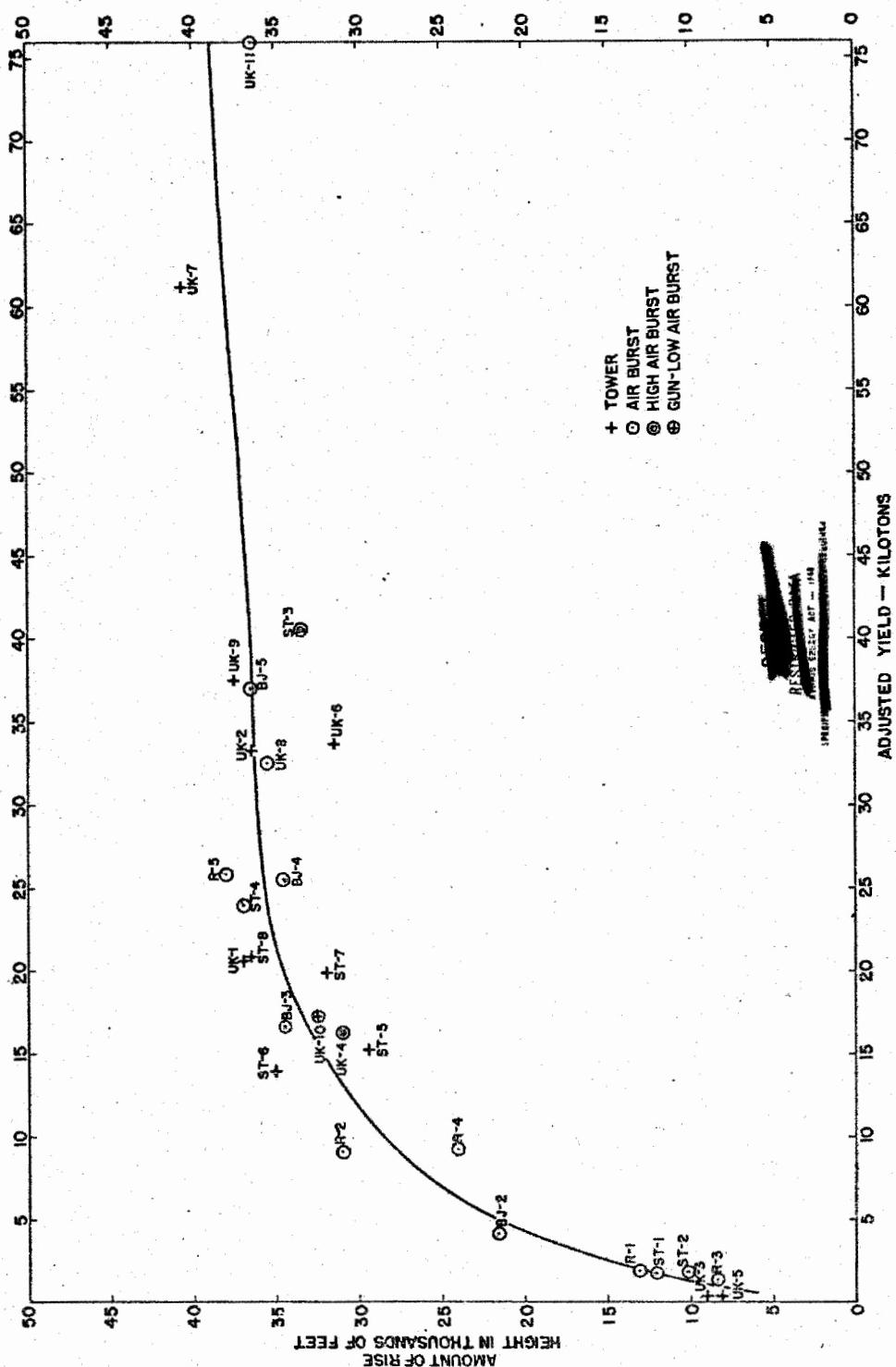
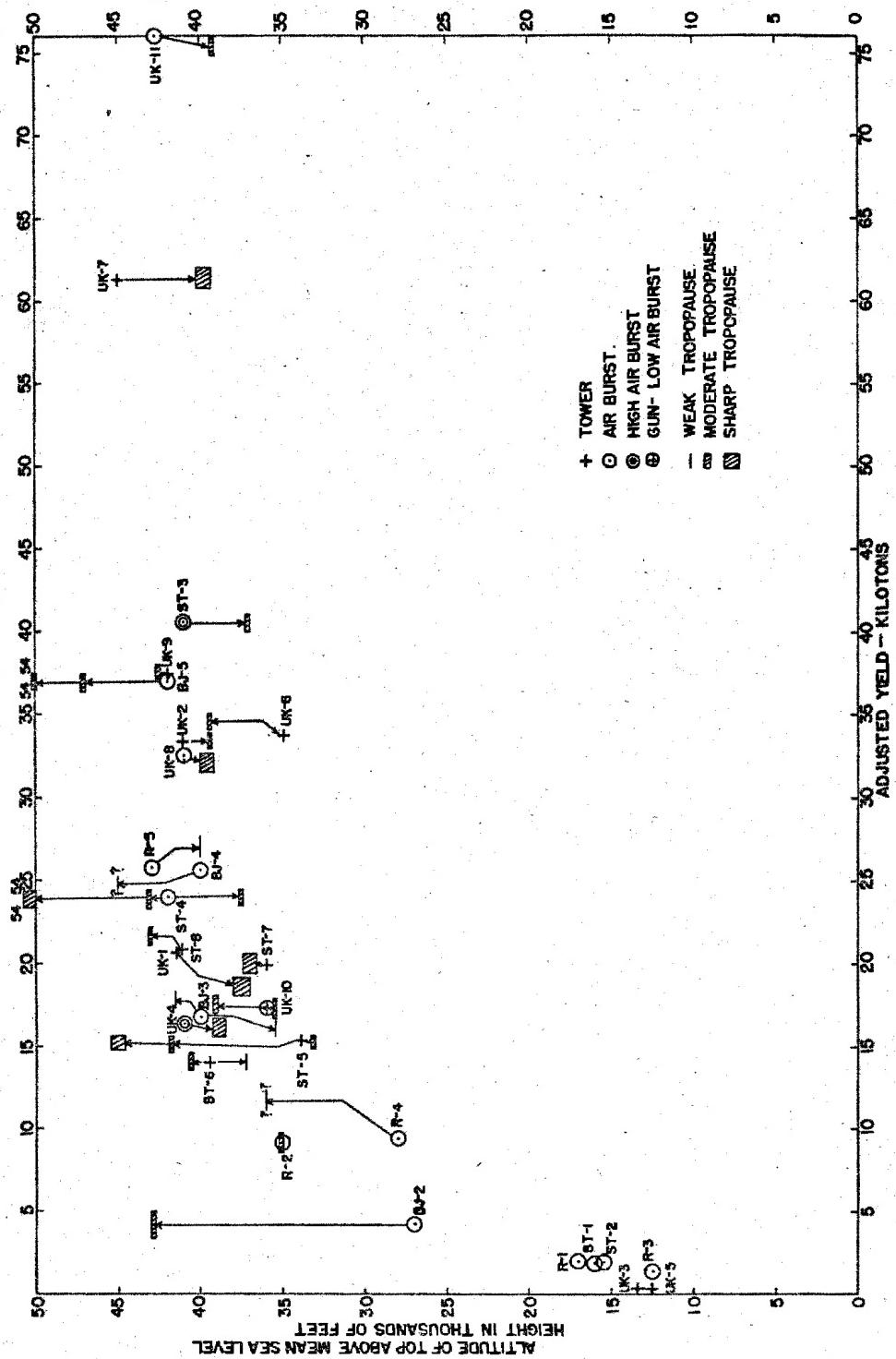


Figure 1  
 Amount of Rise of Atomic Cloud as a Function of the Adjusted Yield



## Altitude (MSL) of Atomic Cloud Top as a Function of the Adjusted Yield

DOE ARCHIVES

210

214

SECRET

In theory, an isolated parcel of air heated above its environment will rise and expand until its density is again similar to that of its new surroundings. Thus, the greater the heating the greater the rise. After the initial effects of radiation loss of the fireball have passed, it is believed that cooling will be accomplished in part by expansion as the parcel moves into regions of progressively lower pressure aloft. During this rapid rise a meteorological property called the potential temperature remains approximately constant even though the actual temperature of the cloud decreases rapidly. If the amount of initial heating available for buoyancy is proportional to the yield of the weapon, then the potential temperature difference of the atmosphere between the elevation of burst and the stopping point of the cloud should, according to one simple concept, be proportional to the yield.

Figure 3 shows the adjusted yield as the abscissa again and the potential temperature difference between point of burst and stopping as the ordinate.  $\theta$  is the symbol for potential temperature. The simple theory states that the cases should arrange themselves so that greater differences in potential temperature go with greater yields. I do not believe that one can argue for more than the vaguest suggestion that the simple theory is verified in the range above 15 or 20 KT.

In a RANGER report, Holzman and Kent recommended using the difference in potential temperature between cloud top and 750 millibars (about 8,000 feet above mean sea level) rather than the top and burst height. Figure 4 shows this potential temperature difference as the ordinate. It is seen that the picture in this figure is very similar to that of the previous one and that the predicted theory is not verified. In passing, you might note that if you look only at the five RANGER shots you can see why with the limited data, the simple theory appeared to be verified in 1951.

I shall not bore you with the details of all the other studies associating the cloud tops with weather elements. The wind shear, the mean wind during ascent and the conditions at the point of burst have so far been looked at with, in my opinion, negative results. I have not by any means exhausted the possibilities nor yet looked into combinations of parameters as controlling the rise of the cloud.

Table 3 emphasizes the present state of ignorance on the part of meteorologists to utilize meteorological factors in predicting the tops of Nevada clouds. Based on regression equations prepared from all the pre-U/K shots in the range between about 10 and 50 KT, LTCOL Spchn made predictions for each of the U/K shots. The equations incorporated the yield, the stability of the air - or essentially something similar to the potential differences shown in the previous figures - and the wind

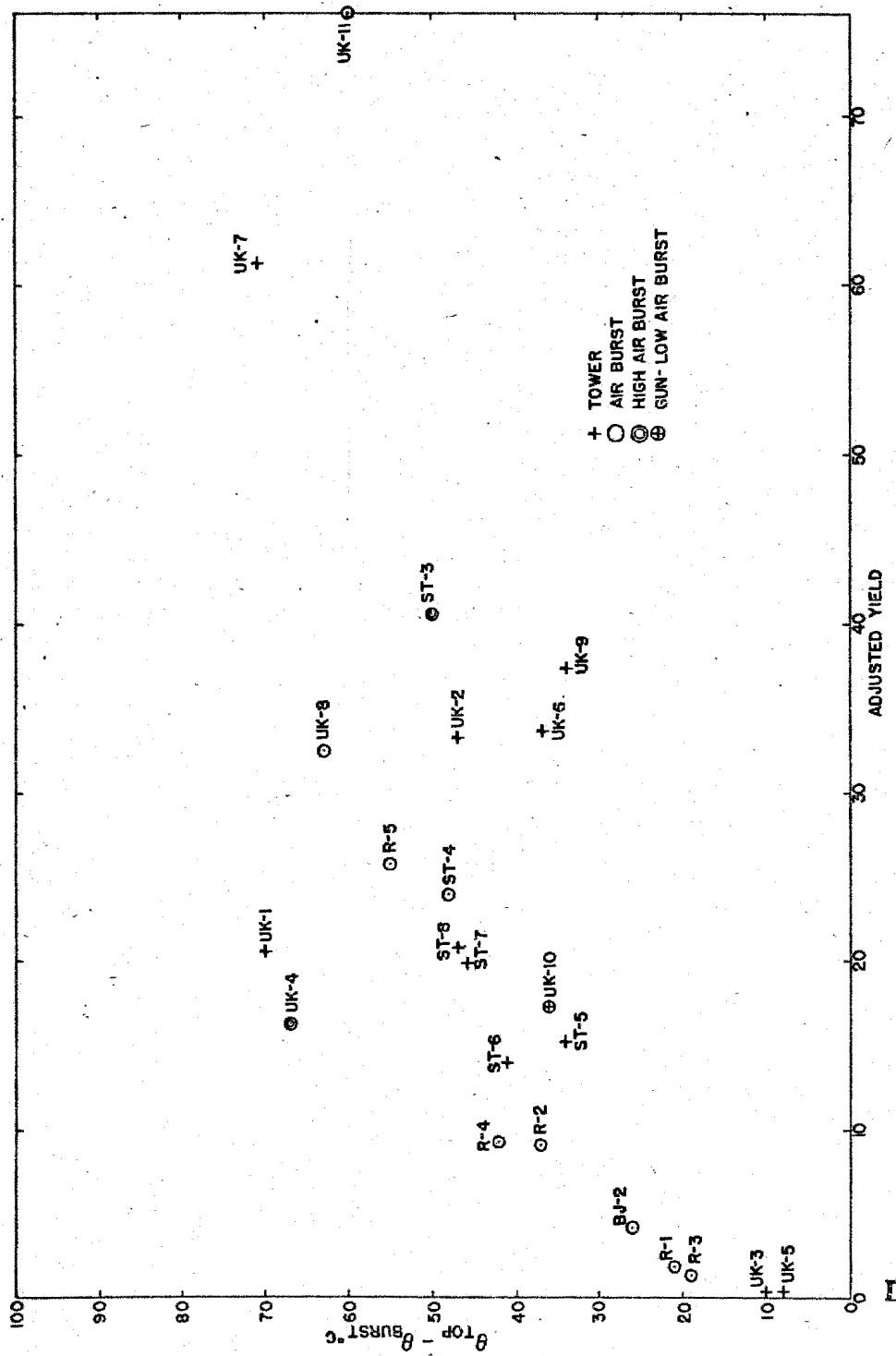
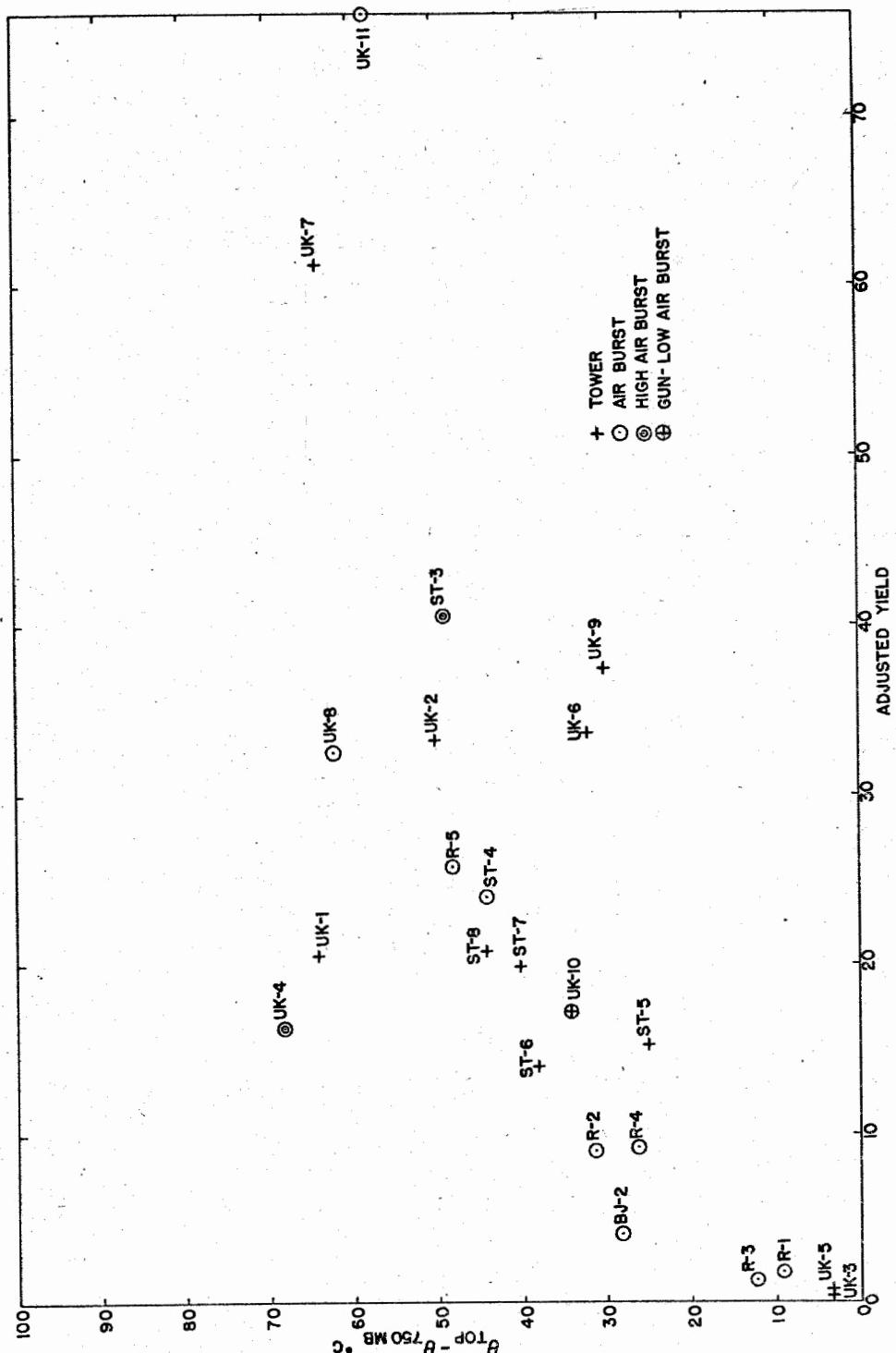


Figure 3  
Potential temperature ( $\theta$ ) difference between the Cloud Top and the Point of Detonation as a Function of the Adjusted Yield.

DOE ARCHIVES

212

216



DOE ARCHIVES

213

Figure 4  
Potential temperature ( $\theta$ ) difference between the Cloud Top and the 750-mb.  
Level as a function of the Adjusted Yield.

217

COSMIC ENERGY DATA

64

Table 3

Verification of U/K Cloud Tops

Absolute Mean Errors in Feet

LASL pre-U/K Regression Equation	Cloud Top at Tropopause	Cloud Top at 40,700 Feet (Mean of pre-U/K Tops)
3,500	3,300	2,800
1. 9 of 11 U/K shots.		
2. U/K tops taken from WT-703.		
3. Tropopause data also taken from WT-703.		

speed. I show here the verification of his predictions for all but the two smaller U/K shots (numbers 3 and 5). The average absolute error is about 3,500 feet and, this error, incidentally, is unchanged for his predictions even if the two smaller shots are included. Two other simple predictive schemes suggest themselves for comparison. First, that the clouds stop exactly at the tropopause. The verification for this case, 3,300 feet, is better than the regression equations, but probably not significantly so. I understand that the present revised version of the Los Alamos regression equations now includes the tropopause height as an additional parameter. Finally, one might argue that all clouds in the 10 to 75 KT yield range stop at the same height above sea level as suggested from one of the earlier figures. The heights of all shots above about 10 KT prior to UPSHOT-KNOTHOLE stopped at about 40,700 feet above mean sea level and using this height for the nine larger U/K shots, the verification, 2,800 feet, turns out to be better than either of the previous cases. Taken literally, it means that, as yet, we have found no reason why the cloud tops should be a function of either the yield or weather conditions for the Nevada shots provided the yield is in the range of about 10 to 75 KT.

I should like to indicate what, in my opinion, represents the most likely explanations for the failure to satisfactorily use meteorology in cloud top analyses.

I feel that there is ample reason for doubting the accuracy of most of the cloud top measurements.

DOE ARCHIVES

Perhaps the changes in atmospheric conditions play little or no role in controlling the cloud rise or if meteorology is important,

we may not be measuring the right meteorological parameters or interpreting the weather observations in the proper fashion.

Perhaps, it is the center of the mushroom or some other feature not yet studied which is related to changes in atmospheric parameters.

If the construction or detonation of atomic weapons possess differences other than their yields of which we are not aware, but which determine, say, the buoyancy of the cloud, this may well account for some of the height differences.

In conclusion, where does this state of affairs leave us? First, I would say that if there is no systematic arrangement of cloud tops in the Pacific for weapons in a broad megaton range, this should not surprise us. Second - for TEAPOT - unless someone produces a rather convincing demonstration of yield and meteorology as controlling features in the cloud tops, I would say that in the 10 to 40 KT range and for normal tropopause elevations, a constant height of about 40,000 feet is as good a predictive rule as any.

DOE ARCHIVES

215

ERASED



~~SECRET~~

THIS PAGE IS BLANK

DOE ARCHIVES

216



220

~~SECRET~~

TYPICAL U. S. AND EUROPEAN WEATHER AS IT AFFECTS  
FALLOUT, WITH EMPHASIS ON WIND STRUCTURE

Dr. Lester Machta  
U. S. Weather Bureau, Washington 25, D.C.

I believe there are two types of fallout information which Civil Defense officials and military commanders would want from the meteorologist; first, material based on past weather records which can be used for planning purposes - it is this which we will discuss primarily - and second, day-to-day forecasts of where and how much fallout would occur from a potential or actual bomb dropped at a specific time and place.

It is clear that what is desired is information both on where fallout will occur and what the distribution of dosages within the fallout area will be. For a variety of reasons, I do not know how to predict dosages from a given wind field. My discussion will describe only the areas of fallout with some clues as to where particles of a given size will fall or when the fallout will occur downwind of the blast. Further, even in providing the areas without giving dosages, I am handicapped because I don't know the width of the radioactive cloud or how high the radioactive part of the clouds from megaton weapons will rise. So, if you will forgive some arbitrary decisions which, strictly, should represent conclusions of this symposium, I can proceed.

The central and northern United States and Europe lie in the temperate latitudes and, by and large, have marked similarities in weather and winds. Thus, though most of what I will show represents data from the United States, the conclusions to be drawn are generally applicable to Europe as well.

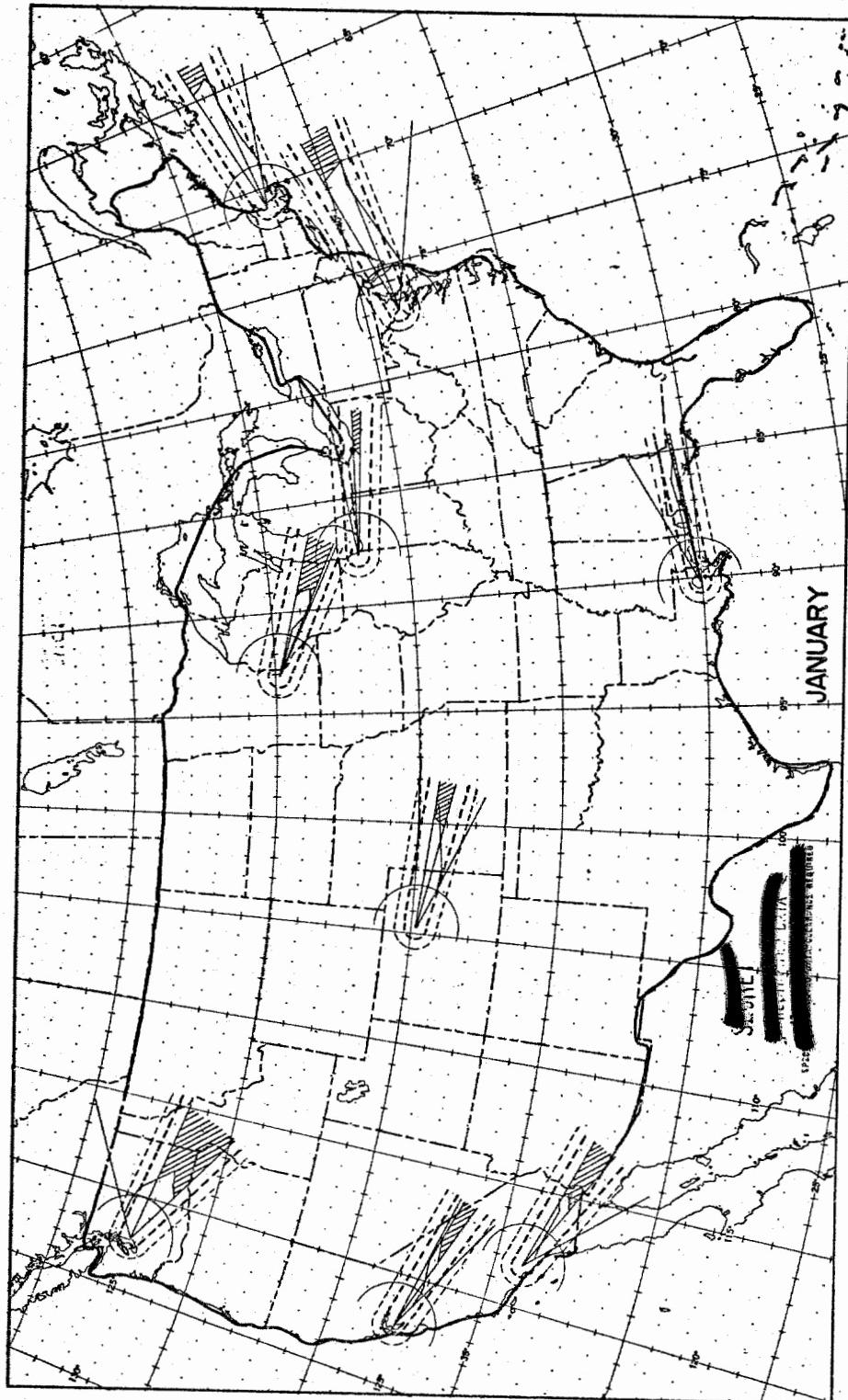
Figure 1 shows the mean fallout sectors in winter. The radial lines show the extremities of the fallout sector for a very narrow cloud. The inner envelope shows the outline of the fallout area if the mushroom (here defined as the portion of the cloud above the tropopause) were 50 miles wide and the outer lines, if the mushroom were 100 miles wide. The shaded area represents the sector in which fallout comes from the center of the mushroom. Fallout is assumed to originate from heights up to 90,000 feet. The heavy line running across the radial lines indicates the approximate position of fallout 6 hours after burst. The arcs are drawn at a distance of 100 miles from the burst to provide a distance scale.

The main feature of the winter chart is that fallout occurs primarily to the east of the burst. The New England area contains many of the stronger wind speeds experienced in the country.

DOE ARCHIVES

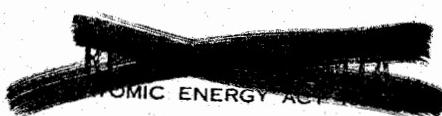


**Figure 1**  
Mean Fall-out Sectors in Winter



218

222



While I feel that the general nature of the picture shown on Figure 1 and Figure 2 is correct, some of the details such as the wider mushroom fallout area at Seattle than Denver, for example, are open to suspicion since the data used to prepare this chart are not homogeneous. That is, at each elevation, we used the best possible average wind, but at, say, 10,000 feet, we used a mean chart based on winds collected from about 10 years of observations, while at 80,000 feet average winds based on records for only 4 years were available. Further, we are always plagued with the fact that high level winds are obtained mainly during periods of fair weather and low wind speeds, while low-level winds are collected more frequently.

Figure 2, the summer patterns, also shows predominant fallout to the east of the burst. The wind speeds become much lighter and the west coast stations actually have a mean northward airflow. The southern tier of States is located in an area of very light winds. Thus, at New Orleans, for example, the mean fallout picture shows no preferential direction. Western Europe would be more like eastern U. S. rather than the U. S. West Coast.

Having viewed the mean picture, we now pass on to the variability of individual cases about this mean. In the troposphere, or up to 30-45,000 feet, where one is more familiar with wind patterns, it is well recognized that above the lowest levels (say above 10,000 feet), the prevailing westerly flow is the result of waves or undulations superimposed on a mean zonal flow. At times, the daily picture in the mid-troposphere looks much like the mean with almost straight west-to-east flow, while at other times, we find large amplitude waves or closed centers.

These waves or closed centers most frequently move across the country from west to east, but occasionally, at certain preferred places such as the southwest U. S., remain stationary for many days.

In the winter, in the stratosphere (Figure 3), the winds normally also blow west-to-east over the temperate latitudes. Although this map shows the flow only at 53,000 feet, direction of the airflow is much the same up to 100,000 feet. However, on anomalous occasions, as in Figure 4, which shows the airflow at 67,000 feet in February 1952, large areas of the temperate latitudes possess easterly winds. In this map, northern U. S. and southern Canada is such an area in which the normal wind direction is reversed. Fallout in such a case would probably still be to the east of ground zero in Northern U. S., but not nearly as far away from ground zero as in the average case.

DOE ARCHIVES

However, the typical and almost invariant summer picture above about 60,000 feet (Figure 5 shows east-to-west flow). This will result in many cases of fallout from the stratosphere occurring to the west of ground zero because of light westerly tropospheric winds.

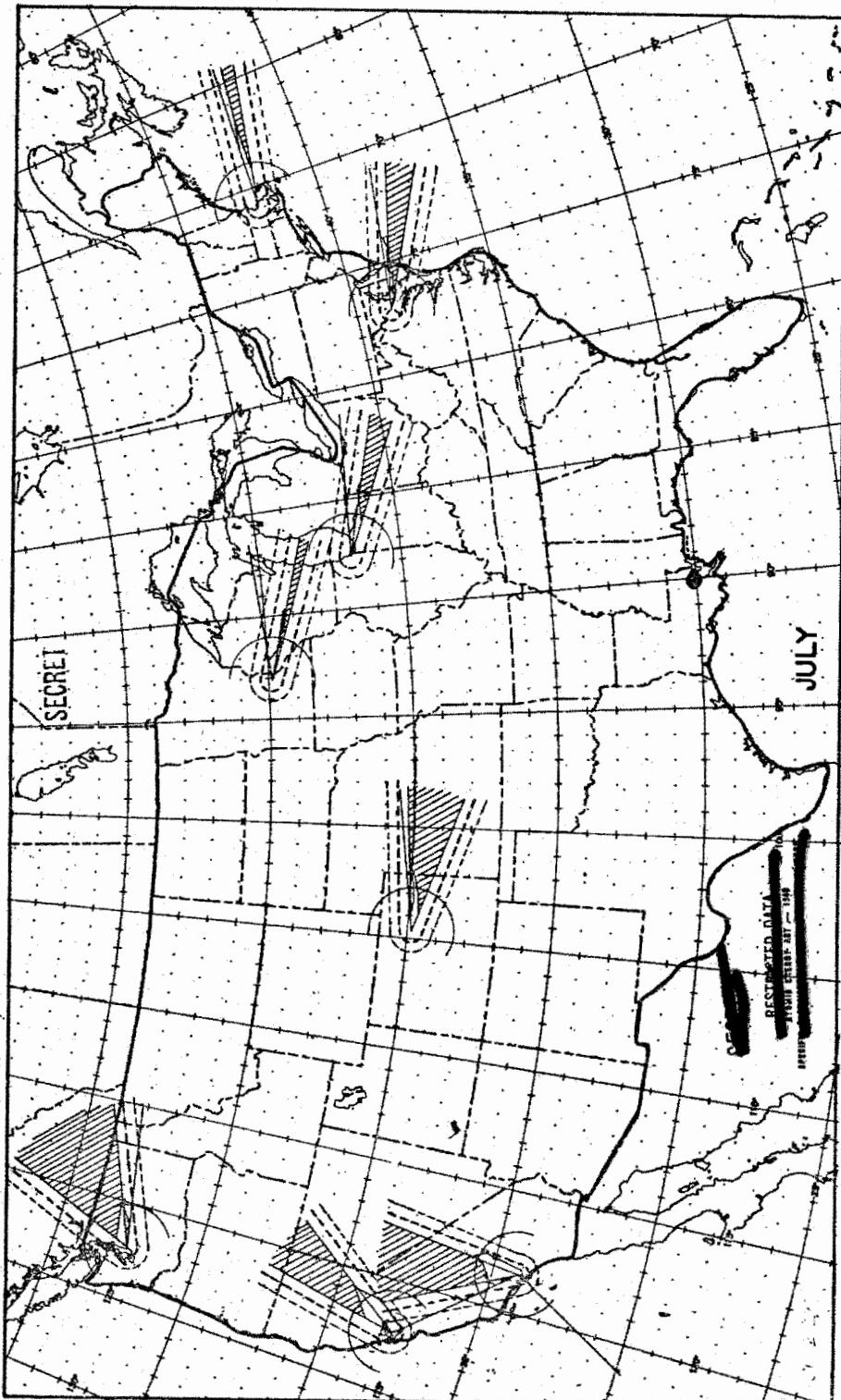


Figure 2  
Mean Fall-out Sectors in Summer

DOE ARCHIVES

220

ATOMIC ENERGY ACT

224

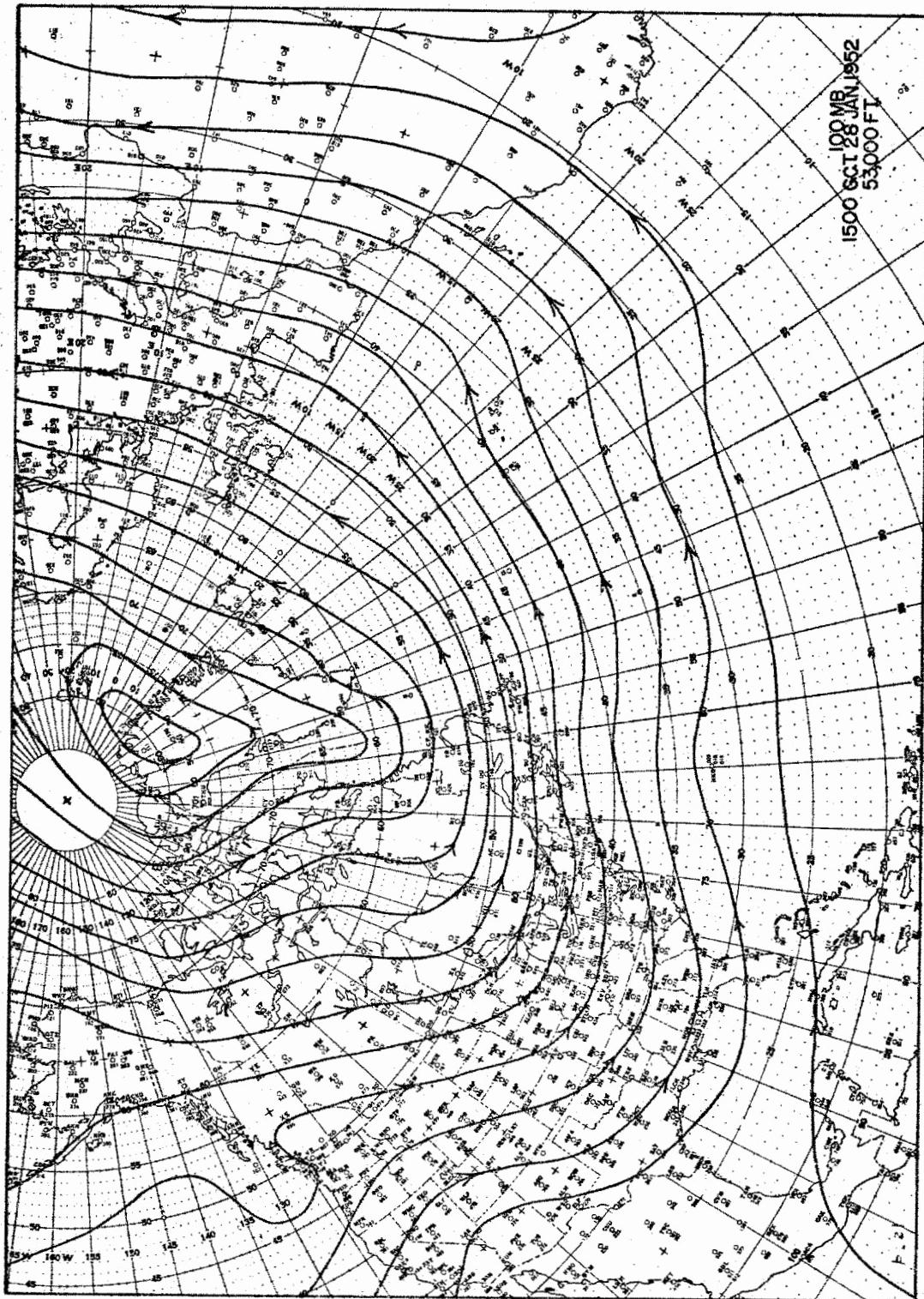


Figure 3  
Example of Normal Winter Flow Pattern in the Stratosphere

DOE ARCHIVES

221

ATOMIC ENERGY ACT 1954

225

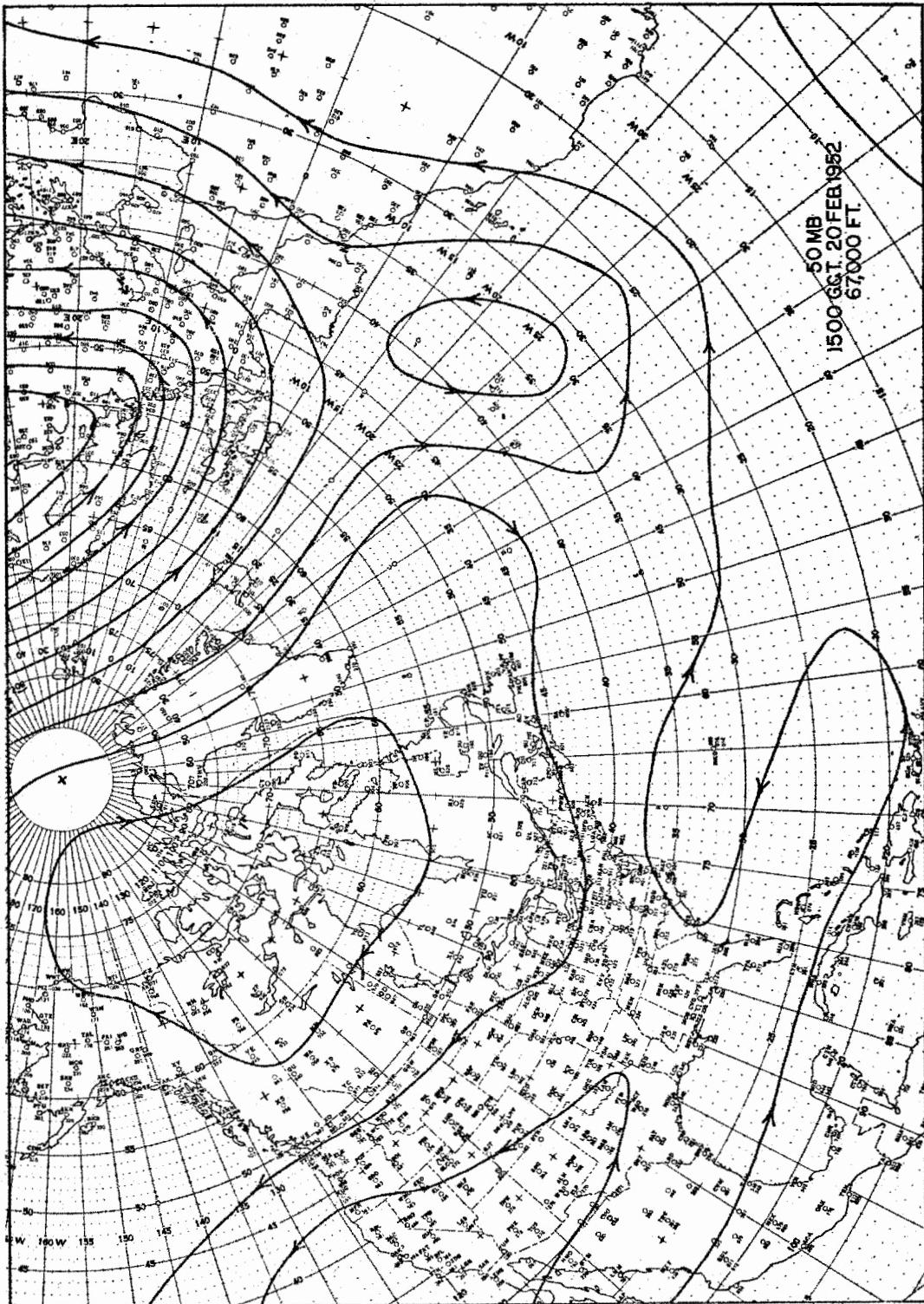


Figure 4  
Anomalous Stratospheric Flow Pattern in Winter, with  
Easterly Winds over much of the United States and Canada

DOE ARCHIVES



Figure 5  
Mean 50-mb. (68,500 ft.) flow for July



DOE ARCHIVES

223

ATOMIC ENERGY COMMISSION

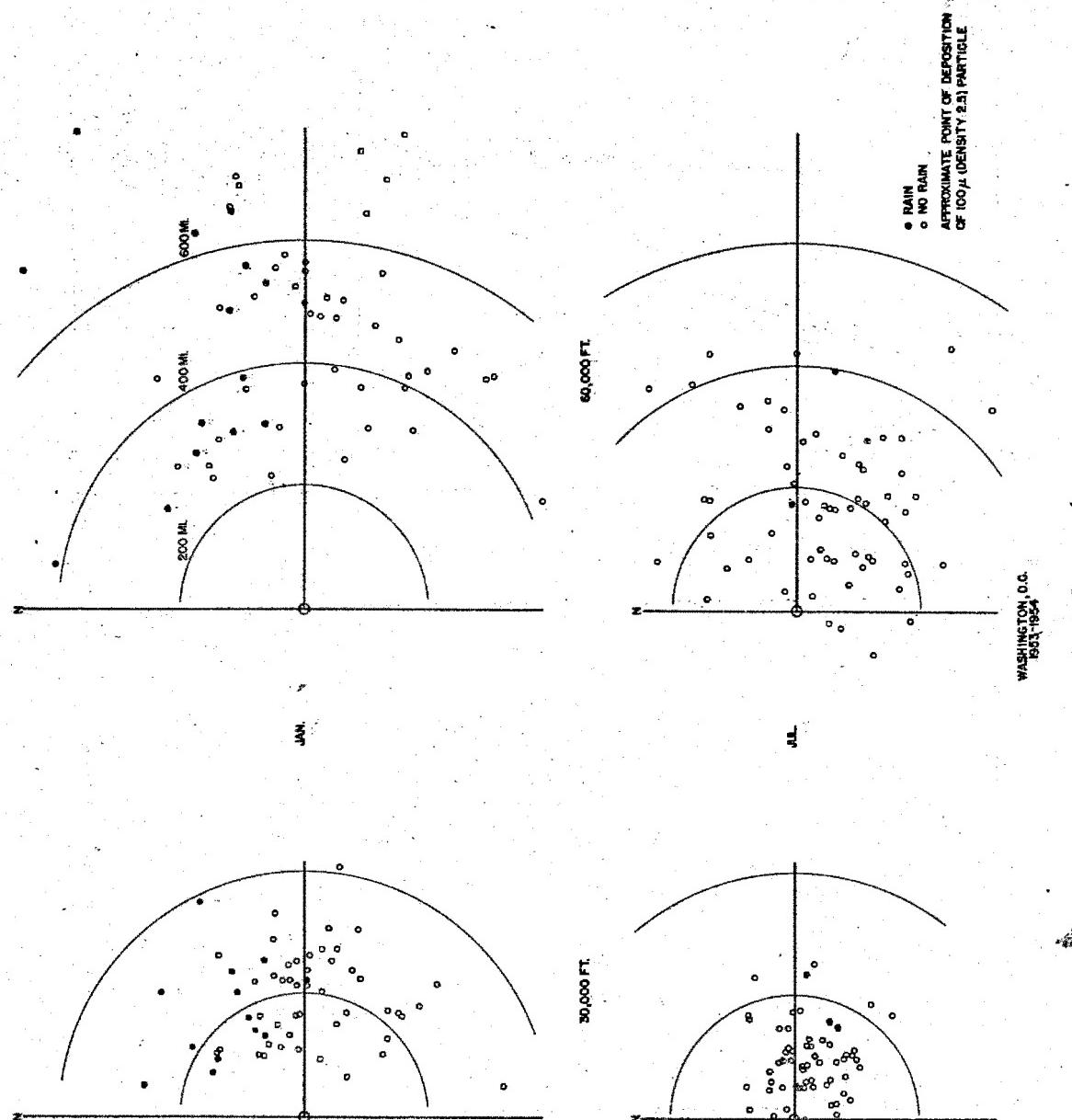
227

Figure 6 shows the distribution of points at which fallout will occur for hypothetical bombs detonated at Washington, D. C. (where the lines intersect) for January and July and coming from two elevations; one in the middle or upper troposphere (30,000 feet), and one in the lower stratosphere (60,000 feet). The points actually indicate where a 100 micron particle of 2.5 density would land if started at the indicated height over ground zero. The arcs are at 200-mile intervals. In the winter, while there are pretty wide departures from direct west-to-east fallout, there are no cases of deposition to the west of ground zero during the two Januaries used in this study from either level. During the summer, not only does the 100 micron particle fall much closer to ground zero, but there actually are cases of fallout to the left or the west of ground zero. The filled-in circles show the cases in which it was raining or snowing at the time of the wind observation. In the winter, it is evident that precipitation is far more likely with fallout occurring northeast of the burst. The distribution of the points provides a measure of the scatter of directions of, say, the effective mean winds for the stem in the left side, and lower mushroom on the right side of the figure.

The last bit of climatological statistics appears in Figure 7. Since the distant fallout is felt to come from the mushroom, the size of the area in which potential danger exists depends, in part, on the amount of the directional shear of the winds in the mushroom. Although the climatological data for this figure was taken from Washington, D. C., the results are drawn for Pittsburgh, Pa. We have on this figure the cumulative frequencies of directional shears in the mushroom. Thus, in January, there is almost a 60% likelihood that the directional shear will be no greater than the smallest angle of  $5^\circ$  and almost 90% likelihood that it will be no greater than  $10^\circ$ , etc. The shear is seen to be much greater in summer. For each of the angles, one may get an idea of the fraction of the northeastern U. S. on which fallout would be observed.

The conclusion to be drawn from this figure is the fact that there is only a small likelihood of large directional shear; especially in winter, a saving factor for some Civil Defense considerations. I have no statistics to confirm this state of affairs everywhere in the temperate latitudes, however.

Figures 8 - 13 illustrate actual cases of fallout with typical weather situations. For example, in Figure 8, on the left is the weather situation near Washington, D. C., at 0630 (Greenwich Time) on 10 January 1953 showing the isobars and fronts in the usual fashion and the precipitation area in shading. A storm is approaching Washington from the south with a wide precipitation area to the north and west. To the right of the weather picture, we find the fallout plot in the event of a hypothetical burst at, say, the Pentagon. The radial lines are the lines along



**Figure 6**  
Distribution of Fall-out from 30,000 and 60,000 feet in January and July, Washington, D.C.

DOE ARCHIVES

225

ATOMIC ENERGY ACT

229

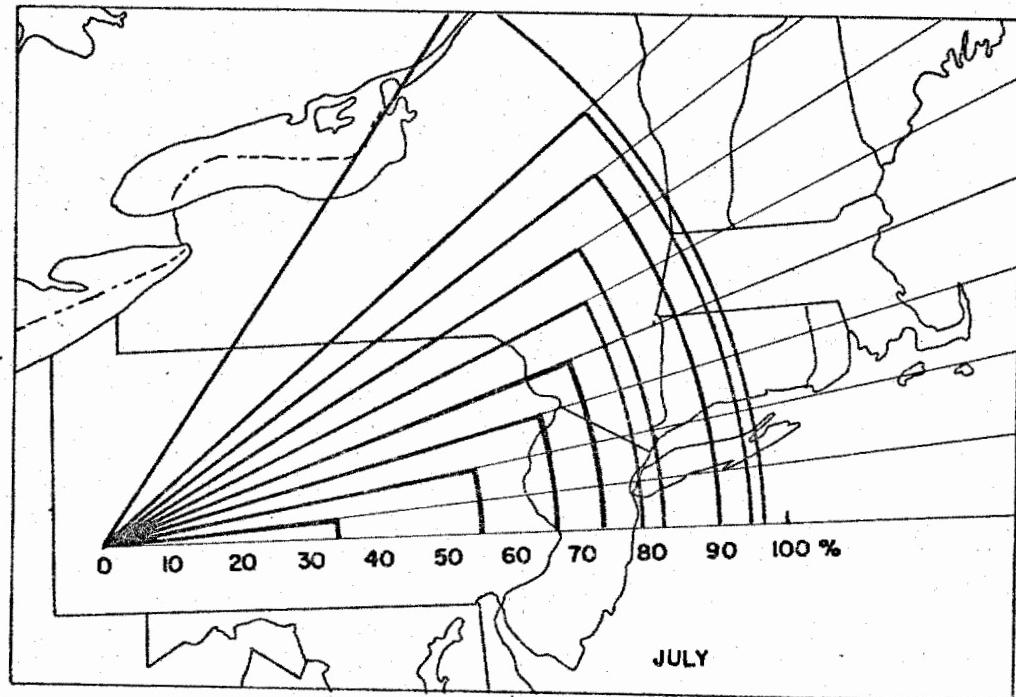
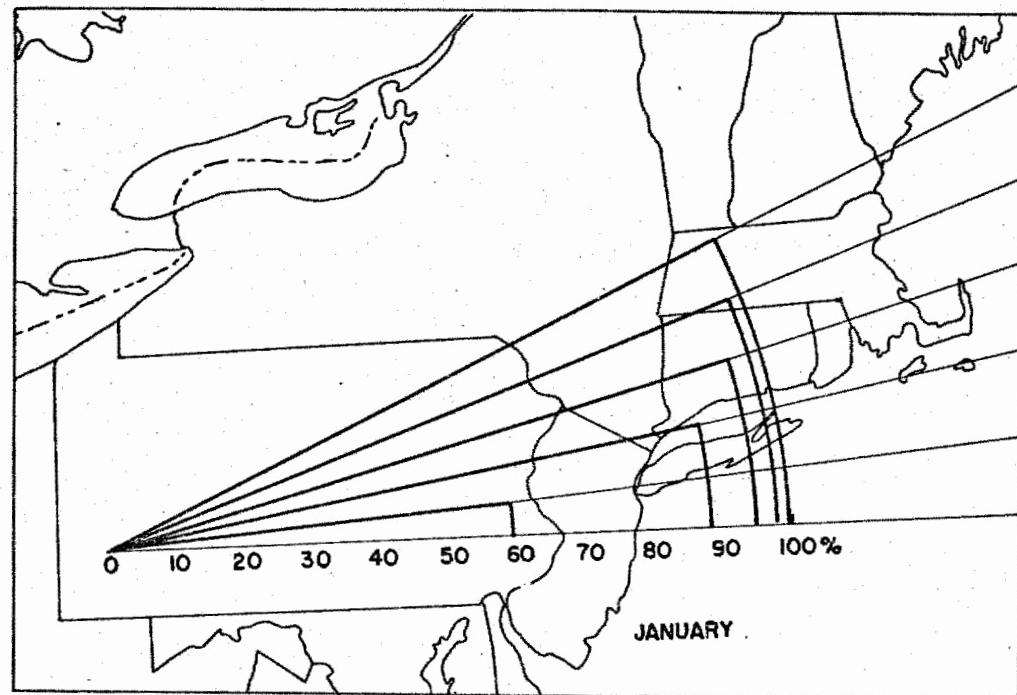
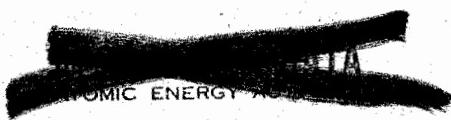


Figure 7  
Frequency of Directional Wind Shear in the Mushroom

DOE ARCHIVES

226



230

which fallout from the indicated height will be deposited. The heavy line shows the places on the ground at which the 100 micron particle of a specific gravity 2.5 will be deposited, while the dotted line shows where fallout will reach at 8 hours after burst. The numbers on the fallout diagram are the heights in tens of thousands of feet: 10,000, 20,000, 30,000 feet and so forth. The direction of motion of the stem below 10,000 feet can be deduced from the surface isobars. No attempt is made to extrapolate beyond the height of observed winds.

It is evident that fallout in Virginia, Maryland, and southern Pennsylvania will be in the rain. No further interpretation of the significance of this fact will be attempted at this time. This is an example of a cyclonic disturbance approaching the target from the south or southwest and shows the fallout to occur typically to the northwest from the lowest levels and the north or northeast from the middle and upper levels.

Other typical winter weather situations are shown in Figures 9 - 11. Figure 9 shows the fallout pattern following the passage of a winter cold front, with fallout occurring to the southeast of Washington. Figure 10 illustrates the conditions well within the cold air, with northwesterly winds in the lowest levels, shifting to southwesterly at the higher levels. Figure 11 typifies conditions after the center of the high has passed Washington and a new low is approaching from the west. Figures 12 and 13 show two examples of summer fallout patterns. Figure 12 illustrates conditions following the passage of a weak summer cold front with northwesterly winds prevailing in the lower levels and very weak easterlies in the stratosphere, while Figure 13 shows a well developed Bermuda high with southerly winds near the surface becoming easterly in the stratosphere resulting in fallout to the northeast of Washington.

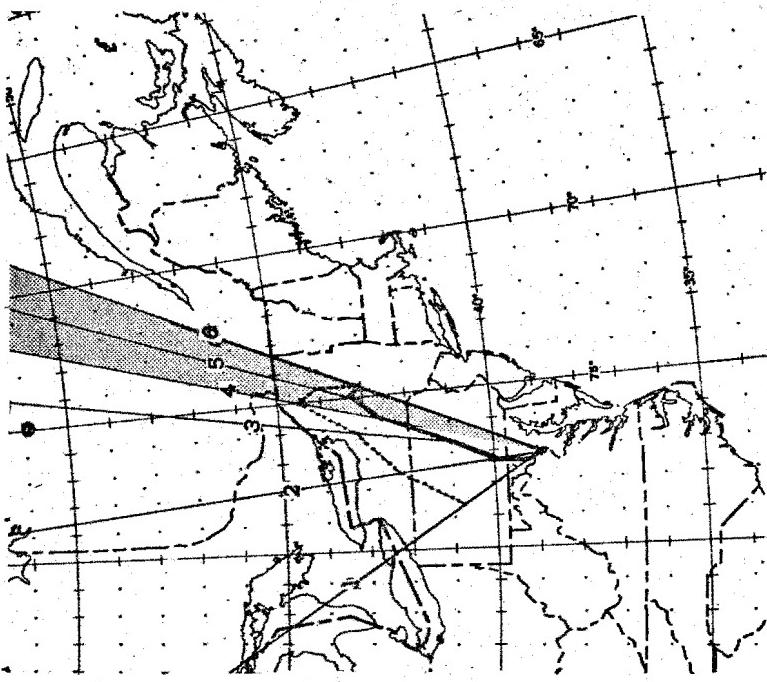
I should like to complete the presentation by returning to the role which meteorology plays in fallout and take a look into the future. The two contributions which the meteorologist can make, as mentioned before, are: Collection of climatological fallout data for planning, and operational fallout forecasts for day-to-day use. I feel that the presentation I have made this morning answers only a very limited number of planning questions. The kind of problem it does not answer is: If the Pentagon were the target for an x megaton bomb detonated at the ground, what is the probability that New York or Philadelphia or Boston might be subjected to a dangerous fallout? If this symposium provides a method by which one may either delineate dosages from the wind data or even delineate, say, two kinds of areas showing different dangers, we feel that we can answer the kind of question which Civil Defense or military commanders are prone to ask. The simple plan to be described represents ideas contributed by many groups besides our own and machine methods may be required in its execution.

DOE ARCHIVES

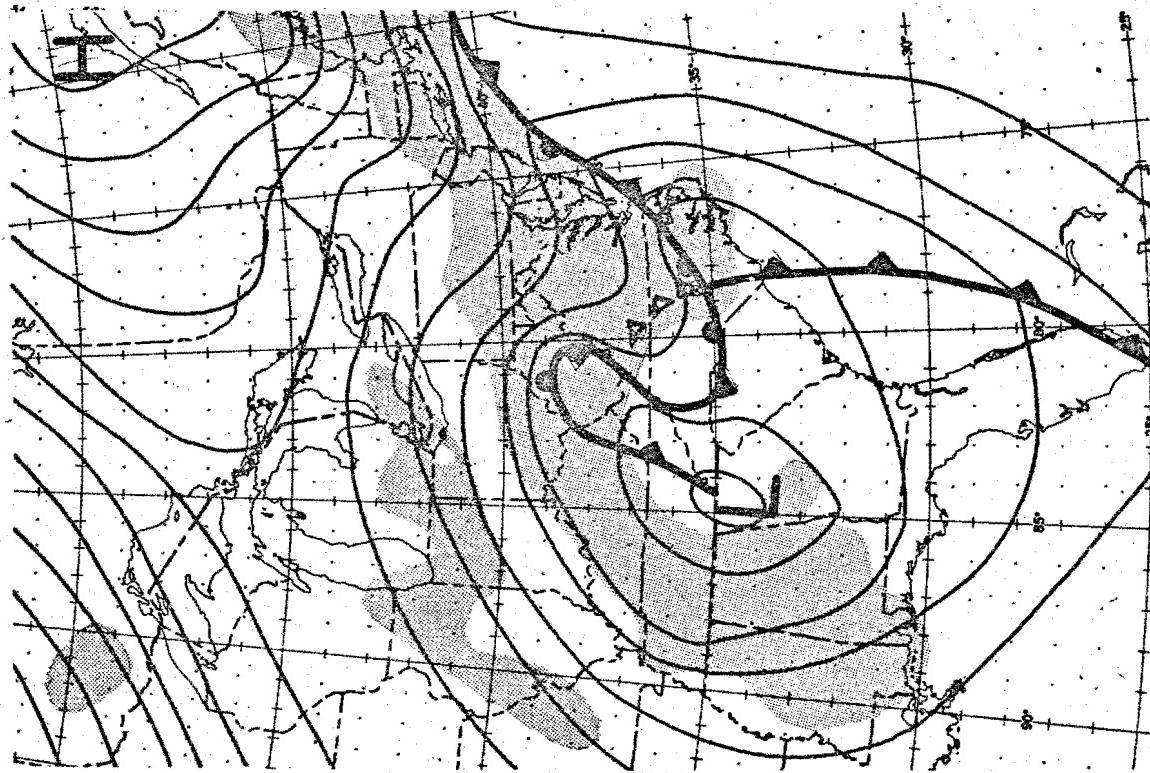
227

DATA  
ATOMIC ENERGY

231



0630Z JAN 10, 1953  
WASHINGTON:  
NIMBOSTRATUS OVERCAST  
CONTINUOUS RAIN  
WIND NE 12 KNOTS

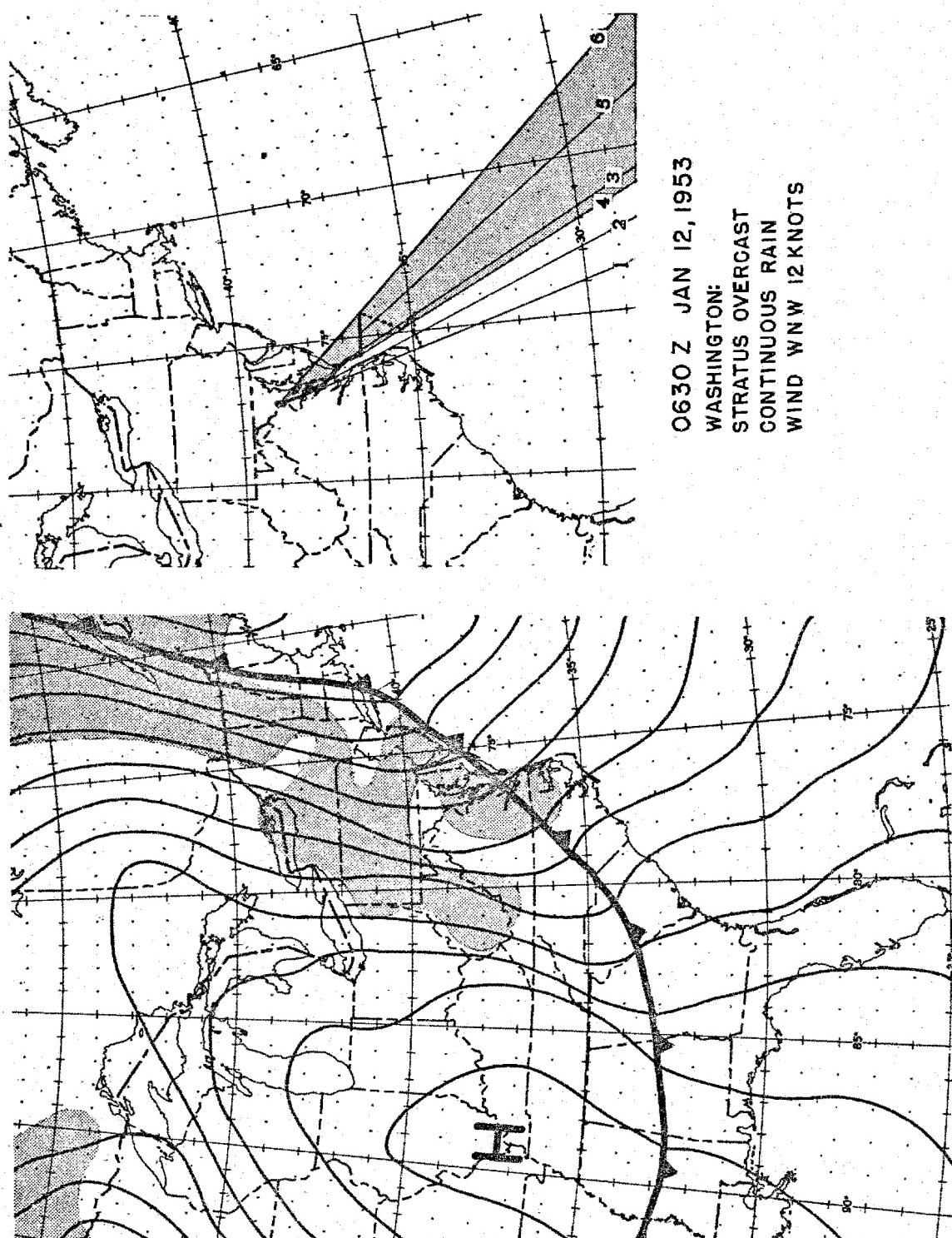


DOE ARCHIVES

228

NUCLEAR ENERGY ACT 15

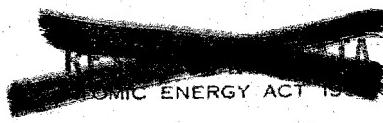
232



0630 Z JAN 12, 1953  
WASHINGTON:  
STRATUS OVERCAST  
CONTINUOUS RAIN  
WIND WNW 12 KNOTS

**DOE ARCHIVES**

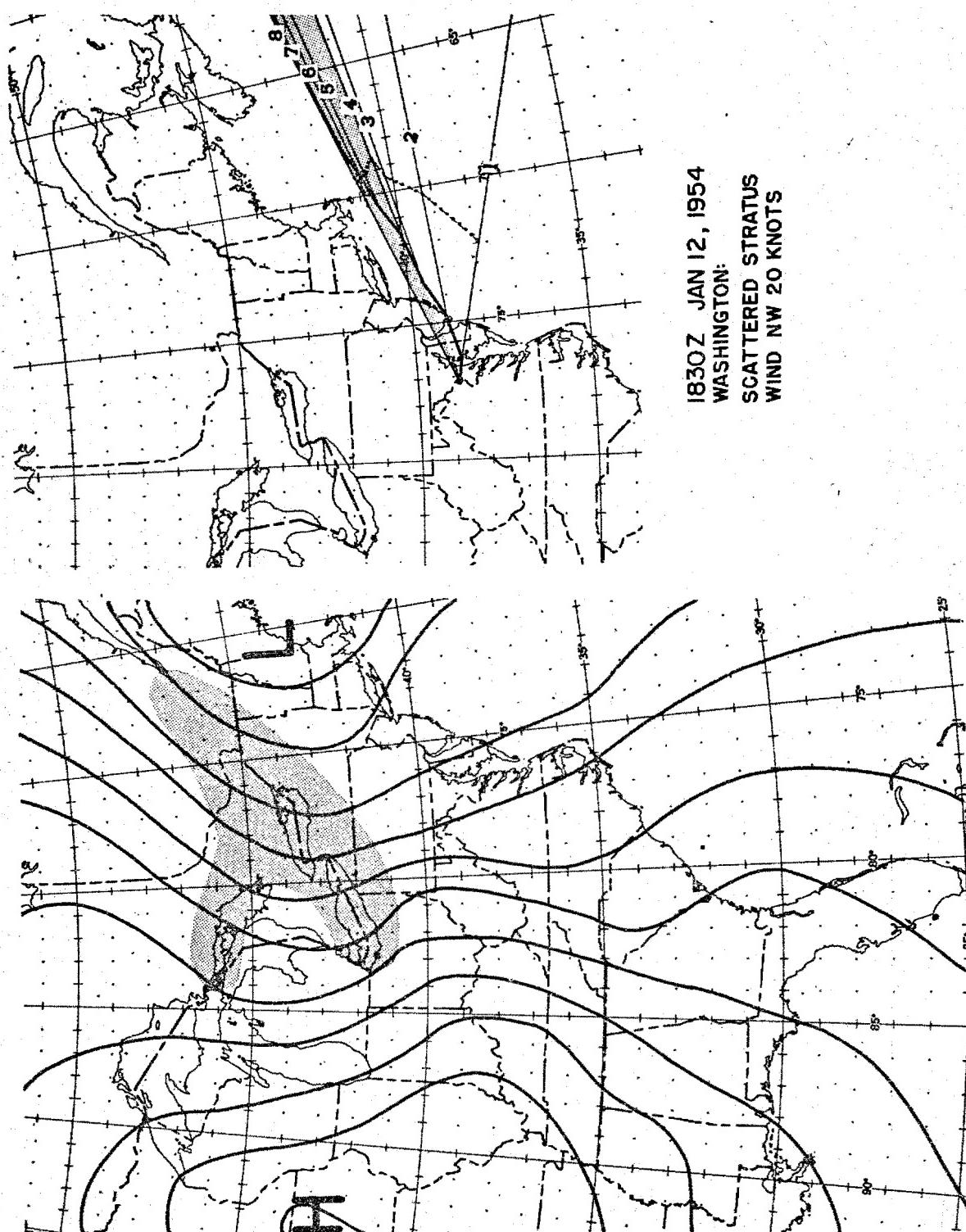
229



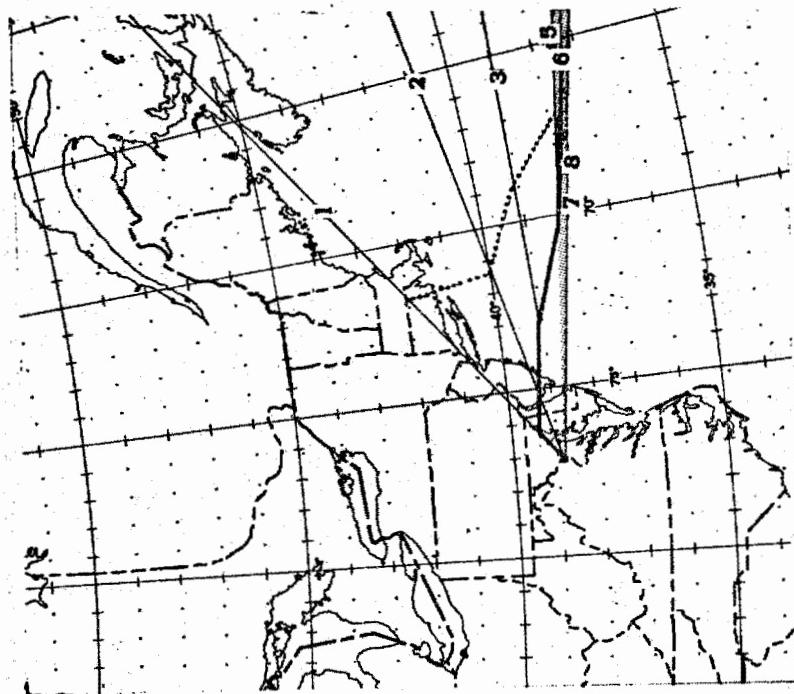
233

Figure 9  
Surface Weather Map and Associated Fall-out Pattern, January 12, 1953

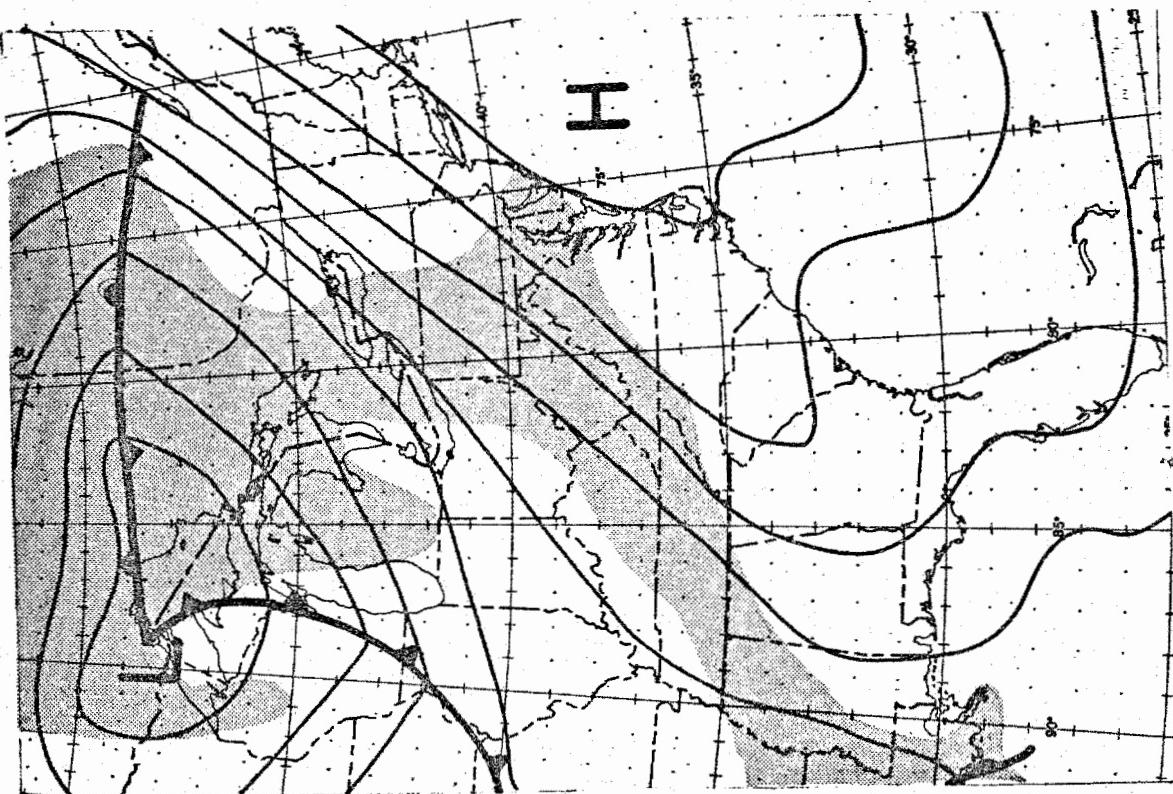
Figure 10  
Surface Weather Map and Associated Fall-out Pattern, January 12, 1954



DOE ARCHIVES



1830Z JAN 14, 1954  
WASHINGTON:  
ALTOCUMULUS OVERCAST  
CONTINUOUS SNOW  
WIND SSW 9 KNOTS



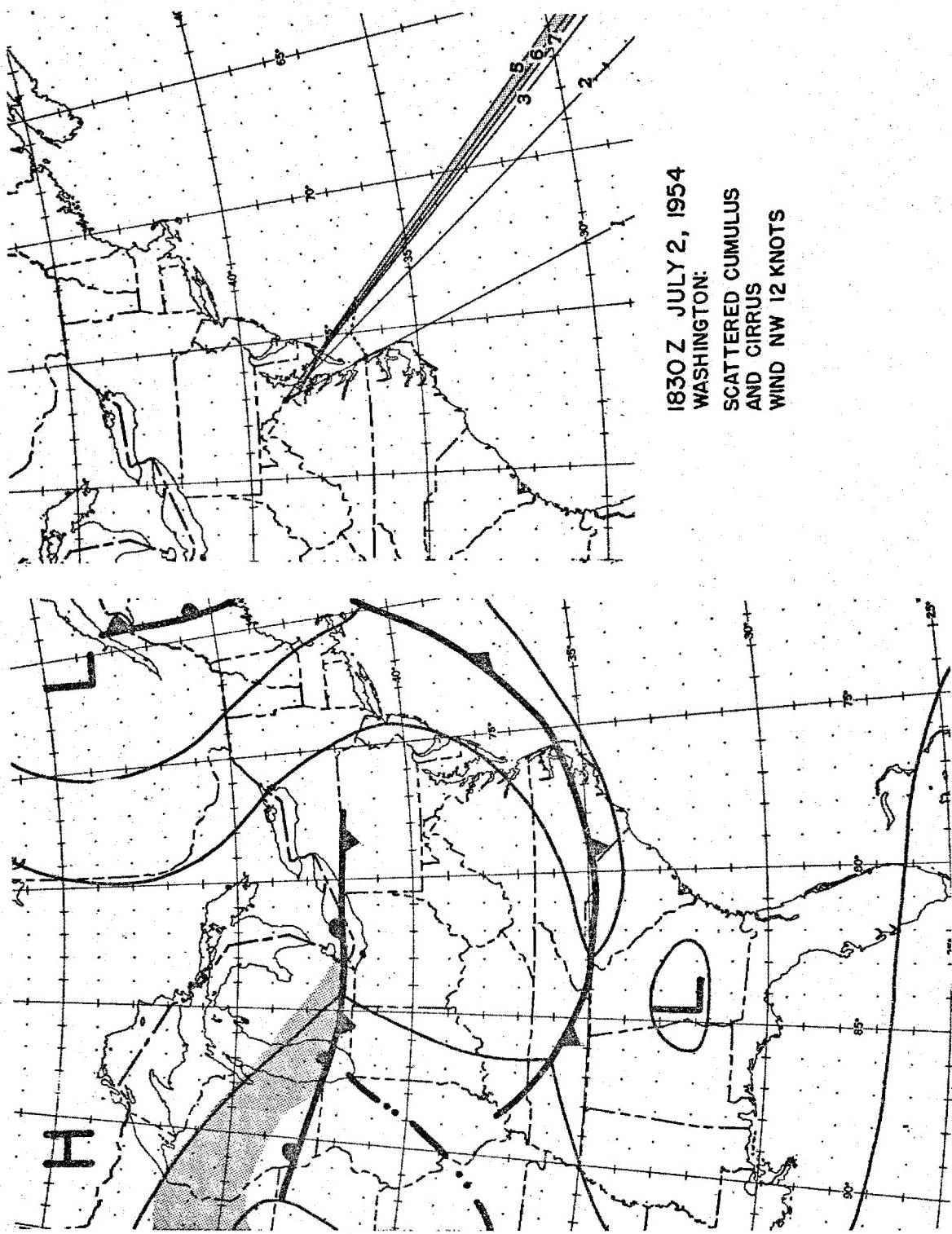
DOE ARCHIVES

231



295

Figure 11  
Surface Weather Map and Associated Fall-out Pattern, January 14, 1954



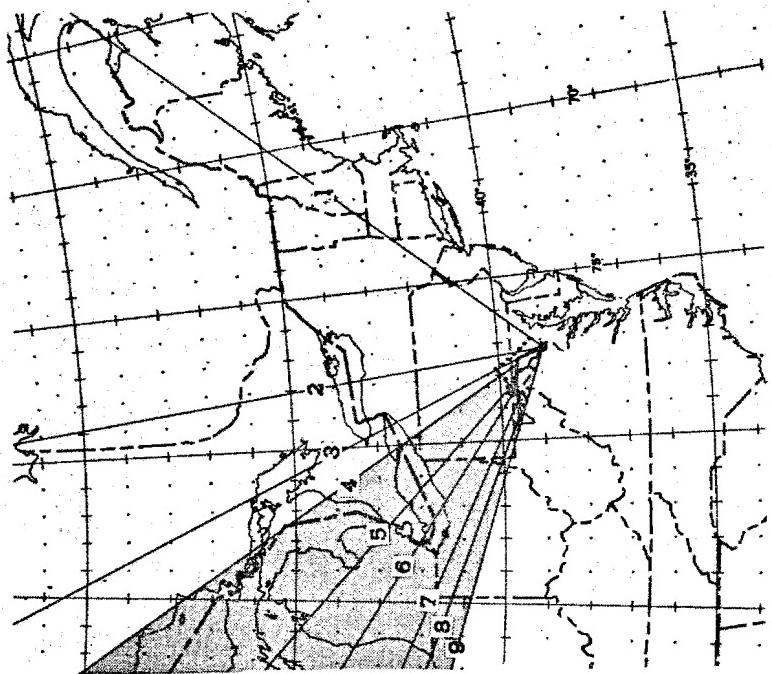
DOE ARCHIVES

232



236

**Figure 12**  
 Surface Weather Map and Associated Fall-out Pattern, July 2, 1954



1830Z JULY 14, 1952  
WASHINGTON:  
BROKEN STRATUS  
WIND S 9 KNOTS

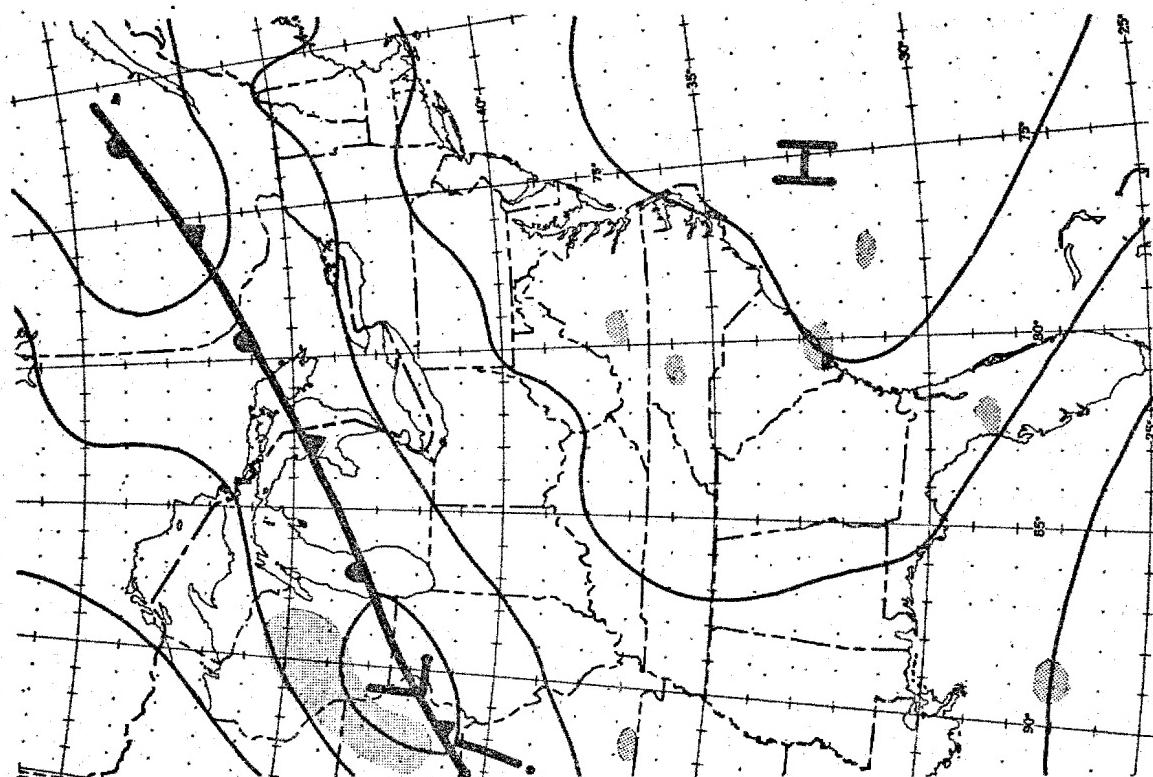


**Figure 13**  
**Surface Weather Map and Associates Fall-out Pattern, July 14, 1954**

DOE ARCHIVES

233

~~RESTRICTED DATA~~  
ATOMIC ENERGY ACT

237

We would first divide the area of interest, for example, the United States, into regions with what we consider to be homogeneous areas of fallout climatology, an example of which is shown in Figure 14. A single upper air wind reporting station would be selected in each region and considered to be representative of the entire region. As we see in Figure 15, fallout diagrams with the areas of, say, dangerous and very dangerous fallout computed from each weather station would then be prepared each day for a number of months of past weather records. For example, the heavy shading might illustrate the very dangerous areas and be surrounded by dangerous areas. On each day, we overlay the same grid of points and then simply count the frequency of occurrence of the point in each area. These may then be tabulated for each season and analyzed to provide probability distributions shown on the right. When the probability distribution for occurrences of very dangerous fallout is superimposed on a potential target, one can readily read off the percentage probability at, say, a nearby city and obtain the likelihood that it would lie within the very dangerous fallout region for the given target.

This, I believe, would satisfy very many planning requirements. A different story must be told for the day-to-day operational capabilities of the meteorologist.

First of all, even if we use persistency as a forecasting tool - that is, take wind observations, say, every 6 hours and use the last observation to transport the fallout debris, I am not even sure our present observational network is adequate. There are two main defects: first, the average height of the wind runs is only 55,000 feet and even at Silver Hill here in the Washington area where ideal operating conditions exist, the average height of the wind runs is only 75,000 feet. Frequently, we do get runs in excess of 100,000 feet, but these are usually in warm climates and with wind speeds which are not excessive. My guess is that, in the winter, with current equipment, the average height of the upper wind observations over northern U. S. is well below 55,000 feet. Second, if the balloon is too near the horizon, it either cannot be tracked at all or the wind data becomes uncertain. Thus, if the speeds are high, making low elevation angles, our wind data becomes much poorer. In addition, the present method of analyzing and reporting upper winds is not particularly suited for fallout computations and certain unnecessary errors are introduced. In Figure 16, we see part of an actual plot of wind speed with height. What is normally used in preparing fallout plots are the winds at 5,000-foot levels rather than vertically integrated winds. The latter would be more desirable from a fallout viewpoint, since winds at all levels transport the particles. Although chosen at random, you can see in Figure 16 that the speed at each 5,000-ft. level is lighter, by chance, than the mean through the layer in which the wind is centered so that the predicted fallout would fall short of where it would actually be.

DOE ARCHIVES

234

SECRET

RESTRICTED DATA  
ATOMIC ENERGY ACT 1954

238

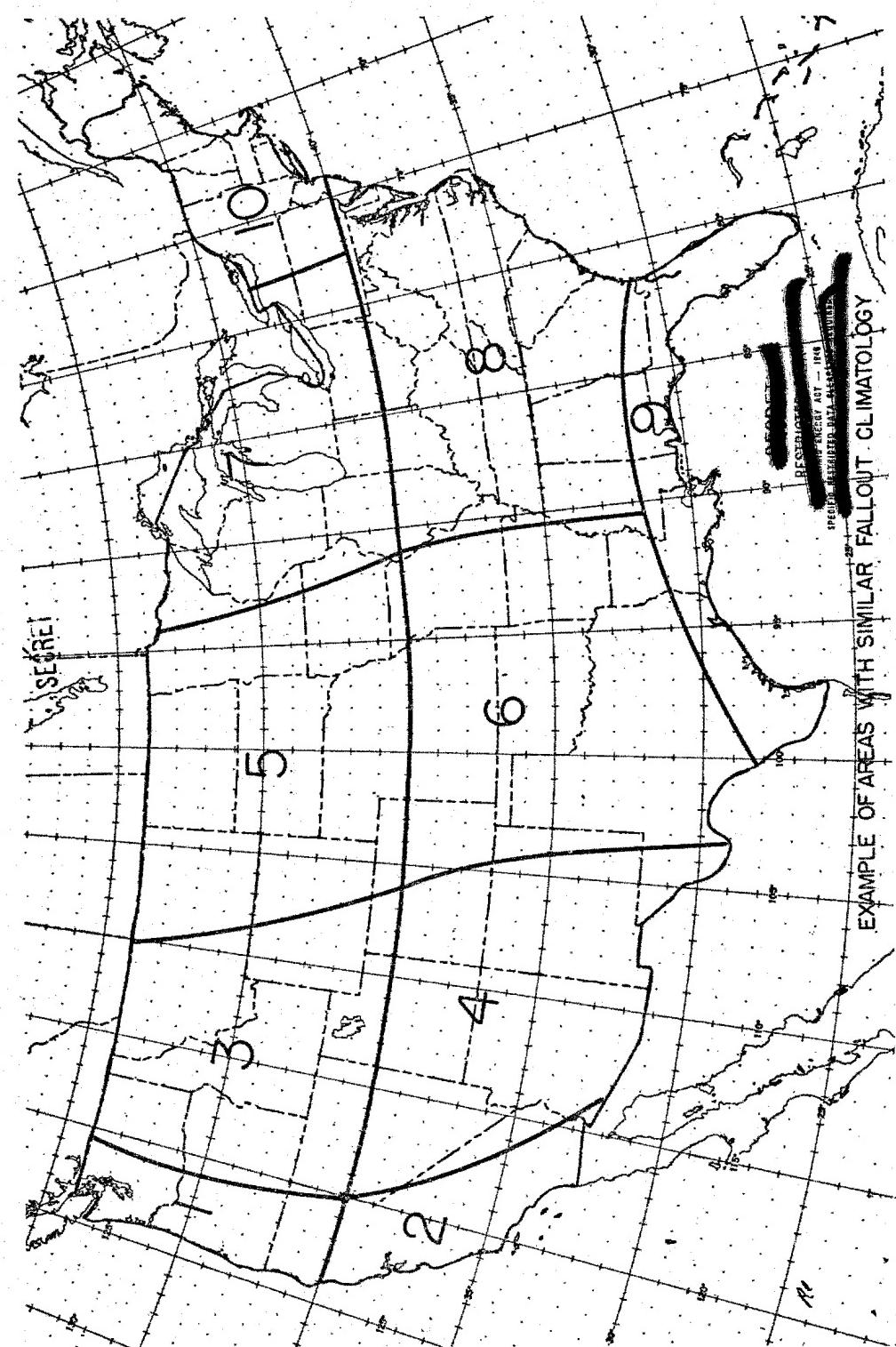
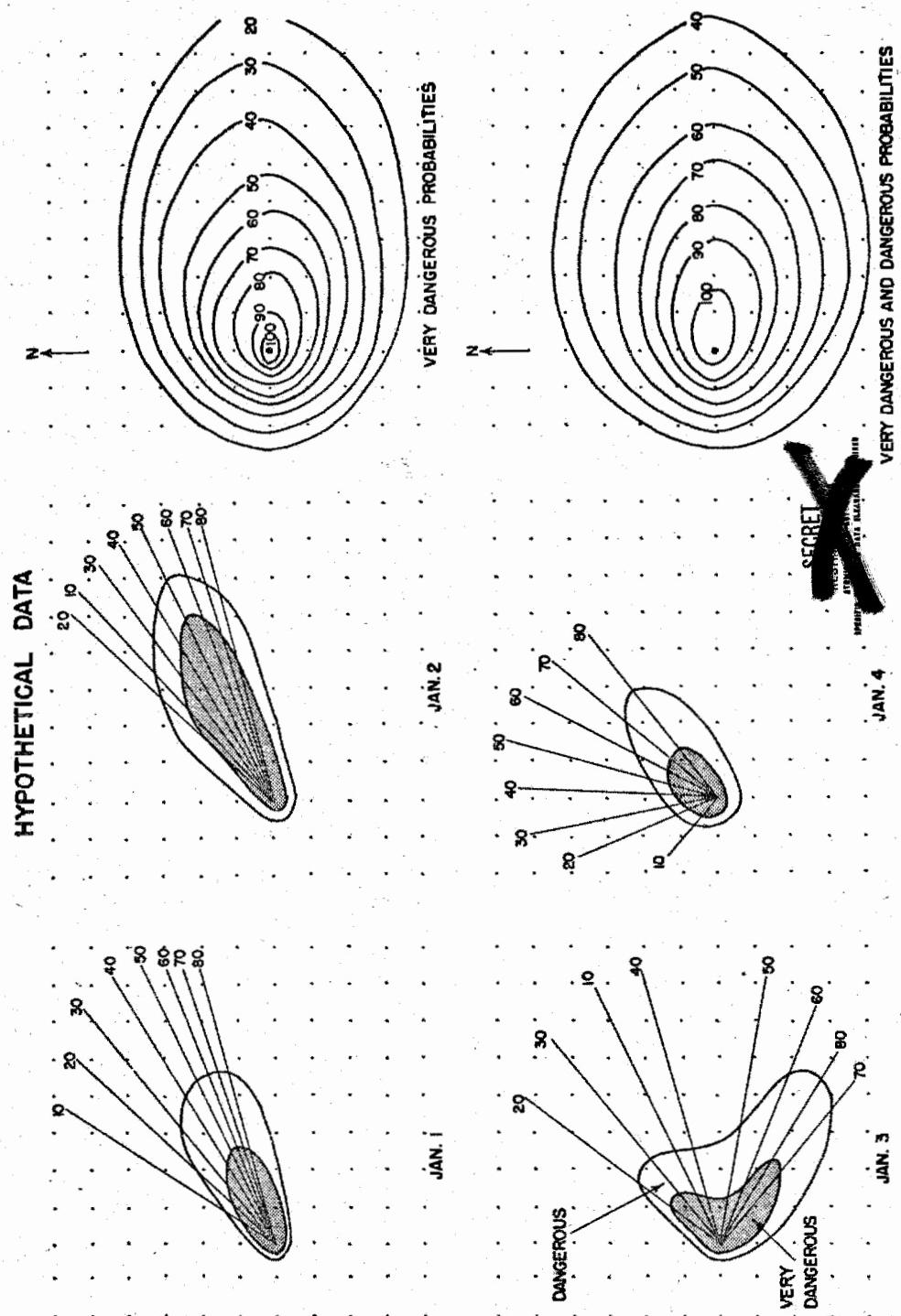
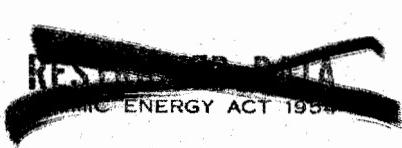


Figure 14  
Examples of Areas with Similar Fall-out Climatology



DOE ARCHIVES

236



240

Figure 15  
Examples of Fall-out Diagrams and Probability of Occurrence of Very Dangerous and Dangerous Fall-outs

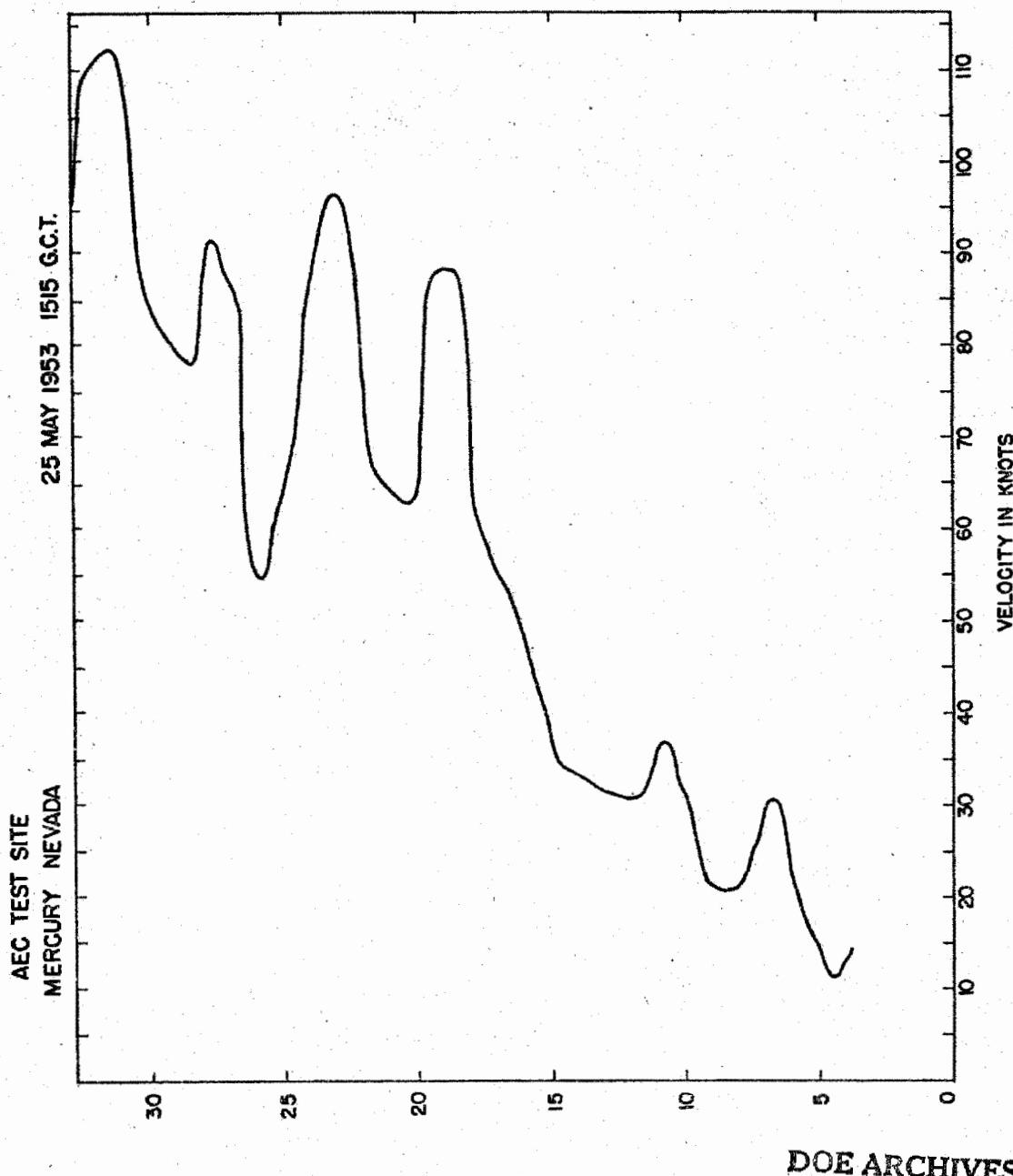


Figure 16  
Typical Wind Variation with Altitude

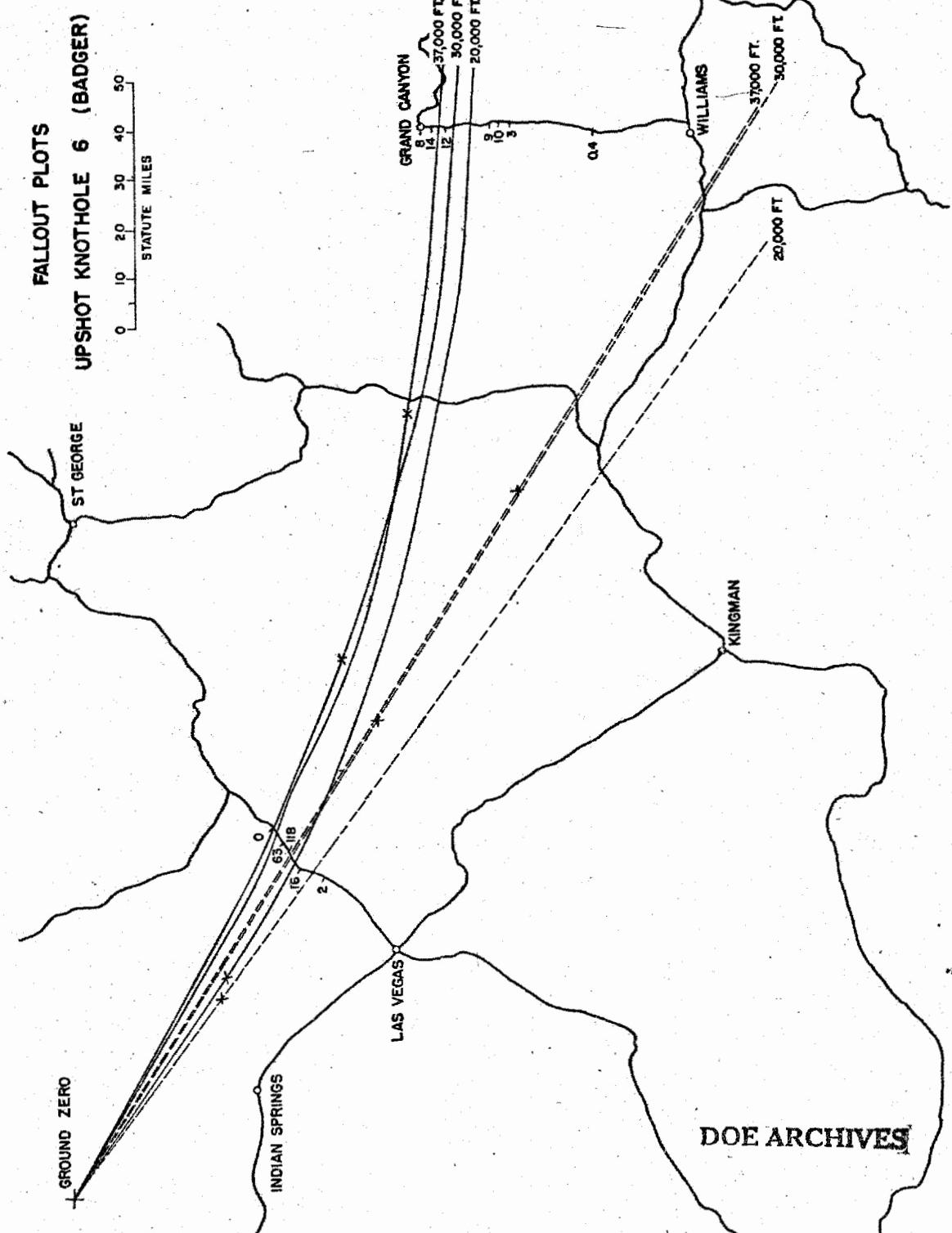
It is highly unlikely, if a bomb is actually detonated or we know one will be detonated, that a persistency forecast will be acceptable. Weathermen will be asked to make best possible forecasts where so much is at stake. Unfortunately, we have practically no forecasting experience at levels above about 30,000 feet, and, in fact, do not routinely even draw weather maps above 55,000 feet. Our experience, in fact, is so limited to the lower atmosphere that, at the Nevada Test Site, the absolute wind forecast error doubles from the 20,000 layer to the 40,000-foot layer. Further, time and space variability of the wind can be adequately included only by the meteorologist. Concerning the need to incorporate time and space changes in the wind, I have an interesting case showing a comparison of using point winds with time and space variable winds, in Figure 17. The straight dashed lines are the lines along which fallout occurs from a given height if the test site wind at burst time alone is used at Nevada while the curved solid lines incorporate time and space variability. The numbers are the observed fallout along the roads. It is clear that the time and space variability is superior, although it may not always provide as good a forecast as shown here. The need for time and space variability is much greater in the case of megaton weapons than in Nevada test operations since fallout is important for longer times and to greater distances.

Finally, the meteorologist must be able to provide the Civil Defense official or military commander with a measure of the uncertainty in the forecast. We can all imagine cases in which, if the uncertainty in fallout forecast is too great, it may do more harm than good.

In conclusion, the meteorologist even today can provide certain valuable generalities about the probable areas of radioactive fallout, but much remains yet to be done to answer questions about dosages or dangerous areas and about the details of the fallout probabilities. Finally, the weatherman needs much more development research and training before he can really assist in operational fallout forecasting.

DOE ARCHIVES





239

REPRODUCED UNDER THE  
AMERICAN ENERGY ACT 1980

243

Figure 17  
Effect of Time and Space Variability of the Wind on the Location of Fall-out

**THIS PAGE IS BLANK**

**DOE ARCHIVES**

**240**



ENERGY ACT

244

PREDICTION OF DOSE-RATE AND DOSAGE CONTOURS AS  
FUNCTIONS OF YIELD AND METEOROLOGICAL CONDITIONS,  
AIR WEATHER SERVICE METHOD

Lt. Col. Clifford A. Spohn, USAF  
Air Weather Service

My talk today is, in a sense, sailing under false colors. The problem under consideration during this portion of the symposium deals with the determination of ground levels of contamination resulting from fallout, and I am listed in the program as presenting the Air Weather Service method. Actually, the method of fallout prediction used by Air Weather Service does not provide an answer giving ground contamination levels. The technique currently used is concerned only with the meteorological portion of the problem, that is, specifying where and when fallout will occur.

The technique itself is a very simple one, and is based on the following assumptions:

That the point winds near the detonation point (observed or forecast) are representative of the time-space wind field through which fallout takes place.

That winds at successive 10,000-foot layers in the atmosphere are representative of the wind flow through their respective layers.

That the various contaminated particles will have constant fall rates, although the fall rates are unspecified, and need not be related to particle size.

That fallout takes place upon a level surface, i.e. terrain variations are ignored.

Given these assumptions, the fallout plot is easily prepared. The wind sounding, observed or forecast, for the place in question, is used to construct composite wind vectors. The 5000' wind vector (representing flow in the layer from sea level to 10,000') is laid off from the ground zero position. From the end of this vector, the 15,000' wind vector (for the layer 10,000' - 20,000') is next laid off. The 25,000' wind vector is laid off from the end of the 15,000' wind vector, and the process continued to as high a level as desired, or to the end of the wind data. Radial lines are now drawn from ground zero to the ends of the various wind vectors and labeled appropriately. Thus, the radial line to the end of the 15,000' wind vector is labeled 20,000'; to the end of the 25,000' wind vector, 30,000', etc. These radial lines are the resultant

DOE ARCHIVES



wind vectors from the specified level to the ground, and indicate the line away from ground zero along which fallout from the given level will take place. The lengths of these resultant vectors is measured and divided by their labeled heights expressed in tens of thousands of feet (i.e., the length of the resultant vector labeled 20,000' will be divided by "2", the 30,000' vector divided by "3", etc.). The numbers obtained represent the speed at which fallout will progress outward from ground zero along the various radial lines.

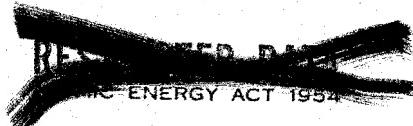
The finished plot is prepared by laying off the resultant vectors, and marking off along them successive hourly positions of fallout. By connecting all of the points corresponding to a given time after zero, the line along which fallout will occur at that time is indicated.

The completed plot thus shows three items. First, the general area in which fallout will take place; second, the lines along which fallout from a given level will occur; and, third, the lines along which fallout will occur at particular times.

The validity of the underlying assumptions must certainly be considered. The latter three assumptions, that of a constant fall rate, fallout on a level surface, and using a wind as representative of a 10,000' layer, will not, in general, introduce much error. The first assumption, however, that a spot wind sounding will be representative of the space-time wind field throughout which fallout takes place, is less dependable. On a comparatively small test sample from the Nevada Proving Ground, using wind soundings taken two hours prior to detonation, and for fallout computed out to not more than nine hours after detonation, 75% of the resultant vectors deviated by less than  $15^{\circ}$  from a post-analyzed position. If the fallout computations are extended considerably beyond nine hours, or if old wind data (i.e., 24-hour forecasts or observations 6 - 12 hours old) are used, this assumption becomes increasingly less reliable, and may lead to quite serious errors in the calculated fallout plot. For this reason, current Air Weather Service practice is to use, if at all possible, observed wind data less than six hours old, and to compute fallout out to 6 - 9 hours from time zero.

DOE ARCHIVES

Note: Examples of problem solutions by the Air Weather Service method are given in the paper, "Comparison of Problem Solutions by Various Methods," by Cdr. R. W. Paine.



PREDICTION OF DOSE-RATE AND DOSAGE CONTOURS AS  
FUNCTIONS OF YIELD AND METEOROLOGICAL CONDITIONS,  
NAVY WEATHER SERVICE METHOD

Dr. F. W. van Straten  
Office of the Chief of Naval Operations

The Navy method for predicting the location of potential radioactive areas after a surface burst of an atomic weapon over land or shallow water is designed to permit routine computations in advance of an actual explosion. It is expected that transparent overlays showing potential radioactive areas will be prepared, when necessary, after each wind sounding. These overlays will then be available for superimposition on a map should an atomic explosion occur during the valid time of the wind sounding. Although it is realized that this procedure gives only approximate results, it is felt that immediate operational decisions can be made on the basis of these approximations. Time and data permitting, more refined computations can be made subsequent to the event.

To permit this computation in advance of an explosion - when the height of the explosion is unknown, the size and nature of the bomb is not known and the terrain characteristics are undetermined - a number of assumptions is required. The limitations resulting from these assumptions are acceptable in view of the availability of a rough diagram from which immediate tactical decisions can be made.

It is assumed that the explosion penetrates the tropopause. This assumption is made so that the diagram will show the maximum area which may be affected. If it is determined, subsequently, that the radioactive cloud did not, in fact, penetrate the tropopause, the diagram can later be reduced.

DOE ARCHIVES

Lack of knowledge concerning the nature of the bomb and terrain necessitates assumptions about the distribution of particles in the radioactive cloud and their rate of radioactive decay. It is assumed that any horizontal cross section through the stem is identical with any other horizontal cross section. In other words, it is assumed that all particle sizes are distributed uniformly throughout the cloud. Further, radioactive decay is postulated to occur at a rate proportional to the square of the diameter of the particle and inversely proportional to the square of the time from the explosion.

Although it is recognized that a complete spectrum of particle sizes is probably present, only a size range between 75 and 150



microns is considered. It is assumed that particles larger than 150 microns will fall out so close to ground zero as to produce no additional hazard. The smaller size particles, less than 75 microns, are of concern, principally, because of the great distances they can travel in the time it takes them to fall from high altitudes. For particles smaller than 75 microns, this time is so great that considerable modification in the wind field is possible, and a computation based on a current wind sounding may lead to completely erroneous results. Particles of 75-micron size are assumed to fall at a rate of 5,000 feet per hour, while those of 150-micron size fall at a rate of 5,000 feet in 3/10 of an hour.

For the original construction of the potential radioactive area, it is assumed that validity is limited to 6 hours in time, and 250 miles in radius.

It should be noted that provision is made for subsequent extension in time and area. Further, while the diagram plotted in advance is designed to show fall-out on the surface, the method also lends itself to subsequent computations to show radioactive areas at any altitude and time - air radex plots - following the explosion.

In brief, the method used by the Navy consists of the following steps:

Determination of the mean wind vectors between specified levels.

From the mean wind vector and the rate of fall, the position of fall-out and the time taken to fall are computed for each size particle.

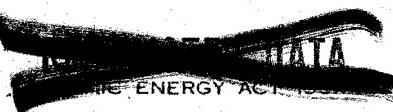
The positions marked along the mean wind vectors permit definition of the area of fall-out.

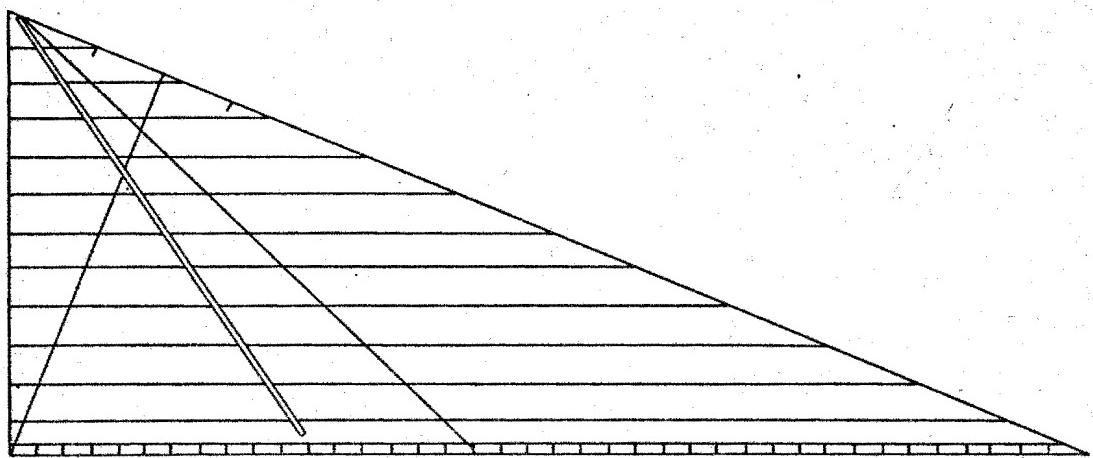
The time marks can be used to draw lines showing the approximate time at which radioactivity reaches the surface within the affected area.

The degree of radioactive contamination in any given unit area is considered to be proportional to the number of mean vectors traversing that area. From the vector concentration and the time lines, it is possible to compare relative radioactivity from unit area to unit area. A series of lines is drawn on the diagram connecting area of equal radioactivity.

DOE ARCHIVES

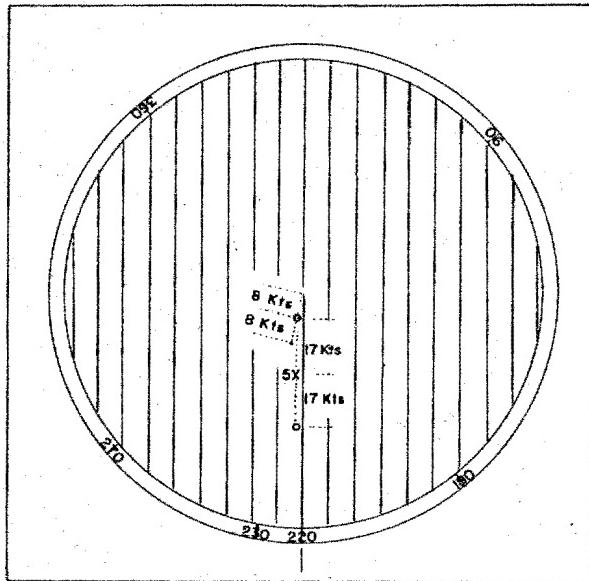
In practice a conventional winds aloft plotting board, a transparent plastic sheet and a radex rule are used. Figure 1 is a diagrammatic sketch of the radex rule.





**RADEX RULE**  
**ML - 502 / UM**

**Figure 1**



PLOT OF SURFACE AND 5000' VECTOR ON PLOTTING BOARD

DOE ARCHIVES

**Figure 2**

245

**RESERVE DATA**  
ENERGY ACT

249

Across the base of the radex rule is a scale used for plotting wind speeds. When a given mean wind vector is placed under the radex rule in such a way that it is parallel to the horizontal lines on the rule and extends from the vertical side to the dark line hypotenuse, the slot in the radex rule marks the position of fall-out of the 150 micron particles and the outer hypotenuse - edge - marks the position of fall-out of the 75 micron particles. The line extending from zero on the base scale to the hypotenuse, together with the tick marks on either side of this line, is used to expand a plotted diagram by  $10^{\circ}$  to take care of dispersion and minor errors in wind information.

The following specific steps are followed to produce the Navy diagram:

On the plotting board, add the 5,000 foot wind vector to 1/2 the surface wind vector. On the end of the 5,000 foot vector add the 10,000 foot vector. Continue this process with each 5,000 foot wind vector to the top of the sounding. The radex rule is used for marking the wind speeds. See figure 2.

Place a transparent, plastic sheet over the plotting board. Mark the center of the plotting board and then mark the  $180^{\circ}$  position of the plotting board as north. Transcribe the mid point of each wind vector on the plastic sheet. Thus the mid point of the 5,000 foot vector is transcribed and labeled 5. The mid point of the 10,000 foot vector is labeled 10, etc.

Connect the center indicated on the plastic sheet with the points marked 5, 10, 15, etc., extending the line well beyond the marked points.

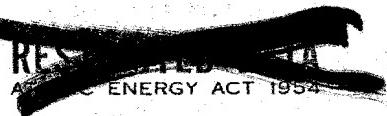
Place the radex rule on each vector in turn so that the center indicated on the plastic sheet is on the vertical edge of the rule, and the numbered point is on the dark line hypotenuse with the vector parallel to the horizontal lines. Mark through the slot on to the vector and mark the edge of the radex rule on the vector. See figure 3.

For the vector labeled 5 the slot marking is labeled 3 indicating  $3/10$  of an hour. The outer mark is labeled 10 indicating one hour. On the vector labeled 10 these corresponding points are 6 and 20. The 15 vector shows 9 and 30, etc. See figures 4 and 5.

Using the radex rule, expand the diagram by adding  $10^{\circ}$  on either side of the outer vectors. See figure 6.

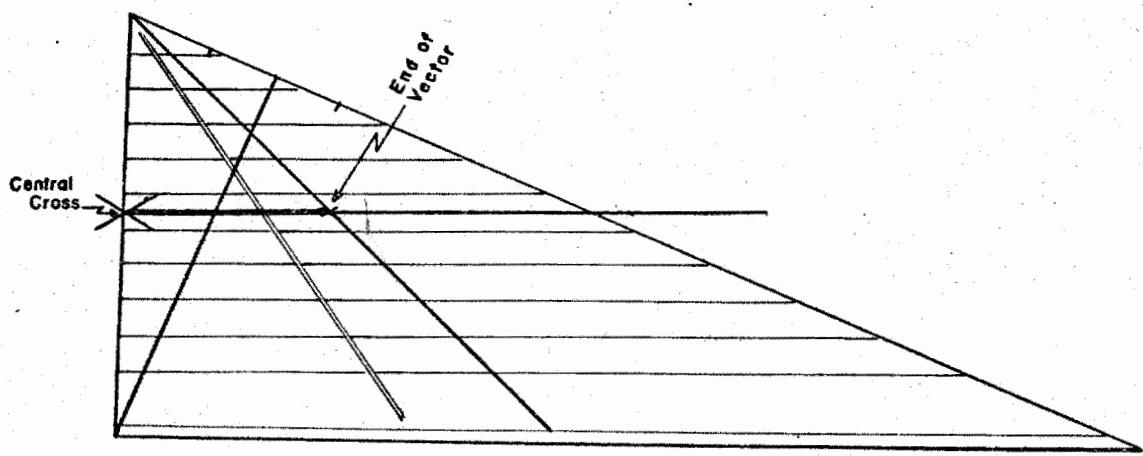
Estimate the position of "10" - the one hour position - on each of the vectors, and draw a line through these points. Repeat for 2 hours, 3 hours, etc.

Enclose an area on the overlay limited by the  $10^{\circ}$  expansion lines, the vector ends, the 6-hour line and the 250 mile radius arc, whichever is smallest (the scale of the radex rule is such that  $20^{\circ}$  is equal to 250 miles).



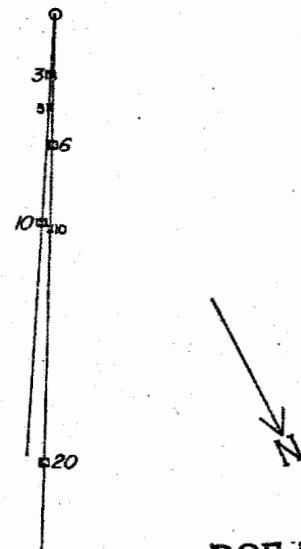
SECRET

250



RADEX RULE IN POSITION ON VECTOR

Figure 3



DOE ARCHIVES

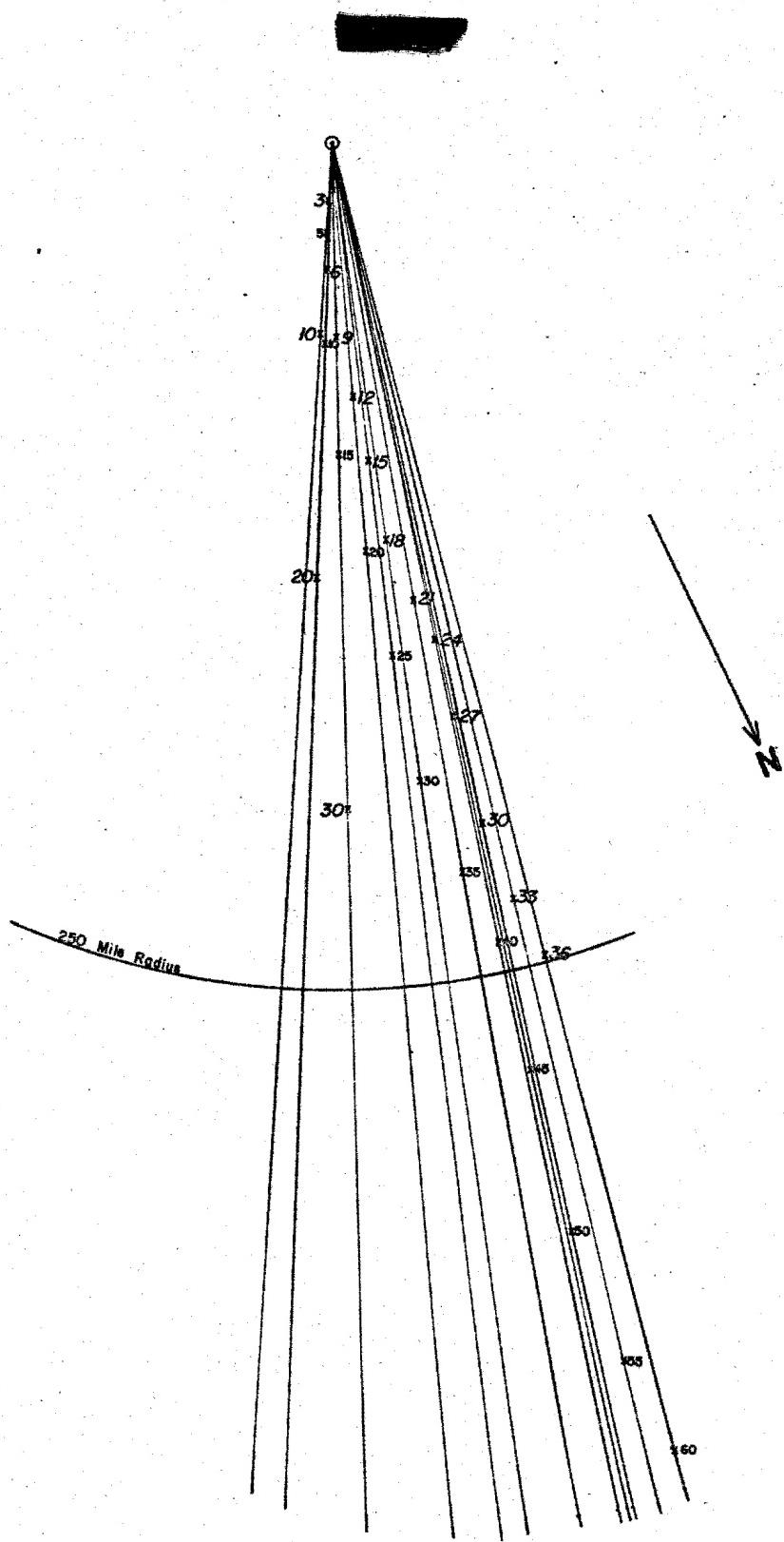
Time Marks are on first two  
Vectors

Figure 4

247

REDACTED  
OMIC ENERGY ACT 1954

251



DOE ARCHIVES

Figure 5  
248

~~RESTRICTED DATA~~  
NUCLEAR ENERGY ACT 1954

252

TABLE I

<u>LARGE</u>		<u>SMALL</u>	
<u>TIME</u>	<u>ACTIVITY</u>	<u>TIME</u>	<u>ACTIVITY</u>
1	1300	1	600
2	600	2	350
3	150	3	60
4	80	4	40
5	60	5	20
6	40	6	16
7	30	7	12
8	20	8	9
9	16	9	7
10	13	10	6
11	12	11	5
12	10	12	4

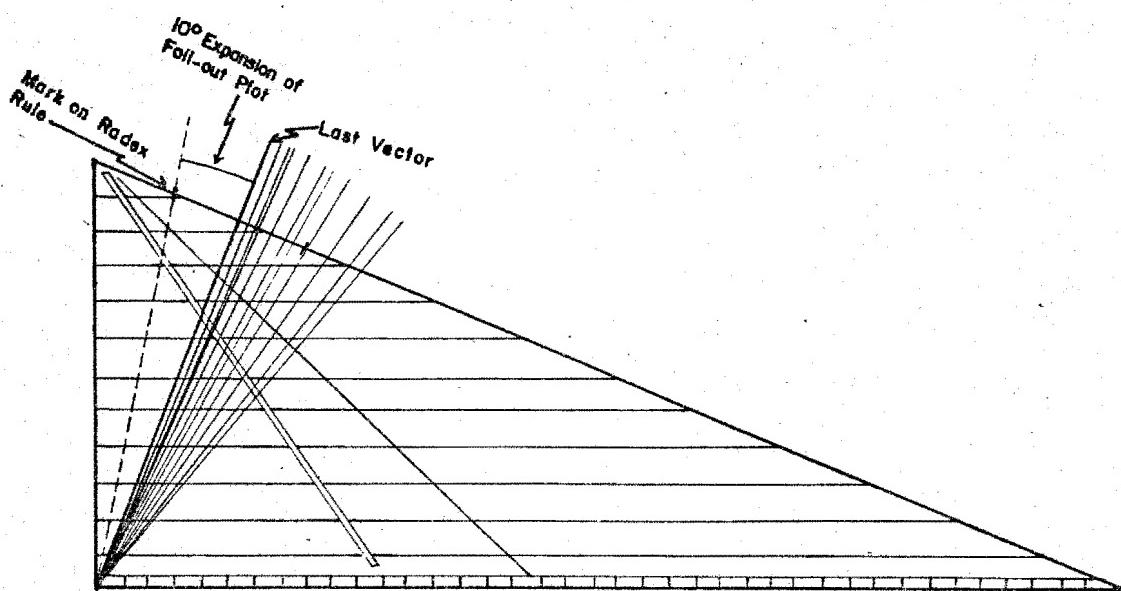


Figure 6

249

DOE ARCHIVES



253

Place a rectangular grid over the diagram and count up the number of vectors traversing each grid area. The grid is drawn in squares 8/10 of an inch from the side. On the grid draw a line connecting the 3, 6, 9, etc., points. Those portions of the vectors which fall closer to the center than this line represent large particle fall-out. The remainder of the vector represents small particle fall-out. Using Table I, the number of vectors and the time lines calculate the relative radioactivity in each area. Connect areas of equal indicated activity. See figures 7 and 8.

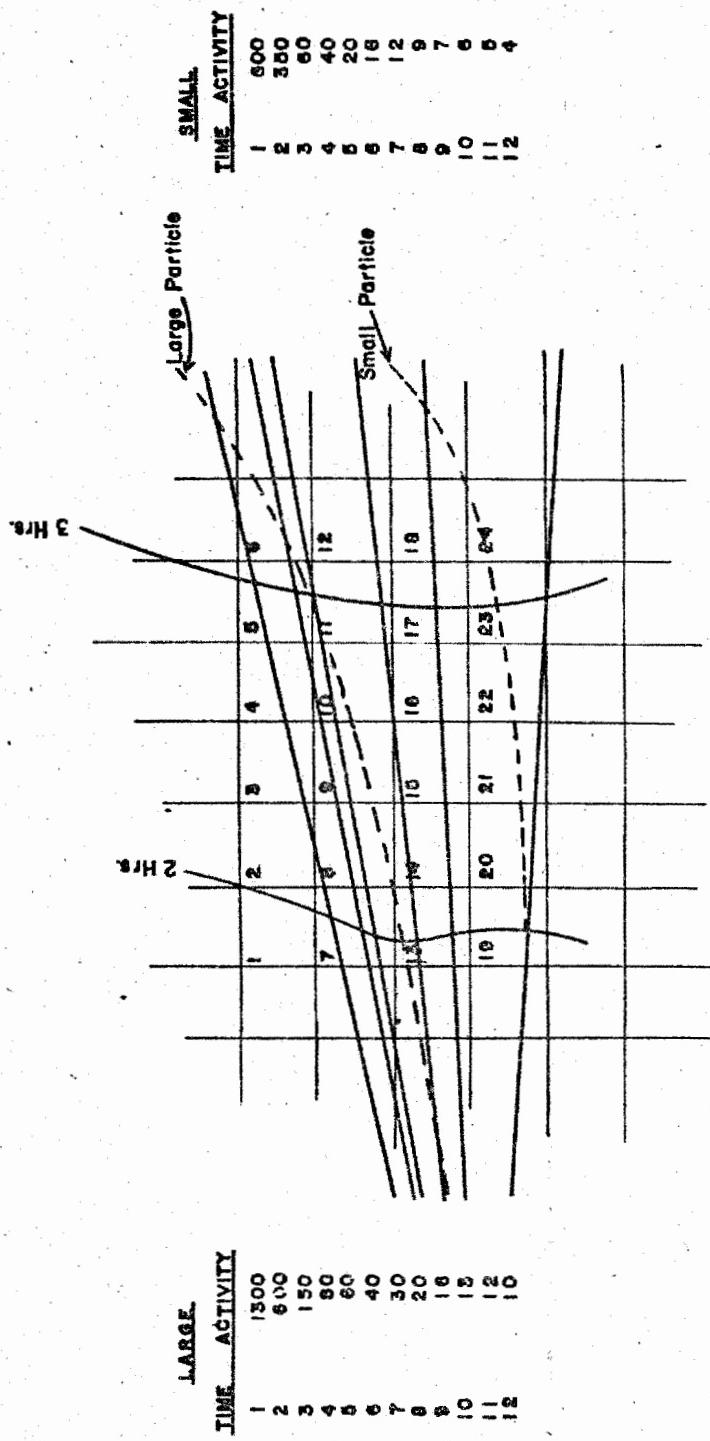
The diagram is now completed since it shows the area of probable fall-out, the time of fall-out and the relative activity.

The steps for preparing an air radex plot will not be outlined in detail. Suffice it to say that appropriate mean wind vectors are selected. For example, if an air radex plot at 5,000 feet and H + 1 hours is required, small particle fall-out will originate from the 10,000 foot level and large particle fall-out from the 20,000 foot level. Thus, only vectors between 5,000 and 20,000 feet are used.

To expand the diagram timewise, an appropriate air radex plot is first constructed and then a new wind field used to determine how particles fall from the selected level to the surface.

One final note is required, it is assumed that the intensity of radiation is proportional to the ratio of the square of the diameter of the particle to the square of time. This ratio is given as relative activity. To convert relative activity to actual activity it is necessary to have a proportionality constant. Presumably a single measurement anywhere within the area can provide this constant and will permit conversion of all relative values to actual values.

DOE ARCHIVES



Grid #	Activity	Grid #	Activity	Grid #	Activity	Grid #	Activity
1	0	7	3 x 600 = 1800	13	2 x 350 = 700	19	600
2	600	8	3 x 600 = 1800	14	2 x 350 = 700	20	0
3	600	9	2 x 600 = 1200	15	2 x 350 = 700	21	0
4	2 x 150 = 300	10	2 x 150 + 60 = 360	16	60	22	0
5	2 x 150 + 60 = 360	11	150 + 60 = 210	17	60	23	0
6	2 x 150 + 60 = 360	12	60	18	0	24	0

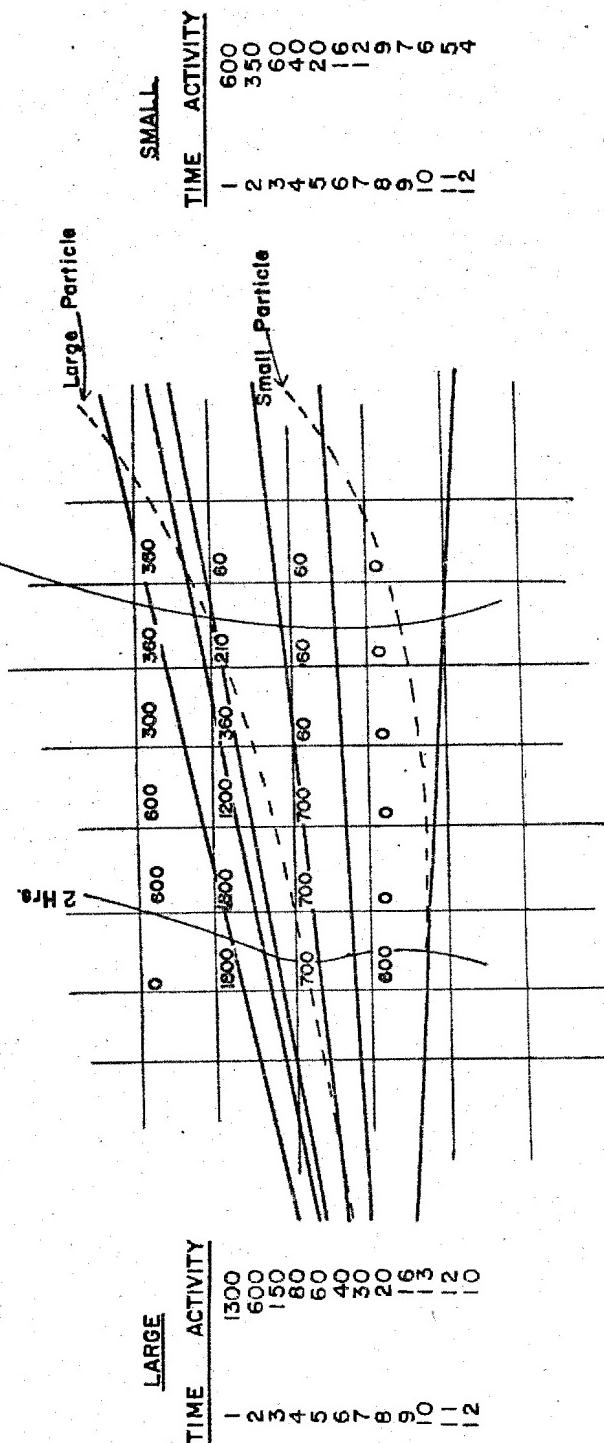
DOE ARCHIVES

RESTRICTED DATA  
AMERICAN ENERGY ACT 1954

261

255

Figure 7



DOE ARCHIVES

252

SECRET



Figure 8

256

PREDICTION OF DOSE-RATE AND DOSAGE CONTOURS AS  
FUNCTIONS OF YIELD AND METEOROLOGICAL CONDITIONS,  
ARMY SIGNAL CORPS METHOD

Donald M. Swingle  
Signal Corps Engineering Laboratories

The Army Problem

During the latter half of 1954 the Signal Corps received an urgent requirement to provide fall-out computations for a study. The two Signal Corps organizations interested in meteorology, i.e., the Signal Corps Engineering Laboratories and the Army Electronic Proving Ground, united to perform the required job. SCEL was to determine or develop a suitable fall-out computation method and AELCTPG was to apply the method to the computation of the patterns required.

The requirements of the Army problem called for the quantitative computation of radioactive fall-out material and dosage under a number of different meteorological conditions. A survey of existing computation methods revealed none that would obtain the required results. It was, therefore, decided to devise a suitable method subject to the following requirements:

The method must be physically reasonable, starting with a specified initial state of the cloud, accounting for modifying influences occurring during fall-out, and yielding quantitative plots of the amount and times of arrival of fall-out material on the ground. Modifying influences would include the effects of wind, diffusion, varying fall velocities, decay of radioactivity during fall-out, and special effects such as the occurrence of precipitation and cloud and details of the terrain on which the fall-out would occur.

The method must yield quantitative plots of dose rate referred to H plus 1, total dose, time of arrival of fall-out and time of ending of fall-out.

The method must yield results in agreement with the observations made at CASTLE BRAVO.

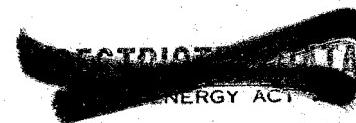
The method must account for real winds in the atmosphere.

The method should be applicable to 15 MT detonations, any day, anywhere.

DOE ARCHIVES

The method must use the best available background information.

The method must be as simple and fast in its application as possible, consistent with not further degrading the existing sparse data on fall-out from high yield weapons.



The method should be amenable to scaling, if possible. The method derived below in this report was based on a 15 MT detonation but may be scaled either by use of the AFSWP scaling laws (which are not based on our cloud model but are convenient) or by the computation of another model of the same nature and having similar treatment but differing in the values utilized.

#### Sources and Acknowledgements

Since the personnel assigned to this task had not had previous contact with the fall-out problem, arrangements were made to visit all groups active in the field which were located in or near Washington, D. C. Contacts were made with AFSWP, JTF-7, Hq. Air Weather Service, Office of the Chief of Naval Operations, Hq. Air Research and Development Command, and the U.S. Weather Bureau.

Personnel interviewed included the following:

Captain Russell Maynard	Hq. AFSWP
Commander R.W. Paine	Hq. AFSWP
Lt. Col. C.D. Bonnot	JTF-7
Lt. Col. House	JTF-7
Lt. Col. C.A. Spohn	Hq. Air Weather Service
Dr. Florence Van Straten	Office of the Chief of Naval Operations
Lt. Col. N.M. Lulejian	Hq. ARDC
Dr. Lester Machta	U.S. Weather Bureau

Source documents utilized included the following:

AFSWP Report TAR-507 and others issued by AFSWP  
RAND Report R-265-AEC  
Instruction books of the various services and offices.

Special acknowledgement must be given to the assistance given us by Captain Maynard and for the information contained in the RAND report. Without his extensive knowledge of sources of information and without the full description of the cloud growth and structure contained in the RAND report, it would have been quite difficult, if not impossible to derive the cloud model utilized in this study.

#### Derivation of the Signal Corps Method

DOE ARCHIVES

The derivation of the computation method used by the Signal Corps is described below in terms of a) basic concepts, b) information on the initial conditions within the cloud structure and related factors, c)



analysis of the basic data, d) derivation of model to obtain the distribution of fall-out material on the ground, and e) the abbreviated method of obtaining total dose.

Concept:

As a result of the understanding which evolved during our inquiry, it was decided to attempt a simple physical model of the cloud and of its fall-out processes. It was conceived that the initial conditions of distribution of radioactivity vs. fall velocity, cloud dimensions, and distribution of cloud radioactivity in height and distance could be specified. This cloud would then be considered as consisting of a number of different "slabs" of suitable thickness. Each slab would be divided into "wafers" representing particles of given size classes located within the slab and each wafer would be followed to the earth from the initial location of the center of the slab in accordance with the fall velocity of the particles and the wind field. The division into slabs and wafers would be so done that each wafer, upon landing on the earth would exert "unit radioactive pressure" URP, i.e., would yield a given unit number of roentgens per hour referred to H plus 1 hour over the area which it covered. The URPs would be tallied over a grid system and summed to indicate the total accumulated radioactivity at that point. This pattern would be analyzed to yield the fall-out pattern. By noting the times of arrival of each wafer, its contribution to total dose could also be evaluated.

Initial Conditions:

It was decided to do the basic analysis in terms of a 15 MT detonation in order to use the relatively good size, shape, and fall-out data obtained from CASTLE BRAVO.

It was assumed that the cloud shape would be as follows: The mushroom top has a radius of 25 miles and extends from 60,000 to 95,000 feet. The stem has a radius of 2.5 miles, extends as a cylinder to 20,000 feet, and then flares out to mushroom diameter. In addition a spike may develop on the top of the mushroom cloud, but is ignored in our analysis since it contains but a small volume of the total cloud.

It was assumed that the particle size distribution and fall velocity curves contained in the RAND report were the best available and sensibly correct. This implied a relationship between radioactivity and fall velocity.

DOE ARCHIVES

It was assumed that the RAND 9:1 ratio of fall-out activity coming from the mushroom to that coming from the stem was correct.

Analysis of Problem:

Having specified the initial data and assumptions we next attempted to obtain as simple a mathematical description of the cloud as possible.

It appeared unreasonable that the radioactivity of the mushroom would be evenly distributed in height but, similar to the distribution of water vapor in turbulent air, it seemed reasonable that the mixing ratio of radioactivity per unit mass of air should be nearly constant within each of the two major regions, mushroom and stem. Uniform height distribution in the mushroom would have placed half the activity in the upper third of the mushroom mass. Any stratification of radicactivity would also tend in the direction of increasing the content of the lower portions of the cloud. It was, therefore, decided to represent the activity in the cloud by a "mixing ratio model." This means that equal pressure thicknesses of cloud contain equal initial radioactivity, subject to the differential of activity between mushroom and stem.

The above decision led to considering all aspects of the problem, including cloud shape and particle fall velocities, in terms of pressure as the vertical coordinate. Pressure has uniformly been related to height through the U.S. Standard Atmosphere.

Representation of the flare of the stem was next considered and an effort made to obtain a simple continuous function which would approximate the reported shape. The flare is concave in height coordinates; in pressure coordinates it must therefore be more so. The simple shape chosen was that of an ellipse in pressure-radius coordinates. It was assumed that for our purposes all detonations could be assumed to occur at low elevations. The nominal surface pressure was taken to be 1000 mb. An ellipse having a vertical tangent at 1000 mb and ground zero, and a horizontal tangent at the lower edge of the mushroom was assumed. The equation of this ellipse in miles and millibars is

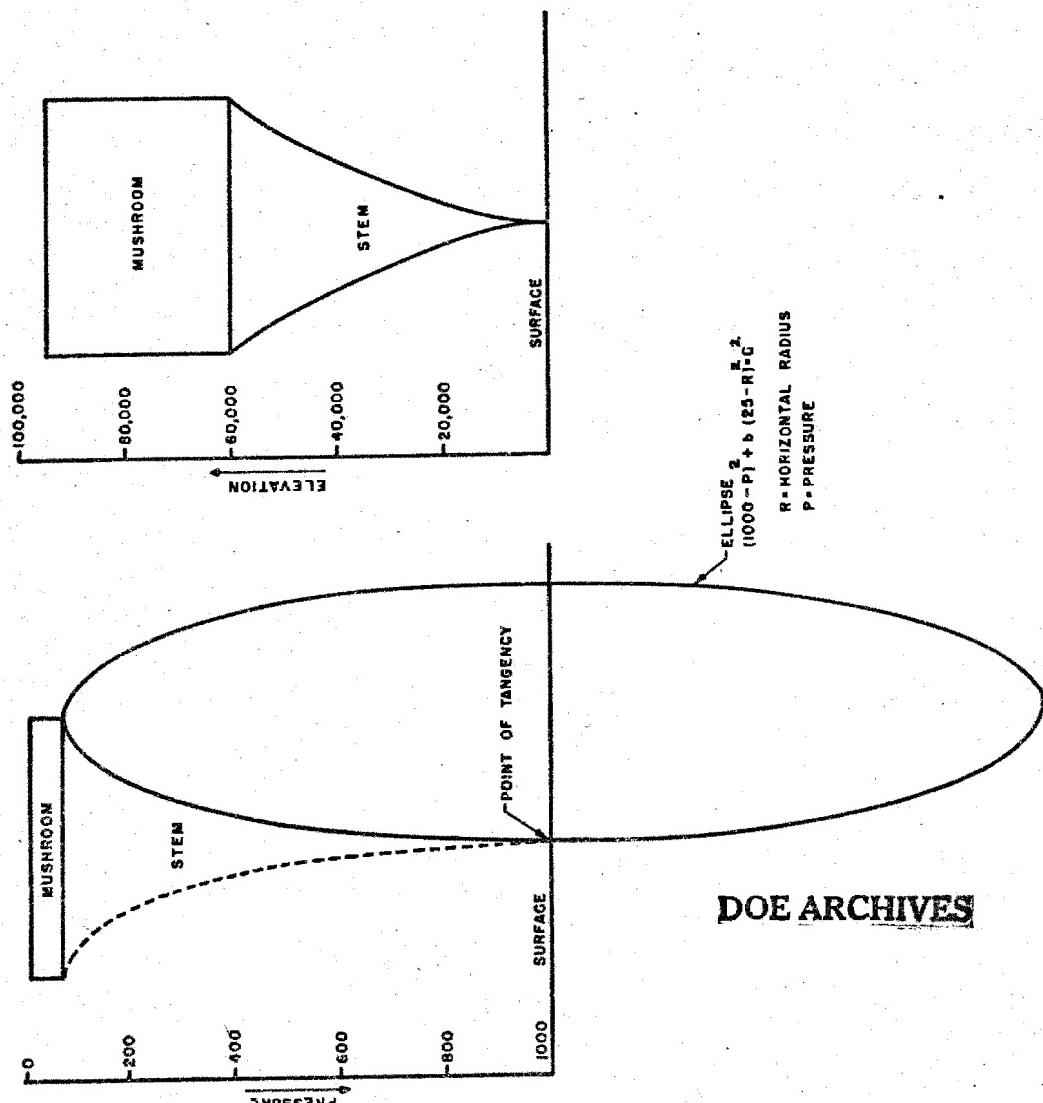
$$(1000 - p)^2 + b^2(25 - R)^2 = c^2$$

Figure 1 illustrates this in both pressure and height coordinates. It will be noted that the only pertinent parameters here are the height of the mushroom base and its radius. This shape was somewhat large at 20,000 feet but, in agreement with the Rand report, assigned little volume, and hence little activity, below 10,000 feet. **DOE ARCHIVES**

The volumes of the mushroom and of the stem in pressure-radius space were next computed taking the mushroom as a cylinder and the stem as a figure of revolution bounded by the ellipse. Using the given ratio of total activity led to determining that the "radioactivity mixing ratio" of the mushroom was about 12 times that of the stem.

METHOD OF DETERMINING THE STEM PROFILE

Figure 1



257

RESTRICTED DATA  
NUCLEAR ENERGY ACT 1954

261

Using the URP concept introduced above, the mushroom was divided into five "slabs" of about 12 mb thickness, with the consideration that this number of slabs would adequately represent the differences of wind and of particle fall time with height. Each slab was to contain nine "wafers" corresponding to various particle size classes so chosen as to account for all the activity within the mushroom and to adequately represent the differences in fall velocity expected between various sizes of particles. Finally, the largest of the size classes (230 microns) was divided into five classes ranging up to 500 microns in order to better represent the fastest falling particles. The 230 micron class was deleted from all slabs and five wafers having an equal total activity and covering the new large sizes were assigned to the middle slab of the mushroom. Each slab then contained 8 wafers and the central slab was assigned the five additional wafers, thus retaining the total of 45 wafers.

Since the stem contains primarily large particles, four large particle size wafers were determined and a thickness of the stem having the previously calculated stem radioactivity mixing ratio was computed which would yield unit radioactive pressure at the center of stem slabs, i.e., the stem was divided into URP wafers. The volume of each such stem pressure slab was determined and an effective cylindrical radius, defining an equal volume, was computed. The stem cloud is then represented by a series of cylindrical slabs having varying radii. These slabs were about 70 mb thick and were assigned from about 70 to 280 mb. Beyond 280 mb, double thickness slabs and double weight wafers were assigned down to about 700 mb.

To obtain the particle size classes mentioned above, the Rand particle size data were replotted and appropriate fractional portions were scaled off. For the mushroom each slab contains wafers representing the following nominal sizes: 20, 42, 68, 85, 100, 110, 125, and 150 microns. In addition the center slab contains particles of 180, 190, 230, 290, and 500 microns. The stem contains wafers representing particles of 180, 260, 375, and 640 microns. Figure 2 shows how these size classes account for the total cloud fall-out radioactivity.

The result of this breakdown is to yield 69 URP or double URP wafers totaling 81 weights in the initial cloud. To obtain a fall-out pattern, each of the wafers is plotted on an overlay at the point where the winds would move it. This process may be rather burdensome but it can lead to quantitative results depending upon the wind. Calibration to CASTLE BRAVO showed that each wafer "weighed" about 100 roentgens per hour at H + 1 hour.

It was noted that the information on which the dimensions of the model cloud was based came entirely from tropical ocean areas. The problem arose of how to account for varying atmospheric conditions. In

DOE ARCHIVES

## MUSHROOM

SIZE GROUP IN MICRONS	20	40	68	85	100	110	125	150	180	210	230	290	500
PERCENTAGE OF TOTAL RADIOACTIVITY	10%	10%	10%	10%	10%	10%	10%	10%	10%	2%	2%	2%	2%
TOTAL 90 %													

## STEM

SIZE GROUP IN MICRONS	180	220	290	640
PERCENTAGE OF TOTAL RADIOACTIVITY	2½%	2½%	2½%	2½%
TOTAL 10 %				

DOE ARCHIVES

259.



263

Figure 2

the present work no account is being taken of cloud, precipitation, diffusion and terrain effects. The possibilities of major changes in cloud height and shape with changes in the hydrostatic structure of the atmosphere, which might occur from the test condition to perhaps polar continental conditions, appeared important enough for some thought. Based on consideration of the increased buoyancy of cold air at low levels, the effects of entrainment of this colder air, and the relatively warm and low tropopause characteristic of polar air masses, it was estimated that the following table of mushroom top and base height would be expected as the tropopause height varied:

Height in  
Feet of:

Tropopause	55,000	45,000	35,000
Mushroom base	60,000	55,000	50,000
Mushroom top	95,000	80,000	65,000

A complete model computation was run on each of these structures. The results of this work are shown in Figure 3, which gives the structures in pressure terms, and in Figure 4, which gives the structures in height terms. It will be noted that the assumed behavior of the mushroom resulted in maintaining the pressure thickness of the mushroom almost constant, resulting in similar mixing ratio ratios between mushroom and stem and in identical numbers of layers having similar radii.

#### Fall Time and Trajectory Calculations:

In order to determine the point on the earth's surface on which any wafer would be deposited, it was necessary to devise a method which would integrate the effect of the winds through which the particles fell. In principle, this required

$$\bar{S} = \int_p^{1000} \frac{V(p)}{W(p,d)} dp$$

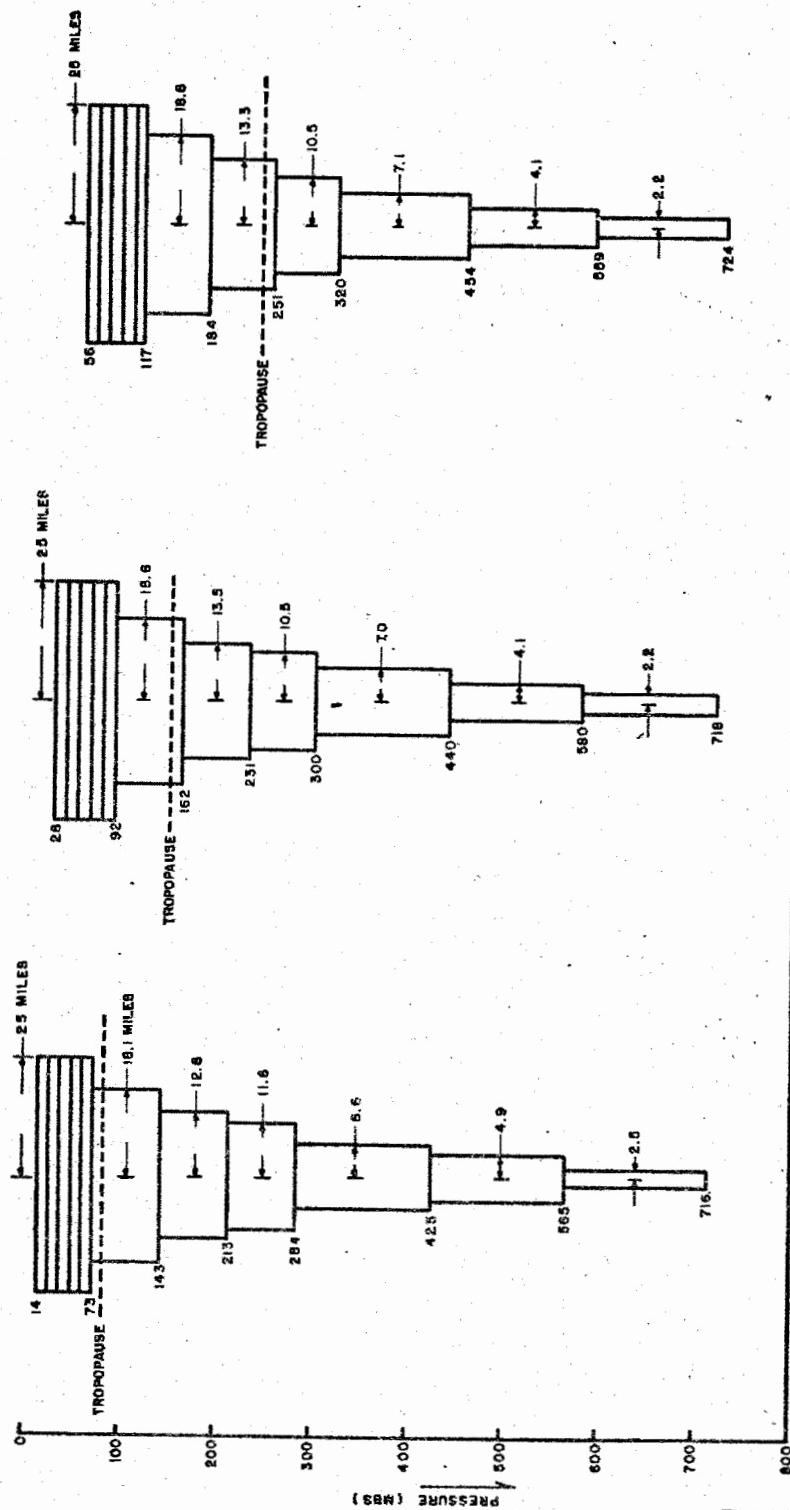
where  $V(p)$  is the horizontal wind at pressure  $p$ , and  $w(p,d)$  is the fall velocity (in millibars per hour), depending on  $d$ , the particle size, and on pressure. Precise evaluation of this would be difficult and unwarranted by the available data. The approximation used was

$$\bar{S} = \frac{1}{W(d)} \sum_{i=1}^n \frac{V_i}{K_i} \Delta p_i$$

DOE ARCHIVES

where  $i$  indicates the reported wind level representing a pressure thickness  $\Delta p_i$ ,  $K_i(p)$  accounts for the deviations of fall velocity from constancy, and  $w(d)$  reflects the fall velocity for different particle sizes.

As indicated above, the Rand fall time curves were assumed. These were replotted in pressure terms for the particle sizes used in the model described above. All curves were found to be concave upward, re-



THE THREE MODELS PLOTTED IN PRESSURE - RATIO COORDINATES

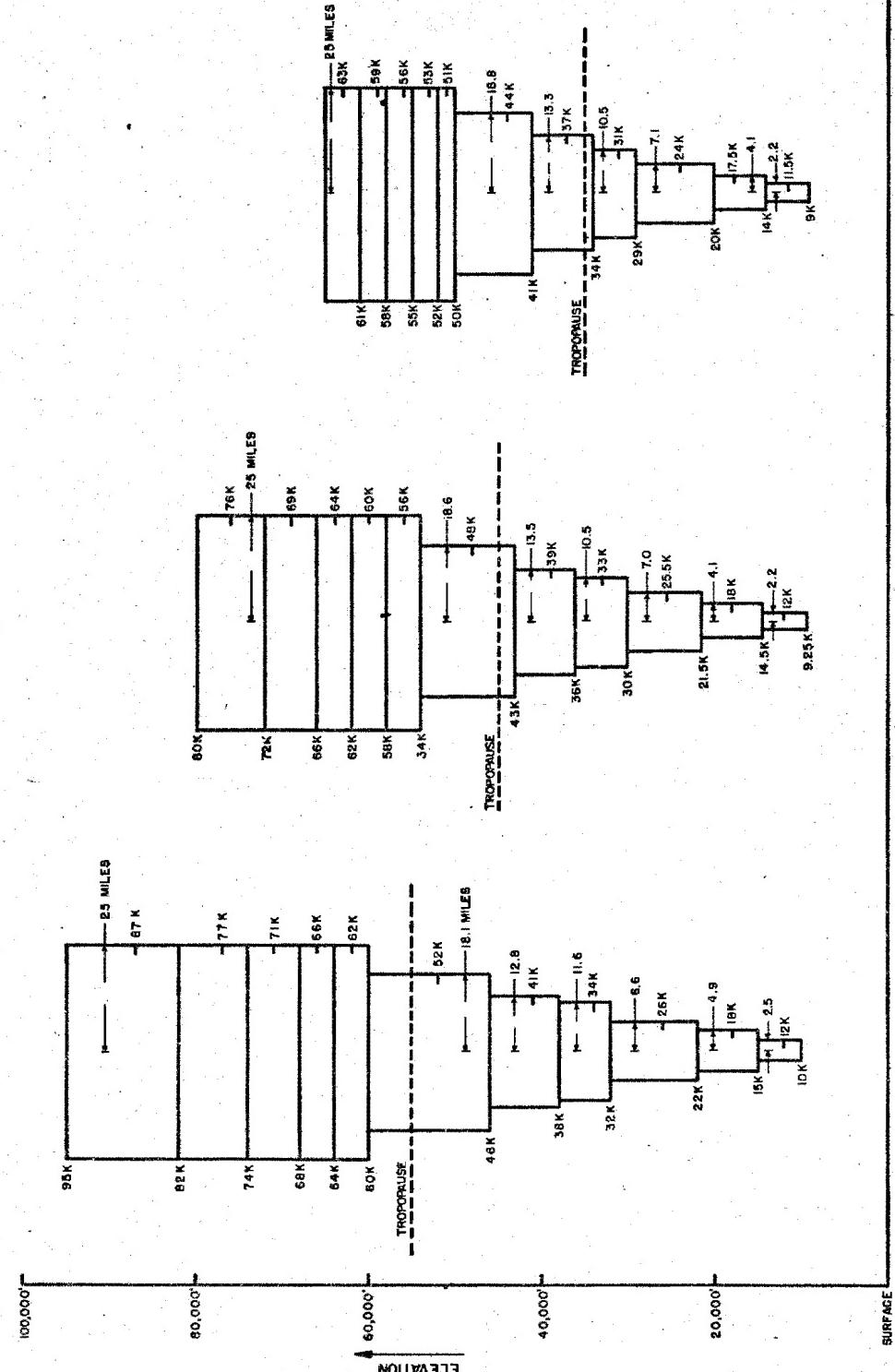
III WINTER CASE  
II MIDSEASON CASE  
I SUMMER CASE

DOE ARCHIVES

~~SECRET~~ DATA ATOMIC ENERGY ACT 1954

Figure 3

265



DOE ARCHIVES



**THE THREE MODELS PLOTTED IN RADIUS - HEIGHT COORDINATES**

I      SUMMER CASE  
II     MIDSEASON CASE  
III    WINTER CASE

Figure 4

flecting a greater fall velocity, in millibars per hour, at the lower pressures. Since this effect was about the same amount percentage-wise for all the smaller particle sizes and since the real effect of such a change in fall time was small for the larger sizes, the effect was treated by determining the reduction in time which the 40 micron particles would spend in any given pressure level as a result of the curvature compared to the time they would spend in an equal slice near the surface. This gave the K(p) factors required to weight the winds representing such pressure levels so that 40 micron particles passing through these levels at a fall velocity assumed constant and equal to that found in the lower atmosphere would be appropriately moved by this modified wind. Fall velocities of all other particle size classes were scaled to this 40 micron fall velocity so as to introduce no error in the center of the mushroom region, yielding the W(d) factors. Thus  $w(p,d)$  was treated as

$$W(p,d) \doteq K(p)W(d)$$

A continuous estimate of the wind as a function of pressure  $V(p)$ , is not available to the meteorologist under normal conditions. In practice, he is given a number of winds representing the air velocity at a number of given heights, commonly based upon averages over time intervals of the order of one minute (i.e. average over height intervals of the order of 1000 feet). Climatological data may not include winds except for the "mandatory levels," i.e. 1000, 850, 700, 500, and 300 millibars. In using wind data to compute trajectories, the winds are weighted in proportion to the pressure thickness for which they are (and must be) taken as representative. For example, the 850 mb wind may be used to represent the atmospheric flow between 925 and 775 millibars and is weighted by 1.5 since it represents 150 millibars in our vertical coordinate.

Thus wind data are weighted to account for the deviation of particle fall velocity from constancy and to account for the thickness of the atmosphere which they represent. A single weighting function table is used. True (i.e. Rand) fall times are used, however, for determining the time of first and last arrival of wafers, since the fall time for each particle size from each of the nominal pressure levels is easily tabulated.

#### Dose Rate and Total Dose:

Since the study for which fall-out computations were required had a number of facets, it was necessary to determine both the dose rate referred to H+1 hours,  $D$ , and the total dose,  $D_T$ , received up to an arbitrary time,  $T$ , later than the ending of fall-out. **DOE ARCHIVES**

The position of each wafer as it arrived at the surface was noted and the number of URP wafers lying over any required point was noted.

For CASTLE BRAVO it was found that each wafer represented about 100 r/hr referred to H+1. This calibration was used for all other calculations, since it was the only good point of contact between wafers on the surface and observed fall-out. Following the approach of AFSWP Report 507, we have assumed a decay rate given by  $t^{-1.2}$  for all times of interest, although deviations from this which would be the same for all wafers could be accounted for without producing significant complication of the computational problem.

The requirement for some sort of integrated dose related to human effects at first appeared to be exceedingly difficult to meet. Inquiry relating to the present knowledge of biological recovery, however, revealed that (a) the facts are not too well known, particularly as they relate to human beings, and (b) the recovery within the first few days following beginning of exposure was estimated to be less than 30%. Within the accuracy of our computation method and considering the uncertainties of the recovery problem, it was decided not to allow for recovery but rather to compute the total dose. Since each URP wafer is followed to the surface and its time of arrival determinable, one could sum the total dose which each delivered up to any given time. This, however, with some 69 wafers per problem, would be rather lengthy. It was felt that some mathematically simplifying assumption regarding the rate of accumulation of radioactivity on the ground would be desirable. The assumption made was that all the fall-out arrived at a constant rate from the time of first arrival,  $a$ , and the time of ending,  $e$ . Assuming total fall-out to be 1 r/hr at H+1, the total dose to time  $T$ , where  $T > e$ , is given by the following simple formula:

$$D_T = 6.25 \frac{e^{-a} - e^{-T}}{e - a} - 5T$$

The first term corresponds to the infinity dose delivered by unit dose rate accrued between  $a$  and  $e$  and the second to the dose which would be delivered between  $T$  and infinity. In use, the dose rate  $D$  is multiplied by the factor given by the formula above, or determined by entering a chart with  $a$  and  $e$ , to obtain the total dose to  $T$ .  $D_T$  so obtained was plotted against coordinates  $a$  and  $e$  and analyzed as a contour chart.

Application of the Model and Method

DOE ARCHIVES

In the practical application of the Signal Corps method devised above, an effective wind trajectory was constructed by connecting the weighted winds corresponding to each interval head to tail. The wind for any given slab was picked off by interpolation along the length of the appropriate vector. These winds were actually plotted on a scale such that the 68 micron particles fell directly along the plotted trajectory. All other particle size destinations, as explained above, then scaled linearly with this wind. In order to simplify the practi-

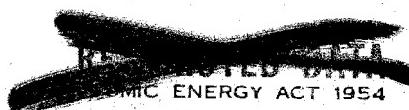
cal work, a triangle was constructed similar to that described earlier by Dr. Van Straten, except that it accounted for a larger number of particle sizes. When the length of the 68 micron trajectory is laid parallel to the base of the scale, with the origin at the left-hand edge and the end of the vector intersecting the 68 micron line, the destination of all other sizes may be plotted at the intersection of the appropriate sloping lines with the 68 micron vector. Thus, all eight (or thirteen) wafers corresponding to a slab within the mushroom can be plotted with ease, and similarly, the four wafers representing each stem slab can be rapidly laid out. A "poker chip" having a diameter corresponding to the proper radius for the slab which it represents (i.e. on the same scale as the 68 micron trajectory plot) is located at each URP wafer destination point. An overlay, ruled in a suitable grid\* is positioned and those grid sections which are at least 50% covered by a poker chip are marked. This is done for each of the eleven slabs corresponding to 11 effective winds, using the same overlay. When all the poker chips have been tallied, the number of URP's lying over each area are summed and the resulting pattern analyzed as a pressure field. Since each URP was determined to represent 100 r/hr at H+1, the fall-out field is readily obtained.

At the same time that the "poker chips" are tallied in the overlay, the leading and trailing edge of the chip are sketched and marked with the appropriate time of arrival. From the field of these values, contours of earliest time of arrival, designated above as  $a$ , and of latest time of arrival, designated above as the time of ending,  $e$ , are drawn. Using the assumption that fall-out (in units of r/hr at H+1) accumulates linearly between  $a$  and  $e$ , and the equation for total dose discussed above, total dose to  $T = a + \frac{1}{2}e$  is computed. In our later practice, a contour chart entered in  $a$  and  $e$  and having contours labeled in terms of total dose to  $a + \frac{1}{2}e$  per unit dose rate is used. The values so obtained are again analyzed to obtain the total dose contours.

Since all three models have the same number of slabs and wafers, there is no modification of the computation method necessary except for the location of the nominal initial pressure of each slab. Having selected the model, the computation procedures may be summarized as follows: (1) The weighted winds to the top of the model are plotted in an effective trajectory, (2) the 68 micron trajectory vectors are drawn for each slab, (3) the wafers are positioned using the scaling triangle, (4) URP contributions are tallied on the overlay along with  $a$  and  $e$ , (5) the sum of tallies and  $a$  and  $e$  are contour analyzed, (6) total dose is evaluated for a suitable number of points and (7) a total dose chart prepared.

DOE ARCHIVES

\* In practical work a 15 mile square grid was used, while for Mr. Barnett's paper a 3.5 mile square grid was used.



### Critique of the Signal Corps Method

A paper of this nature would not be complete without reference to those assumptions which are considered weak and consideration of possible means of improving the method.

#### Weaknesses:

Weaknesses in the method stem from both inadequate basic data and from deficiencies in the development of the method. In the former class the major deficiencies lie in the fact that useful data on total fallout, original distribution of radioactivity for successive fractions of this radioactivity (or, alternatively, distribution of activity by particle size and height and fall velocity), biological recovery effects, decay of radioactivity, diffusion, and terrain effects are either sparse or non-existent. The major deficiencies in the model lie in the length of time required to perform a computation, the linear arrival assumption, and the finite number of wafers considered. It will be noted that, without the use of machine computation methods, an increase in the number of wafers (which would yield somewhat smoother patterns) would further aggravate the time problem.

It is assumed that many of the informational deficiencies will be met by future tests and that more certain estimates of those which cannot be completely met will result from the analysis of the data obtained. With regard to the model and method, a number of improvements appear possible:

Increase the number of slabs and wafers per slab--this would produce smoother patterns.

Perfect an alternate method of obtaining  $\alpha$  and  $\epsilon$  based on the determination of the maximum and minimum effective winds in each azimuth, or

Replace the linear accretion assumption with immediate summation of total contribution from arrival time to  $\alpha + 48$  hours.

Adapt the method to machine computation methods.

Use time-varying trajectories.

DOE ARCHIVES

Use a better approximation of stem shape.

Incorporate any new test results to refine the model and method.

Provide an improved method of scaling either through alternate models or otherwise.

Modify model to take account of diffusion, especially if smaller yield weapons are to be considered.

Use an overlay grid ruled in coordinates suitable to the problem.

Account for variations in particle size distributions of various soils and targets.

Incorporate biological recovery corrections.

Modify method so as to reduce computation time while retaining quantitative results of reasonable accuracy.

DOE ARCHIVES

267

SECRET

DATA  
PROTECTION  
ACT 1988

271

THIS PAGE IS BLANK  
IN ORIGINAL.

DOE ARCHIVES

272

QUESTIONS AND ANSWERS FOLLOWING DR. SWINGLE'S PRESENTATION

Question: LTCOL Spohn, AWS

On the last paper, I am curious of the time interval it takes to actually work through a plot - how long does it take to run a plot?

Answer: Dr. Swingle, OCSO

After some experience in a well equipped office, three or four man hours. Most of the work we have done was not for operational use; we set it up on a production line basis and at one time we had as many as 20 men working on it.

Question: FCDA

What typical times between arrival of the smaller particles and larger particles; that is, in your computation to get dosage figure?

Answer: Dr. Swingle, OCSO

I think you will see that in Mr. Barnett's paper tomorrow, but it runs for something like half an hour to a matter of ten hours, or more.

Question: LTCOL Spohn, AWS

In applying wind data to this, do you use the same assumption as we (AWS) do; that is, assuming point winds apply throughout the time of fall-out?

Answer: Dr. Swingle, OCSO

DOE ARCHIVES

Yes, so far. In the study which we have done we have been concerned with getting what fall-out might be. A single sounding might be just as good as changing it. We have not had an occasion to want to.

PREDICTION OF DOSE-RATE AND DOSAGE CONTOURS AS FUNCTIONS OF YIELD  
AND METEOROLOGICAL CONDITIONS, ARDC METHOD

LtCol N. M. Lulejian, USAF  
Air Research and Development Command

I have analyzed the fall-out from the first shot of CASTLE test operation. The method of analysis is based on Stokes Law of fall and upon the following assumptions of particle size distribution and activity with height within the atomic cloud:

<u>h</u>	<u>d<sub>mean</sub></u>	<u>A</u>	<u>ΣA</u>
0	140	-	-
5	130	3.3	3.3
10	120	7.5	10.8
15	110	3.8	14.6
20	100	4.6	19.2
25	90	6.8	26.0
30	80	10.0	36.0
35	70	17.0	53.0
40	60	12.7	65.7
45	50	6.0	71.7
50	50	5.1	76.8
55	50	2.5	79.3
60	45 <sup>non-scav-</sup> <u>engable</u>	1.7	81.0 <b>DOE ARCHIVES</b>
65	45	1	83.7
70	40	2	86.5
75	30	2	86.9

269

DATA  
OMIC ENERGY ACT

274

<u>h</u>	<u>d<sub>mean</sub></u>	<u>non-scavengable</u>	<u>A</u>	<u>Σ A</u>
80	20	2	2.0	90.9
85	10	2	2.0	92.9
90	< 10	2	2.0	94.9
95	< 10	2	2.0	96.9
100	< 10	2	2.0	98.9
110	< 10		1.0	99.9

where  $h$  = Height above target in thousands of feet (or height in cloud)

$A$  = Percentage activity in each 5000 ft slice of the cloud.  
 $\Sigma A$  is the cumulative percentage activity.

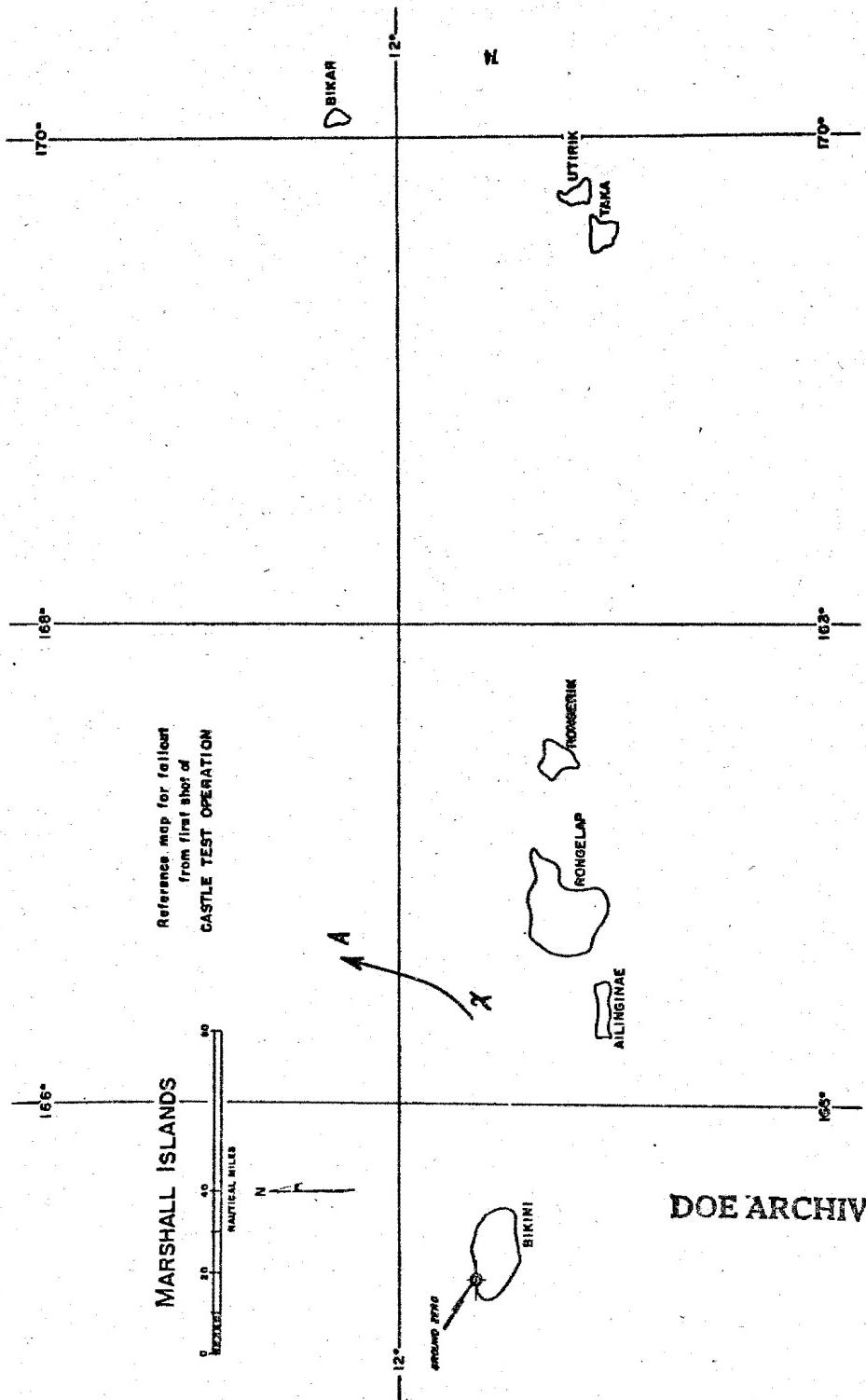
$d_{mean}$  = Mean particle diameter in microns.

I want to now refer to my earlier talk on the percentage fall-out as a function of scaled height. During this discourse I showed that as the scaled height was reduced the percentage activity in the stem of the cloud increased as compared to the activity in the mushroom. Armed with this fact and also with the analysis of particle size in the tower shots of TUMBLER-SNAPPER and UPSHOT-KNOTHOLE test operations, I arrived at the assumptions made in paragraph 1 above. For greater details in this regard, refer to ARDC Report No. C4-23676.

For the winds we have used the composite winds of Eniwetok, Rongerik, and Bikini for  $H -$  hour and  $H + 2:15$  hours. For  $H + 8$  and  $H + 14$  hours we have used the composite winds of Eniwetok and Rongerik weather stations. Figure 2 shows the time variation of the winds, and figures 3 and 4 show the composite wind analysis for different sized particles. Figure 1 gives the names of the islands of interest in the Pacific.

#### DOE ARCHIVES

The main point of difference between our method of analysis and that of RAND is that their assumptions of particle size and activity distribution within the cloud are radically different from ours. I believe this is only possible because the stratospheric winds had a



T

DOE ARCHIVES

271

SMC ENERGY ACT IS

276

Figure 2

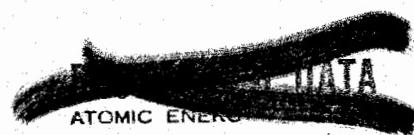
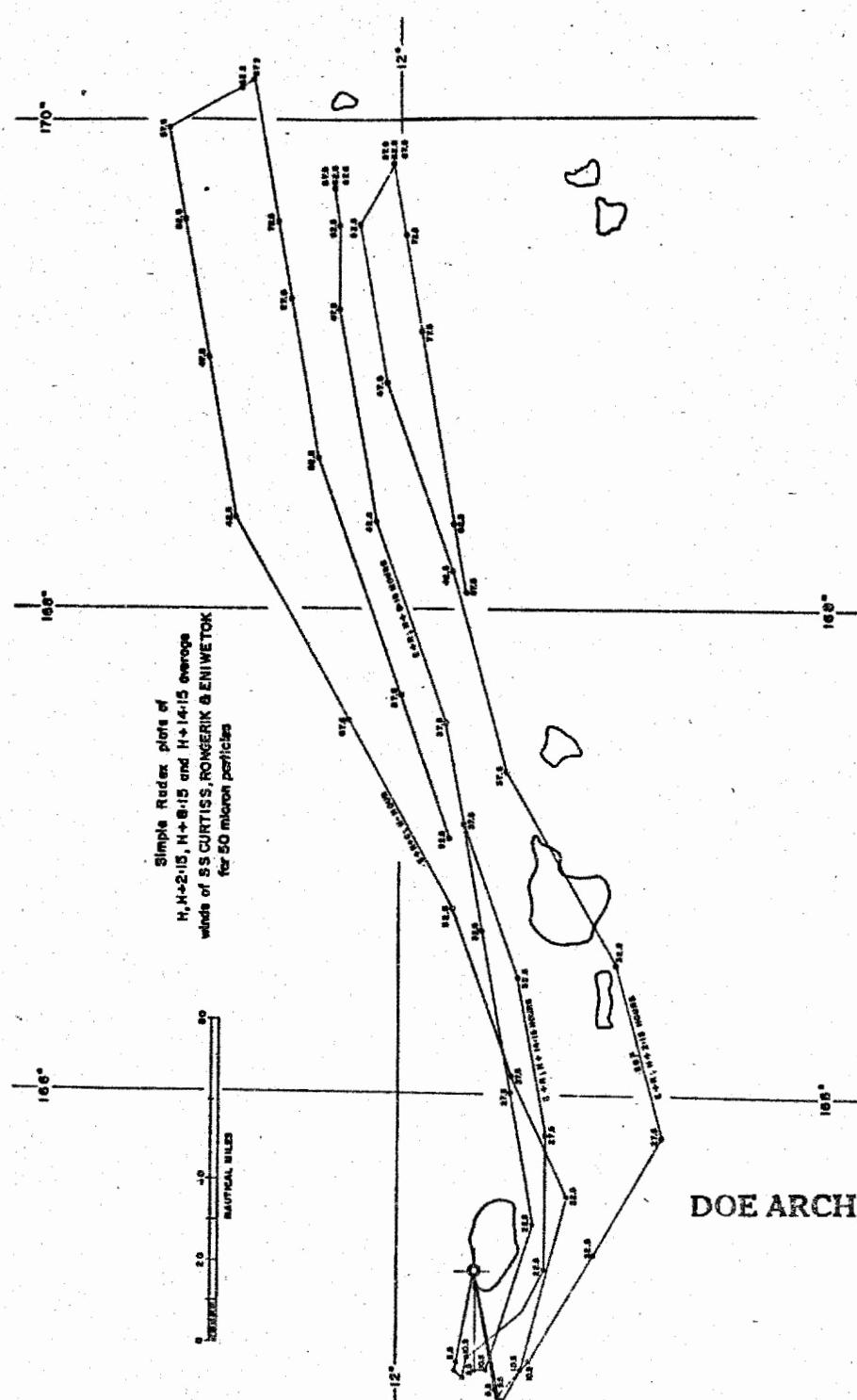


**Figure 3**

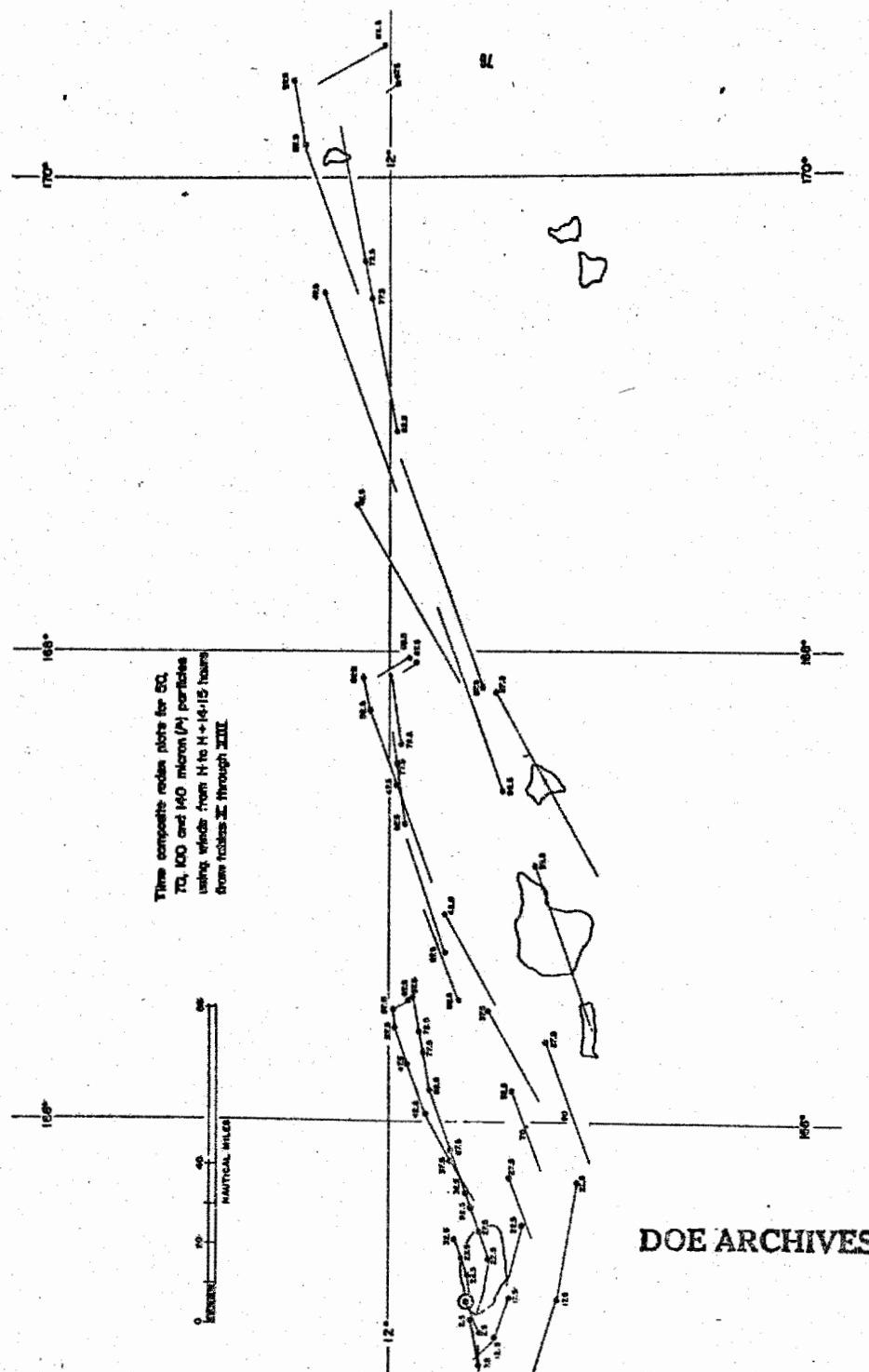
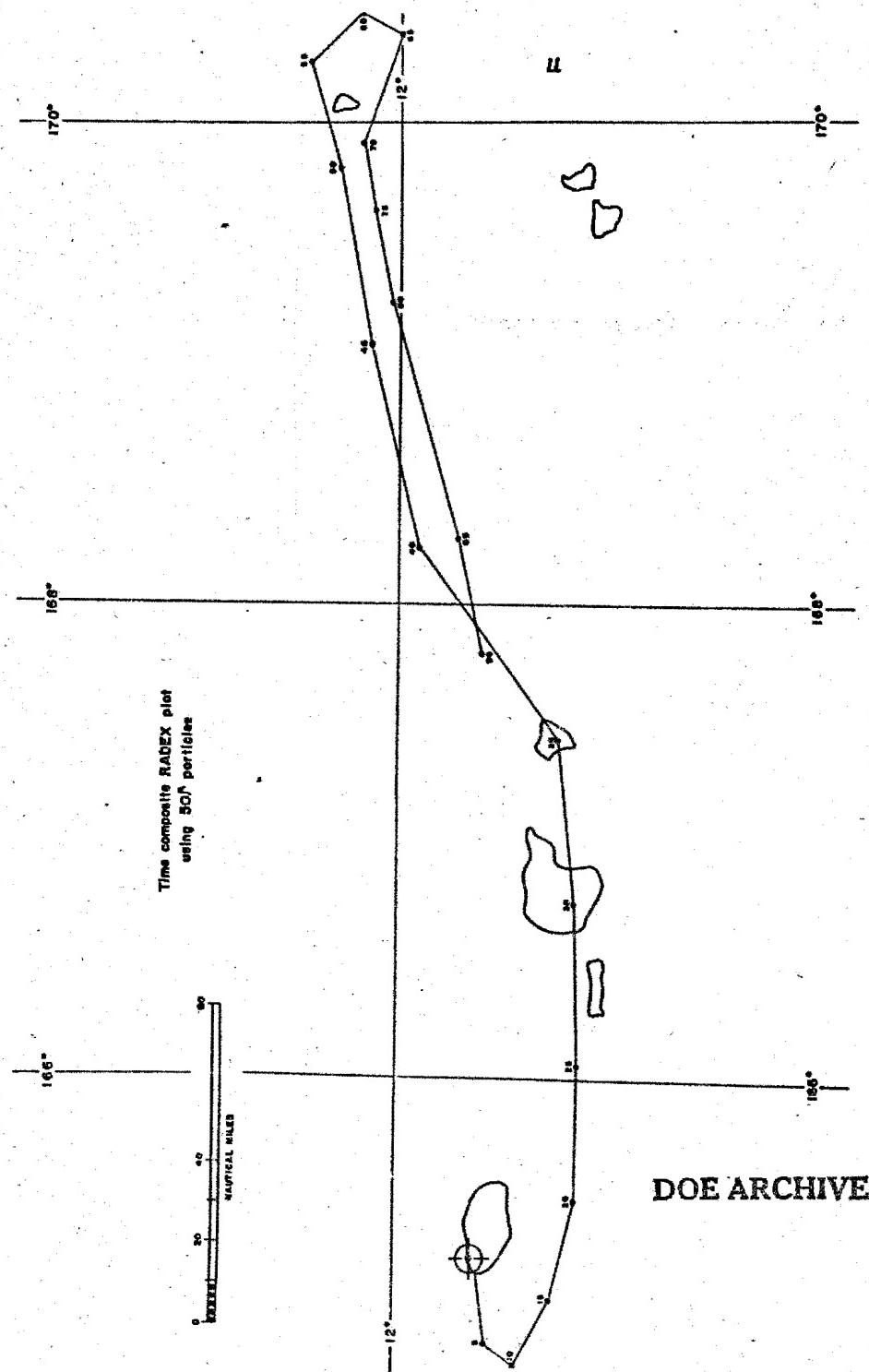
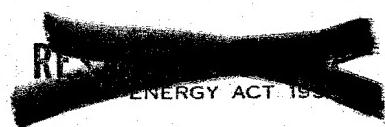


**Figure 4**



274



279

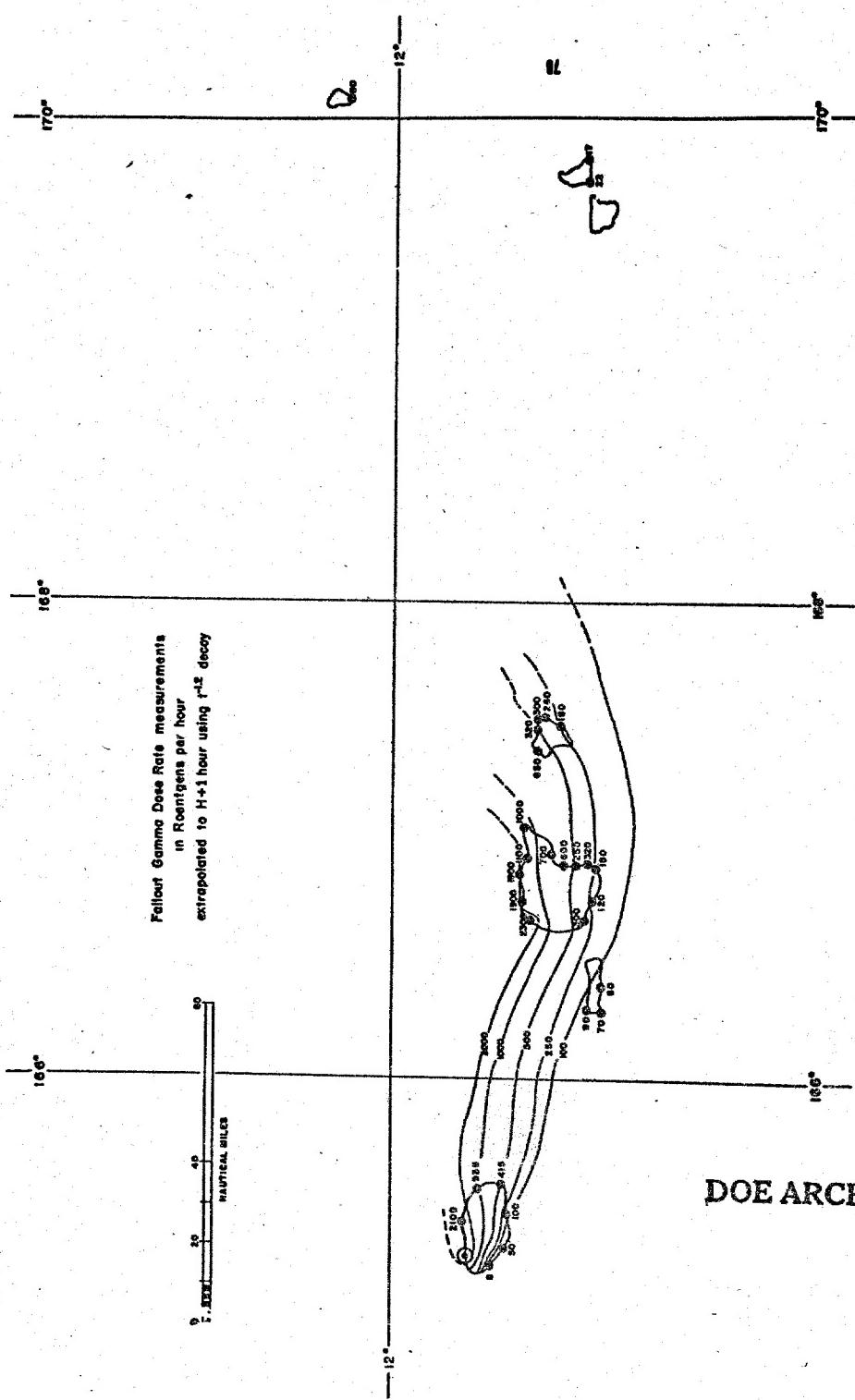
directional shear of approximately  $180^{\circ}$  as compared to tropospheric winds during Bravo shot. I say that the fall-out occurred from the stem; RAND says it occurred primarily from the mushroom; but since the ground trajectory of the stem and mushroom actually coincide in many points (see figure 2), the problem cannot be resolved until at some future test when the wind shears between the troposphere and the stratosphere are at approximately  $90^{\circ}$ . When and if this happens at some future test, we will be able to resolve the problem uniquely, provided we are there to catch the fall-out.

I want to make it clear that my assumptions (given in paragraph 1) apply only to a surface burst on land of an atomic bomb in the range of 10 to 20 MT. It does not apply to a surface burst over water (barge shot). I don't know anything about particle size distribution or activity distribution in a "water" cloud. All I know is that former speakers of this conference (NRDL, Scripps and New York Operations Office of the AEC) have indicated that the total fall-out may be 2 to 5% (Mr. Eisenbud) or it may be 13 to 58% (NRDL-Scripps). All speakers agreed that they make no claim to have caught all of the fall-out. So, as far as I know, fall-out from water shots may be 2 to 58% or more. The activity within a water cloud may be anything. I don't even have a clue as to what it may be.

I have used Stokes Law of fall as compared to aerodynamic fall. The difference between the two rates of fall is relatively small in the size range of 60 to 100 microns, and it is in this very size range that we find most of the activity in the cloud. Therefore, for ARDC method, the use of Stokes Law or aerodynamic fall makes relatively little difference. However, for those other units who assume that particle sizes between 100 and 1000 microns hold most of the cloud activity, the use of aerodynamic fall becomes mandatory. It is my claim that the primary difference in the methods presented is the particle size distribution with activity and height, not the different rates of fall.

#### DOE ARCHIVES

Figures 5 and 6 show the measured dose rates on the islands in the Pacific for the first shot of Operation CASTLE. These two figures are taken from CASTLE Project 2.5a preliminary report by NRDL. They are shown here as the data that we must try to approximate with our plot of fall-out. Figure 7 is the calculated fall-out area using the assumptions made in paragraph 1. Figure 8 shows the ARDC fall-out plot in isodose contour lines of dosage integrated from time of fall-out to 48 hours after the bomb detonation, using the  $t^{-1.2}$  relation. It should be noted that all points on figure 7 are calculated points. They do not show any measured data. All the measured data is in figures 5 and 6.



DOE ARCHIVES

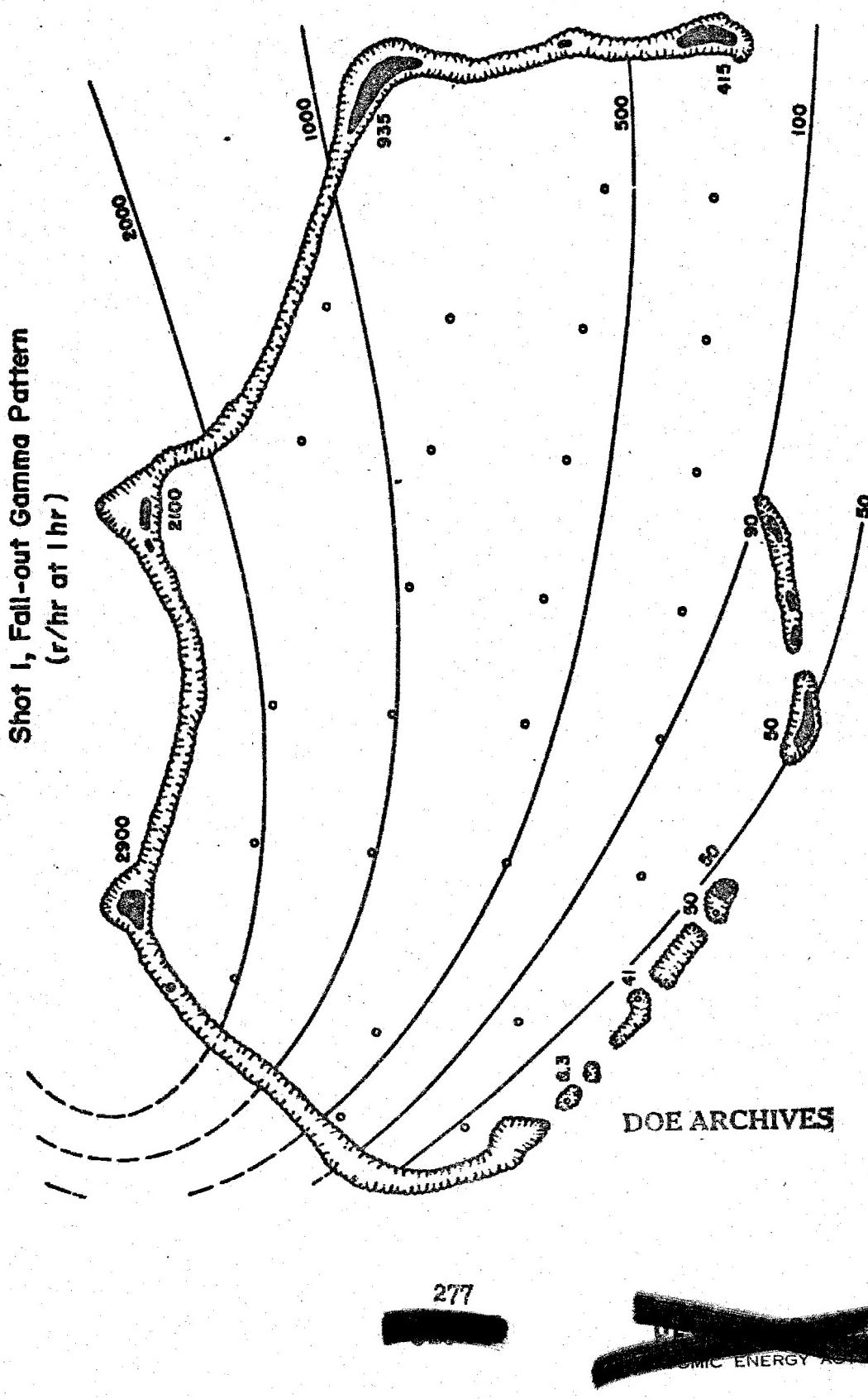
REPRODUCED BY  
ACT 150

276

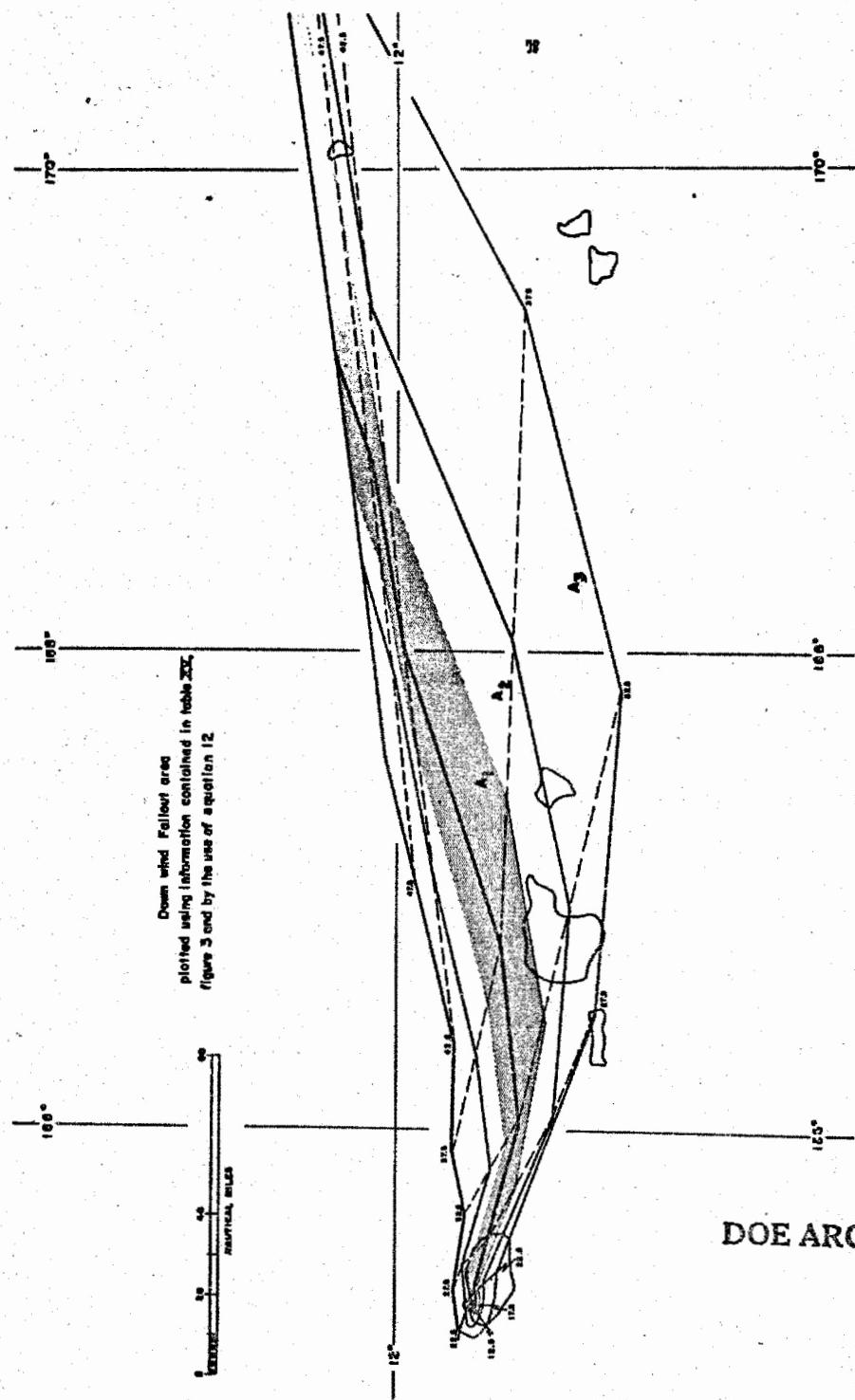
281

FIGURE 5

Figure 6



**Figure 7**

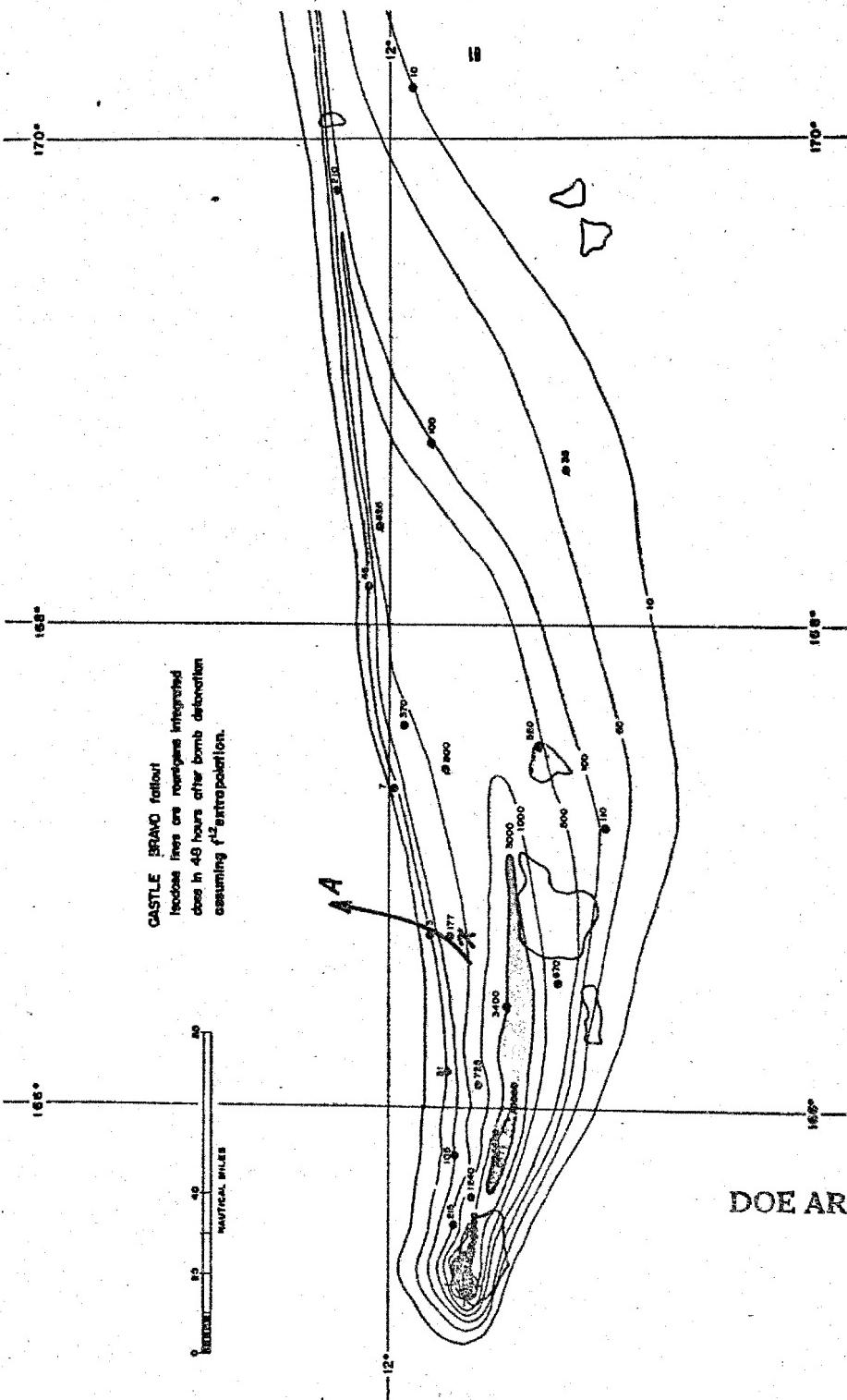


278

~~DATA~~  
AMERICAN ENERGY

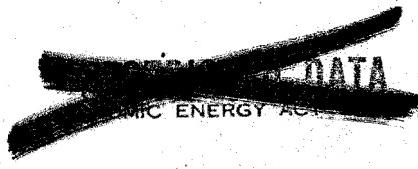
283

CASTLE BRAVO fallout  
Radiation doses are integrated  
dose in 48 hours after bomb detonation  
assuming  $t^2$  extrapolation.



DOE ARCHIVES

279



284

Now let me talk to you about what I call the "Volume-Effect" of fall-out which was found during TUMBLER-SNAPPER and UPSHOT-KNOTHOLE test operations in Nevada. In pages 65 to 67 I discuss this matter in greater detail in ARDC Report No. C4-23676. Figure 9, which is taken from AFSWP Report WT-558, shows this "Volume-Effect" at Lincoln Mine (approximately 40 miles north of ground zero) during TUMBLER-SNAPPER Shot No. 5. Similar "Volume-Effects" of fall-out were obtained during TUMBLER-SNAPPER and UPSHOT-KNOTHOLE tower shots. Figure 9 shows that the 48 hour integrated dose calculated by  $t^{-1.2}$  relation must be multiplied by 1.67 to account for the "Volume-Effect" of fall-out. In ARDC Report C4-23676, we have indicated what would happen if this same "Volume-Effect" is taken into account for the CASTLE Bravo fall-out. During the evening sessions of this symposium I have been advised by AFSWP and NRDL personnel that the "Volume-Effect" was not observed in and around the Bikini Lagoon. I have been told that there were six continuously recording stations on the islands of Bikini Atoll and that these traces did not show the "Volume-Effect" of the type I found in the desert. It was also conjectured by AFSWP personnel (in night session) that if this "Volume-Effect" occurs at all in fall-out from multi-megaton weapons, it would be observed 500 to 1000 miles downwind (where the total fall-out would be small). It is my opinion that this "Volume-Effect" should have appeared on the northern portions of Rongelap and Rongerik quite strongly. It should also have appeared to a lesser extent on the southern sectors of these two atolls. The fact that they were not observed at Rongerik may be due to the fact that there was very little measured data downwind during the fall-out period. I believe that the distinct possibility exists that Rongelap natives may have received from 1.2 to 1.5 times the 48 hour integrated dose used by the investigators in this field of endeavor. I don't know whether this same "Volume-Effect" would occur from fall-out coming from bombs detonated not on the ground, but on water. As I said earlier, I know nothing about fall-out from "water clouds". However, I believe that this "Volume-Effect" will be observed in future tests for surface burst weapons because I believe these things scale from Nevada to the Pacific.

DOE ARCHIVES

It is believed that the ARDC method of fall-out analysis adequately explains the fall-out picture shown in Figures 5 and 6. The important points that must be kept in mind when an attempt is made to fit assumed particle size and activity data to the actual fall-out case are the following:

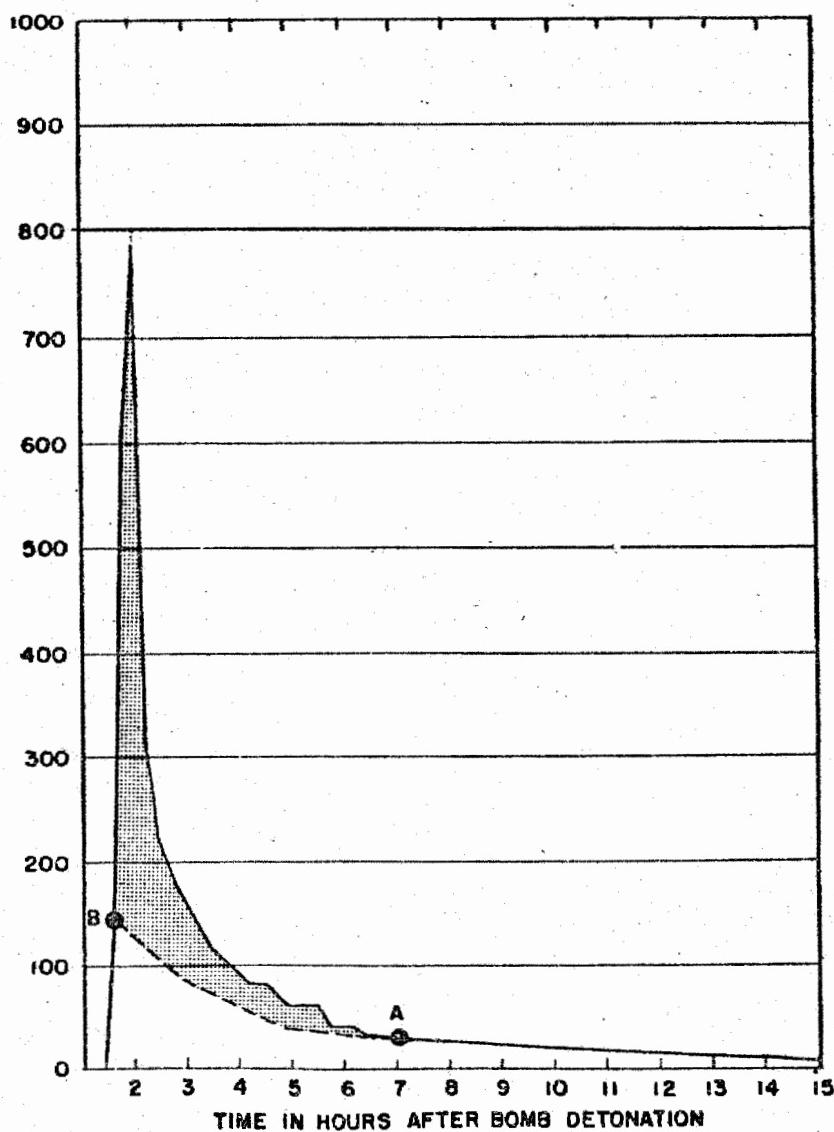
The time variation of the winds was so great that composite analysis of the winds is required. The winds at ground zero are not valid over the downwind path after the lapse of only one or two hours.



Fallout at lincoln mine, Nevada  
from shot 5 of tumbler/snapper  
test operation in 1952.

GAMMA DOSAGE RATE

IN MR/HR



DOE ARCHIVES

Shaded portion shows fallout  
in excess of the  $t^{-1/2}$  RELATION

Figure 9  
281

NUCLEAR ENERGY ACT 1954

286

Any analysis of the fall-out on Bikini Lagoon must take into account the amazing fact that the intensity of fall-out on the lagoon islands to the south and southwest of ground zero is only 8 to 15 r/hr at H+1 hour, even for islands as close as approximately 5 nautical miles from ground zero. On the other islands of Bikini Lagoon, the contamination goes to 1000 to 2100 r/hr at H+1 hour (see figures 5 and 6).

The atoll of Rongelap is contaminated excessively in a steep gradient as shown in figure 5.

The native village on Rongelap Atoll (southern portion of atoll) is in approximately the same radiation intensity field as the weather station on Rongerik.

Ailinginae shows less contamination than Rongelap or Rongerik.

Bikar has less contamination than Rongerik.

Task Force ships 50 miles southeast of ground zero showed less contamination than Ailinginae.

The islands of Taongi and Utirik were least contaminated.

It was later found that the position of the Japanese fishing boat (Fulcuru Maru) was not 10° north of east (80 miles) of ground zero, but thanks to Mr. Eisenbud of NYOC, AEC, the exact position is shown in figures 1 and 8 as point X and the direction of motion of the ship is shown to be from point X to point A. Extrapolation of the Eisenbud data on the Japanese ship shows that it reached the 12° N. latitude line at approximately H+6 to H+8 hours. The fall-out was supposed to have stopped at H+8 hours according to Japanese accounts.

We have kept in mind the measured data mentioned in the paragraph above, and our model fits the above data quite well (see figures 7 and 8). The winds are those obtained from the shot island (Bikini), Rongerik and Eniwetok. Looking over the papers presented by different members of this symposium I note the following:

DOE ARCHIVES

The RAND Aureole report shows CASTLE Bravo analysis that overestimates the fall-out around ground zero (especially on the southerly islands of the atoll). The downwind fall-out misses Rongerik and Rongelap and if memory serves me right, it also misses Bikar. This model then does not succeed in approximating the measured Bravo fall-out. At this symposium, RAND has presented new and as yet

unpublished data which adequately accounts for the fall-out in and around the islands of Bikini Atoll. It also appears to give the correct order of magnitude of the contamination on the northern portion of Rongelap Atoll. The analysis does not go any further than that as far as I can tell.

The NRDL analysis of Bravo event was widened too far to get the fall-out to fall on Rongelap and Rongerik. It is believed that since NRDL used only the ground zero winds (not taking the time variation of winds into account) then they were forced to widen their area of fall-out to account for the observed fall-out.

The particle size and the activity distribution in the cloud shown in paragraph 1 above, was obtained after careful analysis of the TUMBLER-SNAPPER and UPSHOT-KNOTHOLE tower shots and the JANGLE surface shot. Reference is made to ARDC Report C3-36417. On page 40 of this report is shown that the following particle size distribution fits the UPSHOT-KNOTHOLE tower shots (17 to 50 KT from 300 foot towers):

125 microns in lower third of stem  
100 microns in middle third of stem  
90 microns in upper third of stem  
80 to 70 microns in mushroom of cloud for a cloud reaching a maximum altitude of 40,000 feet msl

It is assumed that as the cloud height increases the particle size distribution at the higher levels in the cloud decreases. It is from this background of detailed analysis of the tower shots of UPSHOT-KNOTHOLE and TUMBLER-SNAPPER that the assumptions of paragraph 1 were made. So you see, we didn't pick them out of thin air after all! It is unfortunate that most other units have neglected analyses of the Nevada shots as a guide to Bravo fall-out.

**DOE ARCHIVES**

The next point I want to discuss is my "reasoning" for assuming that the activity in the stem is greater than the activity in the mushroom. During TUMBLER-SNAPPER tower shots (12 to 14 KT from 300 ft towers) the activity in the stem was approximately the same as the activity in the mushroom. However, during the UPSHOT-KNOTHOLE test operation (17 KT to 50 KT from 300 ft towers) the activity in the stem was 2 to 3 times the percentage activity in the mushroom. For the JANGLE surface shot the activity in the stem was approximately thrice times that found in the mushroom. It is for this reason that we assumed in paragraph 1, that approximately 80% of the activity is in the stem and only 20% in the mushroom. This appears to be

contrary to common sense, but I can assure you I'm not doing this to be ornery. I am making this assumption because I believe that we can reasonably scale from tower shots to surface shots and we can also scale for increasing yield.

We employ the following scaling law:

$$P_1 = P_2 \text{ for a given scaled height,}$$

where

$$P = \frac{\sum AR}{kWt}^{1.2} \quad \text{Equation 1}$$

P = Percentage fall-out of residual activity

A = Area in square miles

R = Dose rate at time of fall-out in r/hr

W = Bomb yield in kilotons

t = Time in hours after bomb detonation

k = Constant = 12 in our calculations

This means that we assume that the percentage fall-out from a given scaled height is constant. This refers to residual activity deposited on soil debris which falls out within approximately one day due to the gravity of the particle. Equation 1 may be readily written as:

$$\sum A_2 R_2 = \frac{W_2}{W_1} \left[ \frac{t_1}{t_2} \right]^{1.2} \sum A_1 R_1 \quad \text{Equation 2}$$

Then for any element of Area,  $A_1$ , inclosed by a contour line  $R_1$ , we may be permitted to write:

DOE ARCHIVES

$$\bar{A}_2 = \bar{A}_1 \left[ \frac{W_2}{W_1} \right] \left[ \frac{t_1}{t_2} \right]^{1.2} \quad \text{Equation 3}$$

We can also say:

$$\bar{R}_2 = \bar{R}_1 \left[ \frac{W_2}{W_1} \right] \left[ \frac{t_1}{t_2} \right]^{1.2} \quad \text{Equation 4}$$

We note above that the area scaling with yield depends upon the time.

In the normal formula for scaling it is assumed that

$$A_2 = A_1 \left[ \frac{W_2}{W_1} \right]^{2/3}$$

Equation 5

The time variable from Equation 5 may be eliminated by setting  $t \sim Z \sim W^{1/3}$ , where  $Z$  is distance in the vertical direction.

If we do this we get

$$A_2 = A_1 \left[ \frac{W_2}{W_1} \right] \left[ \frac{W_1}{W_2} \right]^{0.4} = A_1 \left[ \frac{W_2}{W_1} \right]^{0.60}$$

Equation 6

It may be argued that Equation 6 and Equation 5 are not too different; and this may be true, except that we have a problem of extrapolating from 1 KT to 15,000 KT, where the use of the 0.60 exponent produces a factor of two differences from the use of the 0.667 exponent. The reason we have gone through the above analysis is to impress the reader with the fact that the time of start of fall-out is very important in any scaling factor for integrated dose. Paradoxically there is least amount of experimental data on this.

Once we have the Bravo model and we try to extrapolate back to 1 KT, we find that we overestimate the problem by a factor of 3 or 4 using Equation 5 and by 6 to 8 when Equation 6 is used. We have applied a correction factor to compensate for this. We believe that by such a procedure we may be able to use the Bravo shot to scale down to 1 MT and up to 60 MT quite adequately. For details see ARDC Report C4-23676.

**DOE ARCHIVES**

During the conference a number of personnel referred to the ARDC method as implying 90% activity in the stem and 10% activity in the mushroom. Actually in our report (C4-23676) and in the first paragraph above, we showed that our method assumes approximately 80% activity in the stem and 20% in the mushroom, whereas RAND assumed 10% in the stem and 90% in the mushroom. We believe that large particles rise high into the mushroom, immediately as the cloud forms, but it is our opinion that all this falls out fast (within 10 to 30 minutes) and it all lands on or near ground zero or the lagoon. No significant amount of activity falls out downwind in excess of 20% from the mushroom except after 24 hours or so, at which time both dilution and decay would have reduced the radiation intensities to insignificant amounts. For lower yield bombs such as 5 MT, the activity in the mushroom may increase to 30 or 40%, with the stem activity still as high as 60 to 70%. This is because we assume that

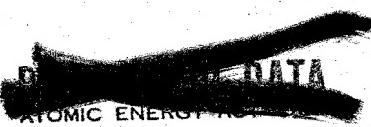
the particle size distribution decreases with height, and the 5 MT cloud would not reach as high as the 15 MT cloud of the Bravo shot.

Figure 10 shows what would happen to this country if 111 bombs of 15 MT are detonated over 106 cities whose population is 100,000 or more and over five other selected areas. For details refer to ARDC Report C4-23676. The slide is here shown to illustrate that if 100 or more hydrogen bombs are used, most of the country will be contaminated almost independently of meteorology. For example, if the winds aloft were all easterly, it would not radically change the contamination pattern over the country. Similarly for northerly or southerly winds. The slide also shows that evacuation and dispersal may not be advisable, for it may clearly be a case of evacuating from the frying pan into the fire.

I would like to make a few rather obvious remarks about worldwide contamination that may be derived from our analysis of percentage fall-out for surface burst bombs. It will be assumed that 80% of the residual activity of a bomb is deposited downwind within 15 to 20 hours after bomb detonation. This means that if we need 10,000 bombs, airburst, of a certain yield to uniformly contaminate the world, then we will need only approximately 200 of the same yield bombs to contaminate this country to the same level.

DOE ARCHIVES

This presentation of the ARDC method of prediction of dose rate and dosage contours was not presented in the manner indicated above. However, the ARDC method has not been altered in this presentation. This paper represents rather the many "conferences" within this conference that were held during these three days. Some of the items, notably the scaling method was not presented at the symposium due to shortage of time, but it is included here for sake of completeness. This paper is in effect a condensation of ARDC Report C3-36417 and its supplement, and ARDC Report C4-23676. The illustrations shown here are from the above reports. This paper in substance indicates not only my talks at this symposium, but also my thoughts by the close of the conference after I had seen the presentation by other members of the symposium. My final comment is that it is unfortunate that RAND and other organizations did not utilize the wealth of information available from analysis of TUMBLER-SNAPPER and UPSHOT-KNOTHOLE tower shots. Had they done so, they would not have placed so much scavengable activity in the mushroom.



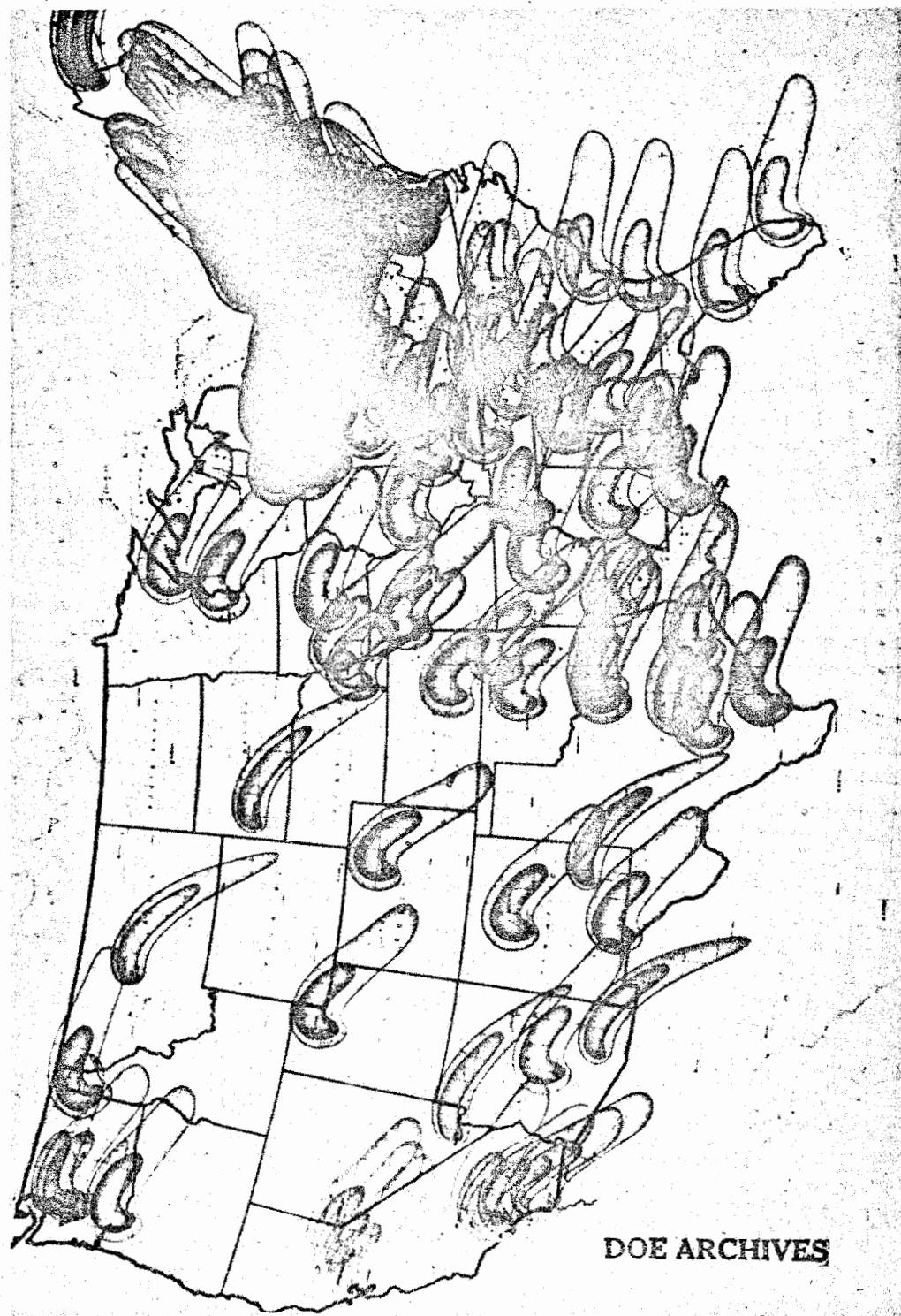


Figure 10  
Fall-cut Pattern of 111 15MT Weapons

287

AMERICAN ENERGY

292

**THIS PAGE IS BLANK**

**DOE ARCHIVES**

**288**

**NUCLEAR ENERGY ACT 1954**

**293**

**SURVEY OF FALLOUT AREA AT SEA FOLLOWING  
YANKEE - NECTAR, OPERATION CASTLE**

Mr. Merril Eisenbud  
U. S. Atomic Energy Commission  
New York Operations Office  
Health and Safety Laboratory

The fallout following Yankee and Nectar was estimated by means of aerial surveys. Evaluation of the data indicated that in the region of from 25 to 150 miles the estimated Yankee fallout of fission product, adjusted to H+1 days, was 1240 megacuries, the estimated Nectar fallout, at H+1 days, was 293 megacuries.

**DELETED**

Since it is possible to measure surface activity by aircraft, it is necessary only to know the law of height attenuation for the characteristic gamma radiations measured. In the case of fission product the height attenuation is shown in figure 1. Figure 2 illustrates also the correlation between the surface gamma activity as estimated from the aircraft, and measurements taken on shipboard. The estimate of total activity could be made since there was also correlation between surface activity levels and total fission product load in depth to the bottom of the thermocline, figure 3.

Figure 4 is the trace of activity taken on H+72 hours following Yankee, figure 5 is the related diagram of wind vectors, figure 6 represents the estimated isodose traces. Figures 7, 8, 9, 10, and 11 bear the same relationship to Nectar. It is interesting to note that the wind vector charts effectively display the probable path of fallout. In the case of Nectar the low level fallout, apparently stem debris, was found on H+24 hours but disappeared during the next 24 hour period.

**DOE ARCHIVES**

The method, beyond providing information on quantity of fallout, supplies data which will permit prediction of the direction of fallout paths, a means of determining safe areas for surface vessel operations and a general source of information for military and civilian defense planning for personnel protection.

Future planning should include the use of telemetering equipment plus automatic altitude compensation of readings to eliminate pilot error. The use of telemetering will permit a central plotting arrangement and is necessary since more than one plane will be required to provide a traverse of a 360° pattern. Sea water surface measurements should be related to depth measurements from the time immediately

~~SECRET~~

following the burst until the main body of activity disappears since no early data has been taken. With better equipment and adequate preparation it may be desirable also to survey beyond the 150 mile radius.

**DOE ARCHIVES**

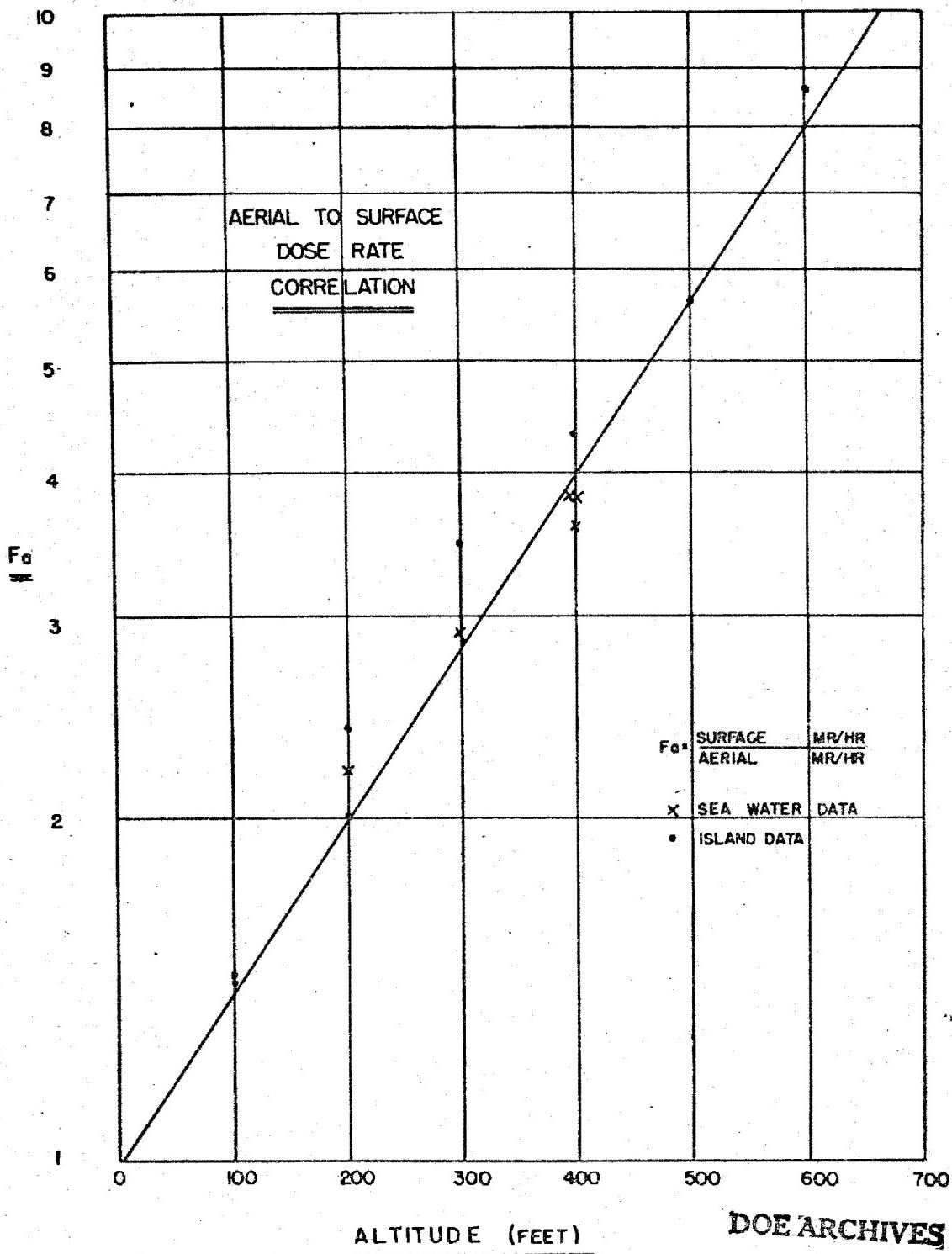
290

~~SECRET~~

ATOMIC ENERGY ACT 1954

295

~~SECRET~~



DOE ARCHIVES

Figure 1  
291

~~DATA~~  
ATOMIC ENERGY ACT 1954

296

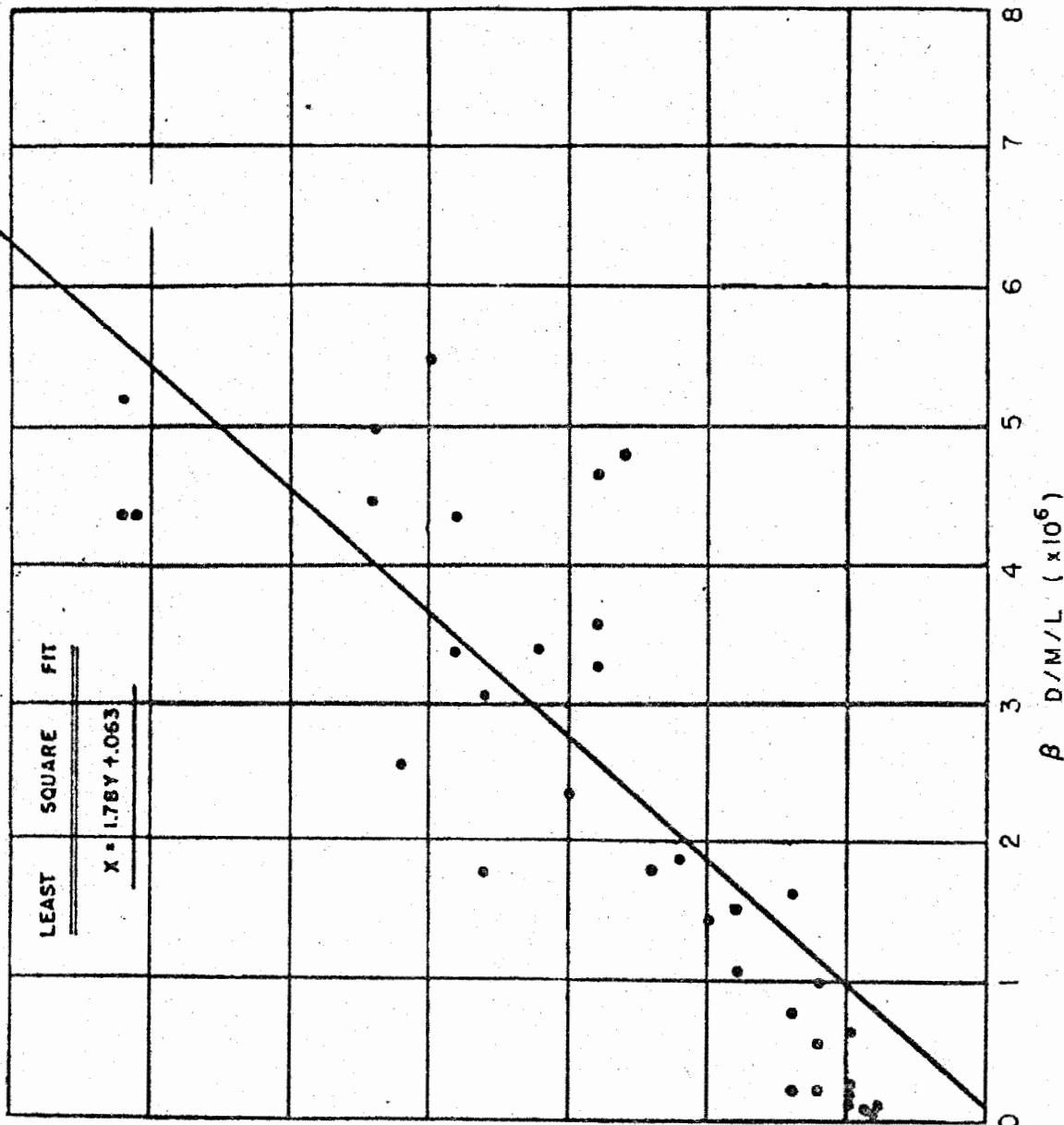


Figure 2

DOE ARCHIVES

2 M/LR

292



291 297

### SURFACE TO TOTAL ACTIVITY CORRELATION

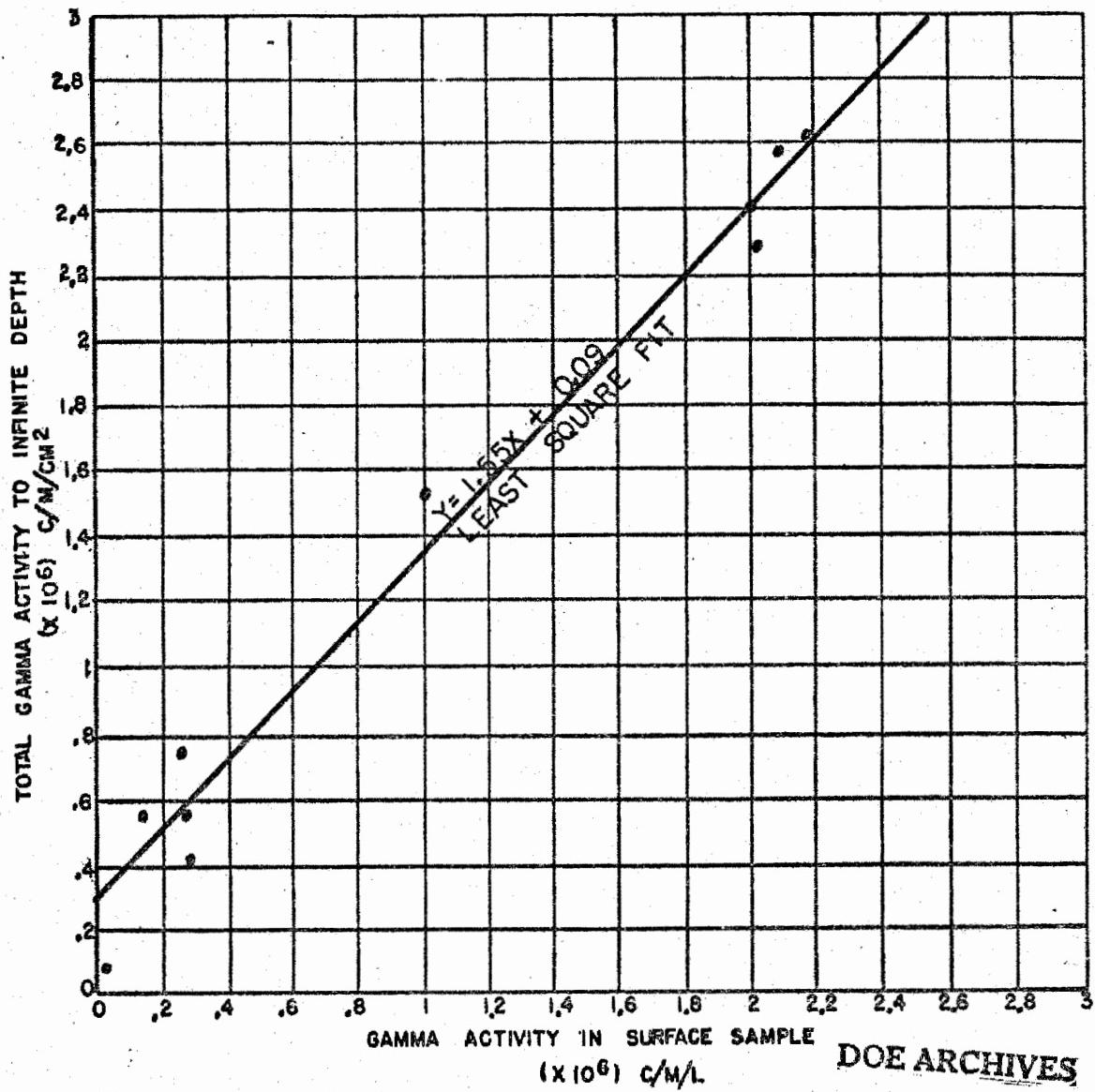
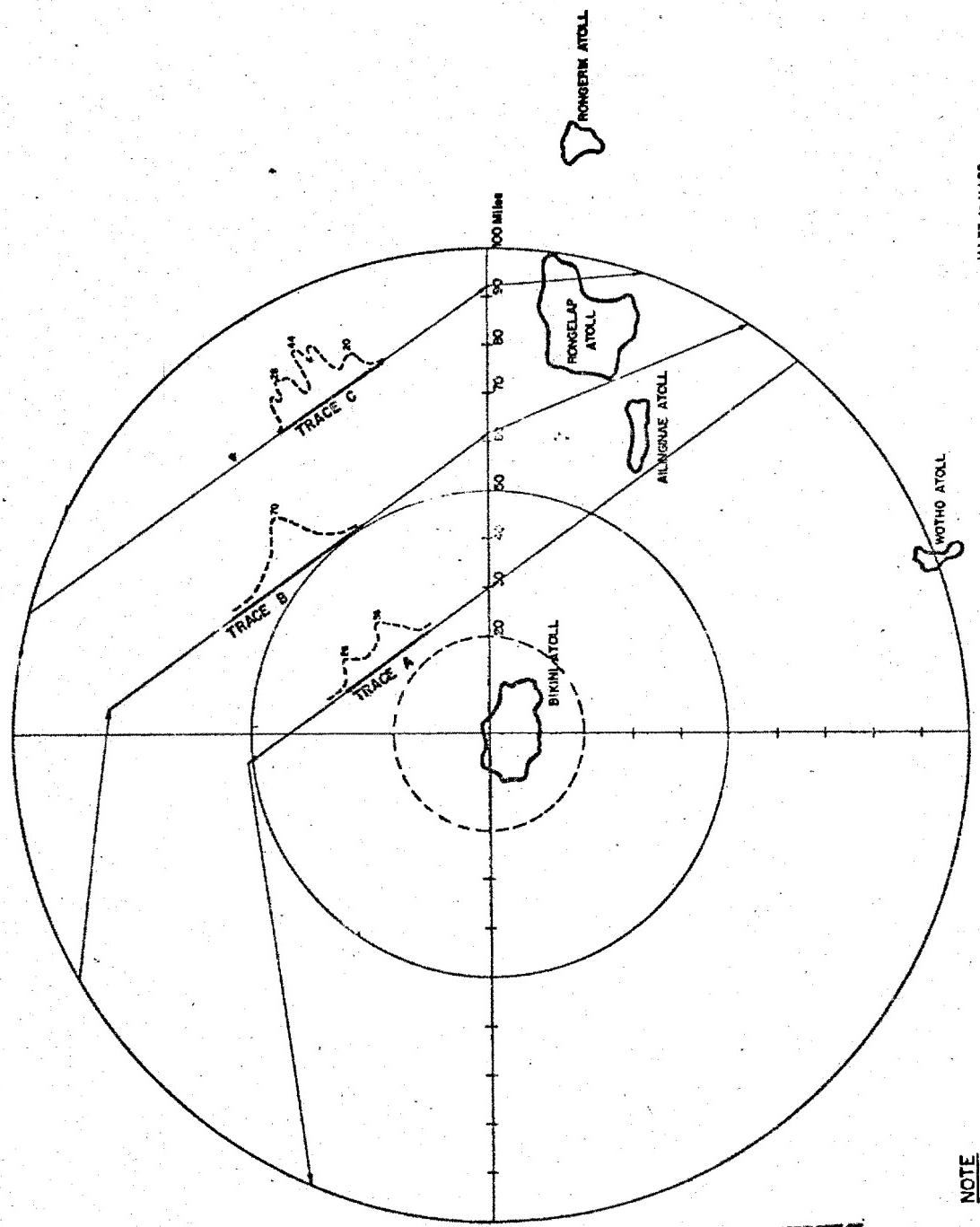


Figure 3

293

RETRIEVED DATA

298



Y-114-F-07192 / No 080345 Z

Figure 4

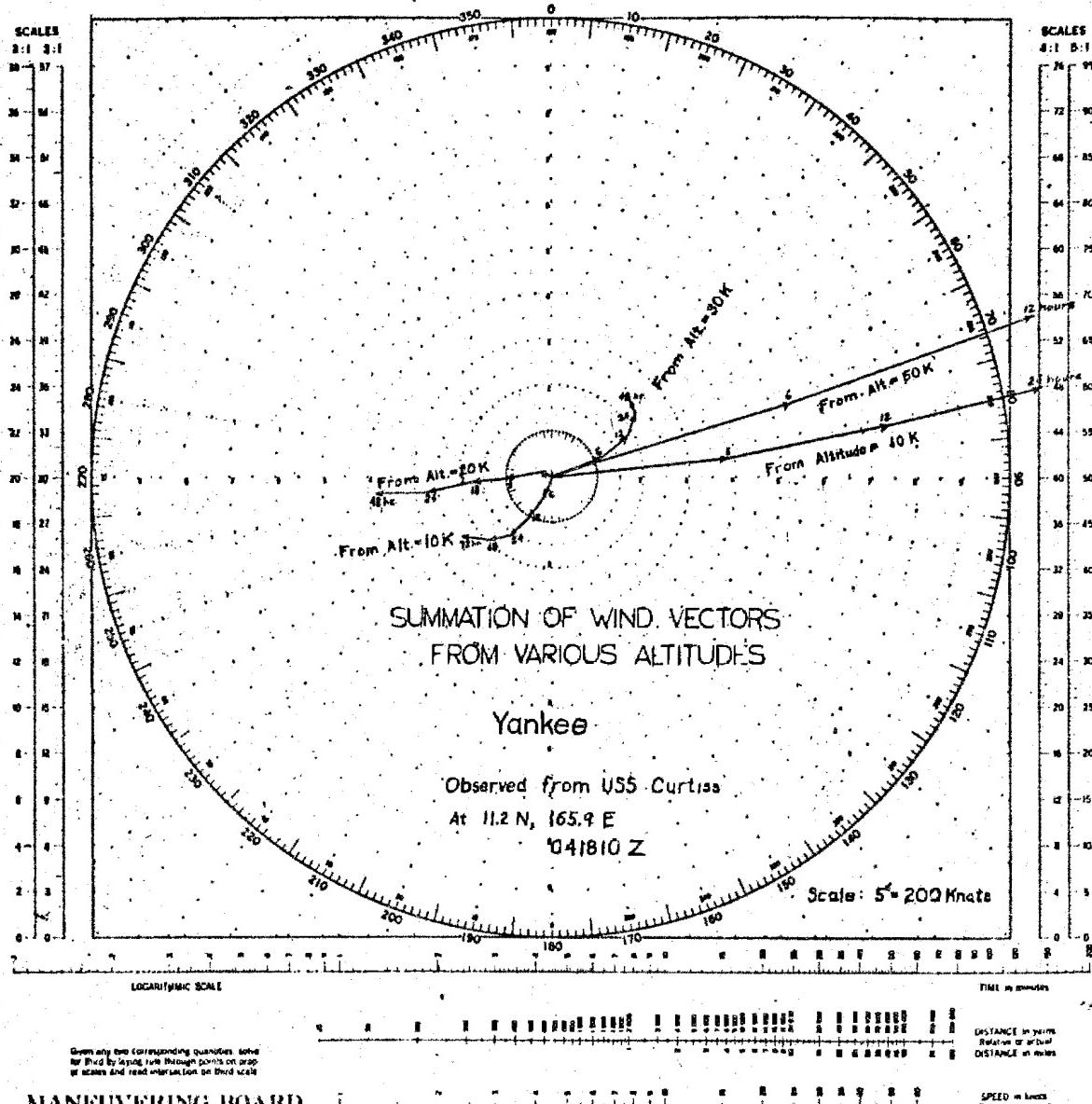


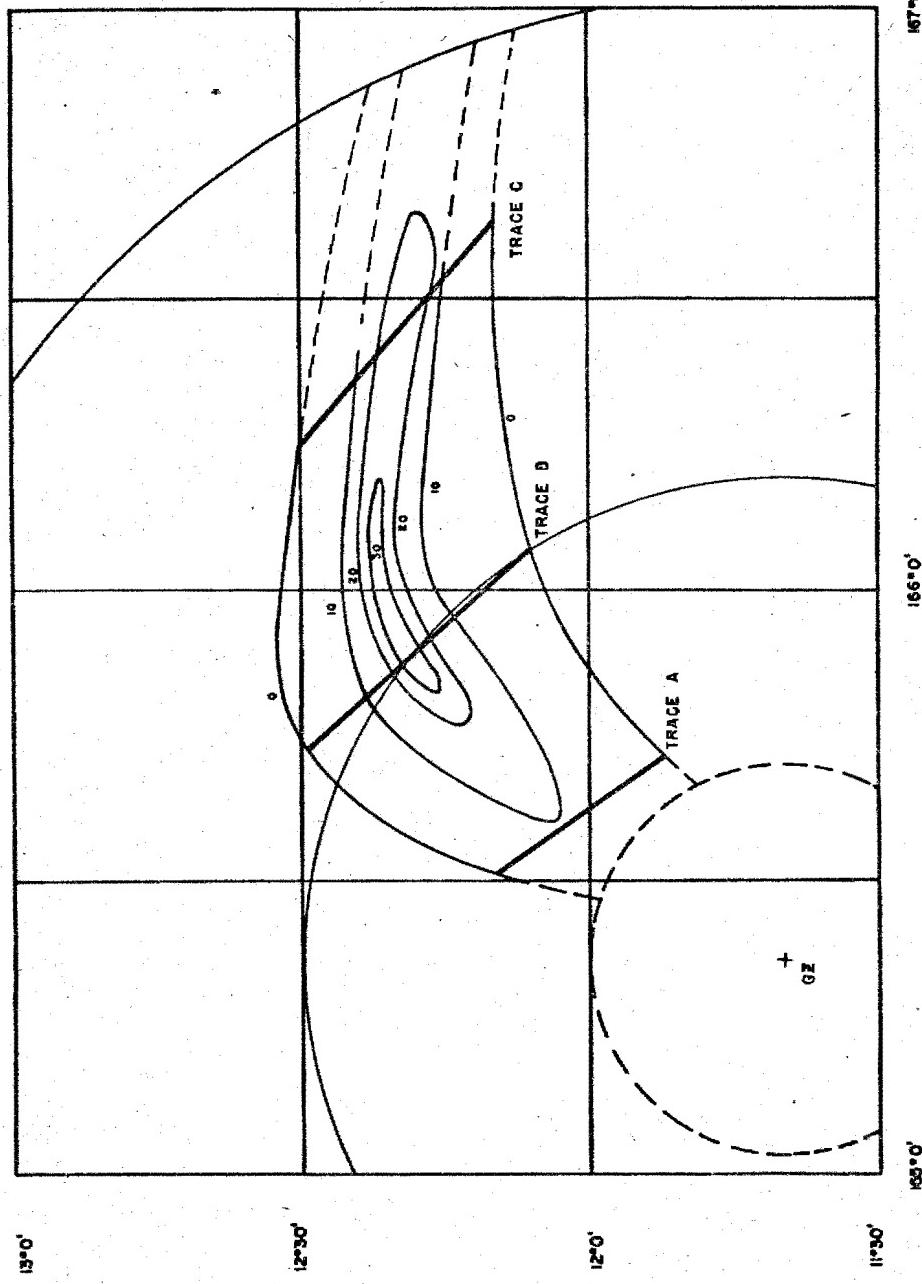
Figure 5

295

DOE ARCHIVES

300

YANKEE ISODOSE



NOTE-- READINGS IN MR/HR EXTRAPOLATED TO SURFACE AND CORRECTED TO H+2 DAYS  
ISODOSE LINES BETWEEN TRACES ARE POSSIBLE CONDITIONS AND SHOULD BE CONSIDERED ILLUSTRATIVE ONLY

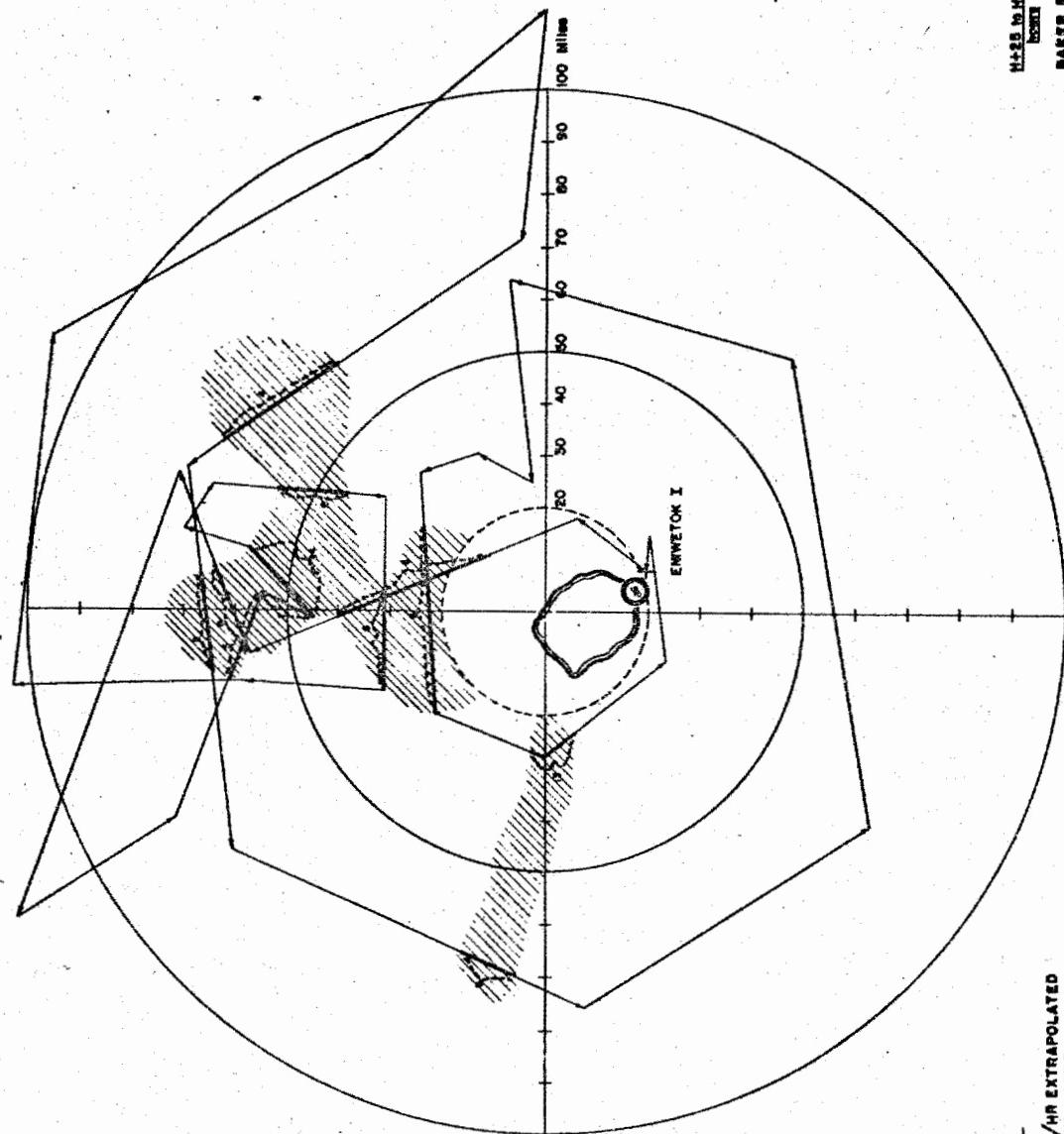
Figure 6

DOE ARCHIVES

296

NUCLEAR ENERGY ACT 1954

301



DOE ARCHIVES

NOTE

PROFILE READINGS IN MPH EXTRAPOLATED  
TO 3 FEET ABOVE SEA, AND CORRECTED  
TO H+46 HOURS

297

— 10 —

卷之三

STUDIO 11 DATA  
MC ENERGY ACT 1934

305

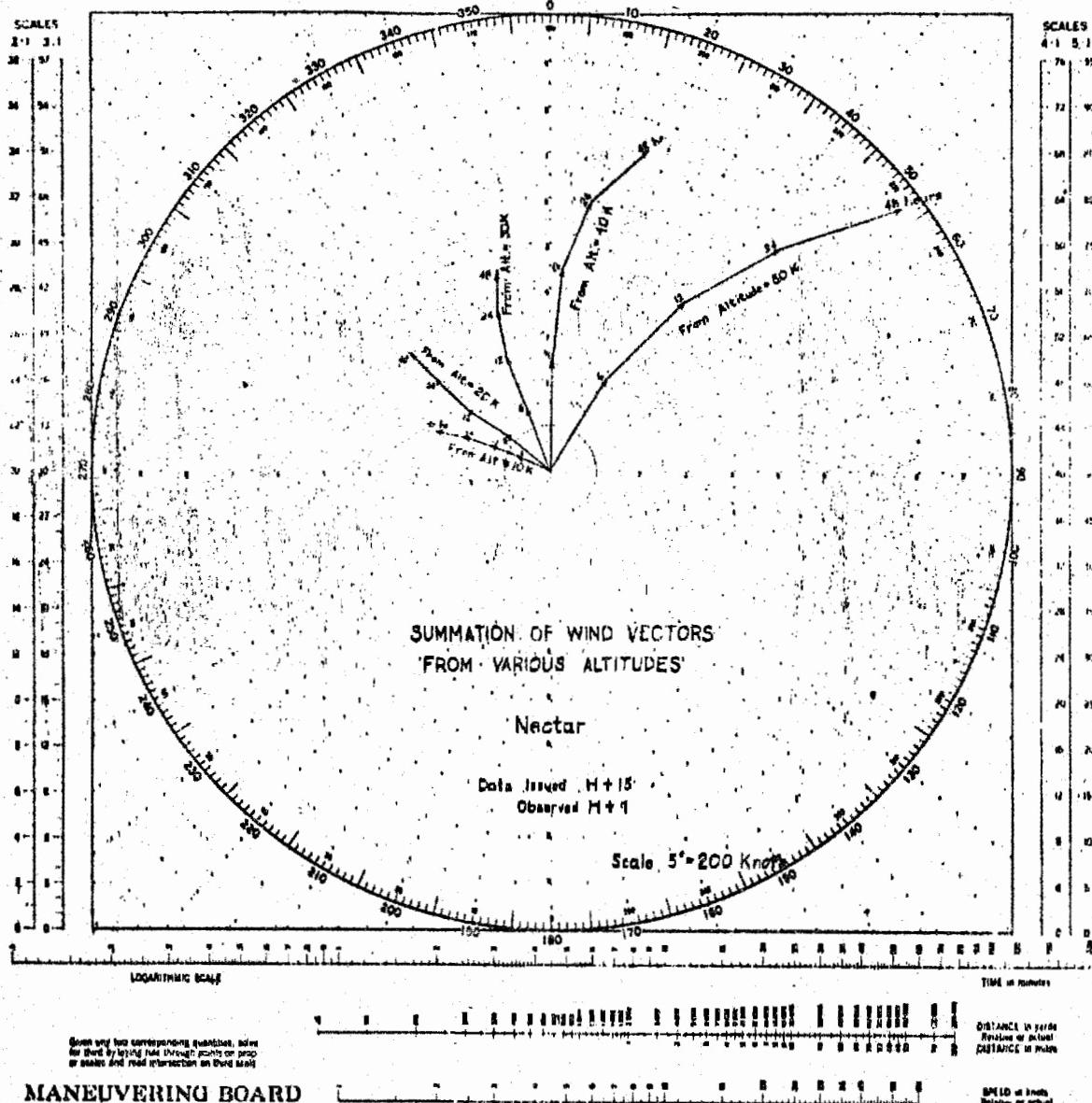


Figure 8

298

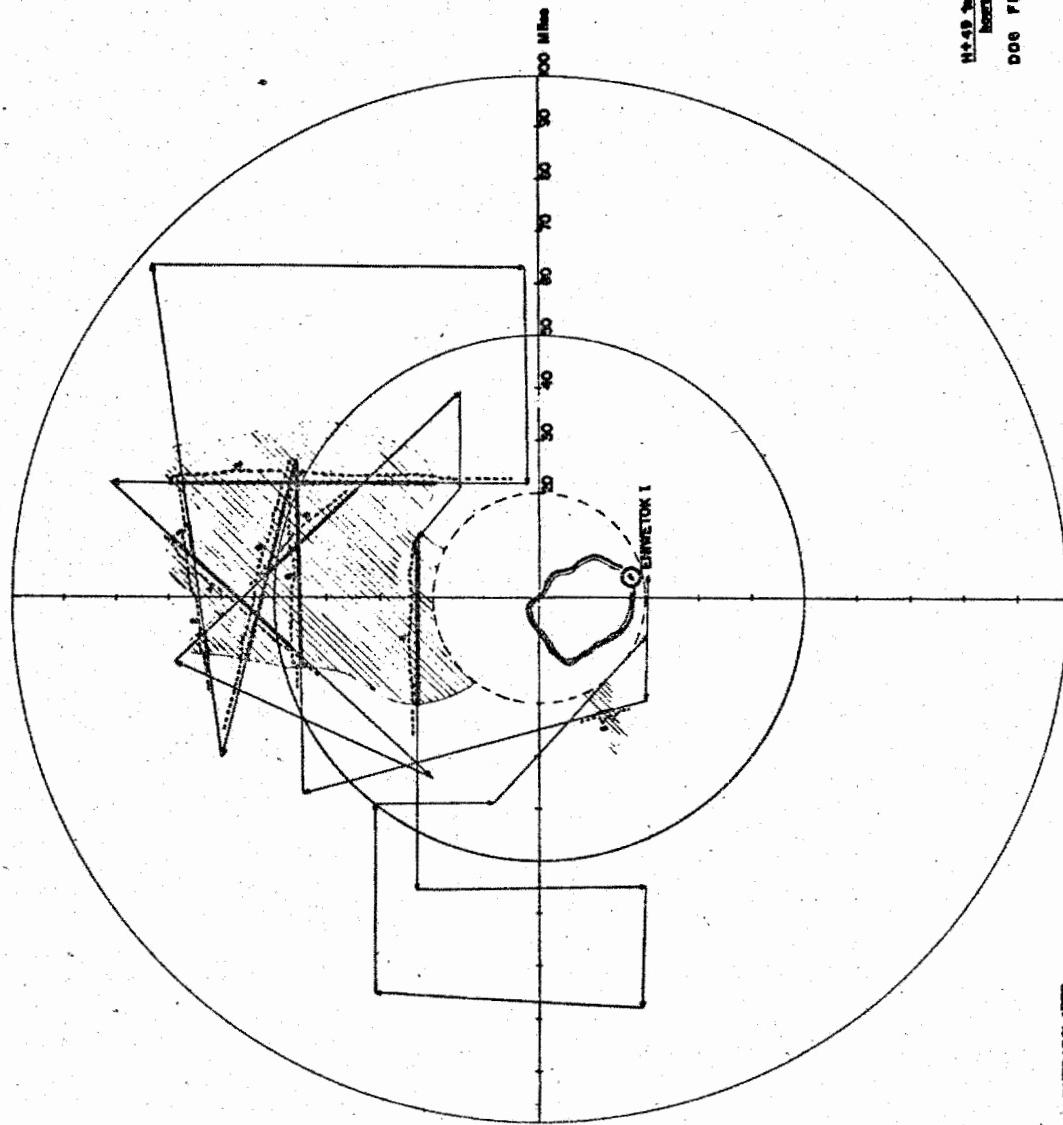


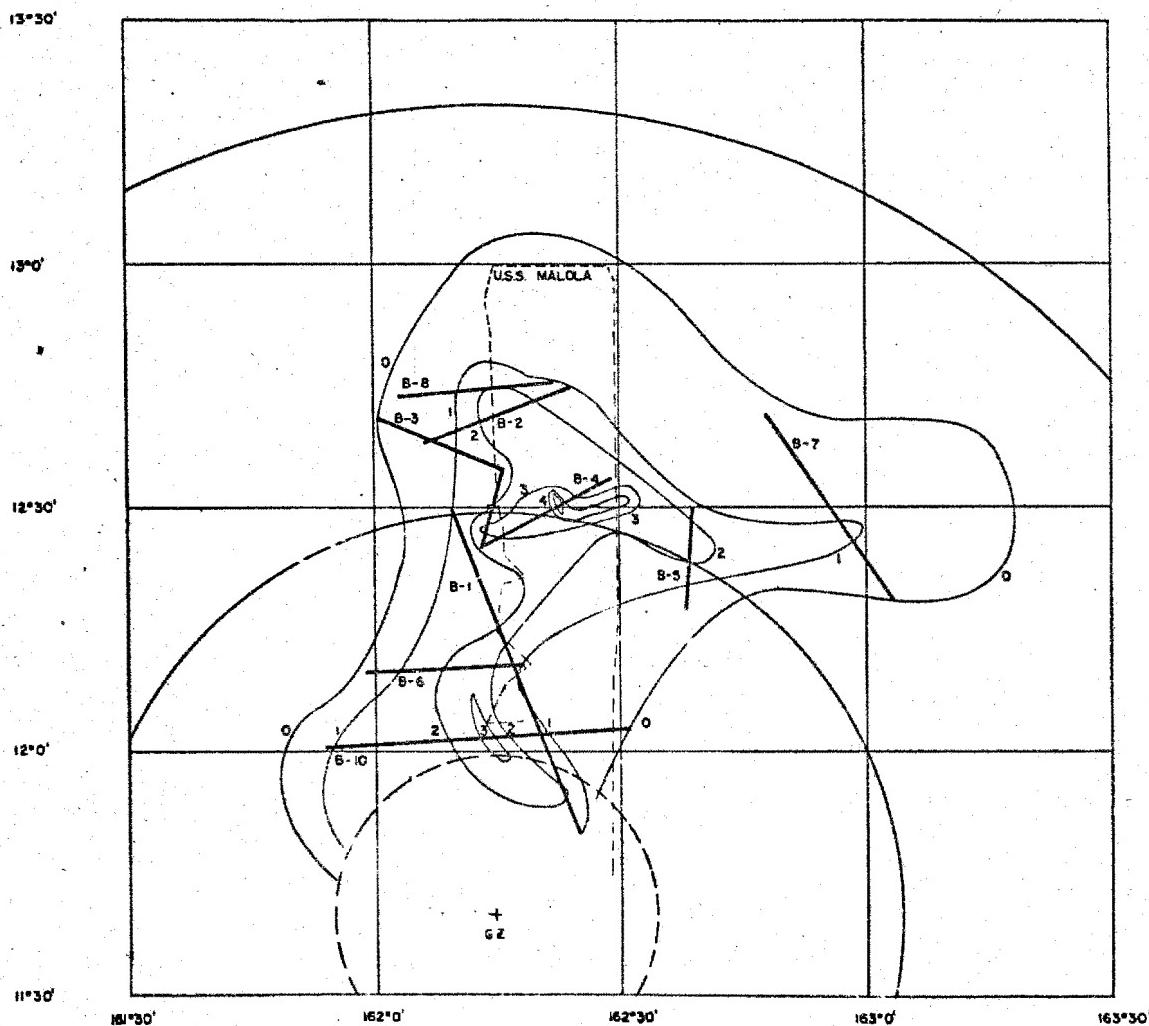
Figure 9

299

~~REFINED DATA~~

304

**NECTAR ISODOSE**



NOTE - READINGS IN MR/HR EXTRAPOLATED TO SURFACE AND CORRECTED TO H+2 DAYS

**DOE ARCHIVES**

ISODOSE LINES BETWEEN TRACES ARE POSSIBLE CONDITIONS AND SHOULD BE CONSIDERED ILLUSTRATIVE ONLY

Figure 10  
300



305

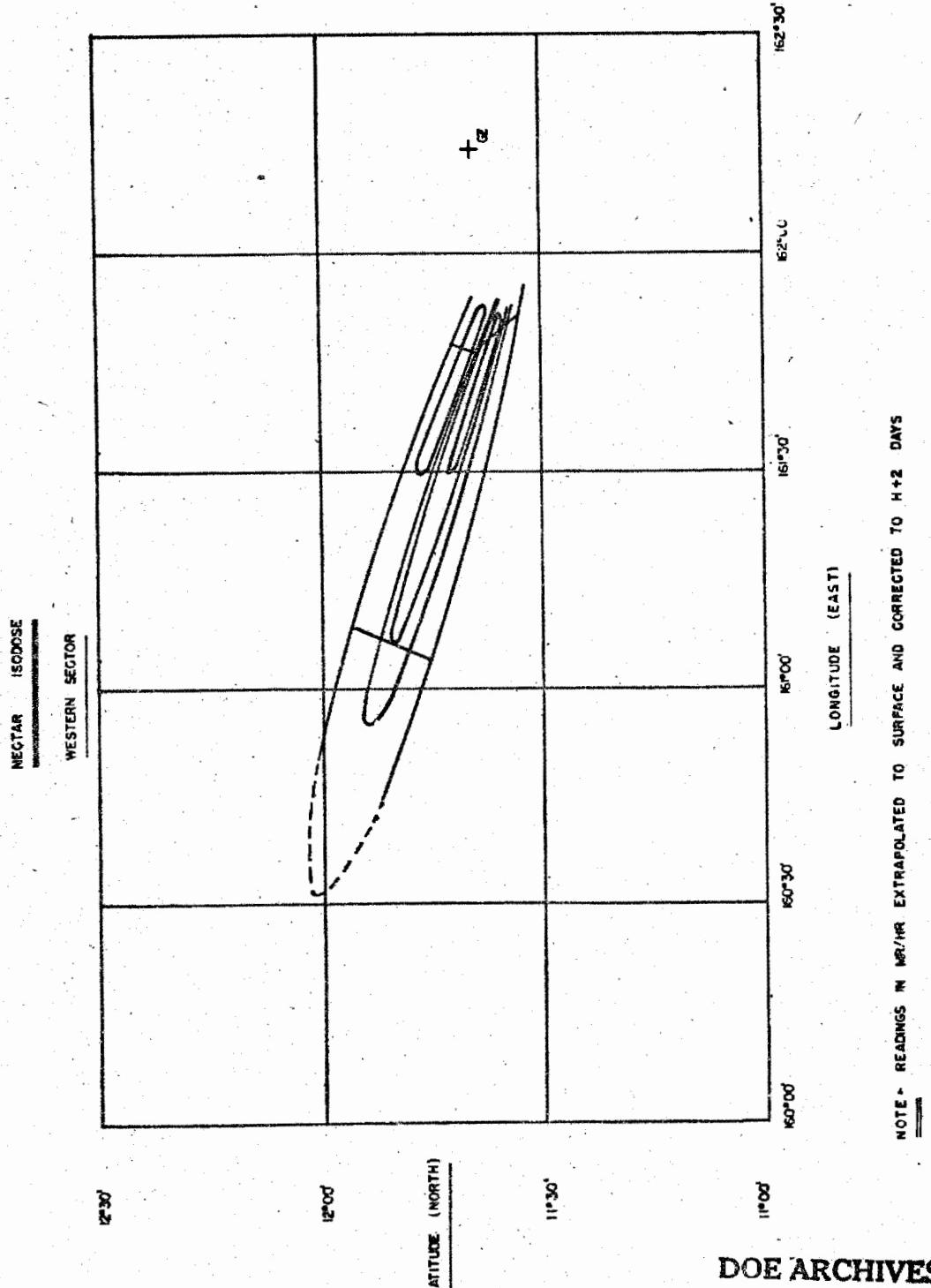


Figure 11

306

**THIS PAGE IS BLANK**

**DOE ARCHIVES**

**302**

**OMIC ENERGY**

**211**

**307**

PREDICTION OF DOSE-RATE AND DOSAGE CONTOURS AS  
FUNCTIONS OF YIELD AND METEOROLOGICAL CONDITIONS,  
LASL METHOD

PART I

FORECASTING OF THE 10 R ISODOSE LINE

Dr. Gaelen Felt  
Los Alamos Scientific Laboratory

Introduction

The problem of long-range fall-out from very large devices (megatons) was first examined prior to Operation IVY. At that time the methods of analysis were based on a simple theoretical model devised to evaluate the hazards from the Jangle shots and on the empirical results from low-yield tests in Nevada. Neither source was truly applicable in detail to Mike, a fact well-known at the time, but the general result, as we know from [REDACTED] was correct; i.e., fall-out from Mike under adverse conditions could have been very severe at distances of 200 to 300 miles. The actual conditions on Mike-Day were, of course, favorable but at the same time rather unusual in that the location of the main fall-out was well clear of all populated areas.

The rare occurrence of ideal conditions, the length of the Castle operation, and the very evident hazards from the devices made necessary a re-examination of the problem of fall-out. In the field such a re-examination could be very crude at best, geared as it was to the immediately practical aim of operational forecasting. It was necessary to devise a system of forecasting simple enough to provide results based on the latest possible weather information, both observations and forecasts, conservative enough to guarantee no repetition of the unfortunate results of [REDACTED] and yet daring enough to enable one to take advantage of weather conditions different from those known to be ideal (no northern components from surface to 100,000 ft and axis of fall-out between about  $315^{\circ}$  and  $045^{\circ}$ ).

DOE ARCHIVES

The treatment generally used in Nevada with moderate success was pretty clearly not well suited to fall-out forecasting at the Pacific Proving Grounds except possible under the condition of "deep easterlies", when all wind vectors from the surface up are easterly (an alternate "ideal" situation, incidentally for Eniwetok Atoll but not for Bikini). The basic difficulty with using the Nevada system for

analysis of the effects of large devices in the Pacific is that the wind structure in the Pacific is not primarily unidirectional in the pertinent altitude range. The usual fall-out pattern in Nevada is a narrow band, broadened at times by the presence of light and variable winds and by the occasional presence of abnormally great directional shear but still confined to a small sector. This general character is not often found in the Pacific, where the directional shear is almost always very great just above the east-northeast flow in the low altitudes and again at the tropopause (usually about 55,000 to 60,000 ft). In the Pacific the sector which includes all the distant fall-out is very frequently 180° and occasionally even greater.

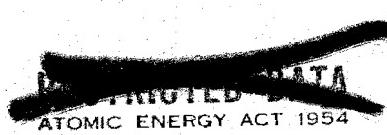
While the sector is very large in the Pacific it is not true that the fall-out is uniformly distributed within it, and it therefore becomes necessary to look closely at the angular distribution of fall-out as well as the radial. It is this new factor in the analysis which makes the Castle system differ fundamentally from the Nevada system. It does not necessarily follow that the Nevada system should not also have this feature since there are evident failings there which may perhaps be removed in this way.

#### The Dose Index

The first step in the new system of analysis was to calculate the relative dose at various points about the origin for a given wind structure. The mechanics of preparing the isodose plots will be described in the following sections. Here we shall discuss the assumptions and general principles of the method. The assumptions used in the calculations are listed below:

The activity is uniformly distributed in height. This assumption is obviously a poor one and was subsequently altered to emphasize the middle region of the cloud and to depress the stem and the top. In the first plot this modification was applied at the plotting stage rather than at the calculational stage.

The distribution of particle sizes is uniform. This assumption <sup>DOE ARCHIVES</sup> is not true but is justified by several arguments. From our point of view--distant fallout--the number of particles two feet in diameter relative to the number 100 microns in diameter makes not the slightest difference since the former all fall in the region of the crater anyway. On the other hand the relative number of very small particles is equally uninteresting since these do not fall quickly enough to affect the results significantly. What we have done in effect is to assume a "white" distribution for simplicity and to restrict the region of validity to distances between approximately fifteen miles and a couple



of hundred miles from the origin. Again, in the absence of any detailed information on the real distribution, the assumption we have made is probably the safest.

The amount of activity deposited by an active particle is proportional to its area. One may fairly argue that in some cases the activity should be proportional to the particle volume. The choice of area dependence is based on the idea of plating on molten solids and on the idea of scavenging by water droplets.

The total activity is proportional to the total yield and decays as  $t^{-1.2}$ .

The particles settle by Stoke's law. This assumption is always challenged but no suitable substitute has yet been suggested. In the range of particle sizes of interest it is probably as good a law as any modification of it.

The area at the surface covered by particles falling from a given height is proportional to the square of the time of fall. This assumption expresses the fact of divergence which may arise from any number of reasons. No numerical value is assigned to the divergence.

The net radial distance that a particle travels is proportional to the time of fall.

With the above assumptions one obtains the dose index in the following inelegant way. At a given point "P" on the surface (Fig. 1) active particles can arrive from certain discrete altitudes of the cloud determined by the intersection with the hodograph of the radius vector from ground zero through the point. In the example these are the altitudes 79,000 ft at "A" and 39,000 ft at "B". The hodograph is customarily drawn for a fall rate of 5,000 ft per hour so that particles with that fall rate which start from 39,000 ft at nominally zero time will land at "B" in 7.8 hours. These particles will have a definite diameter "d". We have said that the activity brought down by any particle is proportional to its area; i.e., the dose index "D" contains a factor " $d^2$ ".

DOE ARCHIVES

The remainder of the argument concerns the time. Two other assumptions contain time terms, the natural decay and the area of deposition. Now the dose rate is expressible in activity per unit area. For example, one megacurie per square mile is roughly equivalent to 3 r/hr about 3 ft above a fission fragment deposition. The dose rate is therefore expressible as

~~SECRET~~

$$\text{rate} \sim \frac{a}{A} \sim \frac{t^{-1.2}}{t^2} \quad (1)$$

and the integrated dose, apart from other factors, is expressible as

$$\text{dose} \sim t^{-2.2}. \quad (2)$$

We chose to define the dose index as

$$D = \frac{d^2}{t^2} \quad (3)$$

where "d" is the particle diameter in microns and "t" is the time at which it arrives in hours. In the event that particles arrive from two heights as indicated for point "P" in Fig. 1, one merely adds the two indices arithmetically. We have felt, in view of the crudeness of these arguments, that very little would be achieved by keeping the power of "t" at -2.2 and have used -2.0 instead.

One will note that in this form the dose index does not yet contain Stoke's law but states merely that particles of size "d" arrive at time "t". The use of Stoke's law and some of the other assumptions permits the dose index to be written in a wide variety of alternate forms. Stoke's law states that the terminal rate of fall is proportional to the area of the particle. In our case the terminal rate is reached so quickly that one may write

$$\frac{h}{t} = K d^2 \quad (4)$$

where "h" is the starting height, "t" is the time of fall, "d" is the particle diameter and "K" is a constant of proportionality containing the density, the viscosity, and numerical factors. The viscosity, incidentally, is temperature dependent, but the variation is small compared to the other uncertainties in this system and we have chosen to keep the viscosity constant. Substitution of equation (4) permits one to write the dose index as

$$D = \frac{h}{K} \cdot \frac{1}{t^3} \quad (3a)$$

and further use of assumption (7) above permits the form

DOE ARCHIVES

$$D = \frac{h}{K'} \cdot \frac{1}{R^3} \quad (3b)$$

~~REF ID: A6514~~

ENERGY ACT 1954

where "K" is some new constant and "R" is the radial distance along a bearing from ground zero.

Numerical values of the dose index can be computed from any of the forms of equation (3) with the proper selection of units.

We defined the numerical value of the dose index as the ratio of the square of the particle diameter in microns to the square of the time of fall in hours. In these units the dose index is of the same order as the dose in roentgens from a 10-megaton yield as determined by a rough match with [redacted] data. The adjustment to other yields in the megaton range is made by direct proportionality as indicated in assumption (4).

#### Preparation of the Plot: Static Case

We proceed now to describe the method of constructing the isodose contours for the simpler case of the static hodograph. The static hodograph presents a plan view of the vertical structure of the forecast winds at zero time and at the origin. Fig. 1 is a sample hodograph constructed from data in Table I. The criticisms against the static hodograph are that it should not be expected to persist unchanged even at the origin throughout the time of fall-out, and that it does not in principle apply at all to points displaced from the origin. These criticisms become more important as one attempts to forecast the low-level isodose lines which are established at considerable distances from the origin and many hours after shot time. The static hodograph does, however, provide a useful guide and has the virtue that a plot can be prepared from it very quickly indeed.

Using the sample hodograph of Fig. 1 let us compute the dose index for point "P" at  $40^{\circ}$  and 60 nautical miles from ground zero. There will be two components for "P" and all other points along the radius from "Z" through "P". From the hodograph the intercept heights and distances are 79,000 ft and 45 miles at "A", and 39,000 ft and 73 miles at "B". As mentioned above the total index for "P" is the sum of the indices computed from the two intercepts.

DOE ARCHIVES

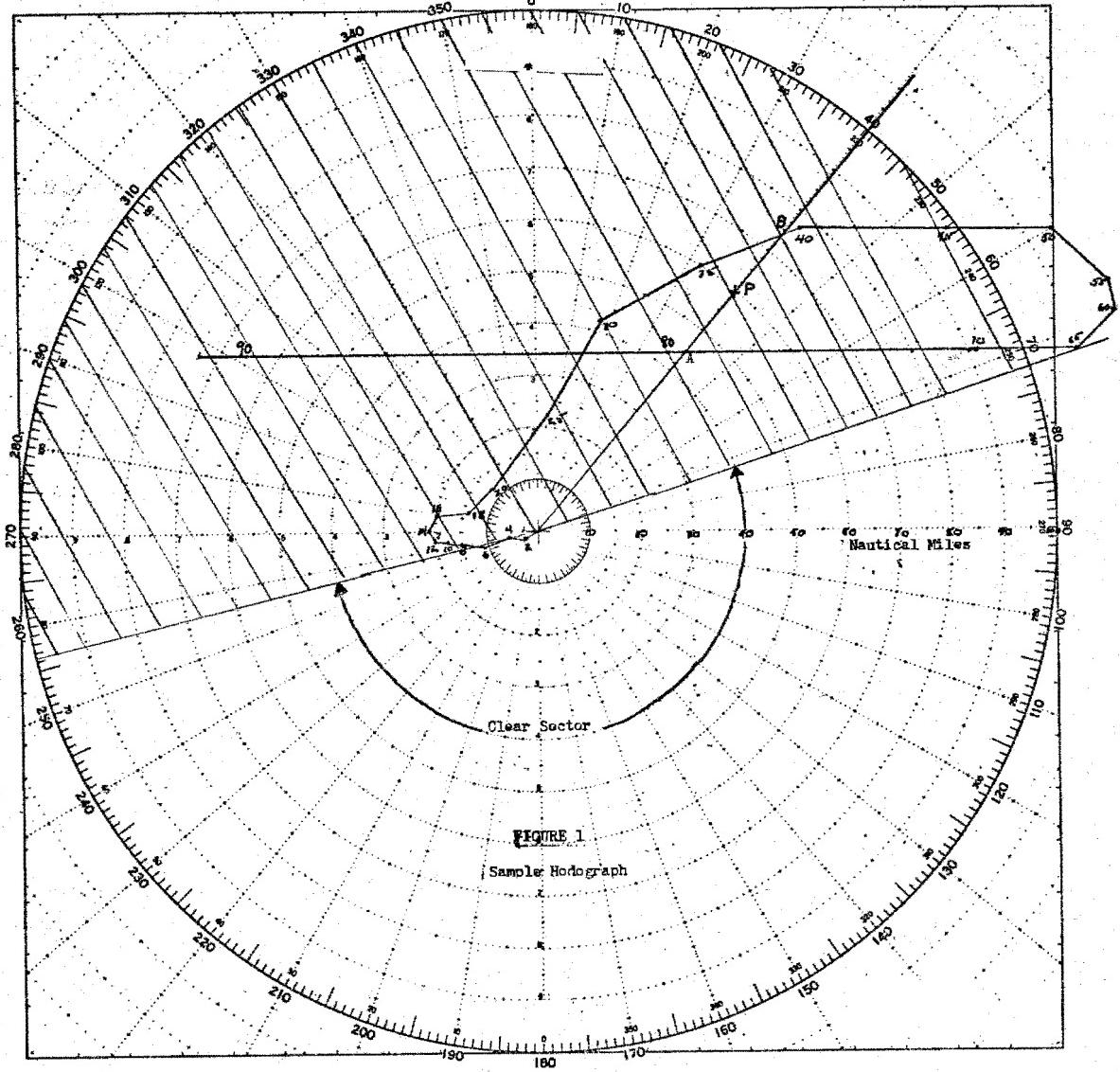
Let us consider first the index from intercept "A". Particles which fall at "A" on the surface start at 79,000 ft above Zero. As they fall to 65,000 ft they travel westward approximately 75 miles. In falling the next 5,000 ft they travel approximately 10 miles southwest. Thereafter they swing around through the south, travel eastward between 50,000 and 40,000 ft, gradually turn to the northeast, and at about 15,000 ft settle into the surface trades for the last 20 miles of westward travel to point "A". Since the hodograph is drawn

Table I -- Sample Wind Forecast

Height in thousands of feet	Bearing in Degrees	Speed in Knots
2	080	08
4	080	10
6	070	10
8	090	10
10	090	08
12	110	05
14	160	05
16	200	08
18	260	13
20	230	15
25	220	18
30	210	20
35	240	23
40	250	20
45	270	28
50	270	20
55	310	15
60	350	05
65	040	10
70	090	20
80	090	30
90	090	40

DOE ARCHIVES

308



DOE ARCHIVES

Figure 1  
Sample Hodograph

309

OMIC ENERGY ACT 1954

314

for the convenient rate of 5,000 ft per hour the particles arrive at "A" 15.8 hours after zero. Particles arriving at "P" from 79,000 ft must spend a slightly longer time in each altitude layer; their trajectory is similar to that for the faster-falling particles but is expanded. The relative time for particles to arrive at "P" compared to "A" is given by the ratio of the vector sums or by the factor  $60/45 = 1.33$ . The time in hours is therefore 21.1 hours.

Now we have assumed a relationship between fall rate and particle diameter given by Stoke's law. Specifically, for land shots at the Pacific Proving Grounds, we assume that 75-micron particles settle at 4,000 ft per hour. Particles arriving at "P" from 79,000 ft settle at 3,740 ft per hour and are therefore slightly smaller than 75 microns. Stoke's law gives 72.4 microns. Using equation (3) with the numerical values 72.4 microns and 21.1 hours one obtains a dose index at "P" from the intercept "A" of approximately 12.

A similar computation for the dose index from intercept "B" gives the much higher value 208. The total index at "P" is therefore 220. This means that for 10 megatons one would expect an integrated lifetime dose of 220 roentgens in the vicinity of point "P".

It is obviously time-consuming to compute the index for a large number of points in the field in the way just described. In order to speed up the computation of dose indices the nomogram in Fig. 2 was constructed from an alternate form of the dose index equation. The most suitable form is

$$D(\theta, R) = \frac{v_o^3}{K_s h_o^2} \cdot \left[ \frac{R_o}{R} \right]^3 \quad (3c)$$

DOE ARCHIVES

(3c)

where " $v_o$ " is the hodograph fall rate (5,000 ft per hour), " $h_o$ " is the intercept height in feet, " $K_s$ " is the Stoke's law constant ( $4,000/5625$  in our units), " $R_o$ " is the intercept radius in miles, and " $R$ " is the distance in miles to a point on the bearing " $\theta$ ". One should note that for constant " $\theta$ " the intercept height and distance are also constant and that the dose index along this bearing decreases as " $R^{-3}$ ". Consequently if one can determine the dose index at one point along the bearing the indices for other points can be read very quickly from a straight line of slope -3, on log-log graph paper. The obvious point to determine an index is at " $R_o$ ". For all bearings the dose index at  $R = R_o$  is determined by the intercept height alone. It becomes very simple therefore to make a suitable nomogram by drawing a line of slope -2 which gives the dose index " $D_o$ " for  $R = R_o$ . The doses at any " $R$ " are then obtained by placing a straightedge with slope -3 through the point " $D_o, R_o$ ". For quick reading several arbitrarily

spaced lines of slope -3 have been drawn in Fig. 2.

Using again the sample wind structure of Fig. 1 one obtains the index for point "P" from the intercept "B" by entering the nomogram at  $h_0 = 39,000$  ft at the top of the page, coming down to the unweighted height line at index 110, moving left to a point above the distance  $R_0 = 73$  miles, then up a line of slope -3 to index 210 above  $R = 60$  miles.

The nomogram in Fig. 2 has two height lines, the curved one corresponding to a weighted height distribution. This second curve is believed to be somewhat more realistic inasmuch as it reduces the weight of the very low and very high parts of the cloud and increases the weight of the middle cloud. This rather general weighting is based entirely on observation and experience and is not derived analytically.

With a very little experience in the use of the nomogram one can from the hodograph prepare the plot shown in Fig. 3 in approximately one-half hour. The weighted height line has been used in this plot.

#### Preparation of the Plot: Dynamic Case

For operational use a 10 R dose is a handy dividing point between "dangerous" and "harmless" levels. A dose index of the order of 10 is therefore perhaps the most important of the family of lines. An index of 10 is however established at rather late times -- it is completed for the 90,000 ft level at approximately 23 hours, and its extreme point may be a considerable distance from the origin. Consequently it is in general desirable to make appropriate corrections for time and space changes in the wind structure.

The method devised is based on the same general assumptions as for the static case and is again simple enough to permit the preparation of a plot in a short time. The complication here was that a complete weather analysis of the entire area could not be made every few hours by the limited crew at the Eniwetok Weather Central. Consequently it was necessary to have a forecaster present to make appropriate corrections as the plot developed.

Since in the dynamic case the trajectories of particles of different sizes falling from the same height are no longer similar, the terminal points do not fall along a straight line running out from the origin. The index falls off inversely as the cube of the distance along the line of terminal points instead of along a line of constant bearing.

DOE ARCHIVES

311

ATOMIC ENERGY ACT 1954

316

Figure 2

INDEX NOMOGRAM

FIG 2 RADIAL DISTANCE (nautical miles)

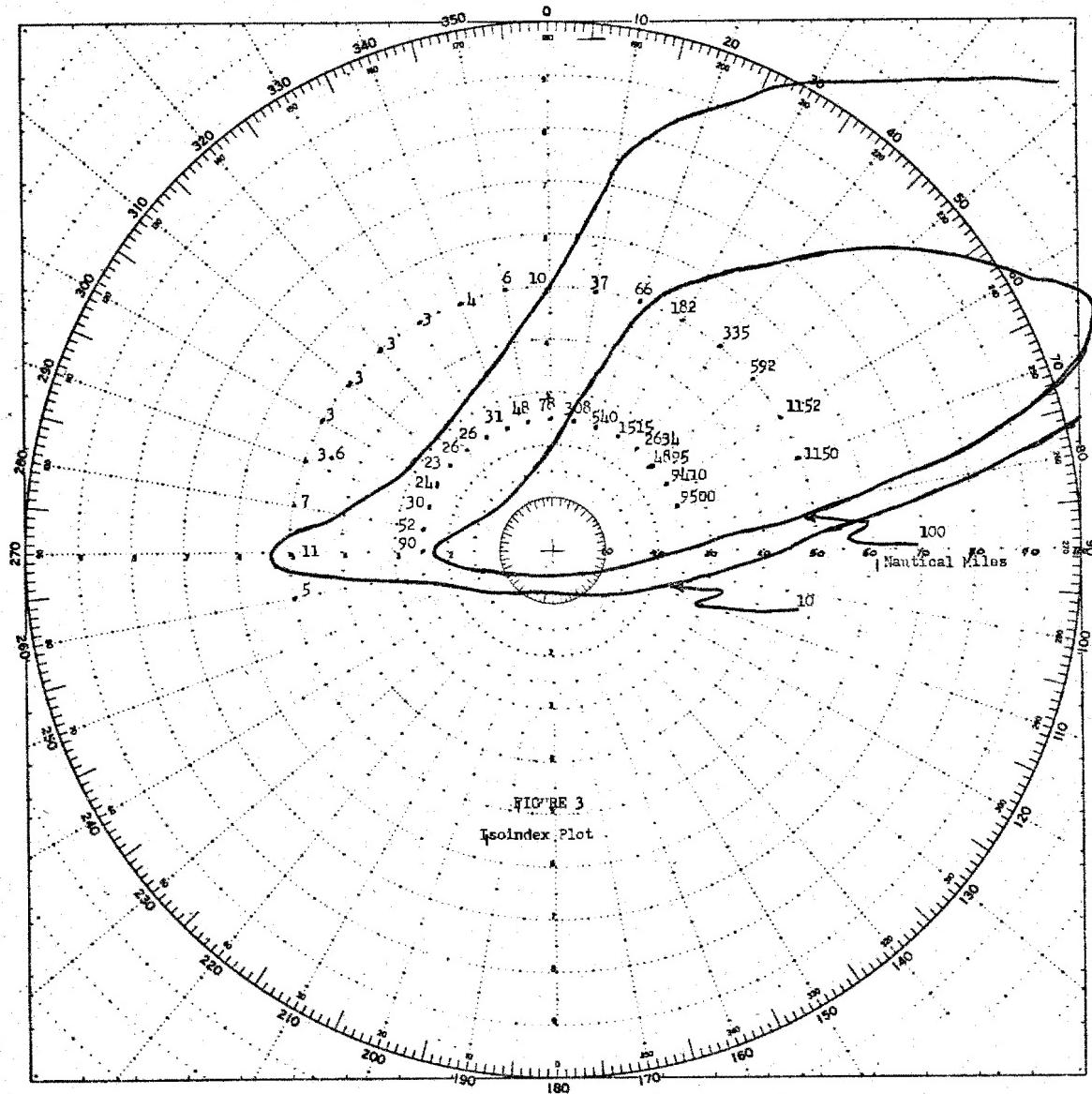


DOE ARCHIVES

312

321

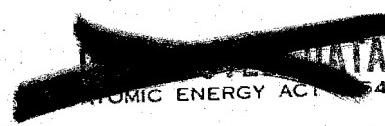
317



**DOE ARCHIVES**

Figure 3  
Isoindex Plot

313



318

It is possible but at present very time-consuming to compute the lines of terminal points for a set of altitudes complete enough for an adequate plot. The best that could be done in the time available was to locate the 10 R point for about a dozen altitudes and base the 10 R line on these points alone. A complication arises when the points fall at different distances on roughly the same angular bearing. This result corresponds to a contribution from two or more altitudes and means that the 10 R line must be drawn some distance beyond the outermost calculated point. The adjustment is easy to make approximately by simple application of the inverse  $R^3$  relation to the inner points to find the contribution at the outermost and a second application of inverse  $R^3$  to the sum. To take into account the height weighting one locates the terminal point and then contracts or expands radially, again by inverse  $R^3$ . These approximate methods are an unhappy feature of the system but are necessary if the plot is to be completed in a reasonable time. We were unable to discover any quick, reliable analytic or graphical method of making these adjustments more precise.

The mechanics of locating the 10 R points (before any adjustments) are straightforward enough. The dose index equation (3) gives the dose in R for 10 megatons. For a predicted yield different from 10 megatons one may write a dose equation

$$I = \frac{W}{10} \cdot \frac{d^2}{t^2} \quad (5)$$

where "I" is the dose in roentgens, "W" is the yields in megatons, and "d" and "t" are defined as before. This equation follows, of course, from assumption (4). The form (5) is not convenient for calculations, since in the construction of a trajectory for a falling particle one is concerned only with the time the particle spends in a stratum characterized by a fixed mean wind. It is convenient then to introduce Stoke's law and to solve equation (5) for the fall rate "v". The result is

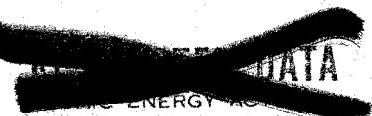
$$v = \sqrt[3]{\frac{10 I K_s h^2}{W}} \quad (5a)$$

DOE ARCHIVES  
(5a)

where "K" is the constant 4000/5625, "h" is the starting height in feet and the unit of "v" is feet per hour. The time spent in a given stratum " $\Delta h$ " is then

$$\Delta t = \frac{\Delta h}{v} \quad (6)$$

Equations (5a) and (6) were used to prepare a worksheet listing the strata, times in the strata, and accumulated times from the start to the strata. Forecast mean winds were then entered on the work sheet as the trajectory plots were made and the times and space



locations became known. In the actual cases computed the changes in wind structure were never very significant and the resulting plots differed little from those made from the static hodograph. The dynamic system does, however, have the capability of handling a rapidly changing situation should it appear.

### Conclusions

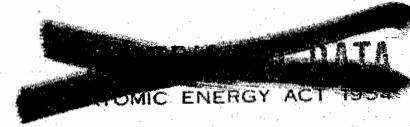
The fall-out forecasting systems described above have a large number of very obvious deficiencies which one would hope to remove by the next operation. For example one would hope to include a good representation of the particle size distribution for both land and water shots. The question whether area or volume of a particle is more significant for the deposition of activity should be investigated. A careful estimate of the height distribution of the activity should be made. Some attention should also be given to the effects of finite lateral cloud dimensions and to the spreading of the cloud. These are points which will refine the system.

Dr. Tom White of LASL began to make such refinements during Castle in an attempt to remove one outstanding defect of this system, its inherent inability to reveal any detail near the origin. His method is described in a separate report.

Two difficulties with the system cannot be removed at all. The case where the hodograph passes directly over the origin is not unlikely and gives embarrassing results, since  $R = 0$  and the dose index vanishes except at the origin. This result is at least circularly symmetric. The other awkward case is that in which one or more elemental wind vectors is radial, since one then has a continuous altitude range contributing to the dose index along a bearing in place of one or two discrete altitudes. This is in reality precisely the kind of wind structure which leads to very intense narrow bands, but the system as set up cannot estimate the magnitude of the dose index along such a bearing. One could perhaps handle this situation by revising the method such that each 5,000-ft altitude interval made a contribution as determined by the mean height of the interval along a bearing line through this mean height. Such a change would introduce difficulties in evaluating the contributions at one point from several heights since the bearing lines through the mean heights would not in general coincide.

DOE ARCHIVES

One difficulty will continue to plague us even with any sort of refined system. At this time it is very difficult to obtain a weather forecast precise enough to justify the effort which must be put into a good fall-out forecast. Because of the inherent uncertainties in



weather forecasting one is tempted to conclude that a refined system of fall-out forecasting will for the time being be most useful for post-shot analysis and that a detailed fall-out forecast based on a normal weather forecast would be misleading. The weather forecasting presently available is of the highest quality but the cumulative errors resulting from small variations about the forecast mean winds can result in a pronounced change in the fall-out pattern. It appears desirable at this time to retain a crude system which is relatively insensitive to small variations in weather structure and which presents conservative upper limits to the fall-out hazard.

DOE ARCHIVES

316

ATOMIC ENERGY

321

## PART II

### A METHOD OF ESTIMATING RADIOACTIVE FALL-OUT

T. N. White  
Los Alamos Scientific Laboratory

The method described herein is designed with an objective that is intermediate between operational requirements, and the requirements of a strictly scientific investigation. It is designed to include what are assumed to be the most important factors that determine a fall-out pattern, with the idea that we might find out enough about what is going on to produce a good simplified method for operational use. One simplified version that was used for local fall-out forecasting is described in Close-in Forecasting by New Techniques Developed after BRAVO, Tab D "Fall-out Forecasting Techniques" of the Task Force Castle Report. It seemed good enough to justify further investigation of the basic ideas as applicable to any range of distances over which a constant wind field could be assumed.

The basic assumptions of the method are as follows:

The whole cloud, up to its height of stabilization, is formed instantaneously at the time of detonation. This is what we call the "initial cloud".

In any height layer of the initial cloud, the concentration (radioactivity per unit volume) is distributed according to the Gaussian Law

$$c(h,r,a_0) = c_0(h) \exp(-r^2/a_0^2)$$

DOE ARCHIVES

where  $c(h)$  is the central concentration at height  $h$ ,  $r$  is the radial horizontal distance, and  $a_0$  is a "spread parameter" (analogous to standard deviation) that is also considered to be a function of height. From this assumption it follows that the total amount of radioactivity in a slice of unit vertical thickness is  $\pi c_0(h) a_0^2$ .

Throughout all of any such layer, the radioactivity is distributed normally with respect to the logarithm of the rate of fall of the particles. Thus at any distance  $r$ , the fraction of radioactivity that falls with speeds in the range  $f$  to  $f + df$  is given by

$$\frac{1}{\sigma(h) \sqrt{2\pi}} \exp \left\{ -\frac{1}{2} \left[ \ln \left[ \frac{f}{f(h)} \right] \right]^2 \right\} \frac{df}{f}$$

where  $f(h)$  is the fall-rate for particles of greatest radioactivity, and  $\sigma$  (also considered to be a function of height) is the standard deviation of the logarithm of fall-rates, weighted according to radioactivity;  $f(h)$  and  $\sigma(h)$  are constant throughout the layer.

The rate of fall of any particle remains constant until it reaches the ground.

Any particle that starts from the central axis will follow a path strictly in accordance with the wind pattern, while all other particles that fall at the same rate from the same level will diffuse laterally from the central particle in such a way that the gaussian distribution is maintained.

During this process, the increase in the spread parameter is described by

$$\frac{a}{a_0} = \left[ 1 + \frac{s}{\beta a_0} \right]^{\frac{m}{2}} = p^{\frac{m}{2}}$$

where  $S$  is the distance travelled by the central particle until it reaches the ground. (It is to be noted that  $S$  is not the straight-line distance from the origin to the landing point unless all winds at all levels are in the same direction.  $\beta$  and  $m$  are parametric quantities that may be used to describe the amount of diffusion. They are not at present regarded as functions of height. (The quantity  $p$  is merely an abbreviation for the quantity in brackets)).

From these assumptions it follows that the dose rate on the ground is

$$I = \frac{K}{\sqrt{2\pi}} \int_0^H \int_0^\infty \frac{c_0(h)}{\sigma(h)p^m} \exp - \left[ \left( \frac{\ln \left[ \frac{f}{f_h} \right]}{\sigma(h)\sqrt{2}} \right)^2 + \frac{r^2}{a^2 p^m} \right] dh \frac{df}{f}$$

where  $K$  is dose rate per unit of surface concentration,  $H$  is the height of the top of the cloud, and  $r$  is now the distance from the point at which the dose rate is estimated to each of the landing points of central particles. These landing points will depend on the wind pattern below the level from which the central particle originated, so that  $r$  is a function of  $h$ . The landing points also depend on the rate of fall, so that  $r$  is also a function of  $f$ . Changing from rate of fall to time of fall, one obtains

$$r^2 = [t \bar{u}(h) - X]^2 + [t \bar{v}(h) - Y]^2$$

DOE ARCHIVES

where  $(X, Y)$  are the rectangular coordinates of the point where dose

rate is estimated, and  $\bar{u}$ ,  $\bar{v}$  are the wind components in the same coordinate system, averaged up to the height  $h$ .

We may also express

$$p = 1 + \frac{tw(h)}{\beta a_0(h)}$$

noting that  $\bar{w}$  is the average speed regardless of direction. ( $\bar{u}$  and  $\bar{v}$  are not, in general, the components of  $\bar{w}$ ). This expression is correct if one is satisfied that the diffusion depends on the total horizontal distance travelled by a central particle. If one wishes to assume that the vertical distance should be included,  $p$  becomes much more complicated.

The significance of  $\beta$  and  $m$  can now be visualized. If  $m = 2$ , then

$$\frac{a}{a_0} = \beta a_0 + tw$$

so that the lateral dimensions of any segment of the cloud will increase as if the segment had come from a point source located at a distance  $\beta a_0$  upwind. The size increases linearly with distance travelled by the central particle. If  $m$  is greater than 2, the borders of the cloud will diverge more rapidly, and if  $m$  is less than 2 they will diverge less rapidly. One can prevent any increase in size either by making  $\beta$  infinite or by making  $m$  equal to zero. This method of describing the diffusive process is similar to that of Sutton, but not exactly the same.

If  $m = 2$ , then at sufficiently large values of  $t$ , the area covered by a segment of cloud is proportional to the square of the time, as in Felt's method. However, the proportionality factor varies, as  $\bar{w}$  varies with height, and further, the overall average proportionality factor changes with the overall strength of the wind field, and in these respects it differs from Felt's method.

Returning to the basic equation, the change of variable from  $f$  to  $t$  changes the argument of the logarithm to

$$\frac{t f(h)}{h}$$

DOE ARCHIVES

and  $\frac{df}{f}$  becomes  $\frac{dt}{t}$

One notes also that concentrations in the initial cloud must be



reduced to those that would have existed at that time for which the dose rate is being estimated.

The information that is needed for a calculation is then:

The winds pattern at heights up to  $H$ .

$H$ , the height of the top of the cloud.

$a_0$ , the initial spread parameter, or radiological radius, as a function of height.

$c_0$ , the central concentration as a function of height in the initial cloud, adjusted to the time of dose-rate estimation.

$f$ , the logarithmic mean rate fall (weighted according to radioactivity), as a function of height in the initial cloud.

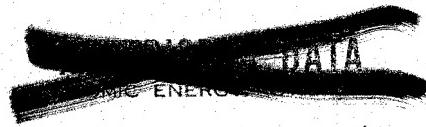
$\sigma$ , the logarithmic standard deviation of this distribution as a function of height in the initial cloud.

$\beta$ , diffusion parameter, described above.

$m$ , diffusion parameter, described above.

Testing of the method requires the use of high speed computing machinery. With such machinery one can make many changes in the quantities described above, proceeding on a trial and error basis. In order to achieve some degree of objectivity, the following approach is adopted.

The logarithm of the ratio of calculated to observed dose rate is estimated at a number of points for a given shot. This quantity is called  $\gamma$  (gamma). Then the mean gamma, and the statistical variance of the individual gamma about the mean gamma, are calculated. This process is repeated for a number of values of some parametric quantity, beta for example. One then plots the variance against beta, and selects as the best value the one that gives the least variance. One then moves on to other parametric quantities, and treats them in the same way, hoping that there is not too much correlation between the effects of the different types of parameters. It will be noted that this application of the "least squares" method discounts the overall ratio of calculation to observation. In principle it is possible to get zero variance (an exact fit) when each calculated value is, for example, exactly ten times the observed value. One would then suspect that 90% of the radioactivity had remained in the crater. If, however, one should obtain a good fit but with only 10% of the observed activity accounted for, one would have to consider other possibilities. One would first look to see whether any large fraction of the activity was excluded from the calculation. In numerical integration it is not practical to go all the way from zero to infinite time, and part of the activity might have fallen outside of the time range chosen. If this explanation fails, and if the fit is really good, one has to conclude



that the least squares criterion, as applied here, is not useful. We have not yet encountered this particular obstacle.

The method of approach is subject to a hackneyed old criticism running as follows: by subdividing the height of the cloud at will, you can obtain as many discrete parametric values of  $a_0$ ,  $c_0$ ,  $f$ , etc. as you wish, so that you should be able to fit any number of observations exactly. This is true, in principle. But if one can get a set of values that look reasonable, and can be scaled in a reasonable way with yield over a wide range, the method can serve a useful operational purpose even though the values might be scientifically unsound.

For machine integration, using the IBM Model 701 "Defense Calculator", those parametric quantities ( $a$ ,  $c$ ,  $\sigma$  and  $f$ ) and the mean wind components ( $\bar{u}$ ,  $\bar{v}$ ,  $\bar{w}$ ), which are functions of height, may be loaded as tables of data. The total height of the initial cloud,  $H$ , is subdivided into  $M$  equal layers, each identified by an integer  $i = 0, 1, 2, \dots (m-1)$ . The time variable is laid on a logarithmic scale, each time being identified by an integer  $j = 1, 2, 3, \dots N$ . Storage limits the maximum value of  $M$  to 32.  $N$  may be any value that doesn't take too much machine time, and the minimum and maximum limits of the time integration may be changed at will. The exponential factor in the formula is recorded as zero if the absolute value of the exponent exceeds a value  $A$  which may be as large as 10.

The coding is so arranged that the time integration is performed first and the height integration second. At each location, the fraction of the dose rate that comes from each initial cloud layer is computed and may be printed along with the calculated and observed dose rates and the co-ordinates of the location. Or one may by-pass this printing and obtain only the statistics: mean gamma and variance for a preselected series of locations.

The codes are not yet frozen, and additional features are being added from time to time. We have two codes (1) a fast "fixed-point" code as outlined above, and (2) a slower "floating-point" code that is more precise and which is more flexible in some respects.

Since starting on this problem about seven months ago, a considerable part of the time has been spent on coding and de-bugging, which we undertook ourselves in order to learn how to use the Model 701. Using Bravo fall-out data, we demonstrated that least squares solutions could be obtained for the various parametric quantities involved. However, the "best" values, as selected in this way, gave distant fall-out predictions that were only 20 to 30% of the observed values, and the

DOE ARCHIVES

"fit" was not good. We then turned attention to Nevada data for a while, and became interested in an approximation that seemed to offer a hope of eliminating one of the two steps in the double integration. Before this possibility had been fully explored, Mr. Vay Shelton, Livermore Operations Division, joined forces with us, and we worked together for a week on UK-1 and UK-7. Mr. Shelton then took our codes to Livermore and continued working on the Nevada data, while we turned attention again to the Bravo shot. Mr. Shelton has reported recently that the method gives satisfactory results for UK-1 and UK-7, and he is continuing work on other shots. We have concentrated on the problem of predicting the Bravo fall-out on the assumption that practically all of the activity in the initial cloud was located above the tropopause. To date, our method of calculation has not been able to give satisfactory results, even when the winds were arbitrarily twisted to make the fall-out occur in more nearly the right place. At this point we feel, therefore, that we do not have any cloud model in which we have confidence. We have merely a mechanism of calculation, the value of which has not yet been proven as far as Bravo is concerned.

Lacking any satisfactory cloud model for Bravo, we tackled the "homework" predictions on a guess-work basis, which does not justify a description. The values that we used in the calculations are:

	<u>1 MT</u>	<u>50 MT</u>
Height of cloud (sea miles)	11.5	19.0
Height of stem (sea miles)	7.0	7.0
a for mushroom (sea miles)	0.94	4.58
for stem (sea miles)	0.41	1.49

Beta: 9.15

m: 1.0

Sigma: 1.0

DOE ARCHIVES

The values of c were taken as constant up to the tropopause, and thereafter decreased with air density. (The machine program requires only the entry of relative values, from which the actual values are adjusted so that the total radioactive content of the cloud is in accordance with the yield). Logarithmic mean rates of fall were assigned to the 16 layers of the cloud as follows, counting from the bottom. (Rates are in knots)

Layers 1 thru 4	20
Layers 5 thru 8	7.4
Layers 9 thru 12	2.7
Layers 13 thru 16	1

322



321

327

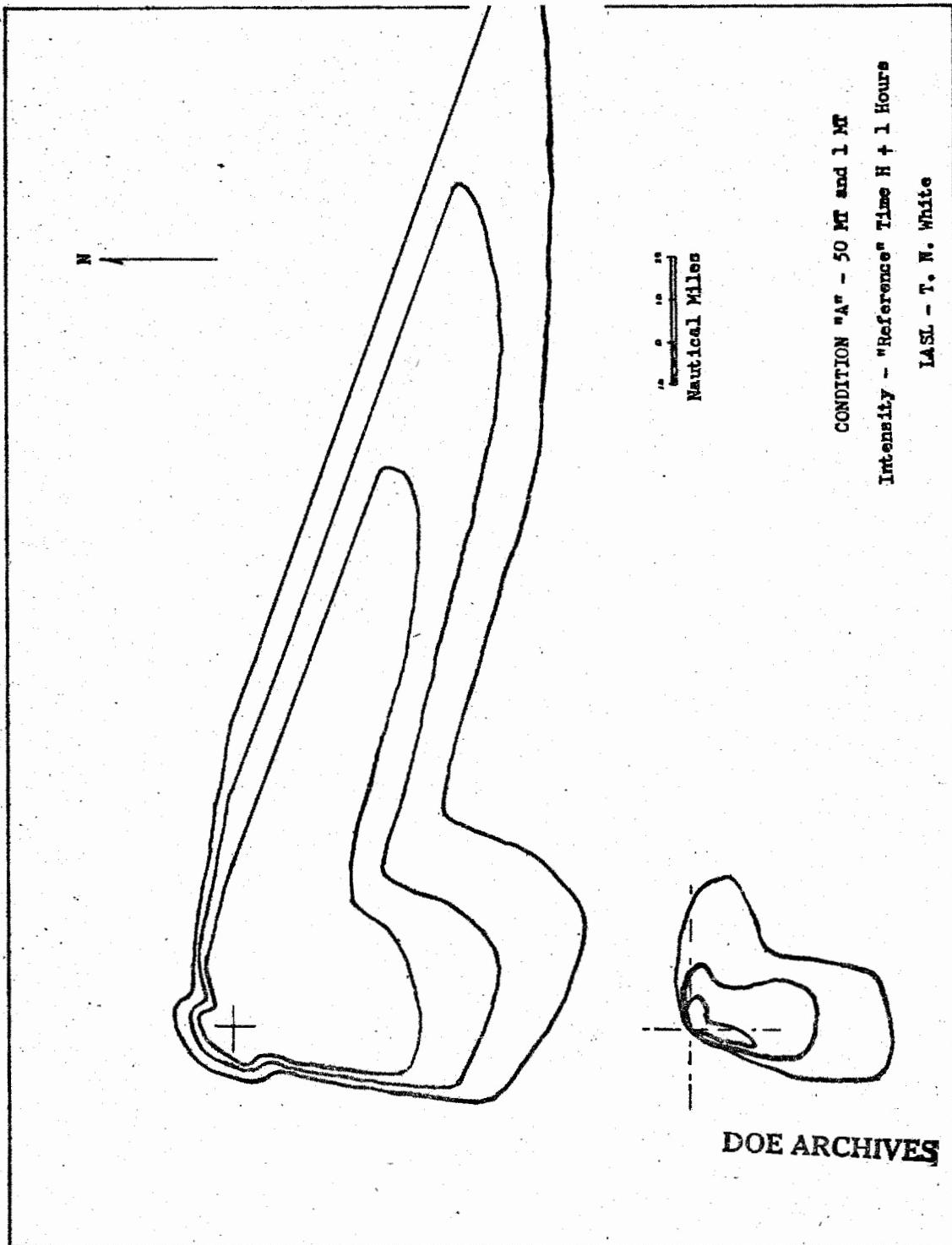
(Editor's note: The four contour figures which follow were received too late for inclusion in the comparison done by Cdr. Paine. The contours shown in that comparison for LASL were submitted prior to the symposium; and, being scaled by simple yield dependence, did not include allowance for different cloud dimensions as those presented here do.)

DOE ARCHIVES

323

ATOMIC ENERGY ACT IS

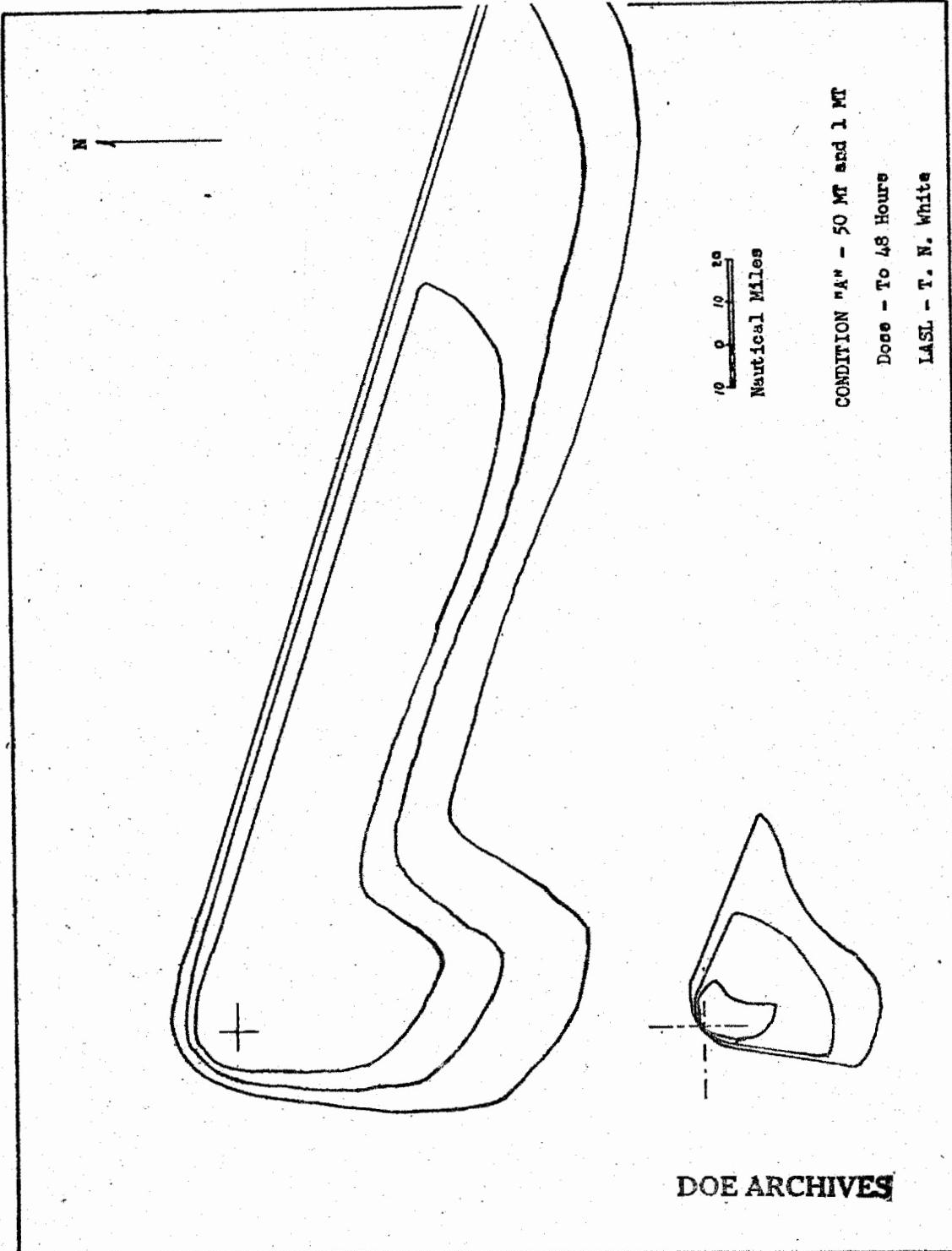
328



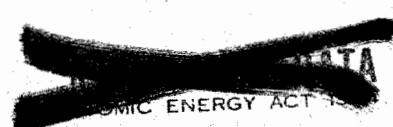
324



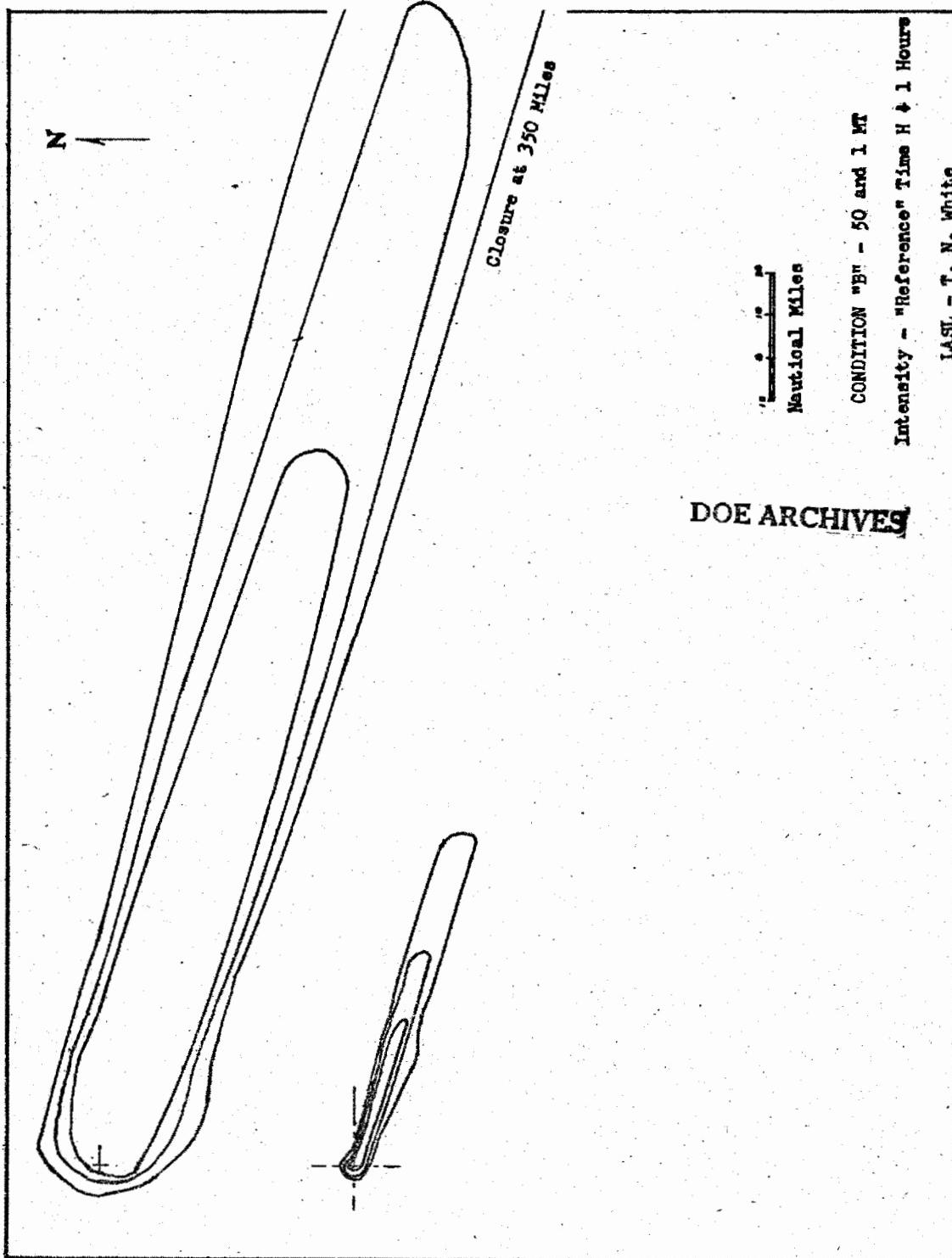
329



325



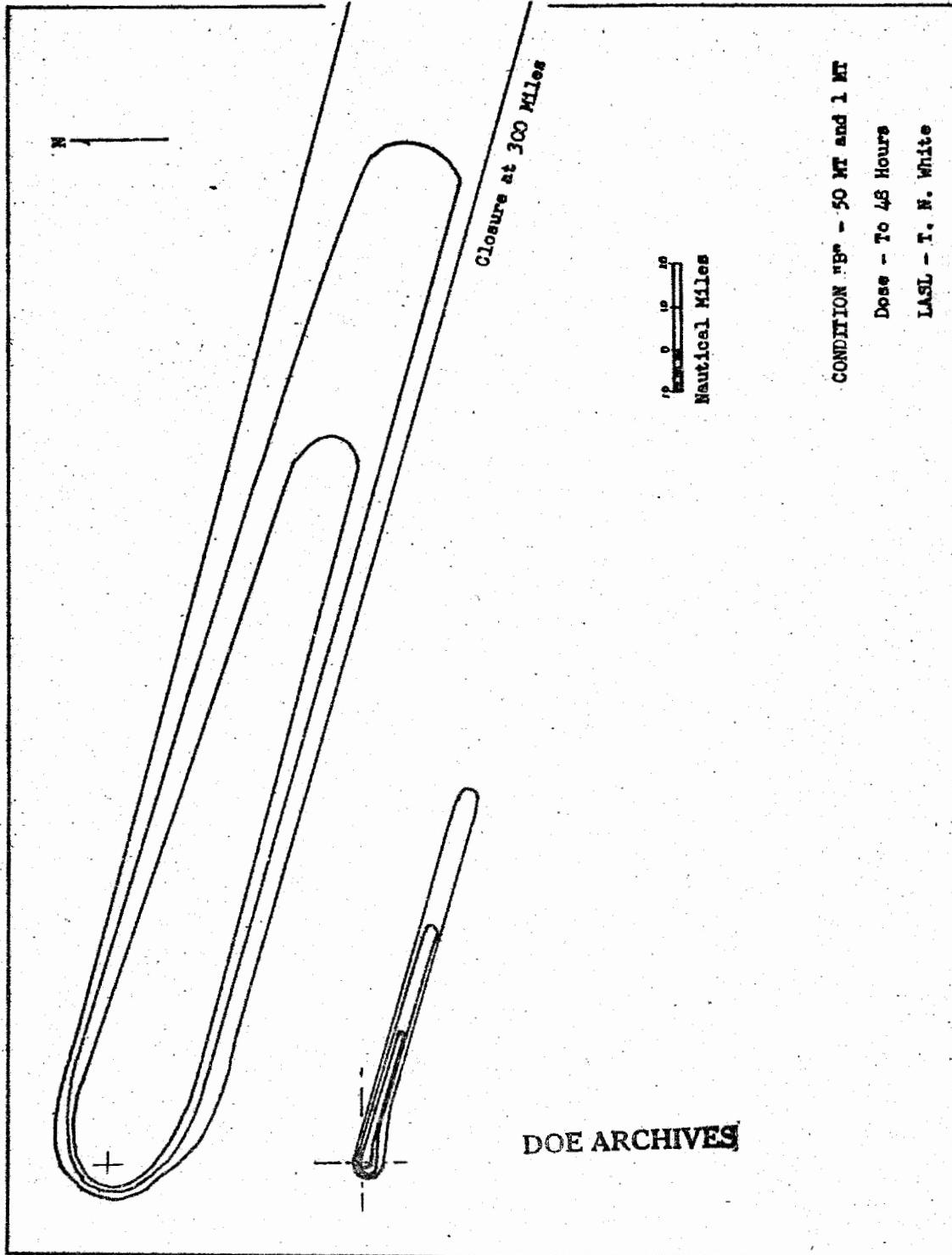
330



326

ATOMIC ENERGY ACT 1954

331



CONDITION "B" - 50 MT AND 1 MT

Dose - To 48 Hours

LAST - T. W. White

327

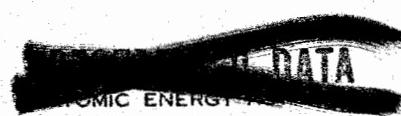


332

**THIS PAGE IS BLANK**

**DOE ARCHIVES**

**328**



**333**

PREDICTION OF DOSE-RATE AND DOSAGE CONTOURS AS FUNCTIONS  
OF YIELD AND METEOROLOGICAL CONDITIONS, RAND METHOD

PART I

Dr. R. R. Rapp  
Rand Corporation

The Formation of the Atomic Cloud

Dr. Kellogg has already presented the physical picture of the atomic cloud upon which the Rand model is posed. There are, however, a few points to stress. First, as shown by the first sketch in Figure 1, there are large amounts of earth taken into the fireball in the very early stages of formation. Next, as is indicated in the other sketches of Figure 1, a large amount of earth is carried aloft with the fission products by the extremely stable toroidal circulation. This toroidal circulation is caused by the intense thermal gradients of the fireball. Thus, large quantities of vaporized, liquified, and pulverized earth are in intimate contact with the newly formed fission products from a few milliseconds to a few minutes after detonation. By way of contrast, it is believed that the earth, which is seen to enter the fireball of an air burst, flows up through the "hole in the doughnut," circles around, and falls to the earth without actually encountering the radioactive material. For the surface burst, where there are large particles, after the cloud stops rising, there will be radioactivity present on particle sizes ranging from thousands of microns to about a very few microns spread through a region of the atmosphere. For a large yield burst, this region may look something like Figure 2. At this point, it is not necessary to quibble about the details of the configuration or the activity distribution with space and particle size, but simply to say that for a given bomb, there exists a space and particle size distribution of the activity produced. It is interesting to note, however, that on the basis of currently available data, there is marked disagreement on the distribution of activity in space. In the Rand model, as will be pointed out later, the size of the active cloud is smaller than the photographic observations of the CASTLE-Bravo cloud would indicate. Thus, although the figure indicates an active particle falling from the edge of the cloud, this is schematic and has no significance in the Rand model.

DOE ARCHIVES

The thermal and kinetic energy which produced the cloud and caused it to rise through the atmosphere has, by the time of stabilization, been dissipated and the particles will begin to fall under the force of gravity. If particles in the size range from 100 to 1000  $\mu$  are considered, it becomes necessary to consider the aerodynamics of the particle. No matter what value is used for a drag coefficient, the density of the air must enter the equations and the particle will fall more rapidly in the less dense atmosphere at high levels.

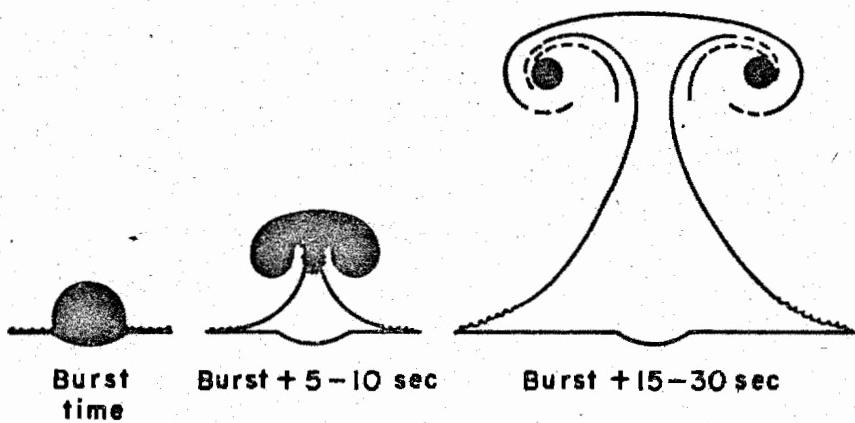
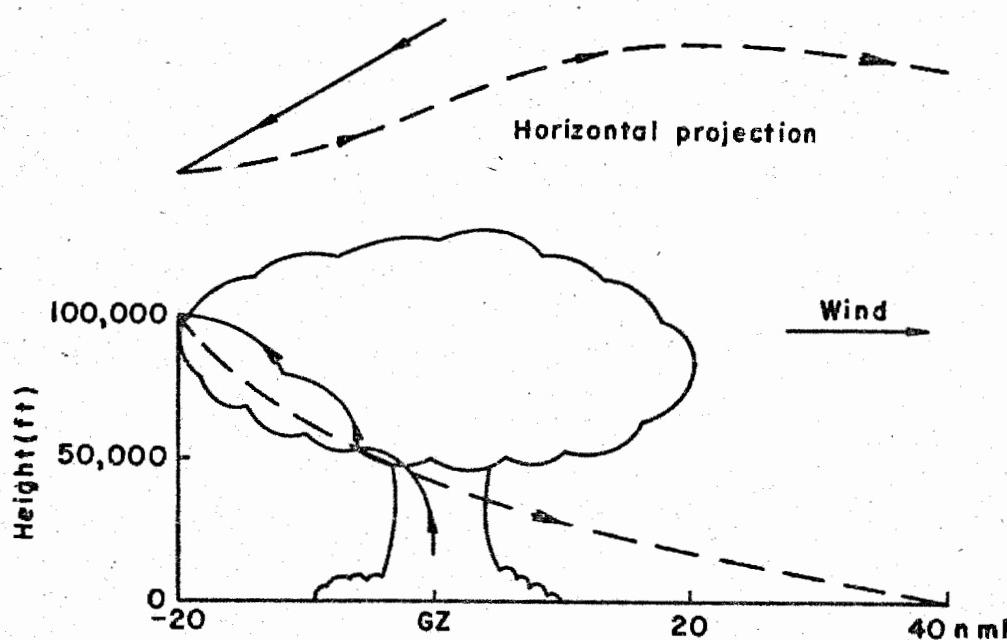


**Figure 1**  
Surface Burst - Schematic Representation of the Manner in which Earth is mixed with Fission Products and carried to great Altitudes



**DOE ARCHIVES**  
**Figure 2**  
Path of a Particle - Schematic showing the Stabilized Cloud and the Idealized Path of One Particle

330

Figure 3 shows some possible assumptions about the fall velocities of the radioactive particles. The Rand curves are based on the aero-dynamic fall of spherical particles as set forth in an article by Langmuir, whereas the NRDL curves are based on the formulae of Dalla Valla. The line labeled Stokes' Law is included mainly to show that it does not give the proper velocity variation with height and that it over-estimates the velocities of all except the very smallest particles. The variation of velocity with height is extremely important when computing the distance a particle will travel, since the more rapid fall through the upper layers means that the particle will spend a relatively shorter time in the upper wind flow than it will in the dense air near the surface. Referring back to Figure 2, it may be noted that the vertical section shows the particle falling faster in the high levels than it does in the low levels. The horizontal section of Figure 2 shows the erratic path a particle may take due to the action of the wind. It should be noted that the term wind implies all the components, scales and variations of the air movement. It may be informative to look at some of the wind factors which must be considered.

The picture of the motions of the atmosphere that one gets is very much a function of the sensitivity and spacing of the measuring instruments. The established weather networks, in which the instruments are spaced at large intervals, indicate a rather smooth flow of air with perturbations from the mean motion which are the size of cyclones and anticyclones. These perturbations change with time so that time and space variations must always be considered. For example, a steady change of a velocity component of 2 knots per hour could make a position error of 24 miles in 12 hours. If more sensitive instruments are used at a closer spacing, it is found that there are smaller perturbations imposed on the larger ones. There have been relatively few experiments with close networks, but the experiments which have been made show that perturbations may be found on almost any scale of measurements. The total motion of the atmosphere can, therefore, be represented by a spectrum of motions on different scales. Such a representation provides a useful mechanism for separating the motions into those which can be readily measured and those which must, for lack of observation, be treated statistically.

**DOE ARCHIVES**

An important feature of the spectrum of motions in the atmosphere is its variability in time and space. Large gaps in the spectrum apparently appear and disappear as the characteristics of a mass of air change with time because of mechanical and thermal effects. Sketch A, Figure 4, shows the effect of the large scale motions which move the cloud bodily. Sketch B shows the effect of motions on a scale comparable to the cloud dimensions. These motions tend to distort the cloud from its original shape and may cause an error up to 20 percent in the computed position of a particle on the ground. Sketch C indicates that motions on a scale, small compared with the horizontal cloud dimensions, tend to spread the cloud by drawing.

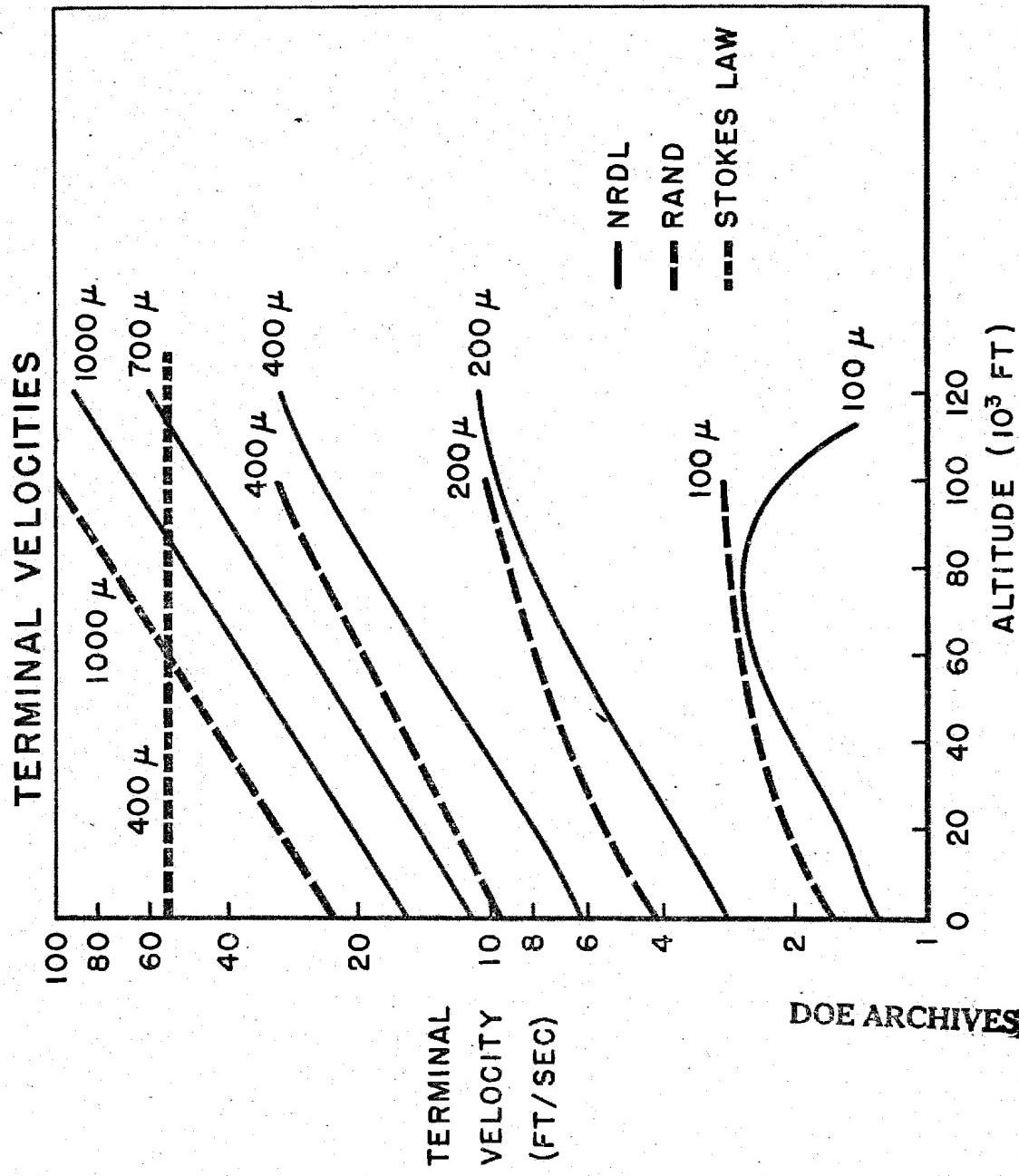
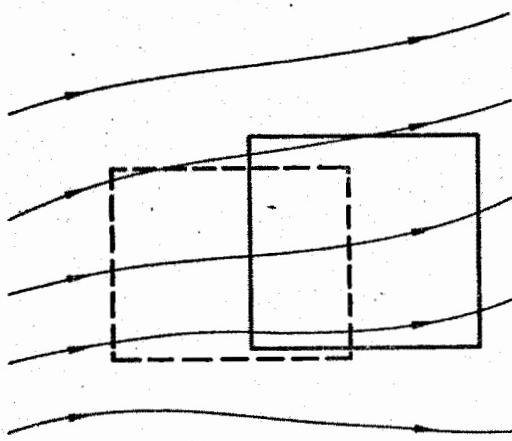
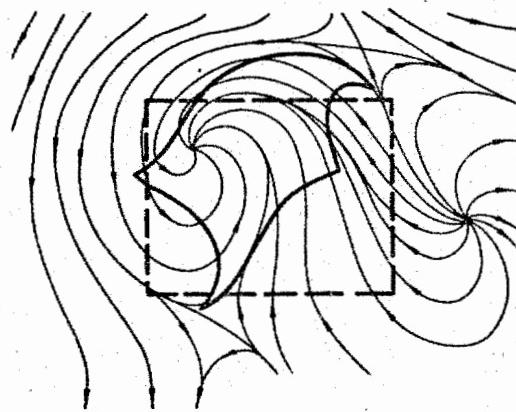


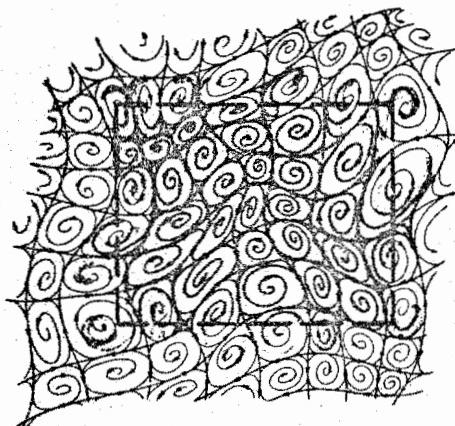
Figure 3  
Comparison of the Fall Velocities under Several Assumptions  
as a Function of Height



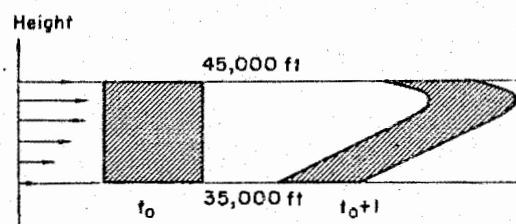
(A) Gross movement—atmospheric motions of a scale large compared with cloud dimensions



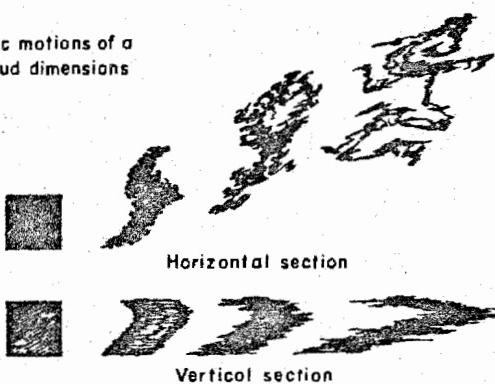
(B) Horizontal deformation—atmospheric motions of a scale comparable to cloud dimension



(C) Eddy diffusion—atmospheric motions of a scale small compared with cloud dimensions



(D) Vertical deformation—shear of horizontal wind in the vertical

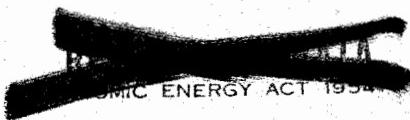


(E) Total effect of gross movement, deformation, and eddy diffusion

**DOE ARCHIVES**

Figure 4  
Schematic Diagram showing Effect of Different Sized Eddies  
on a Cloud of Material

333



338

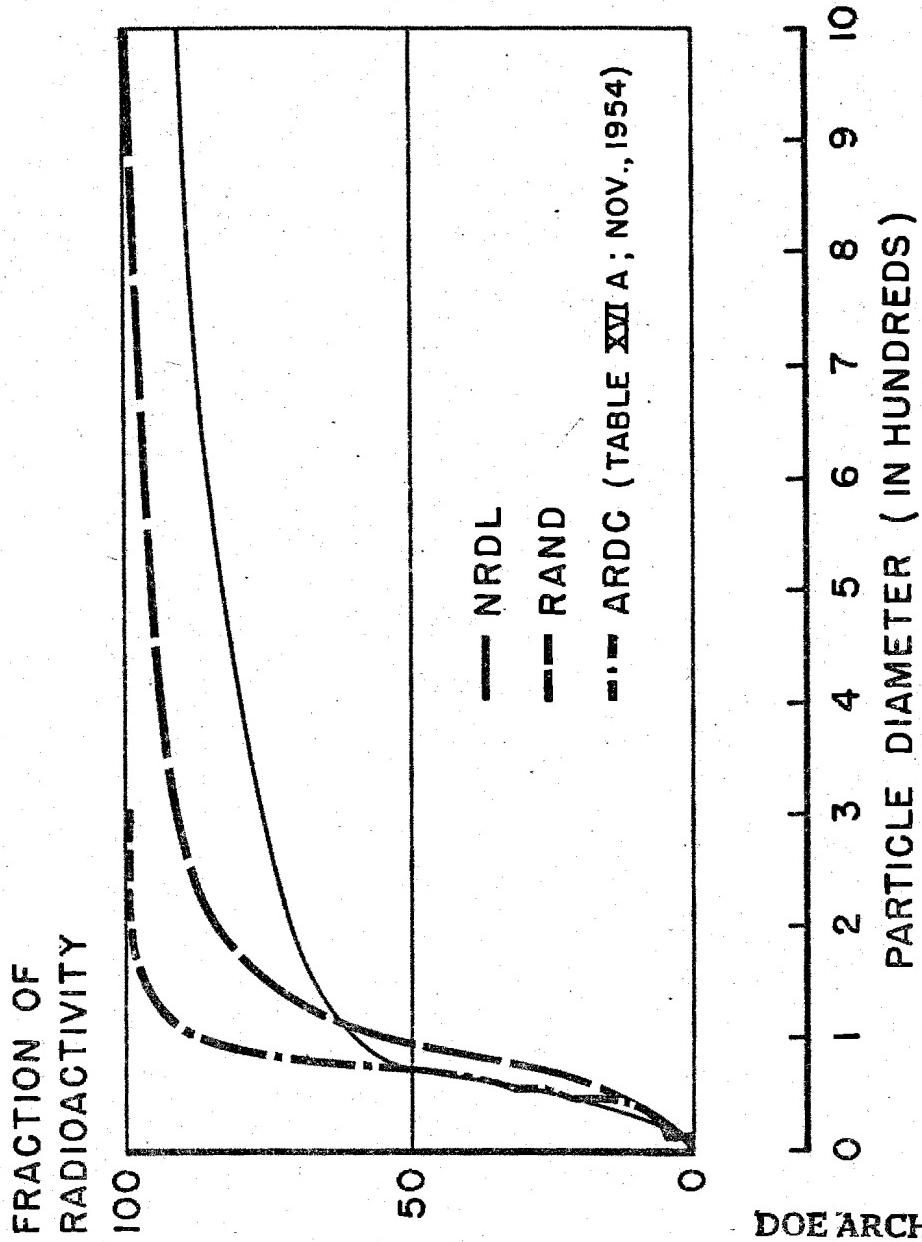
out small wisps of cloud matter from the edges and carrying clear air into the cloud; this type of phenomena is called eddy diffusion. Eddy diffusion spreads the cloud very slowly and may be neglected for short periods. Sketch D shows how the change of wind with elevation tends to shear the cloud into a long ribbon. The last sketch, E, is a schematic view of the integrated effects of these various motions on the cloud.

The breakdown of the atmospheric motion into different scales is, of course, highly artificial. Such a breakdown is dictated by the available measurements and by our ability to analyze them. The gross movement and the gross deformation in the vertical can be conveniently, if not accurately, handled by recourse to actual weather observations. The horizontal deformation and the eddy diffusion are, however, on much too small a scale to be observed by our present network of stations. With such a small scale of motion, it is necessary to resort to some type of eddy diffusion theory or to rely solely upon empirical evidence gathered from the tests that have been made. Since neither the empirical evidence nor the eddy diffusion theories show much spread, diffusion has been neglected.

A bit earlier, the distribution of activity with particle size was mentioned. There are two methods for arriving at such a distribution. One is to measure a large sample of collected particles, as is done by NRDL, and the other is to choose, by trial and error, a distribution which fits an observed case. At Rand, the latter method was applied to JANGLE S to derive a distribution. ARDC uses basically the same technique, but with different assumptions. Figure 5 shows a comparison of Rand, NRDL and ARDC distributions. The studies made by the Weather Bureau Group on reconstructing activity distribution with size and height for tower shots had found still another distribution. It is quite possible that there are changes in the distribution from shot to shot. Thus, in order to compute fall-out, it is necessary to know the space distribution of debris, which is known only by inference; the distribution of activity with particle size, for which no general law is known; the fall velocity of the active particles, which has not as yet been determined experimentally; and the wind in all its particulars, a requirement which is economically unfeasible. It is obvious that with the uncertainties inherent in the data now available, it would be unreasonable to expect any model to reproduce the observed fall-out with a great deal of accuracy. It might be possible to compute within five to ten percent of the relatively close observation where the heavy particles spend the least time in the wind field. For more distant observations, it may be possible to be within a factor of two for the highly significant observations, but on the fringes of an area, fall-out may be computed where none was observed and vice versa due to the unknown factors of the wind variation.

DOE ARCHIVES

# FRACTION OF RADIOACTIVITY ON PARTICLE SIZES SMALLER THAN THAT GIVEN ON THE ABSCISSA



DOE ARCHIVES

335

DATA  
NUCLEAR ENERGY ACT

340

Figure 5  
The Distribution of Gross Fission Activity with Particle  
Size According to RAND, NRDL, and ARDC

### The Model

With all this uncertainty, it is still necessary to fix on some of the physical parameters in order to make computations. Therefore, a model appropriate to CASTLE-Bravo will be presented (see Figure 6). The assumptions used at Rand are, first, the distribution of activity with particle size deduced from the JANGLE surface shot data. We are currently of the opinion that the high temperature and large volumes of soil produce the characteristics of the activity distribution, but at present we have little to offer in support of our thesis. Our computations were based on early measurements of cloud diameters and heights, and have not been modified because the smaller sizes seem to fit the observation adequately. Our early model assumed homogeneous distribution of the material in the cloud and stem. We also assumed that the cloud and stem were cylinders. Recently, we have modified our concepts and adopted an exponential decrease in the activity within the cloud.

The assumption on the fall velocities is that the particles fall as though they were spheres.

For the winds, we have used two assumptions, both quite simple. First, we assumed that the winds at shot time apply to the entire descent of the particles. As the next more complex assumption, we have assumed that the time variation of the wind was more important than the space variation. These assumptions are shown for the Bravo shot in Figure 7.

We have neglected the effects of medium scale motions and turbulence simply because there is no simple way of including these effects. They would tend to spread the cloud, but they would not spread it in a uniform way. Thus, if a spread parameter were included and an even spread of the material were assumed, it would tend to cover a large area, but would smooth out the value of the hot spots. Without a spread parameter, the concentration of material is about right, but the clumps are not distributed over the proper area. Since we do not believe that we can place the debris accurately, we have decided to accept the position error and hope to keep the proper concentrations.

### The Synthesis

DOE ARCHIVES

Having outlined the physical parameters of the Rand model, it is now necessary to go on to a method of computation. The machine method will be discussed later. This paper will be confined to the hand computational scheme.

Consider a section of the cylindrical cloud extending from  $h$  to  $h + dh$  containing particles of a size range  $r$  to  $r + dr$ . Let  $a_1(r, h)$  be the activity contained on these particles in this height interval over

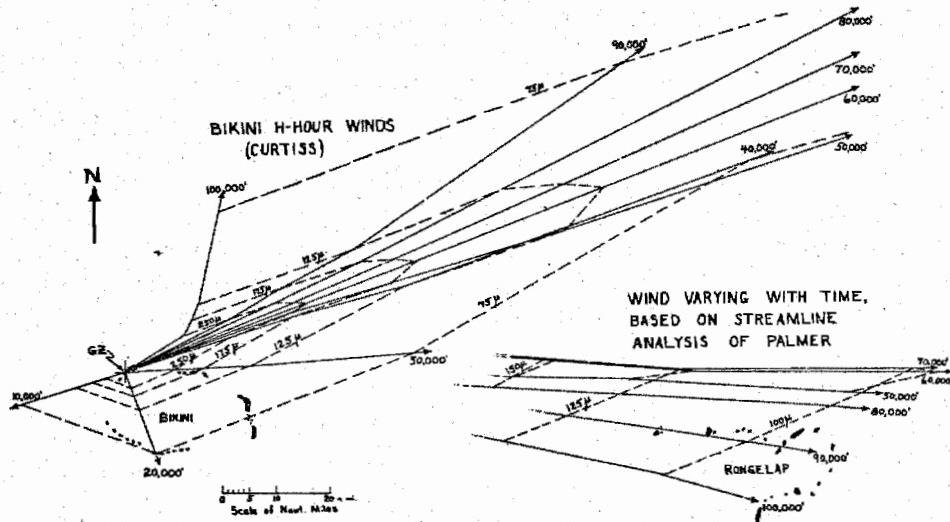
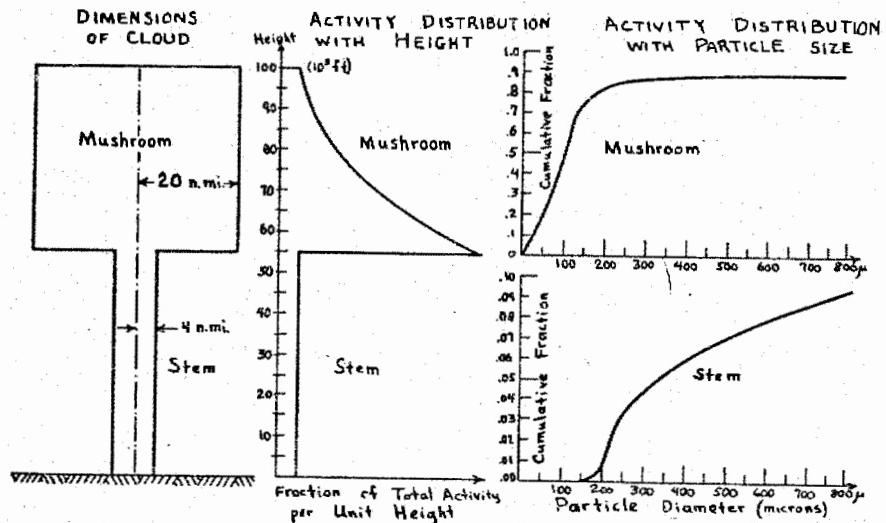


**Figure 6**  
A schematic of the RAND Model showing the Spatial Dimensions of the Cloud, the Relative Distribution of Activity with Height, and the Distribution of Activity with Particle Size

### MODEL FOR CASTLE "BRAVO"



**DOE ARCHIVES**  
**Figure 7**  
A Plot of the Position on the Ground of Particles of Size  $r$ , from Heights  $h$  for the CASTLE-Bravo Event. The Main Plot is Following the H Hour Winds. The added Sector Shows Time Variant Winds according to the Oahu Research Center Report.

~~SECRET~~

a unit horizontal area of the cylindrical section. When all of these particles fall to the ground, the surface concentration will be simply

$$\sigma(r,h) = a_1(r,h)$$

Now it is necessary to determine  $a_1(r,h)$  in the light of the assumptions of the model. First, it is assumed that, within the mushroom, the distributions in the height and particle size are independent. That is,

$$a_1(r,h) = K A(r) G(h) dr dh$$

Where  $K$  is the total activity per unit horizontal area of the cloud and  $A$  and  $G$  are distribution functions. Next, it is assumed that  $A(r)$  is the JANGLE distribution. This  $A(r)$  is now a density function and is the derivative of the curve, presented as the Rand curve in Figure 5. For  $G(h)$ , it has been assumed that the distribution of particles follows the density distribution of air so that  $G(h) = G_0 e^{-a(H - H_B)}$  where  $H$  is the height of a point in the mushroom and  $H_B$  is the height of the base of the mushroom.

Thus for the small cylindrical section

$$\sigma(r,h) = a_1(r,h) = K A(r) G_0 e^{-a(H - H_B)} dr dh$$

This is the surface density of activity for a point on the ground due to the particles of size  $r$  to  $r + dr$  from the height  $h$  to  $h + dh$ .

It is possible to find the coordinates of this point on the ground as follows: If  $v_x(h)$  and  $v_y(h)$  represent velocity components, then

$$dx = v_x(h) dt \quad \text{and} \quad dy = v_y(h) dt$$

But  $W(r,h) = \frac{dh}{dt}$  thus  $dt = \frac{dh}{W(r,h)}$  where  $W(r,h)$  is the vertical velocity. These are derived for all  $(r,h)$  from the aerodynamic fall of spheres, a sample of the variation was shown in Figure 3. Now

$$D_x = \int_h^0 \frac{v_x(h)}{W(r,h)} dh \quad D_y = \int_h^0 \frac{v_y(h)}{W(r,h)} dh \quad \text{DOE ARCHIVES}$$

$D_x$  and  $D_y$  are distances traveled by a particle of radius  $r$ , from a height  $h$ . The actual position of a particle will depend on its initial position in the cloud. If the origin is placed at GZ and  $(x_1, y_1)$  is the initial displacement from GZ,

$$x = x_i + D_x$$

$$y = y_i + D_y$$

$$\approx x_i + \sum_{J=1}^K \frac{v_x(h)}{W(r,h)} \Delta h$$

For any given point, say  $(x_0, y_0)$ , there will be many sets of  $r, h$  values which can reach the spot. If a grid is made of the  $x, y$  positions from the center of the cloud for a large number of  $r, h$  values, any  $r, h$  value from the center of a cloud which lies within a cloud radius will contribute to the activity at the point  $(x_0, y_0)$ , since the spread of the cloud has been neglected.

Since  $\sigma(r, h)$  is the surface density of activity due to one particle size from one height, the total density at  $x_0, y_0$  will be

$$\sigma_T = K \int_{r_1}^{r_2} \int_{h_1}^{h_2} A(r) dr G(h) dh$$

DOE ARCHIVES

If  $R_i = \int_0^{r_2} A(r) dr$

And  $H_i = \int_{H_B}^H G(h) dh$

Then  $\sigma_T = K \int_{r_1}^{r_2} \int_{h_1}^{h_2} dR_i dH_i$

Thus  $\sigma_T$  is equal to a constant, depending on the size of the cloud and the total activity in the mushroom, times the integral which is an area on an  $R_i, H_i$  plot.

In order to compute the activity at a point, assuming all the activity has fallen out, the  $(x, y)$  positions of a set of  $(r, h)$  pairs starting over GZ are mapped onto the ground. A circle the size of the mushroom is

drawn about the point. The  $(x,y)$  positions of the edge of the circle are converted to  $(r,h)$  values. These  $(r,h)$  values are then converted to  $(R_i, H_i)$  values by means of appropriate graphs. These are then plotted on any convenient piece of rectangular graph paper and the enclosed area is measured. This area represents a fraction of a unit area column through the cloud which arrives at the point  $x_0, y_0$ , multiplying this fraction by K gives the surface density of activity at this point.

#### CASTLE-Bravo

Referring again to Figure 7, the time variant winds were used to make the  $(r,h)$  plots shown across Rongelap. The 12-hour dose rate at the northern tip of Rongelap from the time variant winds computed by the method just outlined was 52 R/hr. The time of arrival of the debris was from 5 - 14 hours. By using the same system on the Bikini H hour winds, a 12-hour dose rate of 45 R/hr was computed at a point with similar  $(h,r)$  values. The observed 12-hour dosage at this island was reported to be 96 R/hr. Thus, with the best winds available, our computations are well within a factor of two of the observations. Using the Bikini winds, we are still nearly within a factor of two, but are about 55 miles off in position. The calculations, based on H hour winds which should be valid for this close-in fall-out, close to G-Z appear to be very accurate.

DOE ARCHIVES

340



345

PART II

UTILIZING THE IBM 701 ELECTRONIC DIGITAL COMPUTER

S. M. Greenfield  
Rand Corporation

The previous paper by Dr. R. R. Rapp has indicated that it is possible to construct a model which will adequately represent the physical phenomenon of fall-out. In working with the model he presented, we at Rand have found that it provides us with as much of the fine structure of the fall-out pattern as one might reasonably expect when considering the accuracy of the various parameters that go into it. By these parameters, I mean such things as the accuracy of the wind observations, the dimensions of the cloud at stabilization, etc.

As one might imagine, however, having once established what can be considered a representative model, it is not a simple task to use it for computing a fall-out pattern containing the fine structure that can be expected to result from the quality of the input data under normal conditions. One does not just sit down and, in a short half-hour or hour, construct a complete pattern. Rather, it may take as many as two people as much as a day to finish one of these. While a method requiring this many man-hours is certainly adequate if one were only interested in one or possibly two or three patterns, it falls far short of desirability when one enters into a general fallout study. This is true whether the study involves an investigation of the phenomenon of fall-out or an investigation of the implications of the phenomenon in an operational sense.

We at Rand are faced with both problems in our fall-out study. We would very much like to examine how the patterns change as one varies the wind structure with time and space, the distribution of activity with particle size, and the concentration of activity with altitude. Also, due to the peculiar nature of Rand's work, we have a very definite need for fall-out information as an input into an overall weapons employment study. As such, we have been painfully aware of the shortcomings of the hand computation of the fall-out pattern for many months. However, at Rand we are very fortunate in having available both an excellent digital electronic computer like the IBM 701 and a very capable staff of problem programmers for this machine. Working with two of these people, Miss Shirley Marks and Mr. Dave Langfield of our Numerical Analysis Division, it was recently found possible to place the model that has been described previously, or one with a slight modification, on the IBM 701 for computational purposes. As in the case of the hand computation method, the machine model recognizes the fact that the r,h

341

DOE ARCHIVES

ATOMIC ENERGY COMMISSION 1954

346

plot (that is, the positioning of particles, of different radii starting from different altitudes, on the x,y grid representative of the ground) is the basic bit of information necessary for the pattern calculation, and it is toward this end that the initial (and major) segment of the program calculation is slanted. However, it should be noted that, due to the computational speed of the 701, we have at our command the capability of making a much finer grid of (r,h) than was feasible by means of the tedious hand computations. Because of this advantage, we have chosen to subdivide the atmosphere into 1000 ft. intervals, this being a limit imposed on us as being about the smallest intervals at which winds are reported. In the case of radii of the particles, one-hundred intervals of particle size were chosen as being adequate to treat the problem. These intervals were chosen so as to contain equal fractions of the total activity in the cloud. It was initially assumed that within either the stem or the mushroom, the activity distribution with particle size was invariant with altitude. We then have, essentially, two matrices of particle size and altitude, one representing the stem and one the mushroom. Choosing the value at the center of both the particle size interval and the altitude interval as representative of both the intervals themselves, we can then tag each r,h combination with its appropriate fall velocity as described in the previous paper, assuming that this fall velocity taken for each r,h applies over the entire interval. Due to the fineness of the interval divisions, it is found that this assumption is true to within a maximum of one or two percent. These matrices provide us with the first part of our basic input for the machine. It should be noted that by choosing the particle size intervals so as to contain equal fractions of the activity, we have made these matrices independent of bomb yield. In other words, if we can fix on a distribution of activity with particle size, then each matrix can be constructed so as to include all necessary altitudes and then be included in the program as a semi-permanent part of the memory. For a specific case then, providing the machine with information as to the vertical dimensions of the cloud, and the variation of wind velocity and direction with altitude, will allow it to compute the position of the r,h grid on the ground.

**DOE ARCHIVES**

For this computation, it is assumed that all the particles are distributed along a line extending vertically upward from ground zero (the particles present at each altitude are fixed by the distribution assumed for the stem and mushroom). Under this assumption, the machine then proceeds to solve the following analytical equations:

$$x = \sum_h \frac{v_x(h)}{w(r,h)} \Delta h$$



$$y = \sum_h \frac{v_y(h)}{W(r,h)} \Delta h$$

Where  $v_x(h)$  and  $v_y(h)$  are the x and y components of the wind as a function of altitude,  $\Delta h$  is the 1000 ft. altitude interval and  $W(r,h)$  is the fall velocity applicable to a given particle size and altitude. Choosing an r and an altitude at which to start, the machine then holds the particle size constant and merely sums over the altitude to determine its x or y position on the ground. This process is presented schematically in Figure 1 where each dot represents the ground position of the r,h combination. At the same time, consideration is given to the expression  $\frac{\Delta h}{W(r,h)}$  which is simply the time spent by a particle in each altitude interval. By summing this expression over altitude, we therefore have not only the ground position of each r,h combination, but also the time that it arrives at the ground.

As was stated previously, each r,h combination represents a given fraction of the total activity. Recognizing further that this fraction is contained in a slab whose thickness is 1000 feet and whose cross-sectional area is the cross-sectional area of the mushroom or stem, then the machine, having been given the yield of the bomb and the dimensions of the cloud can calculate the "infinite plane" gamma radiation effect of this slab when deposited on the ground. To do this, we utilize the well known relationships for gamma radiation from fission products

$$\text{Number of 1 hour megacuries/}KT - 300 \quad (3)$$

$$\frac{\text{Roentgen}}{\text{Per Hour}} \text{ at 1 hour} = r_1 = \frac{F(r,h) 300}{A} (3.09) \quad (4)$$

**DOE ARCHIVES**

Where  $F(r,h)$  is the fraction of the total activity associated with a given particle size at a given altitude, and A is a cross-sectional area of the mushroom or stem in square nautical miles, and 3.09 is the conversion factor for megacuries per square nautical mile to roentgens per hour at 1 hour.

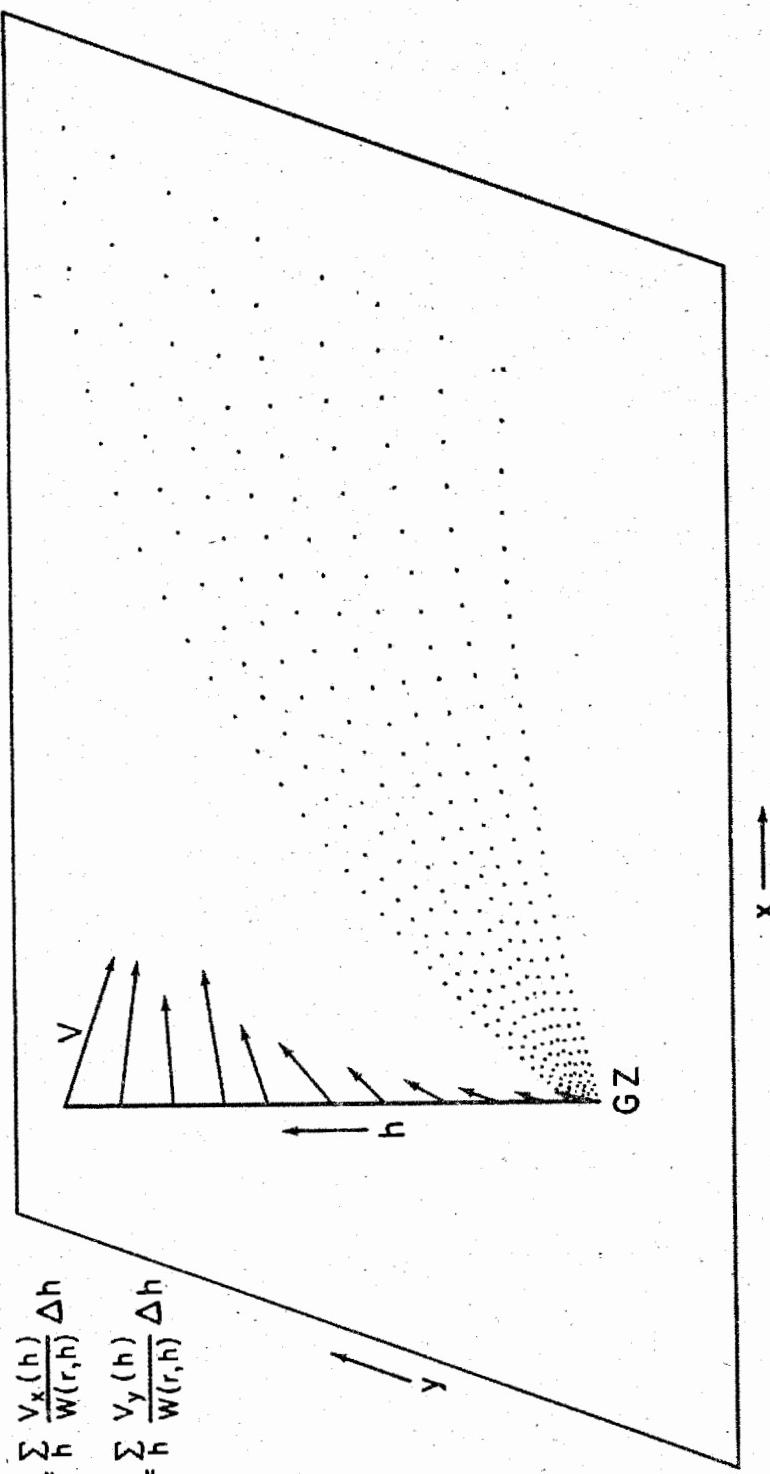
$$r_t = r_1 t^{-1.2} \quad (5)$$

Where t is the time in hours, and  $r_t$  is the dose rate at any time t. And finally

$$R_{\Delta t} = \int_{t_1}^{t_2} r_1 t^{-1.2} dt$$



**COMPUTED X, Y POSITIONS OF PARTICLES FROM  
A LINE SOURCE**



**DOE ARCHIVES**

344

DATA  
ATOMIC ENERGY COMMISSION

349

**Figure 1**

where  $R_{At}$  is the dosage accumulated over a time interval between  $t_1$  and  $t_2$ .

It was decided that the machine would calculate the dose rate at  $t = 6, 12, 24$ , and  $48$  hours after the bomb explodes, and the dosage accumulated between  $0 - 6, 6 - 12, 12 - 24$ , and  $24 - 48$  hours. Implicit in this is the understanding that for any time or time interval occurring earlier than the computed time down for a particle, the dose rate and dosage that the machine will report will be equal to zero.

Having available many thousands of  $r, h$  combinations, positions on the ground and their radiation contribution as a function of the time, we can then proceed to calculate radiation levels at specific points within this pattern. Due to the fact that it has been found that about 100 points scattered representatively throughout the  $r, h$  grid are sufficient to determine the fall-out pattern, it is pointless to attempt to compute the radiation level at each of these many thousands of points and present them as a final output. What was done then was to choose 125 of these  $(r, h)$  combinations in such a way as to make them representative of the entire pattern. As illustrated schematically in Figure 2, this was accomplished in the following way. It is assumed that a representative set of grid points would have a density that was directly proportional to the gradient of density of radioactive material on the ground. Further, it is felt that the variation in time down for particles at the same altitude is a fair approximation to their relative positions on the ground. Under these assumptions, particle sizes were chosen at each 10,000 feet of altitude shot for the following times down:

Every .2 hour for the first hour.

Every .5 hour for the next four hours.

Every hour for the next five hours.

Every 2 hours for the next ten hours.

The  $r, h$  combinations resulting from this type of selection were taken as grid points with some degree of confidence that they truly are representative of the entire pattern. It should be noted that having once chosen our grid points, or  $r, h$  combination, we need not concern ourselves with the problem of how the pattern changes as a function of different wind inputs. This is due to the fact that grid points chosen in this manner will appropriately arrange themselves within the pattern with the wind so as to maintain their representativeness.

DOE ARCHIVES

It is in the final stage of this machine calculation that the dimensions of the cloud really come into play. It should be remembered,

SELECTED PATTERN OF GRID POINTS AT  
WHICH RADIATION WILL BE COMPUTED

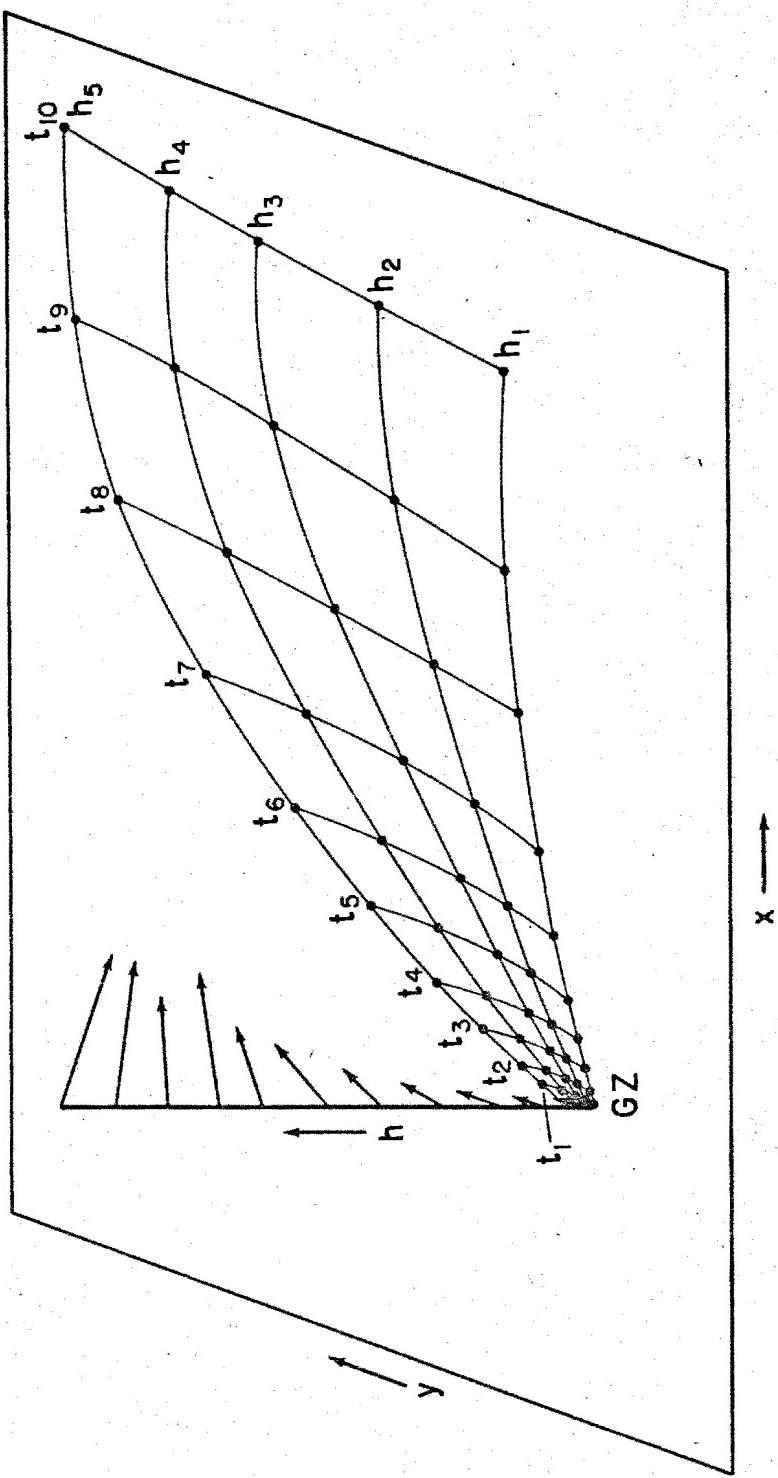


Figure 2

DOE ARCHIVES

346

AMERICAN ENERGY ACT 1954

351

**SUMMATION OF THE RADIATION CONTRIBUTION FROM PARTICLES  
IN THE STEM AND MUSHROOM TO A PARTICULAR GRID POINT**

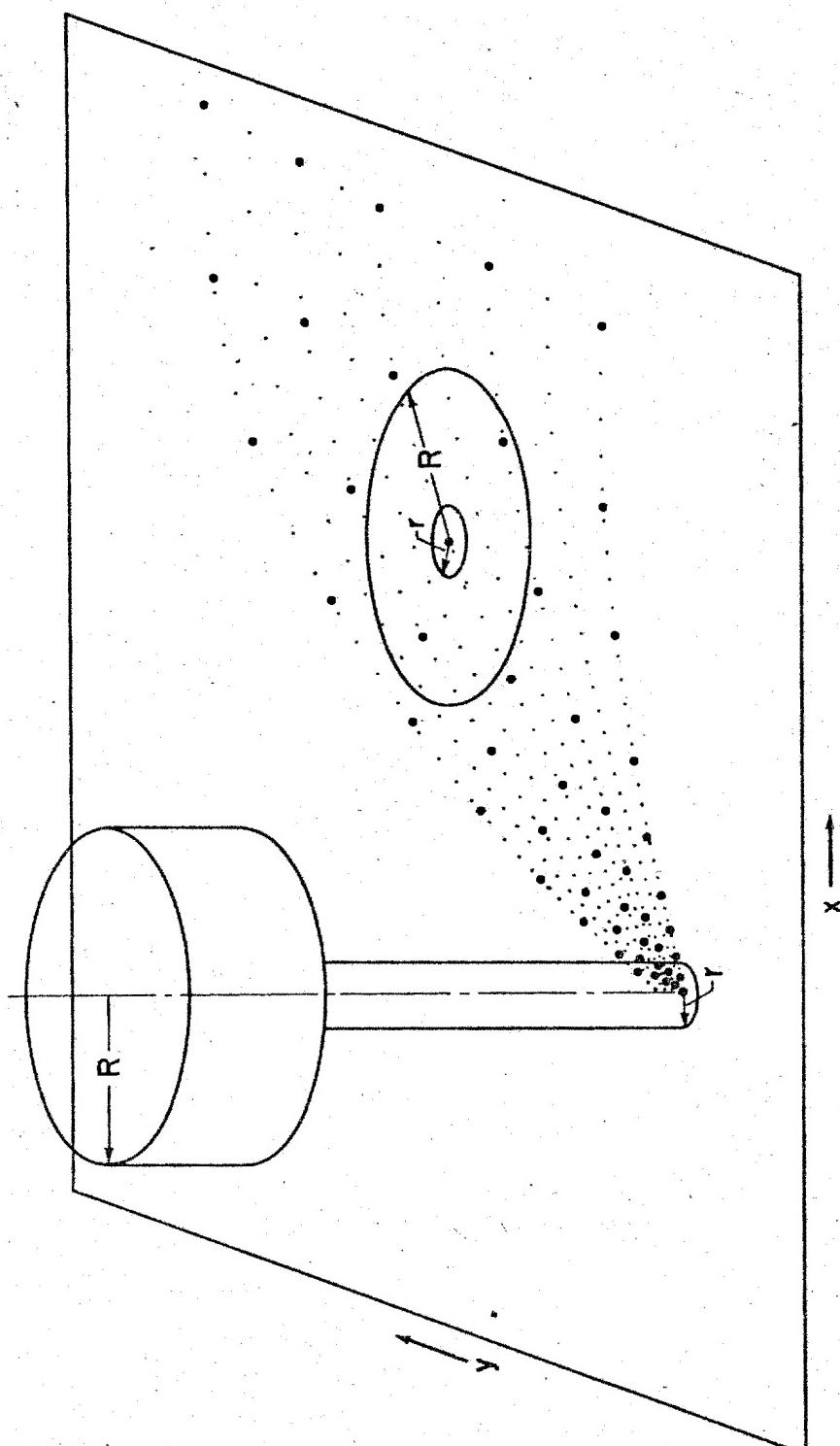


Figure 3

DOE ARCHIVES

347

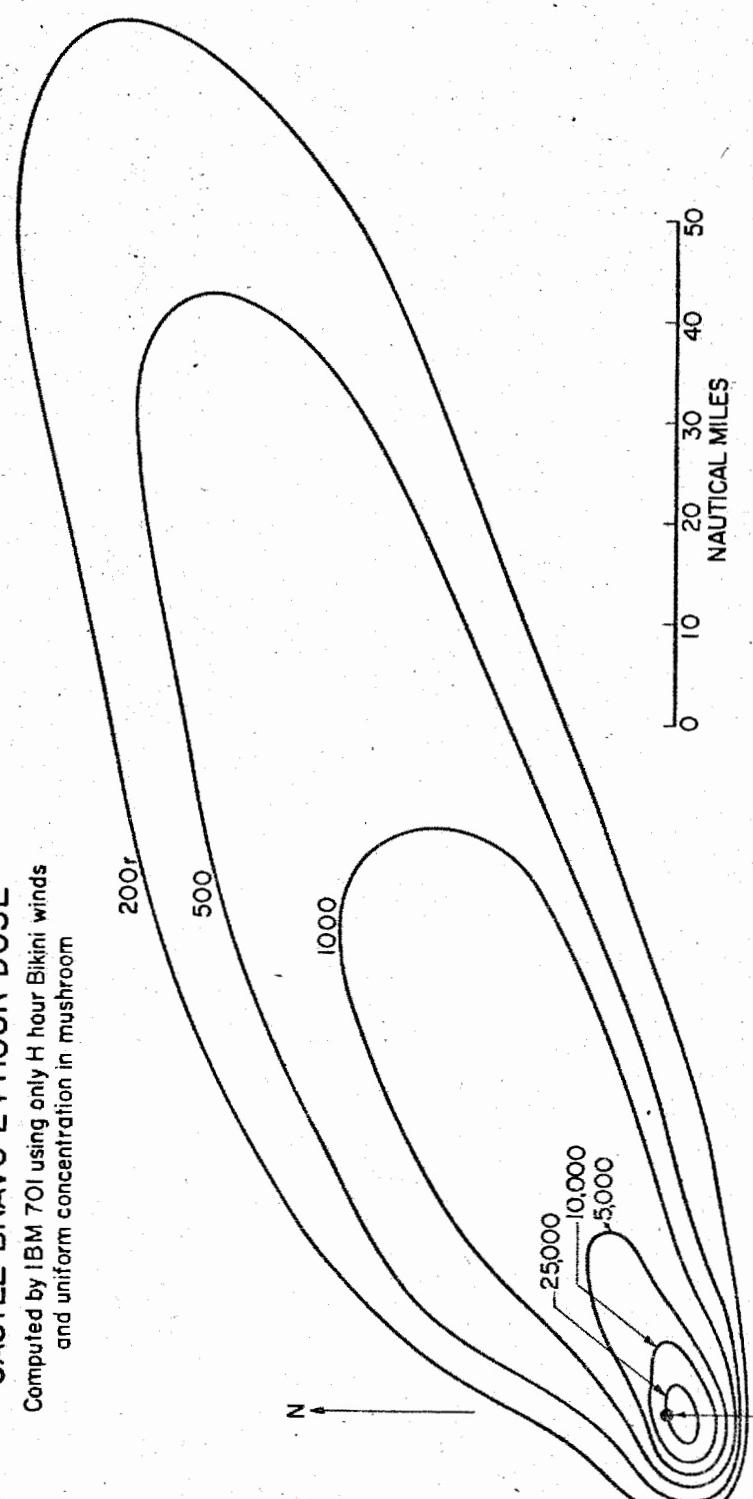
352

as was stated previously, that each r,h point in the grid actually represents the center of a circle that is the projection of a slab of material onto the ground (slab 1000 ft. thick, cross-sectional area equal to the cross-sectional area of cloud). Furthermore, it is assumed that every ground point within this circle receives an equal radiation contribution from this r,h interval. Conversely, it can be seen that if a circle of radius equal to the radius of the stem or mushroom is drawn around any point on the ground, it will include all r,h combinations that will contribute to the radiation found at this point. This is illustrated in Figure 3. Figuratively, then, the machine draws a stem circle and a mushroom circle around each of the 125 grid points and simply sums the contributions from the appropriate r,h combinations. The final output from this machine calculation is, therefore, the coordinates of 125 points on an x,y grid (whose origin is ground zero), the dose rates found at these points at  $H = 6$ ,  $H = 12$ ,  $H = 24$ , and  $H = 48$  hours, and the dosages accumulated from 0 - 6, 6 - 12, 12 - 24, and 24 - 48 hours after burst time. As a secondary output, we have available the many thousand of r,h combinations, their locations on the ground, and their associated radiation contributions. This means, in effect, that any other set of grid points can be utilized in conjunction with this data and their radiation levels calculated.

After the winds are fed into the computer, total machine time for a problem of this type is approximately one hour. Since plotting and analyzing the results takes about one-half hour, we can estimate that the total time from problem to pattern is something under two hours.

Let us now examine some results of these calculations. The first problem that was tried on the machine was the CASTLE-Bravo Shot. This was essentially our test of the machine program in that this particular case had been done by the original hand computing method reported in Rand Report R-265-AEC. An attempt was made, therefore, to duplicate the input data used in the initial calculation. In essence, then, the pattern computed by the machine was as wrong as the pattern in R-265-AEC in that it, too, used only the H-hour winds from the Curtiss (the ship near Bikini). This machine-computed pattern for integrated dosage to  $H = 24$  hours is presented in Figure 4. As was hoped, the machine computation duplicated the hand computation surprisingly well. In fact, due to the greater accuracy of the fall velocities input into the electronic computer and the greater detail possible with the machine, the computed pattern duplicates very closely the observed pattern in the vicinity of Bikini where the H-hour Curtiss winds may be assumed to apply with some degree of confidence. This is illustrated in Figure 5 which presents the observed dose rates in the Bikini Lagoon and the pattern computed by the above method. It should be pointed out that the computed pattern does not fit the far out fall-out observed from CASTLE-Bravo. This is to be expected in that one should not hope to duplicate a pattern that

**CASTLE BRAVO 24 HOUR DOSE**  
Computed by IBM 701 using only H hour Bikini winds  
and uniform concentration in mushroom



**DOE ARCHIVES**

349

NUCLEAR ENERGY ACT

354

**Figure 4**

Fig. 5 - DOSE RATE

AT H + 6 hours  
FOR FALLOUT  
OVER BIKINI  
FROM CASTLE  
"BRAVO"

— XX Computed  
by IBM-701

XX Observed

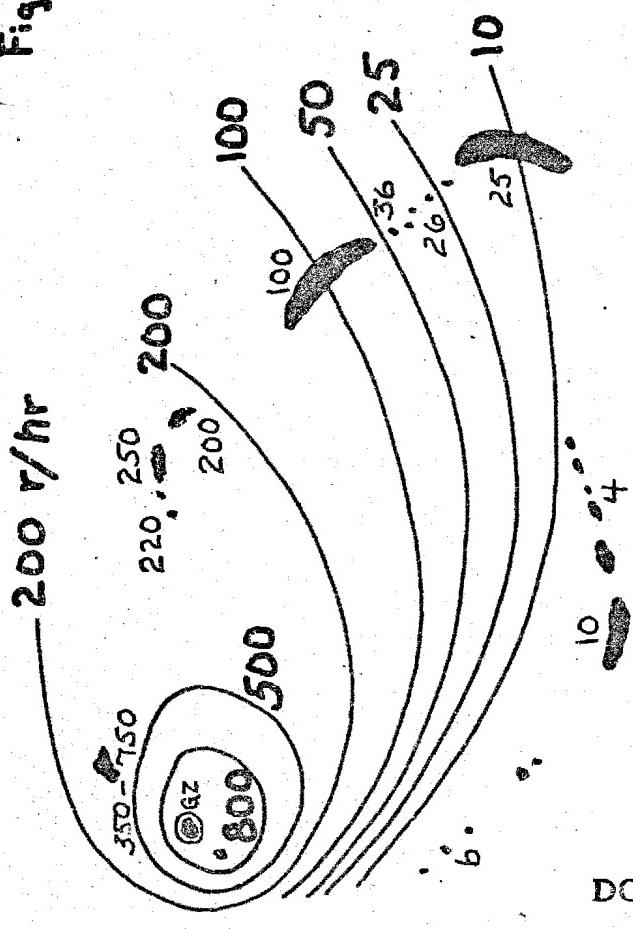


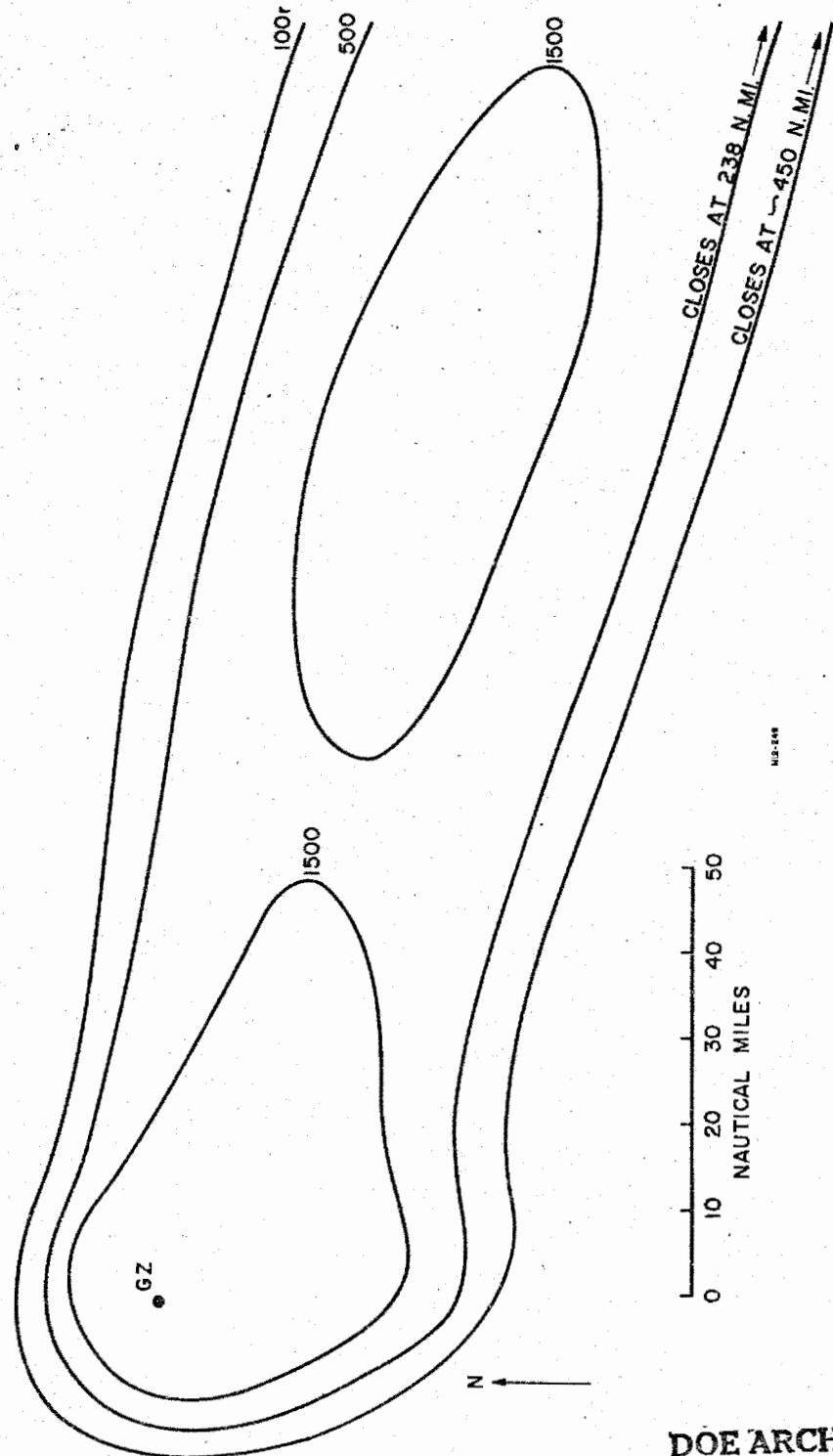
Figure 5

took 17 - 24 hours to deposit on the ground stretching over a distance 200 - 300 miles downwind from ground zero utilizing one set of winds for a particular time and place. As was pointed out in Dr. Rapp's paper, however, when this variation of wind in time and space is taken into account, the Rand model does, indeed, produce an adequate reproduction of the observed Bravo fall-out.

Figures 6 and 7 are the 48-hour dosage patterns for respectively a 50 MT bomb under condition "A" and a 1 MT bomb under condition "B". Conditions "A" and "B" are the wind conditions established by AFSWP for test purposes. Since these will be discussed later in this report, they are presented here just as a further illustration of machine computed patterns. It should be pointed out, that following the suggestion of Dr. F. Henriques of Technical Operations, we have gone over to the assumption that the concentration of activity in the mushroom decreases exponentially with altitude. This assumption has been used in all our calculations for conditions "A" and "B". One final point should be made. As was indicated above, to be truly representative, the computation must take into account the variation of wind in time and space. Although this capability has not been utilized in the past, the 701 program is flexible enough to take this into account with a very small modification. Very simply, sets of winds representative of the variation in time and space are placed in the machine memory (these variations being in terms of finite increments of time and x and y distance) in solving equations (1) and (2). Then, for a given r and h, the machine examines the step-wise buildup of x, y and t over the summation, and switches to the appropriate wind set at the proper time and distance. It is hoped that this added refinement will be utilized in the future wherever feasible.

DOE ARCHIVES

RAND MODEL  
48-HOUR DOSE—50 MT—CONDITION "A"  
COMPUTED BY IBM 701



DOE ARCHIVES

352

GEOR

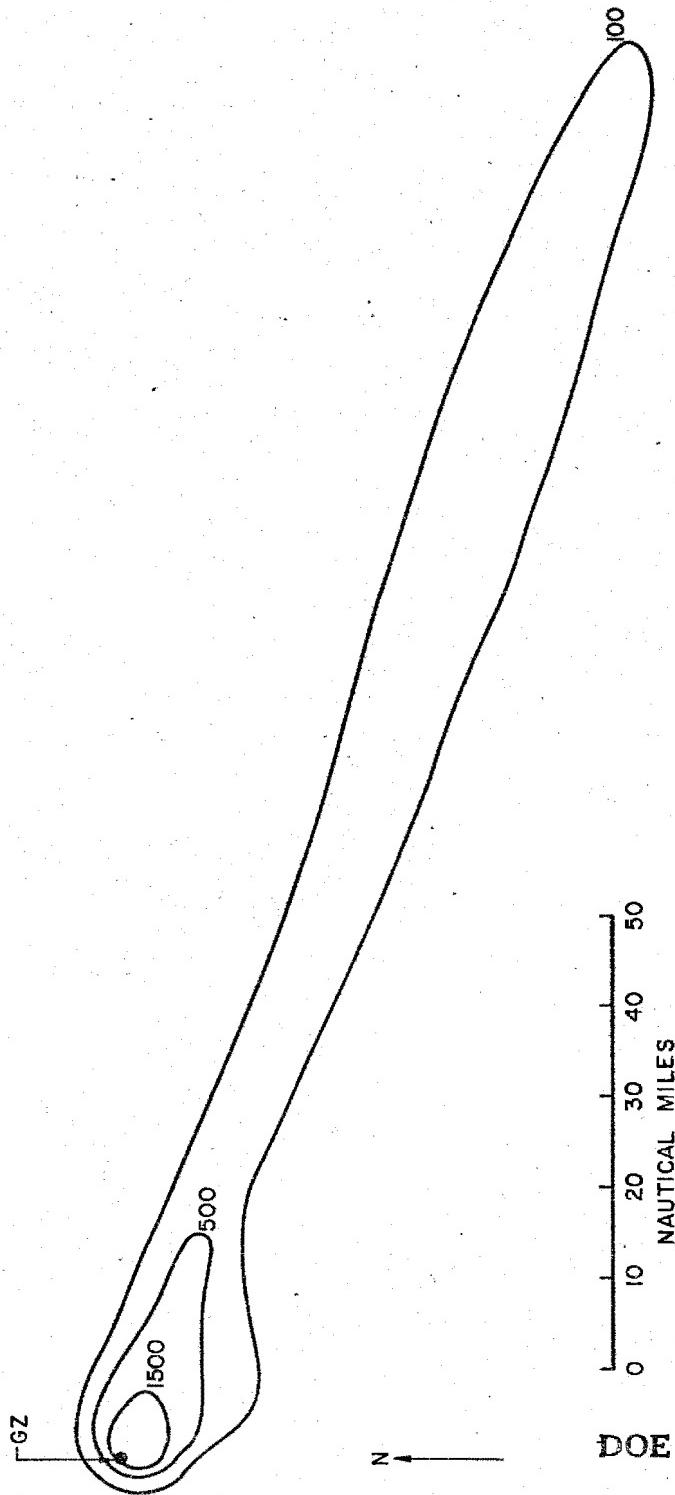


361

357

Figure 6

RAND MODEL  
48-HOUR DOSE — 1 MT — CONDITION "B"  
COMPUTED BY IBM 701



DOE ARCHIVES

353

ATOMIC ENERGY ACT

358

Figure 7

**THIS PAGE IS BLANK**

**DOE ARCHIVES**

**354**

**OMIC ENERGY ACT IS**

**SECRET**

**359**

PREDICTION OF DOSE-RATE AND DOSAGE CONTOURS AS FUNCTIONS OF YIELD  
AND METEOROLOGICAL CONDITIONS, U.S. WEATHER BUREAU METHOD

Mr. K. M. Nagler  
U.S. Weather Bureau

Introduction

Under contract to the Santa Fe Operations Office of the Atomic Energy Commission, the Special Projects Section of the Weather Bureau has attempted to devise a method of forecasting radioactive fall-out for tower bursts at the Nevada Test Site. In the past, fall-out forecasts have been made by various approximate empirical methods. It was felt, however, that enough data had accumulated during the TUMBLER-SNAPPER and UPSHOT-KNOTHOLE tests to provide a basis for a more logical forecasting scheme. Specifically, we had useable amounts of observational data from nine 300-foot tower shots, ranging from about 11 to about 52 kilotons in yield.

Observations of Deposited Activity

The first phase of our work involved the preparation of maps of the observed deposited radioactivity. We have used primarily the ground monitoring data and have considered the aircraft estimated of radioactivity at the ground merely as approximate information which can provide a rough independent check on our method of determining fall-out.

For most of the data outside the test site itself, the monitors drove along the roads taking readings at intervals of 1-5 miles. Where only a single monitoring run was made along a road, we accepted its reports; but for most roads, there were several runs by different monitors, and the concentrations which we used on the maps of observed radioactivity were a compromise - often a difficult one to make. The discrepancies between two or more monitoring runs along the same road may be due to several causes: redeposition of debris that originally landed elsewhere, removal of debris by wind, instrumental errors, a different rate of decay than that assumed, errors in positioning, or to various other human errors. Figure 1 shows the results of several monitor runs along one road, following the ninth UPSHOT-KNOTHOLE burst. This illustrates many of the uncertainties which are encountered in using the observational data. Two runs give similar peak values but differ markedly to the left of the peaks, probably because the fall-out was not complete when the one run was made. A third peak suggests much lower concentration and is displaced from the other two. The two partial runs obviously do not fit the others very well. One seemed to indicate that the reported positioning was wrong, perhaps due to a faulty speedometer on the monitoring automobile.

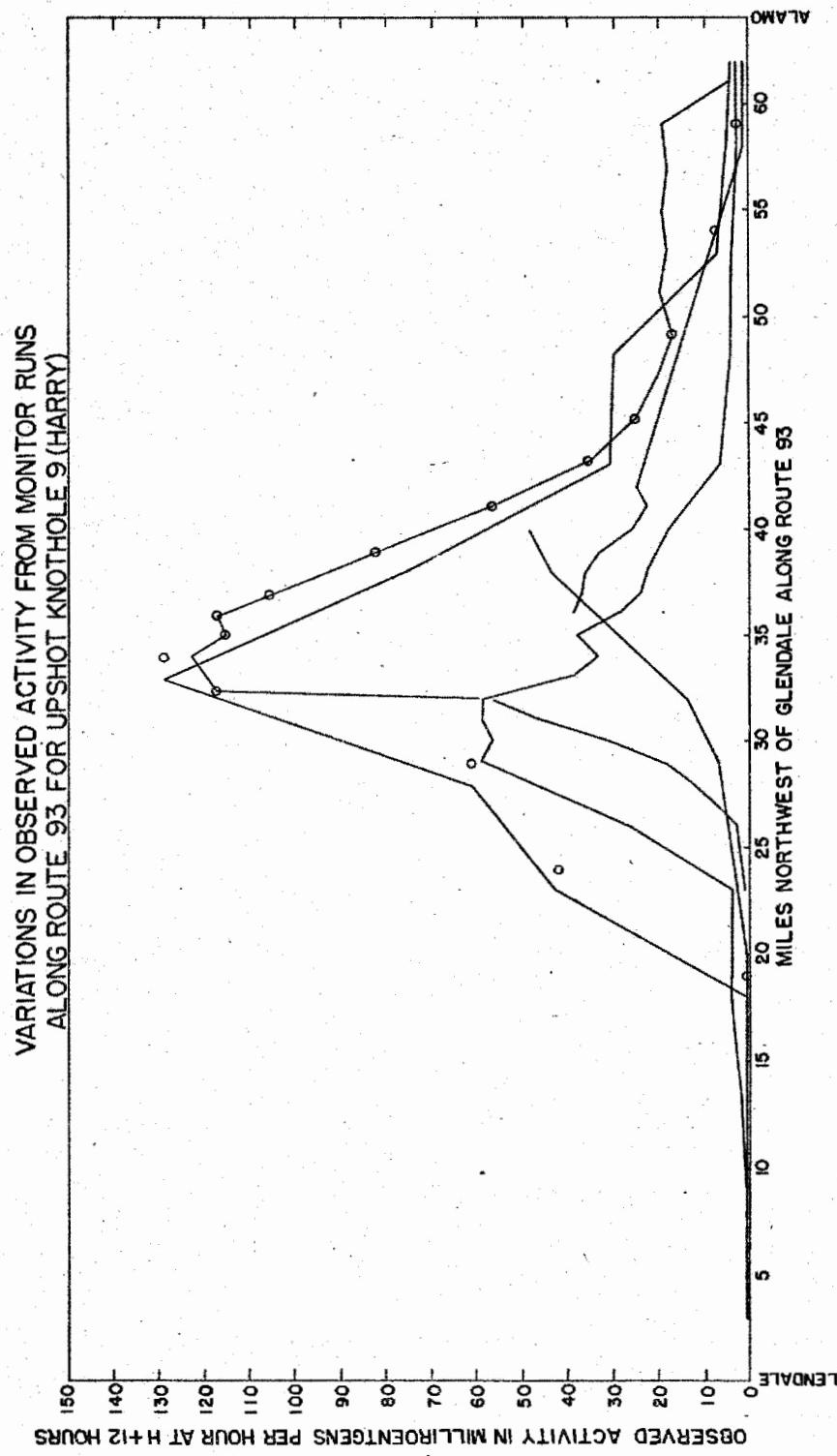


Figure 1

DOE ARCHIVES

356

361

REDACTED DATA  
ENERGY

This series of monitor runs is somewhat more confusing than most, but not as confusing as some. It must be remembered that these observations of deposited activity were not made with the care and accuracy desirable in a scientific experiment. They were made to determine whether there was any radiological hazard.

At any rate, for each tower burst in the TUMBLER-SNAPPER and UPSHOT-KNOTHOLE series, the observations we selected were extrapolated to a common time (12 hours after the burst) and were plotted on maps in units of milliroentgens per hour.

#### Fall-out Plots

The second phase of our work called for the preparation of fall-out plots. A fall-out plot or radex plot is an analysis which shows where particles of various sizes falling from various heights will reach the ground, based on the winds and on the assumed rates of fall of particles of the various sizes. A fall-out plot may also include an analysis of the times at which the different particles reach the ground.

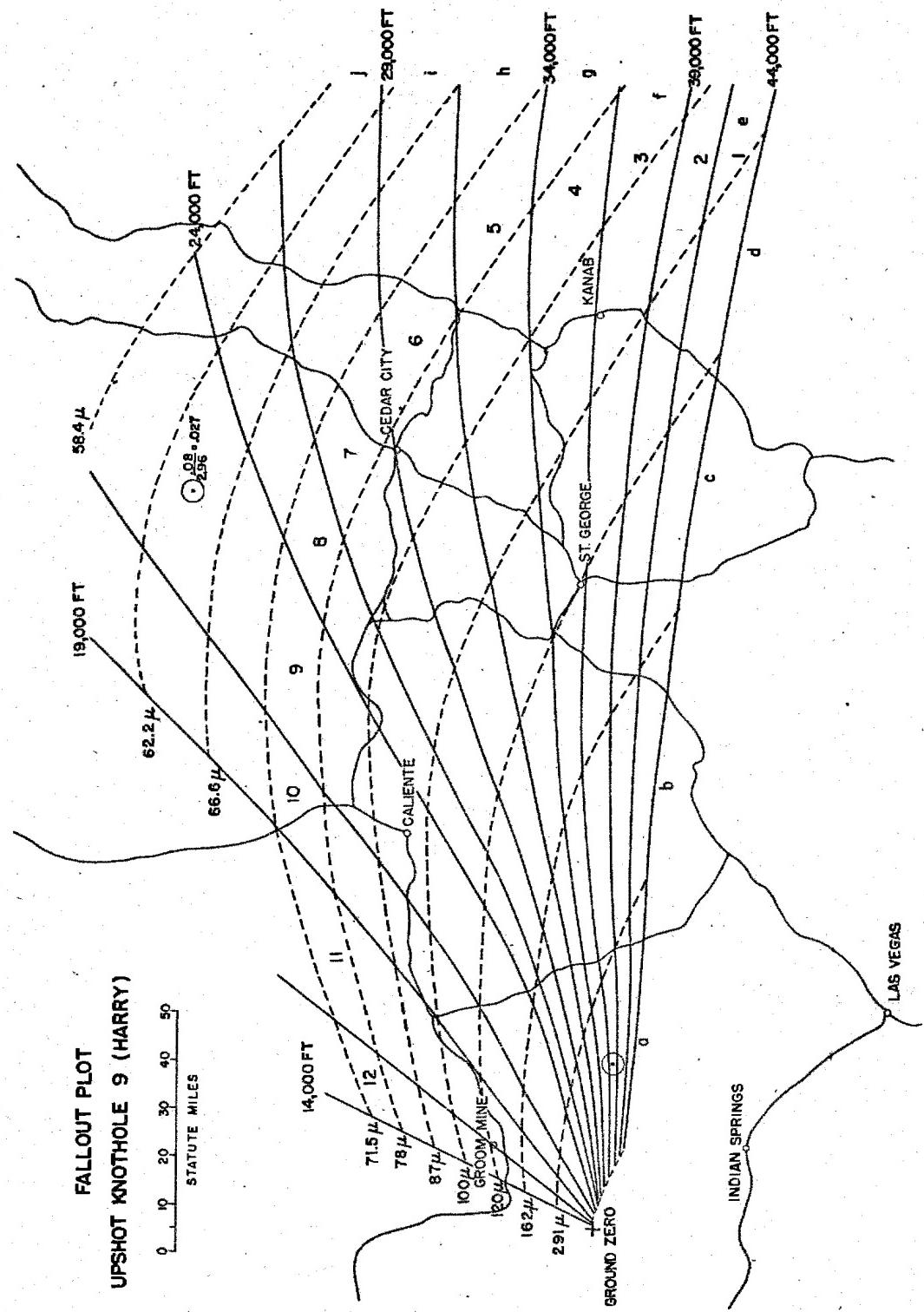
Figure 2 gives an example of a fall-out plot for UPSHOT-KNOTHOLE-9. Each curving line shows the estimates of where particles of a certain size should fall, and each radial line indicates the line along which particles originating at a certain height in the atomic cloud are deposited. A line indicating constant time of reaching the ground would pass through large size, high altitude areas to small size, lower altitude areas.

Our fall-out plots differ from the type used previously at Nevada in two basic ways. In the first place, rather than a uniform rate of fall, we used an aerodynamic fall velocity, derived by means of the formulae given in the Rand report on Project Aureole. For the various altitudes, we used air temperatures and densities obtained from a mean sounding during the UPSHOT-KNOTHOLE series. As an example of the effect of the use of aerodynamic fall velocity, a particle in the 150-200 micron range falls only about 7/10 as fast at 10,000 feet as it does at 40,000 feet.

DOE ARCHIVES

The second basic difference from most earlier fall-out plots is that in computing the path of a falling particle, we used analyses of the space and time variability of the wind, not merely the wind reported at the time and place of the burst. In brief, we prepared maps showing the mean winds for each 5,000-foot layer for each three-hour time when observations were available. On the maps each individual wind observation (for a 5,000-foot layer) was plotted at the point over which the balloon actually was when it passed through that layer, rather than at

Figure 2



the station from which the balloon was launched. Also, the original drift of the rising atomic cloud was taken into account in determining the starting point for the various elevations.

Initially trajectories of particles of six sizes ranging from 60 to 833 microns were drawn, starting from each 5,000-foot level - 10,000, 15,000, 20,000 feet, etc. - and from the reported top of the cloud. Using the space and time changes in wind along the descending trajectory, particles of each size were tracked to the position on the ground or to the 5,000-foot surface (MSL), which with a few exceptions was close to the height of the terrain.

For this initial fall-out plot we interpolated to get convenient intervals of height and particle size, as shown in Figure 2. Our height lines are at 2500-foot intervals, starting with the height of the top of the cloud. The particle size interval was chosen such that the time of fall from 35,000 feet to 5,000 feet is in multiples of an hour. Thus, a particle 291 microns in diameter takes one hour to fall this distance, a 162 micron particle takes 2 hours, etc.

We took considerable care in preparing fall-out plots for the various tower bursts; nevertheless there are still several sources of error.

The trajectories of the falling particle may be in error, due to errors in the wind observations and the analysis. The error in the location of a point is probably less than 10% of the distance away from ground zero. However, the relative error between adjacent points on the fall-out plot is much less.

A further possible source of error is that the rate of fall may be incorrect because the particles are not spherical, have a density different from the 2.5 assumed, or follow a different settling law than the one assumed. However, as far as we have been able to determine, the radioactive particles produced by a tower burst are nearly spherical, particularly those smaller than 200 microns, which contribute mainly to the off-site fall-out. Moreover, data for the few cases for which times of arrival were available agreed with our fall-out calculations. Also, for the second UPSHOT-KNOTHOLE burst, there are particle size observations that seem to verify the aerodynamic law rather than Stoke's law, or uniform descent.

Construction of a Model

DOE ARCHIVES

Equipped with maps of the observed radioactivity along the roads and with fall-out plots for the various shots, we came to our basic

problem, namely to determine the distribution of the debris in the original clouds which would give rise to the ground radiological data.

An explanation of our procedures is in order, however, before we discuss our model of the distribution of debris in an atomic cloud. This fall-out plot, strictly speaking, represents the position where various sized particles from various heights would reach ground, if they originated along the central axis of the cloud or in other words, if the cloud were very narrow. We know, however, that the cloud does have a finite width. We have assumed a cloud to be cylindrical and five miles in diameter at all levels and that the diffusive spread of the cloud over the distances here being considered is negligible compared to the spread by wind shear. As will be pointed out later, the exact diameter chosen is not very important to our computations, so that our use of the same width for both stem and mushroom can be justified.

Let us examine the importance of using a cloud of finite cross-section. If the cloud were not of finite width but were a line source, then each height and particle size in the cloud would correspond uniquely to one point on the ground. With a finite cloud diameter, however, each point on the ground could be affected by a range of particle sizes and heights.

We take the finite dimensions of the cloud into account in a fashion similar to that of the Rand and other groups. We first center a circle of the diameter assumed for the cloud at the point on the fall-out plot for which the fall-out is to be computed. The particle sizes and initial heights which contribute to the activity at the point are those that lie within the circle.

In our model the amount of radioactivity is assumed to be uniform throughout each 2500-foot layer for each particle size range - a, b, c, etc. The mechanical computations of fall-out at a given point are of three types: first, where the circle lies entirely within one of the polygons; second, where the circle contains areas from several polygons; and third, where some or all of the polygons become squeezed into lines or nearly so - that is, the case of little or no directional shear.

DOE ARCHIVES

In the first case, if we know the concentration in appropriate units for each layer and size range, and if the circle lies within the sector, we merely need the ratio of the area of the initial cloud to the area of the sector, as shown by the upper point in Figure 2. This fraction multiplied by the amount of radioactivity assigned to the sector will give an estimate of the concentration at the point.

In the second case, we must find the ratio of each part of the circle to the area in which it lies. Each of these ratios or fractions is multiplied by the amount of radioactivity assigned to the appropriate height and particle size range. The sum of these products gives the estimate of the radioactivity at the center of the circle. The third case - little or no directional shear - will be discussed later.

Here it should be pointed out that the assumed area of the cloud has no effect on the concentration as we would compute it at a point when the circle lies entirely within the bounds of one polygon. And, when the circle covers parts of several sectors, the assumed area is important only when the gradient of radioactivity from one sector to another is large.

The procedure I have just described is the one which would be used when the amount of radioactivity in each height layer and particle size range is known. However, it is this information which was sought.

To get this information, we first obtained the activities which would best fit individually the seven cases with best observational data. Each of these sets of numbers had to be a compromise, as no reasonable model could fit every observation well, and the various sets differed widely. Then, the main problem was to prepare a composite model which would give a best fit to all of the cases.

First, we considered all cases relative to the top of the cloud. Second, to scale for yield, we assumed that the amount of activity is proportional to the area of the ground intersected by the fireball. (This scaling method is a simple one and one which seemed to work reasonably well. Further tests will be made with other scaling methods which are physically more acceptable. Changes in the activity assigned to various ranges of height and particle size may result from changes in the scaling method. The revised values, together with any refinements or simplifications in our procedures, will be given in a forthcoming report.)

#### DOE ARCHIVES

When we completed our initial composite model, we used it to compute a grid of values - one for each sector on the fall-out plot, for each case. Then, considering how patterns and activities fitted the various cases, we continued to change the model to give a better fit. Figure 3 shows the resulting model, which gives the average activity in the various height and particle size ranges for a typical 20 kiloton bomb. In this connection, it should be pointed out that the total deposited radioactivity is not dependent solely on the yield, but also on the nature of the bomb itself. We have considered this effect only qualitatively, but feel that it may be an important one.

AVERAGE DISTRIBUTION OF RADICACTIVITY FROM A 20-KT, 300 FOOT TOWER BURST,  
ASSUMING A CLOUD DIAMETER OF 5 MILES. UNITS ARE THOSE WHICH GIVE  
MILLIROENTGENS PER HOUR AT 12 HOURS AT THE GROUND.

Height in feet (MSL)	Particle size (microns)	Total activity for particle sizes greater than 58.3 microns										Average Meshroom
		a	b	c	d	e	f	g	h	i	j	
40,000	1	50	70	60	50	40	30	20	10	10	360	
37,500	2	100	200	150	150	100	50	30	20	20	850	
35,000	3	150	300	250	250	200	100	60	50	30	1420	
32,500	4	200	350	300	300	250	150	70	60	40	30	1750
30,000	5	250	200	200	200	150	100	60	50	30	20	1260
27,500	6	300	200	150	100	100	70	50	40	20	10	1040
25,000	7	400	200	50	40	40	30	30	30	20	10	850
22,500	8	600	200	50	40	40	30	30	30	20	10	1050
20,000	9	700	300	70	40	40	30	30	30	20	20	1280
17,500	10	750	350	80	50	50	40	40	40	30	30	1460
15,000	11	800	400	80	50	50	40	40	40	30	30	1560
12,500	12	800	400	80	50	50	40	40	40	30	30	1560
10,000												

DOE ARCHIVES

362

367

Figure 3

The model assumes a cloud top at 40,000 feet and a mushroom 15,000 thick. It will be noted that a little more than half of the activity in the particle sizes greater than 58.3 microns occurs in the stem (7760 compared to 6680 units). Most of this, however, reaches ground within about 10 miles of the burst site, much of it within three or four miles, particularly that activity on large particles.

It must be understood that these numbers are only approximate. There are enough observational uncertainties and perhaps enough real differences from one atomic cloud to another, so that errors as large as a factor of two or three are to be expected in parts of the model when it is applied to individual cases.

The units are those which will yield milliroentgens per hour at 12 hours - if a cloud of 5 mile diameter is assumed. However, these units can be converted to units which will give the lifetime dosages (or dosages for any other period), since for each initial height and particle size the time of arrival at the ground can be calculated. In Figure 4 the units are for lifetime dose, in roentgens.

At any rate, we have computed the activity on the ground according to this composite model and our assumptions, for eight of the bursts. Figure 5 shows the observed as well as the computed fall-out for one case, the ninth UPSHOT-KNOTHOLE burst. The data plotted along the roads are a representative selection of the observed values of radioactivity in units of milliroentgens per hour at 12 hours after the burst. The data plotted near the dots are the computed values. The analysis showing activities of 5, 25, and 100 milliroentgens per hour at 12 hours is based on the computed values from our model. This, incidentally, is the case which our model fitted least well of all the cases, largely because of the abnormally great amount of activity observed over fairly wide areas. As can be seen from the figure, we are in error by a factor of about 3 over much of the area, but the general features of the computed and observed data are similar.

Figure 6 shows a similar diagram for UPSHOT-KNOTHOLE 2. In this case, the model, again scaled for the appropriate yield, overestimated the activity as given by the observations by about a factor of 2. Also, the axis of computed peak concentrations differs from the observed peak by about seven or eight miles. This could, of course, be due to meteorological errors in preparing our fall-out plot or to an anomalous distribution of radioactivity in the cloud, with very high concentrations existing near the very top of the mushroom.

DOE ARCHIVES

AVERAGE DISTRIBUTION OF RADIONACTIVITY FROM A 20-KT, 300 FOOT TOWER BURST,  
ASSUMING A CLOUD DIAMETER OF 5 MILES. UNITS ARE THOSE WHICH GIVE  
LIFETIME DOSE AT THE GROUND, IN ROENTGENS.

Particle size (microns)

		a	b	c	d	e	f	g	h	i	j	k	l	m	n	o	p	q	r	s	t	u	v	w	x	y	z
40,000	1	5.5	6.5	5.0	4.0	3.0	2.0	1.5	1.5	0.5	0.5																
37,500	2	11.5	18.0	12.5	11.5	7.5	3.5	2.0	2.0	1.0	1.0																
35,000	3	17.5	28.0	21.0	19.5	15.0	7.0	4.0	3.0	2.0	2.0																
32,500	4	23.5	33.0	25.5	24.0	19.0	11.0	5.0	4.0	2.5	2.0																
30,000	5	30.5	19.0	17.0	16.0	11.5	7.5	4.5	3.5	2.0	1.5																
27,500	6	37.0	19.5	13.0	8.0	6.0	5.5	3.5	3.0	1.5	0.5																
25,000	7	51.0	20.0	4.5	3.5	3.0	2.5	2.5	2.0	1.5	0.5																
22,500	8	80.0	20.0	4.5	3.5	3.5	2.5	2.5	2.5	1.5	0.5																
20,000	9	98.0	31.5	6.5	3.5	3.5	2.5	2.5	2.5	1.5	1.5																
17,500	10	105.0	38.0	8.0	4.5	4.5	3.5	3.5	3.0	2.5	2.5																
15,000	11	112.0	46.0	8.0	5.0	4.5	3.5	3.5	3.5	2.5	2.5																
12,500	12	112.0	50.0	9.0	5.0	5.0	4.0	3.5	3.5	2.5	2.5																
10,000																											

Height in feet (MSL)

DOE ARCHIVES

364

AN ENERGY ACT

369

Figure 4

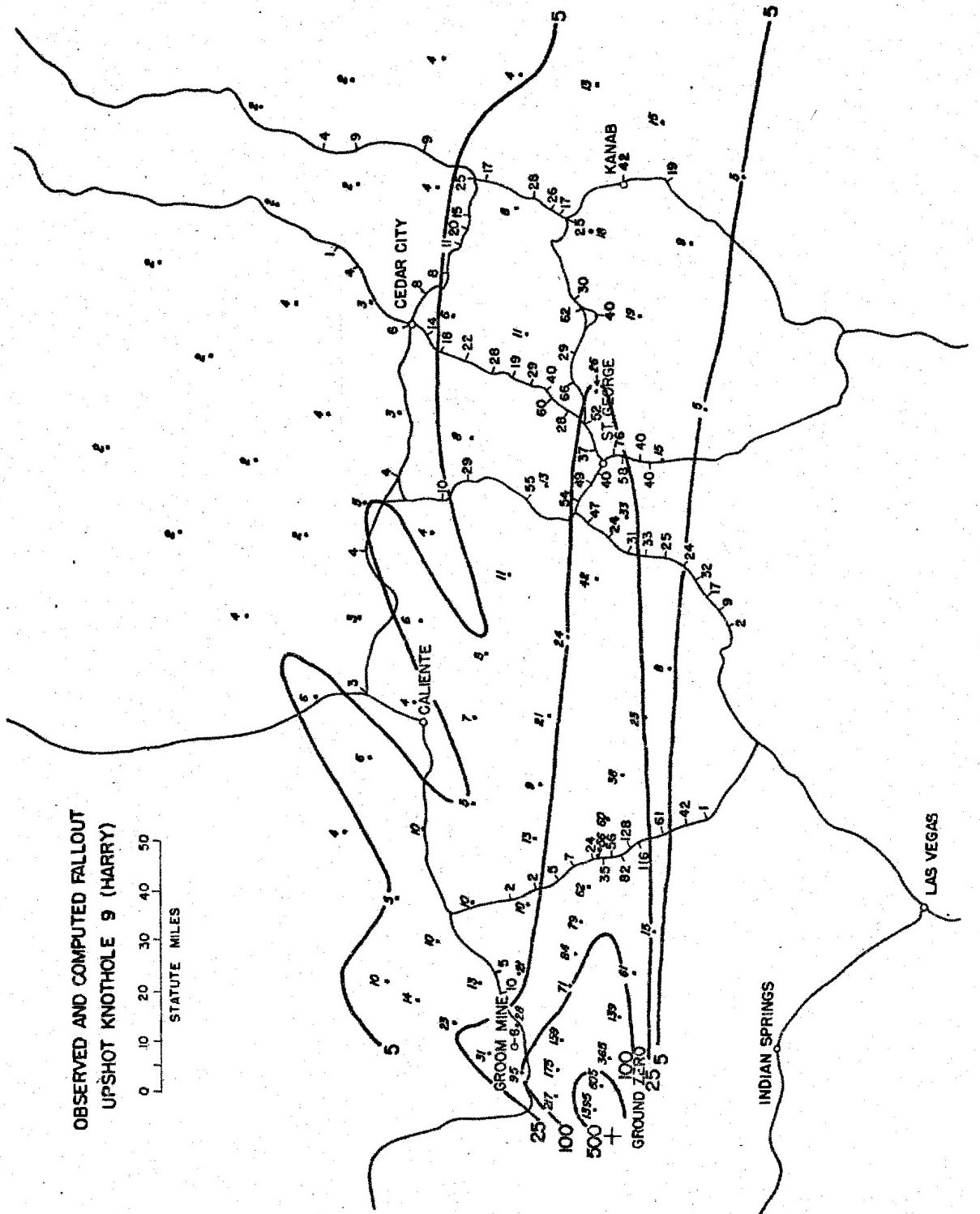


Figure 5

## OBSERVED AND COMPUTED FALLOUT WIPSHOT KNOTTHOLE 9 (HARRY)

STATUTE MILES

365

DOE ARCHIVES

ATOMIC ENERGY

370

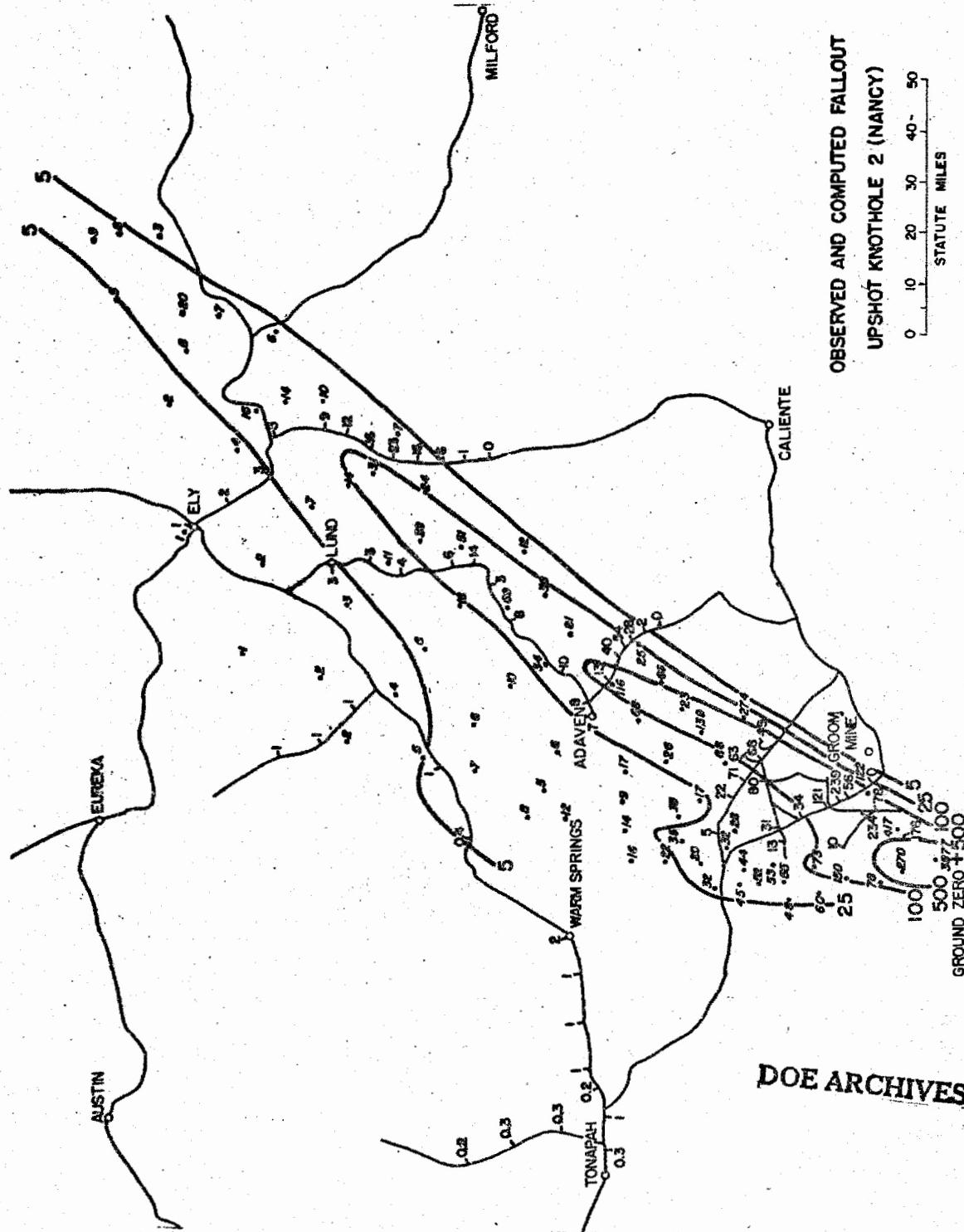


**Figure 6**

**DOE ARCHIVES**

366

371

### Cases with Little Lateral Wind Shear

I have described our physical approach to fall-out prediction only insofar as it applies to wind fields in which there is considerable lateral shear - that is, where the fall-out plot is spread out.

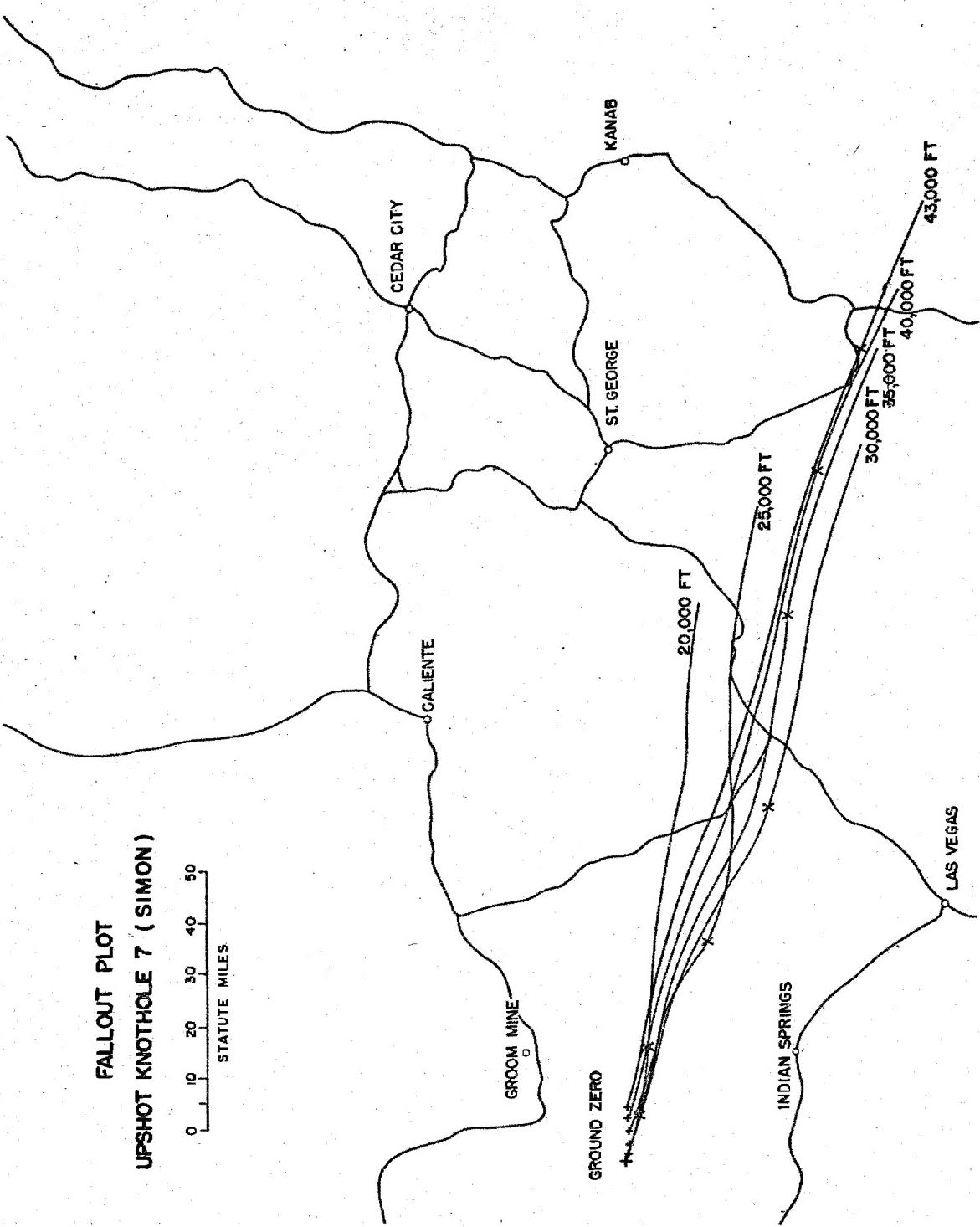
Figure 7 shows a partial fall-out plot for a case (UPSHOT-KNOTHOLE 7) with little lateral spread. A complete fall-out plot would be practically meaningless. The "X's" indicate the position of the 88 micron line and you can imagine the elongated shapes of the polygons. The first and sixth UPSHOT-KNOTHOLE bursts had similar fall-out plots with little lateral spread.

In order to utilize the observational data from these bursts, and to test our composite model, we had to devise an alternate method of treating these cases. What we have done is to assume that there was no directional shear at all. Then, from the distances to the various selected sizes, we prepared a working graph shown in Figure 8. In this graph, we have essentially compressed the fall-out plot into a line. One can see from this graph at what distance along this line a particle of a given size from any initial height will reach the ground. To determine the concentration at any point along the line, using our assumption of a cloud five miles in diameter, we first draw a vertical column five miles wide centered at the appropriate distance from ground zero. Then, to get the contribution, for example, of the top layer of the cloud and our "b" particle size range, we determine the fraction of the total area,  $(l, b)$  which lies within the column. In this case, it turns out to be about 17%. Thus, 17% of the radioactivity in the height range 40,500 to 43,000 feet and in the particle size range 162 to 291 microns in our model would contribute to the deposition at the selected point. To estimate the total deposition at the point, we have to compute similar percentages for each sector cut by the column, multiply each by the appropriate concentration from the model, and sum up the products. This resulting sum must, of course, be multiplied by a scaling factor based on the yield of the bomb. Now, what we get by this method is the deposition at the appropriate point on the ground which would exist if the cloud were five miles wide and if there really were no change in direction of the wind with height. We know that there is some directional shear. Therefore, we would normally expect the value computed by this method to be too high. There is one exception, namely that a narrower cloud than the assumed five mile one exists together with no directional shear. Figure 9 shows the observed fall-out from UPSHOT-KNOTHOLE 7 and shows the computations based on the method just described for several points where the fall-out line crossed roads along which observations were taken. The computed values are shown in italics and the observed values are plotted along the roads as before. In this case, it can be seen that the computed values in

**FALLOUT PLOT  
UPSHOT KNOTHOLE 7 (SIMON)**

STATUTE MILES.  
0 10 20 30 40 50

**SECRET**



**DOE ARCHIVES**

368

**SECRET**  
OMIC ENERGY ACT

373

**Figure 7**

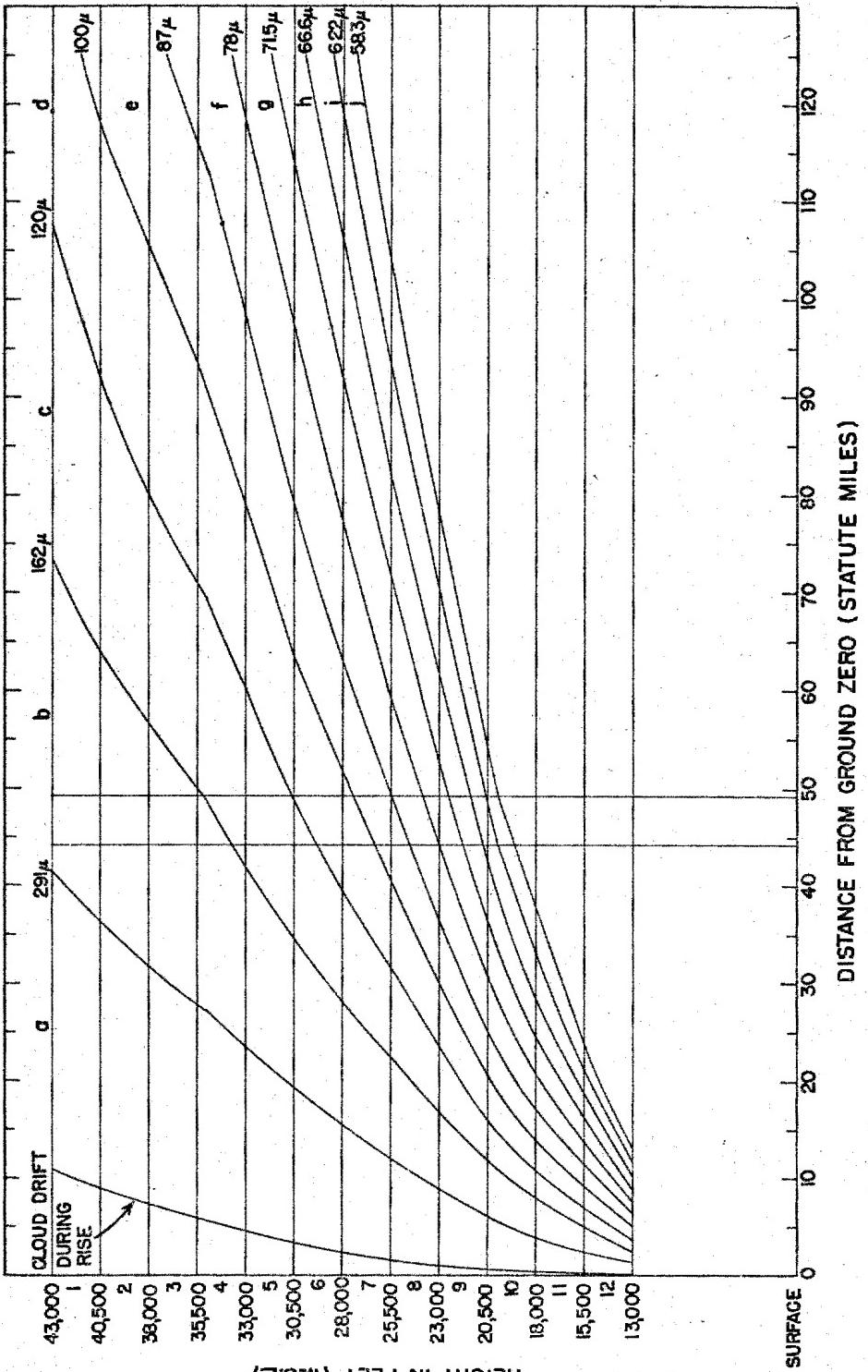


Figure 8  
Working Graph for Computing Fall-out in a Case of Little Directional Shear, UPHOT-KNOTHOLE-7

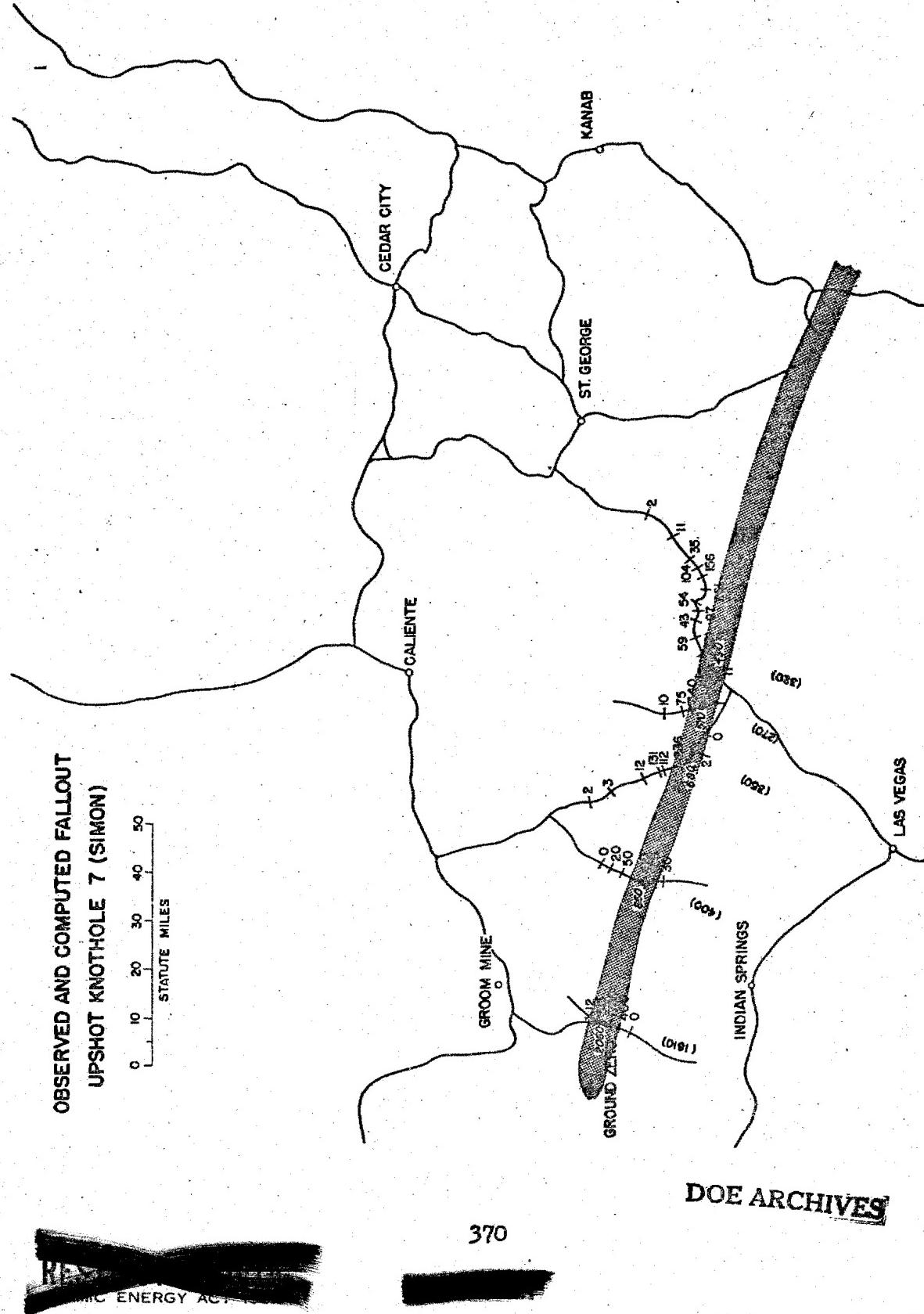
369

DOE ARCHIVES

ATOMIC ENERGY ACT 1954

374

Figure 9



all cases exceed the observed peak values. As a test of our model, however, the observed peak values are not appropriate to use since we have assumed that the fall-out was compressed into a five mile band as shown in the figure. Accordingly, we have integrated the activity along the various roads and have converted to the concentration which would have existed if the cloud had been compressed to a five mile width. These fictitious peaks are shown in parentheses below the observations. It is apparent that in this case our model still gives excessive values but they are generally within a factor of 2 of the observed values. The position of the computed axis of high concentration fits the observed peak values very well.

#### Proposed Procedure for Future Tests

I have discussed the post mortem analysis of the fall-out from the 300-foot tower bursts in previous test series. Now, let us consider how we would use this information in forecasting for a future test.

First of all, unless we had a convincing forecast to the contrary, we would assume that the cloud would rise to 40,000 ft., and that the mushroom would be 15,000 ft. thick. We would assume the amount of debris available for close-in fall-out to be proportional to the area of the fireball intersecting the ground (or we might use some other scaling law if our present investigations indicate that it would work better). This can be estimated from the probable yield and from the tower height. Although in our post mortem investigation, we used trajectories and not merely the winds at the site, the time and effort to prepare such trajectories would not generally be warranted, considering the uncertainty which would occur in forecast winds. Thus, we would base the fall-out plot on the forecast winds at the site only and the height lines would then be straight lines.

DOE ARCHIVES

Figure 10 presents a hypothetical fall-out plot showing considerable directional shear in lower levels, but little directional shear in upper levels. From the lower part of the cloud, where there is considerable lateral spreading by the wind, the fall-out would be determined by the method which we described for the UPSHOT-KNOTHOLE 9 shot. First, we would calculate the size of the various areas, possibly by planimetering, or by some more approximate but quicker method. Then where our assumed cloud lies entirely within a polygon, the ratio of the area of the 5-mile circle to the area of the polygon would yield the fraction of the activity which would fall at a point within the area. Multiplying this fraction by the proper contribution from the model, we get an estimate of the fall-out to be deposited at any point whose circle lies within that polygon. From a grid of these estimated depositions, generally one for the center of each sector, as isoline map should then be prepared.

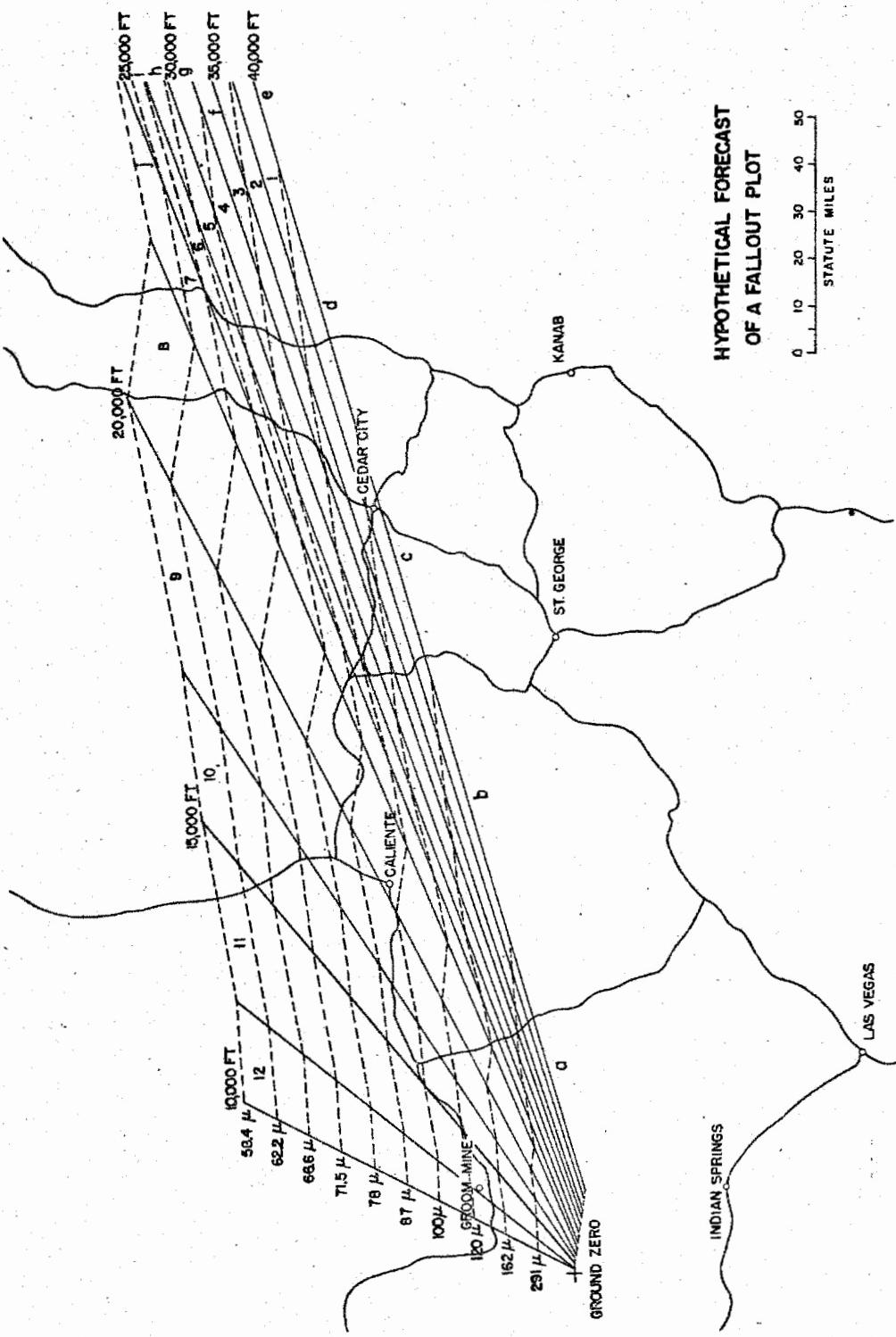


Figure 10

ENERGY ACT 1978

372

371 377

From the higher altitudes of the cloud, where there is little lateral shear, the fall-out can more safely be predicted by the method assuming no directional shear, namely by assuming that the height lines are actually coincident. It must be remembered, of course, that the predicted values are apt to be on the high side unless the initial cloud has a diameter considerably less than five miles. At any rate, we would reduce the upper part of the fall-out plot to a graph similar to that previously shown, but only for the top 17,500 ft. (7 layers). On this graph, we would put columns five miles wide, centered at various distances from the burst site, and we would then determine the approximate fractions of the concentrations in the various layers and particle size ranges. Then, after multiplying the fractions by the appropriate numbers in the model, we would have a series of forecast concentrations in the area to be contaminated by the upper part of the cloud. Now, from the predicted concentrations for both parts of the cloud, an analysis of forecast activity can be made.

As with any forecast, the possibility of a shift in the wind from that forecast and hence a different area of peak concentration must be allowed for as a safety factor and there may also be errors due to incorrect estimates of the cloud height and yield and, of course, there are bound to be errors in the details of the fall-out.

### Conclusions

If anyone expects to find a model which can predict the fall-out from Nevada shots to within a factor of two consistently, we feel he is bound to be disappointed. The errors in the radiological observations, meteorology and doubts about our various assumptions have already been dwelt upon at length.

Our attempt to fit a single model to all the fall-out data, however, uncovered certain interesting features. Two cases were very much different from all the others. Almost any reasonable composite model gives too much fall-out for TUMBLER-SNAPPER 8 and far too little fall-out from UPSHOT-KNOTHOLE 9. If it were not for an attempt to adjust the model to fit UPSHOT-KNOTHOLE 9, all the other cases would verify much better. While there was heavy cloudiness and possibly some rain following UPSHOT-KNOTHOLE 9, we did not feel justified in discarding this case.

DOE ARCHIVES

We have in rough form, maps of our computed and the observed fall-out, in the event that some of you would like to inspect them. The verification of our model by ground monitoring observations leads one to the conclusion that about half of the predictions verify by a factor of two and probably 80 or 90% verify within a factor of three.

**THIS PAGE IS BLANK**

**DOE ARCHIVES**

**374**

OMIC ENERGY ACT

**379**

PREDICTION OF DOSE-RATE AND DOSAGE CONTOURS AS  
FUNCTIONS OF YIELD AND METEOROLOGICAL CONDITIONS,  
USRDL METHOD

PART I

Mr. C. F. Ksanda  
U. S. Naval Radiological Defense Laboratory

Introduction

The Military Evaluations Group at NRDL first got into the business of predicting dose rate and dosage contours somewhat by default. The group was established about four years ago for the main purpose of analyzing the effects of radiological contamination on military operations. It had been assumed that the basic fall-out data would be available elsewhere—but we soon found out it wasn't. We were faced with the dilemma of getting quantitative answers to problems without having even qualitative input data.

Before we could really do very much, we needed at least some kind of rough estimates of expected dose rates and doses for a variety of detonations. At the time, the underwater shot at CROSSROADS was the only significant contaminating shot that had been fired. Also we were concerned with several Navy problems, and the Navy is particularly interested in detonations in and around water. It was natural, then, that the first attempt at prediction was for shallow underwater bursts, and that the predicting method was based on CROSSROADS data. The first approach was to devise a method for scaling the CROSSROADS data to other yields. In principle, this was like the scaling of physical effects—crater formation, for example, where one predicts the influence of yield without necessarily knowing the exact mechanism involved.

At the time of Operation JANGLE the scaling method was extended to land surface and underground detonations. The JANGLE results, for 1 KT, showed considerable areas of significant fall-out downwind beyond the blast damage region. Scaling methods indicated that the areas enclosed by a given dose rate contour would increase more rapidly with yield than the areas of blast damage. So it appeared that the fall-out problem would become increasingly more important with higher operational yield weapons.

DOE ARCHIVES

This scaling process was necessarily quite idealized and was intended only to get from 1 KT to 20-100 KT. No attempt was made to predict twists and distortions in the fall-out patterns which might be caused by wind shear. Instead the main object was to estimate areas contaminated to given levels, and the distances downwind to which these

levels would extend. The area concept is useful when one is considering a target region which is large compared to the fall-out contours. The downwind distance is useful when one wants to estimate the maximum radiation level which might be encountered at any distance from some assumed detonation.

While this kind of information has a number of uses, it was apparent that some kind of quantitative model of the fall-out process was needed, in order to predict dose rates and doses for a wide variety of situations. Some work was started on (the development of) such a model--which I will mention at the end of my talk. After that Mr. McCampbell will describe the recent development of a fall-out model.

Meanwhile, for planning purposes, we have been using the scaling methods--and since they still seem to be useful, I would like to give a brief review of their development.

#### Scaling Method

The general problem required extrapolating a very limited amount of fall-out data to other yields and to other detonation conditions--particularly wind velocities, soil types, and detonation depths. Scaling represents a limited solution; one starts with a known fall-out pattern and extrapolates to other yields.

The method of scaling fall-out contours from one yield to another was developed in the following way. Shortly after the detonation, we visualize a region in the air containing all the radioactive particles. They have just stopped rising, and this region we will call the radioactive cloud. In order to scale fall-out patterns from one yield to another, we make five basic assumptions about this cloud and the particles in it.

DOE ARCHIVES

First, for equivalent scaled depths of detonation, the radioactive clouds from different weapon yields are assumed to be geometrically similar. Both the dimensions and heights of corresponding volumes are assumed to vary as the yield to some power  $\alpha$ .

Second, the total activity is assumed to vary directly with the yield.

Third, for a given soil, the size distribution of active particles is independent of yield.

Fourth, the relative spatial distribution of particles of any given size within the cloud is independent of yield.

Fifth, the rate of fall, for particles of a given size, is independent of the yield.

These assumptions are undoubtedly idealizations of the actual facts. Later, some known departures of the facts from the assumptions will be mentioned. It appears, however, if the scaling is not done over too large a range of yields, these assumptions should lead to reasonable results.

One further assumption is made when field dose rate patterns are to be scaled, rather than activity concentrations on the ground—that the dose rate at any point is directly proportional to the activity per unit area (on the ground).

The scaling method follows directly from these assumptions. It can be stated in this way:

If all linear dimensions of a contour to be scaled are increased as the yield ratio to the power  $\alpha$ , then the associated dose rate will vary as the yield ratio to the power  $1 - 2\alpha$ .

The best value to assign to the cloud scaling exponent  $\alpha$  is somewhat questionable. However, the numerical results are not particularly sensitive to the exact value chosen; and in most calculations we have used a value of  $1/3$ . In this case, the scaling method simply requires that all linear dimensions of the contours, as well as the associates dose rates, be scaled as the cube root of the yield ratio.

The restrictions on this scaling method are that it applies only for: equal wind speeds—or if shear is appreciable, equal wind velocities at equivalent scaled heights; equivalent scaled depths of detonation; and the same soil.

DOE ARCHIVES

We have tried to make some tentative estimates of the influence of detonation conditions on the fall-out patterns for a given yield.

Wind: quantitatively, tends to elongate ideally-circular patterns for no wind. HE data indicates areas of contours of given fall-out concentration quite insensitive to wind speeds; this generalization, together with an empirical estimate of the variation in downwind distance with wind speed, was used to control the wind correction.

Soil type: expected to influence size distribution of radioactive particles formed, and hence the resultant contamination patterns.

Examination of radioactive particles at JANGLE indicates they are formed from fused soil. It appears therefore that HE tests, where the dust fall-out consists of original soil particles, cannot be used to estimate influence of soil type.

Depth: provided cloud dimensions can be estimated as a function of depth of detonation, it is possible to make extrapolations by arguments similar to those used to develop the method for scaling with yield. The main difference is that in the basic assumptions, the total amount of activity is constant, and the cloud heights and dimensions are assumed to vary in some way with depth. If the ratio of cloud dimensions for two depths is denoted by  $\mu$ , then it can be inferred that the dose rate will vary as  $1/\mu^2$  at distances scaled as  $\mu$ .

#### Departures from Idealized Scaling

The scaling method was first applied, for lack of any other data, to dust fall-out measurements from high explosive tests at Dugway Proving Grounds. Dust concentration contours from 320 pound charges were scaled to those from charges as great as 320,000 pounds--or over a charge weight ratio of one thousand. Generally the results were fairly good, the scaled areas being off in the worst case by a factor of less than three.

It is now possible to make a comparison between the JANGLE surface shot and CASTLE Bravo. In this case the yield ratio is about 10,000. The nature of the soil over which the detonations occurred is, of course, quite different, as were the meteorological conditions.

For the 2000 r/hr at 1 hour contour, the Bravo downwind distance is about twice the scaled JANGLE distance. For the 100 r/hr contour, the observed and scaled downwind distances are equal. In all cases, the Bravo contours are considerably broader than the scaled JANGLE contours--by an amount which depends on which estimate of the Bravo contours we look at. On the basis of AFSWP-507 and the preliminary report of Project 2.5a, the CASTLE contours are about 2 to 3 times as wide as the scaled JANGLE contours. The area enclosed by the contours are roughly 4 to 3 times as great as the scaled JANGLE areas. On the basis of the revised 2.5a contours, the discrepancy is considerably greater. The 2000 r/hr contour is about 9 times as wide as the scaled JANGLE value; and the 100 r hr contour about 5 times as wide.

Two possible reasons for discrepancies between scaled JANGLE and Bravo results have already been mentioned: the difference in soil and in meteorological conditions, especially the wind structure. These differences really represent a failure of the tests of conform to the



necessary conditions. There are, however, two additional reasons (at least) where the basic assumptions used to derive the scaling method are not exactly correct. First, the rates of fall of the particles are not entirely independent of yield. The particles fall faster at higher elevations; hence as the yield is increased and the cloud height increases, the average rate of fall for a particle of given size increases somewhat. Second, the clouds are not geometrically similar. Empirical evidence shows a progressive flattening of the cloud with increasing yield. Thus the 1 KT JANGLE cloud was nearly spherical, while the width/thickness ratio of the Bravo cloud was close to 7:1. Scaling measurements as the cube root of the yield, the height of the center of the Bravo cloud corresponds almost exactly to the scaled JANGLE height. However, the depth of the Bravo cloud is only about one-half the scaled JANGLE value, while the width is about 3 times as great as the scaled JANGLE width.

#### Refined Model

Some approximate corrections could be made to account for the variation in cloud shape and rates of fall of particles, in order to improve the scaling method. But the only way to predict actual fall-out patterns for a variety of conditions is by way of a dynamic model of the fall-out process.

Exploratory work on such a model was begun nearly two years ago, to see what kind of agreement with the JANGLE data might be obtained. The first attempt assumed a spherical cloud, uniform wind velocity, and contained a very rough estimate of the distribution of activity with particle size. Somewhat surprisingly, the dose rates predicted from this model looked fairly much like the observed values.

Now it is apparent that any model of the kind that has been discussed here contains quite a few parameters, to which some numbers have been assigned. These parameters are closely related to the things which were mentioned earlier in the five basic assumptions used to develop the scaling method.

DOE ARCHIVES

First, the total activity released must be known—a relatively straightforward calculation.

Second, the cloud height and dimensions must be known. Generally these can be estimated from photographs and extrapolated with the help of some theories--although there is no guarantee that the radioactive cloud is actually coincident with the visible cloud.

Third, activity in the cloud must be known as a function of the particle size.

Fourth, distribution of the particles in space must be known.

Fifth, rates of fall of the particles must be known.

Regarding these last three points, there is some controversy.

Rates of fall depend on the properties of the atmosphere as well as those of the particles. Actually, particle properties vary considerably—those from Nevada being sometimes spherical, sometimes very irregular, and showing density variations of about a factor of 2, mainly because of varying amounts of included air bubbles. In our numerical work, we have assumed that all the particles are irregular and of uniform density.

Distribution in space is clearly not well known. Here we have assumed that practically all the activity is in the mushroom cloud and is uniformly distributed.

Finally, the relation of activity to particle size is not well known either. Rather than try to guess at this, or adjust the distribution to give the best agreement between the predictions of the model and experimental data, we tried to make an independent evaluation from some particle studies at JANGLE.

A fairly large number of fall-out samples were separated into various size fractions at NRDL, and the relative activity of each size fraction was measured. The data were not sufficient to draw activity concentration contours for each size fraction, which is what we would have liked, but it was possible, for the underground shot, to draw curves of activity concentration as a function of distance in the down-wind direction. By integrating these curves, it was then possible to estimate the percentage of activity in each size range which was initially present in a unit width slice of the cloud.

This distribution turned out to be a normal distribution with respect to the logarithm of the particle diameters--and this is the distribution we are using in our numerical calculations.

DOE ARCHIVES

This gives some of the background of the development of our fall-out model, which Mr. McCampbell will describe.

## PART II

Mr. James M. McCampbell  
U. S. Naval Radiological Defense Laboratory

During this Symposium, it has been amply demonstrated that the problem of devising a mathematical model of fall-out consists of two major parts; first, tracing the trajectories of the fall-out particles to determine where they land, and second, summing all the activity that lands at any given point on the ground. These two basic ideas will be developed in their mathematical form.

Concerning the first part of the problem, we consider a particle falling through the atmosphere with a velocity  $u$  and drifting in a wind of velocity  $v$  as shown in Figure 1. During a small interval of time the particle drifts along the vector  $dD$  whose components  $dx, dy$ , and  $dz$  refer to a convenient coordinate system. The magnitude of the time interval equals the distance the particle travels divided by its rate.

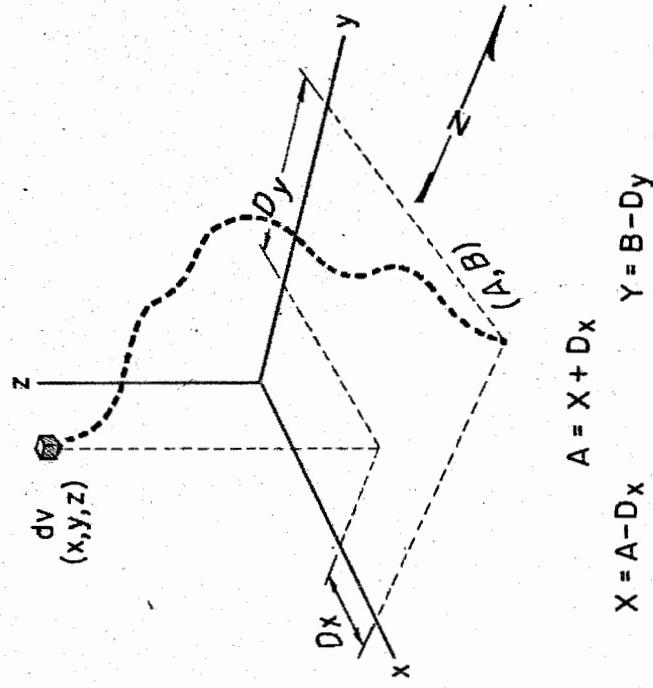
In the vertical direction,  $dt = \frac{dz}{u}$ . The distance traveled in the direction of the wind is  $d\rho = v dt$  and by substitution, equals  $v \frac{dz}{u}$ . But  $dx$  is a component of  $d\rho$ , hence  $dx = d\rho \sin \theta$  where  $\theta$  is the angle between the  $y$ -axis and the direction toward which the wind is blowing. Theta is  $180^\circ$  from the conventional wind angle.

As the particle traverses successive layers of the atmosphere, its path is defined by the sum of the vectors  $dD$ . Therefore, the total drift in the  $x$  direction is the sum of the  $x$  components; that is,  $D_x$  equals the integral from the surface to the altitude of origin of  $v \sin \theta$  divided by  $u$ . A similar expression involving  $\cos \theta$  will of course give the  $y$  component of the total drift. The parentheses indicate that the wind speed and direction vary with altitude and that the particle falling rate is also a function of the altitude. In addition, the falling speed of the particle is a function of its size,  $l$ .

A convenient coordinate system is the one with the origin at ground zero and the  $y$ -axis directed north as in Figure 2. Consider particles of a given size originating in the infinitesimal volume  $dV$  at the point  $(x, y, z)$ . These particles drift along some irregular path indicated by the heavy dotted line, and land at the point  $(A, B)$ . The final displacement of the particles from the origin is the sum of their initial displacement in the cloud and the displacement they experience while drifting with the wind. The  $x$ -component of the final displacement is  $A$ , and it equals  $x$  plus  $D_x$ . Transposing the terms gives

$$x = A - D_x \text{ and by a similar derivation } y = B - D_y$$

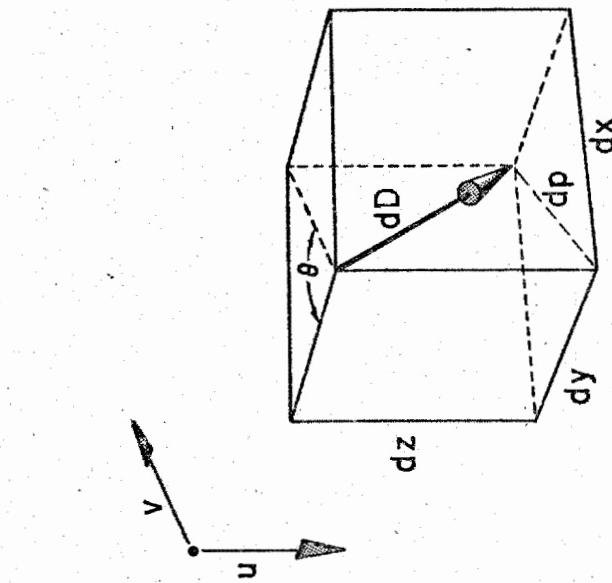
Figure 2



$$A = X + D_x \quad Y = B - D_y$$

$$X = A - D_x \quad Y = D_y$$

Figure 1



$$dt = \frac{dz}{u}$$

$$dp = v dt = v \frac{dz}{u}$$

$$dx = dp \sin \theta = v \frac{dz}{u} \sin \theta$$

$$D_x(z, l) = \int_0^z \frac{v(z) \sin \theta(z)}{u(z, l)} dz$$

DOE ARCHIVES

382

ENERGY ACT 198

387

391

Now what is the meaning of these two equations? For a given point (A,B) and a given wind structure, any value of z determines Dx and Dy, and in turn determines a corresponding x and y. Thus, these equations are the parametric expression of a curve in space. It is along this curve that particles of a given size can possibly originate, traverse the wind structure, and land at the point (A,B). Mathematically, this locus of origins has an infinite extent, but physically, only a segment has significance; that is, that segment which lies within the cloud. We must therefore define the boundary of the cloud.

As shown in Figure 3, an ellipsoidal cloud is assumed. Its semi-axes are a and b and its center is directly above the origin at the altitude H. Such a model will accomodate the very flat clouds from high yield weapons, and will degenerate into a sphere for clouds from low yield weapons. The locus of origins is shown penetrating the cloud at the altitudes  $z_1$  and  $z_2$ . The values for  $z_1$  and  $z_2$  are different for each particle size. The points of intersection are found by the simultaneous solution of the equation of the curve and the equation of the cloud boundary. For a spheriod, the latter is

$$\left[ \frac{Z-H}{a} \right]^2 + \left[ \frac{X}{b} \right]^2 + \left[ \frac{Y}{b} \right]^2 = 1$$

Our equations for the curve were in terms of x and y, so substitution gives

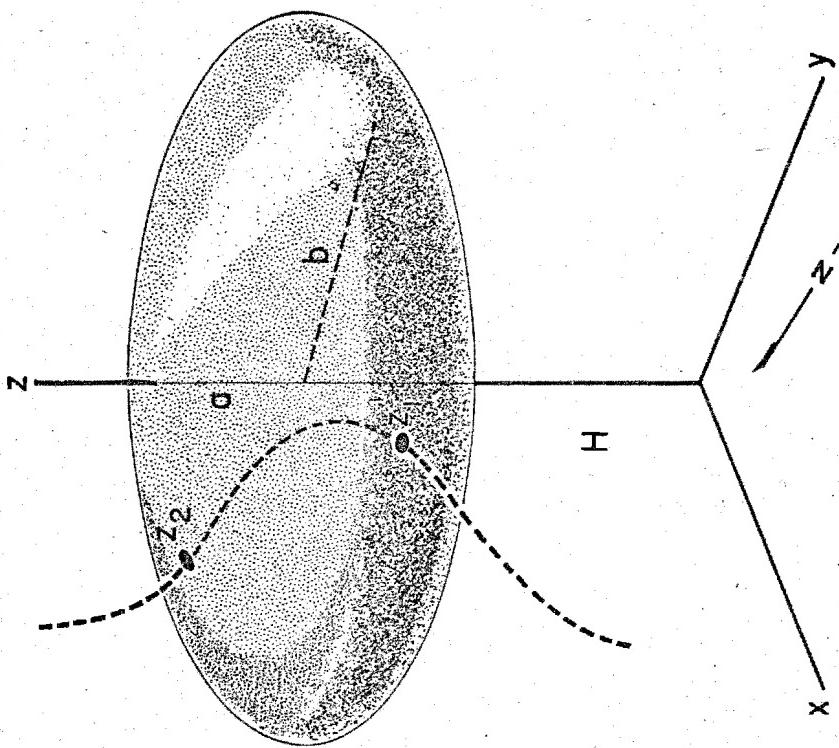
$$\left[ \frac{Z-H}{a} \right]^2 + \left[ \frac{A-Dx}{b} \right]^2 + \left[ \frac{B-Dy}{b} \right]^2 = 1$$

DOE ARCHIVES

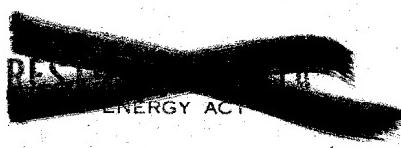
The values of  $z_1$  and  $z_2$  are implicitly given by the last equation. Any point in space which satisfies this equation must lie on the curve and also on the cloud surface; it is therefore a point of intersection. These points may occur in real pairs, imaginary pairs, or singly. Real pairs indicate penetration of the cloud, imaginary pairs indicate that the curve does not touch the cloud, and single points indicate that the curve is tangent to the cloud. The physical meaning of the imaginary case is that particles corresponding to that curve can not reach the point in question. The curve may penetrate the cloud, fold back and penetrate it again; and perhaps again. However, for most wind conditions, the simple case as shown in the figure will probably prevail. Whether or not it does is immaterial—as will be shown later.

Because the cloud height, shape, and size vary with the yield, the cloud parameters H, a, and b will take on values depending upon the yield. Therefore, substituting emperical or theoretical relations between these parameters and the yield would make the last equation applicable for all yields.





384



$$n = P\phi(l)dl \quad dx dy dz \quad \epsilon(l)$$

$$\alpha = P\phi(l)dl \quad dx dy dz \quad \epsilon(l)$$

$$da_l = \frac{P\phi(l)dl \quad dx dy dz \quad \epsilon(l)}{dx dy}$$

Figure 4

$$a_l = P\phi(l)dl \epsilon(l) \int_{z_l}^{z_2} dz$$

$$A(A, B) = \int_{-\infty}^{\infty} a_l = \int_{-\infty}^{\infty} P\phi(l)\epsilon(l) [z_2(l) - z_1(l)] dl$$

$$R(x, y) = K \int_{-\infty}^{\infty} P\phi(l)\epsilon(l) [z_2(l) - z_1(l)] dl$$

Figure 3

Figure 5

389

~~SECRET~~

We must now turn our attention to the second part of the problem, that is, to summing the activity that lands at a given point. In Figure 4,  $P$  is the number of particles per unit volume in the cloud. If  $\phi(l)$  is the size distribution of the particles then  $P\phi(l)dl$  is the number of particles per unit volume of sizes  $l$  to  $l + dl$ . Multiplying by  $dxdydz$  gives the number of particles of that size in the volume  $dV$ .

Let  $\xi(l)$  denote the radioactivity of a particle of size  $l$ , assuming that the radioactivity of particles is in some way related to their size. Then multiplying by  $\xi(l)$  gives the radioactivity of the particles of size  $l$  in  $dV$ . But it was previously shown that these particles were deposited at the point  $(A, B)$ . Assuming that there is no dispersion of the particles in their flight, they will be spread over an infinitesimal area  $dxdy$ . Therefore, the activity per unit area is found by dividing by  $dxdy$  as in the last equation in the figure. It must be pointed out that  $da_1$  is a second order infinitesimal; the two remaining differentials are  $dl$  and  $dz$ . It is apparent that subsequent integration must be performed over the altitudes and the particle sizes.

For particles of each size, the integration with respect to  $z$  must be confined to the applicable altitudes. In Figure 5 we see that  $a_1$ , the activity due to particles of size  $l$ , is found by summing over the range  $z_1$  to  $z_2$ . If our curve of origins had penetrated the cloud twice, we would add another term with limits  $z_3$  and  $z_4$ . Having integrated with respect to altitude, we must now sum over the particle sizes as shown in the middle equation, where the previous integration has been carried out.

Finally, the radiation field produced above a contaminated surface is proportional to the activity on the surface. Therefore, the radiation field  $R$  is obtained by multiplying the activity per unit area by the proportionality factor  $K$ . The value of  $K$  includes the effect of shielding by rough terrain, the mean energy of the gamma rays, and the height above the surface that the radiation intensity is desired. It should be pointed out that the product  $\phi(l)\xi(l)$  is the activity distribution. It is sufficient to know the product of the two functions; they need not be known separately.

**DOE ARCHIVES**

It turns out that solving the problem in this form is virtually impossible. However, it can be readily solved by taking finite increments of particle size and altitude. When formulated in terms of finite intervals, it is ideally suited to machine computation. A computational scheme based on this theory is currently being used in computing fall-out patterns on a Univac. The machine work is being done by the Applied Mathematics Laboratory of the Bureau of Ships.



~~SECRET~~

You will notice that no mention has been made of a very important variable, namely, the time elapsed since the explosion. This variable enters the problem in four specific ways:

In the decay of radioactivity,

In the build-up of the activity at any point and the consequent growth of the fall-out pattern,

In the changes of wind structure that occur during the fall-out process, and finally,

In the change of the mean gamma energy with time.

Recent extensions of the present theory permit a machine solution including the variable time in all four aspects. The output table from the machine could provide the following information:

The coordinates of the point in question,

The radiation intensity at the point at any time,

The dosage accumulated at the point up to any time,

The time in question,

The time that fall-out began to arrive at the point, and,

The time that fall-out ceased at the point.

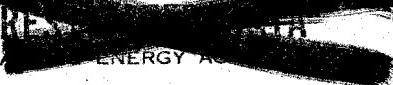
If the preliminary computations now being made confirm the model, there will then be available a useful tool for studying fall-out problems. In particular, investigations could be carried out in such subjects as the:

Scaling of radiation fields,

DOE ARCHIVES

The effect of different wind shears, and,

The effect of different particle and activity distributions.



PREDICTION OF DOSE-RATE AND DOSAGE CONTOURS AS  
FUNCTIONS OF YIELD AND METEOROLOGICAL CONDITIONS;  
PREDICTED CONTOURS FOR THE CASTLE DETONATIONS

E. A. Schuert

U. S. Naval Radiological Defense Laboratory

At Operation CASTLE Project 2.5a had as a primary responsibility the definition of the fall-cut patterns resulting from the 6 detonations. A great deal of analytical work has been expended in the reconstruction of the contours that defined the primary fall-cut pattern resulting from Shot 1. Since the analysis that was employed combined experimental data with particle trajectory evaluations, much of the work is similar to the model developments presented here this week. I will discuss the assumptions made and the techniques employed in this development as well as the relevant experimental data obtained and how this data fits the resulting fall-out contours.

The data available after Shot 1 included the measured fall-out in and about the Bikini lagoon, the negative data from the free floating sea stations west of the atoll, the outer island survey measurements made by Dr. Scoville's team, the observed time of arrival of fall-out at Bikini and on the outer atolls, as well as the measured radioactive particle size, particle density, and particle configuration data for both the Bikini area and the outer islands. There was also data obtained on the time of arrival of fall-out particulate at Bikini.

An attempt to reconstruct the fall-out contours solely from the measured gamma field data offered the analyst a great deal of latitude, for there existed no information that would control the lateral width of the fall-out pattern. Because of this problem an attempt was made to define the area of fall-out by use of particle trajectory analysis. Since we were primarily interested in singularly defining the Shot 1 pattern, data from this detonation was used in defining the trajectory parameters. The parameters necessary to apply the trajectory analysis were:

DOE ARCHIVES

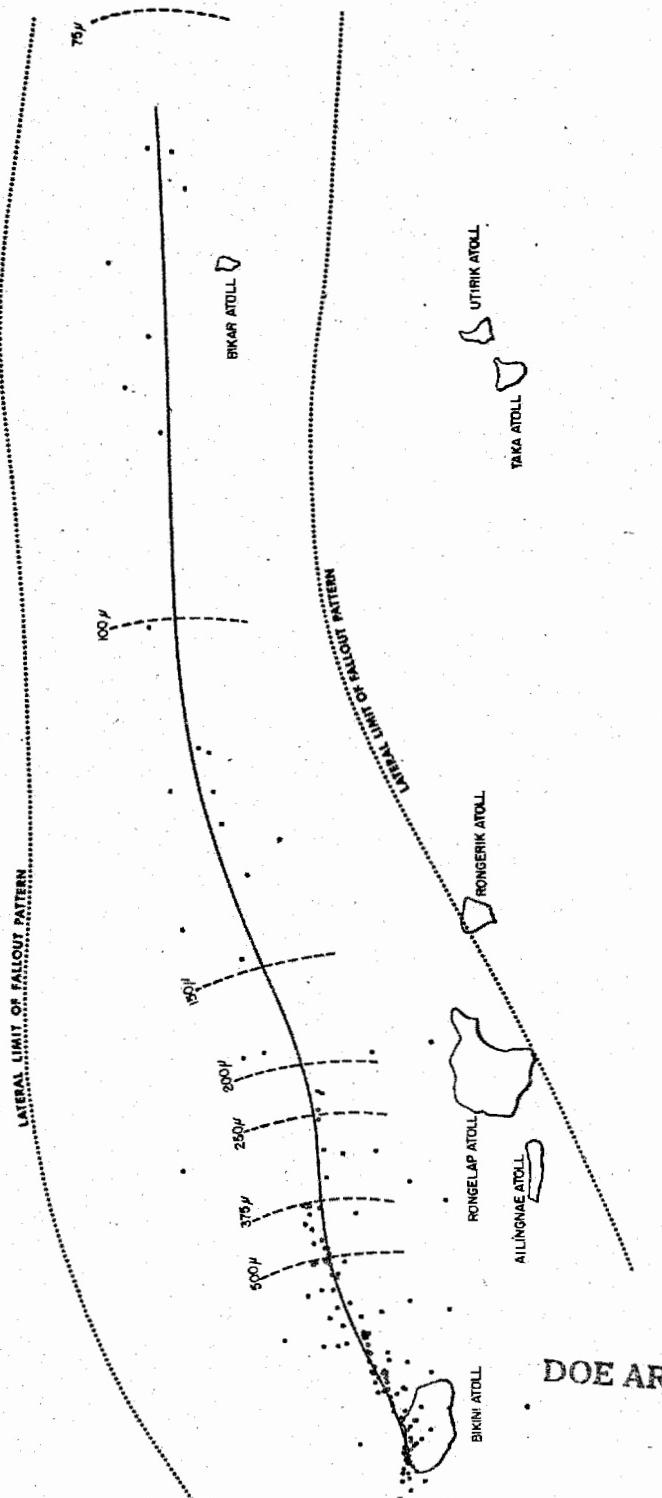
A source of activity.

The initial spacial distribution of the source material.

A mechanism for distributing the source material.

Some of the above parameters were supported by experimental data; others required basic assumptions. The assumed parameters were:





RE  
ENERGY ACT 1980

388

393

**Figure 1**  
General Area of Fall-out, CASTLE-Bravo

The spacial distribution of the source material was described by the visible dimensions of the cloud and stem at time 0 + 10 minutes. This assumption was further simplified by describing the Shot 1 stem and cloud as cylinders.

The distribution of the source material was homogeneous throughout the cloud and stem with all particle sizes at all locations.

The particle trajectories could be defined by their rate of fall under the influence of the existing wind speeds and directions.

The experimental data obtained from analysis of the fall-out material as well as other physical measurements was used as follows:

The measured physical characteristics of the particles were used to determine their rate of fall and to describe the particle size distribution that was actively contributing to the primary fall-out.

The cloud dimensions as measured by cloud photography were used to describe the physical dimensions of the source.

The observed meteorological data both on windspeed and direction and temperature distribution as obtained by the Task Force weather central were used to calculate the particle trajectories.

The trajectory analysis was then defined on both assumed and measured parameters.

In determining the rate of fall of the particles, a size range of from  $2000\mu$  to  $25\mu$  diameter was used. The shape of the particles had been experimentally determined to be almost entirely irregular in shape. The apparent density of 70 particles was measured resulting in a mean density of  $2.36 \text{ g/cm}^3$  with a standard deviation of 9 per cent. The air temperature used in determining the viscosity of the atmosphere with respect to height was taken from that measured at Bikini just prior to shot time. After determining the falling speeds of the particles over the stated size range using the above experimentally determined parameters and applying aerodynamic particle settling rates, a table of average falling speeds was constructed for each 5000 foot increment of altitude to a height of 100,000 feet.

DOE ARCHIVES

With the above falling rates, 231 particle trajectories were computed. These computations were done manually, for at that time application to machine analysis was not available. Particle sizes of 2000, 1500, 1000, 750, 500, 375, 250, 200, 150, 100, 75, 50, and  $25\mu$  in diameter were placed at 5000 foot intervals to an elevation of 100,000 feet and their intersections with the surface of the earth were determined by following each particle as affected by the wind structure. In constructing these trajectories the changes in the wind pattern both with respect to time and location of the particles were

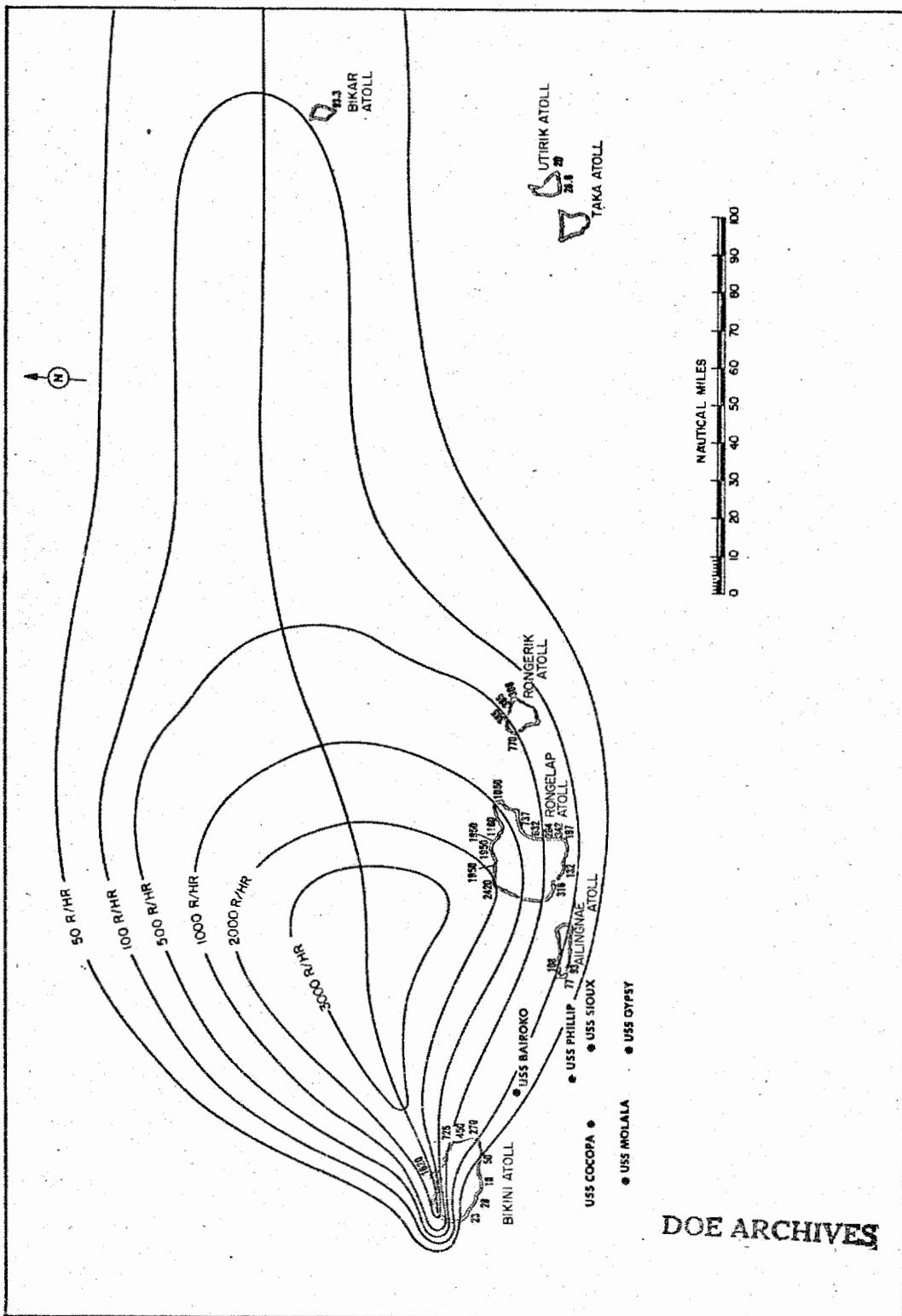


Figure 2  
Fall-out Contours, CASTLE-Bravo

395

considered. This analysis resulted in the plot shown in Figure 1. Here there is a picture of the general area of fall-out based on the stated assumptions. The outer dashed line was constructed by expanding each point by the cloud or stem radius from which the particle originated. The dimensions used were 66 nautical miles cloud diameter and 6.6 nautical miles stem diameter, with the cloud base at 60,000 feet. The dashed arcs show the maximum distance the stated particle size could travel. Because of the wind structure existing at shot time the area of fall-out had a rather well defined axis along which the larger particles were closely grouped. This axis is shown by the heavy solid line in the figure. Because this axis did not change noticeably by varying the particle size distribution, it was reasonable to represent it as an axis of symmetry of the fall-out pattern.

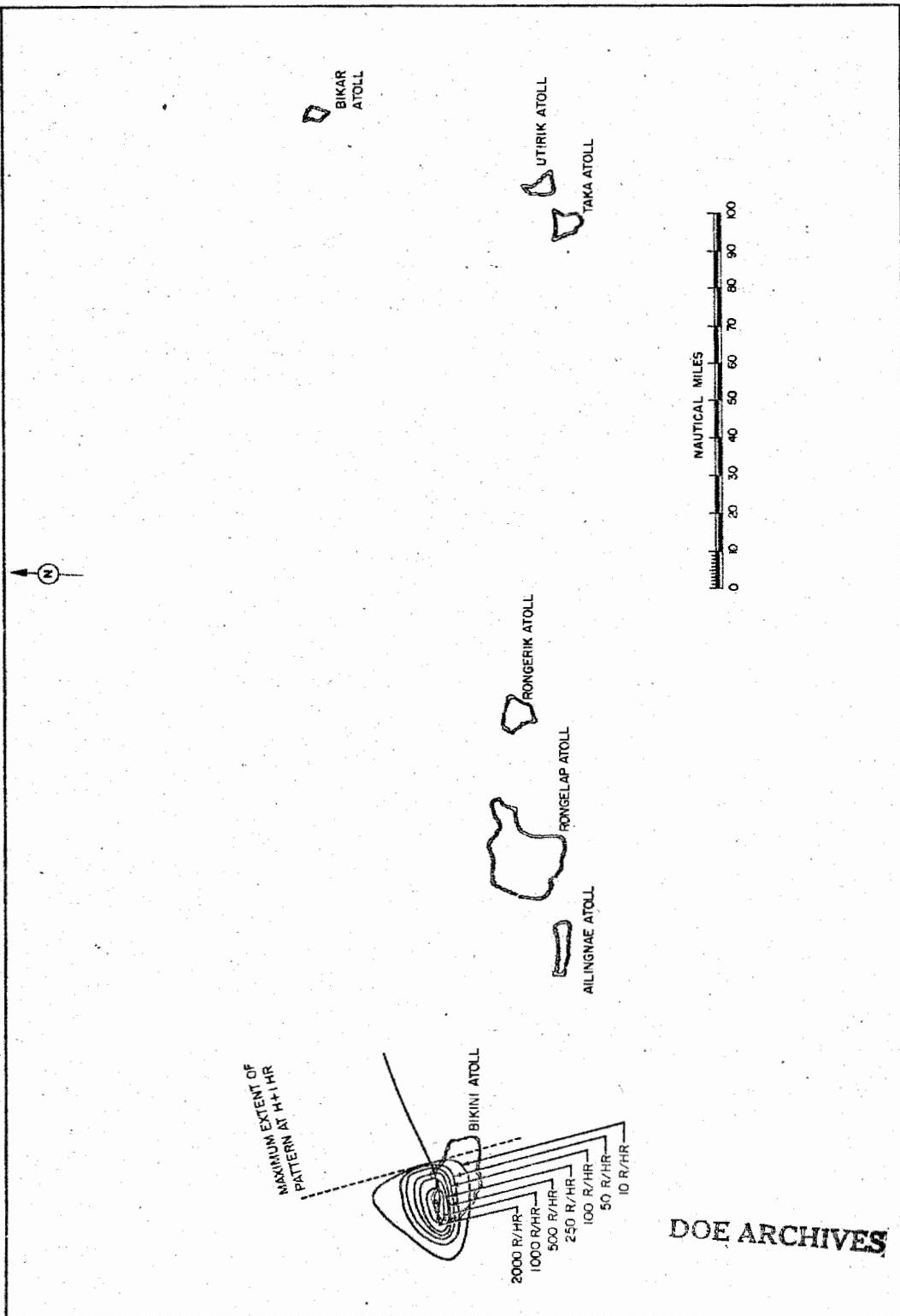
The reconstruction of the fall-out contours for Shot 1 were then made, based solely on the directive axis of fall-out as determined above and the measured gamma field readings. The analysis resulted in the fall-out contours as shown in Figure 2. These contours show gamma activity in r/hr at 1 hr.

The most significant result of this analysis was the unusual width of the fall-out pattern. For comparison, the surface Jangle fall-out pattern was scaled to 15 megatons using the cube root relationship. The most significant observation was again the great difference in the configuration of the two patterns. A reason for this discrepancy was discussed by Mr. McCampbell earlier this morning.

This analysis based on a fall-out axis and the measured gamma fields, created a pattern that fits well with the lateral limit of the pattern as defined by the expansion of the trajectory points as previously shown in Figure 1.

Two material balances were made on the reconstructed pattern. The first material balance based on calculated parameters as described by Dr. Werner earlier this week resulted in from 50 to 70 per cent of the device accounted for within the 100 r/hr at 1 hr. contour. The second analysis based on extrapolation of a radio-chemical analysis of the fall-out material collected at one location, indicated 30 per cent of the device accounted for within the 100 r/hr at 1 hr. contour.

In order to show pictorially the growth of the fall-out pattern with time and the actual existing levels of activity, I have prepared five figures (Figures 3-7), showing the existing gamma field at 1, 3, 6, 12 and 18 hours.



AMERICAN ENERGY

392

401

397

Figure 3  
H+1 Hour Fall-out Contours, CASTLE-Bravo

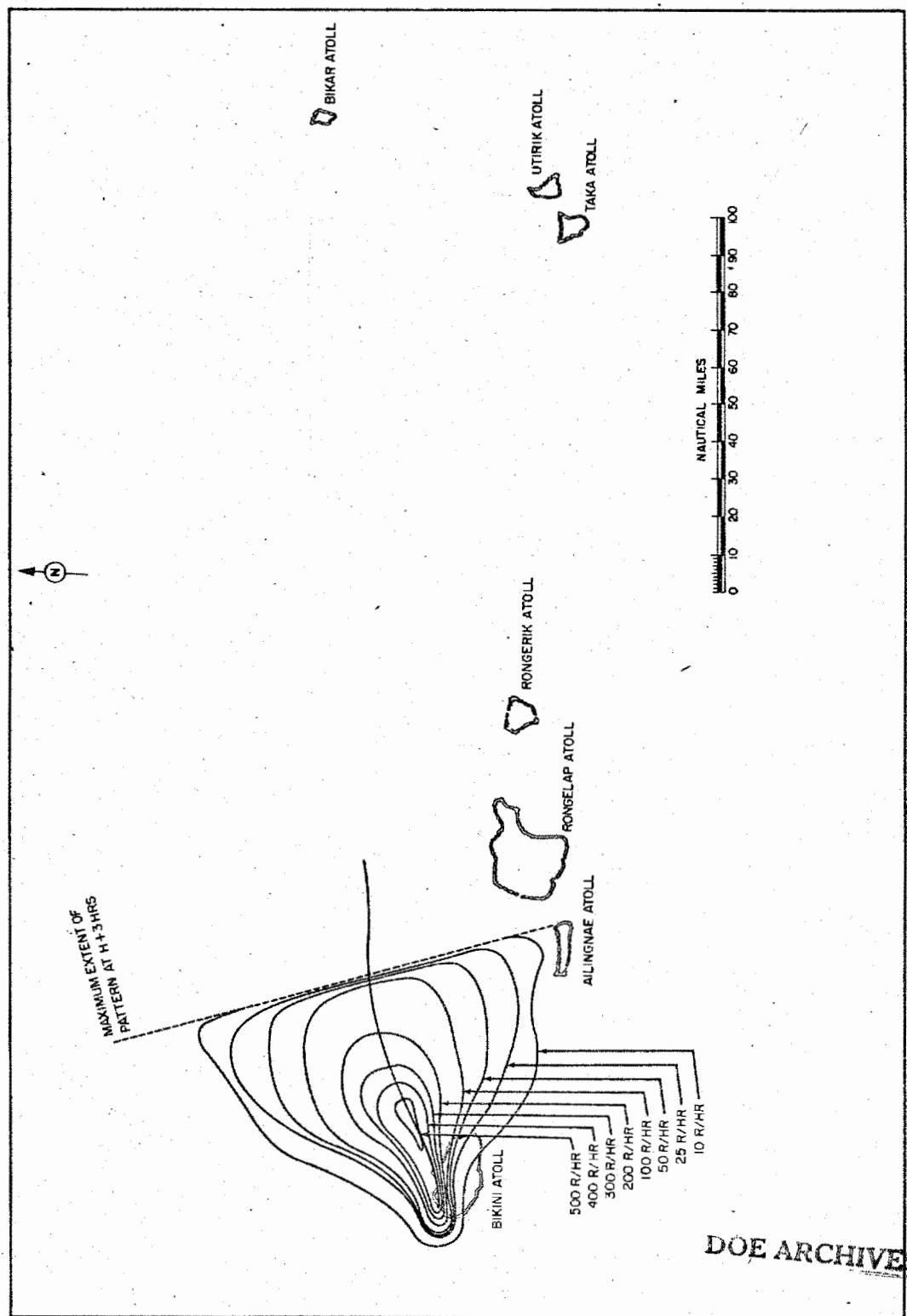
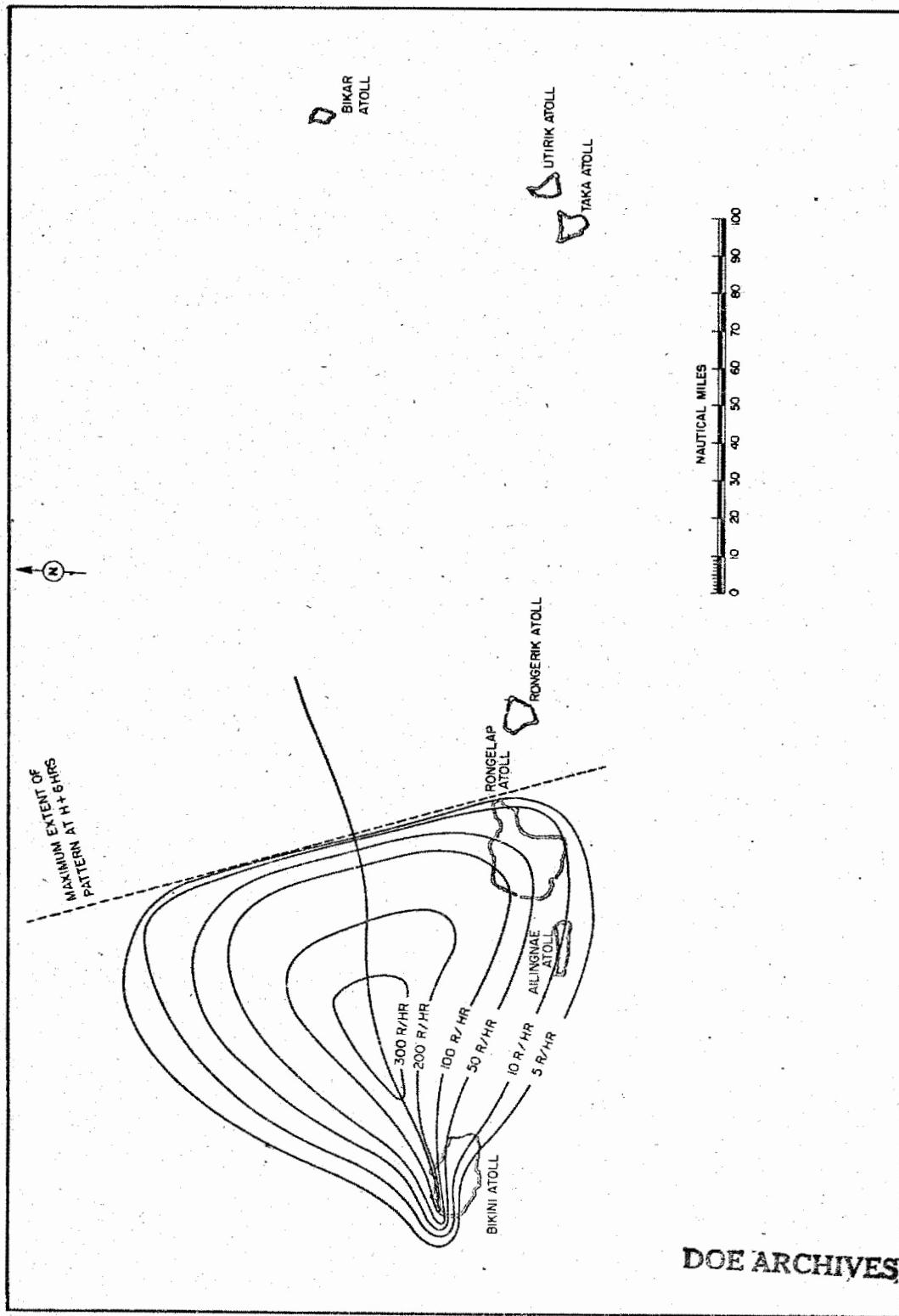


Figure 4  
 H+3 Hours Fall-out Contours, CASTLE-Bravo

398



H+6 Hours Fall-out Contours, CASTLE-Bravo

Figure 5

~~RESTRICTED~~  
NUCLEAR ENERGY ASSOCIATES

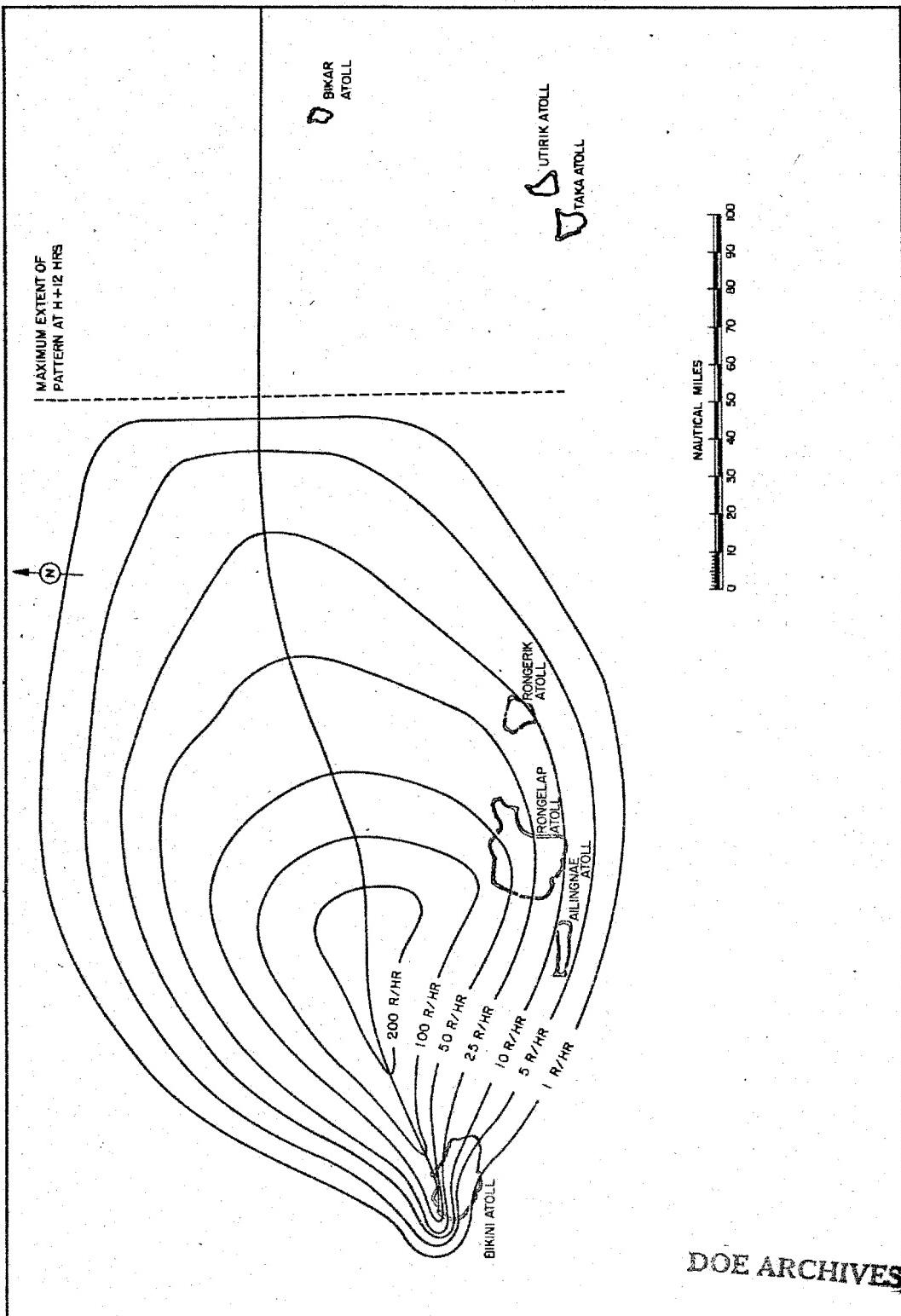


Figure 6  
H+12 Hours Fall-out Contours, CASTLE-Bravo

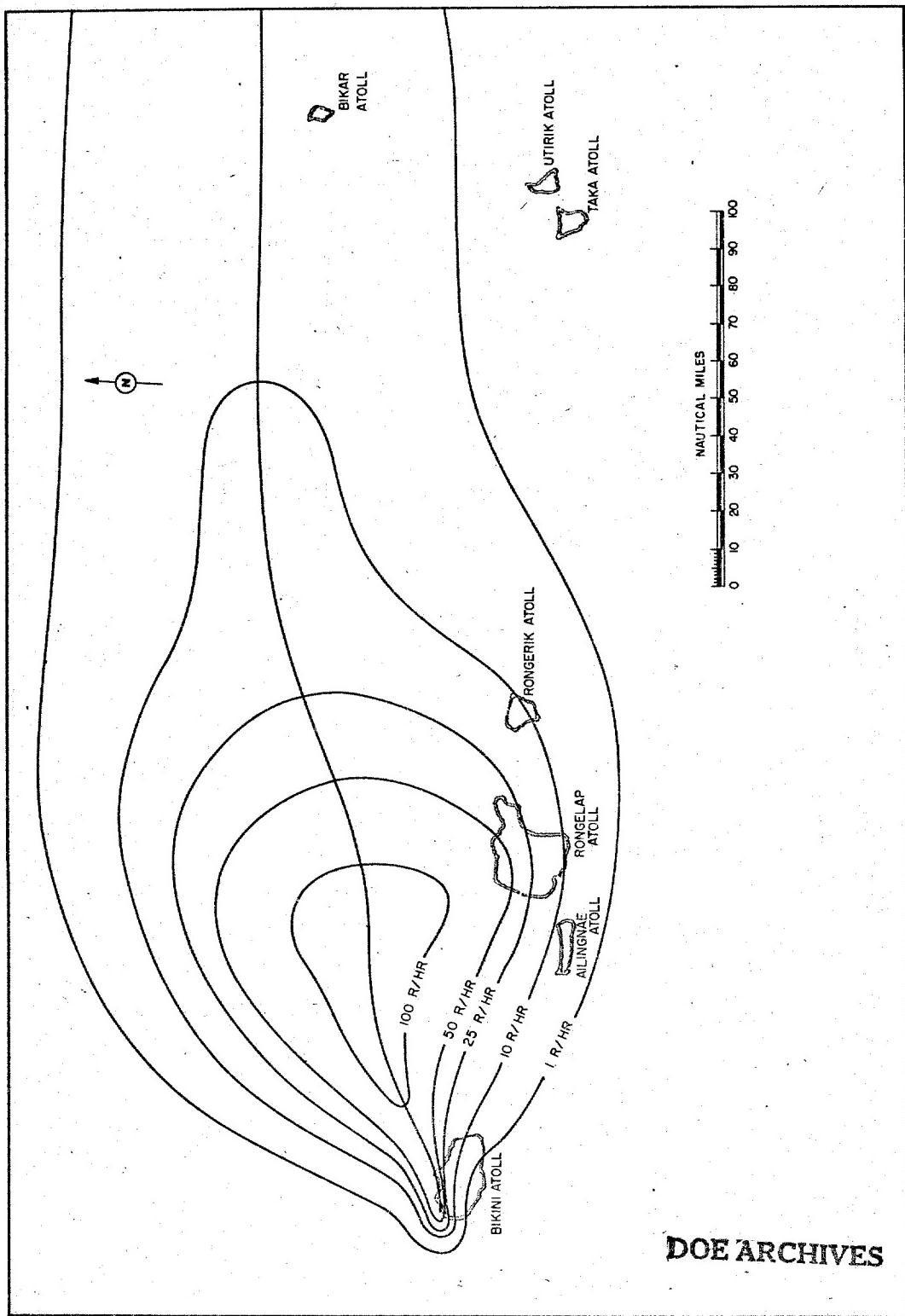


Figure 7  
 H418 Hours Fall-out Contours, CASTLE-Bravo

RE  
 ENERGY ACT

396

401

SECRET

I would like to discuss the experimental data collected that is relevant to the analysis of the fall-out based on trajectory evaluations. Figure 8 shows the computed time of arrival of fall-out based on the 231 trajectories evaluated. It indicates an arrival time of 8.25 hours at Rogerik where the measured time of arrival was 8 hours. It shows an arrival time of 15.4 hours at a distance of 302 nautical miles when the observed time was 18 hours. The analysis appears to satisfy the time of arrival parameter very well.

Figure 9 shows the particle size distribution obtained experimentally from fall-out at Bikini atoll. This is a histogram of some 7000 radioactive particles. The trajectory analysis agrees well with deposition over this size range at Bikini atoll. The data on these particles analyzed with respect to their time of arrival shows positive evidence that of the particles over  $500\mu$  in diameter 50 to 90 per cent had to come from above 60,000 feet.

Figure 10 shows the measured particle size distribution of the fall-out that arrived at the outer islands of Alinginaie, Rongelap and Utirik. The computed size distribution at Rongelap atoll based on the trajectory analysis indicates that particles from 50 to  $150\mu$  diameter would arrive at this location and the  $250\mu$  particles would fall just 10 nautical miles north of the atoll. The measured distribution shows that only 4 particles arrived at Rongelap with diameters larger than  $200\mu$ .

The analysis also indicates no particles above  $75\mu$  diameter could arrive at a distance of 302 nautical miles from ground zero where the measured distribution at Utirik had a geometric mean diameter of  $45\mu$  with only 3 particles being over  $100\mu$  in diameter.

The agreement here is surprisingly good and certainly suggestive of continuation of work along these lines. The major discrepancy in the analysis is the inability to account for fall-out at Utirik. This may be resolved by the use of Dr. Palmers analysis of the wind data existing at and after shot time.

In conclusion, it may be well worth discussing the fields in which serious work should be added both from an experimental as well as theoretical viewpoint. A portion of this work necessary to a more complete understanding of the phenomenology may be listed as follows:

The relation of activity to particle size appears necessary to most model evaluations. At this time data is seriously lacking in this field.

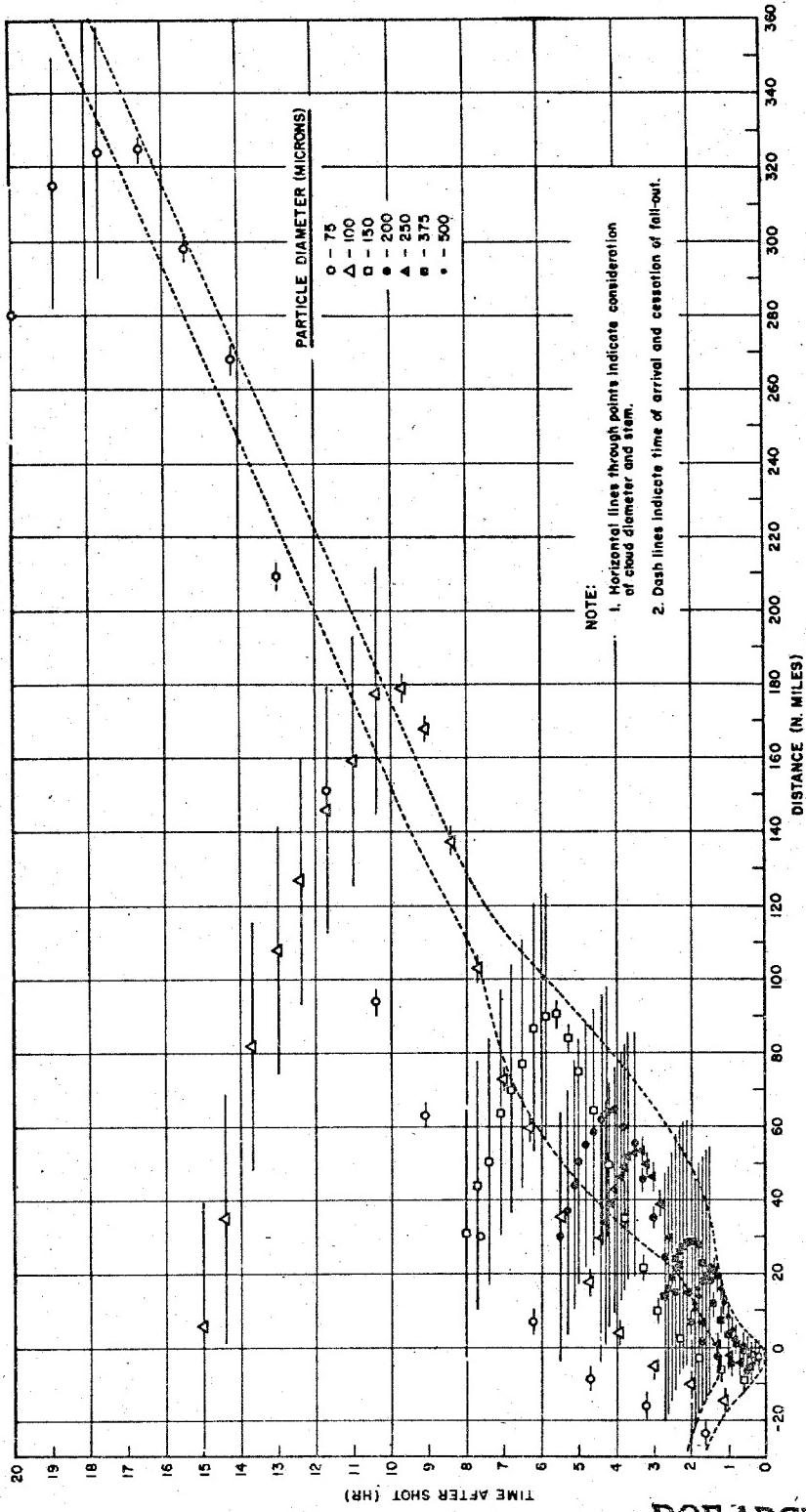
DOE ARCHIVES

397

CROSSED

ATOMIC ENERGY ACT

402



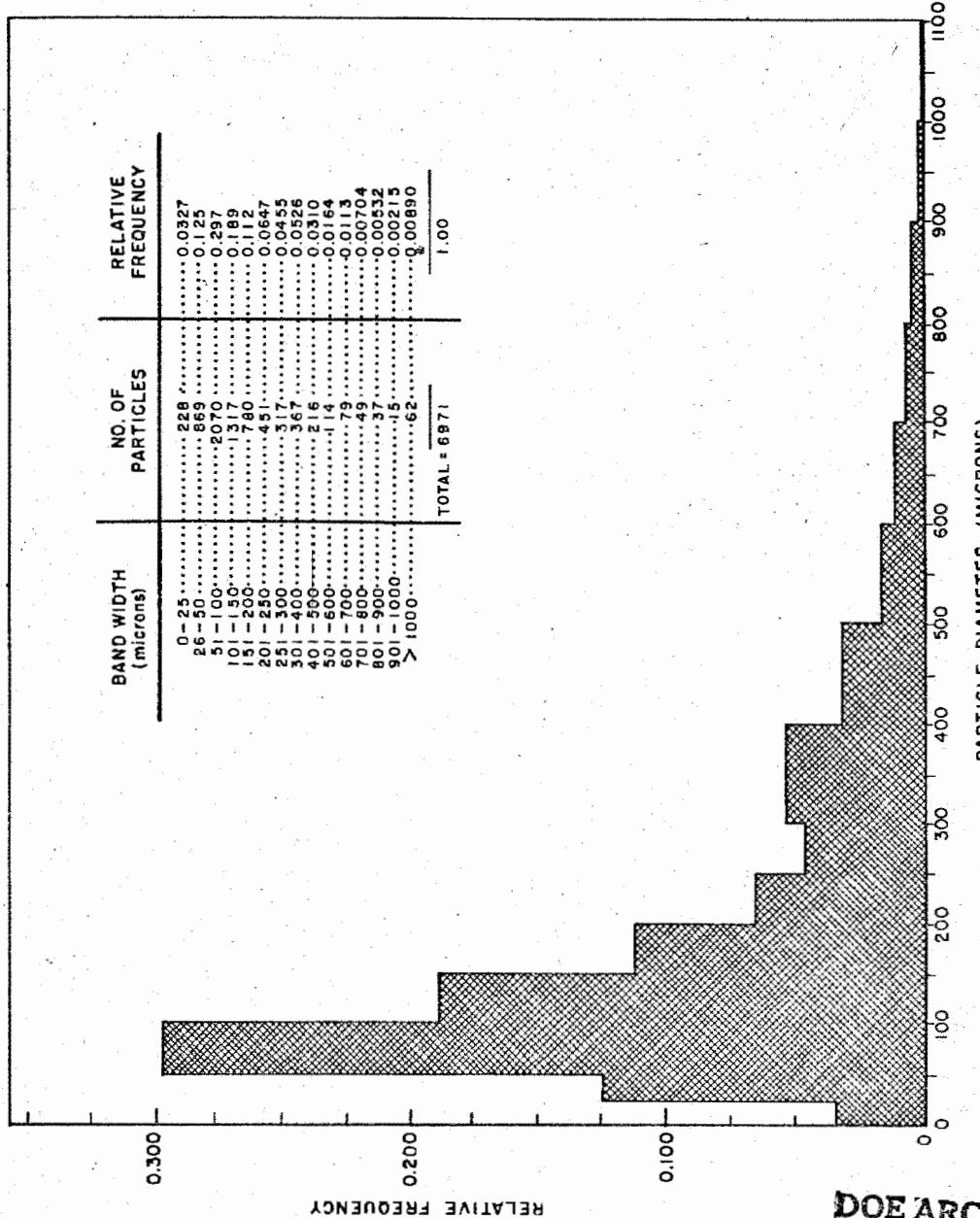
DOE ARCHIVES

398

RESTRICTED  
BY ENERGY ACT

403

**Figure 8**  
**Computed Time of Arrival of Fall-out**



DOE ARCHIVES

399

SECRET

DATA

NUCLEAR ENERGY

404

Figure 9  
Particle Size Distribution at Bikini

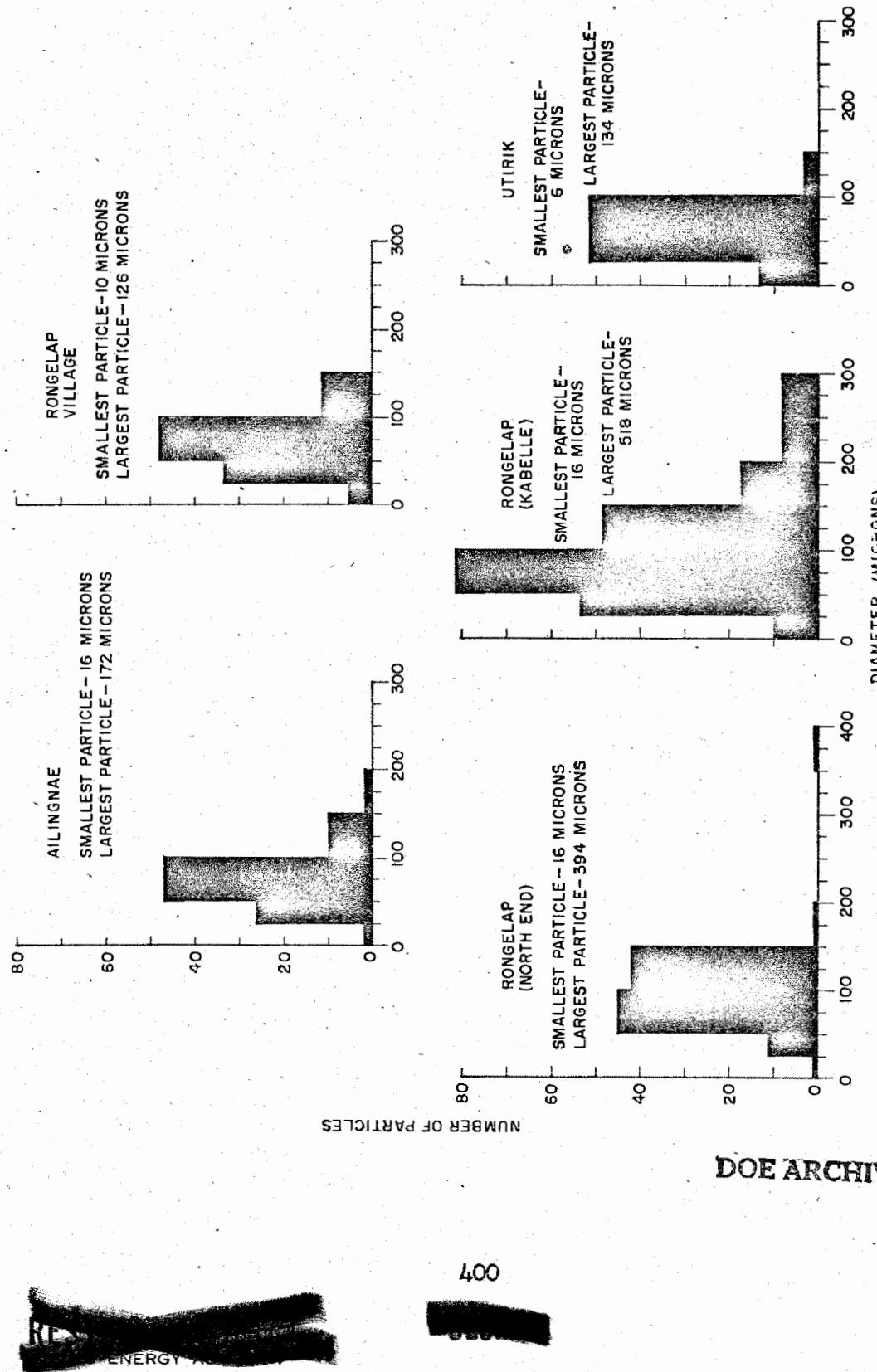


Figure 10  
Particle Size Distribution at Outer Islands

Little is known at this time on particle formation phenomena. Certainly more thought should be given to this field, especially with respect to understanding the complete mechanism of fall-out.

The configuration of the radioactive cloud source as well as the particle size distribution within the source are at this time unknown. This knowledge seems paramount to any resolution of the basic concepts of the models presented at this symposium.

There still remains the small particle anomaly where measured fall-out with respect to time indicates the very small particles arriving at times much too early to account for their trajectory by any falling rate equation.

**DOE ARCHIVES**

401

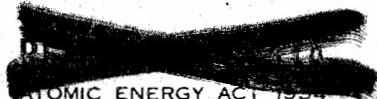
~~THE NUCLEAR ENERGY ACT 1954~~

406

**THIS PAGE IS BLANK**

**DOE ARCHIVES**

**402**



**411**

**407**

PREDICTION OF DOSE-RATE AND DOSAGE CONTOURS AS  
FUNCTIONS OF YIELD AND METEOROLOGICAL CONDITIONS,  
ORO AND TECHNICAL OPERATIONS, INC. METHOD

F. C. Henriques  
Technical Operations, Incorporated

Introduction

Three months ago Technical Operations was requested by the Operations Research Office of the Johns Hopkins University (ORO) to provide 1 Hr-R/hr dose rate and two-day dose contamination patterns which would result from the surface detonation of a 15 MT thermonuclear weapon. These patterns were computed for the thirty wind conditions which resulted from considering wind conditions at six different locations along the Eastern Seaboard during five different but "typical" meteorological situations. Previous to initiation of these computations, conferences were held with those groups at Sandia, NRDL and Rand that are developing fallout models and prediction procedures. Based upon these discussions, a "fallout" model was evolved and a "hand" computational procedure was developed which enabled the calculation of sixty fallout patterns in a one-calendar month with a reasonable number of man months.

The same fallout model and procedural method were used to compute in a two-week period the thirty-six radiological contamination patterns given in this report. These thirty-six patterns result from the calculation of dose rate and two-day dose contours for 1, 15 and 50 MT surface detonations for the six AFSWP wind conditions.

The underlying constraints required for these computations are markedly similar to those which have been described in the Symposium Report by Rand, the Signal Corps, and NRDL. The details of the computational methods employed by the various groups do differ; those recently developed by Rand and NRDL are well suited to machine computations, while those developed by the Signal Corps and Technical Operations have been specifically tailored to "hand" calculation procedures. It is not the purpose of this report to detail our computational procedure; this is reported elsewhere.

DOE ARCHIVES

If the input assumptions used by the above-mentioned groups were identical, identical fallout prediction patterns should result. Unfortunately, since there is a lack of experimental data, assumptions must be made to: (1) the radioactive cloud spacial dimensions; (2) the size distribution and fall times of entrained particles; (3) the fraction of activity associated with a given particle size; and (4) all the conversion factors which ultimately convert this activity once it reaches the ground to roentgen dose rate and biologically effective cumulative dose. Each

of the four above-mentioned groups use different sets of assumptions.

In Section I we outline the constraints which are believed to be common to each of these four methods and list the assumptions inherent in the Technical Operations model. We then discuss the areas and shapes of the 100, 500 and 1500 fission product 1 hr-R/hr dose rate and two-day cumulative dose contours which result from the surface detonation of 1, 15 and 50 MT weapons for the six AFSWP wind conditions. This is followed by an analysis of the similarities and scaling relationships of both the areas and shapes of these contours. Finally we propose a rapid scaling procedure that is believed to be reasonably valid.

In Section II we assume that the 1 hr-R/hr and 2-day dose roentgen readings at any ground location are known input data. We then derive the equations required to compute the biological effective dose from fission products and the contribution of U-239 and Np-239 thereto. The utility of the graphs and tables generated by these equations is illustrated by solving three typical practical problems.

The detailed justification of the information stated in Sections I and II is available elsewhere (ORO report in press).

#### Radioactive Fall-out Constraints, Assumptions and Results

To avoid duplication, it is assumed that the Rand and Signal Corps papers which comprise a portion of the Symposium Report have been read. The constraints inherent to their procedures as well as our approach may first be listed. Some of these could be dropped but only at cost of more complicated calculation procedures.

- A. There is some instant ("instant of stabilization") at which the distribution of activity vs particle size and the spatial distribution of such particles is known.
- B. The range of particle sizes is such that pure diffusion of particles can be neglected and yet the particles as they fall will follow wind currents at each pertinent altitude with no important lag.
- C. The range of particle size is also such that for any two given particles the ratio of their fall times from various altitudes is constant (independent of altitude) to sufficient approximation.
- D. At the instant mentioned in A, the distribution of activity vs particle size is independent of spatial position.
- E. At the instant mentioned in A, the spatial distribution of total activity is laterally uniform (within some area) at any one altitude.
- F. There are no vertical winds, and the horizontal wind pattern vs altitude remains constant over a time sufficiently

DOE ARCHIVES

long for all those particles destined to arrive at locations of interest to complete their fall.

These list only those constraints required to yield a rapid "hand" calculation technique. Before discussing these, it is perhaps worth pointing out several items that need not be assumed to achieve computation rapidity. The vertical distribution of activity in the cloud at the instant of stabilization can be arbitrary, and the cloud can have an arbitrary physical shape. Likewise, the distribution of activity vs particle size can have any shape; the only restrictions here are on the range of sizes, which must satisfy B and C.

Constraint A merely states that the problem is restricted to falling-particle calculations and does not concern the processes which establish the radioactive cloud.

An inertial lag and diffusion analyses show that particles at least in the range 10 microns to 2000 microns satisfy Constraint B. The lower limit is certainly unnecessarily high, but appreciable raising of the upper limit would require more careful investigation. However, the effects of large particles in the model are rather insensitive to this constraint since they all fall close to ground zero in any case.

The rather surprising property postulated in Constraint C is actually satisfied quite well over the same range, 10 to 2000 microns. This is subject to direct calculation. The results of these calculations are given in Tables 1 and 2.

Constraint D is rather ad-hoc; it enables the problem to be broken into independent components. Until actual measurements at the "instant of stabilization" are available, it must rest entirely on the argument that continual mixing occurs during the relatively brief period (10 min) when the "boiling" cloud is rising and that in this way the chances of a given particle being located at a given position are independent of its size and of the activity which it carries. It is doubtful that this is literally true, but the argument seems intuitively reasonable enough to justify its use until data can be shown to seriously refute it.

DOE ARCHIVES

Constraint E simplifies calculation to the extent that only geometric coincidence data need be taken off the plots used in calculation. It could be lifted at the cost of considerably more data-handling during calculation, but it does not affect the over-all scheme of calculation. Very little data seem available on this point, but the few measurements which have been made with drone airplanes at Greenhouse tend to give confirmation.

CLOUD PROPERTIES "AT STABILIZATION"

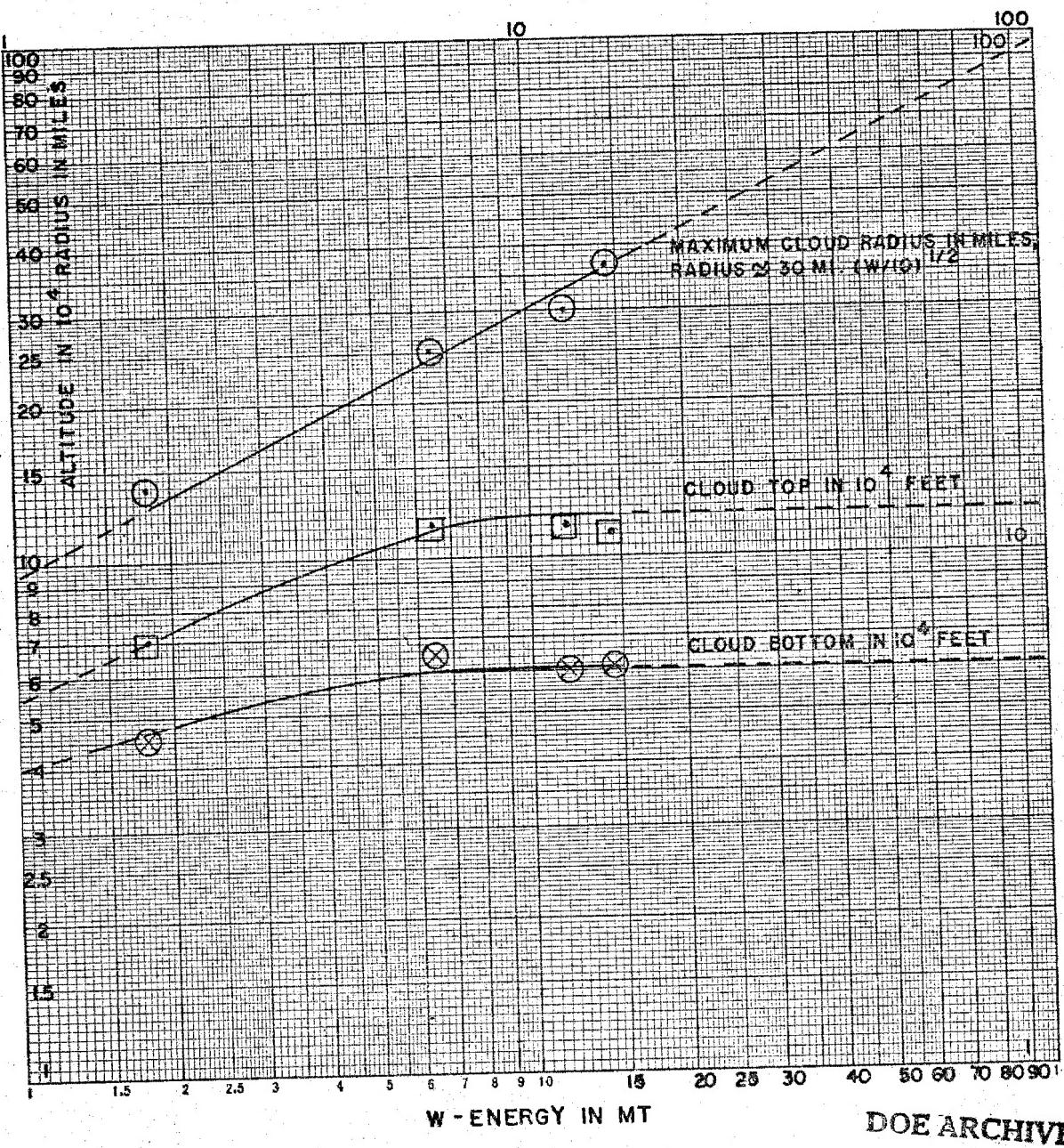


Figure 1

406

RESTRICTED  
BY ACT OF CONGRESS

411

Constraint F is required to avoid plotting the map position of more than one particle size. Vertical winds are probably negligible in a great many cases. Constancy of the horizontal winds over long time periods is probably not too realistic. Provided that the meteorological data were sufficiently well known, Constraint F could be lifted at the cost of plotting in detail the final positions of all particle sizes from all altitudes. Subsequent calculation would not be affected however.

We now proceed to discuss the Technical Operations data assumptions which result in our specific fall-out patterns. These assumptions are not specific to the method of calculation but must, of course, be given before a calculation can be performed.

The cloud properties are shown in Figure 1. The plotted points are experimental surface shots where the radius is the maximum radius of each cloud. The experimental points have been connected by rough curves which have been extrapolated in both directions. These extrapolations are based on the following arguments.

For larger weapon yields, in lieu of data, it seems reasonable to assume that the radius will continue to grow at about the same rate as before; thus the radius is extrapolated as  $W^{1/2}$ . A positive steep atmospheric temperature gradient starting at about 120,000 ft (the "ozone absorption layer") can be expected to limit the cloud top to about this altitude. This is because the cloud must expand as it rises in order to maintain pressure balance with the surrounding air. Because of the expansion, it cools more or less adiabatically. At lower altitudes, however, the surrounding air temperature also drops with pressure approximately adiabatically and the cloud, once much hotter than its surrounding air, remains hotter as it rises and thus continues to have buoyancy. This process reverses, however, at about 120,000 ft and the cloud should very rapidly lose buoyancy and come to thermal equilibrium with the atmosphere. The atmosphere exhibits another positive temperature gradient in the neighborhood of 40,000 - 60,000 feet (the tropopause). However, clouds resulting from nuclear detonations in excess of 1 MT still have sufficient internal energy when they reach the tropopause to punch through it. The cloud top has therefore been assumed to have a ceiling of 120,000 ft. The data for the cloud bottom also appear to indicate a leveling off. This would be expected on the basis of the other two curves, for the mass of the original fireball is known to be nearly proportional to  $W$ . If this is true also of the cloud, the cloud bottom must level off as shown at 60,000 ft. The data seem to support this conclusion.

DOE ARCHIVES

The extrapolation toward lower energies is based on data for the

407

ATOMIC ENERGY ACT

412



Figure 2  
Photograph of IVY-Mike Shot taken at the "Instant of Stabilization"

DOE ARCHIVES

408

RECORDED BY  
THE UNITED STATES  
ATOMIC ENERGY COMMISSION

413

surface shot of 1.2 KT which nearly fall on the straight-line extrapolations shown. In addition, these extrapolations yield a total cloud mass very nearly proportional to yield - assuming the mass-distribution within the cloud is the same as that in the atmosphere it replaces.

An additional property of clouds which is required is their shape. Here data are quite sparse for the "late times" (about 10 min) when the cloud finally stabilizes.

Early calculations were done assuming a cylindrical shape but this leads to rather low peaks of contamination\* and does not agree with photographs and descriptions scattered through the classified literature. The shape finally used was taken from a written description of the Castle-Bravo shot and is substantiated by Figure 2 which is a photograph\*\* of Ivy-Mike shot (11.2 MT) taken essentially at the "instant of stabilization". The result (illustrated in Figure 4) is an inverted cone truncated so that the cloud bottom has a diameter 40% of top diameter given by Figure 1. There is nothing at all sacred about this particular shape; any shape could be used in the calculations but a truncated cone seems to be the best possible assumption at the present state of knowledge, especially since the limiting action of the "ozone ceiling" must enlarge the cloud top with respect to the bottom.

Another piece of required data is the distribution of radioactivity vs. particle size. Such measurements have been made only\*\*\* for the Jangle surface and underground shots of about 1 KT. These data (NRDL, private communication) are plotted in Figure 3 which shows for each particle size, plotted vertically on a logarithmic scale, the fraction of activity associated with particles of that size or less, plotted

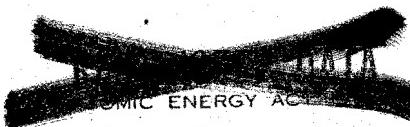
---

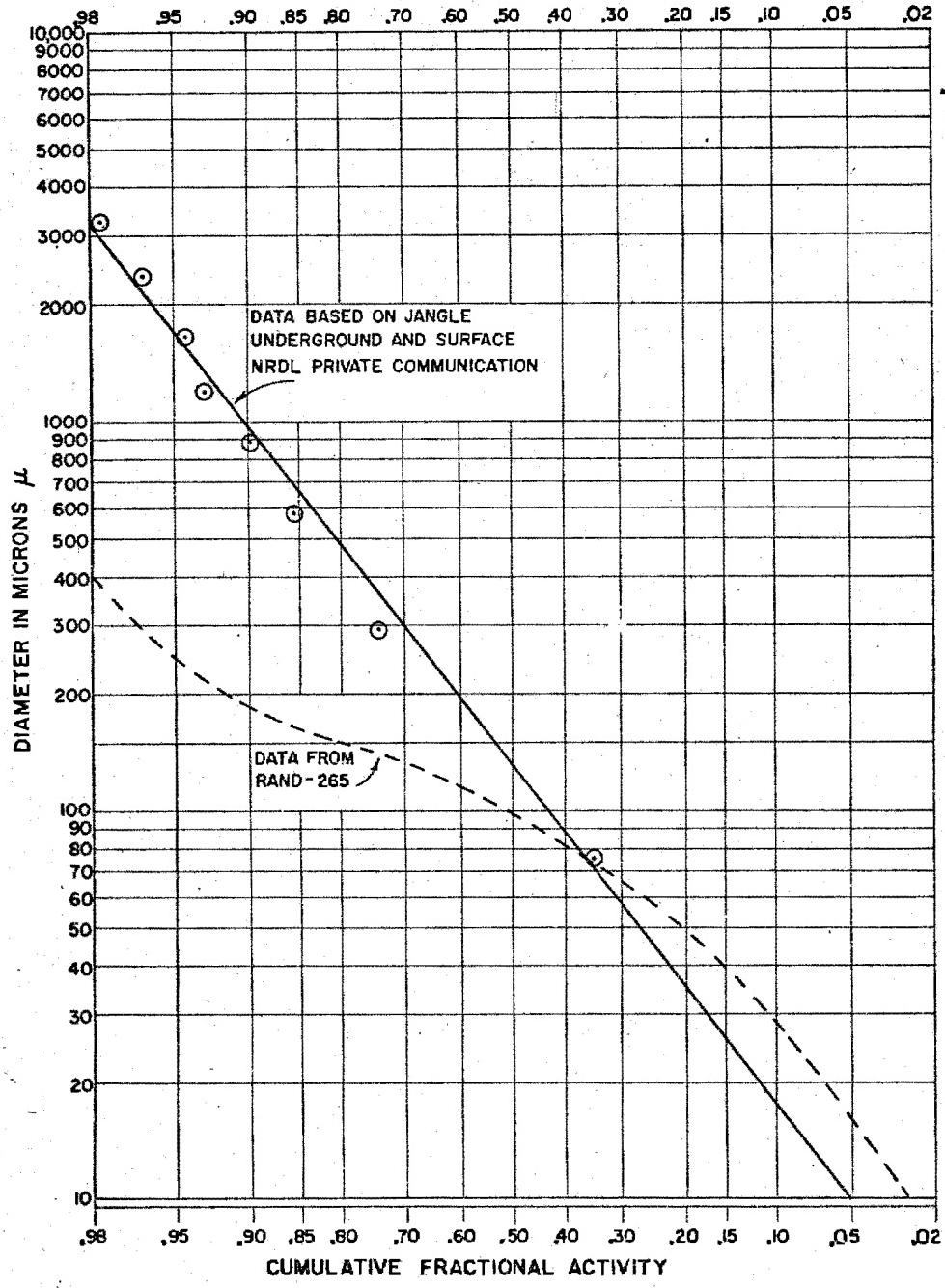
\* This fact has also been recognized by the Rand group. For their calculations they are apparently now using artificial cloud radii which are about 60% of the reported cloud radii.

\*\* Observation of the motion picture of the 15 MT Castle-Bravo shot indicates the same shape at this late time. A still photograph is not available at this writing.

\*\*\* Other measurements have given the size-distribution of particles with some activity, while still other measurements have yielded activity versus particle size but unfortunately for different weapon tests. Neither alone is sufficient. The combination of these is what is required.

DOE ARCHIVES





PROBIT PLOT OF CUMULATIVE PARTICULATE ACTIVITY  
FRACTION OF ACTIVITY IN PARTICLES OF SIZE  $\leq \mu$

Figure 3

DOE ARCHIVES

410

415

horizontally on a probit scale. The straight line plot means that the activity has a Gaussian normal distribution in the logarithm of particle diameter. The data in Figure 3 may be expected to hold for surface shots over most land areas since the intrinsic particle sizes of various soil-particles and concrete are not greatly different. The data may also be expected to hold for a wide range of weapon energies for the following reason. Within the fireball the conditions of formation of radioactive particles must be quite localized and thus depend only upon the energy density per unit mass of debris. The mass of soil blown out of the crater which becomes part of the fireball in a surface shot is proportional to weapon energy. Therefore the energy density per unit mass of soil within the fireball is independent of yield. This leads one to expect that the conditions of formation of the radioactive particles are independent of the weapon energy.

It must be realized, however, that the distribution curve of Figure 3 does not necessarily hold for all other soils. In particular, the coral found in the Pacific area is very different; it is very likely decomposed under the intense heat with  $\text{CaCO}_3$  giving off  $\text{CO}_2$  to become  $\text{CaO}$  which may then be converted to hydroxide by moisture in the air. These processes should still lead to a distribution relatively independent of weapon energy but the curve may be vastly different from the Nevada results. Also shown in Figure 3 is the curve which Rand found necessary to duplicate the results of Castle shot Bravo. Our calculations lead to a similar result.

The distribution of total concentration in the cloud must also be known. (Figure 3 has only specified the breakdown of this total into particles of various sizes.) For reasons discussed under Constraint E, we have assumed the total activity density to be constant within the cloud at any one altitude, but the vertical distribution has not yet been specified.

**DOE ARCHIVES**

The first assumption that generally springs to mind when this question is asked is that the activity is probably uniformly distributed in the vertical direction as well. Consider, however, the fact that a cloud from a large weapon extends from altitude 60,000 to 120,000 ft. Over this range the air density and pressure change by a factor of 8. Now the pressure in the cloud must equal the external air pressure if motion is to cease and the temperature cannot long stay very different from that of the surrounding air. If this is so and if the cloud maintains a stable shape, then the (mass) density must (by the universal gas law) also be near that of the surrounding air. This also balances the buoyancy forces due to gravity.

**TABLE I**  
**Time for Particle to Fall 10,000 Feet from Altitude, H**  
**Tabulated Values in Hours**

Altitude in Thousands Feet, H	Particle Diameter, $\mu$ , in Microns											
	10	20	30	50	70	100	150	200	300	500	1000	2000
0	—	—	—	—	—	—	—	—	—	—	—	—
10	157	39	17.4	6.05	4.05	2.24	1.20	0.84	0.50	0.30	.170	.094
20	149	36	16.5	5.80	3.72	2.15	1.11	0.75	0.45	0.27	.149	.090
30	139	34	15.5	5.43	3.28	1.96	0.99	0.67	0.40	0.23	.127	.077
40	131	32	14.8	5.25	2.99	1.80	0.90	0.60	0.35	0.20	.107	.064
50	125	32	14.3	5.14	2.72	1.65	0.82	0.54	0.31	0.17	.092	.052
60	120	31	14.3	5.04	2.64	1.50	0.77	0.49	0.27	0.15	.084	.043
70	115	30	13.9	5.04	2.62	1.46	0.72	0.45	0.25	0.13	.063	.035
80	109	30	13.5	4.93	2.62	1.39	0.70	0.42	0.23	0.11	.054	.029
90	100	28	13.1	4.78	2.56	1.29	0.69	0.41	0.21	0.10	.045	.024
100	89	26	12.3	4.60	2.44	1.23	0.66	0.39	0.20	0.09	.039	.020
110	73	23	11.2	4.37	2.34	1.18	0.62	0.37	0.18	0.08	.034	.017
120	58	20	10.0	4.09	2.23	1.13	0.59	0.33	0.17	0.08	.030	.014

**DOE ARCHIVES**

**RESTRICTED**  
**ENERGY**

412

421

417

Thus, the mass of the whole cloud must be distributed in the same way as that in the surrounding atmosphere. (As already mentioned, this checks the expected proportionality of total cloud mass to yield, given the data of Figure 1.) If the further assumption of violent mixing during the short (10 min) cloud rise is invoked, the cloud debris must also be distributed in the same way as the density of the atmosphere.

In lieu of detailed data, then, it would appear that the most reasonable assumption is that total activity density is proportional to air density. There is an indication from early drone flights at Greenhouse that ion chamber readings were independent of altitude within the cloud. This is precisely what would be expected on the above assumption since the gamma ray path lengths would vary with air density in such a way as to exactly cancel the variation of activity concentration; in other words, an ion chamber measures activity per unit air-mass which is what we have assumed to be constant. Further data on this point would, however, be most desirable.

In order to compute the fall times of the radioactive particles from various altitudes, they were treated as irregular spheres subjected to the standard aerodynamic fall equation. For very small velocities this equation reduces to Stokes Law and for very high velocities to the law for the turbulent region. At very low air densities, when the mean free path of the air molecules becomes comparable to the particle diameter, the fall velocity must be increased according to a slip-page equation. The fall velocities presented as the time in hours to fall 10,000 ft as a function of particle size and altitude are given in Table I. The computational details are presented elsewhere. Table II has been prepared from Table I. It demonstrates that the relative time for irregular spheres of various sizes to fall to ground is markedly invariant to the originating altitude. Thus Constraint C is satisfied and it is this fact properly exploited which results in the tremendous simplification of the Technical Operations computational method.

Finally, we present the conversion factors used to obtain the fission product dose-rates expressed in roentgen units. These are shown in Table III. In comparing the fallout contour predictions of the various groups, due consideration must be given to the numerical values used by these groups which correspond to those presented in Table III. For example, Rand at this writing uses 1200 in column (A) and unity in column (C).

DOE ARCHIVES

All of the constraints, assumptions and data required to predict fallout patterns have been enumerated above. At this point we will in-

**TABLE II**  
**Relative Particle Fall Time to Ground from Altitude, H**  
**Normalized to 100 Units for  $70 \mu$  Particles**

Altitude in Thousands Feet, H	Particle Diameter, $\mu$ , in Microns							500	1000	2000
	10	20	30	50	70	100	150			
3880	963	430	149	100	55.3	29.6	20.7	12.4	7.41	4.20
3940	965	436	153	100	56.5	29.7	20.5	12.2	7.34	4.11
4030	986	447	156	100	57.5	29.9	20.5	12.2	7.24	4.04
4100	1000	457	161	100	58.0	29.9	20.4	12.1	7.12	3.94
4180	1030	468	165	100	58.5	30.0	20.3	12.0	6.98	3.85
4230	1050	478	169	100	58.2	29.8	20.0	11.8	6.80	3.76
4250	1060	485	171	100	57.9	29.6	19.7	11.5	6.58	3.60
4240	1070	487	173	100	57.4	29.2	19.3	11.2	6.32	3.44
4210	1070	490	175	100	56.8	29.0	19.0	10.9	6.10	3.28
4160	1070	491	175	100	56.2	28.8	18.7	10.7	5.90	3.14
4090	1070	490	177	100	55.8	28.7	18.5	10.5	5.72	3.02
3990	1050	488	177	100	55.5	31.5	18.3	10.3	5.58	2.91
40-120 Average	4160	1050	482	171	100	57.1	29.6	19.4	11.2	6.34
										3.44
										1.98

414

DOE ARCHIVES

REF ID: A6562

419

dicate how this information is employed through reference to Figure 4.

In Figure 4 the cloud sizes containing the radioactive debris at the instant of stabilization for the three sizes of weapons are drawn to scale with the top and bottom altitudes and top-radius given by Figure 1. This shape is then divided into horizontal slabs having equal activity per unit area. (Ten slabs suffice for 15 and 50 MT weapons, and five slabs for the 1 MT.) Due to the assumption that activity density varies as air density, the pressure drops across all slabs are the same. This results in the slabs having the radii and mean altitudes depicted

---

TABLE III  
Roentgen Contour Constants  
(Fission Products Only)

---

Flat Ground		
1 hr-R/hr per		
sq mi/fission	Radioactive	
products on	Decay Law	
Ground per KT	(ii)	
of		
Thermonuclear		
Explosion		
	(AxBxC)	
<b>DELETED</b>		
	550	$t^{-1.2}$

(ii) This  $t^{-1.2}$  law is a good approximation for moderate  $t$  but is known to be inaccurate for times beyond 200 days; however, until better data are available this law seems to be adequate for purposes at hand

---

in the lower portion of Figure 4. In the "zero wind case" all of the activity from each of the slabs must ultimately fall upon the ground with zero lateral displacement. The conversion factors listed in Table III and shown in Figure 4 result in the 1 hr-R/hr dose rates for various

415

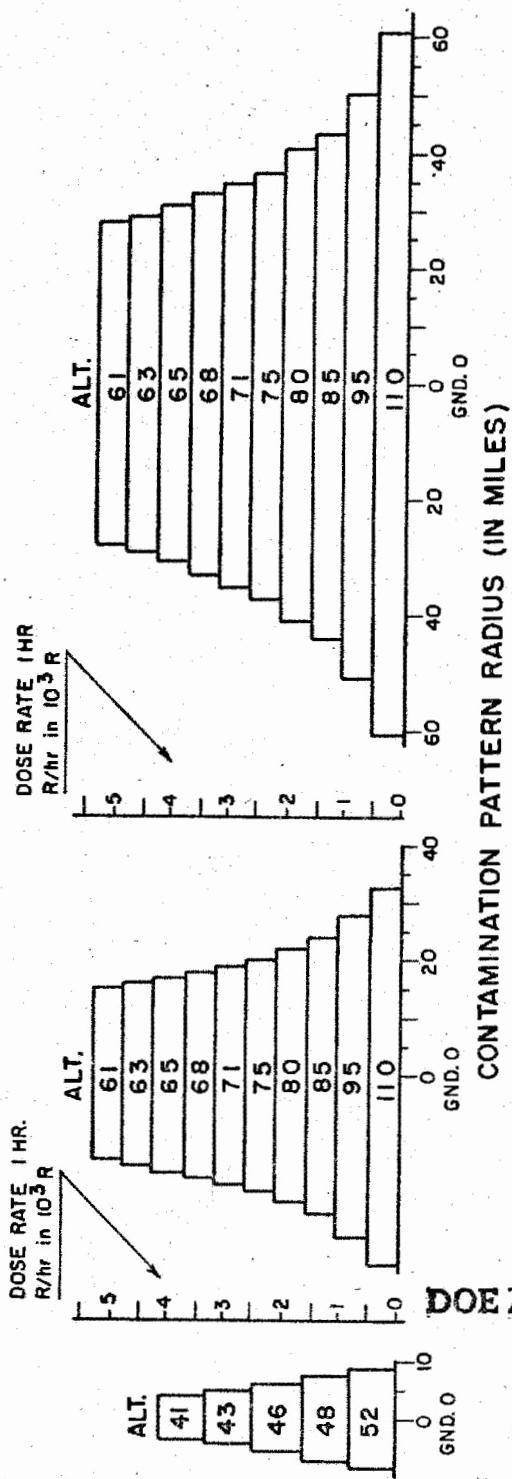
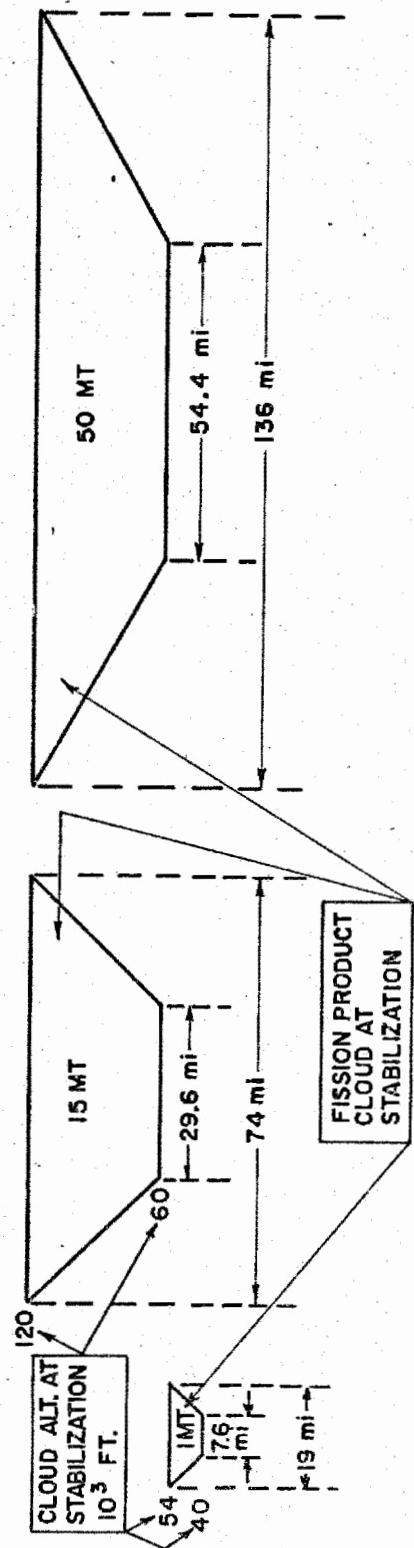
GEORGE

RE

DOE ENERGY AC

420

**DOSE RATE PATTERNS FROM THERMO-NUCLEAR WEAPONS  
ZERO WIND CASE**



**DOE ARCHIVES**

Figure 4

distances from ground zero. Thus the highest possible effective 1 hr-R/hr dose rates which can result from this model under any wind conditions is 5700 for the 15 MT and 50 MT weapons and 4200 for the 1 MT weapon. The additional contamination near ground zero due to the small amount of radioactive debris in the stem is not treated in this model. Although the two-day cumulative dose for the zero wind case is not shown, it is readily calculable since: (a) the fall times to ground of the various size particles from each horizontal cloud slice is predetermined by Table I; (b) the portion of activity associated with the various size particles is given in Figure 3; and (c) radioactive decay is assumed to obey the  $t^{-1.2}$  law.

The effect of wind on zero wind patterns is to change the ground coordinates but not the fall times of the particles contained in each horizontal cloud slice. This distorts the shape and alters the area of the roentgen contours. The degree of distortion and alteration depends upon the meteorological conditions and is calculable from assumptions and constraints discussed above by a method similar in principle to that described by Rand in this Symposium Report. The results of these calculations are the eighteen 1 hr-R/hr and two-day roentgen cumulative dose contours compiled in another section of the Symposium Report. To facilitate comparison, our contours have been renormalized to a terrain factor of unity. We are of the opinion that a terrain factor of 0.55 for flat land is far more realistic. Thus with respect to what would actually be measured with a roentgen dose-rate meter 3 ft above ground, the roentgen levels of our contours as depicted (as well as those shown for the other groups) should be reduced twofold. Table IV tabulates the contaminated ground areas enclosed by fission product roentgen level contours for 1, 15 and 50 thermonuclear surface bursts for all six AFSWP winds.

From the data contained in Table IV, we can draw the following conclusions, some of which in view of the complexity of fallout phenomena could not have been anticipated:

These contour patterns were computed for a variety of rather widely varying wind conditions. Therefore, for a given burst energy, the contaminated area enclosed by any 1 hr-R/hr contour is not strongly dependent upon the meteorology; this is also true for each two-day cumulative dose contour.

DOE ARCHIVES

For each wind condition, except for some of the 1500 R contours resulting from the 15 and 50 MT surface bursts, the areas enclosed by the same numerical value of the 1 hr-R/hr and two-day dose do not differ greatly.

**TABLE IV**  
**Areas of Contaminated Ground Enclosed by the Roentgen Levels Noted for the Six AFSWP Wind Conditions**  
**(Areas Tabulated in 10<sup>3</sup> sq. mi.)**

Fission* Product Roentgen Level	Burst Energy MT	R is 1 hr-R-hr Dose Rate				D is two-day Cumulative Dose			
		Dodge City, In. 28 December Condition A R D	Washington, D.C. 28 September Condition B R D	Caribou, Maine 18 March Condition C R D	Boise, Idaho 14 May Condition D R D	Washington, D.C. 9 February Condition E R D	Washington, D.C. 8 July Condition F R D		
100	1	0.7	0.9	1.0	1.3	0.8	1.8	0.7	0.8
	15	10.7	10.2	12.6	11.4	13.1	13.0	10.0	5.6
	50	32.3	29.0	42.4	28.0	46.0	36.0	27.6	14.4
500	1	0.2	0.3	0.0	0.4	0.0	0.3	0.2	0.4
	15	2.6	3.7	2.8	3.7	2.0	4.3	2.4	3.2
	50	9.3	12.8	10.5	12.1	9.6	14.7	10.3	9.6
1500	1	0.0	0.1	0.0	0.0	0.0	0.0	0.1	0.0
	15	0.0	1.4	0.0	1.6	0.0	0.0	1.1	1.6
	50	1.3	6.2	1.8	6.2	1.0	6.0	5.0	6.0

Condition A - Winter. - Wintertime situation of an abrupt approximately 90° sheer at a height of approximately 40,000 ft.  
 Condition B - Fall. - Gradual sheer of approximately 90 per cent. 30 to 50 knot winds.

Condition C - Winter. - Winds at all levels from approximately the same direction. 30 to 60 knot winds.  
 Condition D - Spring. - Relatively low wind speeds at all levels. 0 to 15 knot winds.

Condition E - Winter. - Relatively high wind speeds above 10,000 ft. 50 to 130 knot winds.  
 Condition F - Summer. - Gradual sheer of approximately 180°. 10 to 30 knot winds.

\* Increasing the roentgen level twofold yields contaminated areas for a terrain factor of unity.

A similar table has been tabulated elsewhere in the Symposium Report for comparative purposes. This latter table gives roentgen levels for our predicted areas based upon a unity terrain factor.

**DOE ARCHIVES**

A Castle-Bravo type weapon (15 MT) detonated on land areas similar to that of the Eastern Seaboard would result in 1 hr-R/hr dose rate and two-day cumulative roentgen dose contours of 100, 500 and 1500 whose contamination areas would encompass about 10,000, 3,000 and 600 square miles, respectively.

For any given wind condition the area encompassed by any dose rate or two-day dose, respectively, appears to be nearly proportional to the weapon size.

Note that Conditions A, B and C are all moderate wind cases with varying degrees of shear; Conditions D and E are of low wind velocity; and Condition F is a high wind case. Thus, if meteorological conditions are classed solely according to wind velocity, namely as low, moderate and high, the phrase, effectively independent of, can be substituted for the phrase, not strongly dependent upon, contained in the first Conclusion.

The last two Conclusions enable Table IV to be reduced to Table V.

---

TABLE V  
The Effect of Low, Moderate and High Wind Velocities on the Amount of Area

Enclosed by the Roentgen Levels Noted

(Tabulated values are average ground area in  $10^3$  sq. mi/MT)

---

Fission Product Roentgen Level	Wind Velocities					
	Low		Moderate		High	
	R	D	R	D	R	D
100	0.6	0.35	0.8	0.7	0.7	1.0
500	0.2	0.2	0.2	0.3	0.1	0.3
1500	0.08	0.1	0.025	0.1	0.0	0.06

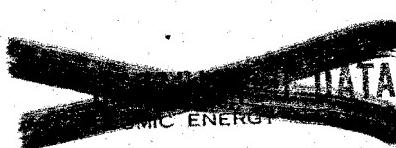
---

R is 1 hr-R/hr dose rate; D is two day cumulative roentgen dose.

---

DOE ARCHIVES

419



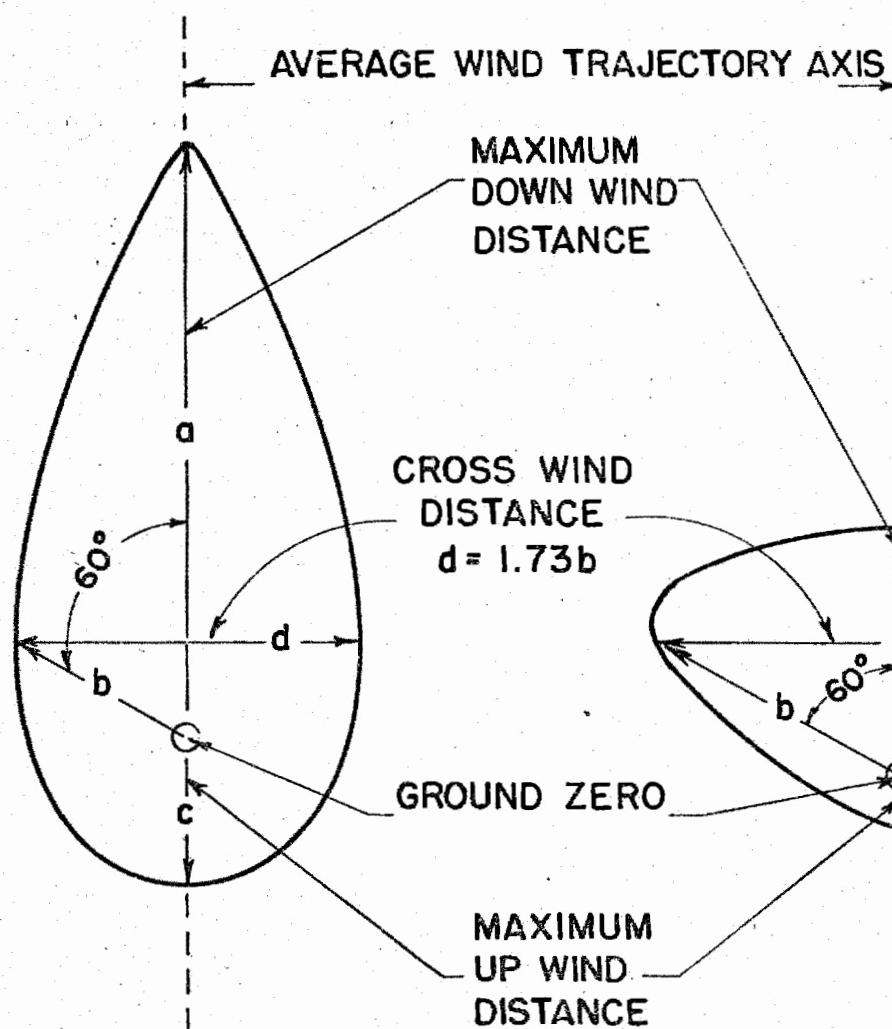
424

## IDEALIZED CONTOUR SHAPES

APPLICABLE TO BOTH 2 DAY DOSE AND 1 hr. - R/hr.  
100 TO 1500 ROENTGEN LEVELS

CURVE A

LOW OR MODERATE  
WIND SHEAR



CURVE B

HIGH WIND  
SHEAR

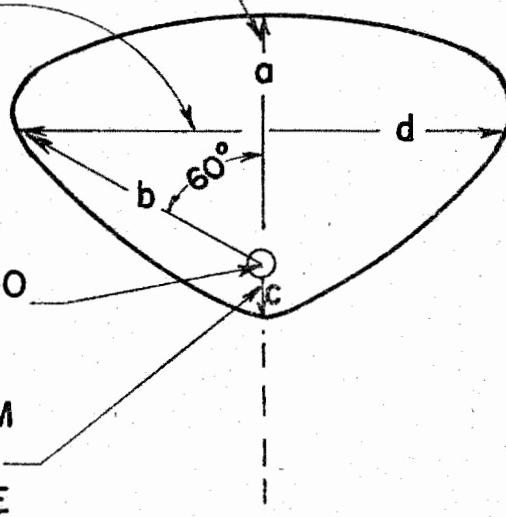


Figure 5

420

DOE ARCHIVES

425

Table V should be a fairly good guide to the roentgen level flat ground area coverage to be expected from the surface detonation of all thermonuclear weapons under most meteorological conditions, provided that the land area is not comprised of coral.

The fact that the contaminated contour areas seem to scale almost directly as the thermonuclear burst energy means that any known contamination pattern for a given energy can be transformed at once into a pattern for another energy if the meteorological condition remains unchanged. Draw vectors from ground zero to various points along the periphery of the contour in question, and scale the length of these vectors by the square root of the ratio of the weapon energies. This working rule is subject to direct verification by measurement of our contour plots for each of the six AFSWP winds. This has been done with excellent agreement between the 15 and 50 MT weapons and fair agreement between the 1 MT and the 15 or 50 MT weapons. Further inspection shows that all of the dose and dose rate contours (somewhat idealized) are lemniscatic in shape, as depicted in Figure 5. Figure 5 shows two curves. Curve A is typical of contours when the wind shear is low or moderate (Conditions A to E). Curve B typifies the contour shape for high wind shear (Condition F). For contour curves both A and B, the terminus of maximum cross-wind dimension, d, is the end of a polar vector which makes an angle of about  $60^{\circ}$  with the average downwind trajectory line. The relative ratios and scaled lengths of polar vectors a, b and c depend, of course, upon the wind velocity, but appear to be relatively independent of wind shear. The numerical values of these three polar vectors for low, moderate and high winds (see Conclusion (e)) are tabulated in Table VI.

In view of the data on the contour areas (Table V), the R and D polar vector numerical values for each case should be nearly identical, except for the 1500 R contours under high winds. This is borne out by Table VI. Table VI indicates that a CASTLE-Bravo type weapon (15 MT) detonated on land areas along the Eastern Seaboard under a moderate wind condition would result in both a 1 hr-R/hr dose rate and a two-day cumulative dose 500 R contour which would extend about 100 miles downwind, 10 miles upwind, and have a maximum cross-wind extent of about 40 miles; the total area encompassed would be about 3000 square miles. (See Table V).

DOE ARCHIVES

TABLE VI

The Effect of Low, Moderate and High Wind Velocities  
 on Figure 5 Polar Vector Distances for the Roentgen Levels Noted  
 (Tabulated Values are Polar Vectors in  $\text{mi}/(\text{MT})^{\frac{1}{2}}$ )

Fission Product Roentgen Level	Polar Vector	Wind Velocities					
		Low		Moderate		High	
		R	D	R	D	R	D
100	a	27	15	80	58	69	70
	b	17	13	8	9	5	8
	c	7	8	4	6	2	4
500	a	11	10	25	25	21	36
	b	8	9	5	7	2	4
	c	5	12	1	4	-7	-2
1500	a	8	8	9	13	0	17
	b	6	6	2	5	0	1
	c	4	4	-1	2	0	-3

R is 1 hr-R/hr dose rate. D is 2-day cumulative roentgen dose.

(-) sign for polar vector c denotes that c is above ground zero in Fig. 5.

a is maximum downwind distance to contour.

b is  $60^\circ$  polar vector;  $1.73b$  is maximum crosswind distance.

c is maximum upwind distance to contour.

DOE ARCHIVES

Figure 5 and Tables V and VI can be used as a rapid method to estimate 2-day dose and 1-hour dose rate contour patterns over contaminated land areas as follows:

Use Figure 1 to determine altitudes of bottom and top of initial cloud resulting from a surface thermonuclear burst of energy in MT.

To characterize wind shear, qualitatively examine wind vector data for only those altitudes which are bounded by cloud bottom and top. If wind shear is high, contour patterns will be similar to Curve B, Figure 5; otherwise it will be like Curve A. Since for altitudes above 40,000 ft, high wind shear is rare, most contour patterns will be like Curve A.

Use an air density table to determine a mean altitude, H, which corresponds to the center of mass of an arbitrary cylinder bounded by the cloud top and bottom altitudes. If the burst energy is 1 MT, H is 45,000 ft; if the energy exceeds 10 MT, H is 70,000 ft.

Consider a  $100\mu$  particle that was originally located H feet directly above zero ground. Use fall times given in Table I together with the wind data to ascertain the location of this  $100\mu$  particle when it reaches the ground.

Draw a line through ground zero and the location of this particle. This is the average wind trajectory axis. Measure distance in miles from ground zero to this particle location. If this distance is less than 150 miles, classify as low wind; if distance is between 150 and 750 miles, call moderate; and if distance exceeds 750 miles, it is a high wind case.

Now draw polar vector distances for the 100, 500 and 1500 roentgen levels as given in Table VI for appropriate wind velocity case and burst energy. Sketch in contour lines as depicted in Figure 5 for appropriate wind shear case. Keep in mind that enclosed areas must satisfy Table V.

**DOE ARCHIVES**

Roentgen levels of these contour lines are valid for the conversion factors listed in Table III. If you are using other values for these factors, alter roentgen levels accordingly.

423  
C5000

DATA ENERGY

428

## Fission Product Biological Damage Dose and Contribution of U-Np Activity Thereto

### Introduction

Biological damage from exposure to radioactivity is complicated by the tendency of the body to repair itself. Thus the maximum effect from a given total dose depends upon the length of time over which the dose was received. If the duration of the dose is less than two or three days, the effect of self-repair on the danger level is slight, but times longer than this are of current interest.

Data on this subject are still rather sparse. However two studies have been made which give two estimates of the effect. The results differ principally at periods of the order of six months or more, where data do not yet exist in sufficient quantity to support either theory. The mathematical forms which summarize the two studies differ considerably, and both will be considered in what follows.

### Method I

A British study states that exposure to a constant dose rate  $d$  per day for  $t$  days is equivalent, at the end of that period, to a one-day dose ("Damage Dose") given by

$$D = d t^{0.64} \quad (t \geq 1 \text{ day}) \quad (1a)$$

Manifestly the restriction " $t \geq 1$ " day is required since for very short times, the effective dose must be more nearly

$$D = d t \quad (t \leq 1 \text{ day}) \quad (1b)$$

Equations (1a) and (1b) fit data taken with a constant dose rate  $d$  per day. To get relations for dose rates which vary in time due to radioactive decay, consider the effect of extending  $t$  by a small amount  $\Delta t$  which is added at the beginning of the interval  $t$ . The additional damage dose due to this increment is easily seen to be:

$$\Delta D = \begin{cases} \frac{d\Delta t}{0.64 t^{-0.36}} & \text{if } t \leq 1 \text{ day} \\ d\Delta t & \text{if } t \geq 1 \text{ day} \end{cases} \quad \text{DOE ARCHIVES}$$

This relation says that the effect of a pulse ( $d\Delta t$ ) of radiation is (a) unreduced for times less than 1 day, and (b) reduced by a factor ( $0.64 t^{-0.36}$ ) after times,  $t$ , longer than one day. If then, exposure

occurs from time  $t_1$  to  $t_2$  at variable fission product dose rate of  $c/t^{1.2}$ , the final damage dose will be (provided  $t_2 \geq t_1 + 1$  day):

$$D = \int_{t_2-1}^{t_2} \frac{cdt}{t^{1.2}} + \int_{t_1}^{t_2-1} \frac{0.64 cdt}{(t_2-t)^{0.36} t^{1.2}} \quad (2)$$

If  $t_2 \leq t_1 + 1$  day:

$$D = \int_{t_1}^{t_2} \frac{cdt}{t^{1.2}} \quad (3)$$

Therefore if  $t_2 \leq t_1 + 1$  day

$$D = 5 c(t_1^{-0.2} - t_2^{-0.2}) \quad (4)$$

In equations (2) and (4) time is in days and the dose rate from decaying fission products is taken as  $c/t^{1.2}$ . The constant  $c$  is therefore in roentgens per day at one day. To convert to more usual units let  $R_o$  be the dose rate due to fission products in roentgens per hour at one hour. It is then easily seen that

$$c = R_o / (24)^{0.2} = (0.530)R_o \quad (5)$$

In equations (2) and (4), time is still measured in days.

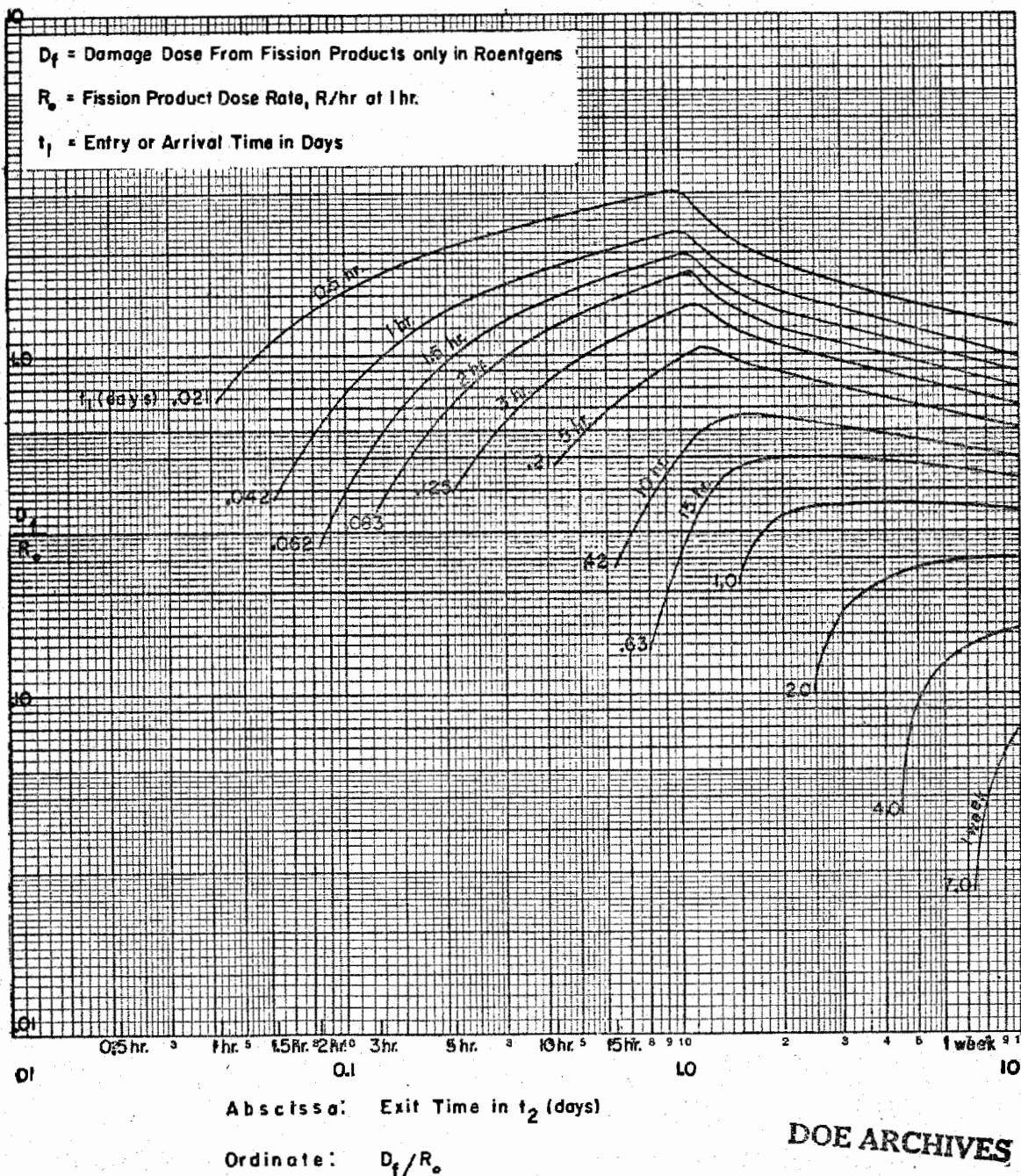
The second integral of equation (2) has been computed numerically. The results along with those from equation (4) have been plotted in Figures 6a and 6b which give directly the ratio  $D_f/R_o$ , for fission products alone and various entry and exit times, as implied by the British results, equations (1a) and (1b). An example will be given after discussing other approaches and refinements.

#### Method II

DOE ARCHIVES

An American investigation of the same questions has yielded a different expression. The concepts used here are those of a "permanent

BIOLOGICAL EFFECTIVE DOSE FROM FISSION PRODUCT DECAY (BRITISH DATA)



DOE ARCHIVES

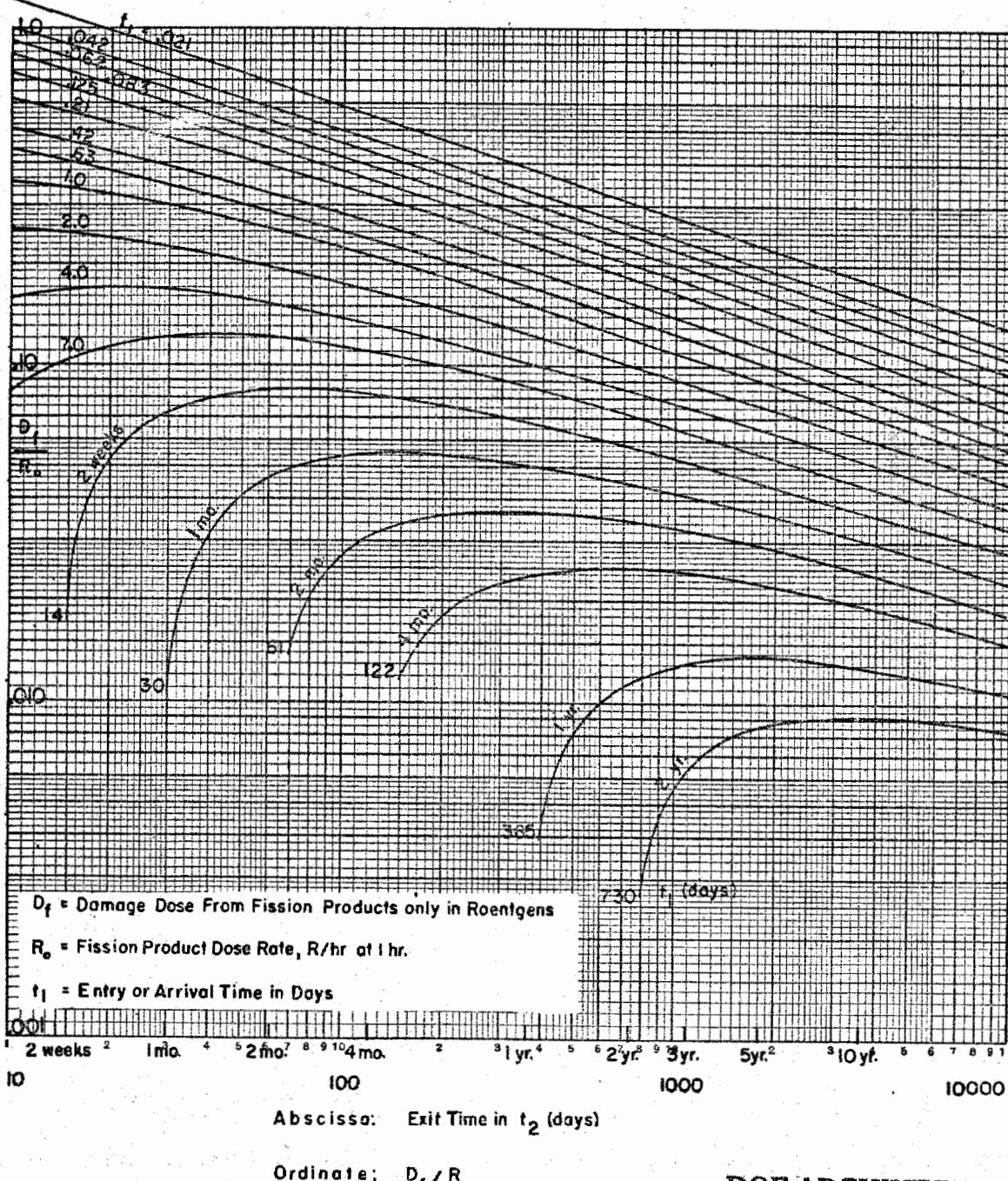
Figure 6a

426



431

**BIOLOGICAL EFFECTIVE DOSE FROM FISSION PRODUCT DECAY (BRITISH DATA)**



**DOE ARCHIVES**

Figure 6b

427

ATOMIC ENERGY ACT

432

"injury" and a "recoverable injury". The former is empirically 20% of the "instantaneous injury" while the latter decays exponentially with an apparent recovery half-life of about 2.4 days. In symbols, if  $I_p$  is the permanent injury dose,  $I_r$  the reparable injury dose, and  $R$  the dose rate then

$$\frac{dI_p}{dt} = 0.2 R \text{ and } \frac{dI_r}{dt} = 0.8 R - k I_r \quad (6)$$

where  $k = \frac{0.693}{2.4} = 0.29$  per day.

The damage dose at time,  $t$ , is then

$$D(t) = I_p(t) + I_r(t) \quad (7)$$

For the case of fission product decay  $R = c/t^{1.2}$  and exposure from  $t_1$  to  $t_2$ , equations (6) and (7) may be integrated. The result is

$$D = (0.2) c \int_{t_1}^{t_2} \frac{dt}{t^{1.2}} + (0.8)c \int_{t_1}^{t_2} \frac{e^{k(t-t_2)}}{t^{1.2}} dt \quad (8)$$

Here time may also be measured in days and equation (5) again applies:

$$c = (0.530)R_0 \quad (5)$$

where  $R_0$  is the dose rate in R/hr at one hour due to fission products.

Equation (8) has also been computed numerically. The results are given in Figures 7a and 7b which are completely analogous to Figures 6a and 6b.

#### Integral Dose Without Recovery (Fission Product Cumulative Dose)

To emphasize the effect of biological recovery, there is displayed in Figures 8a and 8b the integral dose, which would correspond to the case of no self repair. The equation for the integral or cumulative dose is simply equation (4) without the restriction that  $t_2 < t_1 + 1$  day. It will be noted that such a computation is in error in two respects. First the time of maximum danger would always appear to be the exit time.

**ELECTRA**

Secondly, the maximum dose may be much too high. These points are illustrated in Figure 9 which shows the integral and damage doses versus time for an entry or fallout arrival time of 10 hours. For long times, the integral dose is at least a factor of 5 above the actual biological damage dose. The spread between the "American" and "British" curves in Figure 9 gives some idea of the accuracy (or rather, paucity) of the original data as a function of exposure time.

### Neptunium Activity

Before discussing further the application of results obtained above, it is necessary to consider an additional factor. The curves developed above concern only the gamma activity from fission products. There is in addition another activity which has a different decay law. This arises from capture of neutrons by U-238 to yield U-239 which decays to Np-239. Both give off biologically significant radiation. U-239 gammas have a mean energy of 0.074 MEV while that of Np-239 (including the effect of internal conversion) is 0.225 MEV per disintegration. The half lives are 23.5 min. and 2.36 days, respectively.

Calculations lead to the following results. If  $R_0$  is the dose rate in R/hr at one hour for fission product activity, the integral dose from U and Np assuming unity capture to fission ratio is

$$\frac{I_{Np}}{R_0} = 0.315 \left[ e^{-42.5 t_1} - e^{-42.5 t_2} \right] + e^{-0.29 t_1} - e^{-0.29 t_2} \quad (9)$$

The units for  $I_{Np}$  are R/day and  $t_1$  and  $t_2$  are the entry (or arrival) and exit times in days. The biologically effective dose (damage dose) is

$$\frac{D_{Np}}{R_0} = 0.2 \frac{I_{Np}}{R_0} + 0.254 e^{-0.29 t_2} \left\{ e^{-42.2 t_2} - e^{-42.2 t_1} \right\} + 0.232 e^{-0.29 t_2} (t_2 - t_1) \quad (10)$$

where the units are the same and  $I_{Np}/R_0$  is given by (9). **DOE ARCHIVES**

The damage dose (10) is to be added to that previously computed for fission product gamma rays. To give an indication of the relative importance of the two terms (for unity capture to fission ratio), Table VII gives the relative dose rates from the two processes as a function of time for a unity capture to fission ratio. Table VII shows that from 1 to 10 days after shot time, U-Np-239 make a significant contribution to the dose rate.

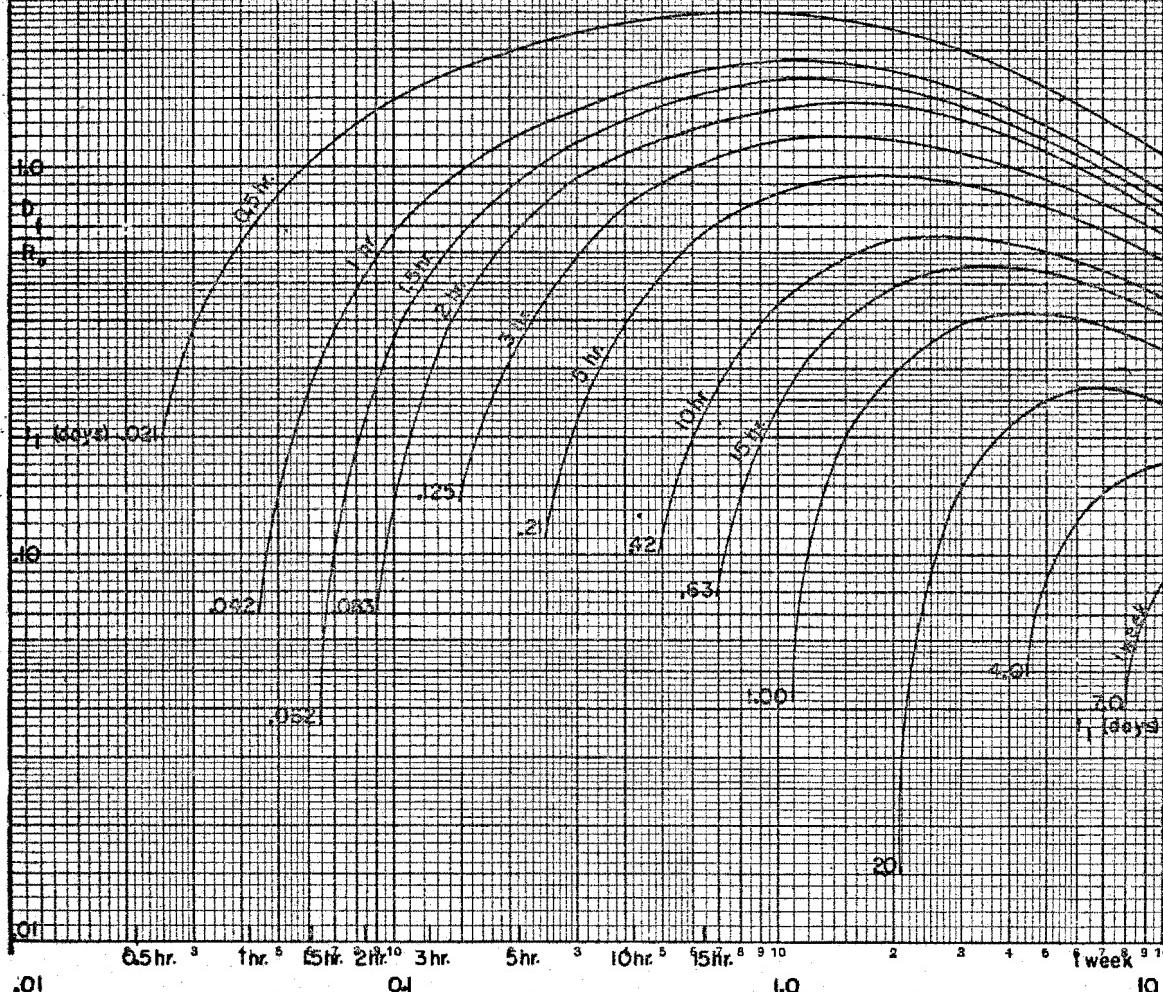
## BIOLOGICAL EFFECTIVE DOSE FROM FISSION PRODUCT DECAY (AMERICAN DATA)

10

**D<sub>f</sub>** = Damage Dose From Fission Products only in Roentgens

$R_e$  = Fission Product Dose Rate, R/hr at 1 hr.

**t<sub>1</sub>** = Entry or Arrival Time In Days



Abscissa: Exit Time in  $t_2$  (days)

Ordinate:  $D_t/R_s$

DOE ARCHIVES

Figure 7a

430

ATOMIC

495

BIOLOGICAL EFFECTIVE DOSE FROM FISSION PRODUCT DECAY (AMERICAN DATA)

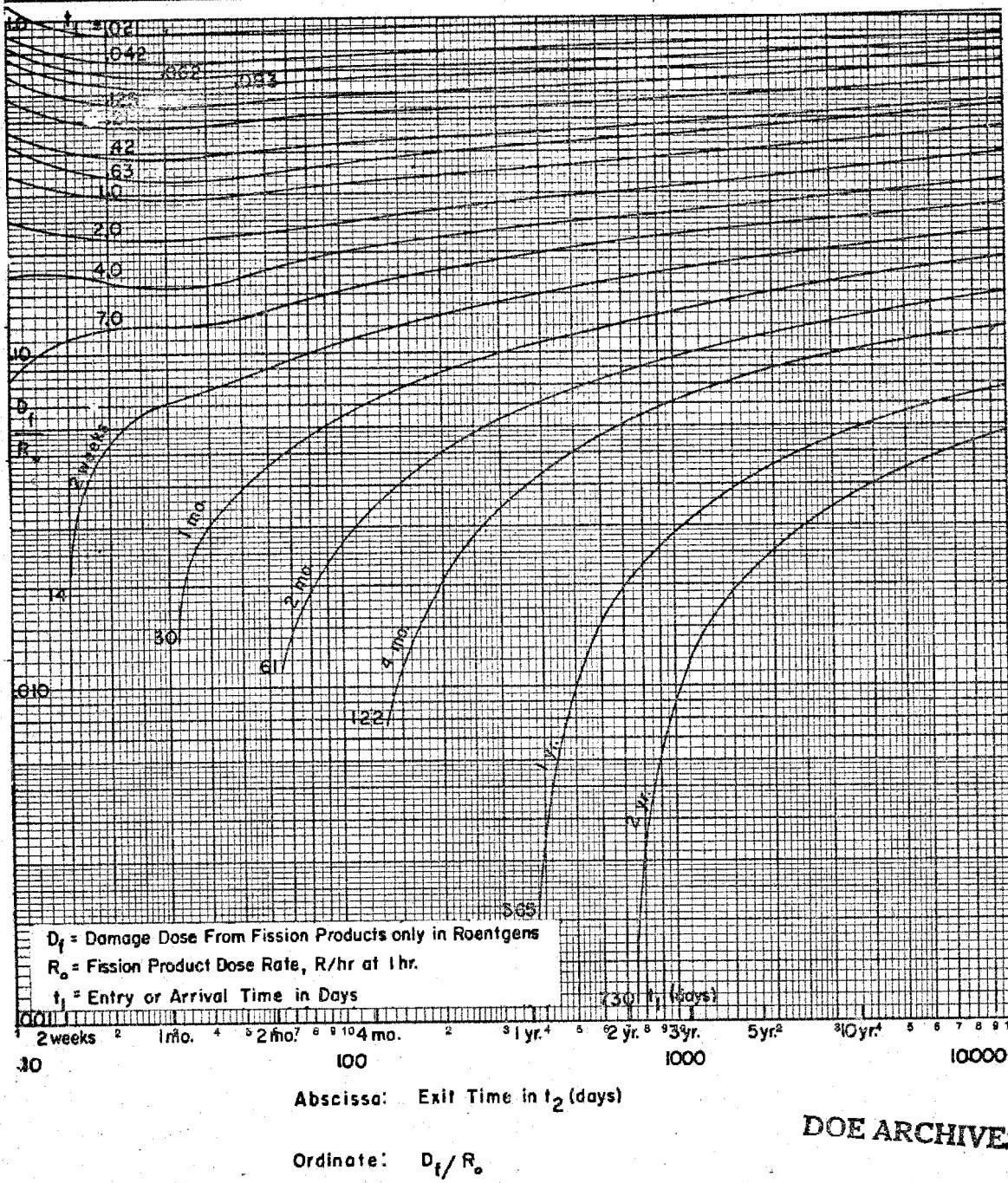


Figure 7b

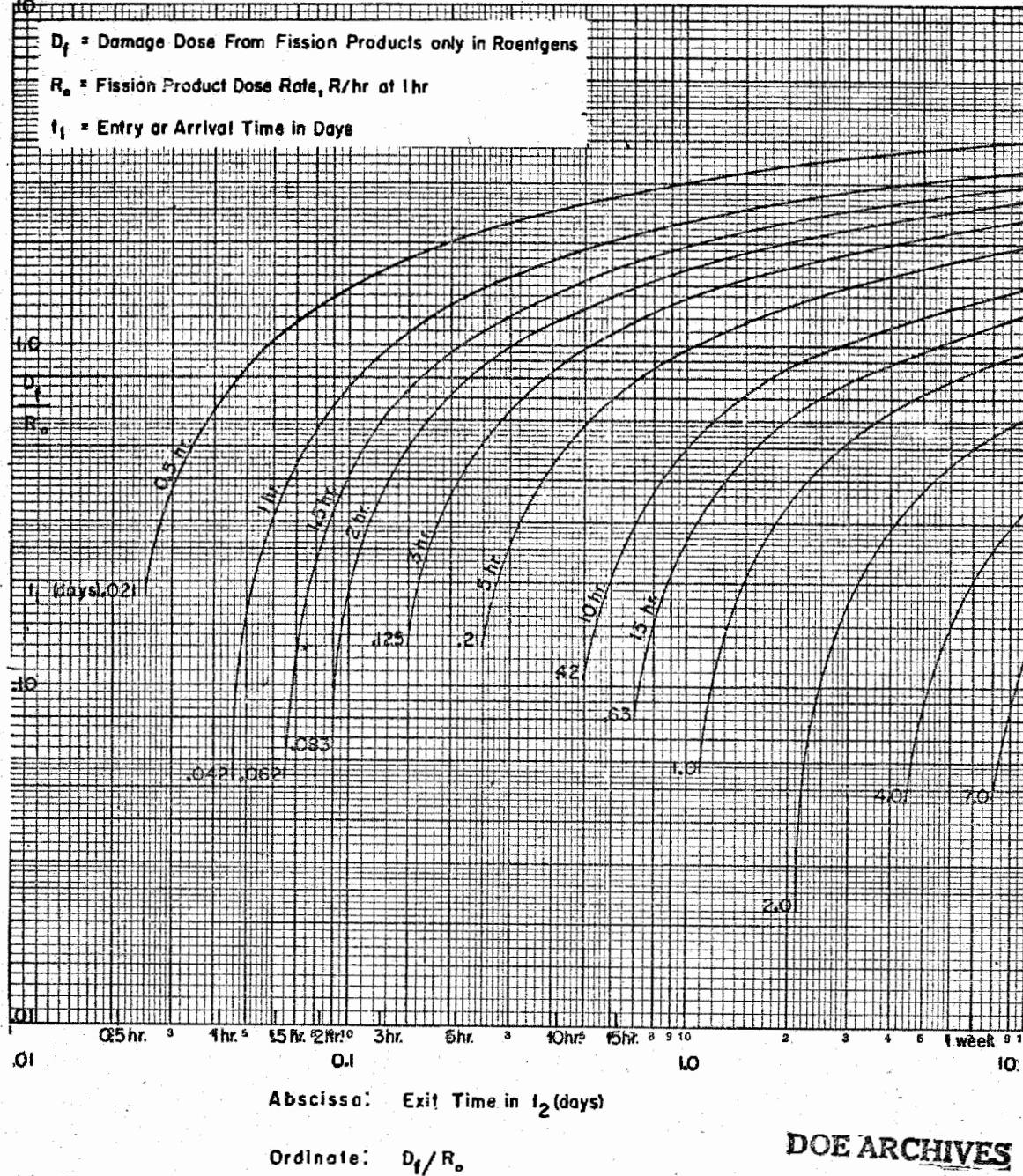
431.

OMIC ENERGY ACT 34

436

## INTEGRAL DOSE FROM FISSION PRODUCT DECAY

10

 $D_f$  = Damage Dose From Fission Products only in Roentgens $R_o$  = Fission Product Dose Rate, R/hr at 1hr $t_1$  = Entry or Arrival Time in Days

DOE ARCHIVES

Figure 8a

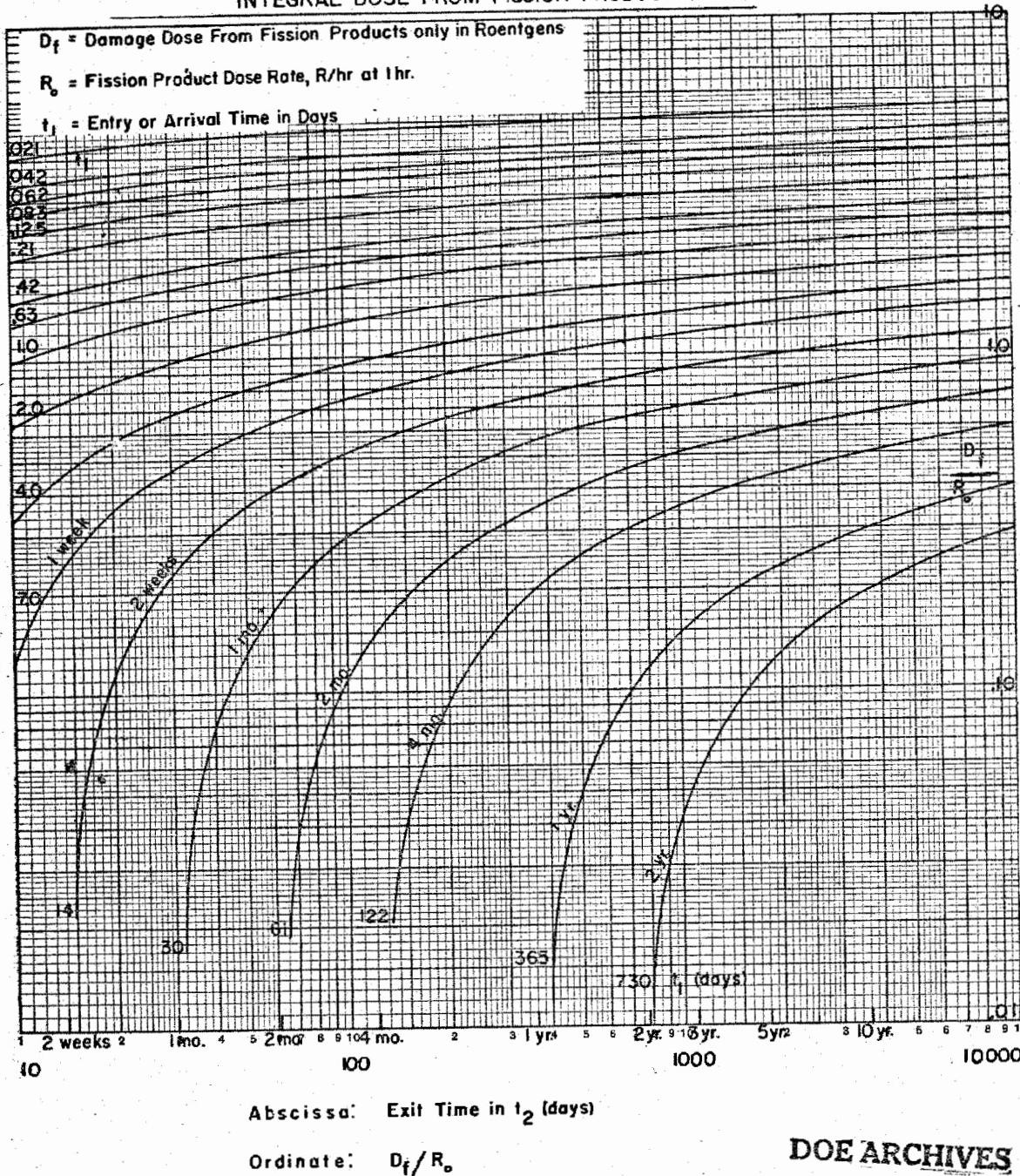
432



441

437

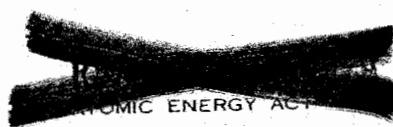
### INTEGRAL DOSE FROM FISSION PRODUCT DECAY



DOE ARCHIVES

Figure 8b

433



438

**COMPARISON OF PREDICTED DOSES FROM FISSION PRODUCTS  
ONLY, FOR 10 HOUR ENTRY OR ARRIVAL TIME.**

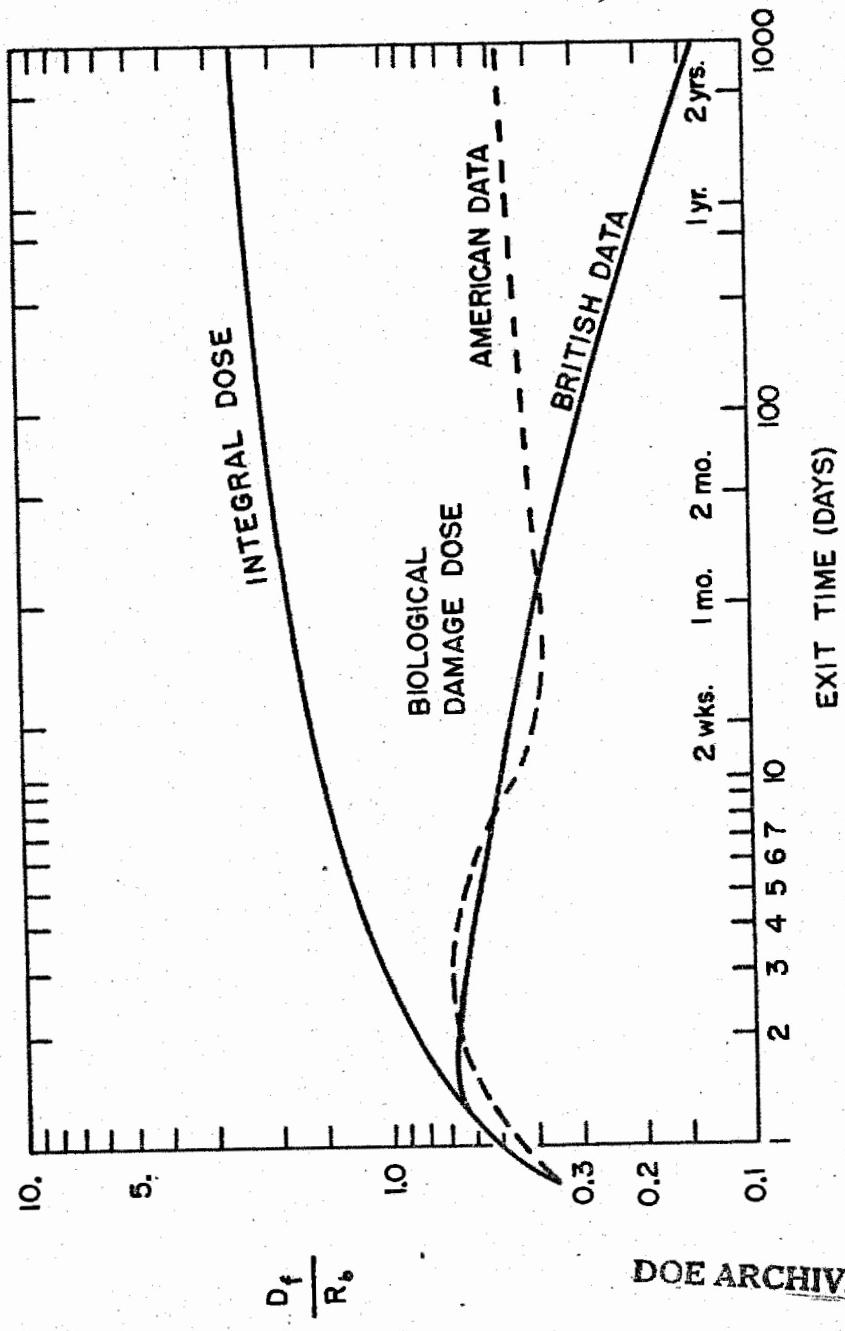


Figure 9

TABLE VII

## Dose Rate Ratio of Np-239 and U-239 to Fission Products

at Various Times Following Detonation

(Unity Capture to Fission Ratio)

Time	Hours						Days					
	0.1	0.3	0.5	2	5	10	24	2	4	7	14	30
Dose Rate Ratio Np and U/F. P.	0.03	0.14	0.11	0.06	0.08	0.17	0.41	0.66	0.84	0.71	0.20	0.04

In order to simplify the addition of this extra activity to that of the fission products, there is presented in Figure 10,  $\alpha$ , the ratio of the biological damage dose due to Np and U to that due to fission products alone (for unity capture to fission ratio):

$$\alpha = \frac{D_{Np}}{D_f} \quad (\text{Ratio of equation (10) to equation (8)}) \quad (11)$$

Figure 10 presents calculations for  $\alpha$  for various entry and exit times, where  $D_{Np}$  is given by (10) and  $D_f$  is the ("American") damage dose given in Figures 7a and 7b.

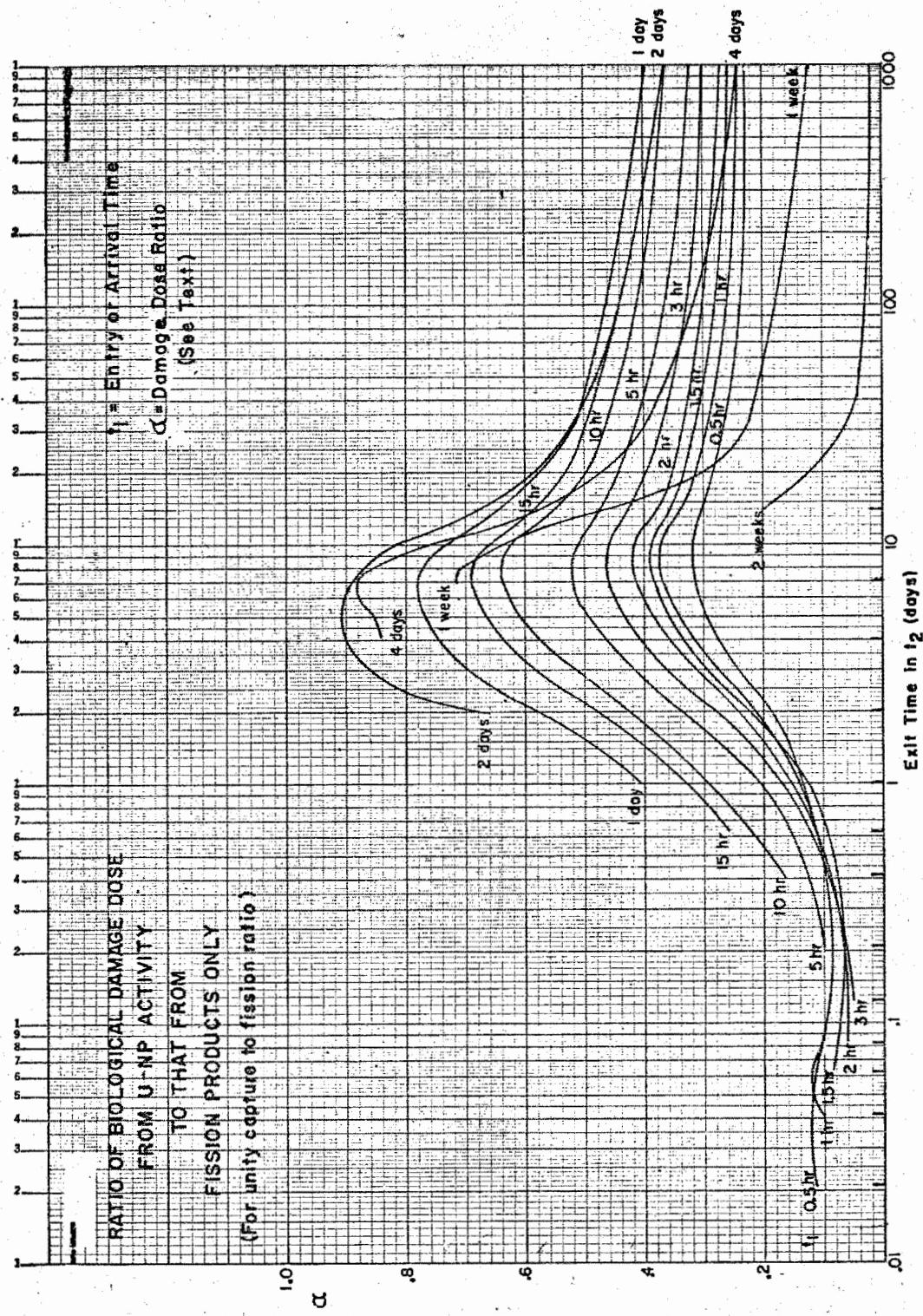
To use the information in Figure 10 the damage dose  $D_f$  due to fission products alone is first determined from Figures 7a or 7b for given values of  $t_1$  and  $t_2$ . These same times are then used to obtain a value of  $\alpha$  from Figure 10. The complete damage dose  $D$  is then found by

$$D = D_f(1 + F\alpha) \quad (12)$$

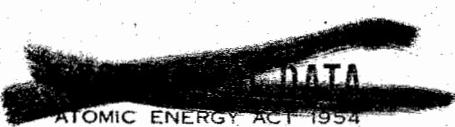
where  $F$  is the capture to fission ratio for the weapon in question. ( $F$  = number of neutrons captured in U-238 for each fission which takes place at the instant of detonation.)

To complete the presentation, Figure 11 shows the analogous ratio,  $\beta$ , for integral doses as computed from (9) and the standard integral-dose formula (Figures 8a and 8b).

DOE ARCHIVES



DOE ARCHIVES



441

Figure 10

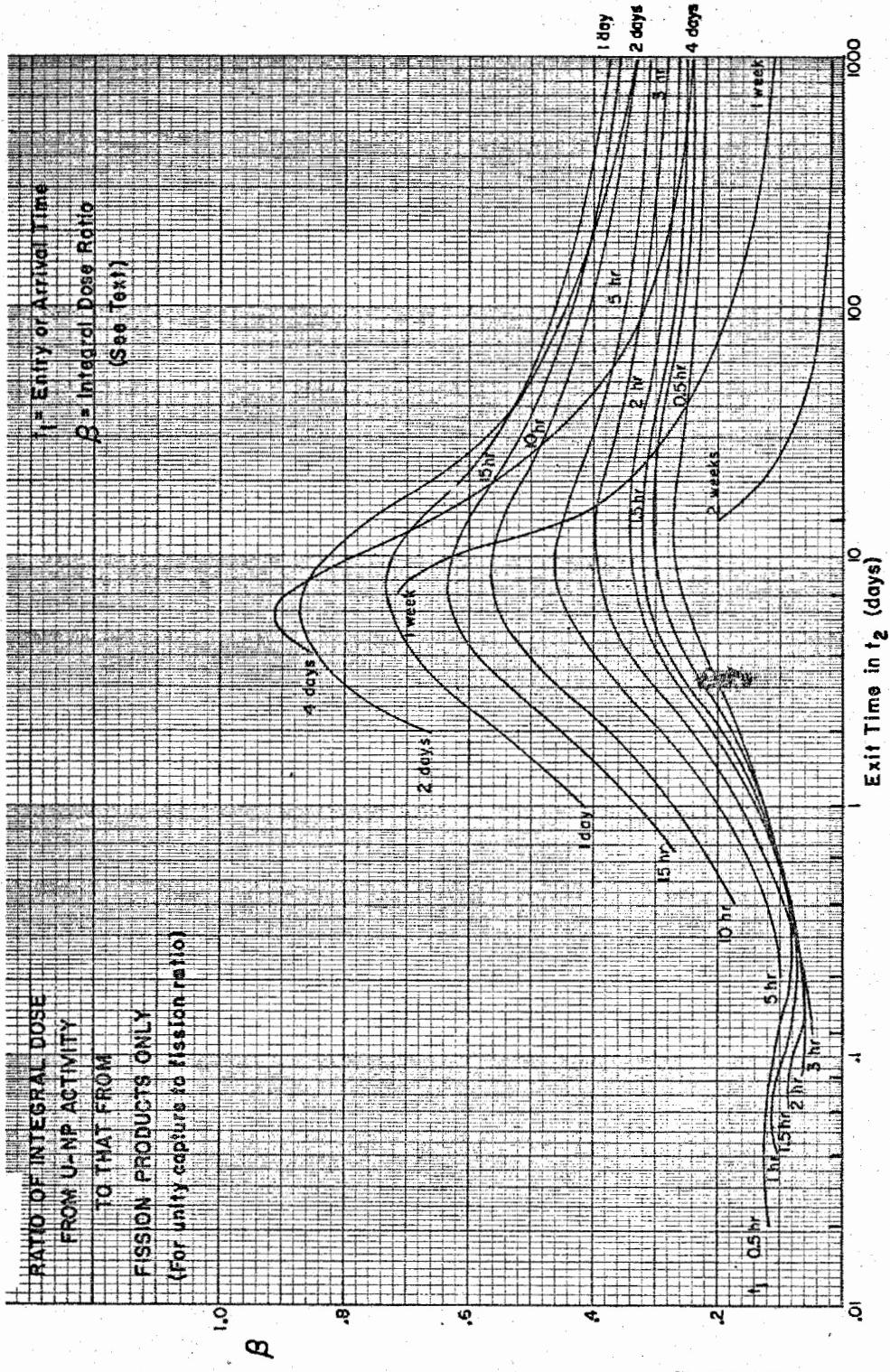


Figure 11

437

ATOMIC ENERGY ACT 1954

442

### Use of the Data in Fallout Calculations

In calculations such as discussed in Section I, the final results are presented in the form of 1 hr-dose-rates and 2-day integral (cumulative) dose. The employment of the data presented in this section to modify dose rate patterns is straightforward but the effect on integral dose is more complicated. We will first consider the effect on dose rate.

Dose Rate. - The 1-hr dose rate contour cannot be used to predict actual dose rates on the ground until most of the radioactive debris contributing to the roentgen rate has reached the ground location of interest; depending upon the distance from ground zero, this may be as long as twenty hours following shot time. Thus the dose rate contours should not be used to predict dose rates as would be measured on the ground by a roentgen dose-rate meter for times less than twenty hours after explosion. The following example illustrates the use of these contours to predict the dose rates at a given location:

#### Example. -

Surface detonation of 15 MT weapon with capture to fission ratio of unity.

Contour predicts 1500 1 hr-r/hr due to fission products, 70 miles NW of ground zero.

What is dose rate as measured by roentgen dose meter 24 hours after detonation?

$$\text{fission product dose rate} = \frac{1500}{24^{1.2}} = \frac{1500}{46} = 33 \text{ R/hr}$$

$$\text{From Table VII, } (U-Np/F. P.)_{24 \text{ hr}} = 0.41$$

$$U-Np \text{ dose rate} = 0.41 \times 33 = \underline{\underline{14 \text{ R/hr}}}$$

$$\text{Total roentgen dose rate at 24 hrs} = \underline{\underline{47 \text{ R/hr}}}$$

Integral Dose. - It must first be emphasized that all graphs in Figures 6 through 11 are plotted on the assumption that the amount of contamination is constant. No further fallout particles are considered to arrive during the time of exposure. The modifications due to arrival during exposure will be discussed below; for simplicity we shall first suppose that, as predicted in Figures 6 through 11, all contamination is already present at time  $t_1$ .

DOE ARCHIVES

With this proviso, consider first a simple example: Exposure occurs at a location where the fission product dose rate is 500 R/hr at 1 hr. Exposure starts at  $t_1 = 10$  hr = 0.42 days and exit occurs at  $t_2 = 2$  weeks = 14 days.

From Figure 6b we find that the "British" curve for  $t_1 = 0.42$  has the value  $D_f/R_o = 0.47$  when  $t_2 = 14$  days. Thus the damage dose due to fission products only is  $0.47 R_o = 235$  roentgens at the exit time of 2 weeks. The American data predicts approximately the same biological effect; from Figure 7b the damage dose is  $0.42 R_o = 210$  roentgens at 2 weeks.

Note, however, that both curves have an earlier maximum. From Figure 7a, for example, the damage dose (from fission products only) at 2.6 days was  $0.66 R_o = 330$  roentgens. In effect, the mechanism of biological repair was unable to "keep up" with the damage at early times when the radioactivity level was high. After 2.6 days, however, the activity decayed to the point where repair mechanisms could somewhat more than make up for the damage.

Consequently, the danger is measured not by the final damage dose but by its maximum value during the time of exposure. The (possibly delayed!) manifestations of injury will in general correspond to this maximum and not to the final value.

So far, we have considered only the damage dose due to fission products alone. This must be further increased by the effect of U-Np activity. From Figure 10, for example, the  $t_1 = 10$  hr curve shows that  $\alpha = 0.56$  at  $t_2 = 2$  weeks. The total damage dose at the exit time is thus  $210(1 + 0.56F) = 322$  roentgens if the capture to fission ratio F of the weapon was unity.

Recall, however, that it is the maximum dose which represents the actual danger. We must therefore maximize  $D_f(1 + \alpha)$  (if  $F = 1$ ) where  $D_f$  is obtained from Figure 7a and  $\alpha$  from Figure 10. Calculating this quantity for the 10 hr curve in the two figures, one soon finds that the maximum is very flat and occurs at about 3 days where  $(D_f/R_o)(1 + \alpha) = 0.99$ . Thus the maximum danger in this exposure occurs at 3 days and the total damage dose is then 500 roentgens. (Assuming  $F = 1$ )

This result is to be contrasted with integral dose which may be determined from Figures 8b and 11. The former gives a fission product dose of  $1.6 R_o$  for the same times while the latter leads to a correction factor of  $(1 + 0.55F)$ . If  $F = 1$ , the total integral dose is therefore

DOE ARCHIVES

1240 roentgens. Not only is this 250% too high in terms of actual biological damage but the maximum always occurs at the exit time, thereby leading to the false conclusion that earlier evacuation would be helpful. We saw above, that unless evacuation occurs before 3 days, there is no reduction of the danger.

At this point, it may be noted that even moderate shielding can provide considerable protection. The maxima which measure the danger of biological damage all occur earlier than about one week and their high values are due almost entirely to the very high dose rates occurring at times earlier than this. Protection during these early times is therefore very important and helpful. Thus retreat to a shelter for a period of one week under the circumstances already used in the above example changes all calculations to the curves for  $t_1 = 1$  week. Suppose the shielding reduces the earlier 3-day maximum by a mere factor of 10 leading to a dose of 50 roentgens while in a shelter. The one week curves in Figures 7 and 10 then show that the quantity  $(D_F/R_0)(1 + F\alpha)$  has a maximum (assuming  $F = 1$ ) of 0.16 at the exit time, 2 weeks. The maximum damage dose is then 80 roentgens due to exposure after leaving the shelter plus  $(0.42)(1 + 0.56)(R_0/10) = 33$  roentgens lingering damage dose from that received while in shelter. The net result is thus a dose of 113 roentgens instead of 500. If the arrival time is smaller than 10 hrs, the effect of even moderate shielding is even greater.

Finally, we consider the result of lifting the restriction stated earlier on the arrival of contamination. All of the above discussion assumed that fallout was complete before exposure started.

We will consider the contribution to the 2-day biological effective dose from radioactive debris that arrives at a ground location five hours after shot time. It will be comprised of two parts, that due to fission products alone and that due to U-Np. We will again assume a unity capture to fission ratio. If the fission-product-only 1 hr-R/hr dose rate of this debris is  $R_0$  then from Figure 7a,

the fission product contribution to the

$$\text{2-day biological effective dose} = 0.95 R_0$$

while from Figure 11 the Np-U contribution

$$\text{is given by } 0.34 \times 0.95 R_0 = \underline{0.32} R_0$$

Hence the total 2-day biological effective dose

$$= 1.27 R_0$$

440

DOE ARCHIVES

DATA  
ATOMIC ENERGY

445

We will now compare this total value with the fission product only 2-day integral dose from 5 hrs arrival time debris whose 1 hr-R/hr dose rate is also  $R_o$ . We refer to Figure 8a and find this to be 1.3  $R_o$ , and note that this is identical to the value for the 2-day biological effective dose. If we repeat these calculations for any other arrival time between 0.5 and 15 hrs and again make the above comparison, we reach the same conclusion. Now it can be proved that the location of the perimeter of any two-day dose contour equal to or greater than 100 R is determined solely by radioactive particles which arrive at a ground location in 15 hours or less.

In view of the above, the following conclusion can be stated, namely:

Conclusion (A). -

Irrespective of arrival times of the radioactive debris, for all thermonuclear surface detonations where the capture to fission ratio is about unity, the fission product two-day contour is the two-day damage (biological effective) dose contour, provided that the contour in question is at least 100 roentgens.

We will now consider damage dose for periods greater than two days.

Biological damage is apparently additive. The effects of self-repair require one to successively "down-grade" earlier doses before adding them to obtain the total effect, but the addition otherwise appears to reproduce the data on damage. (This additivity is implicit in both the British and American damage dose relations, equations (1a, 1b, 6 and 7).) Further, two days after shot time, the 1 hr-R/hr dose rate is a real measure of the actual dose rate at any ground location within the two-day dose 100 R contour, since by this time all radioactive particles have arrived.

The information in the preceding paragraph plus Conclusion (A) means that the biological effective (damage) dose at a non-shielded reasonably flat location at any time,  $t$ , is given by the following equation:

For  $t \geq 2$  days,  $D_{2d} \geq 100$  roentgens and capture to fission = 1; then the damage dose at the time,  $t$ , is

$$D_t = D_{2d} \left\{ 0.2 + 0.8 e^{-0.29(t-2)} \right\} + R_o \left( \frac{D_f}{R_o} \right) (1 + \alpha) \quad (13)$$

where  $t$  is time in days.  $D_{2d}$  and  $R_o$  are the respective fission product

two-day dose and 1 hr-R/hr dose rate levels in roentgens at the ground location in question. The right hand term is the "down-grading" of the 2-day damage dose with time and comes from equation (6). The left hand term is the damage dose which results from an exposure starting at 2 days and ending at  $t$ . It comes from equation (12) where  $D_f/R_0$  and  $\alpha$  at the time,  $t$ , can be found from the curves labeled two-day entry time on Figures (7) and (10), respectively.

Equation (13) can be rearranged to read:

$$D_t = D_{2d} M(t) + R_0 Q(t) \quad (14)$$

where the functions  $M(t)$  and  $Q(t)$  are obvious by comparison with equation (13). For convenience they are tabulated in Table VIII.

TABLE VIII

Values of  $M(t)$  and  $Q(t)$  of Equation (14)

	Time after Shot in Days						
	2	3	4	5	7	10	20
$M(t)$	1.00	0.80	0.65	0.54	0.39	0.28	0.20
$Q(t)$	0.00	0.28	0.40	0.50	0.51	0.45	0.35

These values are based upon continuous exposure to radioactive fallout for time periods of at least two days duration where time period is measured from shot time. See equation (13) for other restrictions.

From Table VIII we see that the time after shot at which maximum damage dose due to continuous exposure to radioactive fallout can never exceed 7 days. The time at which the maximum damage dose takes place and its numerical value depend only upon the 2-day dose and the 1 hr-R/hr fission product roentgen contour values of the ground location in question. To illustrate the use of equation (14), we will now give two numerical examples; Example (i) leads to a practical working rule, while Example (ii) illustrates the use of equation (14) to solve a problem which involves protective shielding.

**Example (i).-**

Surface detonation of 50 MT weapon with capture to fission ratio of unity.

Contours predict 300 R 2-day dose and 350 1 hr-R/hr due to fission products 270 miles NW of ground zero.

What is maximum biological effective (damage) dose due to continuous exposure and when after shot time will it occur?

From equation (14) and Table VIII we obtain

<u>Days after Shot</u>	<u>Damage Dose</u>
2	$300 \times 1.00 + 350 \times 0.00 = 300 \text{ R}$
3	$300 \times 0.80 + 350 \times 0.28 = 340 \text{ R}$
4	$300 \times 0.65 + 350 \times 0.40 = 335 \text{ R}$
5	$300 \times 0.54 + 350 \times 0.50 = 335 \text{ R}$
7	$300 \times 0.39 + 350 \times 0.51 = 295 \text{ R}$

Thus maximum damage dose is 340 R and will occur 3 days after shot time.

In Example (i), where ratio of  $R_{2d}/D_{2d}$  is 1.2, the maximum damage dose is only 10% greater than  $D_{2d}$ . Examination of all of the contour patterns for roentgen values of interest for all of the AFSWP winds shows that  $R_{2d}/D_{2d}$  is usually of the order of unity, and essentially never exceeds 1.2. This fact results in the following working rule:

**Conclusion B.-**

For a surface burst thermonuclear weapon with a capture to fission ratio of about unity, the maximum biological damage dose that can ever be received at any geographic location (with no shielding) is essentially the 2-day fission product integral dose and hence can be read directly from a 2-day fission product dose prediction contour map.

We now proceed to Example (ii).-

DOE ARCHIVES

443

RECD/CDL/SP/AM

448

Example (ii).-

Surface detonation of 15 MT weapon with capture to fission ratio of unity.

Contour predicts 1500 1 hr-R/hr and 2000 R 2-day dose due to fission products, 70 miles NW of ground zero.

A person is in shelter of shielding factor 10, for the first two days after shot. After first two days he leaves shelter and is exposed in open flat area for 8 hours each day; remaining 16 hours spent in shelter.

What is maximum biological dose received by the person and when will it occur?

$$\text{Effective } D_{2d} = \frac{2000}{10} = 200 \text{ R}$$

$$\text{Effective } R_o = \frac{1500 \times 8}{24} + \frac{1500 \times 16}{10 \times 24} = 600 \text{ 1 hr-R/hr}$$

From equation (14) and Table VIII we obtain

<u>Days after shot</u>	<u>Damage Dose</u>
2	$200 \times 1.00 + 600 \times 0.00 = 200 \text{ R}$
4	$200 \times 0.65 + 600 \times 0.40 = 370 \text{ R}$
5	$200 \times 0.54 + 600 \times 0.50 = 410 \text{ R}$
7	$200 \times 0.39 + 600 \times 0.51 = 380 \text{ R}$

Thus the person will receive a maximum damage dose of 410 roentgens and this will occur 5 days after shot time.

DOE ARCHIVES

444

DATA

ATOMIC ENERGY AGENCY

449

QUESTIONS AND ANSWERS FOLLOWING DR. HENRIQUES' PRESENTATION

Question: Dr. Kellogg, Rand Corp.

This last slide Dr. Henriques showed brought up a question. Would you include the attenuation factor for the terrain or are they based on the infinite flat plain?

Answer: Dr. Henriques, TOI

Mine include both the [REDACTED]  
terrain factors. [REDACTED]

DELETED

Question: Dr. Genevese, AFOIN

DELETED

Answer: Dr. Henriques, TOI

When you have a nuclear explosion, two main things happen. One is you get fission products that fall to the ground; and you get some U-239 which goes into Neptunium-239 and these are normally not considered with the fission products. These curves provide a means to do it if you know what fraction of the bomb goes to fission products and what goes to U-239. It makes no contribution to the fission products dose rate early but it does in time, because of the difference between the 1.2 law and the exponential decay.

Question: (Unknown)

Could you amplify your remarks about the degrading effects of terrain? How much does it vary with different types of terrain? What is the cause of it and so forth?

Answer: Dr. Henriques, TOI

There are magic numbers you can use and they are all available in reports and all roughly the same. I just don't know how to answer it. It depends on whether you are in the city and it comes down on buildings or if you are on the ground. The reason for using .55 instead of .7 is not basically important. Any open terrain or open field will not be as flat as the Salt Lake flats.

DOE ARCHIVES

445

ATOMIC ENERGY ACT 1954

450

Question: Dr. Krey, CRL

You think the different types of soil around ground zero will have an effect?

Answer: Dr. Henriques, TOI

Yes. Two different things, coral and Nevada dirt, there is a real basic difference. If you use the NRDL curve, it is impossible to duplicate Bravo with the NRDL particle.

Comment: Dr. Kellogg, Rand Corp.

There was one point you mentioned - the geometry of the cloud and that altitude is an important point. The height of the cloud as being constant through a rather large range of yields - this seems not to be borne out when you plot the CASTLE results with IVY results. The entrainment at each altitude is relatively insensitive to yield. When you put in more energy, the cloud would become higher. The difference might not be very large, but I think it would be incorrect to assume that the altitude is not a function of yield.

Question: Dr. Scoville, AFSWP

Isn't the bottom of the cloud likely to be at the bottom of the tropopause?

Answer: Dr. Kellogg, Rand Corp.

I don't know.

Comment: Dr. Felt, LASL

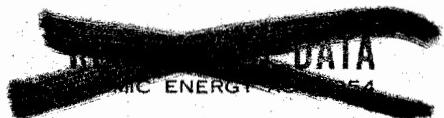
The Chemical or physical nature of the soil are more important to the fall-out. Dr. Henriques mentioned coral and I think I was talking mainly about soil. Some have proposed that the physical nature is more important.

Comment: Dr. Rapp, Rand Corp.

I would like to clarify our position. Our way of looking at it is the earth that will eventually become active must get into the fireball almost instantaneously.

DOE ARCHIVES

446



451

Comment: Dr. Krey, CRL

At CASTLE, we found quite a lot of particles over 100 microns to have activity principally on their surface. It was hard to see how they could get into the fireball and have activity strongly on their surface. These were actually found at CASTLE.

Comment: Dr. Rapp, Rand Corp.

I will quote some work that was done at Rand. They investigated this condensation principle. According to this model, the silicates come out and then some of the fission products are condensed at a later time, so this model definitely accounts for not having the fission products evenly distributed throughout the fall-out particle. Most of it is from the condensation particles.

Comment: LTCOL Lulejian, ARDC

I think I remember reading in a GREENHOUSE report where they found a small piece of chlorophyll which had fission products on it. Apparently everything is happening. Condensation, vaporization, and other things. Hence, a leaf coming down with a lot of activity on it.

DOE ARCHIVES

447.

REF ID: A671452  
DATA  
ATOMIC ENERGY ACT

452

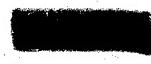
**THIS PAGE IS BLANK**

**DOE ARCHIVES**

**448**



**AMERICAN  
ATOMIC ENERGY**



**453**

PREDICTION OF DOSE-RATE AND DOSAGE CONTOURS AS FUNCTIONS  
OF YIELD AND METEOROLOGICAL CONDITIONS; RECENT DEVELOPMENTS  
IN WEATHER FORECASTING TECHNIQUES FOR THE PACIFIC PROVING GROUND

PART I  
LTCOL C. D. Bonnot, USAF  
Joint Task Force SEVEN

Introduction

We have been talking the last few days about fall-out, and now we will talk about weather. We know we can only have as good fall-out analysis as we have weather forecasts. We have discussed that pretty thoroughly. From the various fall-out models given, I thought it would be well to go back and discuss the Bravo weather situation. I want to give credit for this work to the Oahu Research Center in Hawaii. The work was not done by me personally, but by Ohmstead and Dean under Dr. C. E. Palmer's direction. The report is unclassified and it was deliberately made that way; there is no reference to Bravo or to shot times. They selected this date because there is a lot of good weather data, so the report states. The Oahu Research Center is part of the Institute of Geophysics, UCLA, and operates under contract to the Air Force Cambridge Research Center. They have both military and civilian personnel assigned and the Task Force works with them. They assist during the test period and then we give them all the raw weather data. They now have data from all the Pacific tests. They are a storehouse of all the raw data and weather information for the tropical Pacific. It might be well for everyone interested in Bravo to get this report. It has now been published in its final form as Special Report No. 1, Oahu Research Center. The report is unclassified and available to anyone who wants it. Just ask AFCRC at Boston, or contact me and I'll see that you get a copy.

This presentation will be in three sections. I am going to talk about just the horizontal field, or streamline analysis, for Bravo day. Commander Rex will speak of the vertical motions for Bravo day, which are also analyzed in the report mentioned above. He also will discuss five other situations which he has analyzed for vertical motions, and then I will close with a short discussion of the proposed rawinsonde observing net for the Southwest Pacific which we feel is necessary if adequate analyses and forecasts of the weather and wind fields are to be furnished to the Commander, Joint Task Force SEVEN.

Horizontal Fields

The synoptic situation changed very little during the three day period between February 28 and March 2, 1954. At any given level, the wind directions and speeds did change slowly but these changes were due to systematic internal developments within the cyclones and anticyclones

in situ. No synoptic systems moved through the area; no new synoptic systems developed in the area during this three day period.

In the vertical, two transition levels (shear levels) happened to intersect various parts of the analysis levels. The transition levels occurred near 10,000 and 60,000 feet. The apparent synoptic changes at these analysis levels are due to small height changes in the shear levels together with some slow internal synoptic intensifications.

During the three day period, at 10,000 feet, there was a gradual intensification of two cyclonic vortices that lay in a trough oriented east-west between Wake and Rongerik. (Figures 1, 2, 3. Note: These maps have been analyzed by the isogon-isotach method on a 1:7,500,000 scale. All time changes of the winds in the horizontal as well as in the vertical have been incorporated into the isogon-isotach analysis.) Only one cyclonic vortex appears on the analyses. It is located north of Rongerik; the other lies in the area covered by the legend box. These vortices slowly intensify during the period, but do not descend to the surface. They are reasonably well fixed by reconnaissance reports (10,000 feet only) on February 28, March 1, and later again on March 3. The gradual intensification of the trough in which they are imbedded is apparent by the westward movement of the neutral point from Eniwetok on February 28 to the Guam area by March 2. In other words, the higher level westerlies have descended into the analysis level.

An anticyclone at 10,000 feet is located near Kwajalein on February 28 (Figure 1), and during the period it moves slowly southwestward to Kusaie. At the same time another anticyclone appears to the north of Ponape (based on off-time reconnaissance reports). It also moves slowly southwestward towards Truk during the three days. Both systems descend further into the 10,000 foot surface during the period. The combined effect of the slow intensification of the cyclones and the equatorial anticyclones at 10,000 feet over the Marshall Islands is to maintain northerly wind components over the Rongerik area below 20,000 feet.

The subtropical anticyclones are located north of 20°N at 10,000 feet (just off the map). (Figures 2 and 3.) They weaken vertically north of Wake, completely disappearing as wind singularities above 10,000 feet, and cannot be found in the speed field above 20,000 feet. The systems have very little effect on the weather of the Marshall Islands.

DOE ARCHIVES

At 30,000 and 40,000 feet the flow pattern around the equatorial anticyclones is the same with height and with time, giving southwesterly

450

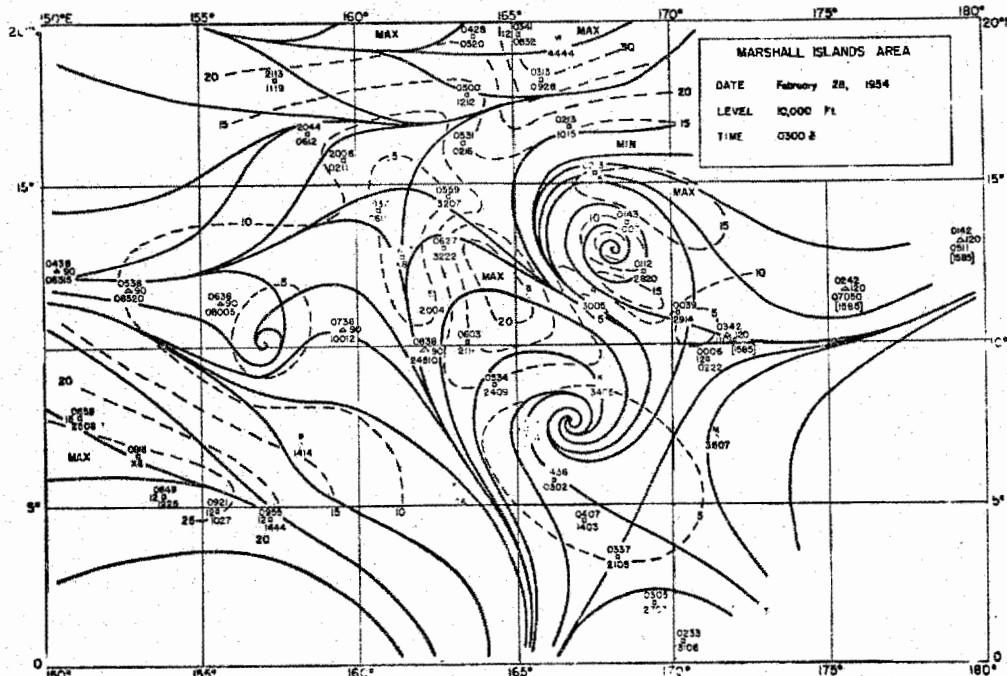
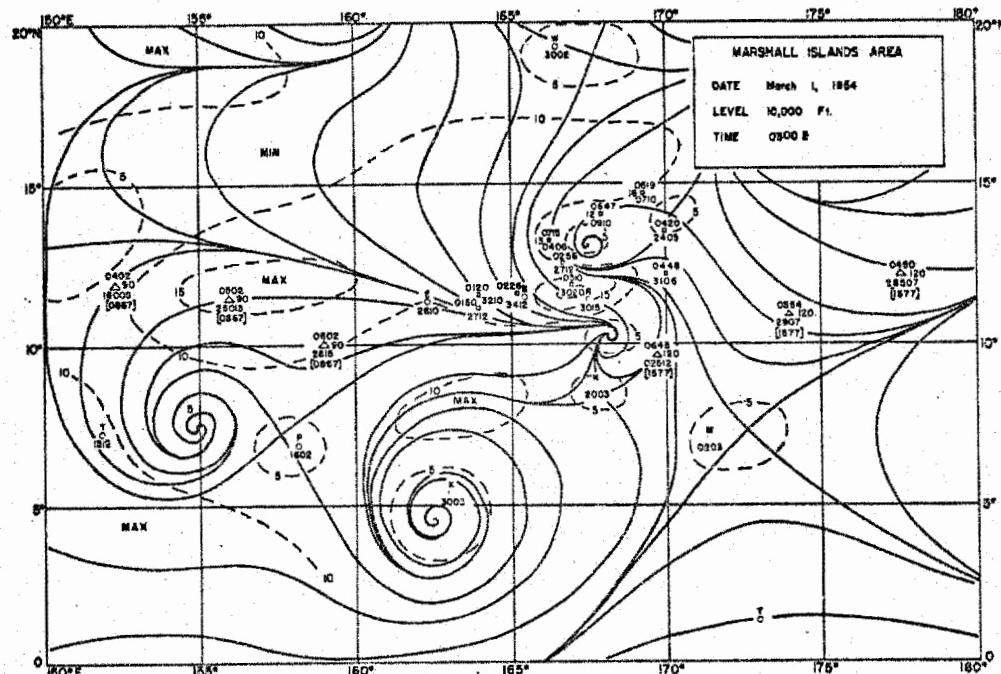


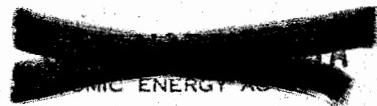
Figure 1



DOE ARCHIVES

Figure 2

451



456

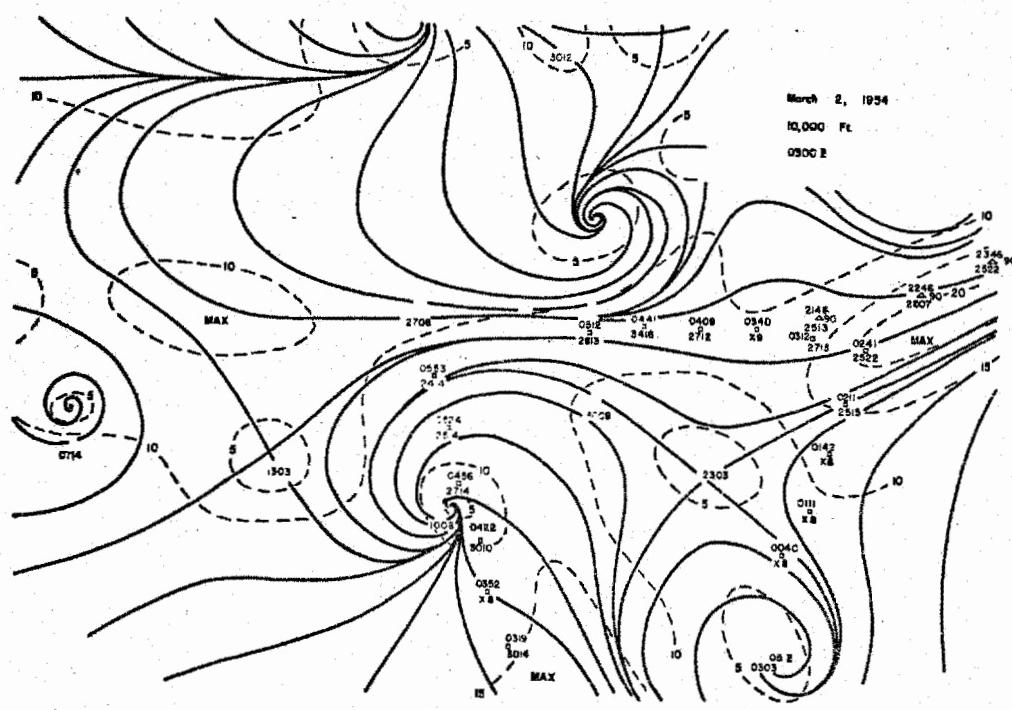


Figure 3

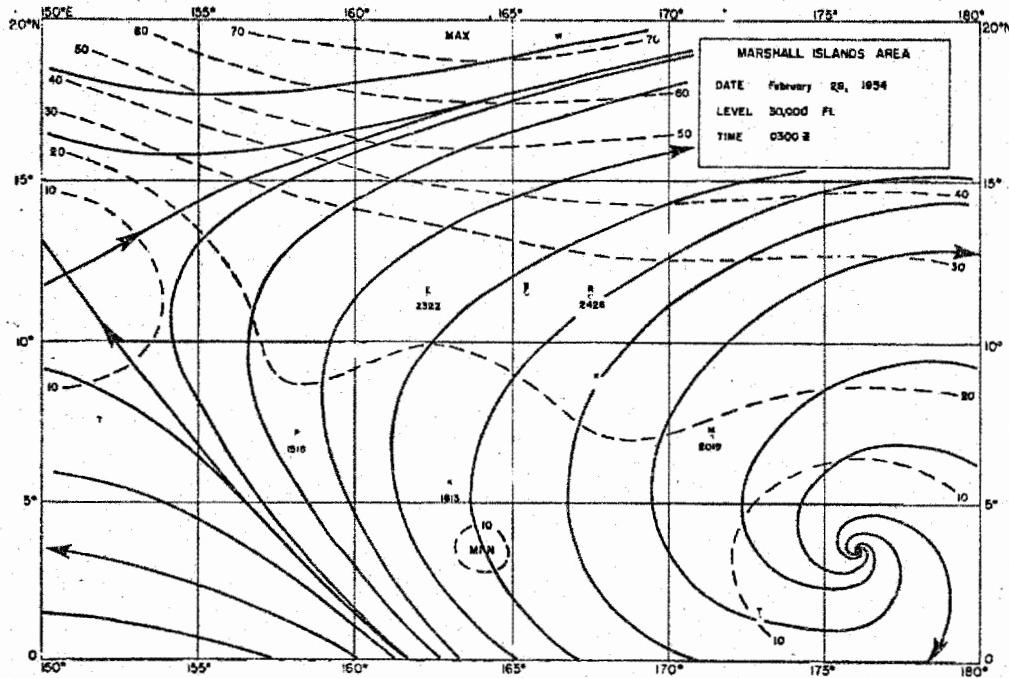
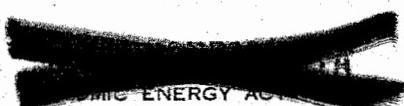


Figure 4

DOE ARCHIVES

452



457

components over the Bikini area. (Figures 4, 5, 6, 7) A gradual southwestward shift of this belt occurs with time, in agreement with the southwestward displacement of the anticyclones at 10,000 feet.

At 50,000 feet southwesterly flow appears on February 28. (Figure 8) On March 1 an anticyclone descends into the analysis level at map time, but ascends again after a 6 hour period, and is not evident at 50,000 feet on 2 March. (Figures 9 and 10)

The horizontal picture of the wind flow at 60,000 and 70,000 feet is complicated by the presence of the tropopause and the low level stratospheric easterlies. (Figures 11 and 12) Any horizontal analysis in these layers represents only the height changes in all of these shear levels, and therefore has not been performed except for March 1. (Figures 13, 14, 15) Wind speeds at these levels are light.

Steady and strong easterly winds persist at 80,000 feet throughout the period.

In conclusion, analyses for all levels from the surface through 80,000 feet for 1 March 1954 are shown (Figures 16, 17, 2, 18, 5, 6, 9, 11, 12, 14).

DOE ARCHIVES

453

AMERICAN ENERGY ACT

458

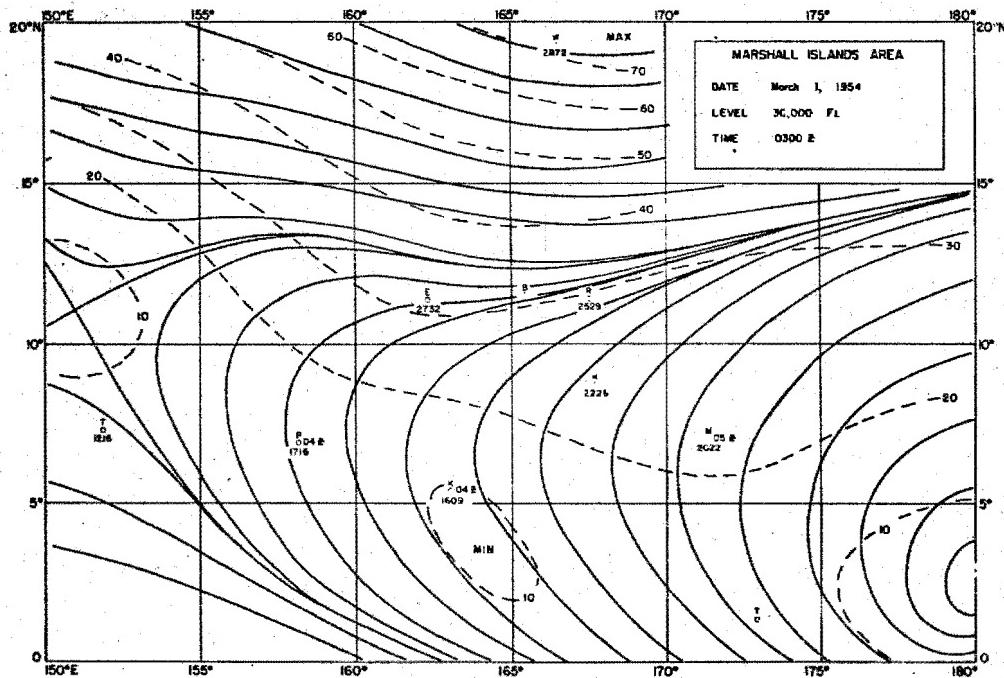


Figure 5

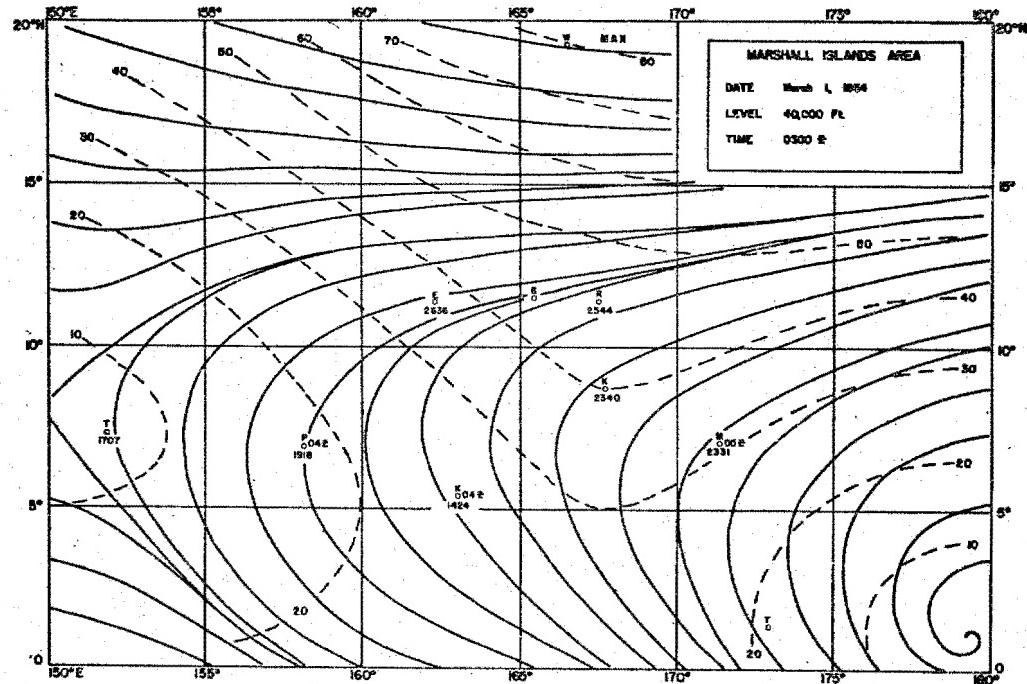


Figure 6

DOE ARCHIVES

454

**THE  
NATIONAL  
ENERGY  
POLICY**

459

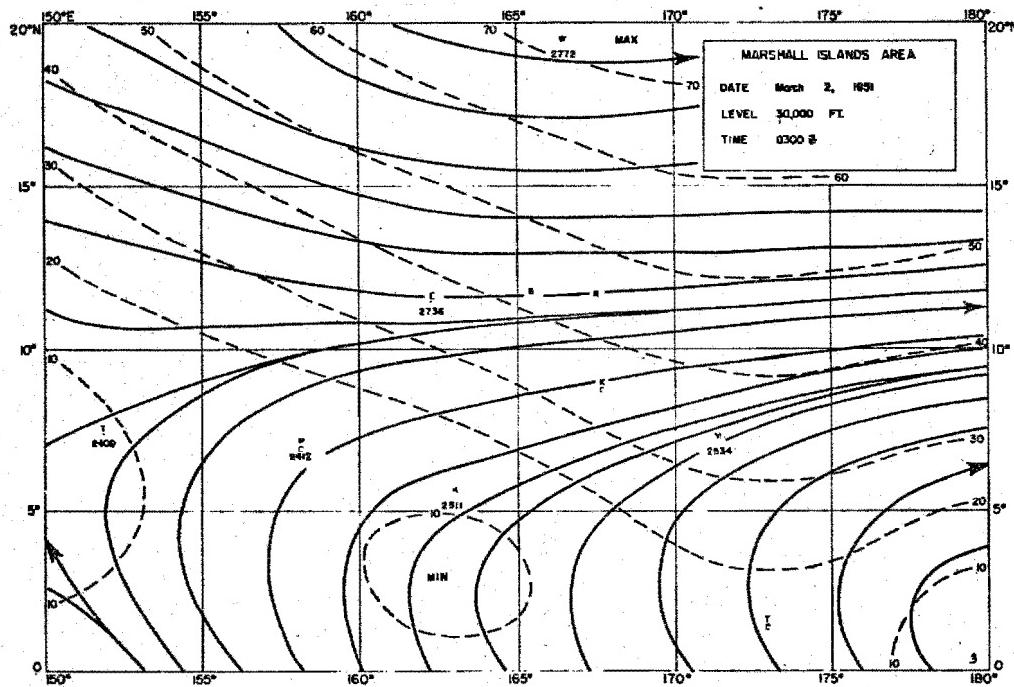


Figure 7

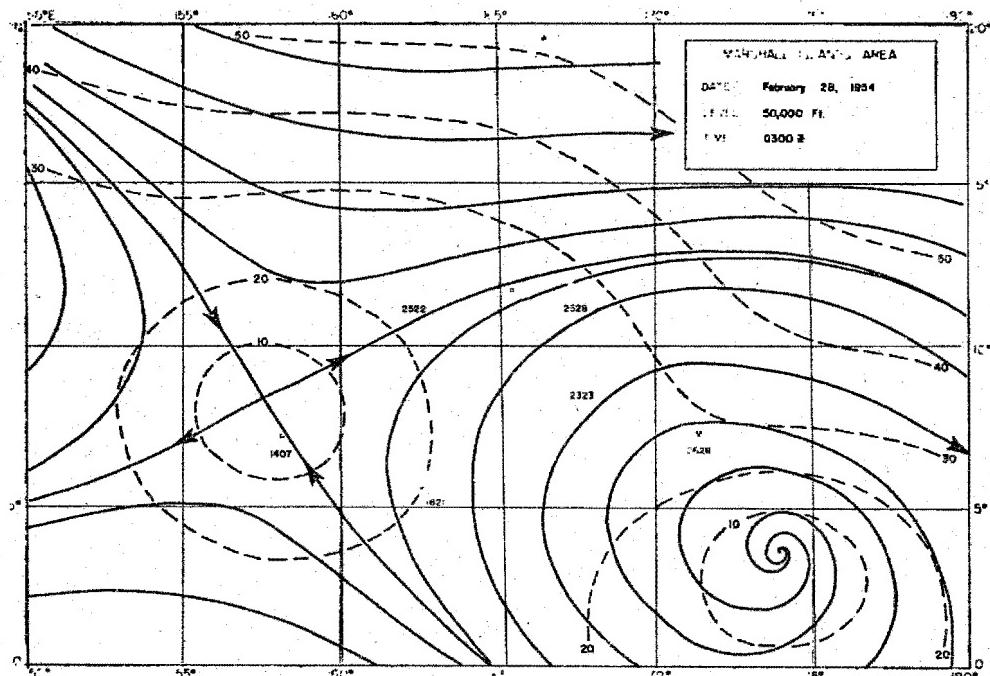


Figure 8

DOE ARCHIVES

455



460

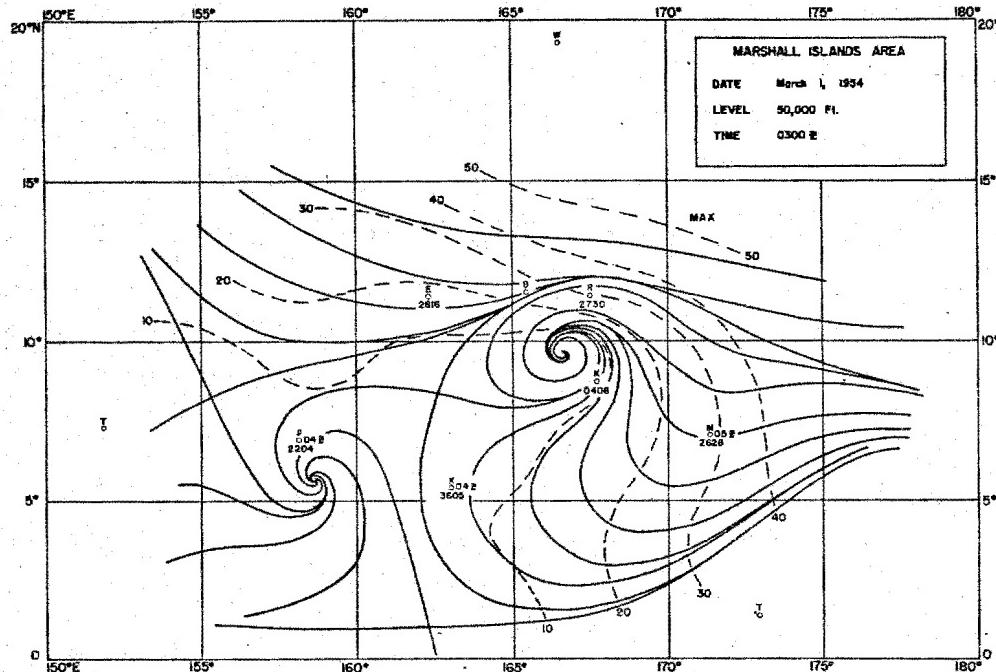


Figure 9

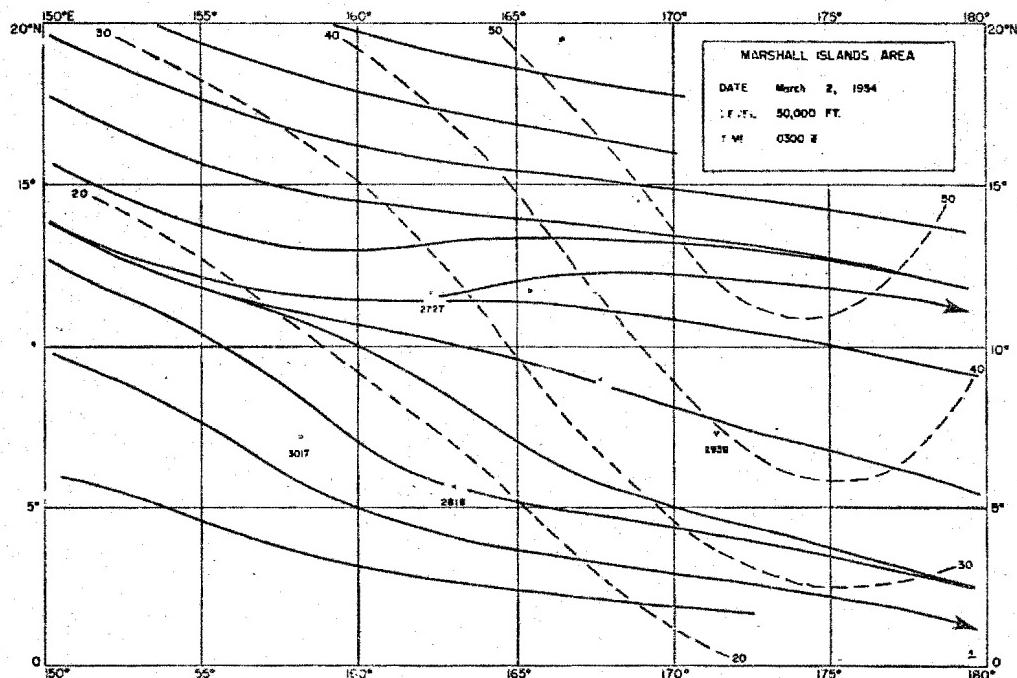
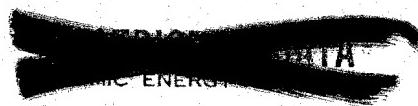


Figure 10

DOE ARCHIVES

456



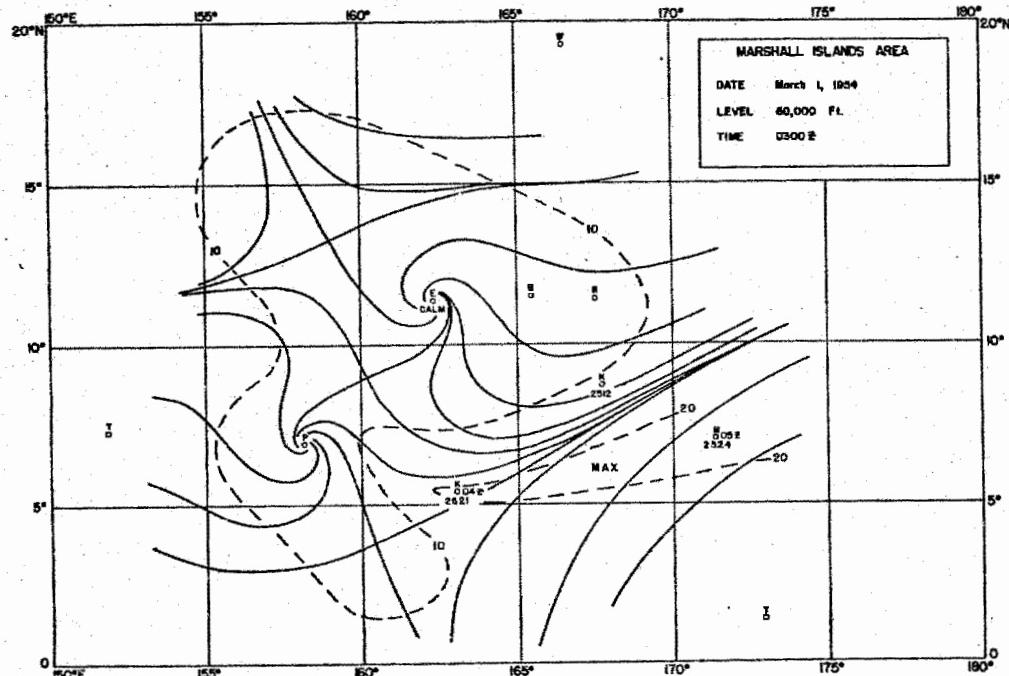


Figure 11

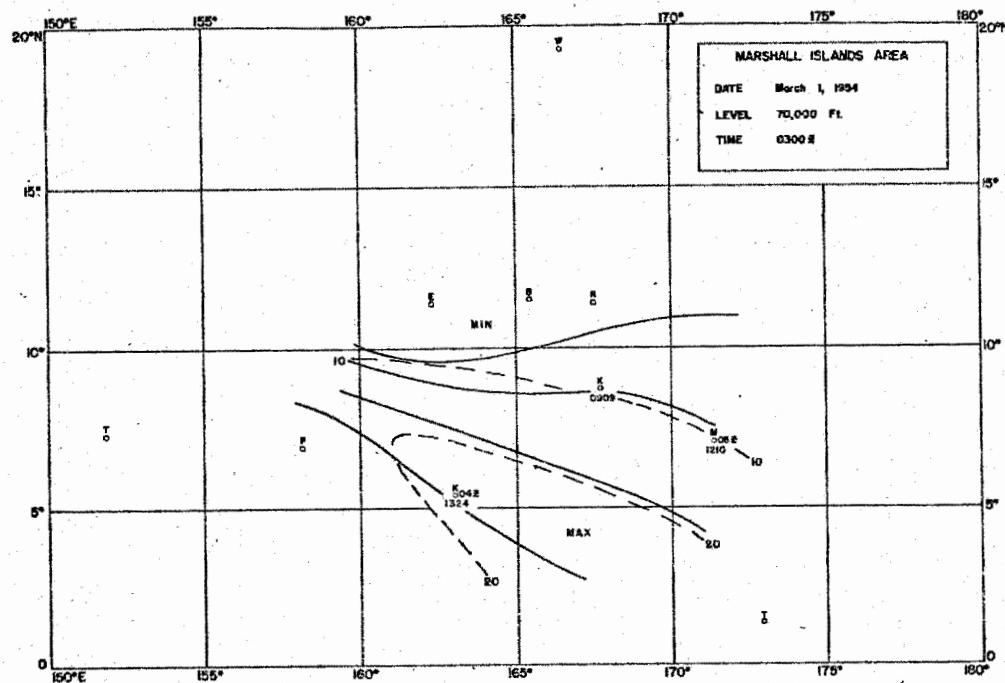


Figure 12

DOE ARCHIVES

457

ENERGY ACT 195

462

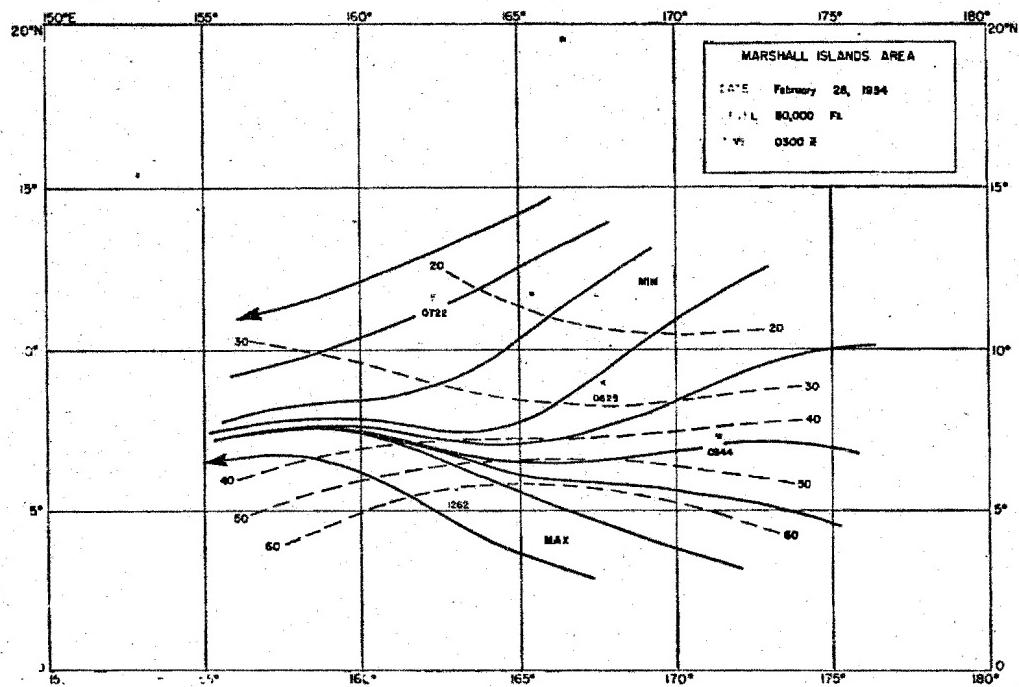


Figure 13

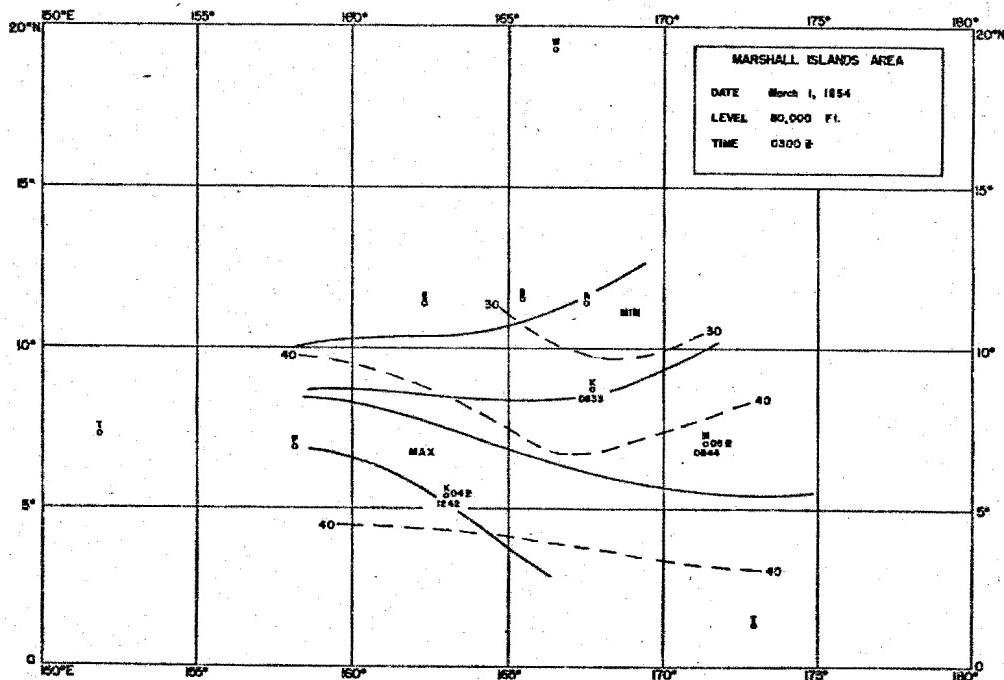


Figure 14

DOE ARCHIVES

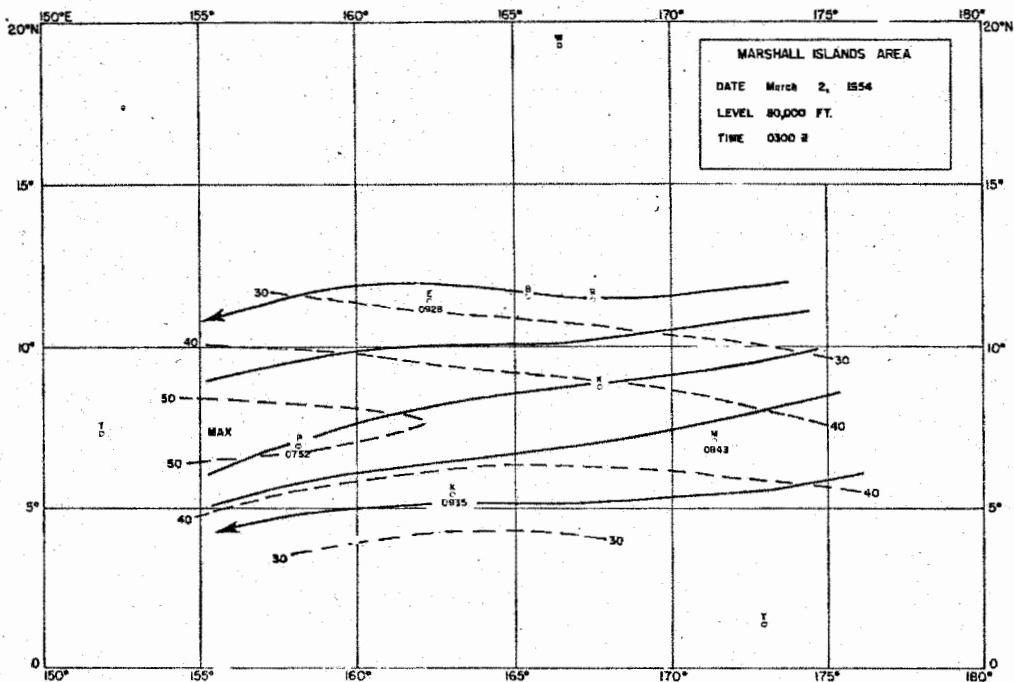


Figure 15

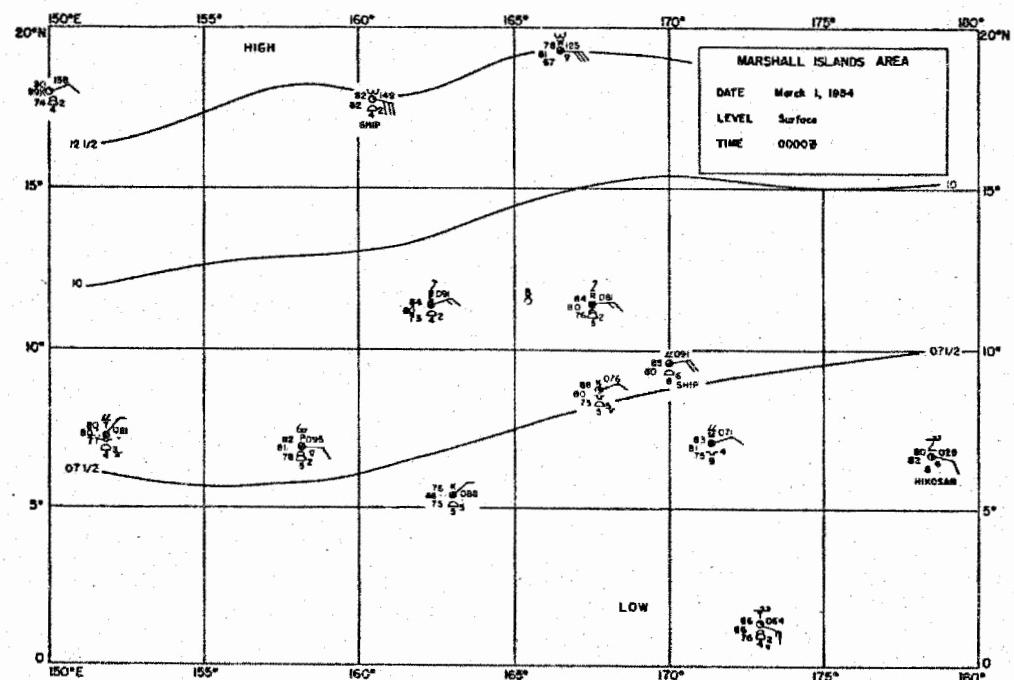


Figure 16

DOE ARCHIVES

459

**NUCLEAR ENERGY ACT**

464

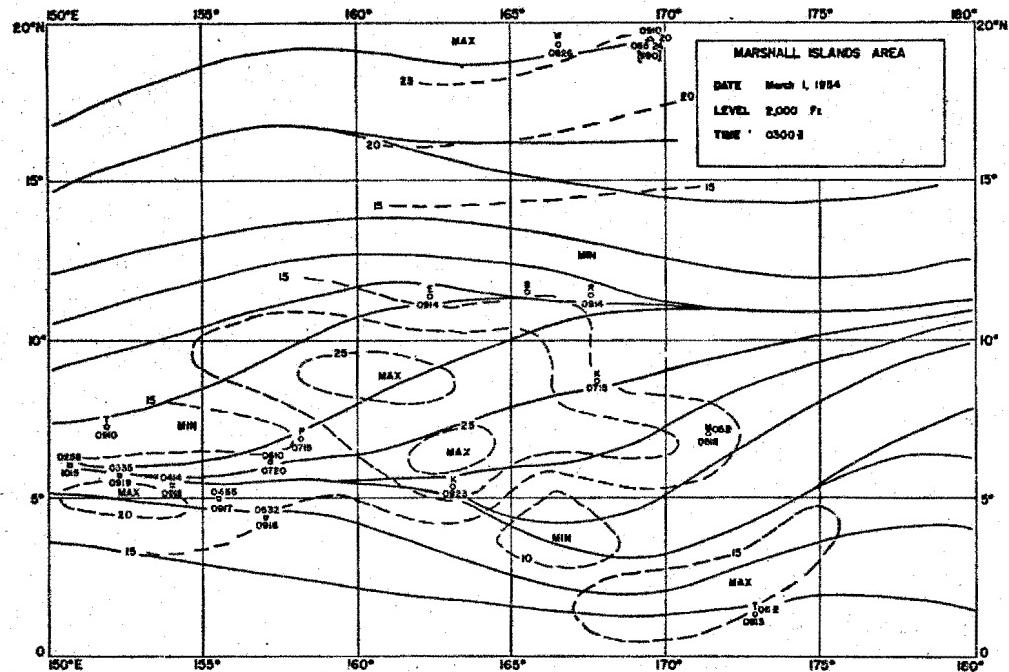


Figure 17

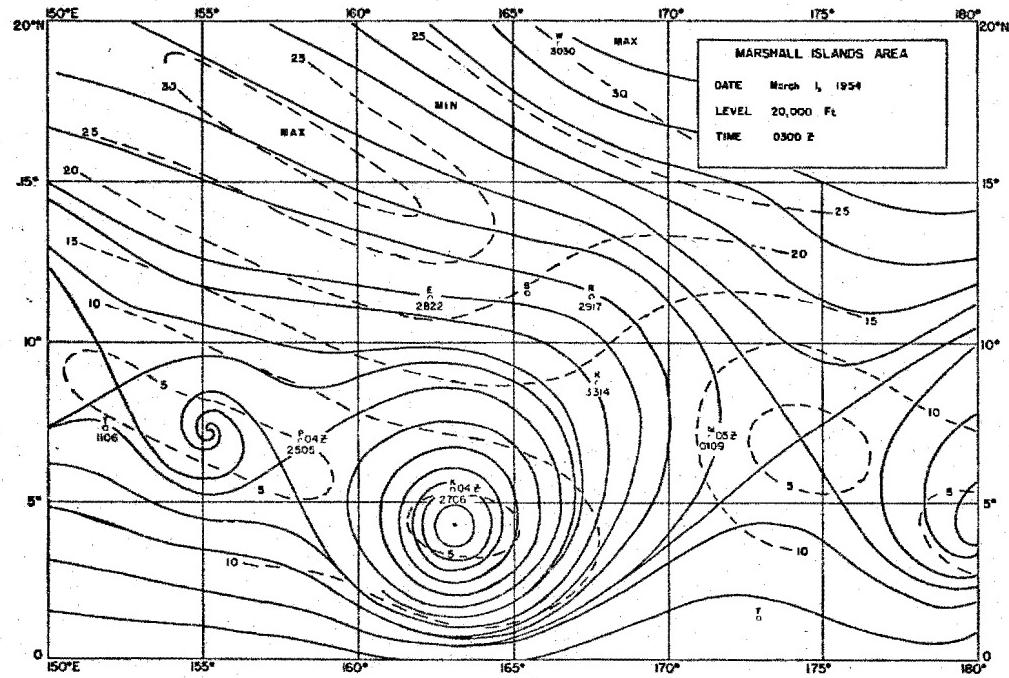


Figure 18

DOE ARCHIVES

~~SECRET~~  
**PART II**  
**VERTICAL MOTION IN THE MARSHALL ISLANDS AREA**

CDR Daniel F. Rex, USN  
Joint Task Force SEVEN

In the Task Force we are interested in the field of vertical motion for two reasons; first of all, through an analysis of vertical motions we may be able to gain a better understanding of the circulation in the tropical atmosphere and secondly, if the vertical components are sizeable they will certainly affect the fall-out pattern produced following an atomic explosion. G. A. Dean and W. D. Ohmstead, in Oahu Research Center Special Report No. 1 under Air Force Contract No. AF 19(604)-546, have computed the vertical motion at various levels for 1 March 1954 at 0300Z from streamline analyses of the horizontal wind field. In order to extend their interesting results it was decided to compute the same and other cases using a different technique. So my purpose is first, to describe the vertical motions "typically" observed in the Marshall Islands area and second, to demonstrate the computational method which was used—a method which is perhaps simple and objective enough to be applied successfully under operational conditions.

We have available six cases in which the vertical motion in the area of interest has been computed; 0300Z 1 March 1954 by Dean and Ohmstead; 2100Z 28 February 1954, 0300Z and 1500Z 1 March 1954, and 0300Z 2 March 1954 by Rex; and one case during GREENHOUSE computed by Dr. C. E. Palmer and published in the GREENHOUSE meteorological report. It is obvious that no general conclusions may be drawn from such a meager statistical sample. Nevertheless, one can perhaps obtain a gross, qualitative picture of vertical fields common in the Marshall area. Figures 1 though 6 illustrate the fields of vertical motion obtained at the 2000, 10000, 20000, 30000, 40000 and 50000 foot levels by Dean and Ohmstead and are generally typical of the computational results for all cases both with respect to the magnitude of the values and to the geometry of the patterns obtained. A comparison between the vertical wind speeds drawn in Figures 1 through 6 with those obtained in each of the other cases computed, gives a maximum variability of  $\pm 25\%$  of the values illustrated for any particular level. It may be seen from the figures that the vertical motions are organized into upward and downward moving currents or cells having horizontal dimensions of many hundreds of miles. It is also apparent that the magnitude of the vertical component increases with increasing altitude, and there is a tendency toward larger cell dimensions at the higher levels. In a very brief way this summarizes the computational results. For comparison purposes it should perhaps be noted that all vertical speeds in Figures 1 through 6 are given in centimeters per second; one centimeter per second is equal to one hundred and twenty feet per hour or thirty centimeters per second is equal to 3,600 feet per hour.

DOE ARCHIVES

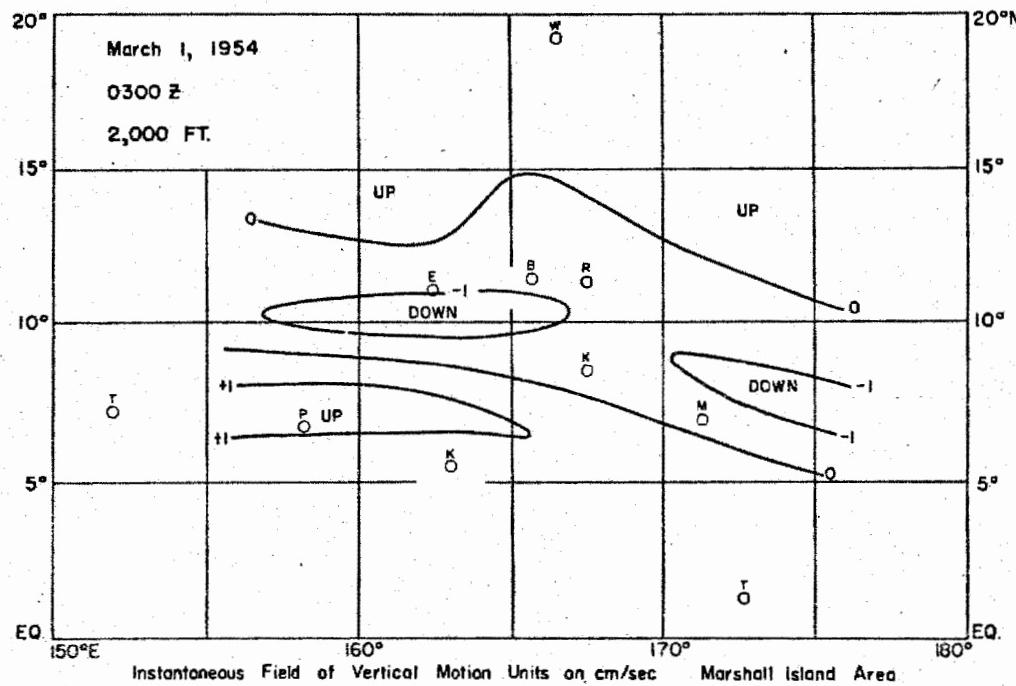


Figure 1

DOE ARCHIVES

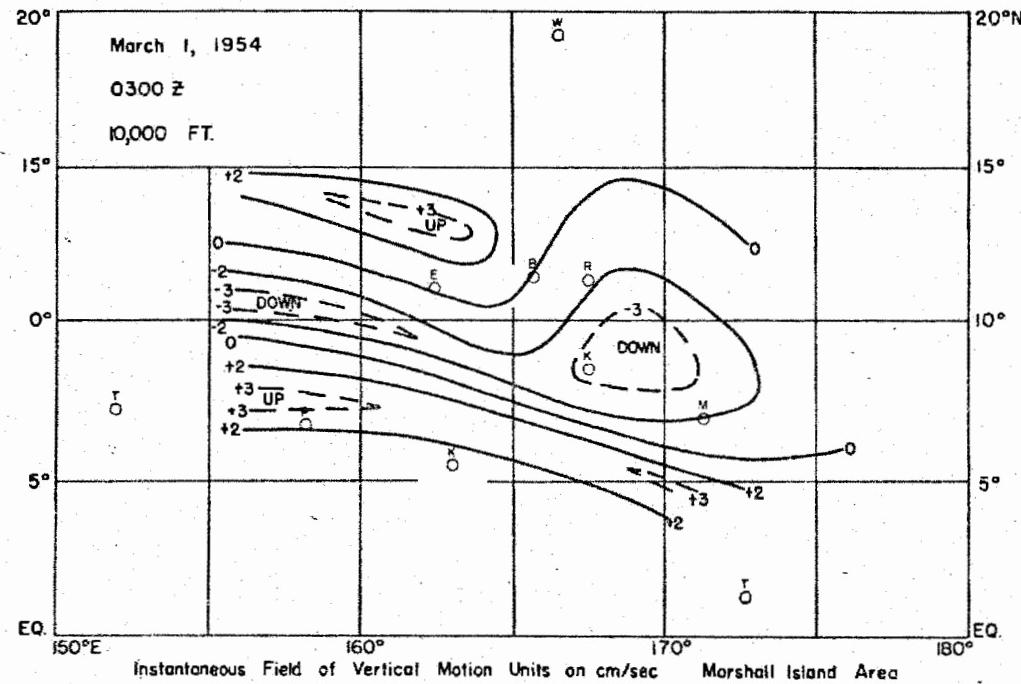


Figure 2

462

467

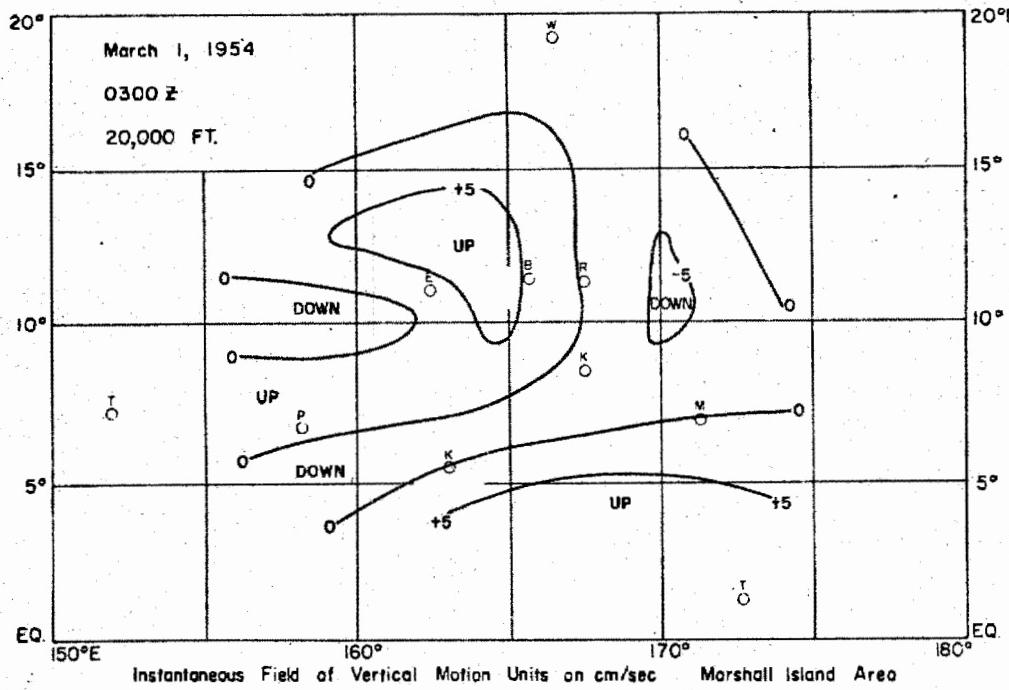
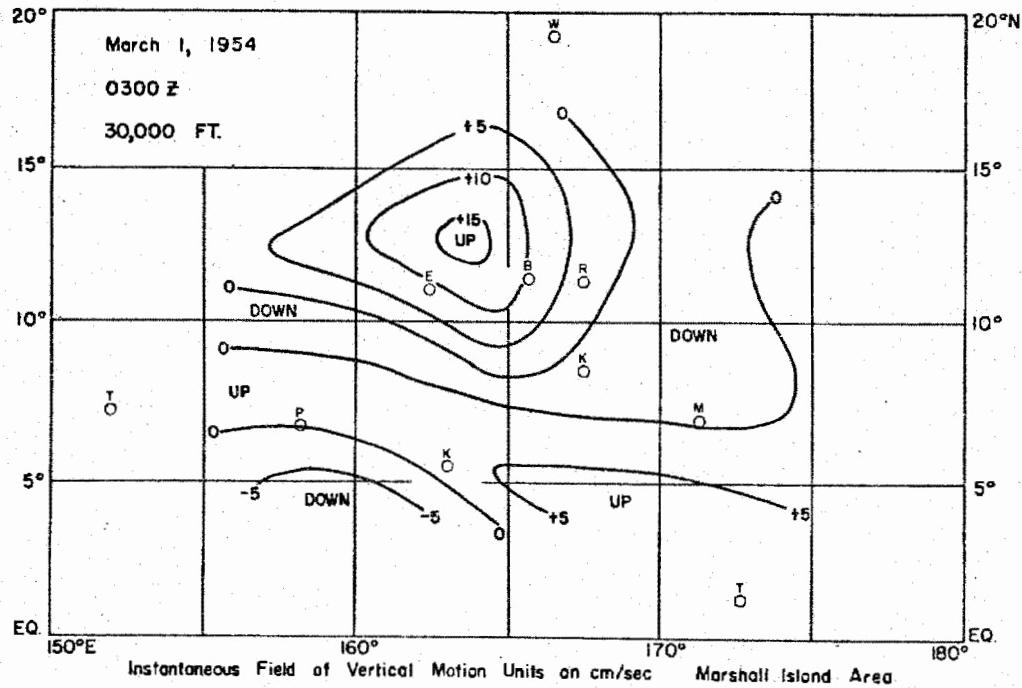


Figure 3



DOE ARCHIVES

Figure 4

463

ATOMIC ENERGY ACT

468

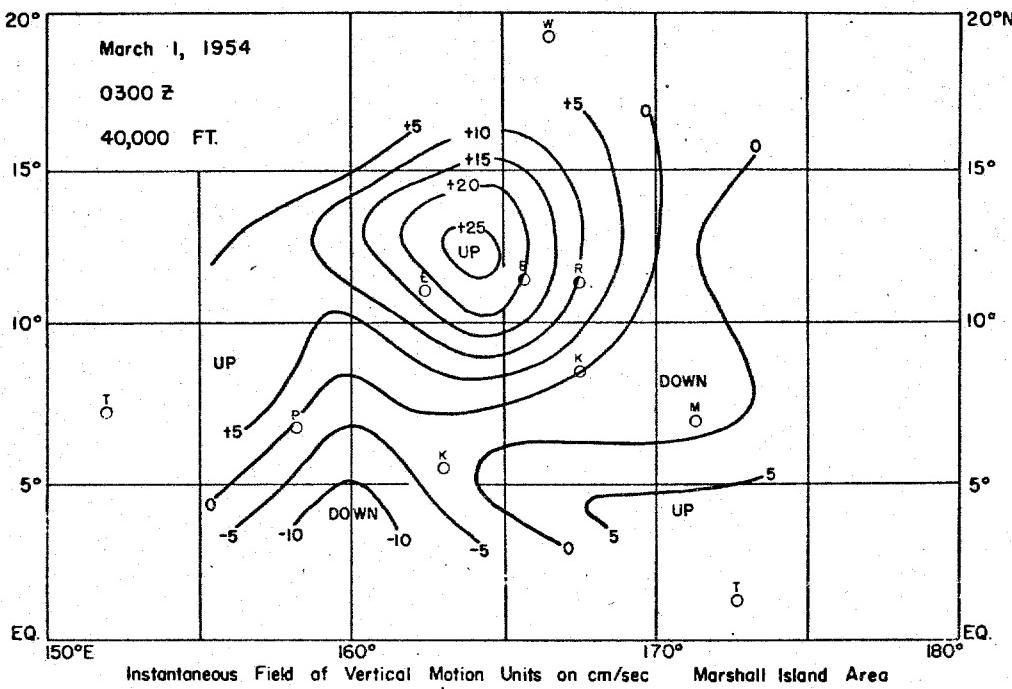


Figure 5

**DOE ARCHIVES**

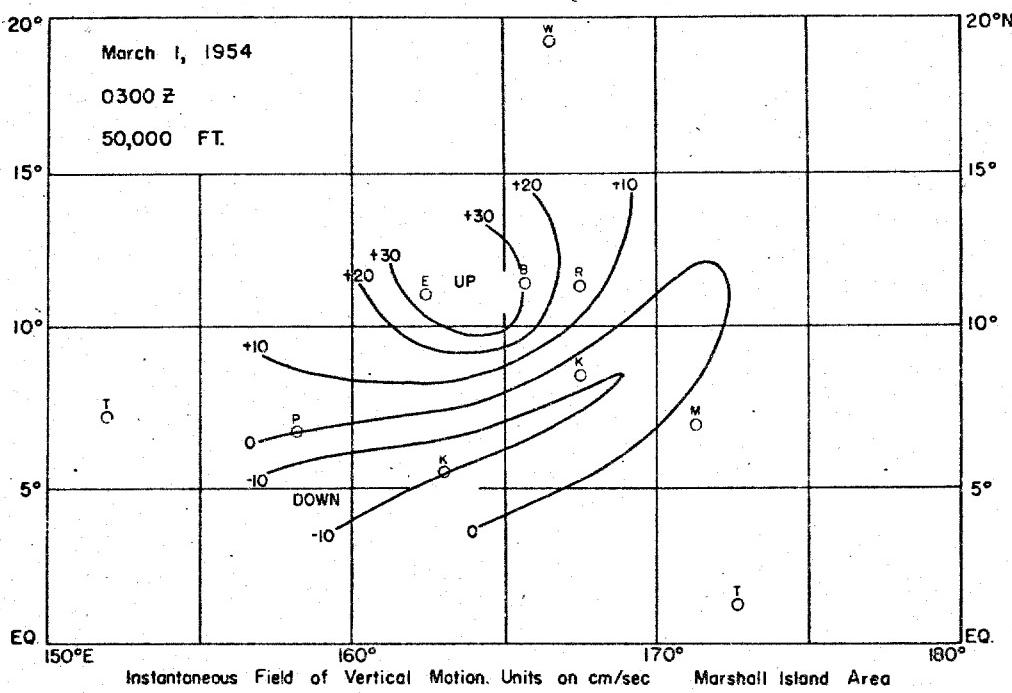


Figure 6

464

DATA  
ATOMIC ENERGY

469

Because the fields of vertical motion are obtained indirectly through computation of the horizontal divergence it is important to investigate the reality of the computed patterns. For this purpose two checks were used: the distribution of observed weather was compared with the computed motion; and vertical motions, computed for the same time by two different methods, were compared. In Figure 7 is shown the distribution of weather in the Marshall Islands area at 2300Z on 28 February 1954; the observed cloud amounts and types and the location of precipitation elements are indicated by the following symbols:

- RAIN  
 - - Rain
- SHWRS  
 - - Showers
- TSTMS  
 - - Thunderstorms
-  - - Cumulonimbus
-  - -  $\frac{1}{8}$  to  $\frac{3}{8}$  Cumulus (low cloud)
-  - -  $\frac{4}{8}$  to  $\frac{6}{8}$  Cumulus (low cloud)
-  - -  $\frac{7}{8}$  to  $\frac{9}{8}$  Cumulus (low cloud)
-  - -  $\frac{1}{8}$  to  $\frac{3}{8}$  Stratus or Stratocumulus (low cloud)
-  - -  $\frac{4}{8}$  to  $\frac{6}{8}$  Stratus or Stratocumulus (low cloud)
-  - -  $\frac{7}{8}$  to  $\frac{9}{8}$  Stratus or Stratocumulus (low cloud)
-  -  $\frac{1}{8}$  to  $\frac{3}{8}$  Cirrus, Cirrostratus or Cirrocumulus (high cloud)
-  -  $\frac{4}{8}$  to  $\frac{6}{8}$  Cirrus, Cirrostratus or Cirrocumulus (high cloud)

Blank areas are cloud and precipitation free

DOE ARCHIVES

Figure 7 was taken without modification from the original weather briefing chart used just prior to the Bravo event; it is simply a reproduced section of the original and was constructed many months before the vertical field computations were begun. Figure 8 shows the field of vertical motion computed for the 2,000 foot level (Figure 9 for the 30,000 foot level) at 2100Z on 28 February 1954 or just two hours prior to the time of Figure 7. Comparing Figures 7 and 8 we find the greatest

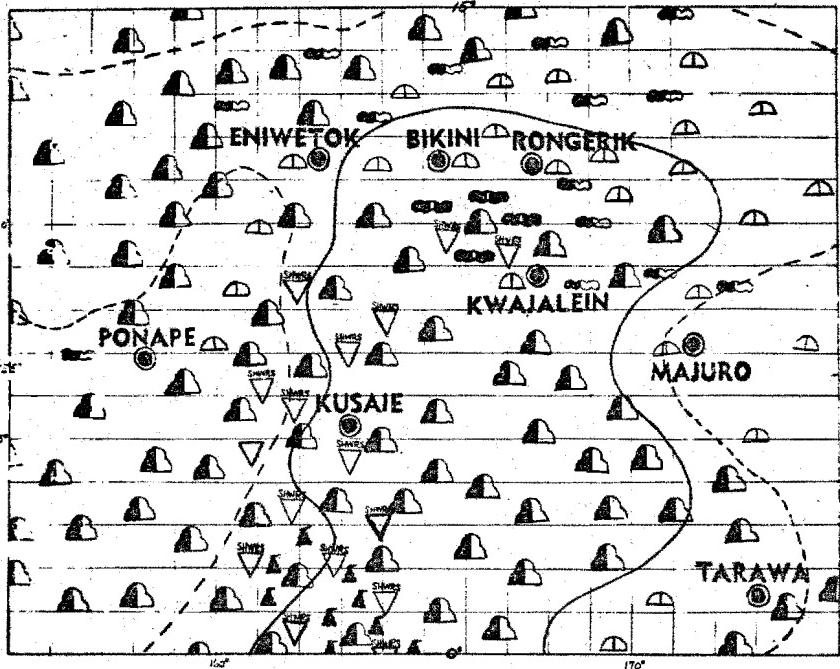


Figure 7  
Weather Chart, Marshall Islands Area, 2300Z 28 Feb 54

DOE ARCHIVES

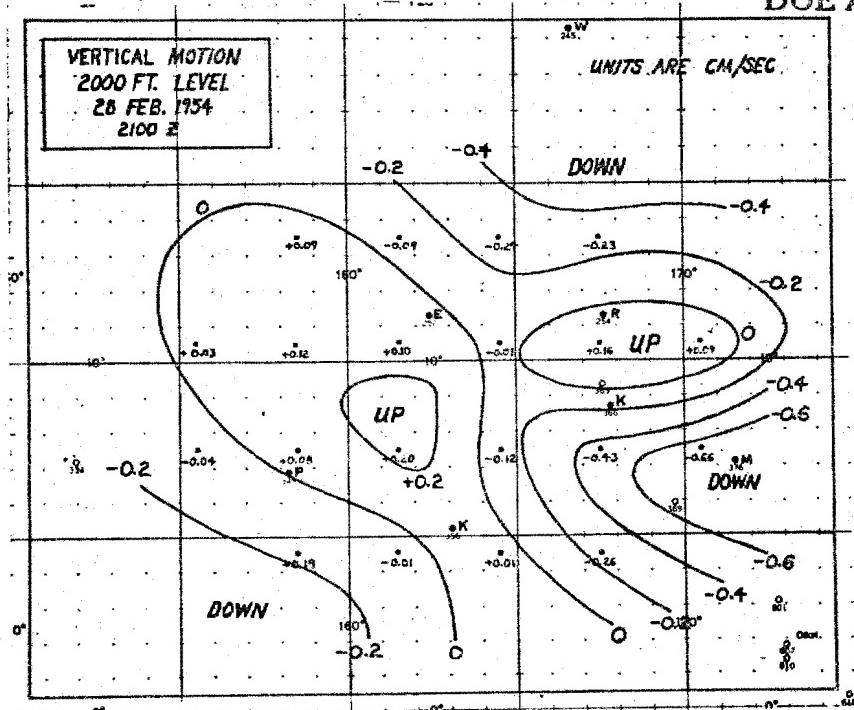


Figure 8

466

REF ID:  
AT ENERGY ACT

471

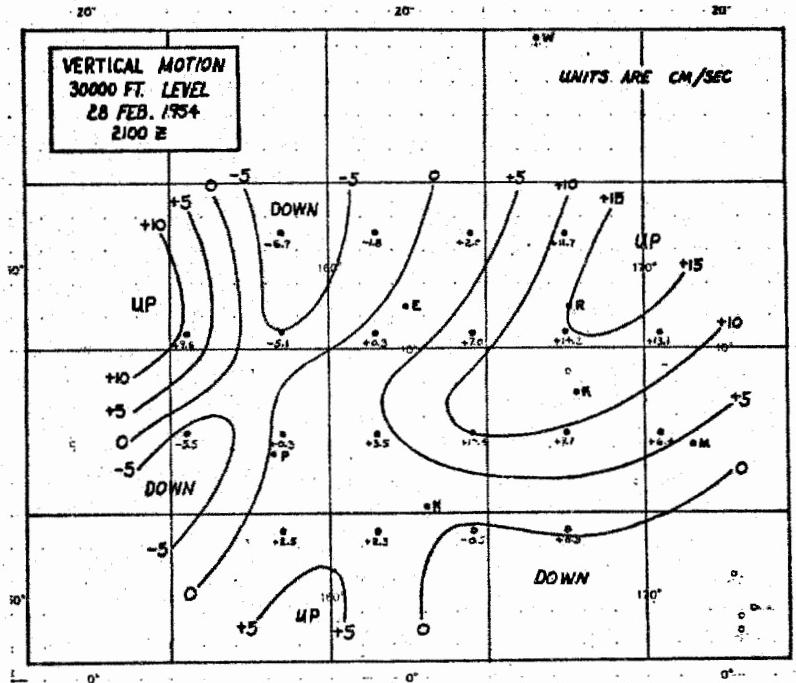


Figure 9

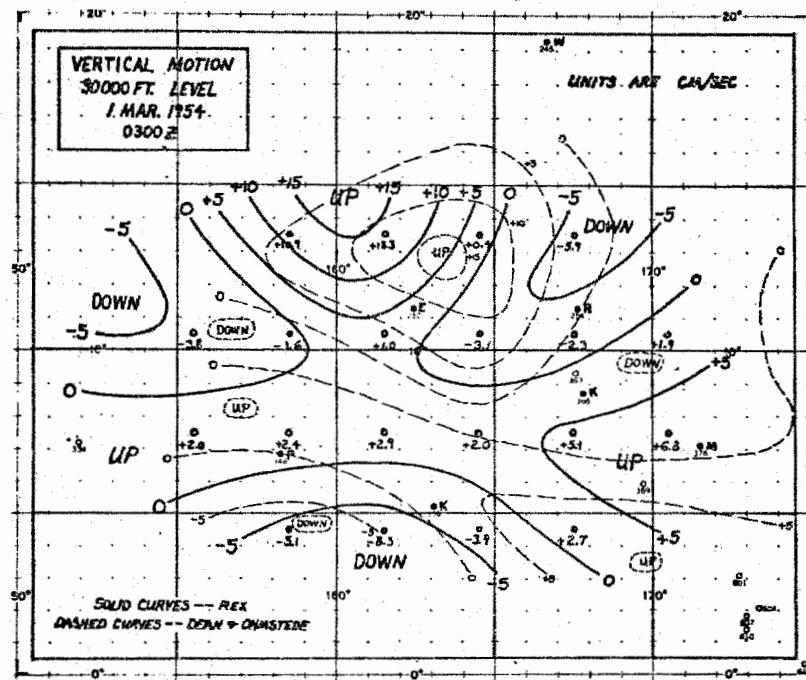


Figure 10

DOE ARCHIVES

convective activity (showers, thunderstorms and cumulonimbus) in the areas of upward motion. The similarity between the two patterns is quite striking. In a similar fashion comparing Figures 7 and 9 we find high cloud amounts greatest in the areas of upward motion at the 30,000 foot level. Figure 10 shows the field of vertical motion at the 30,000 foot level at 0300Z on 1 March 1954 as computed by two independent methods, that of Dean and Ohmstead which is described in their report mentioned earlier and is based upon the calculation of horizontal divergence from streamline analyses and a method, suggested by Dr. C. E. Palmer, which I have used and which will be described later. Inspection of Figure 10 will show that the vertical wind speeds obtained by the two methods are of the same order of magnitude and further, that the geometry of the two patterns is quite similar. From the studies which have been completed and were briefed in the preceding paragraphs, it appears to be possible to compute fields of vertical motion which are at least qualitatively representative of the actual atmospheric motions.

Now I should like to discuss briefly the method of computation which we have used. There are in general two approaches to the computation of vertical velocity; the thermodynamic and the kinematic. Thermodynamic methods are derived from the fact that changes in the vertical temperature and humidity structure are largely the result of vertical motions. Such changes as may be produced by non-adiabatic processes such as radiative effects, the release of precipitation, etc., are either neglected or treated empirically. It is for this reason that the thermodynamic approach is not especially useful in tropical areas where non-adiabatic processes are maximized. Kinematic methods are derived from the continuity equation; they involve the computation of the divergence of the horizontal wind field at various levels and a vertical integration to determine the vertical velocities. The simplest kinematic methods involve the calculation of horizontal divergence within a polygon (usually a triangle) having observation stations at its vertices; the observed winds being averaged along each side of the polygon. This method produces good results in an area of dense observations where the sides of the figure are not long but cannot be applied in the Marshall Islands area with any assurance of success because of the extremely sparse observing network. The method used by Dean and Ohmstead, as has been mentioned before, required a streamline (isogon-isotach) analysis at various, rather closely-spaced, levels. Divergence fields are computed from the streamline charts and the vertical velocities computed over a set of grid points from smoothed values of the divergence at each point.

DOE ARCHIVES

The method which I have used was originally suggested by V. Bjerknes in Dynamic Meteorology and Hydrology, Part II and was further

~~PROTECTED DATA~~  
NUCLEAR ENERGY

developed by C. E. Palmer during GREENHOUSE. In Figure 11 is shown the derivation of the computational function as I have used it. Using standard nomenclature the of continuity (1) is integrated in the vertical direction and by substitution the variable is changed to pressure resulting in equation (4). Defining the vector components  $\bar{u}$  and  $\bar{v}$  as indicated in equation (5) we may write the vertical velocity at the level of interest,  $w_i$  is equal to the horizontal divergence of the vector field  $\vec{V}$  divided by the product of density times gravity. The computational procedure used was developed from this relationship, equation (6). The two assumptions made in the derivation of equation (6), i.e., that the local rate of change of density and the vertical velocity at the surface are both negligible, have been shown to be essentially valid over low oceanic stations in the tropics.

To determine the  $\bar{u}$  and  $\bar{v}$  values for any particular case, the  $u$  and  $v$  components of the observed winds at each station available within the area of interest are plotted as a function of pressure as illustrated in Figure 12. In the figure, which is for Eniwetok at 2100Z on 28 February 1954, the heavier curves represent the  $u$  and  $v$  values. These curves are then graphically integrated with respect to pressure by the method of equal areas to determine the corresponding  $\bar{u}$  and  $\bar{v}$  values; a pressure interval of 5 centibars was used in the computation. The  $\bar{u}$  and  $\bar{v}$  values are then plotted as a function of pressure; the lighter curves in Figure 12 represent these graphs. Finally the value of  $\bar{u}$  and  $\bar{v}$  at any particular height can be read from the graphs by means of the pressure-height relationship. In Figure 12 the average values of the wind components  $u$  and  $v$  in each 5 centibar pressure interval are denoted as  $\bar{u}_j$  and  $\bar{v}_j$  respectively. In order to interpolate between the few stations available in the Marshall Islands area it has been found best to plot and analyze the  $\bar{u}$  and  $\bar{v}$  fields. This step is illustrated in Figure 13 showing the  $\bar{v}$  field as solid isolines and the  $\bar{u}$  field as broken isolines. An analysis must be made for each level at which it is desired to compute the field of vertical motion, but it should be emphasized that the  $\bar{u}$  and  $\bar{v}$  fields may be analyzed as scalar fields thus greatly simplifying the labor involved. From the charts of the  $\bar{u}$  and  $\bar{v}$  fields the field of vertical motion at any level can be computed as indicated in Figure 14. A square grid was drawn on a transparent overlay in order to facilitate reading off the required  $\bar{u}$  and  $\bar{v}$  values; values were read off at each solid black dot shown in Figure 14. The average value of  $\bar{u}$  along the east side of square 3 is denoted as  $\bar{u}_{3E}$ ; other averages are indicated by a similar nomenclature. Also shown in Figure 14 are the locations of the nine observing stations which were available in the Marshall Islands area for the cases investigated.

From the preceding discussion we conclude that if any appreciable percentage of the active material producing radioactive fall-out is

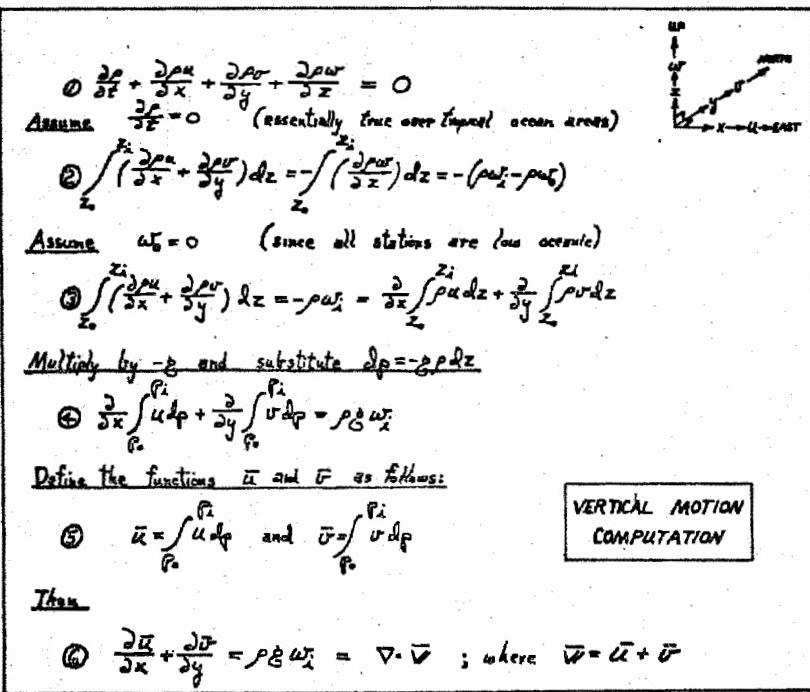
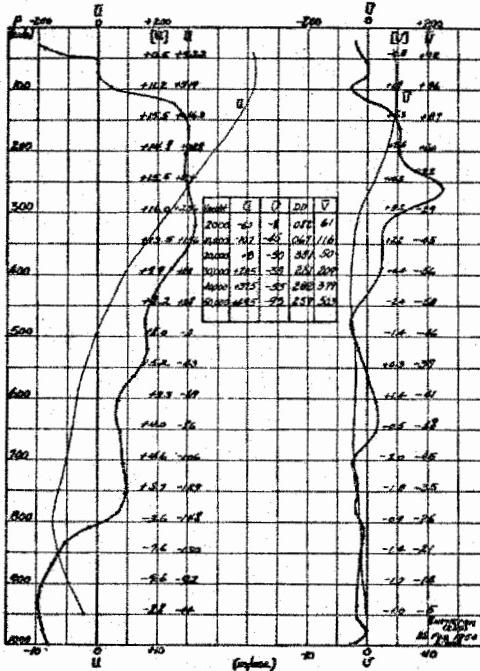


Figure 11



DOE ARCHIVES

Figure 12  
Vertical Motion Computations

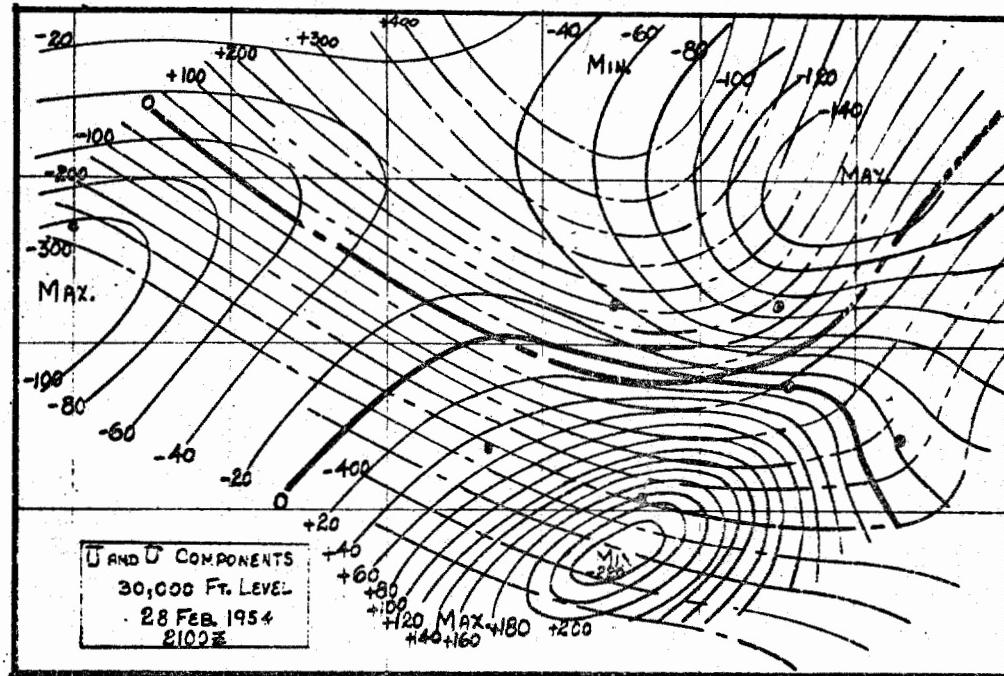


Figure 13

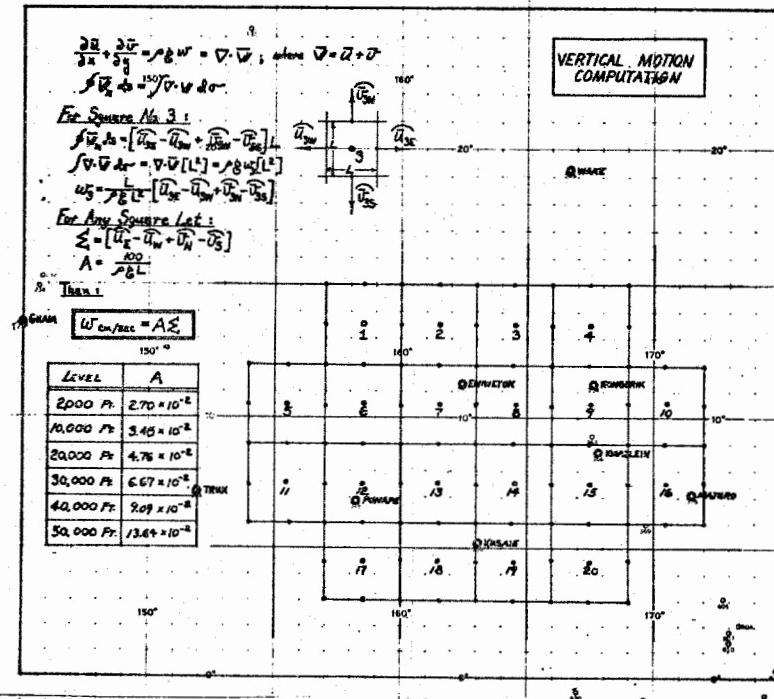
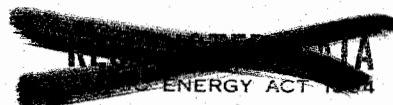


Figure 14

DOE ARCHIVES



carried above the 30,000 to 40,000 foot level in the atomic cloud and if such material, or any large part of it, is carried on particles having a falling velocity less than about 5,000 feet per hour, then any quantitative calculation of the fall-out pattern geometry and activity will certainly have to take into account the existing field of vertical motion within the area in question. Furthermore, if computations of the vertical field are required in connection with future test operations, it would appear to be feasible to compute them on a routine basis by means of the technique described in the preceding paragraphs.

DOE ARCHIVES

472

A [REDACTED] ENERGY ACT

481 477

PART III  
CONCLUDING REMARKS

LTCOL C. D. Bonnot, USAF  
Joint Task Force SEVEN

Figure 1 is a map of the Southwest Pacific area, centered on Enewetak. This map presents the presently operational rawinsonde stations, as well as several new sites which we are proposing. You will note that Yap, Koror, Truk, Ponape, and Majuro are to give us additional information; this was obtained through contract with the Weather Bureau by the Task Force. There are several sites south of the equator which we are asking the British Commonwealth to establish. Also, there are two ocean station weather ships we are requesting the Coast Guard to operate for us on a continuing year-round basis. Lastly, you will note that we plan to establish temporary stations during test periods at Kapingamarangi, Kusaie, Bikati, and Taongi. This net will give us what we feel is an absolutely minimum observing net to support the Task Force.

If such a weather observing net is operating, we feel that adequate information will be available to those required to predict the fall-out and radiation hazards at the Pacific Proving Ground. Work is being continued at the Oahu Research Center by Dr. Palmer toward improving our weather forecasting procedures for this area.

DOE ARCHIVES

473



478

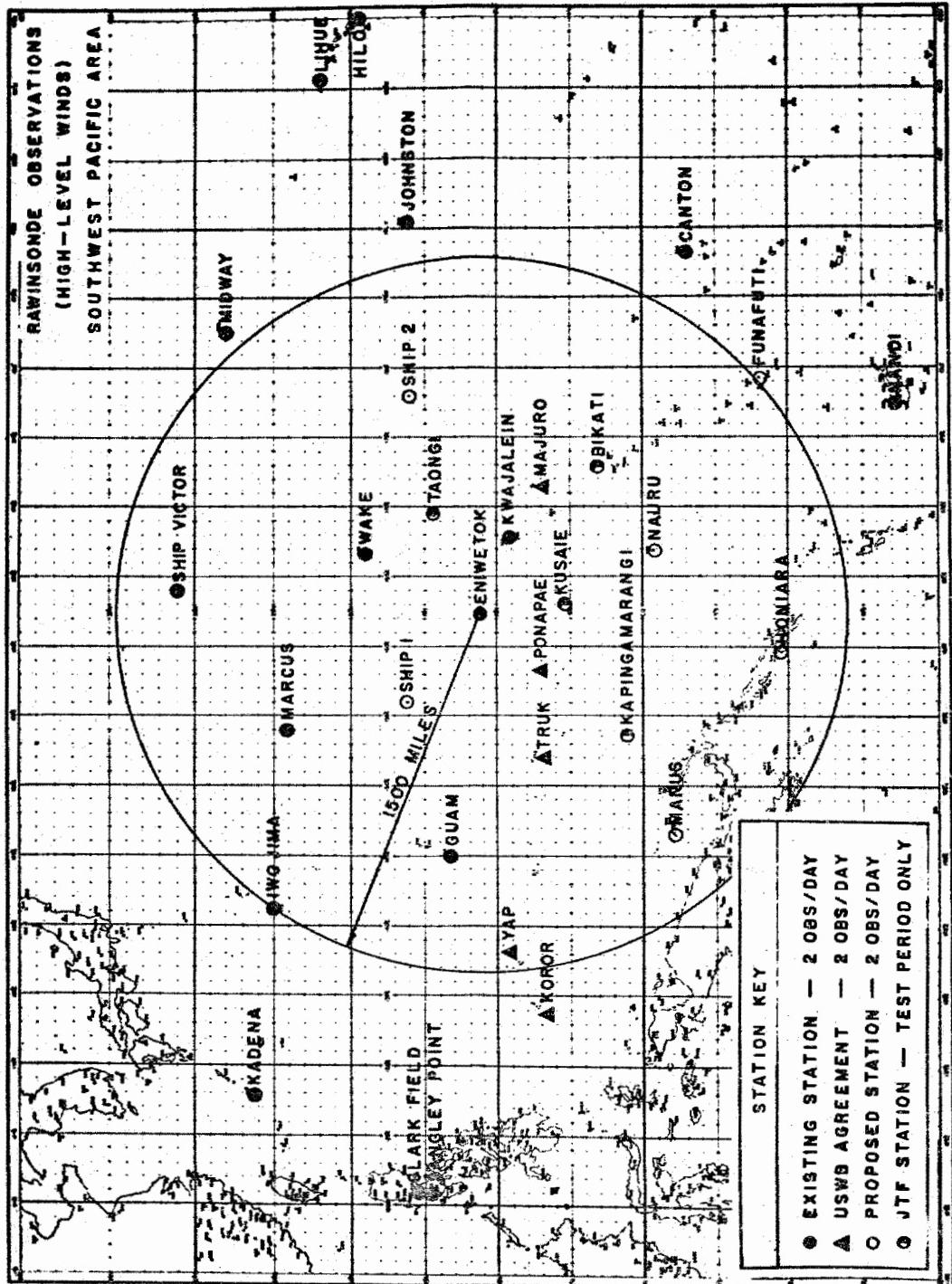


Figure 1

DOE ARCHIVES

474

ATOMIC ENERGY

479

PREDICTION OF DOSE-RATE AND DOSAGE CONTOURS AS  
FUNCTIONS OF YIELD AND METEOROLOGICAL CONDITIONS;  
EFFECTS OF SPECIFIC WING STRUCTURES USING THE ARMY  
SIGNAL CORPS METHOD

Kenneth Barnett  
Office Chief Signal Officer

Dr. Swingle has explained to you the Signal Corps procedure for making forecasts of the radiological fall-out patterns that result from 15 megaton explosions in the tropics. I would like to show you three things. First, how this forecast procedure was calibrated by comparison with CASTLE Bravo observations. Second, the forecast made by using this procedure with different wind conditions, and third, some suggestions for making better fall-out forecasts in the future. In Figure 1, we have the trajectory of the 68 micron particles which fall out from the center of the cloud. These winds are the winds taken at shot time at CASTLE Bravo with some changes in the higher altitudes to account for the changes that occurred eight hours after the shot time. Since it required about one hour for the 68 microns particles to fall through 5,000 feet, this trajectory is very similar to a hodograph. In Figure 2, we have the iso-chrones of the arrival time of the first particles and the ending times of the particles. Both are in hours, and using the predicted data from CASTLE Bravo. In the upper part we have two points where the fall-out time, the arrival time of the first particles, was observed. We have one point at 5.7 hours; it is right on the 5 hour predicted line. We have another point at 7.8 hours that is almost exactly correct. The comparison of these few pieces of observed data fit quite well and give us confidence in the dimensions of our model. It is interesting to point out that somewhere between 30 and 35 hours the particles begin to drift backwards, as would be indicated by the 180 degree wind shift around 55,000 feet. Likewise in the lower curve, the ending time of particles, we also see how the ending time begins to change. In Figure 3, we have at the top the predicted dose rate, and this requires a calibration. As you will recall, we determine our dose rate by bringing out each of the disks or slices from our model according to the wind velocity and according to the rate of fall of the median particle size for that particular disk. We let these fall over a square, cross-sectional grid. We make a tally of the total number of cylinders that fall on each grid and then we draw lines for total numbers of each of these tallies. In order that these total numbers for each square will be in roentgens per hour, we have compared the top figure of Figure 3 with the bottom figure, which is the observed data from AFSWP Report 507. You will notice that in the top figure, our predicted figure, as drawn here, our 100 line encloses an area a little larger than the area enclosed

**CASTLE BRAVO COMPOSITE WINDS**

LEVEL	DEG.	KNOTS	FACTOR	VECTOR LENGTH (NM)	MILES
SEC.	.060	12	.98	11.8	10.6
3,000	.097	10	1.14	11.4	9.45
10	.307	11	1.15	12.4	10.9
15	.295	12	1.12	13.4	11.84
20	.283	13	1.11	20.0	18.05
25	.251	25	1.10	27.5	23.96
30	.241	31	1.09	33.8	30.3
35	.246	38	1.08	47.1	42.6
40	.251	45	1.07	48.1	42.09
45	.257	44	1.06	46.7	41.8
50	.260	30	1.05	31.5	28.2
55	.098	18	1.04	16.7	14.6
60	.350	04	1.03	4.1	3.6
65	.090	03	1.02	3.1	2.7
70	.090	18	1.01	16.8	15.5
75	.090	20	1.00	20.0	18
80	.080	22	.99	21.8	19.7
85	.090	37	.98	36.2	32
90	.070	39	.97	37.6	32.9

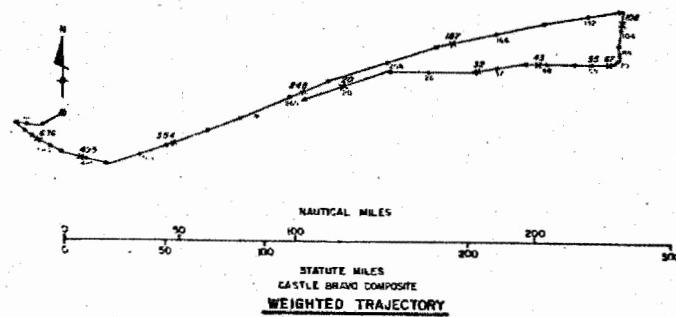
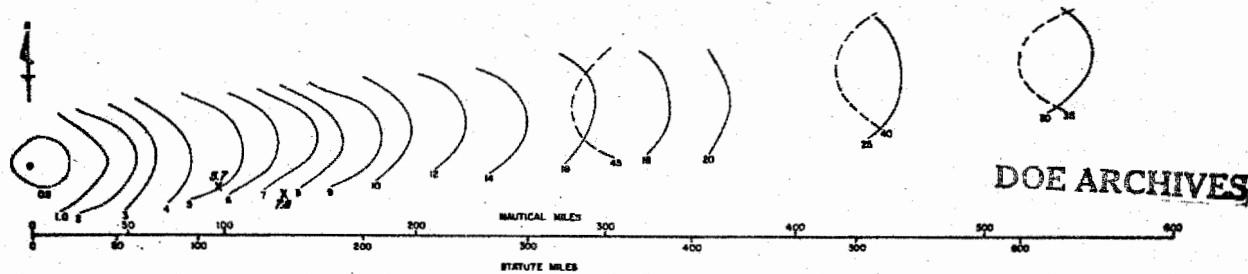
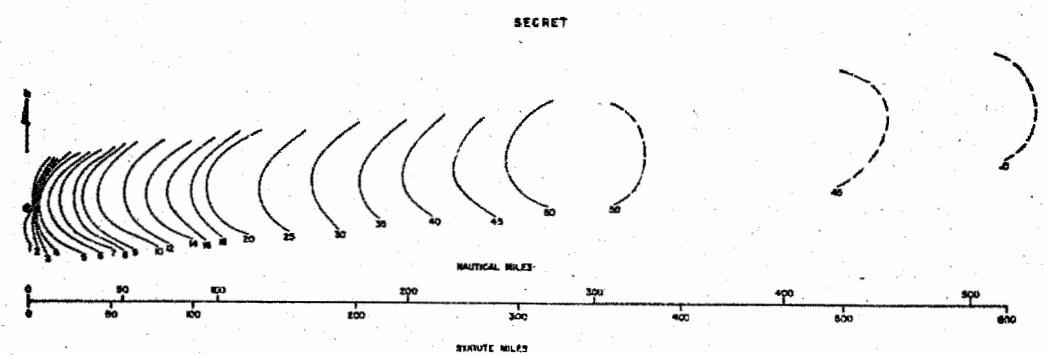


Figure 1



DOE ARCHIVES

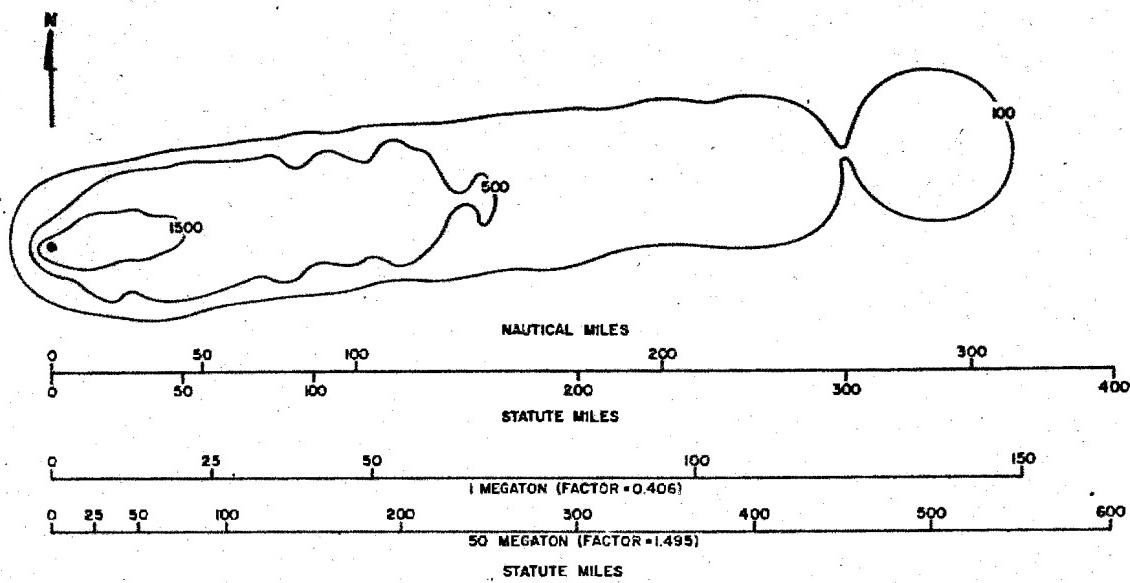


T<sub>s</sub>, ENDING TIME OF LAST PARTICLES IN HOURS, PREDICTED USING CASTLE BRAVO WIND DATA

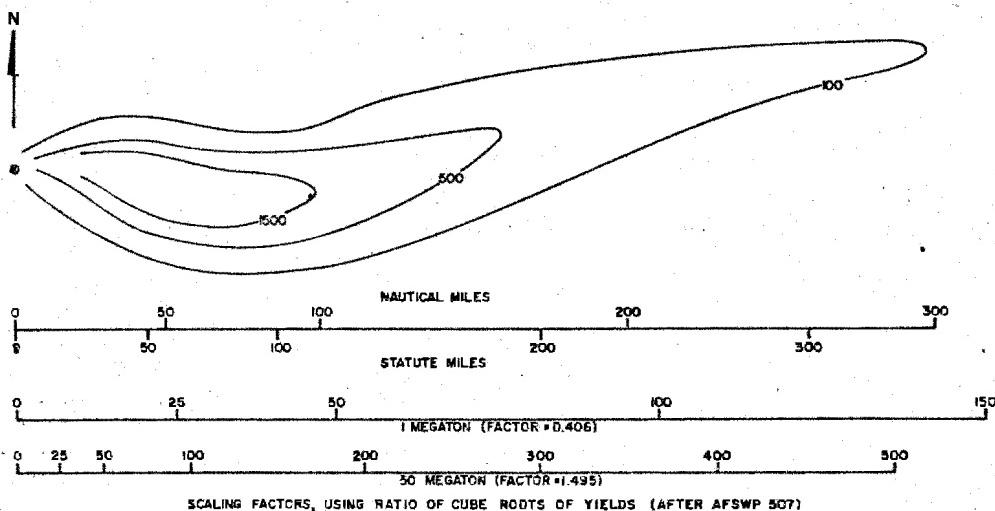
Figure 2

476

491



#### PREDICTED DOSE RATE, R/HR, USING CASTLE BRAVO WIND DATA



CONTOURS FROM CASTLE BRAVO DOSE RATE, ROENTGENS PER HOUR AT H+1 (FROM AFSWP REPORT 507)

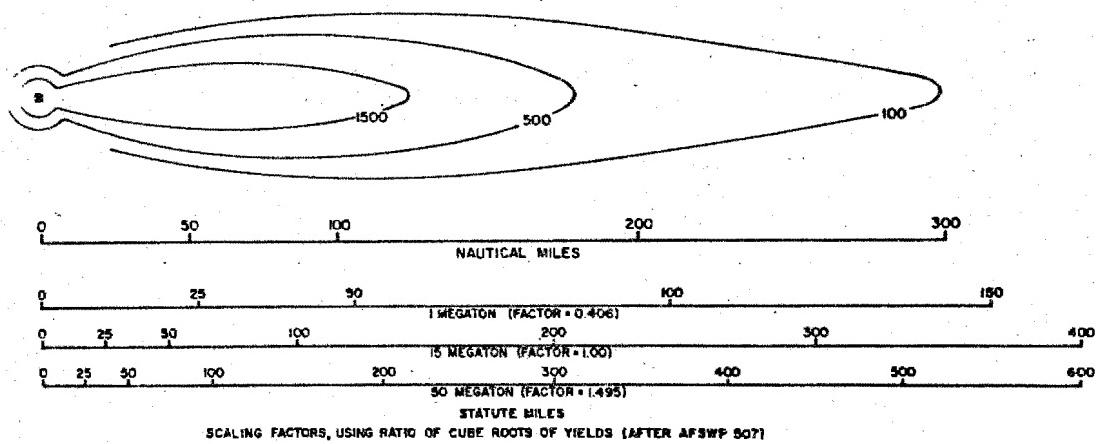
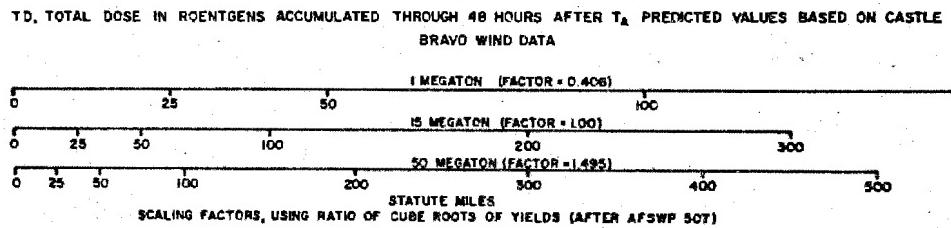
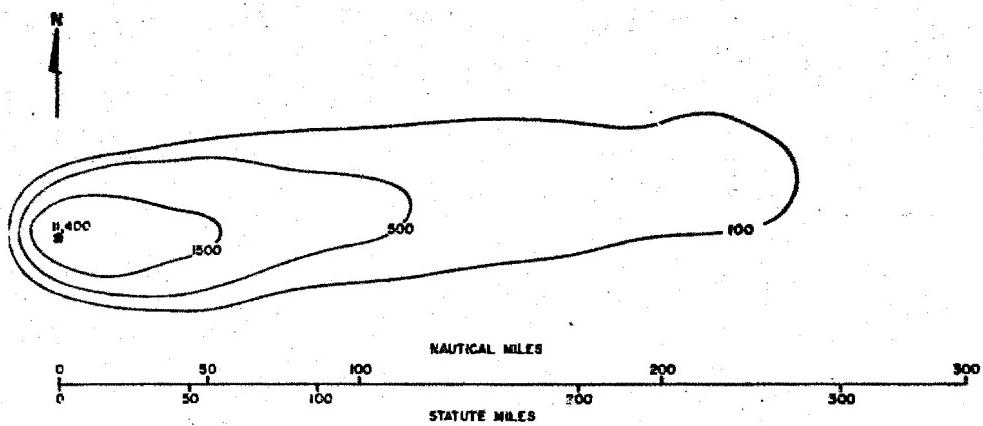
DOE ARCHIVES

Figure 3

477

CASTLE BRAVO  
NUCLEAR ENERGY

482



DOE ARCHIVES

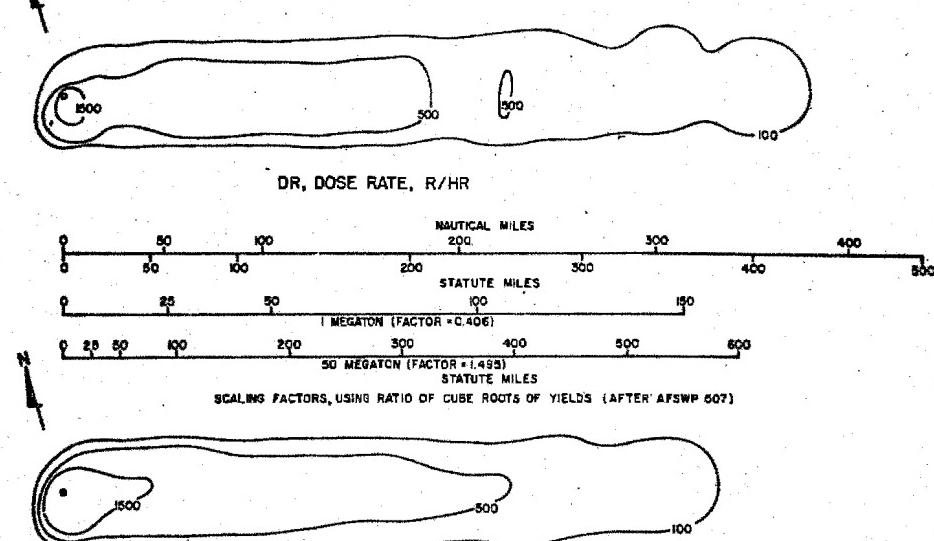
Figure 4

478



483

by the 100 line in the bottom or observed figure. Likewise in our predicted pattern, the area enclosed by the 1500 r/hr line is slightly smaller than the observed area enclosed by the 1500 r/hr line. We used a calibration factor of 100 to obtain this tip figure and somewhere, probably around the 600 roentgen per hour line, the areas are the same in the predicted model and in the observed areas. Looking at our predicted dose rate, you will see that there is one problem rather obvious, that is the lumping of it. For example, out towards the end of the 100 line there's almost a perfect circle which indicates that one disc alone fell at that point. And right next to it, to the left, are the other circles. Later on I'll discuss some ways we have we hope will improve this. All of our calculations have been for the 15 megaton model and we did not have the time to make models for one and 50 megatons for this symposium. So we used a simple scaling factor to give some idea of what this procedure should give for a one megaton and 50 megaton yield. You'll see the two scales here in Figure 3 and in later Figures. In Figure 4 we have a comparison of our predicted total dose pattern with the idealized observed total dose pattern from CASTLE Bravo. The total area included by our predicted 100 total dose line and the idealized observed 100 total dose line is almost the same. However, the area included by our 1500 total dose line is a little smaller than the observed area. We think we have some procedures that will improve this, that is, that will make our 1500 total dose line a little larger relative to our 100 predicted total dose line. Again here in Figure 4 we have these scaling factors to go from 15 megatons to either one megaton or 50 megatons. I would now like to go on to the examples that were furnished to us by AFSWP. You know their example 1 was the condition of an approximately 90 degree shear at a height of about 40,000 feet at Dodge City, Kansas. In the lower 40,000 feet, the mean vector is generally towards the south, from the ground zero; above that the vector goes out toward the east, and I think in our resulting patterns we should see some indications of these two vectors. In Figure 5, we have the isochrones for the arrival times and the ending times. The arrival time curves are quite symmetrical and go out steadily. This suggests that we might develop a short-cut method in which we extend one vector out along one azimuth and then space the isochrones at equal spaces there and draw them off, more or less, as circles. I think we could use that to get an approximation that would be very close to this and would save us a great deal of time. Looking at the predicted ending values we see that at one hour, there is a little irregularity which I think is the lower vector which points toward the south. In Figure 6, we have our predicted dose rates and our predicted total dose. You will see that in both of those there is a little extension of the 1500 area toward the south, which is a reflection of the fall-out in the lower 40,000 feet which is extended toward the south. And again we have our scaling factors here to give



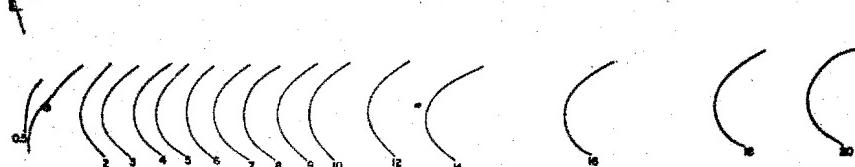
TD, TOTAL DOSE IN ROENTGENS ACCUMULATED OVER 48 HOURS AFTER  $T_A$

PREDICTED VALUES USING WIND CONDITION "A"

Figure 5



NAUTICAL MILES  
STATUTE MILES



PREDICTED VALUES, 15 MT, USING WIND CONDITION "A"

DOE ARCHIVES

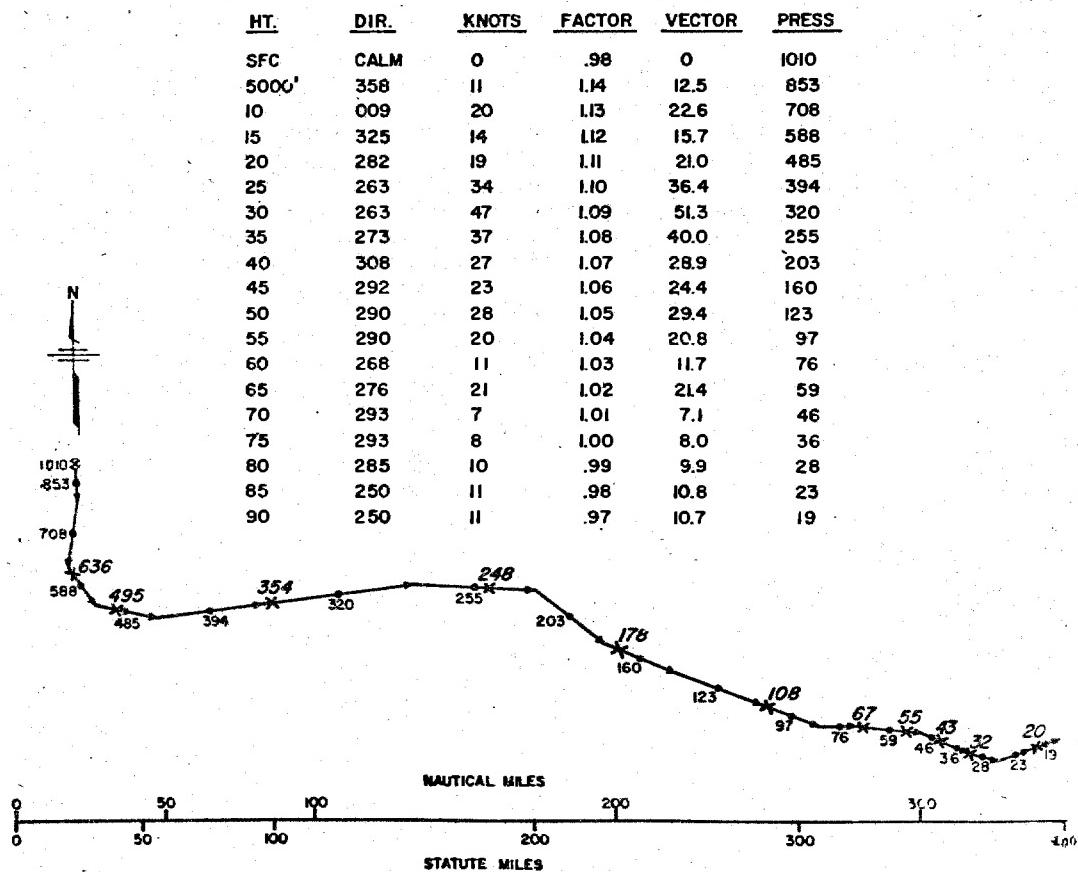
Figure 6  
480



485

the approximate dimensions for a one megaton and a 50 megaton yield. Going on to Case B, which is a gradual wind shear of approximately 90 degrees (Figure 7), I think we should find a fairly symmetrical pattern because the mean wind vector from the surface up to various altitudes is almost constantly towards the east-southeast. In our Figure 8, we see that the arrival time of the first particles, the isochrones for those and the ending time are quite symmetrical and extend out towards the east-southeast. Likewise, in Figure 9, the dose rate contours and total dose contours were quite symmetrical and point straight out towards the east-southeast. Case C should give us very symmetrical results too, since the winds are from almost the same direction at all levels. And Figures 11 and 12 give the isochrones for ending and arrival times for dose rates and total dose. Case D, in my opinion, is the most interesting one, and that is the condition of relatively low wind speeds at all levels. In fact, the effective wind from the base of the fireball on down to the ground is only about six miles per hour. Figure 14 shows the arrival time of the first particles and you notice that up to about 25 or 30 hours it is quite regular and then due to an almost 180 degree wind shift, the lines bunch up together and begin to go down towards the south. We likewise have a pattern for the ending time (Figure 15), which might be the super-position of two symmetrical patterns, one on the other. Figure 16 shows by the dose rate contours that, at least the 1500 contour is almost a circle, with a long piece sticking up towards the northeast where the winds had begun to shift around and there was an unusually large amount of fall-out at that distance out in this particular case. Figure 17 shows us the total dose and the contours here are nearly circles and up towards the northeast those we have are very small, much smaller than the dose rate values in that area. This is due to the deterioration factor because it is further out from the source. Figures 19 and 20 show the results of condition E, which is a case of relatively high wind speed above 10,000 feet. (Figure 18) As would be expected, it is a long, thin pattern in the dose rate and total dose. Condition F is a case of a gradual shear of approximately 180 degrees (Figure 21), and again this might be broken down into two major vectors; the lower half and the top half. Then we see that reflected in Figures 22, the idochrones of arrival time that are fairly symmetrical out to about 10 or 12 hours and after that the upper shear which goes down toward the south and makes itself apparent. In Figure 23 we have the dose rate and the total dose. Notice that on the right hand side there is quite a big lump out by itself in both cases. This is due partly to the wind shift at high levels going down towards the south. It is also the result, partly, of the lumpiness problem that we have in this model. In Figure 24 we have a summary of the dose rate and total dose areas for all of the conditions as well as for the observed CASTLE Bravo results and our predicted results. One interesting thing that should

GRADUAL WIND SHEAR OF APPROXIMATELY 90°



CONDITION "B"  
WEIGHTED TRAJECTORY

DOE ARCHIVES

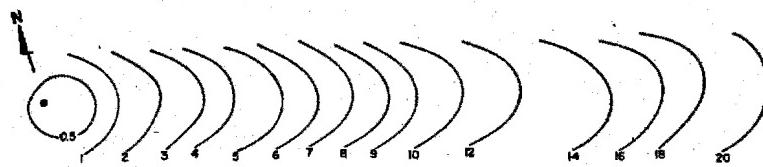
Figure 7

482

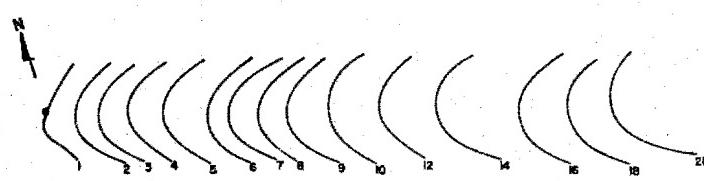
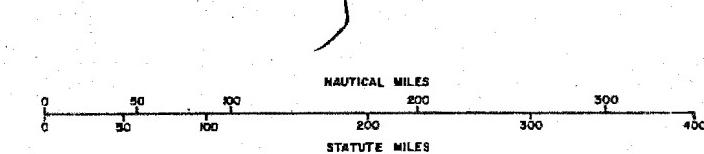


491

487

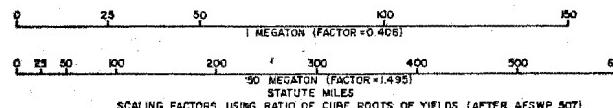
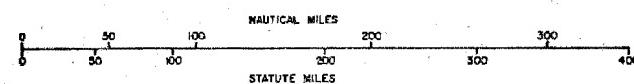
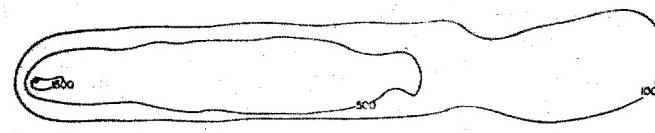


$T_A$ , ARRIVAL TIME OF FIRST PARTICLE, HRS., PREDICTED USING WIND CONDITION "B"

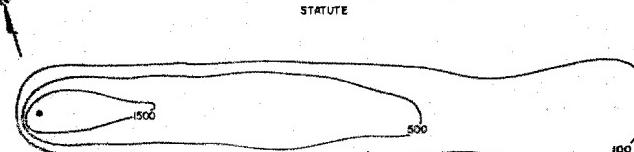


$T_E$ , ENDING TIME OF LAST PARTICLE, HRS., PREDICTED USING WIND CONDITION "B"

Figure 8



SCALING FACTORS, USING RATIO OF CUBE ROOTS OF YIELDS (AFTER AFSWP 507)



DOE ARCHIVES

TD, TOTAL DOSE IN ROENTGENS ACCUMULATED OVER 48 HOURS AFTER  $T_A$   
PREDICTED VALUES, 15 MT, USING WIND CONDITION "B"

Figure 9

483

ATOMIC ENERGY ACT

488

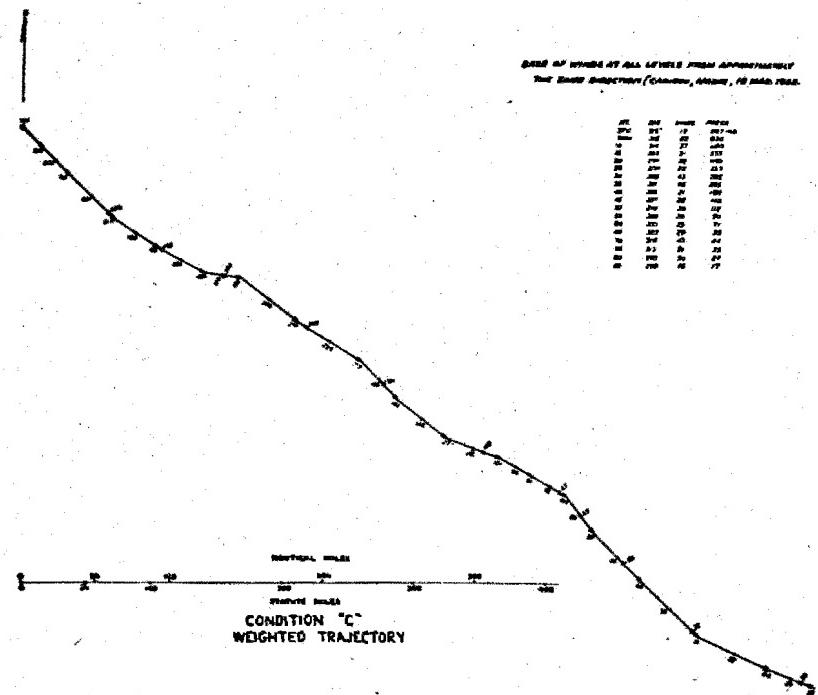
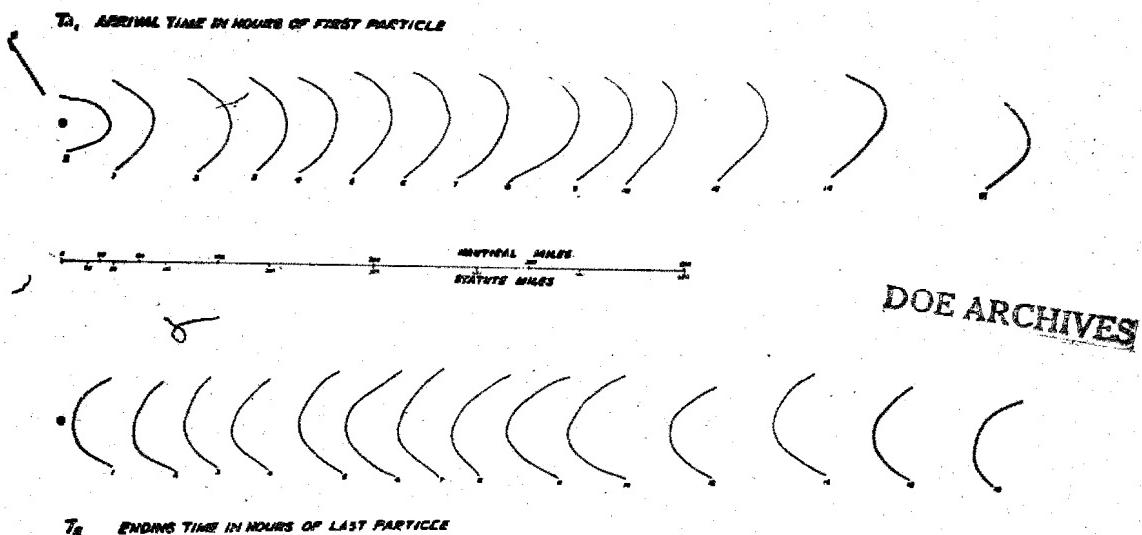


Figure 10



T<sub>A</sub> ARRIVAL TIME IN HOURS OF FIRST PARTICLE

T<sub>B</sub> ENDING TIME IN HOURS OF LAST PARTICLE

PREDICTED VALUES 15 MT USING WIND CONDITION "C"

Figure 11

484



489

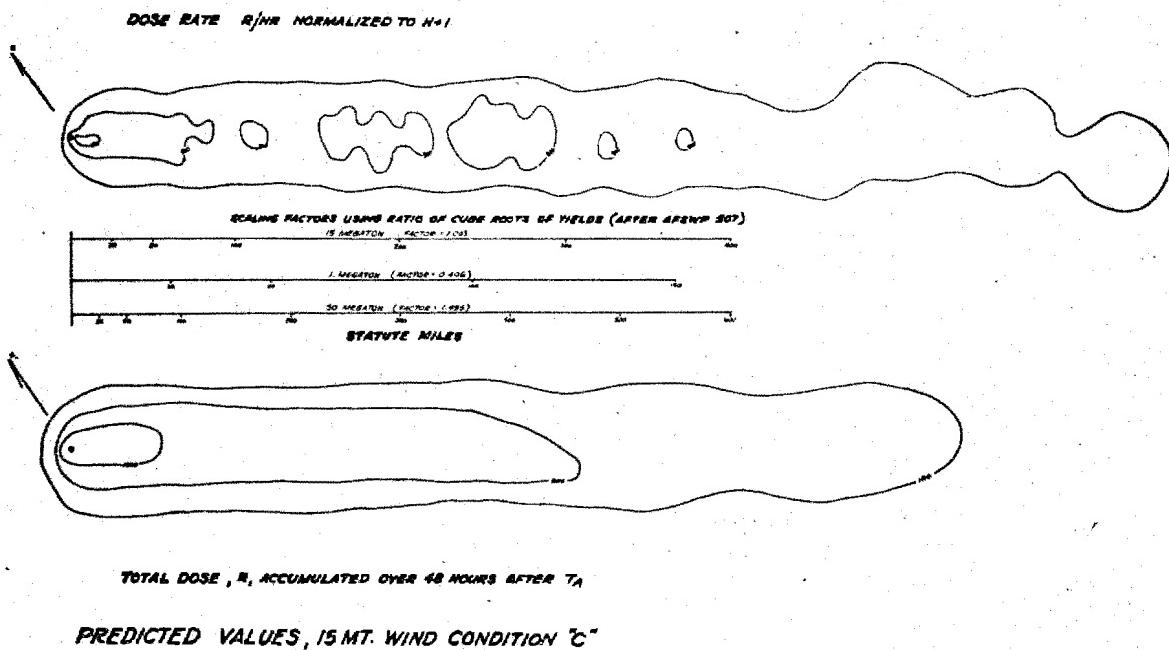
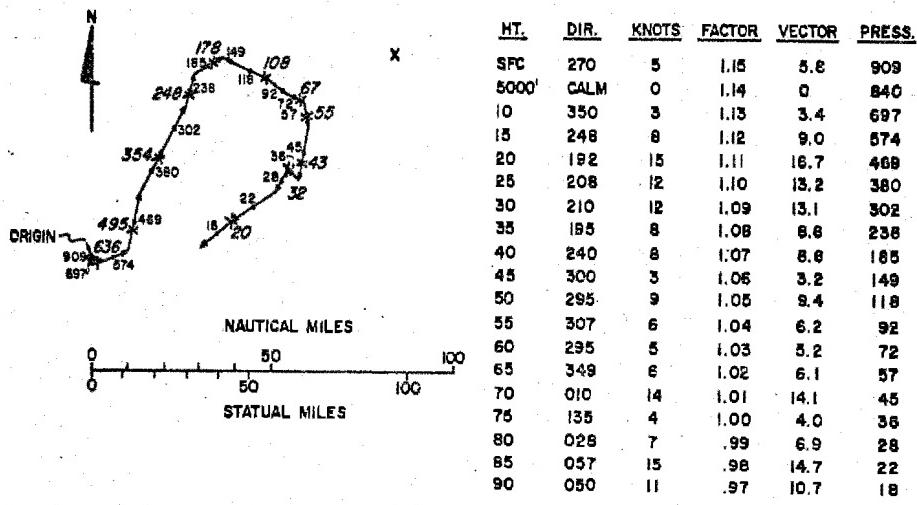


Figure 12

CONDITION OF RELATIVELY LOW WIND SPEEDS AT ALL LEVELS  
(BOISE, IDAHO, 14 MAY 1953)



CONDITION "D"  
WEIGHTED TRAJECTORY

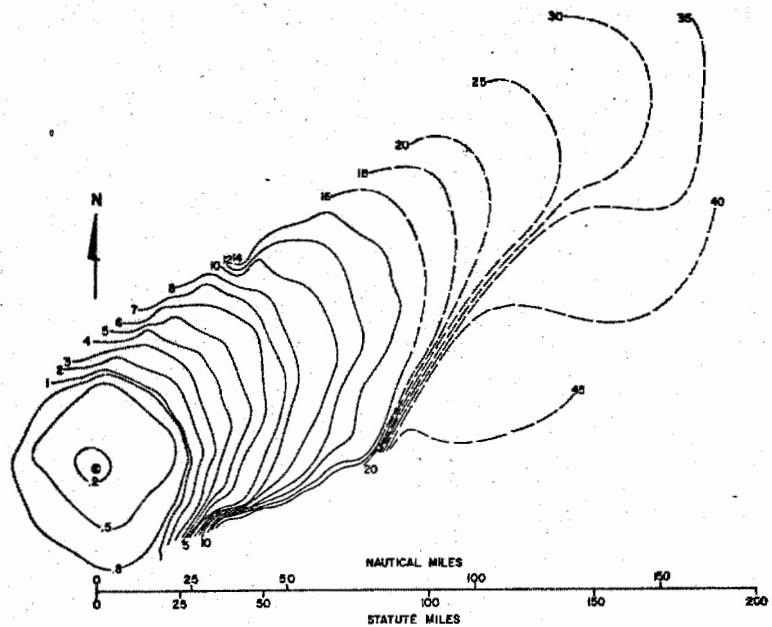
DOE ARCHIVES

Figure 13

485

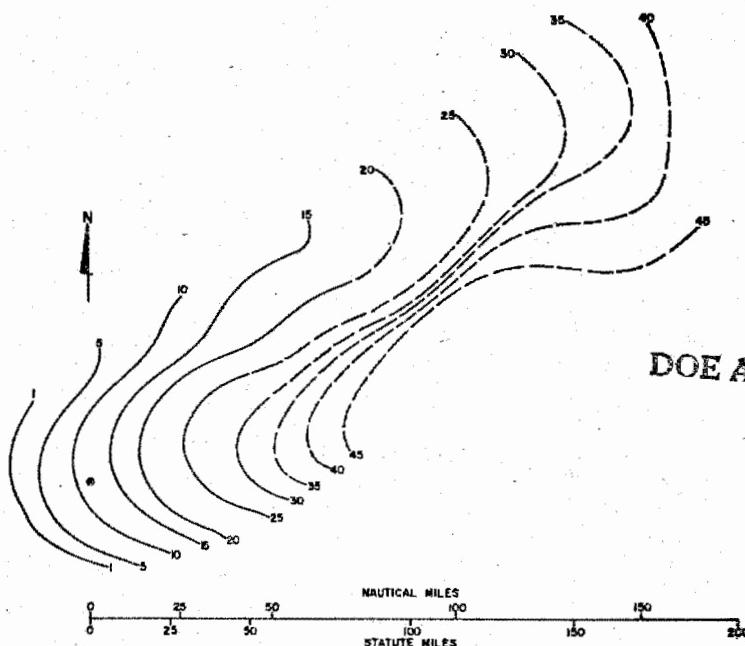


490



$T_A$ , ARRIVAL TIME OF FIRST PARTICLE, IN HOURS, PREDICTED USING  
WIND CONDITION 'D'

Figure 14



DOE ARCHIVES

$T_E$ , ENDING TIME OF LAST PARTICLE, IN HOURS, PREDICTED USING WIND  
CONDITION 'D'

Figure 15

486

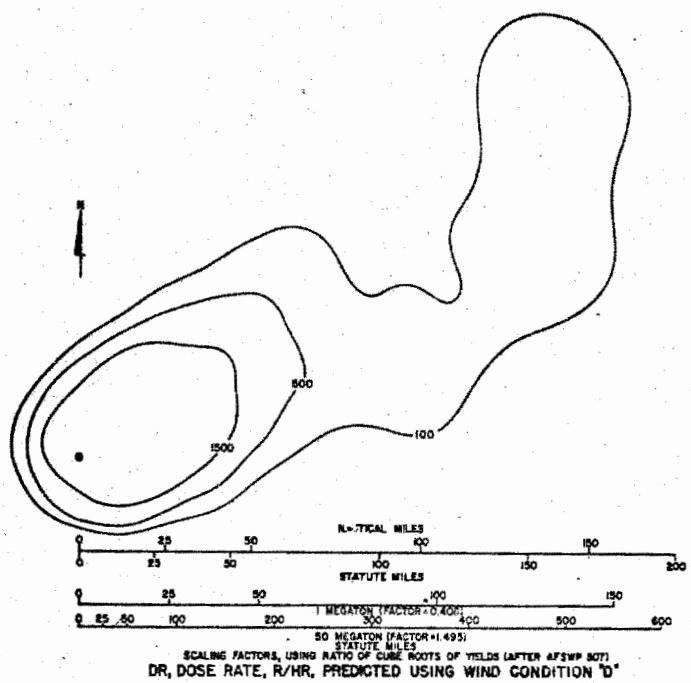


Figure 16

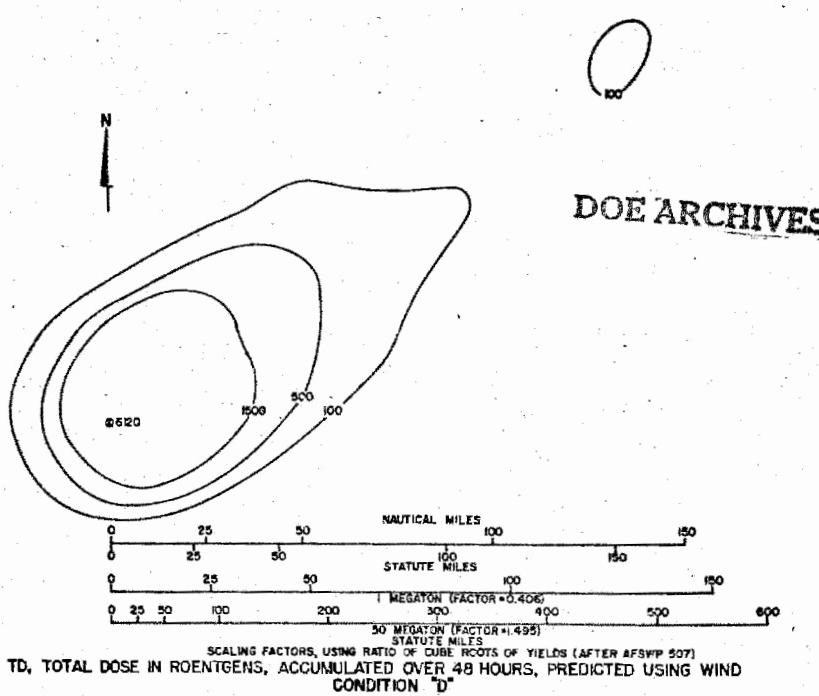
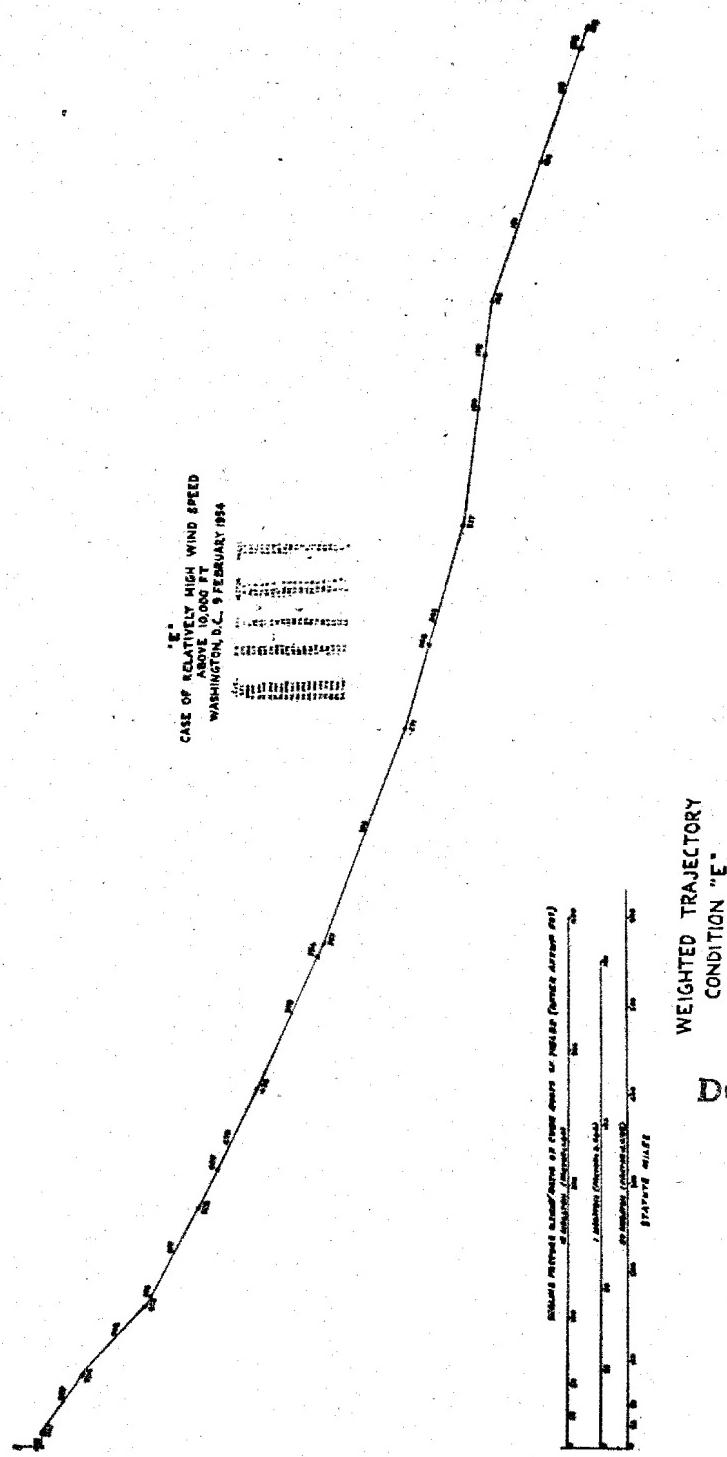


Figure 17

487

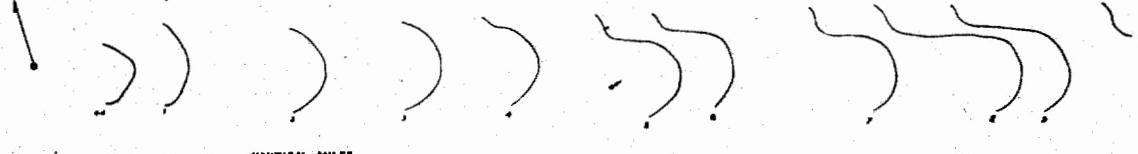
492

Figure 18



DATA  
ENERGY

493



~~MUTICAL MILES~~

THE ENDING TIME IN HOURS OF LAST PARTICLE

PREDICTED VALUES IS MT USING WIND CONDITION "E"

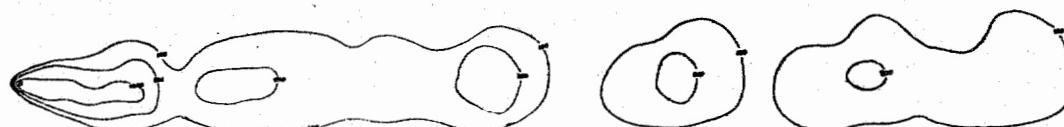
Figure 19

**DOSE RATE IN R/HR NORMALIZED TO H+I**



BLADING FACTORS GIVING RATIO OF CHARGE ROOTS OF TURBINE (AFTER ADJUSTING FOR WINDAGE AND FRICTION)				
No.	100	200	300	400
1. INTEGRATOR (FACTOR 0.400)				30
2. 20	100			
3. INTEGRATOR (FACTOR 1.025)				
4. 200	100	200	300	400
5. STATUTE MILES				

DOE ARCHIVES



TOTAL DOSE, R. ACCUMULATED  
OVER 48 HOURS AFTER T<sub>A</sub>

PREDICTED VALUES FOR 15 MT WIND CONDITION<sup>E</sup>

Figure 20

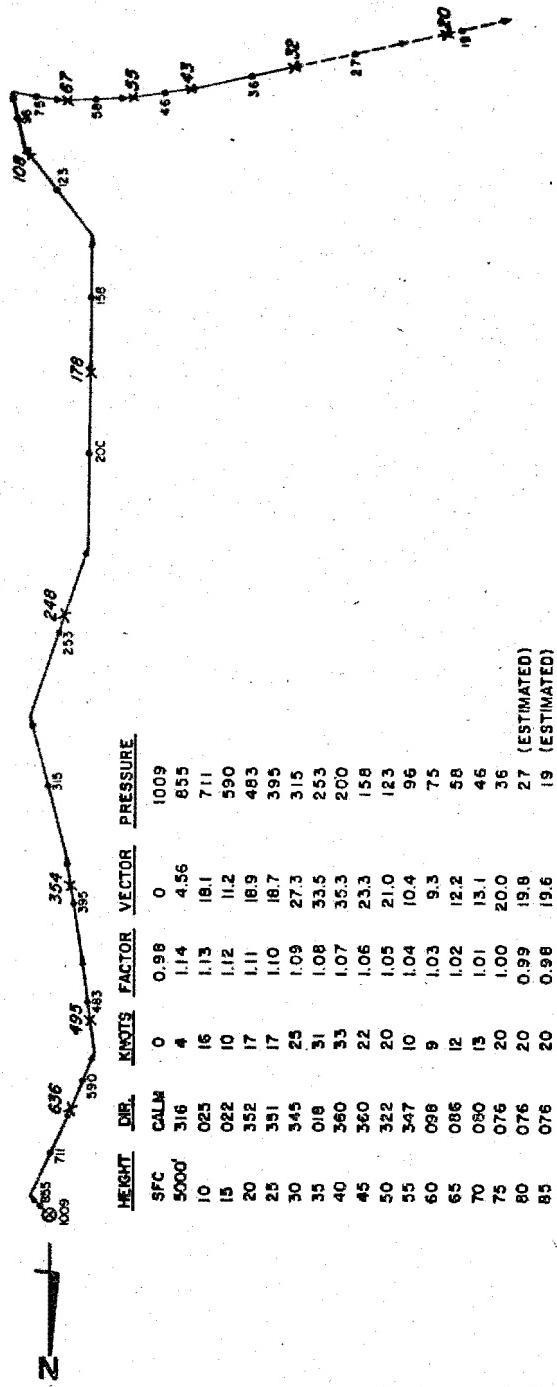
489

SECRET

NUCLEAR ENERGY A

494

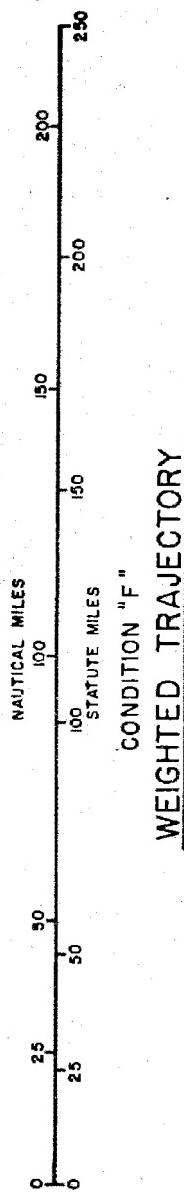
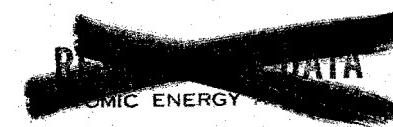
GRADUAL SHEER OF APPROXIMATELY 180° (WASHINGTON DC, 8 JULY 1951)



SFC CALLS      DIR.      KNOTS      FACTOR      VECTOR      PRESSURE

SFC	CALLS	DIR.	KNOTS	FACTOR	VECTOR	PRESSURE
5000	316	0	0.98	0	1009	
5000	316	4	1.14	4.56	855	
10	025	16	1.13	18.1	711	
15	022	10	1.12	11.2	590	
20	352	17	1.11	18.9	483	
25	351	17	1.10	18.7	395	
30	345	25	1.09	27.3	315	
35	018	31	1.08	33.5	253	
40	360	33	1.07	35.3	200	
45	360	22	1.06	23.3	158	
50	322	20	1.05	21.0	123	
55	347	10	1.04	10.4	96	
60	098	9	1.03	9.3	75	
65	086	12	1.02	12.2	58	
70	080	15	1.01	13.1	46	
75	076	20	1.00	20.0	36	
80	076	20	0.99	19.8	27 (ESTIMATED)	
85	076	20	0.98	19.6	19 (ESTIMATED)	

490

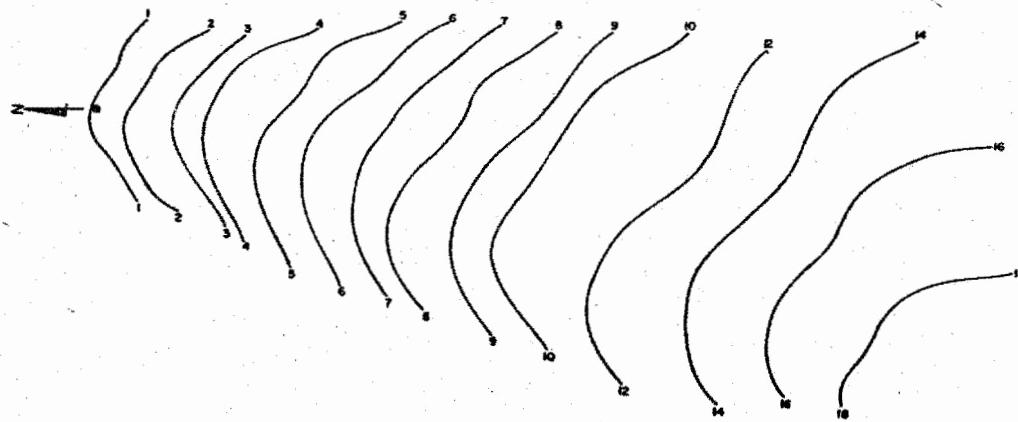
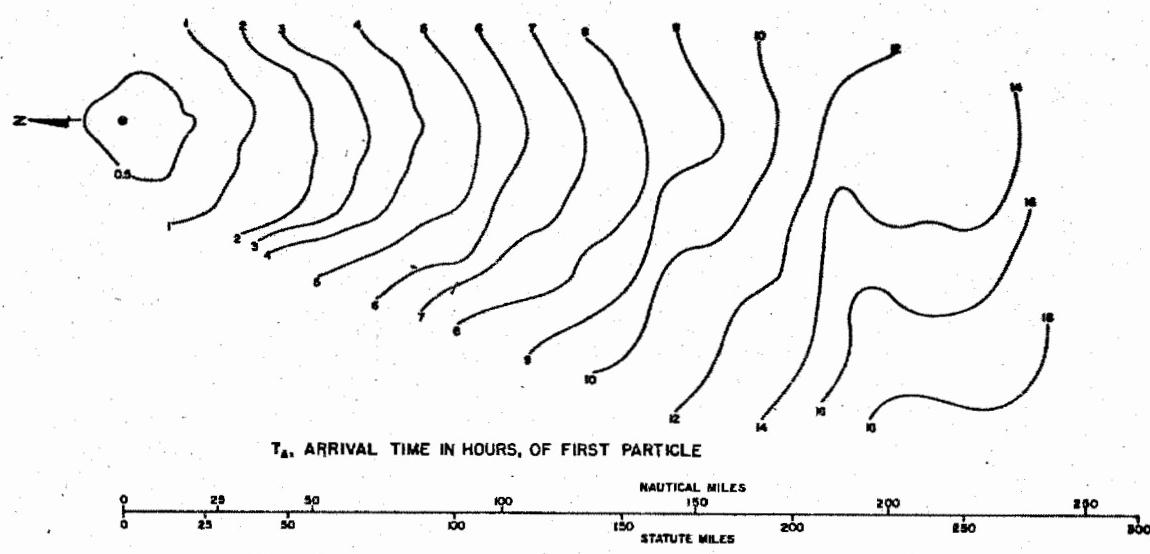


WEIGHTED TRAJECTORY

Figure 21

DOE ARCHIVES

495

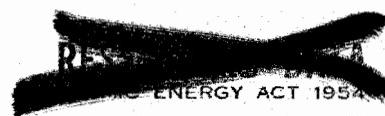


PREDICTED VALUES FOR 15 MT USING CONDITION "F"

**DOE ARCHIVES**

Figure 22

491:



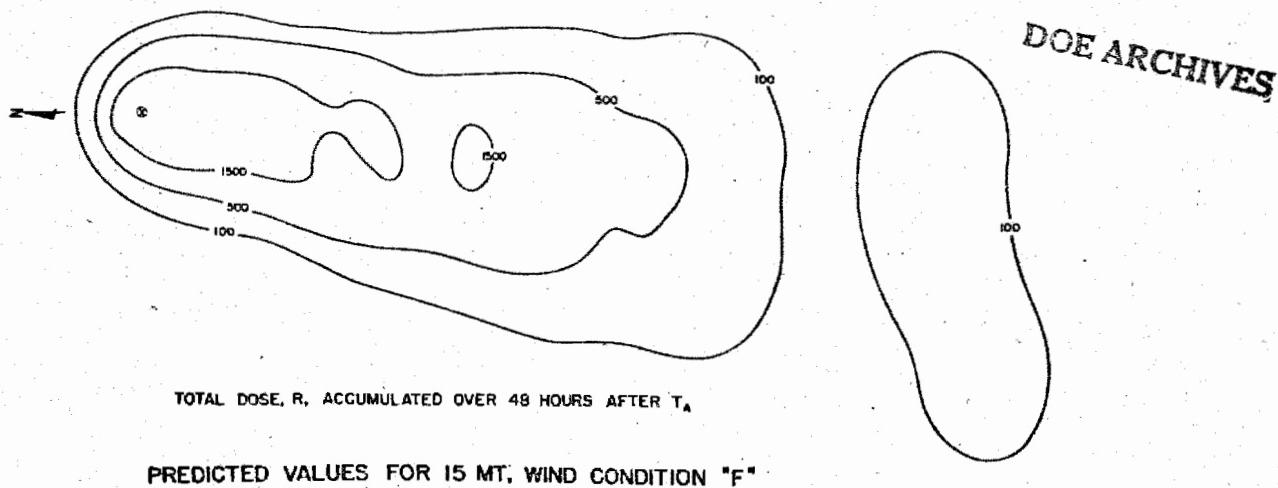
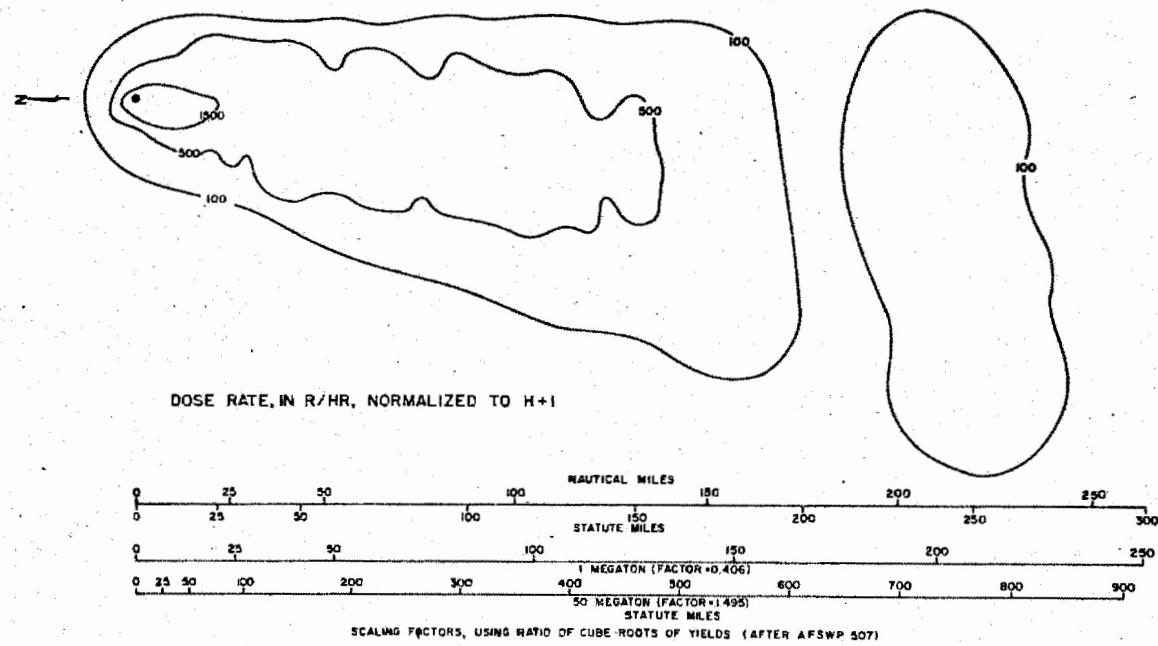


Figure 23

492

501 497

SUMMARY OF DOSE RATE AND TOTAL DOSE AREAS, 15 MT

Wind Condition and Method	Value of Dose Rate (DR) and Total Dose (TD)					
	100		500		1,500	
DR	TD	DR	TD	DR	TD	
Castle Bravo Observed Or Idealized Results. (Approx. Wind Surface To Base of Mushroom 19.4 mph)	13,240 sq mi	17,200	4,520	7,600	1,500	3,240
Castle Bravo Predicted Results, Using Composite Winds and Signal Corps Procedure	20,800	16,200	6,950	5,970	540	1,890
Predicted Results, Using The following Wind Conditions & Signal Corps Procedure:	35,000		9,000		250	
"A" Abrupt 90° Shear At 40,000 Ft. Wind 19.0)		23,000		10,600		1,440
"B" Gradual 90° Shear Wind 23 mph)	35,300	24,800	9,900	10,900	100	1,690
"C" Constant Wind Direction Wind 36 mph)	39,000	37,800	6,180	13,000	60	1,330
"D" Low Wind Speeds Wind 6 mph)	15,750	8,780	4,850	4,730	2,700	2,480
"E" High Wind Speeds Wind 94 mph)	46,600	50,800	2,400	7,860	None	1,240
"F" Gradual 180° Shear Wind 17 mph)	23,400	21,900	6,750	9,100	280	2,620

NOTE: Dose Rates Are In Roentgens Per Hour Normalized To H / 1  
 Total Dose in Roentgens Accumulated Over forty-eight (48) hours After First  
 Particle With No Biological Recovery Factor  
 Areas Are In Square Statute Miles.

DOE ARCHIVES

Figure 24

be noticed is that for very high wind speeds, the area enclosed by the 100 roentgen total dose line is much larger than in the low wind speeds. However, in very high wind speed cases the area enclosed by the higher roentgen values, such as 1500, are much smaller than those enclosed in the low wind speeds. I mentioned to you earlier that we had some suggestions for improving this forecast procedure and we have two. The first one is to get rid of the lumpiness by increasing the total number of discs in particle size categories. To make any significant correction in this direction is going to require a great deal more work. For example, in working up the example of this type, if we use a 15 mile grid for tallying the dose rate, it requires three or four hours for an example. If we use a smaller grid, such as the  $\frac{3}{4}$  mile grid which we employed for these examples, it requires from 15 to 20 man-hours. Now if we were to increase the disc and particle size categories, say ten times, it would increase our work ten times which is beginning to get unreasonable. The obvious answer to this is to apply it to machine methods which we hope to do. The second improvement we would like to make to our procedure applies to the case of the CASTLE Bravo where we made predicted values using the composite winds in that test. Our results would have been better if the area enclosed by the 1500 roentgen total dose lines had been better and larger relative to the area enclosed by the 100 roentgen total dose line. I believe that this is partially the result of the assumption we made in developing our total dose formula. This assumption was that between the arrival time of the first particle and the ending time, at any one point, the accumulation of particles is constantly timed. Now, this does not hold, and particularly near ground zero in the first few hours. I believe that our total dose values near ground zero would be significantly larger if we integrated instead of once, if we integrated several times, and particularly with each particle disc as it came down. Naturally this is going to be a great deal more work and again it implies the necessity for machine methods. One additional advantage that might come from a procedure like that is that we can use a different deterioration rate with time; that is, in the first few hours we might use a  $t^{-0.8}$  or  $-1$ , and later on, after 8 to 10 hours, we might use values  $t^{-1.5}$  or something of that nature. In any case, we are attempting to do this and see if we can compute the CASTLE Bravo pattern by electronic calculating machines employing the improvements that I have just discussed. There are several obvious advantages to electronic calculations; first it is much faster and this allows one to compute a great many cases of fall-out patterns which are necessary if we are to determine realistic probabilities. For example, suppose we wanted to know what the probability was of a lethal dose occurring 50 miles west of a certain town. The only really reliable way to do that is to compute daily patterns for several years and then add up these patterns and see what the probabilities are of having the lethal

dose 50 miles to the west. At the present we can make some approximations to this by using statistical wind data but this can lead to misunderstandings, if not used very carefully. Another advantage of computing these faster is that it admits the possibility of very detailed forecasts for tactical purposes; that is, ones that can be made in perhaps an hour or two. A last advantage to electronic computations is that it will make it practical for us to consider more factors in our procedure. For example, we should take more accurate account of the time space variations of wind during fall-out. We should take more accurate account of the stability of the atmosphere, dispersion, the terrain effects, and perhaps even precipitation. All of these things will greatly complicate the calculations and would only be practical with electronic computations.

If we can look into the crystal ball for a few minutes here I would like to make some suggestions on something that might develop as a result of the electronic calculations. Suppose we develop a series of wiring panels, each of which contains a different model; another series which contains a number of particle size distributions. Once we have those and have tested them to the point where we feel they are reliable then it would be possible to get a prediction of the fall-out pattern for any yield bomb for a wide variety of soil types and for any part of the world. For example, the yield of the explosion and the atmospheric stability would indicate the model size, so that the appropriate wiring panel for that model size could be chosen. Likewise, if we knew the soil type, we could choose the particle size distribution for that soil type, we could choose the particle size distribution for that soil type and put that into the machine. Then our dose rate calibration factor, which you recall in our CASTLE Bravo prediction was 100, could be varied with the condition of the soil and the height of the explosion. That is, if the soil were frozen, there certainly would be much less soil sucked up in the explosion than if the soil were not frozen. Likewise, if the explosion were 500 or 1,000 feet above the surface, it probably would suck up much less dirt. The dose rate calibration factors take account of these things.

DOE ARCHIVES

One final point comes up and that is the question: Are we trying to do something that is more accurate than the data we are working with? I think perhaps we are. The data we have of the actual resulting fall-out patterns, some of the wind conditions, are not as accurate as we are trying to do. However, we can surely expect that this data will be more accurate in the future and ultimately we are going to need the most accurate prediction procedures possible. So I think we are justified in going ahead in trying to develop a fall-out prediction procedure as accurate as possible.

In closing I would like to say that I believe that we have a procedure that gives relatively good results and we have immediate prospects of some improvement. However, there are problems that need to be solved along with problems of this procedure. We need more information about soil types, particle size distribution, biological factors. We need more information about the winds to high levels. We need more accurate forecasts of winds. Last but not least, we need more observed data of fall-out patterns to thoroughly test forecast procedures.

DOE ARCHIVES

496

~~RESTRICTED~~  
ATOMIC ENERGY ACT 1954

~~SECRET~~

501

COUNTERMEASURES; AN ANALYSIS OF NEW WEAPONS EFFECTS  
INFORMATION REQUIRED FOR FALL-OUT COUNTERMEASURES

Paul C. Tompkins  
U. S. Naval Radiological Defense Laboratory

A symposium on fall-out would not be complete if the need for information were not analyzed in the light of countermeasures needed to offset the effects. It is the purpose of this paper to consider that type of information which will lead to reliable countermeasures systems.

The general conclusions derivable qualitatively from an analysis of existing information may be summarized as follows:

Radioactively contaminated areas can be expected to be encountered with sufficient frequency and at sufficient gamma intensity levels to demand direct countermeasures.

Existing facilities and equipment are not adequate to provide the necessary protection.

Areas which can be affected are too large to permit use of evacuation or avoidance of a radiological area as the predominant control measure.

Protection of both personnel and installations from the initial and subsequent effects supersedes recovery as a primary objective. Alternatives to protection and recovery from the effects of the event decrease as areas affected increase.

The primary countermeasures system must be based on provision of sheltered living areas with shielding for protection against the gamma radiation, and recovery through pre-protection of an installation or its subsequent decontamination.

The objective of countermeasures studies is to arrive at a determination of the provisions that must be made to permit people to live through a contaminating event, and still perform essential functions. This implies that not only must one deal with the effects of radioactive contamination under emergency conditions, but one must also know how to live with radioactive contamination under long-term exposure conditions.

Let us now turn to a consideration of the essential elements of countermeasures systems. These elements are:

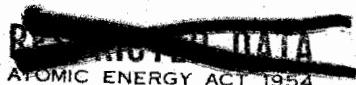
DOE ARCHIVES

Reduction of gamma radiation intensities by shielding.

TABLE 1  
Comparison of Fall-out vs Non-fall-out Conditions on Radiological Practice

Peacetime (non-fall-out conditions)	Fall-out Area
1. Environment Clean. Radioactive materials restricted to limited areas and/or conditions.	1. Environment Contaminated. Clean areas restricted to those protected in advance.
Objective. Keep activity greater than background confined to sharply limited regions.	Objective: Keep activity out of critical localities.
2. Shielding around the source.	2. Shielding around the person.
3. Control points at entry to confined area. Time in restricted area limited.	3. Control points at exit from confined area. Time in environment limited.
4. Contamination monitoring done under low and constant background conditions.	4. Contamination monitoring done under high and variable background conditions.
5. Food supply unlimited and generally not exposed to contamination.	5. Food supply sharply limited and generally exposed to contamination.
6. Clean water supply not limited.	6. Clean water supply very limited.
7. Material control requirements increase with increasing specific activity and total activity.	7. Personnel contamination protective measures increase with increasing specific activity and total activity.
8. Requirement for exposure limited to few people under good administrative control.	8. Requirement for exposure affects many people not under administrative control.
9. Assume things in contaminated area are affected until proved clean.	9. Same.
10. Acceptable dosage/unit time decreases with increasing frequency and duration of exposure.	10. Same.

DOE ARCHIVES



Reduction of gamma radiation fields caused by loose radioactive weapon debris by removal of such debirs. This includes both post event reclamation methods and protective measures such as the "washdown" system employed by the Navy.

Reduction of ingestion, inhalation, and beta radiation burn hazards by the use of proper doctrines, clothing, respirators and effective decontamination.

Reduction of dosage by control of exposure time. This requires an intimate knowledge of time and motion involved on the part of personnel, and an equally intimate knowledge of the radiation intensity and radiological conditions under which these personnel must operate.

Exclusion of contaminated material from critical areas such as those designed for occupancy, food and water sources, etc.

The first requirement of countermeasures is to provide enough protection to permit survival during the acute phase immediately following a detonation. This must be done primarily through an adequate shelter program. Such shelters must provide a shielding factor of the order of 1000, if military forces are to retain the capability of operating despite the presence of fall-cut.

DOE ARCHIVES

The second requirement is to establish the capability of recovering and occupying the affected regions as normally as possible. To do this it is necessary that "living areas" be designated. These areas must have maximum shielding available and provisions for excluding the entry of radioactively contaminated material. This requirement must be met if dosage control is to be possible. It is from these centers that personnel would then emerge into the surrounding contaminated area to discharge their assigned duties. The decontamination of "work areas" will be a requirement in many cases. The provision of clean food and water supplies will be the predominant practical problem encountered in this phase. The acceptance of a single, sub-lethal acute dose as the criterion of acceptable dosage is not sound practice. It is required that a new set of medical standards be developed to cover continued exposures at various rates, comparable to the 30 roentgens per two years which is the current standard for peacetime operations permitted by the Navy. Criteria for properly prorating the revised acceptance doses are needed.

Unlike industrial practices, fall-out influences the environment. Although this fact does not affect the currently practiced principles of radiological procedure, there are drastic practical influences on the conditions to which these principles are applied. Table I illustrates some of the more obvious differences brought about by the radiological effect on environmental conditions. Notice that only items 9 and 10 stay the same under the two situations.

Figure 2  
Contamination Pattern

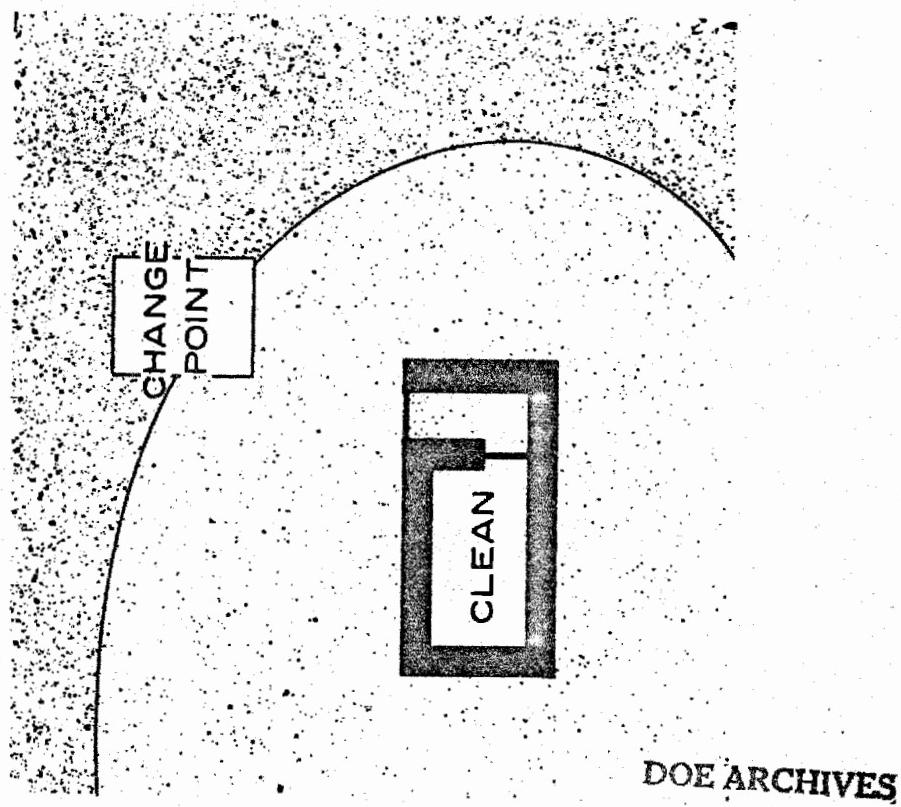
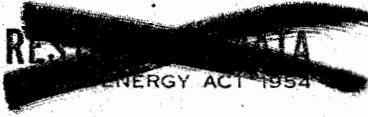
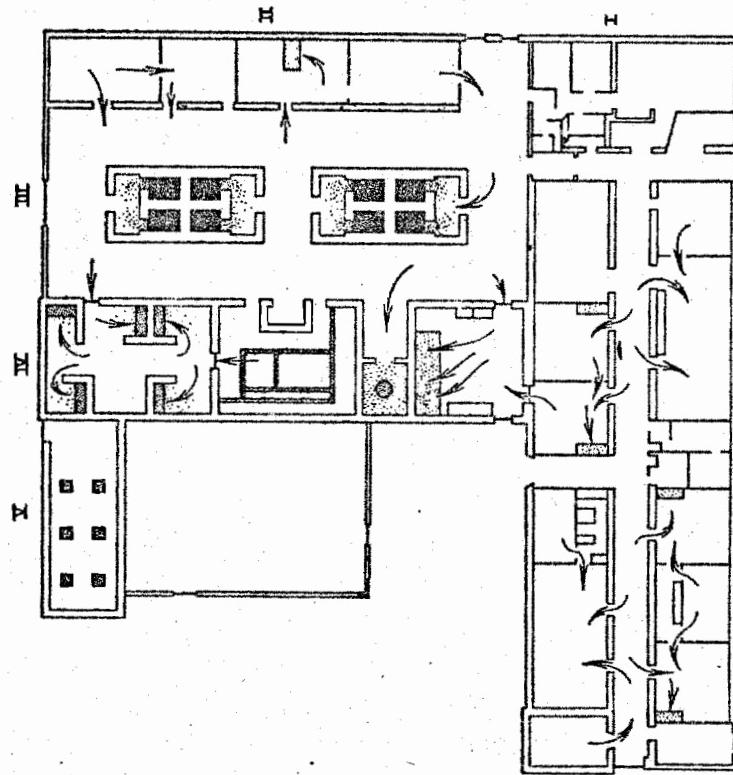


Figure 1  
Floor Plan



505

These differences are further illustrated by Figures 1 and 2. Note particularly the relationships between areas and contamination density. Figure 1 shows the lay-out of a building designed to conduct research work with multicurie quantities of radioactive materials. The highest activity area marked by the heavy stippling is the interior of the cells which are surrounded with 3-foot concrete walls for shielding, maze entrances to further reduce radiation levels when the cell doors are open, doors to confine activity to the interior, and air flow (shown by the arrows) for regions of low contamination to those of higher contamination. In Figure 2, the principles employed are identical, but the pressure is in the opposite direction. The situation in Figure 2 is that which one encounters when one is required first to survive and subsequently live with the effects of a major fall-out event without evacuation. The same principles of ventilation control would lead to positive pressure ventilation in the shelter.

This completes the summary of the qualitative picture. Let us now consider the more quantitative aspects which determine the character and ultimate cost of countermeasures systems. Quantitative knowledge is essential because any protective system can be overwhelmed by increasing either the gamma radiation levels or the contamination densities. Also, any system can safely handle any radiological condition lower than that for which it was designed. However, when applied unnecessarily, this usually involves very high costs and excessive impediments to normal practice, since remote or semi-remote control operations are usually involved in coping with severe radiological conditions.

Three types of protection are required: from whole-body gamma radiation; from skin burns arising predominantly through direct contamination of the person; and internal deposition of radionuclides from all methods of entry into the body.

It is recommended, with limitations to be noted presently, that the absolute maximum dosages considered acceptable for countermeasures systems design purposes be:

For gamma exposure,

- Not over 500 r accumulated over 5 years,
- Not over 200 r in any one year,
- Not over 20 r in any event under maximum protection.

DOE ARCHIVES

For beta exposure,

- Not over 5,000 rep in 5 years,
- Not over 2,000 rep in any one year,
- Not over 200 rep in any single exposure.

TABLE II (a)

Reference Contours Related to Delivery of 1000 Rep  
or 10,000 Rep in One Week

Time After Burst of Start of Initial Exposure	Reference Contour (b) Leading to 1000 rep in 1 week (r/hr at 1 hr)	Reference Contour Leading to 10,000 rep in 1 week (r/hr at 1 hr)
1 hr	7.8	78
1 wk	107	1,070
1 mo	455	4,550
1 yr	7,500	75,000

(a) Calculations by Broido, A., and Teresi, J.

(b) The calculations assume the applicability of the  $t^{-1.2}$  decay law, and uniform contamination over the whole body. Whole-body beta exposure LD<sub>50</sub> assumed to be about 5000 rep. The 10,000 rep column applies to small particles only.

DOE ARCHIVES

For internal deposition;

The accumulation of  $5 \mu\text{c}$  Sr<sup>89-90</sup> as the body burden should be considered the absolute upper limit.

It must be stressed that these criteria have a limited biological safety factor and those personnel getting the maximum of any one of these might be expected to show a high incidence of delayed effects. Further, a quantitative basis for reduction in allowable whole-body exposure in the presence of radionuclides deposited in the bone is not available.

The problem of controlling gamma exposure has been dealt with many times. Suffice it to say that exposure time control is the essential ingredient and that design appears to call for a shielding factor of the order of 1000 or more.

The probable scope of the beta burn problem is shown in Table II. Here one sees an estimate of the reference contour lines expressed in r/hr at 1 hr which would be expected to give 1000 rep and 10,000 rep in one week. The selection of these two levels was based on the assumptions that:

The burns would come largely from weapon debris in direct contact with the skin.

No immediate burn would be developed with less than 1000 rep.

A local burn would be certain above 10,000 rep from a small particle (point source). The current effects table (AFSWP) states that incapacitation will occur in 3 to 6 hours from 3000 to 5000 rep over a relatively small area (a few square centimeters) of the body.

Health habits will insure that no contamination stays in one particular locality on the body for more than 1 week.

No subsequent contaminating material will expose exactly the same area of the skin by depositing in exactly the same place.

Note that the reference value shifts upward as the initial time of exposure increases from  $T_0$ .

DOE ARCHIVES

The internal deposition problem can be assessed from the Sunshine project which reached the conclusion that the Sr<sup>90</sup> tolerance level in soil would be reached at about the 120 r/hr at 1 hour reference line. During the first 18 months, the activity of Ba<sup>140</sup> - La<sup>140</sup> and Sr<sup>89</sup> is about 10 times this amount or more. Allowing for build-up from detonations occurring over a period of time and the possible addition of inhalation as a source of internal deposition, reference contour of 1 r/hr at 1 hour can be taken as defining the point at which one must start becoming concerned.

The general character of the applicable countermeasures systems as related to the reference contour lines from a single detonation are summarized in Table III.

#### Summary of Effects Data Needed to Guide Countermeasures Development

##### **Biological:**

Maximum "acceptable" dosages prorated over 5 years. Particular attention should be paid to late biological effects occurring between 5-10 years.

Medical Effects Table for skin effects as functions of time and area. Particular emphasis should be paid to burns from small "hot" particles.

##### **Instruments:**

Contamination meters for clothing, water, air, food, etc. must be able to cancel out surrounding radiation field between ~ 0.1 mr/hr to 1 r/hr.

Dosimetry should distinguish between deep dose and surface dose.

Calibrations with a point source appear to be inadequate. Calibrations should reflect the distributed geometry which is actually encountered.

##### **Characteristics of radionuclides:**

Beta energy and amount as function of time up to 2 years.

Gamma energy and amount as function of time up to 2 years.

Fission Yields.

Solubility in the range of  $10^{-3}$  to  $10^{-6}$ .

Exchange properties with soil and other surfaces, particularly Sr and Pu.

Uptake of radioelements into growing foods.

DOE ARCHIVES

##### **Radiation Fields characteristics:**

Radiation fields from contamination distribution other than the infinite flat plane. Knowledge of important variations in either the spectrum or air ionization are needed.

A "simulated" or "synthetic" gamma spectrum as a function of time is needed for both dosimetry and shielding development work.

Typical radiation fields from basic geometric models should be developed schematically so that actual situations can be analyzed by a summation of parts.

**Shielding:**

Basic types of construction geometry should be schematized. Build-up factors should be measured for energies of about 0.4 Mev, 0.7 Mev, and 1.5 to 2.0 Mev. Build-up factors should be based on data for slab, edge, and corner orientations.

**Fall-out:**

Mathematical model should cover region to the 1 r/hr at 1 hr. reference contour line.

Meteorological conditions leading to deposition of "hot" spots in lower activity areas should be identified possibly through refinement of the model. Probable number and size but not location should be statistically predictable.

Chemical composition of the weapon debris is extremely important in relation to contamination density and solubility.

**Countermeasures:**

Reduction in the radive field without shielding by removal of the weapon debris should aim at 90 to 99 per cent reduction.

Water treatment should aim at a reduction of  $\sim 10^5$  in total activity and  $\sim 10^3$  for Sr.

Contaminability of clothing and skin from the environment must be quantitated at least roughly.

**DOE ARCHIVES**

505

NUCLEAR ENERGY ACT 1954

510

TABLE III  
Comparison of Countermeasures Requirements as Related to Initial Contamination Level

Reference Contour Line	Ingestion	Surface Burn	Whole-body Gamma
Less than 1 r/hr at 1 hr	No severe problems. Good hygiene required. Radioactive decay will prevent serious consequences.	No severe problems. Good hygiene required. Radioactive decay will prevent serious consequences. Probable total body dose less than 20 r for the total event.	No severe problems. Good hygiene required. Radioactive decay will prevent serious consequences. Probable total body dose less than 20 r for the total event.
1 r/hr at 1 hr to 10 r/hr at 1 hr	Upper limit controllable by procedural methods alone. Availability of clean water essential. Fresh vegetables grown and consumed within the 6 mo. period following fall-out may cause some trouble. Methods for assessing level of contamination in food and water predominant requirement.	Probably no problem if reasonable precautions against unnecessary exposure are observed.	Protection at a factor of 2 to 10 r required. Can still operate uninhibited at a total dosage of less than 100 r for the whole event.
10 r/hr at 1 hr to 100 r/hr at 1 hr (Approaching Rongelap region)	Intermediate level of protection. Food & water definitely affected, but area may be recoverable by biological scavenging plus decay within ~1 year.	Upper limit for reasonably normal behavior.	Upper limit is approaching the LD <sub>50</sub> unless shielding or evacuation can cut the dose by at least a factor of 5 to 10. Burns will definitely develop in a few people unless good hygiene and precautions are used.

DOE ARCHIVES

TABLE III (continued)  
Comparison of Countermeasures Requirements as Related to Initial Contamination Level

Reference Contour Line	Ingestion	Surface Burn	Whole-body Gamma
More than 100 r/hr at 1 hr.	(a) Protection of food and water supplies essential. Hydroponics best technique for growing new crops. (b) Soil scavenging essential if agriculture is to be resumed within 5 years.	Full protective covering between contaminated areas and living areas must be introduced. Contamination control is predominant problem.	Minimal shielding of 10 to 100 required on lower side. Between 100 to 1000 required for higher contours. Operations must be planned on basis of limited exposure in unshielded condition.

- (a) Since contours of ~ 10,000 r/hr at 1 hr can be encountered, this region covers approximately a factor of 100 in severity. Doses as high as 50,000 r can be received and beta burns can be initiated with contact times of minutes.
- (b) Rongelap region is probably between the 100 r/hr at 1 hour and the 200 r/hr at 1 hour reference line.

507

DOE ARCHIVES

ATOMIC ENERGY

512

**THIS PAGE IS BLANK**

**DOE ARCHIVES**

**508**

**ENERGY ACT 1954**

**513**

PREDICTION OF DOSE RATE AND DOSAGE CONTOURS AS FUNCTIONS  
OF YIELD AND METEOROLOGICAL CONDITIONS; COMPARISON OF  
PROBLEM SOLUTIONS

CDR Roger W Paine, Jr., USN  
Headquarters, Armed Forces Special Weapons Project

Early in the planning phase of the fall-cut symposium, it was decided that a ready means of comparing the various methods of generating fall-out contours would be a desirable addition to the symposium summary report, and to the symposium itself if such a means of comparison could be made ready in time. In the last analysis, the contours generated by a model for a specific weapon yield and for a specific weather situation probably form the best means of comparison with other models. Accordingly, speakers who had consented to present their methods at the symposium under Topic F were sent six actual weather soundings taken at various localities in the United States in recent years and asked, time permitting, to work out a series of contour solutions for two or more of these weather situations. In order to make a distinct break with the CASTLE BRAVO event, against which most of the methods had already been calibrated, yields of 1 MT and 50 MT were chosen. The participants were asked to generate by their methods for surface bursts of each of these yields, contours of 100, 500, and 1500 r/hr referred back to H-1 hour, and contours of 100, 500, and 1500 r total dose accumulated up to 48 hours after burst time.

DOE ARCHIVES

This "homework", as the participants chose to call it, represents a considerable amount of hard work by the agencies involved, some of whose methods are not easily adaptable to generate the particular contours asked for. It is therefore very gratifying that complete problem solutions by each method were turned in for one of the weather situations, and at least partial solutions by each method for a second. Particular thanks are due the Army Signal Corps, the Air Weather Service, and Technical Operations Incorporated for completing work on all six weather situations.

Owing to the great volume of material involved, only problem solutions for the two situations for which almost complete returns are available will be compared in detail in this report. Solutions for these situations are sufficient to point out the

more important conclusions which can be drawn from the comparisons, which are:

For situations which do not involve abrupt wind shears, the contours generated by the several methods, although differing in detail, do not differ greatly in the direction of fall-out nor in the order of magnitude of the area covered.

Because of the basically different assumptions as to the location of radioactive materials in the stabilized cloud, the presence of an abrupt wind shear between 15,000 and 50,000 feet is apt to cause considerable differences in the predicted direction of fall-out for certain contours, although predictions of the magnitudes of the areas covered do not differ greatly.

None of the methods predict very high intensity dose or dose rate contours, even for the hypothetical 50 MT yield. A maximum dose rate of the order of 10,000 r/hr or less at H+1 hour appears to be indicated, and this is likely to occur only in a very small area at or near surface zero.

In comparing the problem solutions, it is well to keep in mind the basic assumptions and limitations of the methods being compared. Some of these account directly for the differences observed. Examples are:

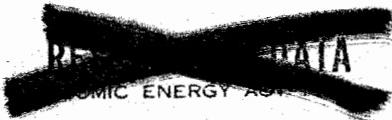
#### AFSWP Method

This method is based on ground surveys at JANGLE-S and CASTLE BRAVO, and consists of "idealized" contours, which follow a single scaling wind direction. Abrupt wind shears and unusual weather conditions are not easily handled. The method is suitable for planning purposes only; not for post-shot analysis. An order-of-magnitude contour can be drawn for any weapon yield between 0.1 KT and 100 MT in two or three minutes by untrained personnel.

#### ARDC Method

#### DOE ARCHIVES

The model assumes that 90% of the bomb debris activity is in the stem of the stabilized cloud, and 10% is in the mushroom. Mean effective particle sizes are assumed for the cloud and parts of the stem, and Stokes Law fall rates for spherical particles are used. Wind and weather conditions are allowed for. The method is calibrated to CASTLE BRAVO, but is adaptable over a wide range of yields. A problem solution requires several hours by trained personnel.



### Army Signal Corps Method

The model divides a hypothetical stabilized bomb cloud consisting of super-posed cylinders into disc or cylindrical wafers or compartments, each associated with a particular particle size category and fall rate. Each disc is then brought to the ground according to the winds acting on it, and ground values are then summed over all the discs to obtain contours. A different model must be generated for each weapon yield, and for different localities (tropical, polar, etc). Wind and weather conditions are allowed for. A particle size distribution hypothesized by the Rand Corporation is used. Aerodynamic particle fall rates are used. The method is calibrated to the AFSWP-507 reported survey of CASTLE BRAVO. Because of the finite number of discs in the model, contours are often lumpy and may involve artifact "hot spots". A problem solution requires several hours by trained personnel. (The dose contours presented are for 48 hours after arrival time, rather than for H+48 hours).

### Air Weather Service Method

The method is essentially a radex plot resulting in rough sectors within which fall-out may be expected, together with estimated times of arrival along vectors from ground zero for particular altitudes from which it is assumed particles start their fall. The method does not generate contours, and thus is not directly comparable to methods that do. The plot can be drawn in about 15 minutes by trained personnel.

### Los Alamos Method

The method was devised for use during CASTLE in forecasting the gross results to be expected from surface bursts of about 10 MT fired in the northern Marshalls. The plots submitted are modified only by direct yield dependence. The effect of yield on initial cloud geometry is not included, nor is the effect of the different tropopause height of the middle latitudes from that in the Marshalls. The method gives very little detail anywhere and none at all near the origin. It is not intended for use in detailed post-shot analyses, but rather for radsafe planning. A problem solution probably requires about an hour for an individual familiar with the method.

### Navy Method

DOE ARCHIVES

This method, which is based largely upon a radex wind plot, is a system of weighting incremental square areas according to the degree of fall-out expected, relative one to another. It results in wind-sensitive contours which have only relative values. Actual values may be fitted to the contours as a result of one or more post-shot survey

readings taken in the contaminated area. For purposes of this comparison, the contours submitted have been roughly normalized in area to the corresponding contours of another method or methods (e.g., LASL) in order to show agreement in shape. A problem solution requires something more than an hour for personnel familiar with the method.

#### NRDL Method

This is a wind and weather dependent system which assumes the bulk of the radioactive material originates in the lower portion of the mushroom, and utilizes an aerodynamic particle fall rate which varies considerably with the altitude of the particle. A problem solution requires several hours by personnel familiar with the method.

#### Rand Corporation Method

The method gives wind and weather-sensitive contours, based on an assumed particle size distribution and the hypothesis that 90% of the fission product radioactivity falls out from the mushroom cloud and 10% from the stem. An aerodynamic rate of fall is used which is somewhat different from that used by NRDL, but which also varies markedly with altitude. A problem solution requires a great amount of hand calculation. The method has also been programmed for machine solution, and the machine method was used for the solutions presented here.

#### Technical Operations, Incorporated, Method

The method utilizes an inverted cone cloud model, the NRDL assumption of particle size distribution, and fall rates which increase with increase in altitude.

DELETED

A problem solution requires somewhat more than an hour, utilizing trained personnel.

DOE ARCHIVES

The problem situations presented for comparative solutions were as follows:

CONDITION "A"

Wintertime situation of an abrupt, approximately 90° shear at a height of approximately 40,000 feet.

Dodge City, Kansas

1500 GMT 28 Dec 1953

37° 46'N, 99° 58' W.

Height ft, msl	Wind Direc- tion Degrees	Wind Speed Knots	Pressure Millibars	Elevation: Temperature Degrees C	Relative Humidity -%
Surface	260	7	925	-7.4	84
5,000	247	12	842	-3.0	36
10,000	273	19	695	-8.7	30
15,000	307	13	570	-13.2	MB
20,000	008	16	463	-24.0	
25,000	045	41	373	-34.2	
30,000	036	52	300	-45.5	
35,000	357	29	238	-53.5	
40,000	213	47	187	-55.5	
45,000	255	43	118	-58.0	
50,000	255	55	115	-60.2	
55,000	260	47	90	-60.6	
60,000	272	54	71	-61.0	
65,000	289	40	55	-58.8	
70,000	285	36	43	-59.3	
75,000	285	38	34	-56.5	
80,000	285	45	27	-56.0	

DOE ARCHIVES

513

AMERICAN ENERGY ACT 1955

518

## CONDITION "B"

Gradual Shear of Approximately 90°

Washington, D. C. (Silver Hill)

0300 GMT 28 Sept 1952

38° 50' N, 76° 57' W.

Elevation: 289 feet

Height Ft, msl	Wind Direc- tion Degrees	Wind Speed Knots	Pressure Millibars	Temperature Degrees C	Relative Humidity-%
Surface	Calm	0	1010	9.7	85
5,000	358	11	853	11.8	16
10,000	009	20	708	5.8	39
15,000	325	14	688	-0.2	MB
20,000	282	19	485	-10.9	
25,000	263	34	394	-21.4	
30,000	263	47	320	-31.0	
35,000	273	37	255	-41.0	
40,000	308	27	203	-51.5	
45,000	292	23	160	-60.2	
50,000	290	28	123	-66.5	
55,000	290	20	97	-65.4	
60,000	268	11	76	-64.0	
65,000	276	21	58	-61.5	
70,000	293	7	46	-59.0	
75,000	293	8	36	-55.5	
80,000	285	10	28	-54.3	
85,000	250	11	23	-52.0	

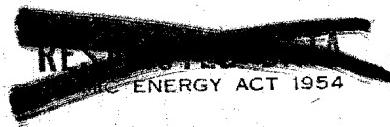
The salient features to note about Condition "A" are that the winds are generally from the west, except for a band between 15,000 and 35,000 feet, wherein the winds are from the north and the north-east. The mean wind is about 40 knots.

DOE ARCHIVES

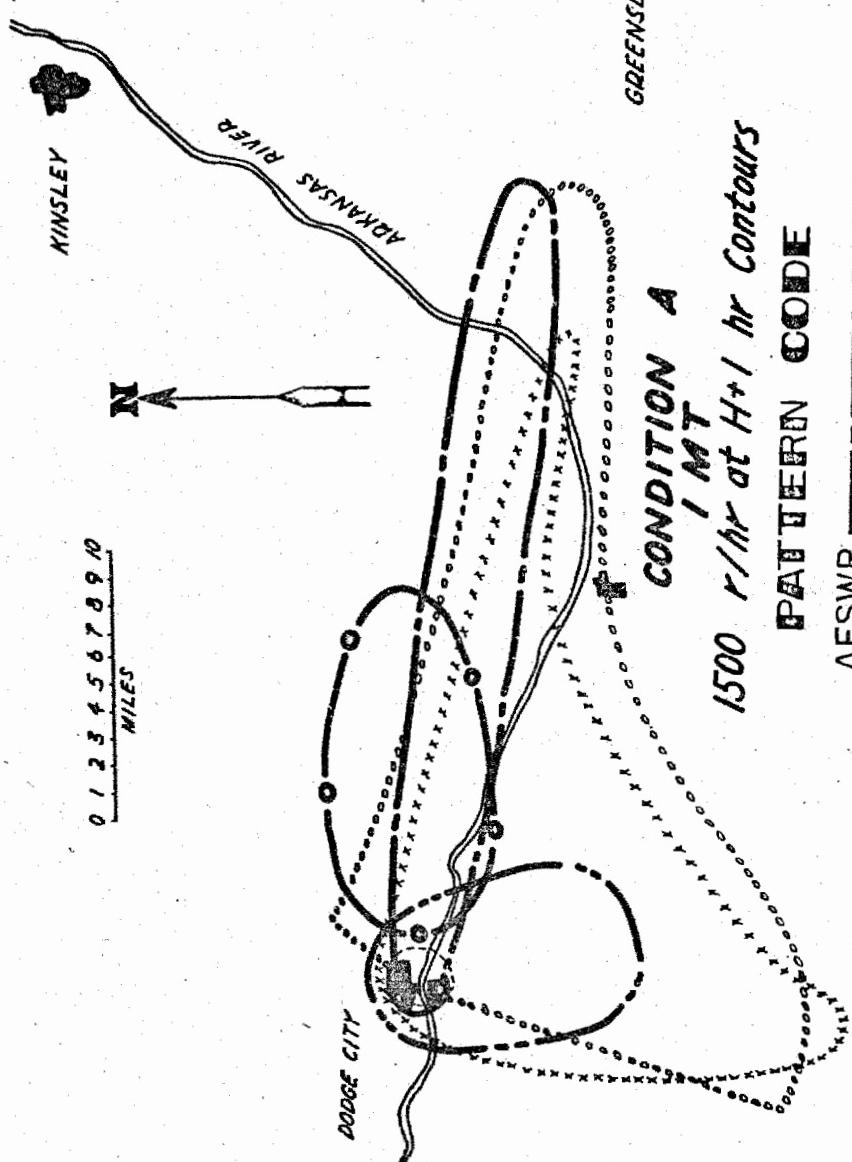
For Condition "B", the winds are again generally from the west, except for the region between the surface and about 15,000 feet, within which the winds are northerly. The mean wind is about 20 knots.

The problem solutions are compared by superposition on the charts which follow, using coded overlays as indicated on each chart. Missing solutions either had not been received in Headquarters, AFSWP, at time of press make-up (1 February 1955), or the material received was not readily adaptable for comparison. Tables giving numerical comparisons of contour areas and downwind and crosswind extents follow the charts.

514



519



### CONDITION A

1500 r/hr at H+1 hr Contours

### PATTERN CODE

AFSWP	—	—	—	—
ARDC	—	X	—	X
ARMY SIG	—	—	—	—
LASL	X	X	X	X
NAVY	0	0	0	0
NRDL	—	—	—	—
RAND	—	—	—	—
TECHOPS	—	O	—	O

**DOE ARCHIVES**

515

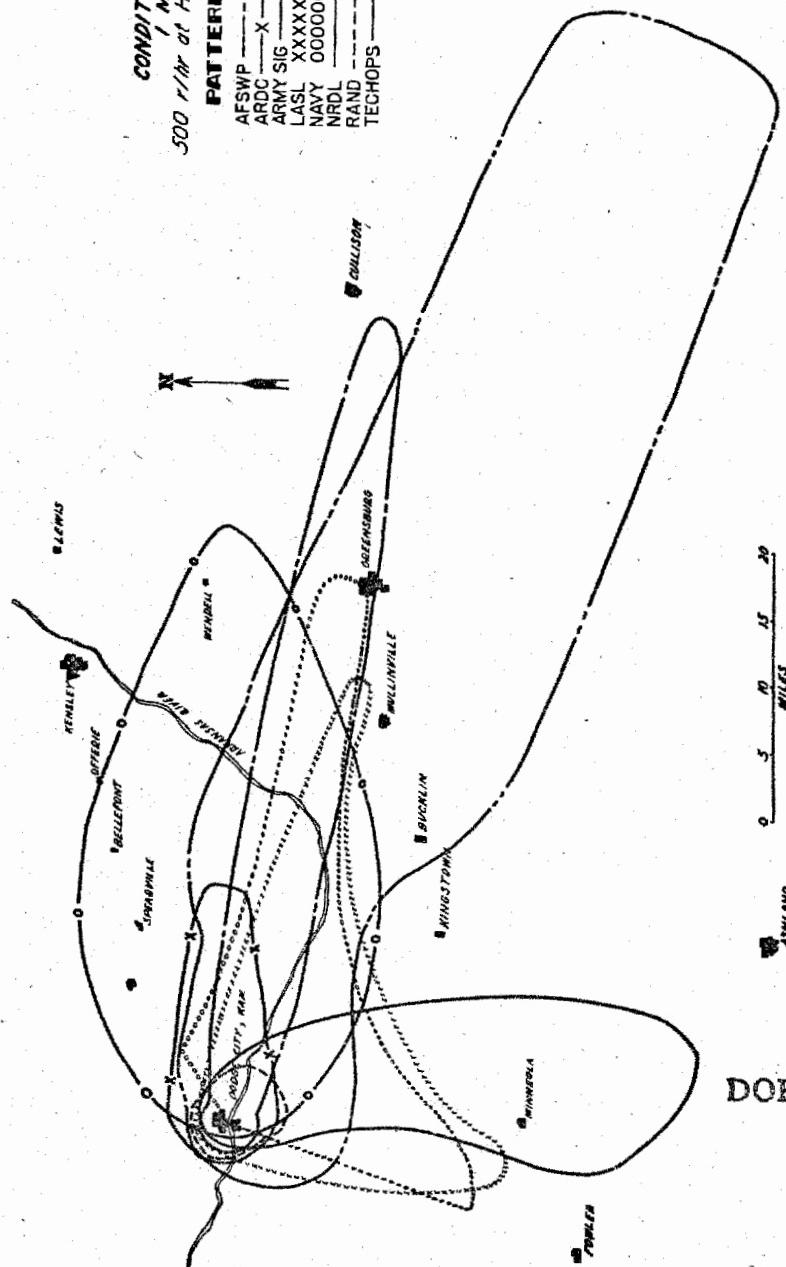
AMERICAN ENERGY ACT

520

**CONDITION A**  
1 MT  
500 r/hr at H+1 hr Contours

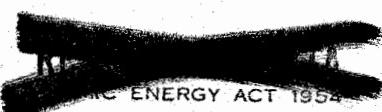
**PATTERN CODE**

AFSWP	- - - - -
ARDC	X - - X - - X
ARMY SIG	X - - - - -
LASL	X XXXX XXXX XXXX
NAVY	0000000000000000
NRDL	- - - - -
RAND	- - - - -
TECHOPS	0 - - 0 - - 0



DOE ARCHIVES

516



521

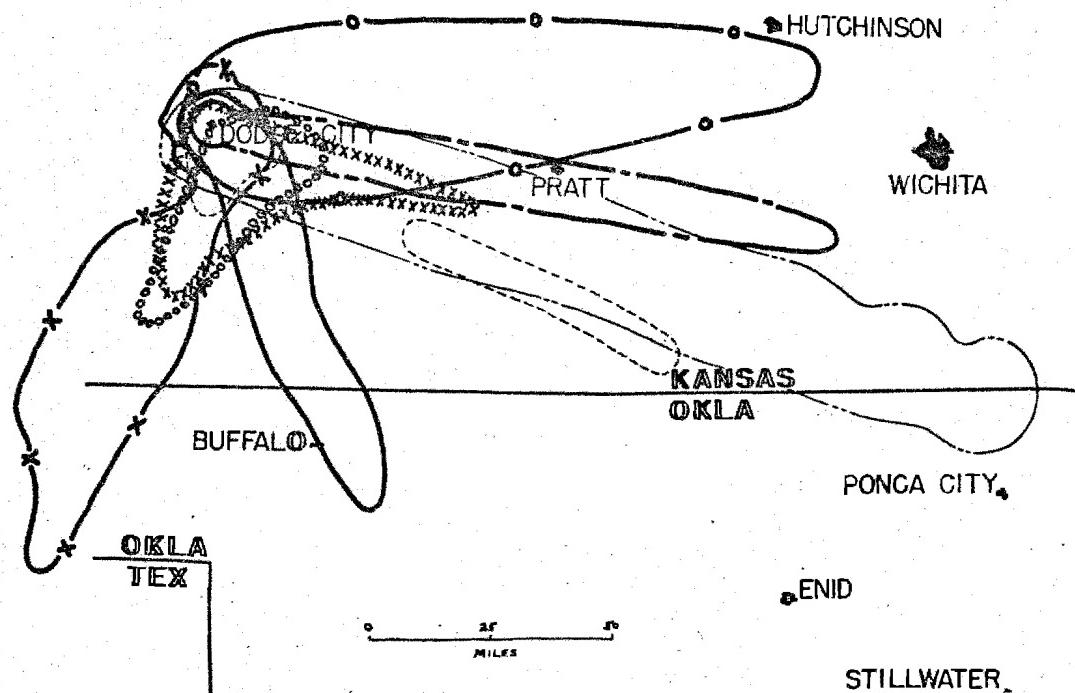
**CONDITION A**

I MT

100 r/hr at H+1 Contours

**PATTERN CODE**

AWSWP \_\_\_\_\_  
ARDC X X X → SALINA  
ARMY SIG \_\_\_\_\_  
LASL XXXXXXXXXXXXXXXX  
NAVY 0000000000000000  
NRDL \_\_\_\_\_  
RAND \_\_\_\_\_  
TECHCPS O O



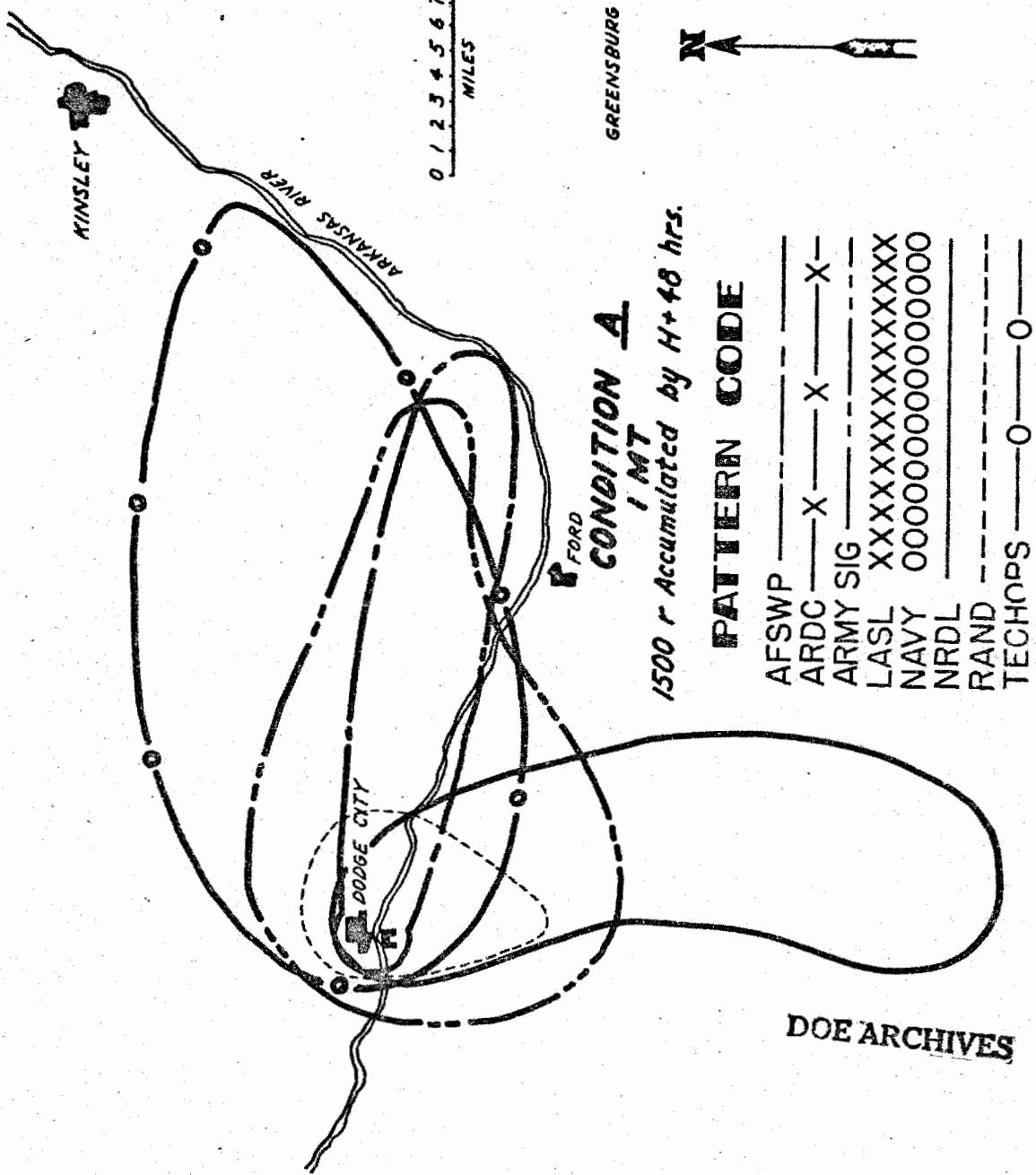
STILLWATER

**DOE ARCHIVES**

517

ENERGY ACT

522



518

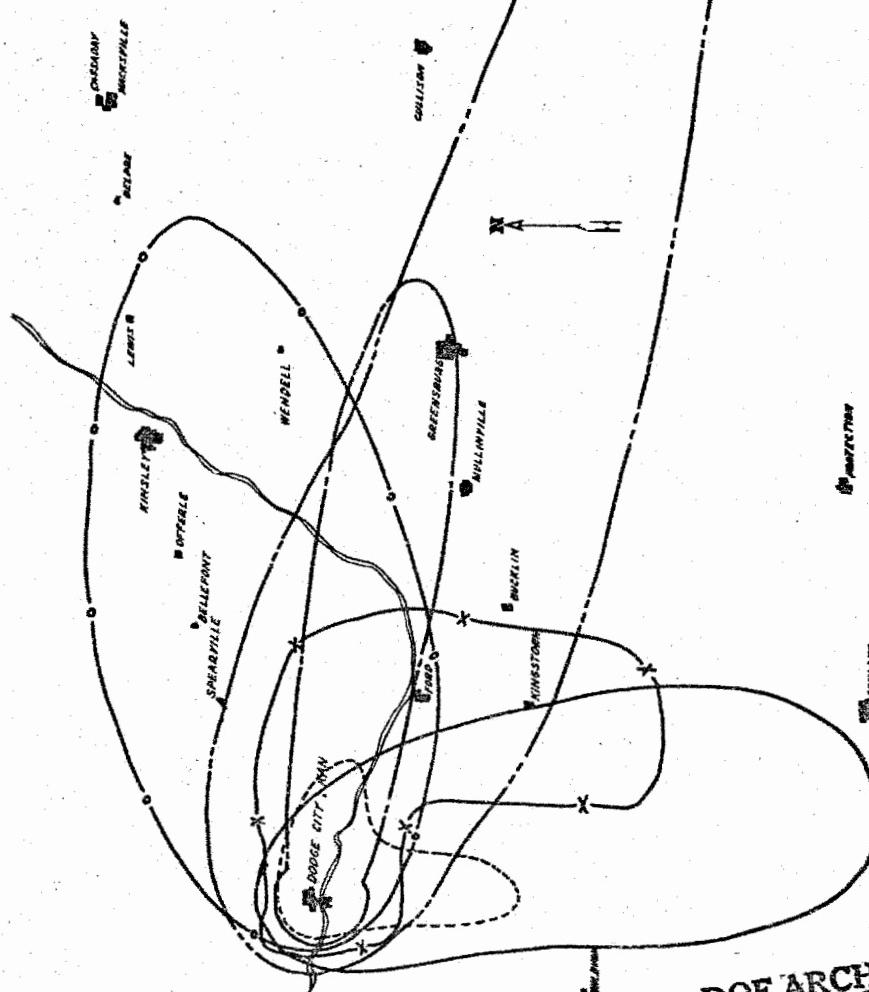
NUCLEAR ENERGY ACT 1954

523

**CONDITION A**  
1 MT  
500 m Accumulated by H-48 hours

**PATTERN CODE**

AFSWP	X	X
ARDC	X	X
ARMY SIG	X	X
LASL	XXXXXX	XXXXXX
NAVY	0000000000000000	0000000000000000
NRDL		
RAND	O	O
TECHOPS	O	O



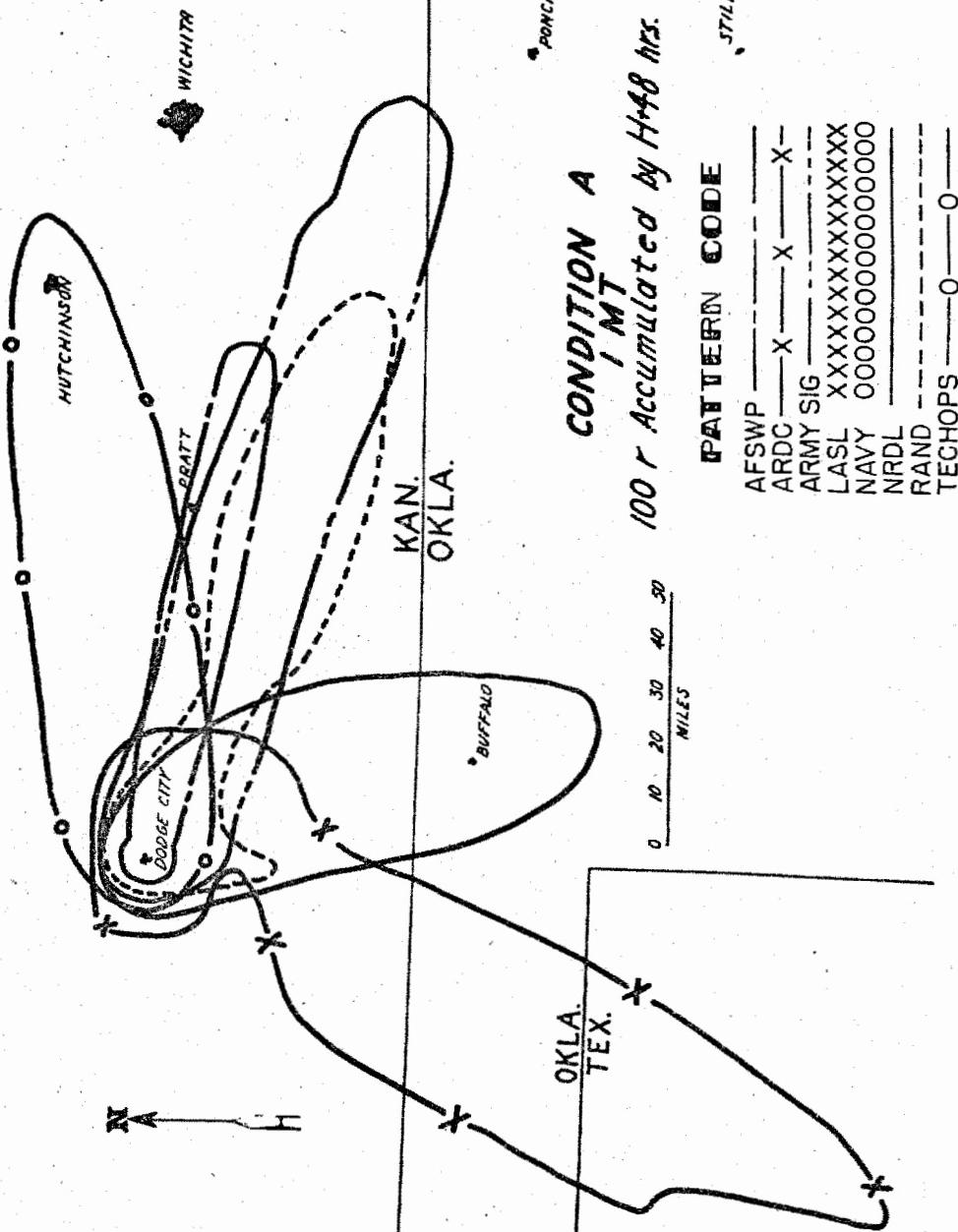
519

**SECRET**

ATOMIC ENERGY ACT

524

EMPIORIA

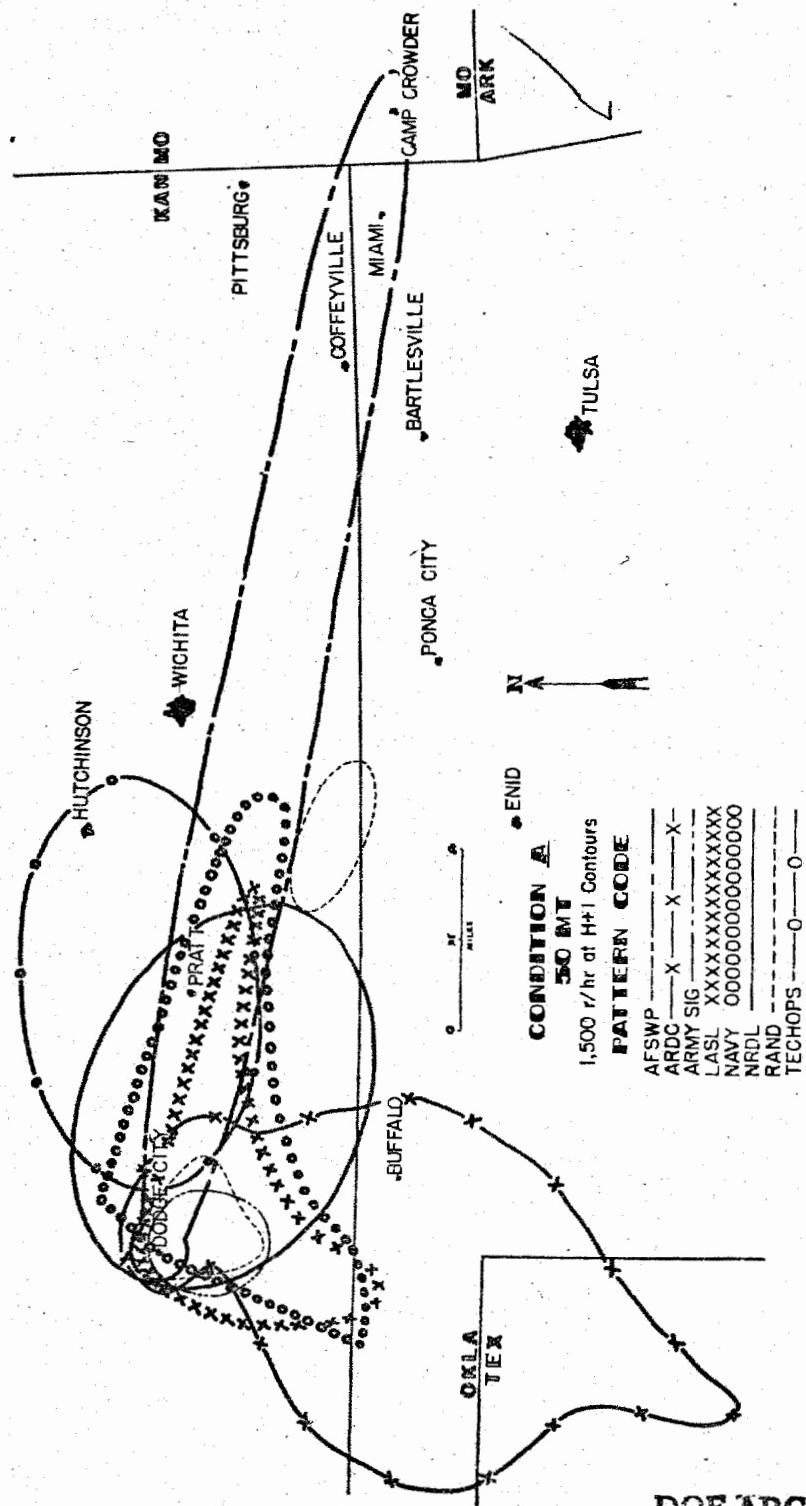


DOE ARCHIVES

520

OMIC ENERGY ACT 1954

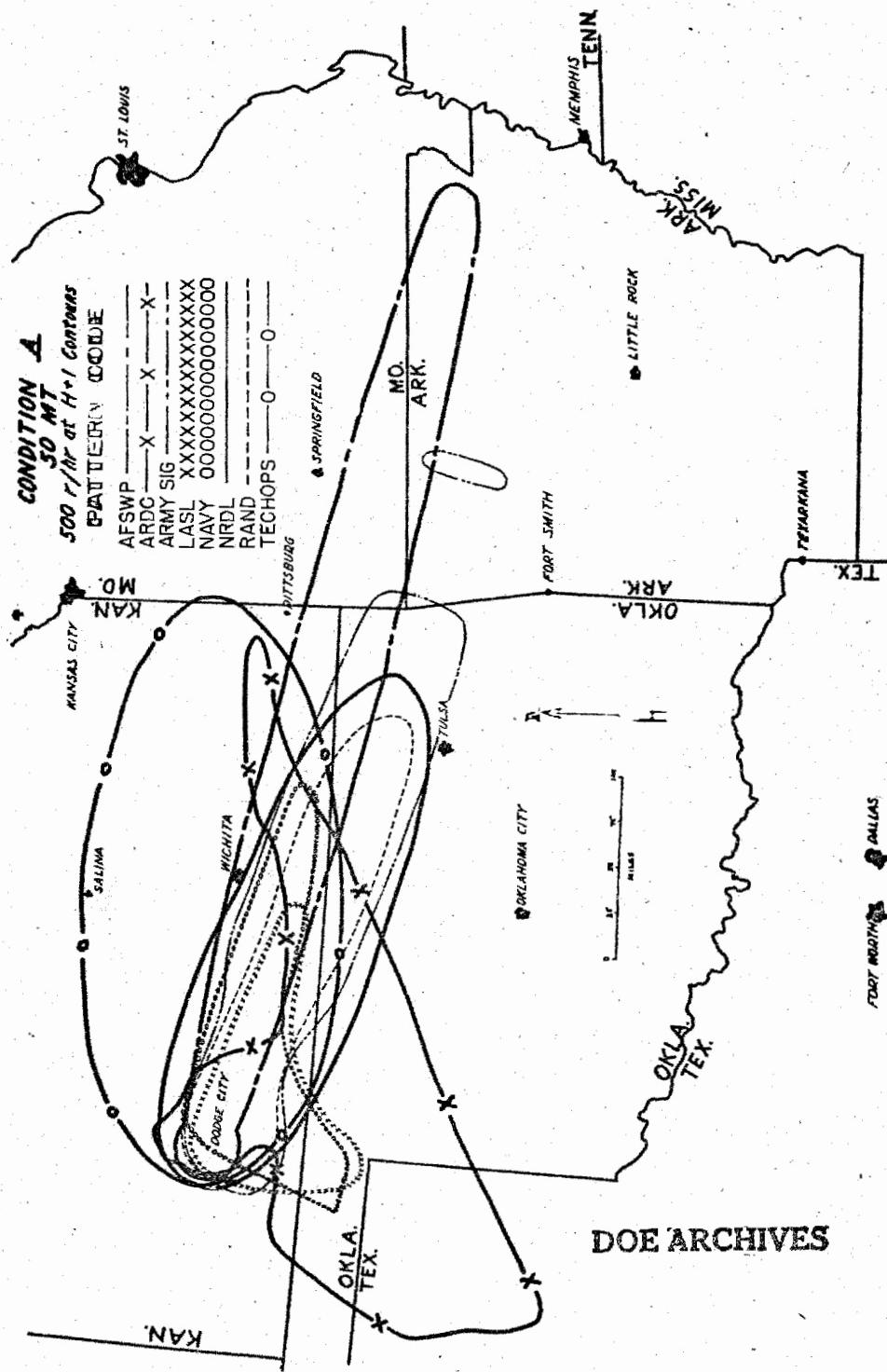
525



521

ATOMIC ENERGY ACT 1954

526

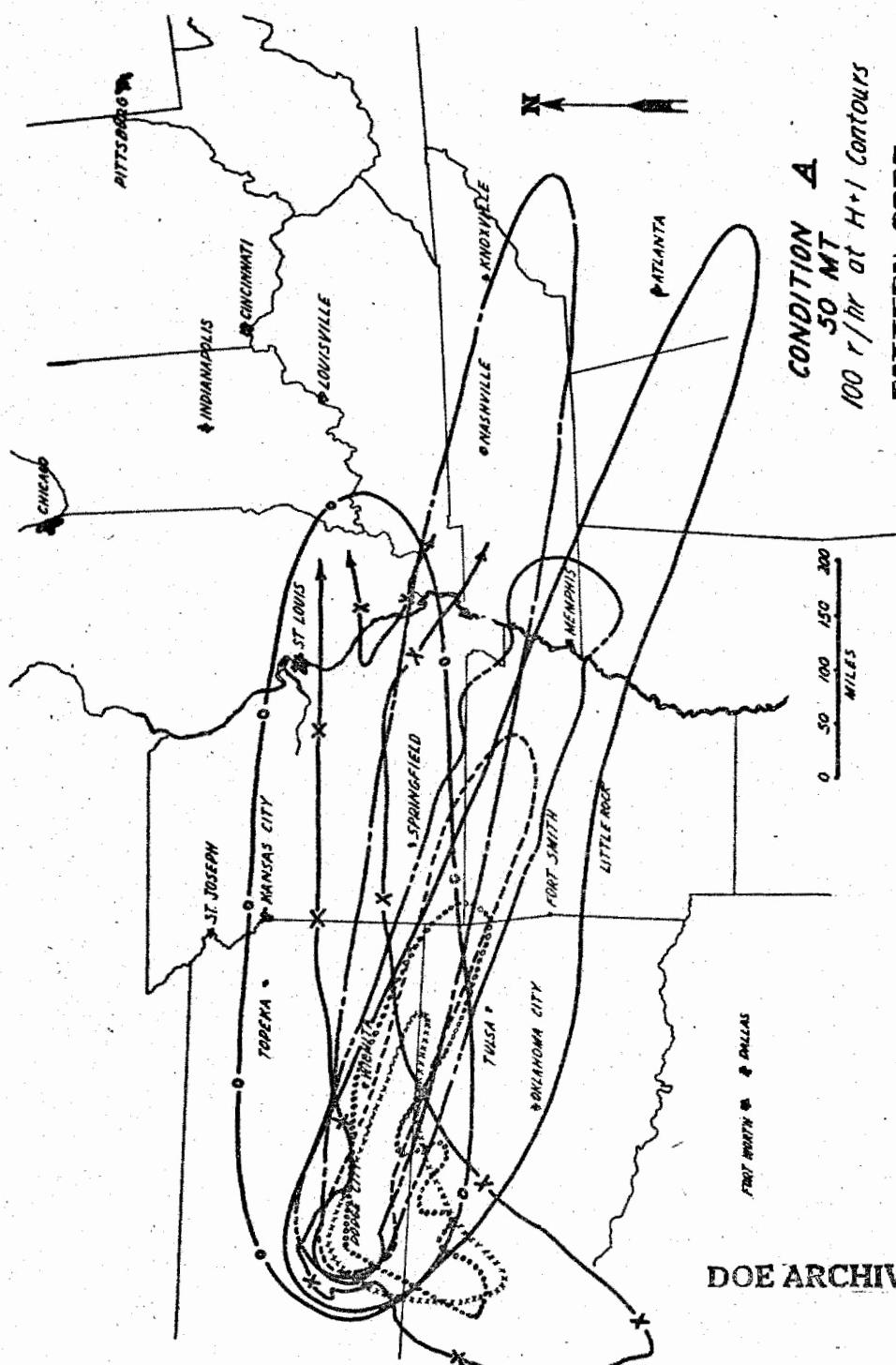


DOE ARCHIVES

522

#### ENERGY ACT 1983

527  
531



**CONDITION A**  
**50 MT**  
**100 r/hr at H+1 Contours**

**PATTERN CODE**

AFSWP	-----
ARDC	X ----- X ----- X
ARMY SIG	-----
LASL	XXXXXX XXXXXXXXXX
NAVY	0000000000000000
NRDL	-----
RAND	- - - - - O ----- O
TECHOPS	-----

523

ATOMIC ENERGY ACT 1954

528

TOPEKA

HAYS SALINA

0 2.5 50  
MILES

HUTCHINSON

WICHITA

CHANUTE

COFFEYVILLE

KAN.

OKLA.

BARTLESVILLE

PONCA CITY

TULSA

STILLWATER

CONDITION A  
50 MT  
1500 r Accumulated by H<sup>48</sup> hrs END

PATTERN CC DE

AFSWP	- - -	- - -	- - -
ARDC	X	X	X
ARMY SIG	- - -	- - -	- - -
LASL	X	X	X
NAVY	0	0	0
NRDL	- - -	- - -	- - -
RAND	- - -	- - -	- - -
TECHOPS	O	O	O

OKLA.  
TEX.

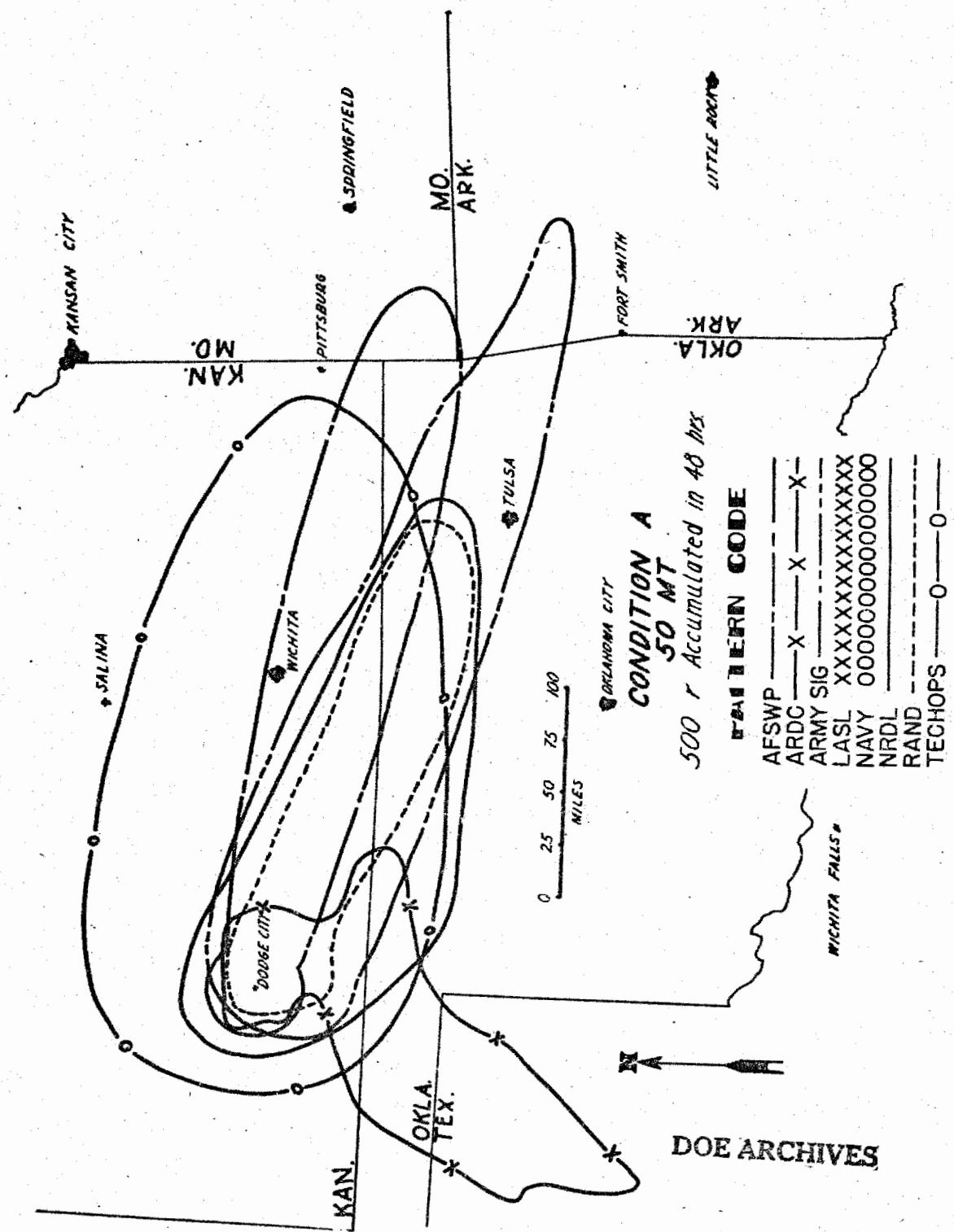
DOE ARCHIVES

524

SECRET

AMERICAN ENERGY ACT 1980

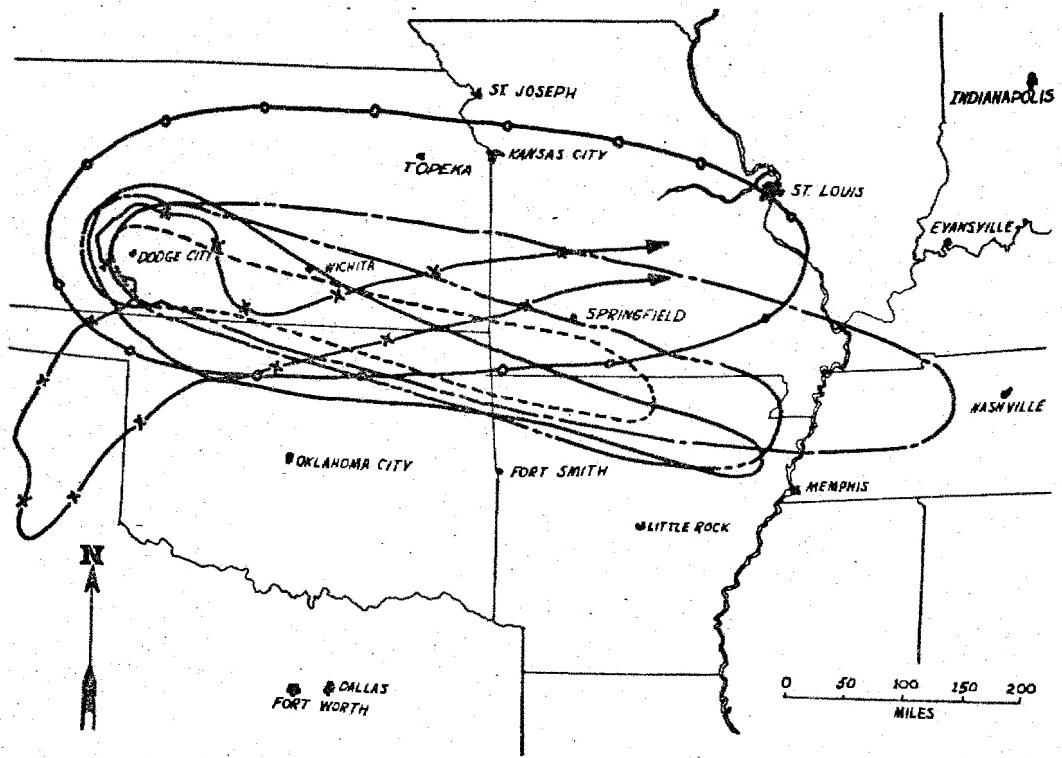
529



525

ATOMIC ENERGY ACT

530



**CONDITION A  
50 MT**

100% Accumulated in 48 hrs.

**PATTERN CODE**

AFSWP	-----
ARDC	-X-X-X-
ARMY SIG	-----
LASL	XXXXXXXXXXXXXX
NAVY	00000000000000
NRDL	-----
RAND	- - -
TECHOPS	0-0

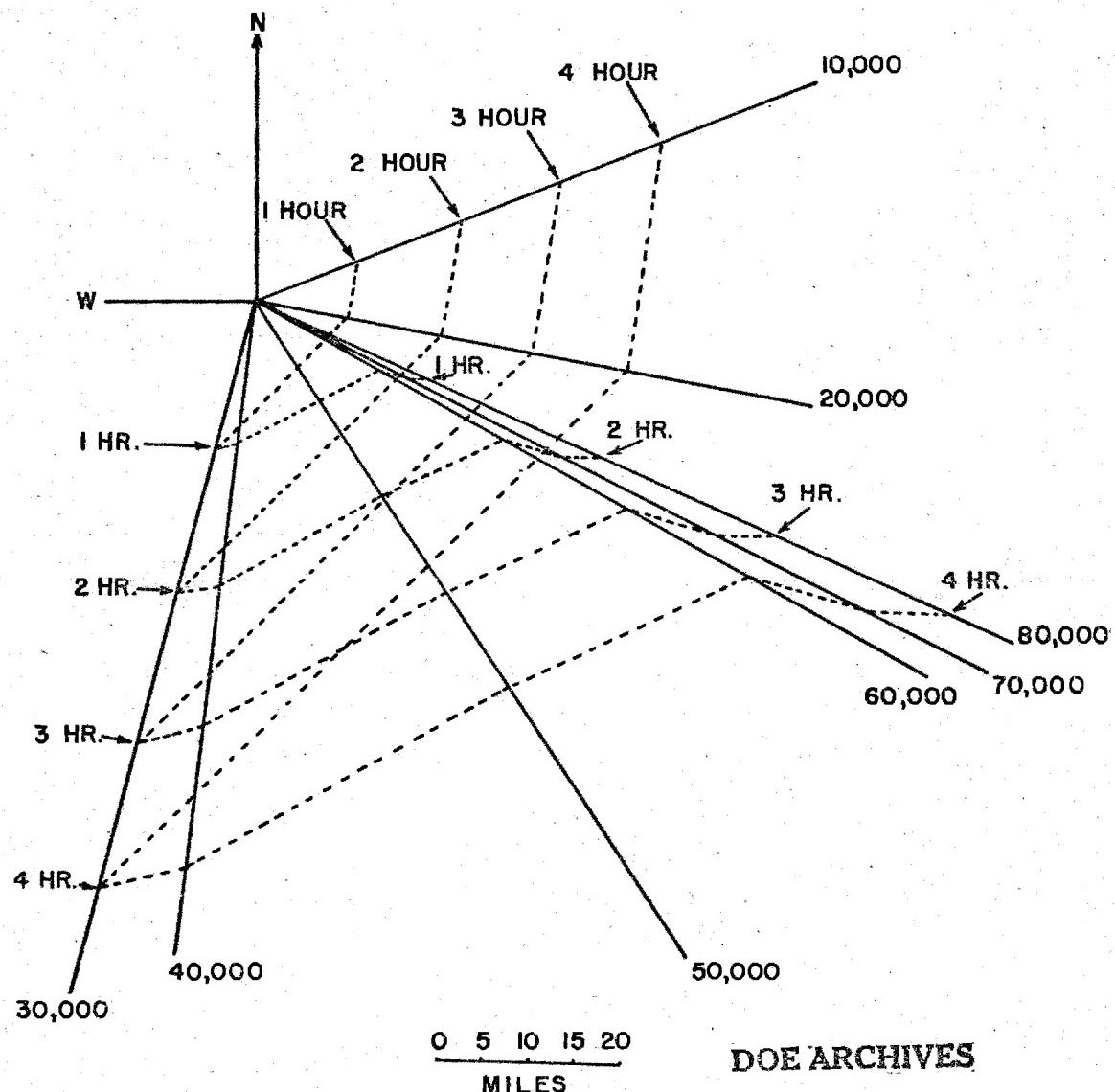
**DOE ARCHIVES**

526



531

FALL-OUT PREDICTION  
AIR WEATHER SERVICE METHOD  
CONDITION "A"

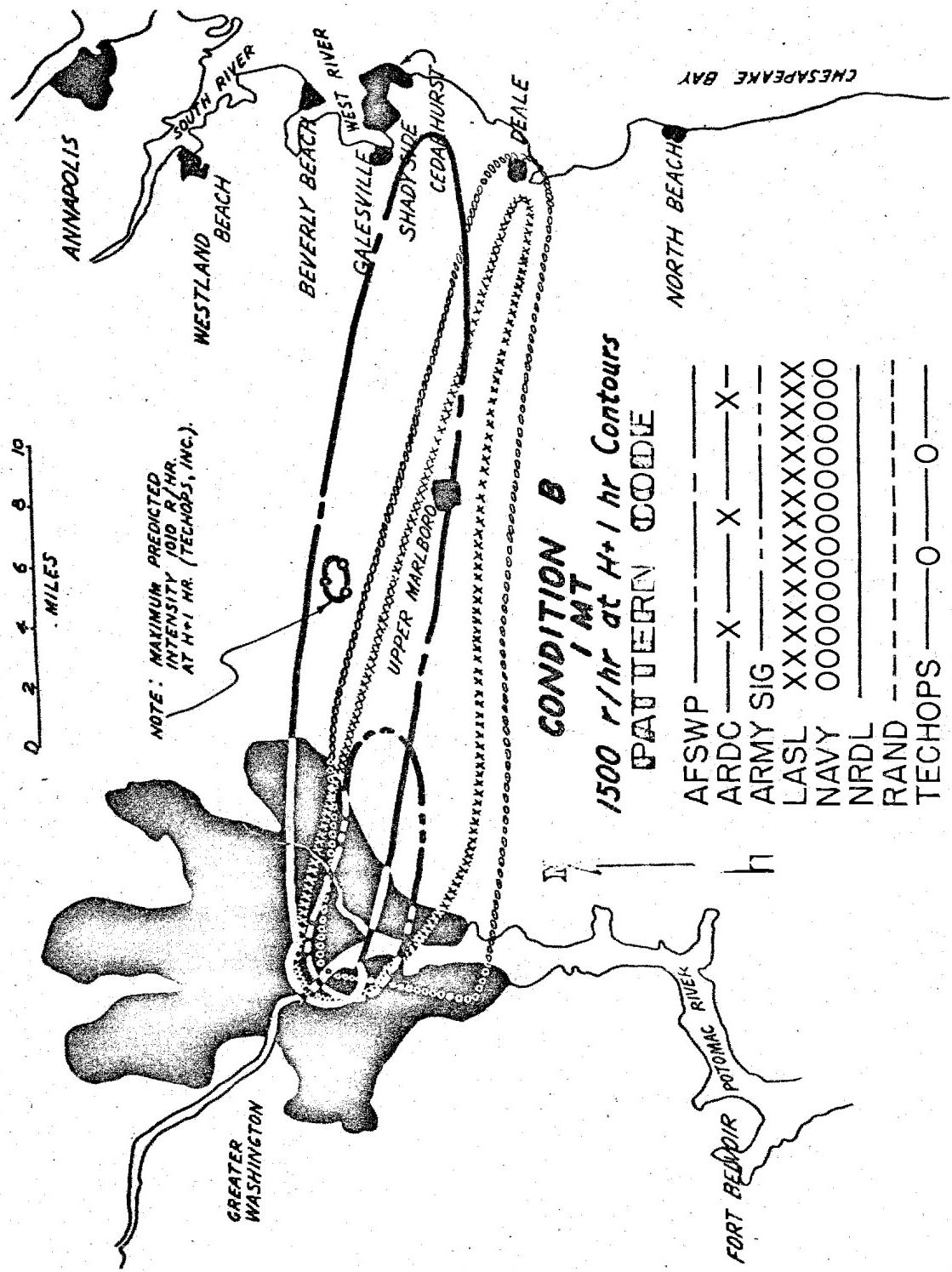


DOE ARCHIVES

527

AMERICAN ENERGY ACT

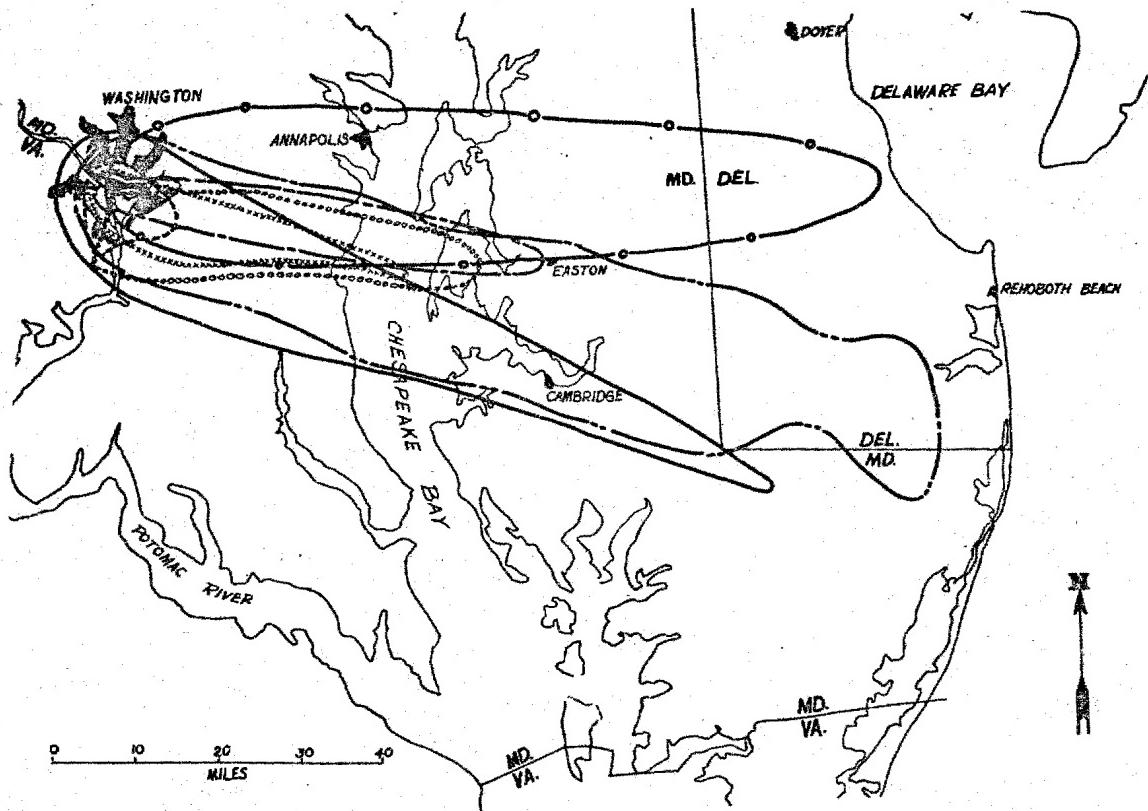
532



DOE ARCHIVES

528

593



**CONDITION B**  
**1 MT**  
*500r/hr At H+1 Hour Contours*

**PATTERN CODE**

AFSWP	-----		
ARDC	-X-	-X-	-X-
ARMY SIG	-----		
LASL	XXXXXXXXXXXXXX		
NAVY	00000000000000		
NRDL	-----		
RAND	-----		
TECHOPS	-O-	-O-	

**DOE ARCHIVES**

529

NUCLEAR ENERGY ACT OF 1954

534

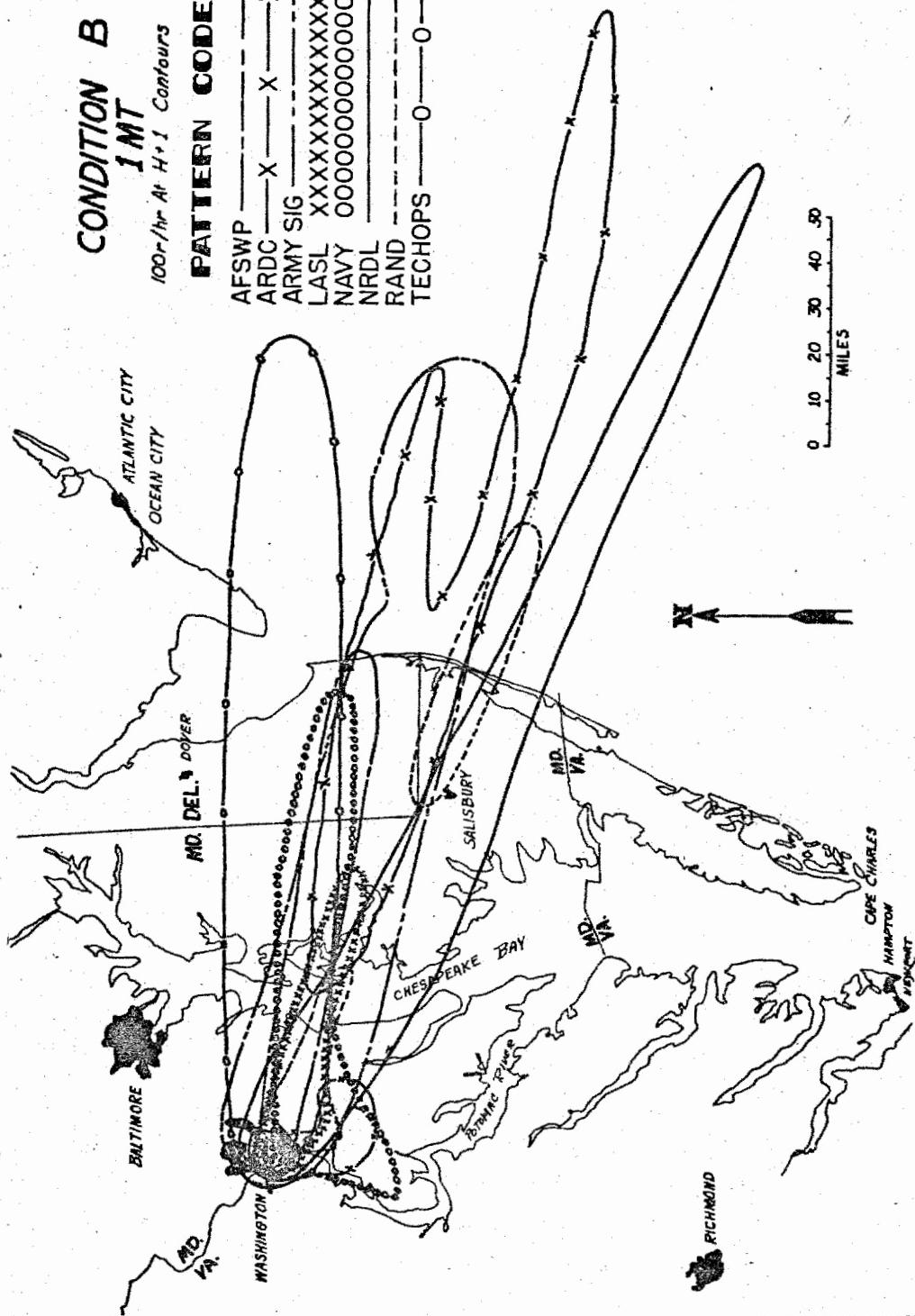
**CONDITION B**

**INT**

100r/hr At H+1 Contours

**PATTERN CODE**

AFSWP	- - -
ARDC	X - - X - - X
ARMY SIG	- - -
LASL	XXX XXX XXX XXX
NAVY	00000000000000
NRDL	- - -
RAND	- - - O - - - O
TECHOPS	- - -

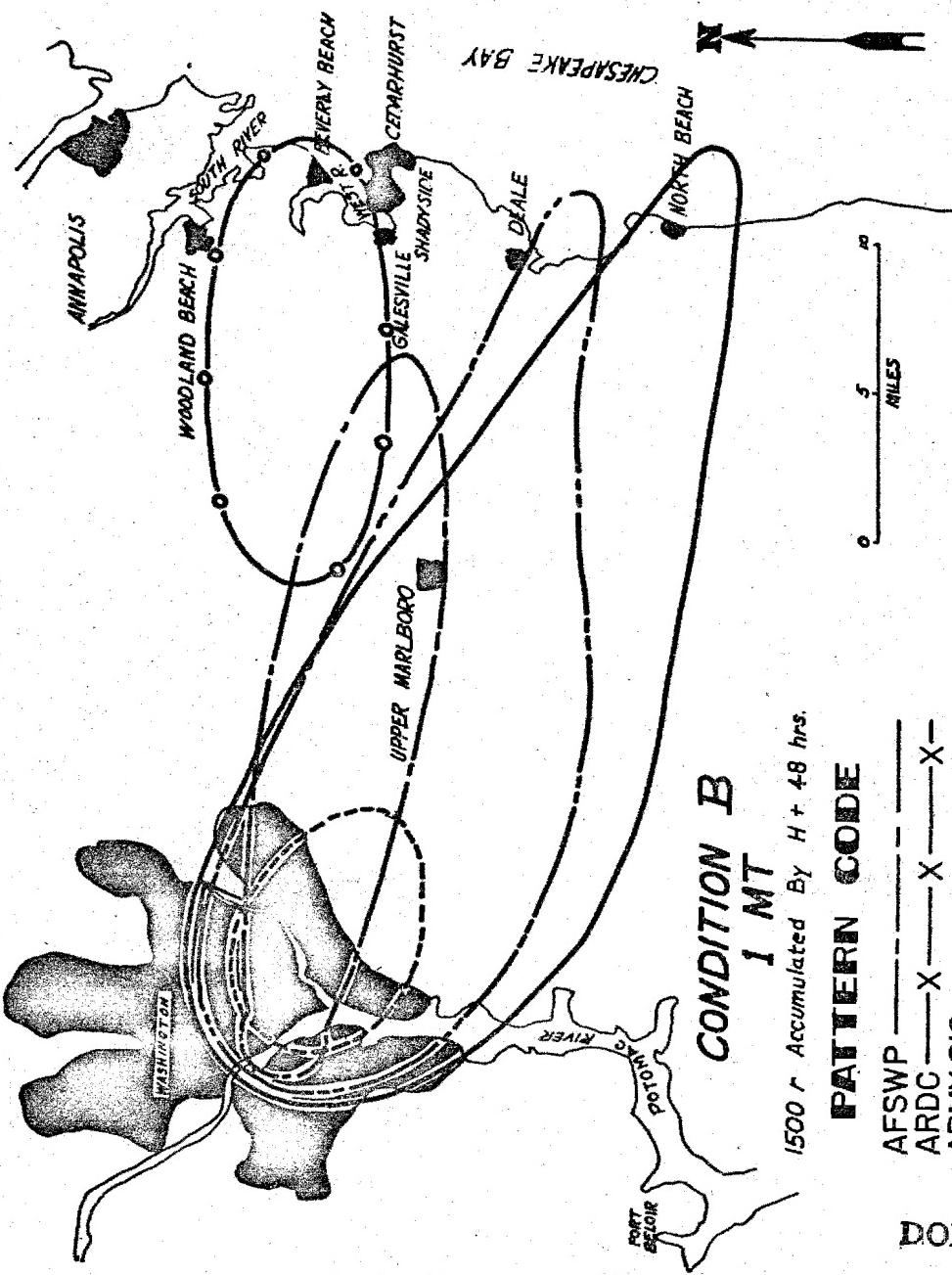


DOE ARCHIVES

530

ATOMIC ENERGY

535



### CONDITION B

1 MT  
1500 r Accumulated By H + 48 hrs.

### PATTERN CODE

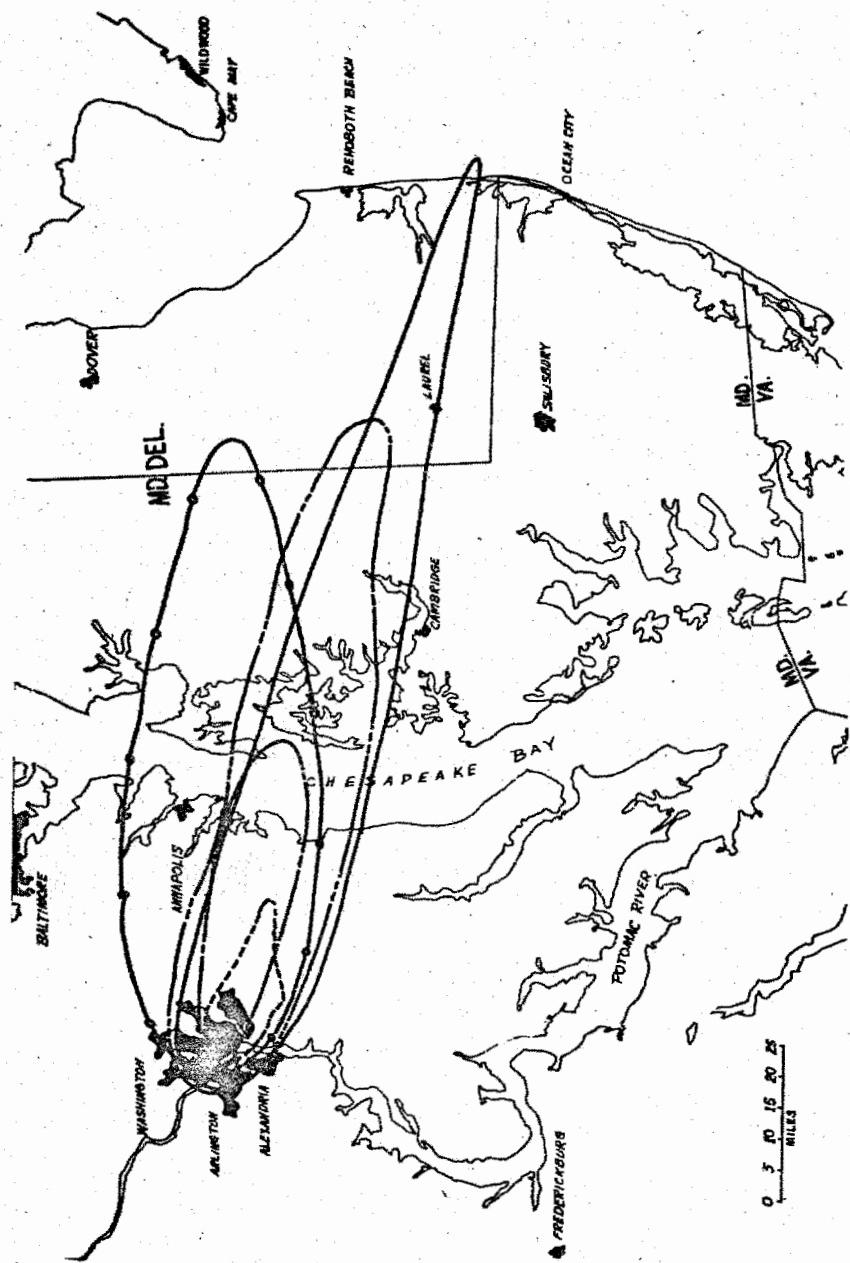
AFSWP	—	—	—	—
ARDC	—	X	—	X
ARMY SIG	—	—	—	—
LASL	XXXXXX	XXXXXX	XXXXXX	XXXXXX
NAVY	0000000000000000			
NRDL	—	—	—	—
RAND	—	—	—	—
TECHOPS	—	O	—	—

**DOE ARCHIVES**

531

DEPARTMENT OF ENERGY  
ATOMIC ENERGY ACT 1954

536



**CONDITION B**

**1 MT**  
500 m Accumulated By 1148 hrs.

**PATTERN CODE**

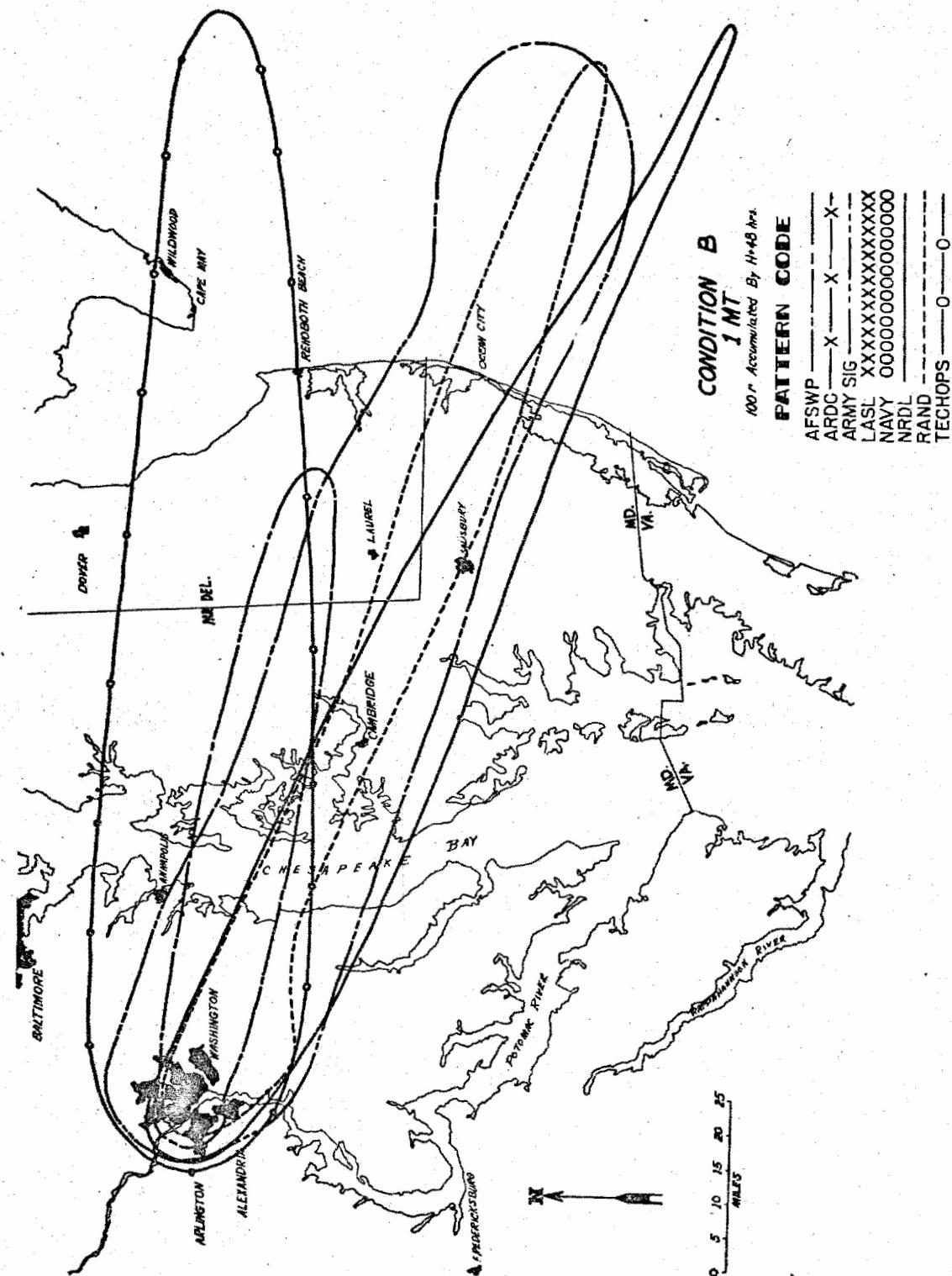
AFSWP	—	—	—
ARDC	X	—	X
ARMY SIG	—	—	—
LAISL	XXXXXX	XXXXXX	XXXXXX
NAVY	0000000000000000	0000000000000000	0000000000000000
NRDL	—	—	—
RAND	—	—	—
TECHOPS	—	O	—

**DOE ARCHIVES**

532

107  
DOE ENERGY DATA

537

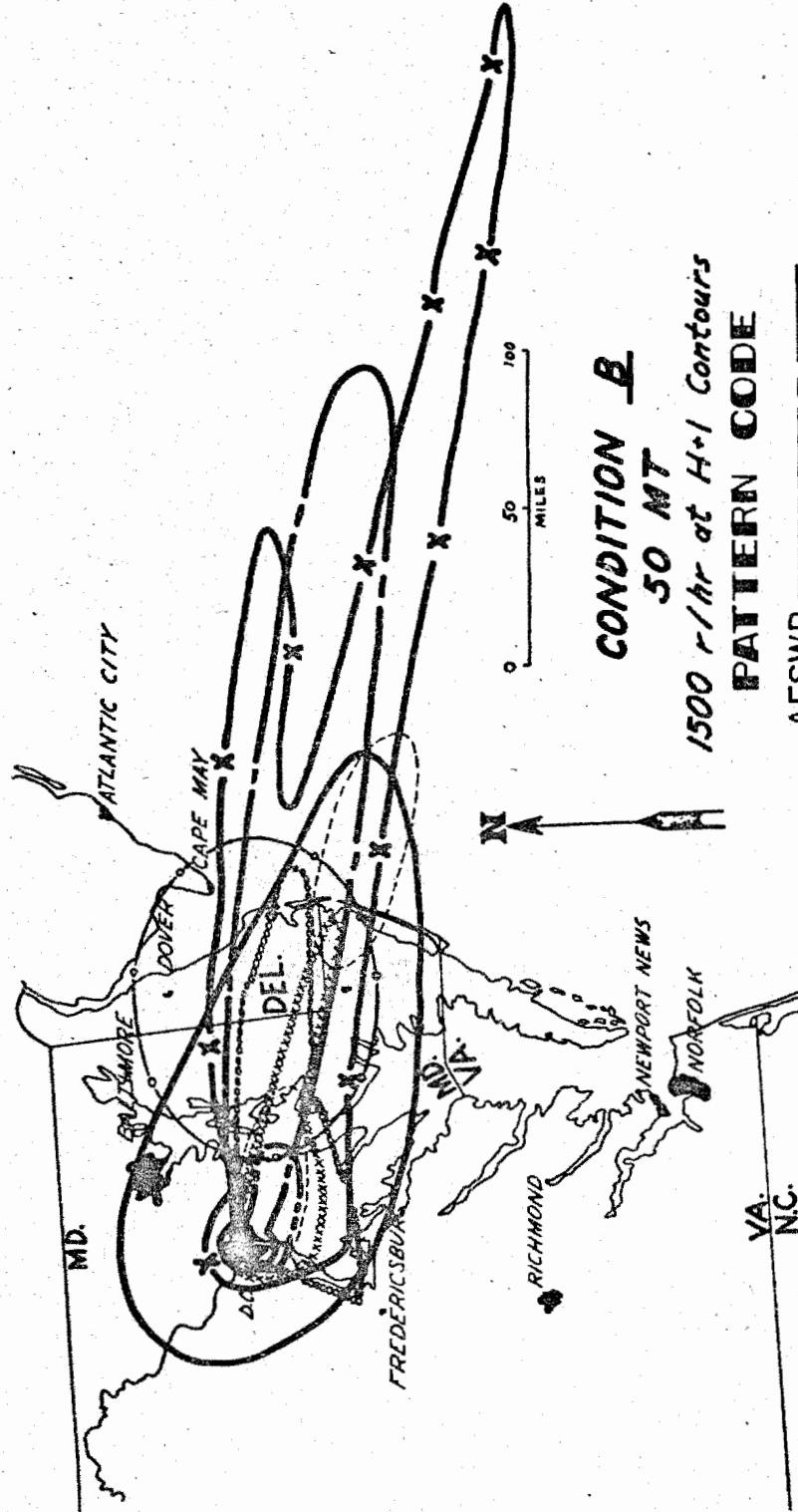


DOE ARCHIVES

533

ATOMIC ENERGY ACT 1954

538

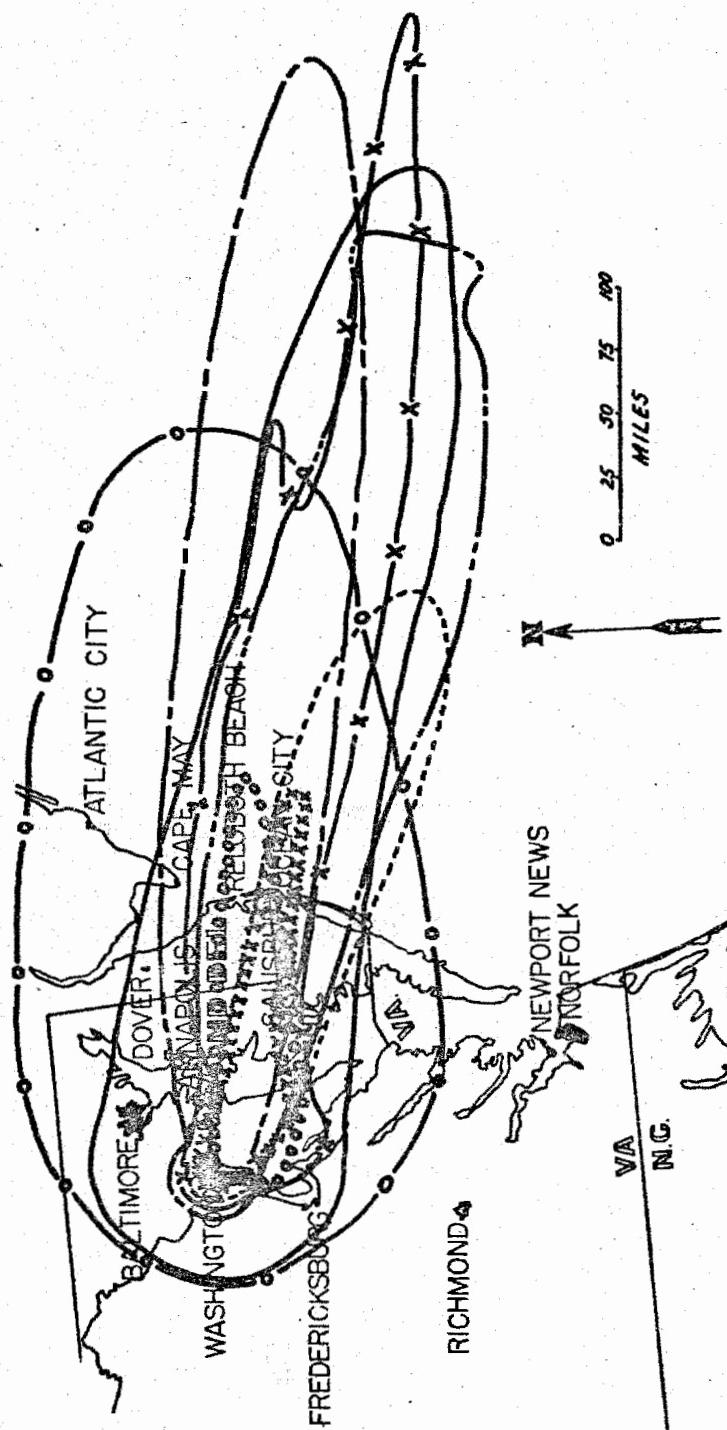


DOE ARCHIVES

534

AMERICAN ENERGY ACT  
ENERGY ACT 1954

539



**CONDITION B**  
**50 MT**  
500 r/hr at H+1 Contours

**PATTERN CODE**

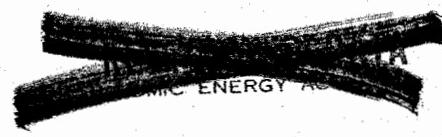
AFSWP	—	—	—	—
ARDC	X	—	X	—
ARMY SIG	—	—	—	—
LASL	XXXXXX	XXXXXX	XXXXXX	XXXXXX
NAVY	00000000000000	00000000000000	00000000000000	00000000000000
NRDL	—	—	—	—
RAND	—	—	—	—
TECHOPS	—	—	—	—

CAPE HATTERAS  
CAPE LOOKOUT

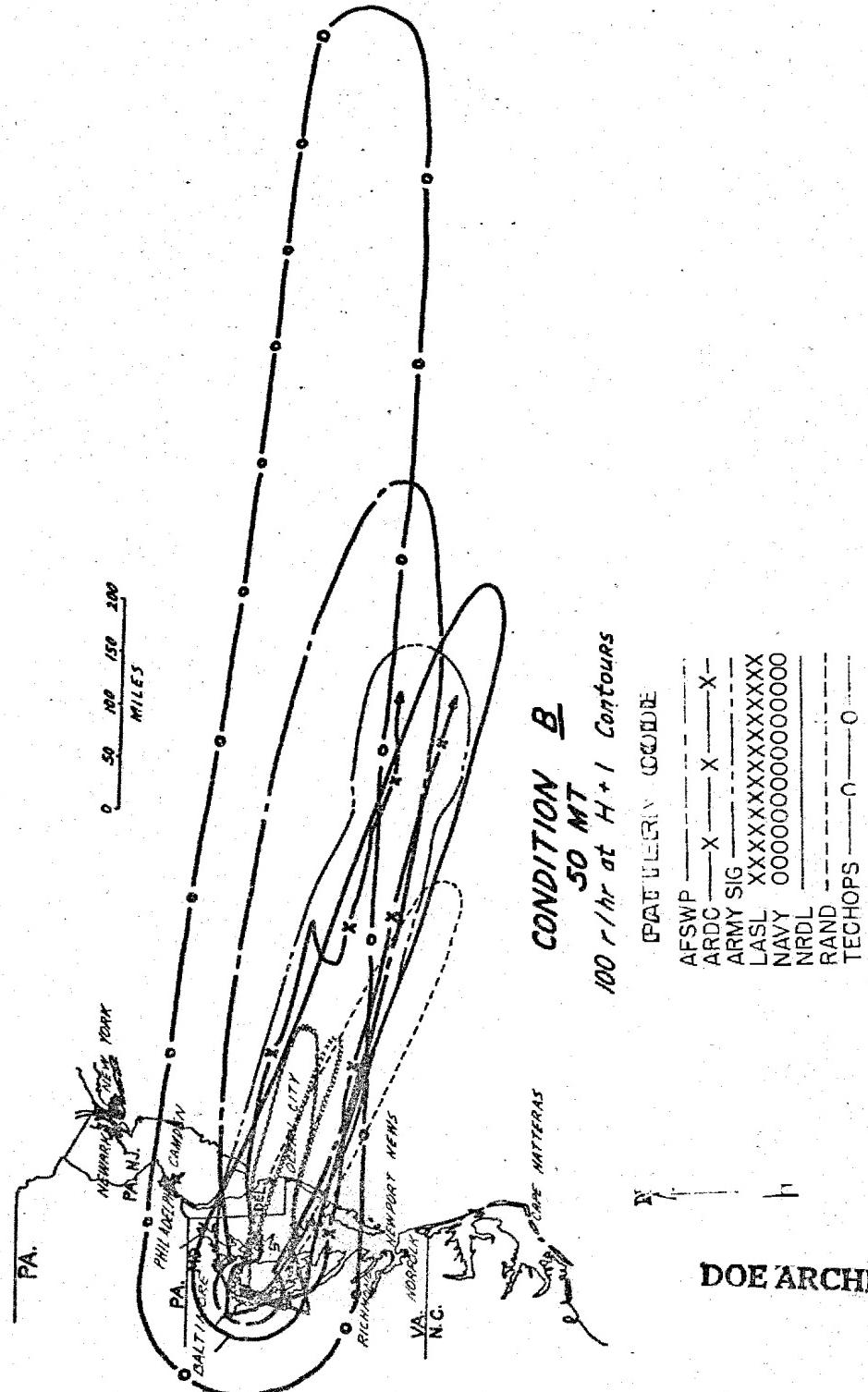
RALEIGH

**DOE ARCHIVES**

535



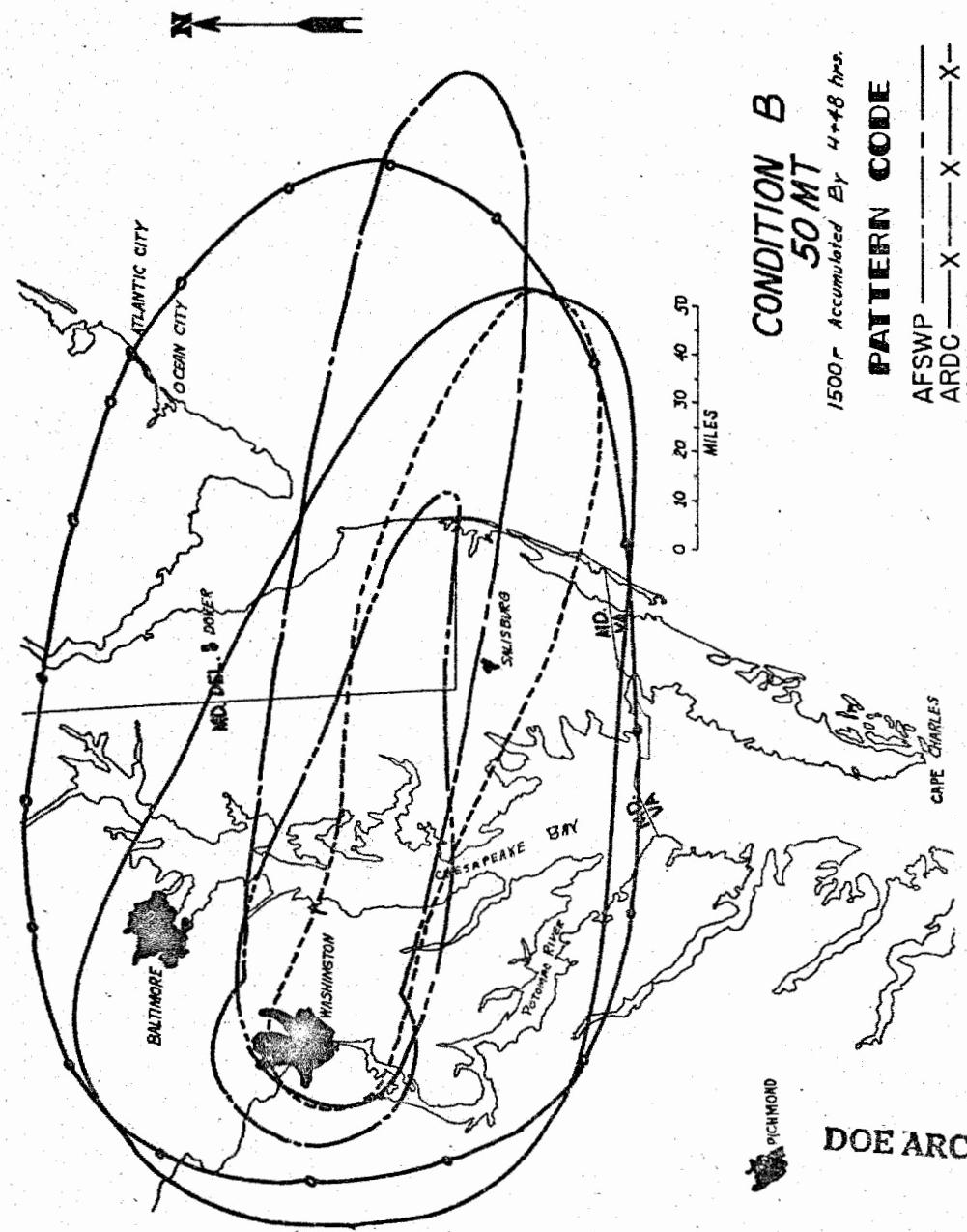
540



536

DOE ARCHIVES

541



DOE ARCHIVES

537

## ATOMIC ENERGY

542

7/18/88

INCOMPLETE DOCUMENT REFERENCE SHEET

The archive copy of this document is incomplete.

Pages missing 538

Enclosures missing \_\_\_\_\_

Attachments missing \_\_\_\_\_

Other \_\_\_\_\_

CR8  
signature

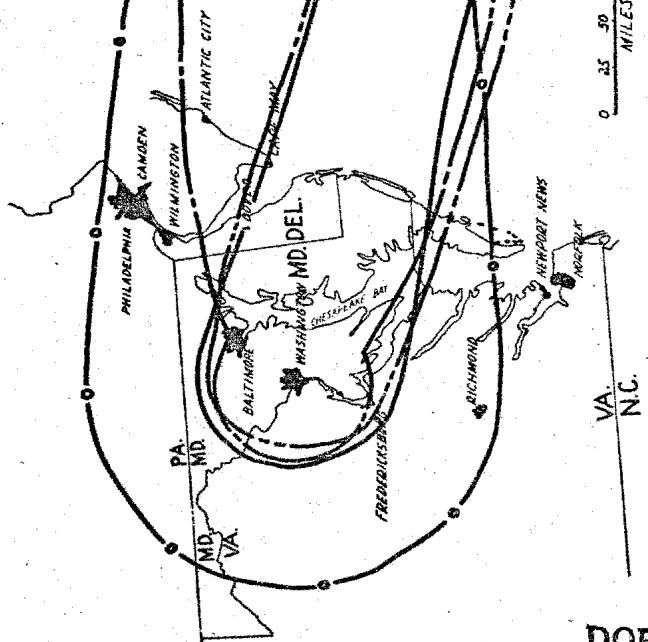
2-11-92  
date

542A

**CONDITION B**  
**50 WT**  
100 r Accumulated by H+40 hrs

**PATTERN CODE**

AFSWP	-----
ARDC	-X-----X-----X-
ARMY SIG	XXXXXXXXXXXXXX
LASL	00000000000000
NAVY	NRDL
RAND	TECHOPS



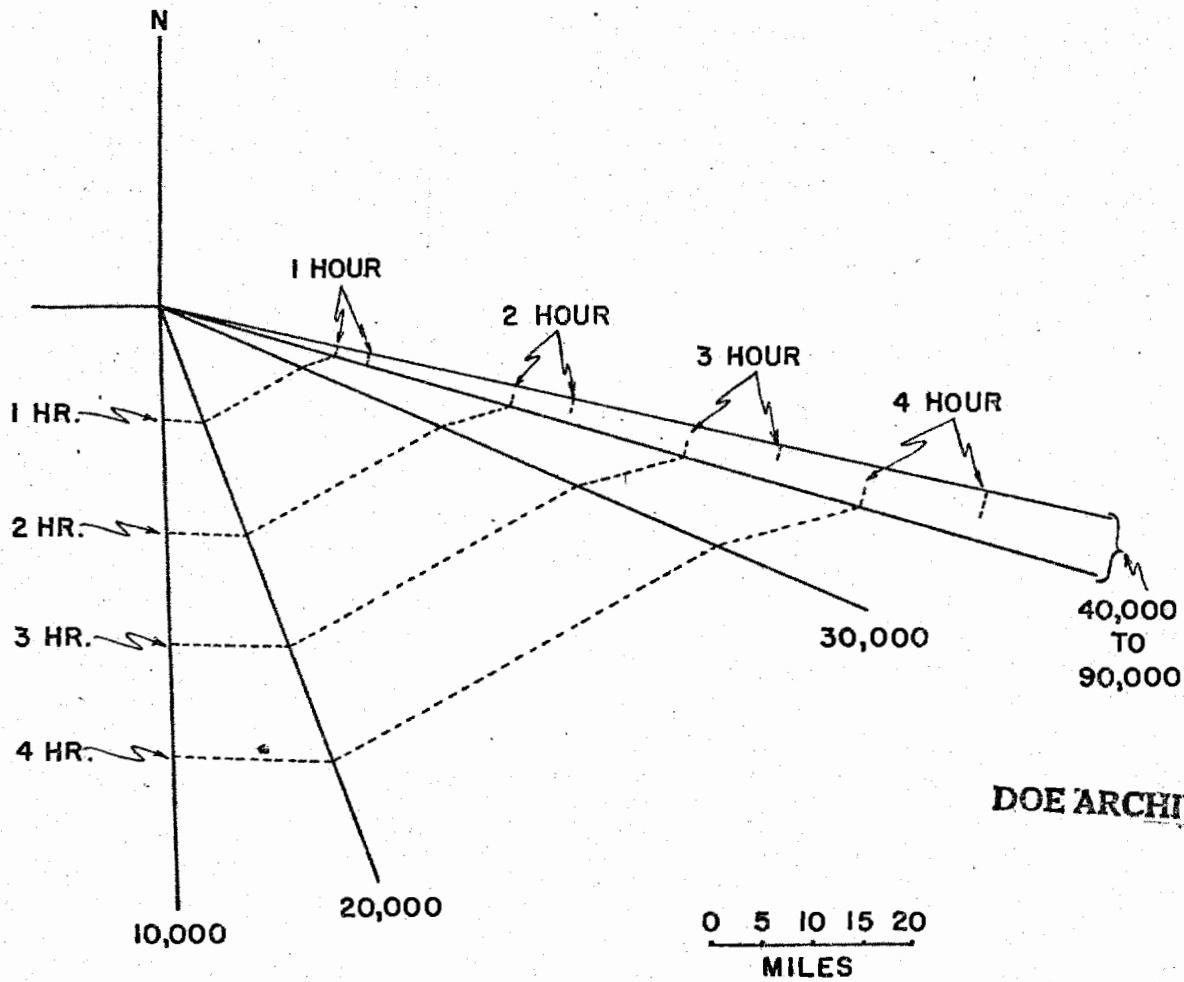
DOE ARCHIVES

539

ATOMIC ENERGY

543

FALL-OUT PREDICTION  
AIR WEATHER SERVICE METHOD  
CONDITION "B"



540

NUCLEAR ENERGY

544

Comparison of Certain Contour Parameters

CONDITION "A"

1 Mt Surface Burst

AFSWP	Arty Sig	ARDC	LASL	NAVY	NDRL	RAND Tech Ops
1500 r/hr at H+1	92 30 <u>4</u>	52 9 7	(**) 25 20	180 350 350	260 30 22	(**) 330 330 330
500 r/hr at H+1	330 60 (6)	1590 107 20	115 18 9	33 40 25	350 34 30	(33) (4) 13
100 r/hr at H+1	1,200 130 (10)	3,900 180 26	1,850 95 20	(950) (55) 35	650 70 40	1,150 83 29
1500 r/48 hrs	75 25 (5)	240 22 15	(**) ** *	*	190 26 10	(40) (7) 7
500 r/48 hrs	350 45 (9)	1620 105 22	450 26 (9)	*	670 40 22	(120) (14) 12
100 r/48 hrs	(1,300) 105 (13)	3,600 156 26	5,350 160 38	*	3,150 (92) 40	2,500 120 24

541

ATOMIC ENERGY

DOE ARCHIVES

545

The first figure given is the contour area in square miles; the second is the greatest downwind extent of the contour from ground zero in miles; and the third is the greatest crosswind extent of the contour in miles.

\* Indicates contours not received for this condition at time of press make-up.

\*\* Indicates method does not predict a significant contour for the conditions specified.

( ) Indicates smallest value predicted.

Underlining indicates largest value predicted. (Navy and Tech Ops values not included in this comparison, since the contours had to be normalized from data furnished.)

Comparison of Certain Contour Parameters

CONDITION "A"

50 Mt Surface Burst

AFSMP	ARMY SIG	ARDC	'LASL	NAVY	NDRL	RAND	TECH OPS
1500 r/hr at H+1	7,500 330 27	(650) (30) (25)	2,700 160 50	2,850 100 65	4,500 125 75	6,200 100 80	1,100 113 (25)
500 r/hr at H+1	23,000 550 50	20,000 400 65	27,000 280 80	(6,800) (134) 100	8,800 200 130	20,500 275 108	7,000 260 (47)
100 r/hr at H+1	92,000 1,000 110	57,000 660 98	>76,000 >600 270	(18,000) 215 120	24,000 250 150	119,000 1,000 152	28,000 500 (65)
1500 r/48 hrs	6,700 210 70	(2,900) (76) 56	5,700 160 38	*	*	2,000 125 80	3,000 153 (39)
500 r/48 hrs	18,000 340 60	22,000 395 75	12,200 (200) 70	*	*	20,000 (10,500) 110	22,000 238 (50)
100 r/48 hrs	81,000 700 135	55,000 580 96	>39,000 (>380) 95	*	*	114,000 (24,000) 152	111,000 560 (62)

The first figure given is the contour area in square miles; the second is the greatest downwind extent of the contour from ground zero in miles; and the third is the greatest crosswind extent of the contour in miles.

\* Indicates contours not received for this condition at time of press make-up.

\*\* Indicates method does not predict a significant contour for the conditions specified.

( ) Indicates smallest value predicted.

Underlining indicates largest value predicted. (Navy and Tech Ops values not included in this comparison, since the contours had to be normalized from data furnished.)

Comparison of Certain Contour Parameters

CONDITION "B"

1. MT Surface Burst

AFSMP	ARMY SIG	ARDC	LASL	NAVY	NRDL	RAND	TECH OPS
1500 r/hr at H+1	97 28 4	15 8 2	(**) (**) 6	72 26 5	116 27 (**)	6 2 3	**
500 r/hr at H+1	300 52 7	1,800 105 22	(**) 36 8	200 40 8	375 950 16	44 6 8	1,350 92 18
100 r/hr at H+1	2,400 110 (11)	4,100 172 27	3,500 250 28	(600) (64) 14	2,750 100 14	3,250 235 26	4,000 176 (11)
1500 r/4.8 hrs	110 (5)	220 30 11	*	*	*	290 33 14	(38) (8) 6
500 r/4.8 hrs	325 40 (10)	1,900 105 22	*	*	*	1,200 115 20	(140) (26) 12
100 r/4.8 hrs	(1,100) (95) (11)	4,000 165 28	*	*	*	2,100 176 26	1,500 165 17
							3,900 160 30

The first figure given is the contour area in square miles; the second is the greatest downwind extent of the contour from ground zero in miles; and the third is the greatest cross-wind extent of the contour in miles.

\* Indicates contours not received for this condition at time of press make-up.  
\*\* Indicates method does not predict a significant contour for the conditions specified.  
( ) Indicates smallest value predicted.

Underlining indicates largest value predicted. (Navy and Tech Ops values not included in this comparison since the contours had to be normalized from data furnished.)

543

DOE ARCHIVES

ATOMIC ENERGY ACT 1954

547

Comparison of Certain Contour Parameters

CONDITION "B"  
50 FT Surface Burst

AFSMP	ARMY SIG	ARDC	LASL	NAVY	NEDL	RAND	TECH OPS
1500 r/hr at H+1	7,500 260 32	350 (33) (12)	11,600 110 116	1,500 106 22	3,000 120 25	11,000 160 80	1,700 168 22
500 r/hr at H+1	27,000 435 62	24,000 380 76	17,500 150 56	(2,600) (152) (30)	3,700 155 35	31,000 400 26	8,500 240 52
100 r/hr at H+1	92,000 775 110	56,000 630 100	>34,000 >500 70	(6,000) (250) (50)	10,000 250 50	54,000 700 100	22,000 425 63
1500 r/18 hrs	7,500 200 40	(3,100) (115) 42	*	*	*	11,000 160	11,500 160 98
500 r/18 hrs	21,000 300 80	25,000 380 75	*	*	*	20,500 250 100	19,500 (225) (50)
100 r/18 hrs	76,000 550 170	47,000 600 100	*	*	*	35,000 450 100	28,000 (18,000) (350) (63)

544

ENERGY ACT 1954

The first figure given is the contour area in square miles; the second is the greatest downwind extent of the contour from ground zero in miles; and the third is the greatest cross-wind extent of the contour in miles.

\* Indicates contours not received for this condition at time of press make-up.  
\*\* Indicates method does not predict a significant contour for the conditions specified.

( ) Indicates smallest value predicted.  
Underlining indicates largest value predicted. (Navy and Tech Ops values not included in this comparison since the contours had to be normalized from data furnished.)

DOE ARCHIVES

547

## CLOSING REMARKS

Dr. Herbert Scoville, Jr.  
Armed Forces Special Weapons Project

Before opening the general discussion of the conference, I should like to summarize briefly my own impressions of what has been accomplished. First, we should remember that the prime objectives of this symposium were to make all the data on fallout available to everyone who has been making studies in the field. The second objective was to put forth the various theories and fallout models so that their assumptions and methods could be compared. Obviously, it is not possible to reach any decision as to a best method at a meeting of this sort. Actually, there is probably no such thing as a best method since different groups have different requirements for information.

I believe this symposium has rather graphically shown, in case anyone had previously doubted it, that the radiological fallout involves very complex phenomena. The initial stages in the process depend upon reactions occurring in the fireball and the properties of the atomic cloud. Later stages include atmospheric transport problems, particularly those related to the settling velocity of particulate matter. Finally, one has the radiological phenomena which determine the radiation fields in actual locations and which are effected by the radiochemical properties of the bomb debris. The entire fallout process is moreover strongly dependent on such external variables as the nature of the soil at the point of detonation and the meteorological conditions. It is, therefore, no wonder that all the data are not self-consistent and that a variety of models can be developed to explain the test observations.

With respect to the data, I believe that it is important to remember that to a large extent it derives from one or two actual test shots. For example, the data from the BRAVO shot has been used for calibration of all theories. Other shots have produced bits and pieces of data which are very useful in checking parts of the theories but with the exception of the JANGLE surface shot, all others have certain basic differences from the situation of greatest operational interest; i.e., surface land detonations of high yield weapons. Furthermore, as Lt Colonel Lulejian has pointed out, the weather conditions which actually existed at the BRAVO shot were not good for differentiating between some of the proposed models. In particular it was not satisfactory for determining what fractions of the active material are in the cloud and stem. I think it is also important to remember that obtaining data on fallout at the Pacific Proving Grounds is an extremely difficult process. A great deal of credit is due to those who have

struggled to get this information, where most of the fallout was occurring over the open ocean. In this respect, there is a new bright ray of light for the future as a result of the very fine work which was done on the spur of the moment, using the ocean itself as a collecting medium. It is indeed a rare event when a project produces important results within a week of its conception, and all who participated deserve a great deal of credit for the success of the oceanographic sampling project. In the future it would seem that oceanographic sampling combined with aerial surveys would provide a very practical solution to obtaining good fallout data at the Pacific Proving Grounds.

Despite all the difficulties in obtaining good data and the complexity of the phenomena, I think it would be a mistake to get the impression that we are completely ignorant of the magnitude of the fallout problem in operational situations. Actually, I believe that the general scale of the phenomena, as derived from the BRAVO fallout data, can be believed with a great deal of confidence. The available data from both the JANGLE surface shot which took place over a silicate sand and the ocean data from the lagoon barge shots all support the thesis that an appreciable fraction of the radioactive material produced in the explosion will fall out in the neighborhood of the detonation. We must conclude that a surface burst of a yield comparable to that of BRAVO will produce large areas, approximately 5,000 square miles, where the fallout will be lethal to exposed personnel. In certain specific situations this area might be only half as great and in others the area might be even greater, but I believe it can be guaranteed that this area will not be limited to a few hundred square miles. Likewise, I believe it is important to note that none of the speakers indicated that the contamination level outside the area of blast and fire damage would be likely to exceed ten or twenty times this lethal level. This is extremely important from a defensive point of view since it means that adequate radiation shielding can be obtained anywhere without construction of massive, expensive shelters.

Coming to the models, one has seen during the past two days a large number with widely varying degrees of complexity. Some will solve problems in a few minutes; others will require hours or fancy machines to produce the specific fallout patterns. Each of these models have their specific operational usefulness. While the complicated models can not be used directly to give operational information immediately following an attack, they are particularly useful in arriving at a detailed understanding of the phenomena. Furthermore, if a wide variety of typical meteorological situations are studied by means of these machine calculations it may be possible to get a rough picture which would be satisfactory for operational purposes by merely comparing the

DOE ARCHIVES

actual wind conditions with those which had been previously used in a machine solution. This approach would be similar to that described by Dr. Felt, who indicated that at the Nevada Test Site it is possible to predict with considerable confidence, based on previous experience, the fallout levels which will occur.

In summary, I believe that we can conclude that: (a) the general scale of the fallout problem under various detonation conditions can be reasonably well defined, (b) a number of models are now available which will provide reasonable estimates of the specific fallout patterns which are likely to occur under different meteorological conditions, and finally, (c) there is a real need for further experimental data to check the various theories. In this connection, the oceanographic techniques offer considerable promise in the Pacific, but truly satisfactory results will be obtained when it is possible to detonate large yield weapons on the surface of a large land mass.

DOE ARCHIVES

547

OMIC ENERGY

551

THIS PAGE IS BLANK

DOE ARCHIVES

548

## NUCLEAR ENERGY A

552

**SECRET**

## GENERAL DISCUSSION

Question: Dr. Kellogg, Rand Corp.

Is there any initial dosage rate at which it would be advisable to evacuate a contaminated area? It would seem that there must be a limit somewhere.

Answer: Dr. P. C. Tompkins, USNRDL

No. In my opinion, it is completely feasible to reduce the radiological effects at any location down to a safe value so that the limiting factor will be blast or fire. I am equally sure that one can design shelters to provide blast protection quite close to the limits of the crater, but here the problem may become economic.

Question: (Unknown)

Does this hold for civilian populations too?

Answer: Dr. P. C. Tompkins, USNRDL

In principle yes; however, practically there may be situations where evacuation is the best.

Question: Dr. Langer, FCDA

When you said you rule out evacuation, does this mean you rule out permanent evacuation also?

Answer: Dr. P. C. Tompkins, USNRDL

**DOE ARCHIVES**

In general, yes. I do not believe that we are going to run off and leave 5,000, 10,000, or 15,000 square miles deserted. If a single weapon were going to be dropped, then evacuation might be more practical but in a situation where many weapons may be released then this measure does not appear too useful.

Comment: LTCOL Lulejian, ARDC

I should like to show this slide of 111 bombs exploded over this country, 106 on cities of 100,000 or more. This points out that in such a situation there are very few locations to which it is safe to evacuate. Furthermore, it points out that when you have large numbers of bombs, meteorology becomes less important since the over-lap tends to blanket such large areas.

Comment: Dr. Knapp, OEG

This last chart certainly makes evacuation not look very good, up in the north, anyway. However, I would like to point out that people living within 5 or 6 miles of the center of a city might be killed by blast. The only solution for these people if they have an hour or two warning time might be to go upwind and take shelter.

Comment: Dr. Felt, LASL

In the event that we find ourselves forced to live in a contaminated area following an attack, I might point out that about twenty-five of us lived almost two months in such an area and after the first week people adjusted to it quite readily. After a couple of mistakes, it never occurred to us to go outside without taking necessary precautions.

Comment: LCDR Miller, BuAer

If one is planning to measure fall-out by surveying wide areas with aircraft, I believe that the accuracy of the method should be checked more thoroughly. My experience at CASTLE indicated considerable variation in the correction factors to reduce aerial readings to surface values.

Comment: Dr. Werner, USNRDL

DOE ARCHIVES

I believe that the aerial techniques for obtaining the intensity over the water are reasonably well established. However, care should be exercised to avoid the impression that these can give you the total amount of material in the water without additional information on the distribution of activity with depth. Perhaps the apparent correlation which was observed at CASTLE resulted from a constant distribution with depth which can not be relied on in all cases.

Comment: Mr. LeVine, NYOO, AEC

We too had difficulty initially in correlating aerial data with ground surveys but by the last shot the techniques had been sufficiently well developed so that we obtained a constant correction factor in almost every case. It should be noted that the aerial surveys picked up activity which went off to the northeast and which was not detected by other

means. This activity disappeared on the second day indicating that particles had settled below the surface. There is, of course, considerable question as to how much activity had disappeared before the first survey was made. This observation may give some clue as to the presence of activity in the stem since the fall-out pattern from the stem was to the northeast in contrast to the pattern from the cloud which was to the west.

Comment: Dr. Scoville, AFSWP

One of the reasons for the discrepancies in aerial survey measurements results from the non-uniformity of the source. When a large area is uniformly contaminated, the altitude correction factors should be constant. However, for the Enewetak situation, where the contamination is heavy on a small land mass and low over the water, it is quite natural to expect big variations from one location to the other. I do believe, however, that it will always be necessary to calibrate the aerial surveys over the ocean with oceanographic measurements in order to obtain depth distribution.

Comment: LTCOL Lulejian, ARDC

We did lots of aerial measurements at Nevada and these show the importance of the geometric factors. If the contamination is not uniform or if there is shielding, then the altitude relationships will vary.

Question: MAJ Hord, AFSWP

DOE ARCHIVES

What is there about the thermocline which traps the fission products?

Answer: Mr. Isaacs, Scripps

In the ocean there is a layer, about 100 meters thick, in which there is considerable mixing; but there is very little mixing between this layer with the water below it. Therefore, diffusion of fission products through this boundary, i.e., the thermocline, is very slow.

Question: Dr. Scoville, AFSWP

Both the shots at which oceanographic measurements were made were lagoon shots where the fall-out was primarily associated with very small particles. In a surface land shot where the

particles are 100 micron or larger, would they be expected to have an appreciable settling velocity through the thermocline?

Answer: Dr. Folsom, Scripps

We do not know. In order to check this at an actual shot it will be necessary to collect water samples below the thermocline and, where possible, even on the bottom.

Comment: Dr. Kellogg, Rand Corp.

With respect to fall-out model construction, it is interesting to note that a great many agencies have started by using a simple model, finding that it does not satisfy the experimental results and finally going to more and more complex models, including eventually machine calculations. It should be pointed out that the machine calculations, once they are developed, will again reverse the trend and decrease the time required to solve a specific fall-out problem.

Comment: Dr. Graves, LASL

I think what Dr. Kellogg said is true. It is possible that complicated calculations may now be made by machine. On the other hand, we have seen examples of various computations here and they do not disagree enough to be able to evaluate them with the available data. I wonder whether we are yet at the stage where these more complicated calculations are justified until we have more input data.

Question: Mr. Isaacs, Scripps

DOE ARCHIVES

In this connection, one matter worries me. This is the type of material over which the bomb is exploded. We have talked about particles produced from soil but soil does not enter into it if one has a surface burst in New York City. In such a case, what would be the particle size? I also question how realistic a very careful model would be.

Answer: Mr. Tompkins, CRL

As far as cities are concerned the Chemical Corps is looking into this now. I think this problem can be approached by trying to develop a better understanding of the mechanism of the formation of the original particles in the cooling

[REDACTED]

fireball. If we understand this mechanism, we should be better able to predict what will happen for different types of surfaces.

Comment: Dr. Felt, LASL

I think that Dr. Scoville mistakenly gave the impression that it is not worthwhile for people to consider data resulting from other types of shots, particularly those at Nevada. These produced lots of information, some good, some poor. The models should be able to say something about the Nevada shots if they are good models, and these shots provide a lot more data for checking the various systems.

Comment: Dr. Scoville, AFSWP

I agree. I only meant to imply that the only test which approaches the situation which one is most interested in operationally was the Bravo shot, but certainly other shots can be useful in providing checks on various steps in the different fall-out models.

Question: Dr. Tompkins, USNRDL

I wonder if Mr. Young of NOL would be willing to discuss some of his work on mass subsidence which might explain some of the other fall-out observations.

Answer: Mr. Young, NOL

DOE ARCHIVES

We have observed mass subsidence from HE tests and underwater shots. A few pictures we have seen at CASTLE indicated that this may have occurred during the first five minutes but unfortunately there was insufficient light to get good pictures. This effect might have contributed to the early spreading out of the active material along the surface.

**THIS PAGE IS BLANK**

**DOE ARCHIVES**

**554**



**558**

ATTENDANCE LIST

<u>NAME</u>	<u>RANK</u>	<u>ORGANIZATION</u>
ADAMS, Charles E.	Civ	USNRDL
ADKINS, W. H.	LtCol	AFMPC-AE
AITKEN, Harold L.	Civ	FCDA
ALLEN, Philip W.	Civ	Weather Bureau
ANDREWS, Howard	Dr	Health, Education & Welfare
ANDREWS, Thomas J.	LtCol	OASD (R&D)
ARMSTRONG, W. W.	Civ	BuShips
BALLINGER, Edwin R.	Capt	Hq, ARDC
BALLOU, Nathan E.	Dr	USNRDL
BARNETT, Benjamin	Dr	Chem & Radiological Lab
BARNETT, Kenneth M.	Civ	Sig Corps
BASCOM, Williard	Civ	Nat'l Academy of Science
BEERS, B. W.	Col	OSD
BEHNKE, A. R.	CAPT	USNRDL
BENNETT, B. F.	CAPT	BuShips
BENNETT, W. F. V.	CDR	CNO OP-36
BIRD, D. C.	LtCol	Hq, AFSWP
BLIFFORD, Irving H. Jr.	Civ	NRL
BODINGER, Norman B.	Maj	CONAD
BONNOT, Carlos D.	LtCol	JTF-7
BOOGHER, Arnold	LtCol	AFMLP
BOUSE, Therman	LtCol	DA, Research & Development
BOWMAN, Donald	Civ	OSD
BRENNAN, John W.	Capt	Army Map Service
BRENNAN, James T.	Col	Walter Reed
BRETTLER, Benjamin J.	Civ	EG&G Inc
BRICE, Charles S.	LtCol	DA, Research & Development
BRILL, Heber C.	Maj	DA, Research & Development
BROOKS, W. K.	CIR	CNO OP-341E1
BROWN, B. F.	CAPT	Hq, AFSWP
BROWNING, L. E.	LtCol	Hq, AFSWP
BROWNYARD, Theodore L.	Dr	BuOrd
BURRISS, Richard C.	Capt	Air Weather Service
BYARS, David O. Jr.	Col	JTF-7
CADLE, Richard D.	Dr	Stanford Research Inst
CALLAHAN, Cornelius J.	Civ	Air Weather Service
CARP, Gerald	Civ	Evans Sig Lab
CHAPMAN, Rupert D.	LtCol	DA, Research & Development
CHUBBUCH, James B.	LtCol	OCE
CLARK, Francis	Civ	Nuclear Dev Assoc
CLARK, Fred J. Jr.	Maj	DA, Research & Development

CLARK, Joseph T.	Col	OSD
CLAUS, Walter D.	Dr	B&M, AEC
COATES, J. K.	LCDR	BuShips
CONANT, Frank D.	Capt.	DA, Research & Development
CONDIT, Richard I.	Dr	G3
COOK, Clarence S.	Dr	USNRDL
COOK, Thomas B.	Civ	Sandia Corp
COONS, Richard David	Civ	Hq, ARDC
COWAN, Maynard	Civ	Sandia Corp
CRISTADORO, M. A.	LtCol	AFDAP
CURTIN, G. P.	LtCol	G3
CRUMLEY, Harold J.	Civ	ARDC
DALE, C. R.	CIR	OP-533
DAVIDSON, Harold O.	Dr	ORO
DAVIDSON, Glenn M.	Civ	BuOrd
DAVIES, John M.	Civ	DA, Research & Development
DHEIN, Ernest H.	Civ	Corps of Engineers
DUDLEY, Robert A.	Civ	AEC
DUNNING, Gordon	Dr	B&M, AEC
DURHAM, A. C.	Civ	BuShips
EDDY, Leonard A.	LtCol	Hq, AFSWP
EISENBUD, Merrill	Civ	NYOO
ELY, Strode L.	Civ	AFCIE
ERICKSON, Kenneth Warne	Dr	WSEG
ERNST, Martin L.	Civ	CNO Oper Eval Grp
ETTER, Harry S.	CIR	Med Corps USN
FACCI, Hugo A.	Civ	AFCIE
FAIR, William R.	Civ	Stanford Research Inst
FANO, Ugo	Civ	Nat'l Bureau of Standards
FAVORITE, W. M.	Maj	AFDRQ
FELDMAN, David	Civ	DA, Research & Development
FELT, Gaelen	Civ	LASL
FIESTER, Irving	Civ	AFOOA
FINE, Paul C.	Dr	DOE ARCHIVES
FLETCHER, Robert Dawson	Civ	DMA-AEC
FOLSOM, Theodore R.	Civ	Air Weather Service
FRENCH, Joseph E.	Maj	ONR
GAGGE, Adolph Pharo	Col	Air Weather Service
GALE, Donald I.	Civ	AFDRD-HF
GARCIA, Luis F.	Civ	NRL
GARDNER, J. H.	Dr	NRL
GAYER, H. Kenneth	Dr	OCAFF
GENEVSE, Frank	Dr	AFOOA
		AFOIN

GETZINGER, P. L.	LtCol	OCAFF
GIBSON, Thomas A. Jr.	Maj	Hq, AFSWP
GILFILLIAM, Edward S.	Dr	Tech Operations
GILLER, Edward B.	Col	AFSWC
GOLDTHWAITE, Robert	RADM	JTF-7
GRAVES, Alvin C.	Civ	LASL
GREENBERG, Norman D.	LtCol	DMA-AEC
GREENE, Jack C.	Civ	FCDA
GREENFIELD, Stanley M.	Civ	Rand Corp
GROSSMAN, Bertram H.	Civ	AFCRC
GUILD, Walter A.	Col	Health, Education & Welfare
GUTHRIE, William L.	Capt	DMA-AEC
HAFSTAD, Katherine	Civ	ORO
HALLOCK, H. E.	Civ	Sig Corps
HANSEN, Carl L., Jr.	Maj	Hq, AFSWP
HARDIN, Luther M.	Civ	Chem & Rad. Lab
HARMAN, Leo V.	Col	AFDDC-ND
HARRIS, D. Lee	Civ	Weather Bureau
HARTMANN, Gregory K.	Dr	BuOrd
HAYES, George T.	Civ	Stanford Research Inst
HENRIQUES, F. C.	Dr	Tech Operations
HILCKEN, John A.	Maj	MSC
HILL, Jerald Everett	Dr	Rand Corp
HINNERS, Robert A.	CAPT	USNRDL
HODGES, Charles T.	LtCol	USMC JCS
HOLLAND, Willis D.	Capt	Army Med Service Grad School
HOLZMAN, Benjamin G.	Col	AFSWC
HOME, William M.	Capt	Chem & Radio. Lab
HOOKS, D. E.	BrigG	AFOAT-1
HORD, John d'H	Maj	Hq, AFSWP
HORTON, H. Burke	Civ	Office of Defense Mobilization
HUGHES, James Henry	Civ	ONR
IRVINE, James Jr.	Maj	Corps of Engineers
ISAACS, John Dove III	Civ	Scripps Inst Oceanog.
JACKSON, John Early	Civ	OASD (R&D)
JAMES, Jack G.	LtCol	Field Command, AFSWP
JENNINGS, Feenan Dee	Civ	Scripps Inst Oceanog.
JOHNSON, Robert F.	LTJG	USNRDL
JOHNSON, William S.	Civ	LASL
JONES, John Junior	Col	DOE ARCHIVES
JONES, William L.	Maj	Air Weather Service
		OSD



KAESSER, Herman H.	LtCol	Hq, AFSWP
KANE, John Joseph	Civ	ONR
KELLOGG, William Welch	Civ	Rand Corp
KENNEDY, William R.	Civ	LASL
KESLING, Earl W.	Col	AFOAT
KESSLER, Irving J.	Civ	AFOOA
KNAPP, Harold A.	Dr	CNO Oper Eval Grp
KORTY, Vernon M.	Civ	BuOrd
KOTSCH, W. J.	CDR	OP-533
KREY, Philip W.	Civ	Chem & Radiological Lab
KRIEGER, Firmin Joseph	Civ	Rand Corp
KSANDA, Charles F.	Civ	USNRDL
LANGER, Rudolph	Civ	FCDA
LANGEVIN, R. A.	Civ	Tech Operations
LaRIVIERE, Philip D.	Civ	USNRDL
LA VIER, Eugene C.	LtCol	Hq, AFSWP
LAURINO, Richard K.	Civ	USNRDL
LAWTON, Alfred H.	Dr	AFIRD-HF
LAY, Dent L.	Col	Hq, AFSWP
LE VINE, Harris D.	Civ	NYOO,AEC
LIFTON, S. E.	Maj	USAF(MC)
LIST, Robert J.	Civ	Weather Bureau
LOCKHART, Luther B. Jr.	Civ	NRL
LOWRY, Philip	Dr	ORO
LUKES, George D.	Civ	OSD
LULEJIAN, Norair M.	LtCol	Hq, ARDC
McCAMPBELL, James M.	Civ	USNRDL
McCOWN, Dean A.	LtCol	AFOAT
McGINLEY, Eugene	MajG	JTF-7
McLAUGHLIN, Earl W.	CDR	BuAir
MACHTA, Lester	Civ	Weather Bureau
MAHAFFEY, George W.	Civ	USNRDL
MARCIANO, Joseph J.	Civ	NEL
MARFING, T. E.	LtCol	OCAFF
MARGENAC, Henry	Civ	ONR
MARTELL, Edward A.	Dr	Inst of Nuclear Studies Univ. of Chicago
MASSEY, Donnell	Col	JTF-7
MASTERSON, John E.	LCDR	ONR
MAUPIN, Clinton S.	Civ	Field Command, AFSWP
MAXWELL, Richard	Civ	Tech Operations
MAXWELL, Roy D.	Col	Hq, AFSWP
MEYER, George R.	LCDR	DOE ARCHIVES Field Command, AFSWP

MILLER, Carl F.	Dr	USNRDL
MILLER, Charles A.	Col	CONAD
MITCHELL, Harold H.	Lt	Hq, AFSWP
MITCHELL, James P.	Civ	Chem & Radiological Lab
MITTELMAN, Don I.	Civ	DA, Research & Development
MOMSEN, Charles B.	RADM	JTF-7
MORGAN, Bruce H.	Civ	OM Food & Cont (Chi)
MORRIS, Wilford E.	Dr	BuOrd
MULLER, Ragnwald (NMI)	LCDR	BuAir
MURDEN, Charles H.	LtCol	School of Aviation Med
MURPHY, Howard L.	CDR	Hq, Cmd, Bolling AFB
MUTCH, William W.	Civ	BuDocks
NAGLER, Kenneth M.	Civ	NRL
NASH, Russell J.	Maj	Weather Bureau
NELSON, Robert K.	LtCol	AFOAT-1
NEUNDORFFER, J. D.	Dr	SCC
NEWELL, John F.	Civ	CNO Oper Eval Grp
NIEMAN, A. S.	Civ	AEC
NORTHROP, Doyle L.	Civ	AFCIE
O'DONOGHUE, John A.	CIR	AFOAT-1
O'KEEFE, Bernard J.	Civ	Med Corps, USN
OWNBY, Frederick L.	Maj	EG&G Inc
OYSTER, Dale E.	Civ	AFIRD-HF
		USAF OPN
PACK, Donald H.	Civ	Weather Bureau
PAINES, Roger W.	CDR	Hq, AFSWP
PARSONS, Edgar L.	Dr	FCDA
PARTHUM, Alfred H. Jr.	LtCol	Hq, AFSWP
PENLAND, J. R.	Capt	JCS
PENNINGTON, Ralph W.	Civ	SWD Ft Bliss, Tex
PERLEY, R. H.	CDR	JTF-7
PFEIFFER, Edward G.	Capt	Air Weather Service
PICKLER, D. A.	CDR	JTF-7
PINSON, Ernest A.	Col	AFSWC
POOLER, Francis Jr.	Civ	Weather Bureau <b>DOE ARCHIVES</b>
POSEY, James T.	Col	JCS
POWELL, Clinton C.	Dr	Health, Education & Welfare
FRITCHARD, William C.	Col	OSD
PURCELL, W. P.	LtCol	G3
RAPP, Ralph Robert	Civ	Rand Corp
REEVES, James E.	Civ	SFOO
REX, Daniel F.	CDR	JTF-7

559

ATOMIC ENERGY ACT 1954

563

RICHIE, Frank G.	Maj	JTF-7
ROBERTS, William K.	Maj	Field Command, AFSWP
ROCK, Donald H.	Civ	AFOAT-1
ROSE, Howard C.	Maj	Hq, AFSWP
SCHORR, Marvin	Dr	Tech Operations
SCHUERT, Edward A.	Civ	USNRDL
SCHUYLER, Garrett L.	Civ	FCDA
SCOVILLE, Herbert Jr.	Dr	Hq, AFSWP
SHAPIRO, Maurice M.	Civ	NRL
SHIELDS, Buren R.	Capt	Hq, RECOM
SINGER, S. E.	Maj	AFSWC
SINGLEVICH, Walter	Civ	AFOAT-1
SMITH, James W.	Civ	ONR
SMITH, Scott W.	Civ	Bureau of Standards
SMITH, Sherwood B.	Civ	Hq, AFSWP
SPOHN, Clifford A.	LtCol	Air Weather Service
SPREEN, William C.	Civ	Air Weather Service
STEEL, Charles L.	Maj	Army Map Service
STETSON, Robert L.	Civ	USNRDL
STOPINSKI, Orin W.	Civ	LASL
STROCK, Alan M.	LtCol	USA JCS
STUDER, Robert	LtCol	G3
SUNDSTROM, Harold J.	Civ	Corps of Eng
SVENDSON, E. C.	CDR	BuShips Code 850
SWOMLEY, Neely M.	Maj	Sig Corps
SWINGLE, Donald M.	Dr	Evans Sig Lab
TARRANT, Legare K.	BrigG	Hq, AFSWP
TAYLOR, P. H.	LtCol	AFCIE
TAYLOR, Robert L.	Capt	AFOOP
TERRILL, James G.	Civ	Health, Education & Welfare
TEST, Herbert H.	Civ	AFDRQ
THOMAS, Norman C.	Civ	DA, Research & Development
THOMSON, Warren	Civ	OSD
TOMPKINS, Edward R.	Dr	USNRDL
TOMPKINS, Paul C.	Dr	USNRDL
TOMPKINS, Robert C.	Civ	Chem & Rad Lab
TORBETT, Oscar C.	Capt	Army Map Service
TYLER, George W.	Civ	AFOOA
UNDERWOOD, Warren N.	Col	DOE ARCHIVES
UNGAR, Stanley H.	Civ	Corps of Eng
VAN HORN, William H.	Civ	Evans Sig Lab
VAN STRATEN, F. W.	Dr	
VANN, James O.	LtCol	Corps of Eng
		OP-533
		AFSWC

VINE, Allyn C.	Dr	BuShips
WALLACE, Duane G.	Maj	AFOPD
WALSH, Thomas	Civ	Corps of Engineers
WATSON, William W.	Dr	ONR
WEIDLER, Roy C. Jr.	Maj	Hq, AFSWP
WERNER, Louis B.	Dr	USNRDL
WHEDON, Frances	Civ	OC Sig 0
WEYLER, Harry	Civ	Weather Bureau
WHITE, Fred D.	Civ	Weather Bureau
WHITE, Thomas N.	Civ	LASL
WHITE, William L.	Civ	Stanford Research Inst
WIENER, Martin	Civ	AFOIN
WILKINS, James Jr.	Civ	Nuclear Dev Assoc
WILLIAMS, Edwin G.	Civ	FCDA
WILSEY, Edward F.	Civ	Chem Radiological Lab
WYCKOFF, Harold L.	Civ	Bureau of Standards
YOUNG, George A.	Civ	BuOrd
ZIGMAN, Paul E.	Civ	USNRDL
ZIRKIND, Ralph A.	Civ	BuAir

**DOE ARCHIVES**

561

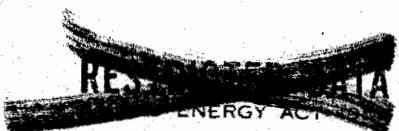
ATOMIC ENERGY ACT

565

THIS PAGE IS BLANK

DOE ARCHIVES

562



566  
571